UCRL-16580

University of California

Ernest O. Lawrence Radiation Laboratory

NUCLEAR CHEMISTRY DIVISION ANNUAL REPORT

1965

TWO-WEEK LOAN COPY

This is a Library Circulating Copy which may be borrowed for two weeks. For a personal retention copy, call Tech. Info. Division, Ext. 5545

DISCLAIMER

This document was prepared as an account of work sponsored by the United States Government. While this document is believed to contain correct information, neither the United States Government nor any agency thereof, nor the Regents of the University of California, nor any of their employees, makes any warranty, express or implied, or assumes any legal responsibility for the accuracy, completeness, or usefulness of any information, apparatus, product, or process disclosed, or represents that its use would not infringe privately owned rights. Reference herein to any specific commercial product, process, or service by its trade name, trademark, manufacturer, or otherwise, does not necessarily constitute or imply its endorsement, recommendation, or favoring by the United States Government or any agency thereof, or the Regents of the University of California. The views and opinions of authors expressed herein do not necessarily state or reflect those of the United States Government or any agency thereof or the Regents of the University of California.

Research a[illegible]velopment

UCRL-16580
UC-4 Chemistry
TID-4500 (46th Ed.)

UNIVERSITY OF CALIFORNIA
Lawrence Radiation Laboratory
Berkeley, California

AEC Contract No. W-7405-eng-48

NUCLEAR CHEMISTRY DIVISION ANNUAL REPORT, 1965

January 1966

I. Perlman, Director, Nuclear Chemistry Division
Editors: J. M. Hollander, F. Reynolds, and B. B. Cunningham

Work done under the auspices of the U. S. Atomic Commission

Printed in USA. Price $6.00. Available from the Clearinghouse for Federal Scientific and Technical Information, National Bureau of Standards, U. S. Department of Commerce, Springfield, Virginia.

NUCLEAR CHEMISTRY DIVISION ANNUAL REPORT, 1965

Contents

A. RADIOACTIVITY AND NUCLEAR STRUCTURE

1. Measurements of g Factors of Excited States with a Digital Time-to-Height Converter (E. Matthias and D. A. Shirley) 1
2. g Factor of the 90-keV Level in Ru^{99} and the Paramagnetic Correction in Transition Atoms (E. Matthias, S. S. Rosenblum, and D. A. Shirley). . . 4
3. Half-Life and g Factor of the 75-keV Level in Rh^{100} (E. Matthias, D. A. Shirley, J. S. Evans, and R. A. Naumann) 9
4. Nuclear Spin and Moment of Ag^{110m} by Paramagnetic Resonance (Warren Easley, Norman Edelstein, Melvin P. Klein, D. A. Shirley, and H. Hollis Wickman) . 14
5. Nuclear Moments of Americium-241 and 16-h Americium-242 and Analysis of the Hyperfine Fields (Lloyd Armstrong, Jr. and Richard Marrus) . . . 15
6. Direct Measurement of the Magnetic Moment of Plutonium-239 (John Faust, Richard Marrus, and William A. Nierenberg) 16
7. Hyperfine Structure and Nuclear Moments of Promethium-148 and Erbium-165 (Dolores Ali, Isaac Maleh, and Richard Marrus) 17
8. The Decay Scheme of Es^{254} (W. McHarris, F. S. Stephens, F. Asaro, and I. Perlman) 18
9. Energy Levels of Am^{239} and Am^{241} (I. Ahmad, F. Asaro, and I. Perlman). . 21
10. Odd-Parity Rotational Bands in Cm^{246} (F. S. Stephens, Frank Asaro, Sherman Fried, and I. Perlman) 26
11. A New Particle-Conserving Variational Wave Function for the Nuclear Pairing-Force Problem (Oliver Johns and J. O. Rasmussen) 29
12. Measurement of Pair Production Cross Section Near Threshold (T. Yamazaki and J. M. Hollander) 34
13. The Effect of the Chemical State on the Lifetime of the 24-Second Isomer of Nb^{90} (J. A. Cooper, J. M. Hollander, and J. O. Rasmussen) 35
14. New Weak Beta Transition from Y^{88} (M. Sakai, T. Yamazaki, and J. M. Hollander) 39
15. An 8- Isomaric State in the 106-Neutron Nuclei: W^{180}, Os^{182}, Pt^{184} (J. Burde, R. M. Diamond, and F. S. Stephens) 40
16. An Isomer of Spin $25/2^+$ in Re^{183} (M. J. Emmott, J. R. Leigh, J. O. Newton, and D. Ward) 43
17. Angular Distribution of γ Rays in $La^{139}(p, 2n)Ce^{138}$ (Mitsuo Sakai, Toshimitsu Yamazaki, John R. Meriwether, and David L. Hendrie) 46
18. Spin and Parity of Be^8 States at 16.6 and 16.9 MeV (H. E. Conzett, P. Darriulat, H. G. Pugh, E. Shield, and R. J. Slobodrian) 48
19. (d, α) Reactions on C^{12}, N^{14} and O^{16} Induced by 24 MeV Deuterons (Richard H. Pehl, Joseph Cerny, Ernest Rivet, and Bernard G. Harvey) . . 49
20. Investigation of High Spin Levels Preferentially Populated by the (α, d) Reaction (Richard H. Pehl, Ernest Rivet, Joseph Cerny, and Bernard G. Harvey) 52
21. Energy Levels of O^{18} from Shell Theory (Martin G. Redlich) 54
22. Corrected Na^{20} Mass and Levels in Na^{20} and F^{16} Using the (He^3, t) Reaction (R. H. Pehl and J. Cerny) 57
23. Observation of $T = \frac{3}{2}$ Levels in Li^7-Be^7 and the Uncharacterized Nuclei He^7, B^7, and He^8 (Claude Détraz, Joseph Cerny, and Richard H. Pehl). . . . 59

24. Li^4 and the Excited Levels of He^4 (Joseph Cerny, Claude Détraz, and Richard H. Pehl) 61

25. He^3 and He^4 Scattering on B^{11} (D. L. Hendrie, Marc Chabre, H. G. Pugh, and E. Boschitz) 64

26. The $C^{12}(d,t)C^{11}$ and $C^{12}(d,He^3)B^{11}$ Reactions (M. Chabre, D. L. Hendrie, H. G. Pugh, and C. Détraz) 68

27. The Scattering of α Particles by Cr^{52} (John R. Meriwether, Italo Gabrielli, David L. Hendrie, Jeannette Mahoney, and Bernard G. Harvey) 71

28. Charge and Energy Distributions of Recoils from Th^{226} Alpha Decay (K. Gunter, F. Asaro, and A. C. Helmholz) 74

29. The Mass 13 T = 3/2 Quartet (J. Cerny, R. H. Pehl, G. Butler, D. G. Fleming, C. Maples, and C. Détraz) 76

30. New Neutron-Deficient Isotopes of Emanation (Matti Nurmia, Kalevi Valli, and Earl K. Hyde) 80

31. Decay Properties of Zr^{86} (E. K. Hyde, W. J. Treytl, A. Siivola, D. H. Sisson, and D. J. Horen 81

32. Shell-Model Calculation for Po^{212} Norman Glendenning and Kichinosuke Harada 82

33. Restudy of Alpha Decay of Fr^{212} (Kalevi Valli and Earl K. Hyde) 85

34. Radiations of 14-Minute Nb^{88} (E. K. Hyde and M. Nitschke) 87

35. The Radiations of 1.9-Hour Nb^{89} (E. K. Hyde and J. M. Nitschke) 88

36. High-Resolution Study of Transitions in the Decay of U^{237} (T. Yamazaki and J. M. Hollander) 91

37. Internal-Conversion Coefficients of the 381-keV and 389-keV M4 Transitions from Y^{87m} and Sr^{87m} (M. Sakai, T. Yamazaki, and J. M. Hollander). . . 92

B. FISSION

1. Identification of Heavy-Ion Reaction Products by In-Beam x-Ray Measurement (H. R. Bowman and S. G. Thompson) 95

2. Gamma-Ray and Internal-Conversion Electron Studies of Primary Cf^{252} Fission Fragments (R. L. Watson, H. R. Bowman, S. G. Thompson, and J. O. Rasmussen) 96

3. Fragment Angular Distribution in the Fission of Bi^{209} and U^{238} Induced by α Particles of Energies up to 115 MeV (Shyam S. Kapoor, Hiroshi Baba, and Stanley G. Thompson 99

4. Fission Properties of Some Elements Below Radium (A. Khodai-Joopari, R. C. Gatti, and S. G. Thompson) 101

5. Fission of Uranium-238 by Argon-40 (Torbjörn Sikkeland) 105

C. NUCLEAR REACTIONS AND SCATTERING

1. Correlations as Revealed by the (p, t) Reaction (Norman K. Glendenning) . . 107

2. Inelastic Scattering Based on a Microscopic Description of Nuclei (Norman K. Glendenning and Marcel Veneroni) 109

3. Inelastic Scattering of 40.5-MeV Alpha Particles by C^{12}, C^{13}, N^{14}, N^{15}, O^{16}, and O^{18} (B. G. Harvey, J. R. Meriwether, J. Mahoney, A. Bussière de Nercy, and D. H. Horen) 112

4. Comparison Between Phase Shift and Complex Potential Descriptions of Elastic Scattering (Jonas Alster and H. E. Conzett). 114

5. Energy Dependence of the Polarization in p-O^{16} Elastic Scattering Between 21 and 53 MeV (E. T. Boschitz, M. Chabre, H. E. Conzett, and R. J. Slobodrian). 118

6. Polarization in p-He^4 Scattering Between 27 and 63 MeV (E. T. Boschitz, M. Chabre, H. E. Conzett, E. Shield, and R. J. Slobodrian) 120

7. Proton Polarization in Small-Angle p-He^4 Scattering at 38.7 MeV (E. Boschitz, M. Chabre, H. E. Conzett, E. Shield, and R. J. Slobodrian) 122

8. The Real Part of the Scattering Amplitude at High Energies (Homer E. Conzett) 124

9. Study of the $He^4(p, d)He^3$ Reaction with Polarized Protons at 55 and 63 MeV (E. T. Boschitz, M. Chabre, H. E. Conzett, and R. J. Slobodrian) . . . 126

10. On the Determination of the Proton-Proton $^1S_0$ Shape Parameter (R. J. Slobodrian) 128

11. The $C^{12}(p, 2p)B^{11}$ Reaction at 50 MeV (H. G. Pugh, D. L. Hendrie, Marc Chabre, and E. Boschitz). 130

12. Inelastic Scattering of α Particles on Fe^{56} (J. Valentin, I. Garbrielli, B. G. Harvey, D. L. Hendrie, J. Mahoney, and J. R. Meriwether) . . . 133

13. Comparison of the Elastic Scattering of He^3 and He^4 by Ca^{40} (A. Springer, Marc Chabre, D. L. Hendrie, and H. G. Pugh) 136

14. High-Energy Deuteron Cross Sections (V. Franco and R. J. Glauber) . . 139

15. Qualitative Aspects of Neutron-Nuclear Interactions and the Optical Model (V. Franco) 140

16. Extended Charge Effects on Low-Energy Proton-Proton Scattering (R. J. Slobodrian) 142

17. The $Li^6(p, pd)He^4$ and $Li^7(p, pt)He^4$ Reactions at 55 MeV (D. L. Hendrie, Marc Chabre, and H. G. Pugh) 146

D. CHEMISTRY

1. Systematic Variation of Quadrupole Crystal-Field Shielding in Rare-Earth Ethylsulfates (Johan Blok and D. A. Shirley) 149

2. Systematic Variation of Hyperfine Fields at Nuclei of Solutes in Ferromagnetic Lattices (D. A. Shirley) 152

3. Hypersensitive Transitions in Rare-Earth Ions (B. R. Judd) 154

4. Second Quantization and Atomic Spectroscopy (B. R. Judd) 154

5. Three-Particle Operators for Equivalent Electrons (B. R. Judd) 155

6. Zeeman Effect as a Prototype for Intra-Atomic Interactions (B. R. Judd) . 156

7. The Hyperfine Magnetic Fields at Nuclei of Indium in Iron and Nickel (R. J. Holliday, D. A. Shirley, and N. J. Stone) 156

8. The Temperature Scale for Neodymium Ethylsulfate Below 1°K (Johan Blok, D. A. Shirley, and N. J. Stone) 161

9. Crystal Structure and Lattice Parameters of Curium Trichloride (J. C. Wallmann, J. Fuger, J. R. Peterson, and J. L. Green) 163

10. The Heat of Solution of Curium Metal and the Heats of Formation of $Cm^{+3}(aq)$ and $CmCl_{3(c)}$ (J. C. Wallman, J. Fuger, Hermann Haug, Sayed A. Marei, and Brij M. Bansal) 164

11. The Absorption Spectrum of Cf^{+3} and Crystallography of Californium Sesquioxide and Californium Trichloride (J. L. Green and B. B. Cunningham) . . 166

12. Hyperfine Fields in Gold-Manganese Compounds (M. O. Faltens and D. A. Shirley) 169

13. Atomic-Beam Method for the Study of Isotope Shifts (Richard Marrus and Douglas McColm) 173

14. Measurements of the Fano Factor and the Energy Per Hole-Electron Pair in Germanium (Sven O. W. Antman, Donald A. Landis, and Richard H. Pehl) 175

15. The Production and Characterization of Am^{+2} in CaF_2 Crystals (N. Edelstein, W. Easley, and R. McLaughlin) 178

16. Optical Pumping Transients in Rb^{87} and Application to Disorientation Cross Sections (Richard Marrus and Joseph Yellin) 178

17. Crystal and Molecular Structure of a Double Complex of Manganese with Phthalocyanato and Pyridine Ligands (Lester H. Vogt, Jr., Allan Zalkin, and David H. Templeton) 179

18. The Crystal and Molecular Structure of $C_5H_5FeB_9C_2H_{11}$ (Allan Zalkin, David H. Templeton, and Ted E. Hopkins) 182

19. Crystal Structure of Thorium Nitrate Pentahydrate by x-Ray Diffraction (Tatzuo Ueki, Allan Zalkin, and David H. Templeton) 185

20. The Structure of Cycloaliin Hydrochloride Monohydrate (K. J. Palmer (and Kay Sue Lee) 189

21. Mass Spectroscopy. The Determination of First Ionization Potentials by Surface Ionization Methods (F. L. Reynolds) 192

22. Metastable Peaks in the Mass Spectra of N_2O and NO_2 (Amos S. Newton and A. F. Sciamanna) 194

23. Metastable Ion Peak Shapes in Dempster-Type Mass Spectrometers (Amos S. Newton) 198

24. Application of High-Resolution Semiconductor Detectors in x-Ray Emission Spectrography (H. R. Bowman, E. K. Hyde, S. G. Thompson, and R. C. Jared) 202

E. RADIATION CHEMISTRY

1. Reactivity of the Hydrated Electron with Organo-Nitrogen Compounds (Rodney L. S. Willix and Warren M. Garrison) 207

2. Formation of Unsaturated Products in the Radiolysis of Peptides in the Solid State (Mathilde Kland-English and Warren M. Garrison) 210

F. INORGANIC CHEMISTRY

1. The Extraction of Perchloric Acid by Trilaurylamine. I. Aromatic Diluents (J. J. Bucher and R. M. Diamond) 213

2. Spectrophotometric Determination of Gold with Azide (Ray G. Clem and E. H. Huffman) 215

G. INSTRUMENTATION

1. 88-Inch Cyclotron Research and Development (David J. Clark, Elon Close, and Hogil Kim) 219

2. Energy Levels of Pu^{+3} on $LaCl_3$ (John G. Conway and K. Rajnak) . . . 222

3. A Preamplifier with 0.5-keV Resolution for Semiconductor Radiation Detectors (E. Elad and M. Nakamura) 222

4. Nuclear Instruments (William Goldsworthy) 223

5. A 4096-Channel Analog-To-Digital Converter (F. S. Goulding, L. B. Robinson, and F. Gin) 224

6. Instruments Developed for the New AEC Modular System (F. S. Goulding, S. Wright, D. Schurr, and D. Landis) 225

7. Germanium Gamma Ray Detector Development (W. L. Hansen and B. V. Jarrett) 226

8. Nitride and Oxide Bands of Molybdenum (John C. Howard and John G. Conway) 227

9. Beam Current Integrator System with Built-In Preset Dump Scaler and Control Circuitry (D. A. Landis and F. S. Goulding) 227

10. Implementing Automatic Data Handling (Richard Leres) 228

11. Silicon Radiation Detectors (R. P. Lothrop, M. D. Roach, H. E. Smith, and B. V. Jarrett) 228

12. Detection of 30- and 40-MeV Protons by a Thin-Window Lithium-Drifted Germanium Counter (Richard H. Pehl, Donald A. Landis, Fred S. Goulding and Blair V. Jarrett) 229

13. Computer System for Nuclear Spectroscopy Program (L. Robinson, M. Myers, J. Meng, and H. Cingolani) 231

14. Computer System at the 88-Inch Cyclotron (L. Robinson, T. Schaeffer, and J. Mahoney) 231

15. An Advanced Multiscaler (A. A. Wydler) 232

16. Improved Accuracy in Measurement of Low Gas Flow Rates with a Bubble Meter (Amos S. Newton and G. W. Kilian) 233

17. Electron-Gamma Angular Correlation Apparatus Using Semiconductor Detectors (T. Yamazaki, D. A. Landis, R. S. Stone and J. M. Hollander) 236

18. A Three-Counter Particle Identifier for Studies of Low-Yield Nuclear Reactions (F. S. Goulding, D. A. Landis, J. Cerny, and R. H. Pehl) 238

19. Application of Lithium-Drifted Germanium γ-Ray Detectors to Neutron Activation Analysis: Nondestructive Analysis of a Sulfide Ore. (J. Lamb, S. G. Prussin, J. A. Harris, and J. M. Hollander) 240

20. A. Mica Track Scanner (R. LaPierre, M. Nakamura, and K. Ward) 242

21. Modification of Internal Conversion Coefficient Spectrometer (A. J. Haverfield and J. M. Hollander) 242

22. Phenomenological Correction of the Field Shape of the Berkeley Iron-Free $\pi\sqrt{2}\beta$ Spectrometer (Karl-Erik Bergkvist and J. M. Hollander) 245

23. Azimuthally Varying Magnetic Field with Small Aperture Defect for β-Spectrometer Application (Karl-Erik Bergkvist and Andrew M. Sessler) 248

H. CHEMICAL ENGINEERING

1. Kinetics of Bacterial Sulfate Reduction (V. H. Edwards and C. R. Wilke) . . 251

2. Interphase Mass and Heat Transfer in Laminar Flow (Charles H. Byers and C. Judson King) 253

I. THESIS ABSTRACTS

1. Development of Some High-Speed Chromatographic Methods (M. S. - Ajuria-Garza) 255

2. Nuclear Spectroscopic Studies of Polonium-204 (M. S. - An) 255

3. Quadrupole Coupling in Rare Earth Crystals (Ph. D. - Blok) 256

4. Collective Excitation of Neutron-Deficient Barium, Xenon and Cerium Isotopes: Centrifugal Stretching Treatment of Nuclei (Ph. D. - Clarkson) 256

5. Nuclear Studies Using Semiconductor Detectors (Ph. D. -Frankel) 257

6. Oxygen Initiated Pyrolysis of Ethylbenzene (M. S. - Hausmann) 257

7. Isomeric Chemical Shifts and Electronegativity (M. S. - Keller) 258

8. Reaction of He^3 with Light Elements: Applications to Activation Analysis (Ph. D. - Mahony) 258

9. Magnetic Properties of Curium Metal and Its Compounds (Ph. D. -Marei) 259

10. Decay Schemes of Odd-Odd Einsteinium Isotopes (Ph. D. - McHarris) 259

11. Axial Dispersion in Liquid Flow Through Packed Beds (M. S. - Miller) 260

12. The Production of Tritium Labeled Methane and Ethane in the CH_4 - T_2 System (Ph. D. - Nash) 260

13. Theoretical Alpha Decay Rates of Deformed Nuclei (Ph. D. - Poggenburg) 260

14. Effects of Collective Excited States on Alpha Particle Barrier Penetrability (M. S. - Rauscher) 261

15. The Electromagnetic Levitation of Metals; The Design, Construction, and Operation of a Differential Micromanometer; Studies of Atomic Hydrogen at Low Pressures (Ph. D. - Rony) 261

16. Decay of the Zn^{64*} Compound Nucleus Formed by Nuclear Reactions of p, He^3, He^4, and C^{12} with Cu^{63}, Ni^{61}, Ni^{60}, and Cr^{52}, Respectively (Ph. D. - Smith). 262

17. Scattering of 50.9 MeV Alpha Particles from Ne^{20} and Ca^{40} (Ph. D. - Springer) 263

J. AUTHOR INDEX

1. Papers Published and UCRL Reports Issued, 1965 265

2. Contributions to this Report 285

NUCLEAR CHEMISTRY DIVISION ANNUAL REPORT, 1965

Lawrence Radiation Laboratory
University of California
Berkeley, California

December 1965

A. RADIOACTIVITY AND NUCLEAR STRUCTURE

1. MEASUREMENTS OF g FACTORS OF EXCITED STATES WITH A DIGITAL TIME-TO-HEIGHT CONVERTER

E. Matthias and D. A. Shirley

The method of measuring a perturbed angular correlation in a known magnetic field has been widely used to determine g factors for excited nuclear levels.[1] Surprisingly, however, major emphasis has been spent on very short-lived levels with half-lives in the nanosecond or subnanosecond region. This time range is very difficult, as large magnetic fields are needed and only the time-integral method can be employed, giving a limited accuracy. Internal perturbations are not well controlled and often make the result questionable.

In the range where time-differential observations are possible, hyperfine interactions can be measured with a much better accuracy. In general, the longer the half-life, the higher the precision of the result. The narrowness of the nuclear level permits the measurement of small energy variations. In spite of this perspective only four cases with half-lives between 100 and 500 nsec have been measured. For half-lives longer than 500 nsec there has not been any angular correlation measurement reported. It is worth noting that presently there is no method known with which nuclear g factors or, more general, hyperfine interactions can be investigated for isomeric states ranging between microseconds and seconds. It is our belief that the perturbed angular correlation method can be employed successfully at least in the range up to milliseconds, provided that sufficiently unperturbed source structures can be found.

To use the time-differential correlation method with half-lives beyond microseconds, two major difficulties have to be overcome: (a) the poor signal-to-noise ratio, and (b) the fact that only very small magnetic fields can be used due to the poor time resolution of the analog time-to-height converter system, which usually is of the order of 1% of the total time range. An improvement of the signal-to-noise ratio by decreasing the source strength of the radioactive source is possible only to a limited extent. A better way would be to produce the isomeric state in a nuclear reaction process and study the time-differential angular distribution following the beam bursts. Still, with an analog converter one would have to use extremely small magnetic fields. This difficulty can be avoided by employing a digital time-to-height converter, which has been described in the literature.[2]

The advantage of a digital converter is that its time resolution is determined only by the driving frequency and is independent of the desired time range. The lower limit of the resolution is, of course, given by the intrinsic time uncertainty of the detectors. In our system[3] a crystal-stabilized 100-Mc/sec frequency is fed into a correspondingly fast scaler which is started and stopped by the signals coming from γ_1 and γ_2, respectively. Each number occurring in the scaler is dumped on a paper tape recorder, and the randomly occurring numbers on the tape are later processed by computer.

After the numbers are ordered they form a distribution identical with the time spectrum recorded with an analog converter. A typical example is the 84-74.8-keV cascade of Rh^{100}, shown in Fig. A.1-1. The measurement was carried out with NaI(Tl) detectors which could not resolve the two γ lines. The activity was embedded in Pd metal and placed in an external magnetic field of 2.22 kilogauss. In Fig. A.1-1 poor statistics obscure the modulation effect present in this measurement. A simple analysis of the data, however, makes the presence of a Larmor precession visible. In the upper part of Fig. A.1-2 the results of two measurements with opposite field directions are displayed. The points for field up are calculated from the data shown in Fig. A.1-1. The ratio R is defined as

$$R(\tau) = 2 \frac{\sum_n a_{2n+1}(\tau) - \sum_n a_{2n+2}(\tau)}{\sum_n a_{2n+1}(\tau) + \sum_n a_{2n+2}(\tau)} \qquad n = 0, 1, 2, 3, \cdots$$

and plotted as a function of the time interval τ. The quantities $a_{2n+1}(\tau)$ and $a_{2n+2}(\tau)$ are actually the sums of the coincidences within the respective time intervals of length τ. If the difference $\Delta = R\downarrow - R\uparrow$ between the two field directions is formed the effect occurs more enhanced, as shown in the lower part of Fig. A.1-2. The second overtone, which should appear at 5/4 T_L, is missing, as there were too few cycles in the spectrum. From the time at which the two resonance peaks occur a g-factor value for Rh in Pd of

$$g = 2.0 \pm 0.1$$

is inferred.

The most satisfactory method for obtaining the Larmor precession frequency consists of a harmonic analysis of the data.[4] In this way one obtains the frequency spectrum $P(\nu)$ as the Fourier transform of the autocorrelation function $C(\tau)$:

$$P(\nu) = 2 \int_0^\infty \frac{C(\tau)}{C(0)} \cos 2\pi\nu\tau \, d\tau,$$

with

$$\frac{C(\tau)}{C(0)} = \frac{\text{ave } \{R(t) \cdot R(t+\tau)\}}{\text{ave } \{R(t) \cdot R(t)\}} .$$

The autocorrelation function is calculated by comparing the coincidences at time t, R(t), with the ones at time $(t+\tau)$, using all data and a shift τ ranging from 0 up to times larger than the period T_L. A typical frequency spectrum for Rh in Pd and an external field of 5.00 kG is shown in Fig. A.1-3. The g-factor value corresponding to the resonance frequency is

$$g = 2.02,$$

in very good agreement with the above result and other measurements with an analog converter.[5] The sign of the g factor can be obtained from the phase of the Fourier transform. The fact that the resonance is determined by two points only depends on the use of a 100-Mc/s driving frequency. It is obvious that the accuracy will be appreciably improved by using a higher resolution 1000-Mc/s system; such a system is presently being tested.

References

1. See E. Karlsson, E. Matthias, and K. Siegbahn, Perturbed Angular Correlations (North-Holland Publishing Company, Amsterdam, 1964).
2. See, e.g., R. E. Bell, in Alpha-, Beta-, and Gamma-Ray Spectroscopy, Vol. 2, editor K. Siegbahn (North-Holland Publishing Company, Amsterdam, 1965) Chap. XVII, p. 913; also J. K. Whittaker, Nucl. Instr. Methods 28, 293 (1964).
3. The 100-Mc system has been designed and constructed by F. S. Goulding and L. B. Robinson of Lawrence Radiation Laboratory.
4. The computer program for a complete Fourier analysis has been developed by Esther Coleman of Lawrence Radiation Laboratory.
5. E. Matthias and D. A. Shirley (Lawrence Radiation Laboratory), work in progress.

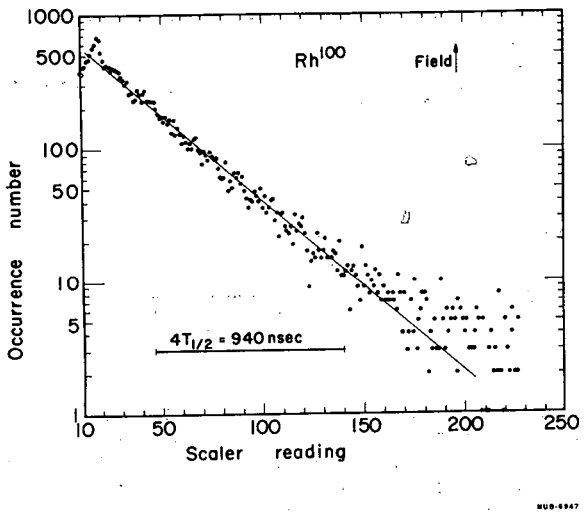

Fig. A. 1-1. Time spectrum of the 84-74.8 keV cascade in Rh^{100} obtained with a 100 Mc/sec digital time-to-height converter system. The measurement was done with NaI(Tl) detectors and a Pd metal source placed in a magnetic field of 2.22 kgauss.

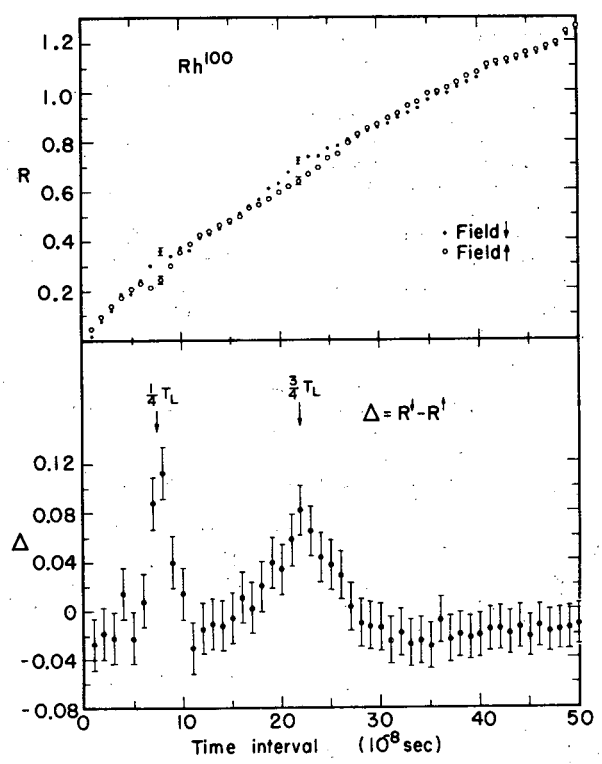

Fig. A. 1-2. Result of a simple treatment of the data shown in Fig.A.1-1 and another measurement with opposite field direction. The resonance effect shows up at a time interval which corresponds to a coherent successive addition and subtraction of the positive and negative half-waves, respectively.

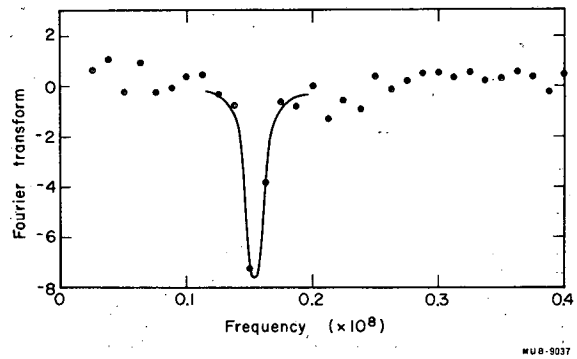

Fig. A. 1-3. Frequency spectrum of the Fourier transform for a measurement of the 84-74.8 keV cascade in Rh^{100} embedded in Pd metal and an applied external field of 5.00 kG. The data were obtained with a 100-Mc/sec digital time-to-height converter system.

2. g FACTOR OF THE 90-keV LEVEL IN Ru^{99} AND THE PARAMAGNETIC CORRECTION IN TRANSITION ATOMS*

E. Matthias, S. S. Rosenblum, and D. A. Shirley

The isotope Ru^{99} has recently been the subject of Mössbauer studies.[1,2] By using an iron absorber containing 2.3 atomic percent of Ru^{99} Kistner and Segnan[2] were able to observe the hyperfine splitting, from which they obtained the spin I = 3/2 for the 90-keV level and the ratio of the magnetic moments for the ground and the excited state, $\mu_1/\mu_0 = +0.455 \pm 0.010$. The fact that the half-life of the 90-keV state is 20 nsec[1,3] offers the possibility of measuring the g factor of this state with good accuracy by studying the rotation of the angular correlation pattern in an external magnetic field. This is interesting especially because the ground-state moment is not accurately known, while the ratio μ_1/μ_0 is.[2] This nucleus lies in a region of the periodic table where nuclear properties are neither thoroughly explored nor well understood. Also, the knowledge of this g factor allows determination of magnetic hyperfine fields at the nuclei of Ru atoms embedded in ferromagnetic lattices.

The first step in our investigation was to reexamine the γ-ray spectrum of 16.1-day Rh^{99}. A detailed decay scheme is given in the Nuclear Data Sheets with reference to a conference report.[4] However, when studying the γ-ray spectrum of the 16-d Rh^{99} activity with Ge(Li) detectors we were not able to reproduce the decay scheme of Ref. 4, except for the lowest four excited levels. The part of the decay scheme of interest for our work is shown in Fig. A. 2-1.

In connection with the Mössbauer experiments on Ru^{99} Kistner et al.[1,3] reported a half-life of $t_{1/2} = 20 \pm 1$ nsec for the 90-keV level. Recently, in connection with their g-factor investigation, Bodenstedt et al.[5] redetermined the half-life and obtained $t_{1/2} = 19.7 \pm 0.4$ nsec. We measured this half-life by observing delayed coincidences for both the 354-90-keV and 529-90-keV γ-ray cascades. In Fig. A. 2-2 a typical time spectrum is shown. As a final value we give

$$t_{1/2} = (20.7 \pm 0.3) \text{ nsec.}$$

This result is in good agreement with the value reported by Kistner et al.[1,3] but disagrees with the half-life reported by Bodenstedt et al.,[5] which lies somewhat outside the limits of error of our value.

The anisotropies of the photopeaks at 340 and 520 keV may be used to measure the g factor of the 90-keV level in Ru^{99}. This was done by observing the rotation of the angular correlation pattern in an external magnetic field in the conventional way, described elsewhere.[6] The γ_2 detector was placed at an angle of 135 deg with respect to the detector for γ_1. The time spectrum

of the coincidences was measured for a magnetic field pointing upward ($C_i^{\uparrow}$) and downward ($C_i^{\downarrow}$), and the ratio

$$R_i = 2\,\frac{C_i^{\downarrow} - C_i^{\uparrow}}{C_i^{\downarrow} + C_i^{\uparrow}}$$

was formed for each channel number i. For $A_4 << A_2$ the ratio R_i can be described by the function[6]

$$R_i = a \cos 2(\omega_L t_i - \phi) + c \ ,$$

where ω_L is the Larmor precession frequency, $\omega_L = -g \cdot H \frac{\mu_N}{\hbar}$. The four parameters a, ω_L, ϕ, and c are obtained from a least-squares fit of the experimental data, R_i. Several measurements with two different liquid sources have been performed for both the 354-90-keV and the 529-90-keV cascade. The results of all runs with liquid sources are summarized in Table A. 2-I. A typical set of data for the 529-90-keV cascade obtained with a liquid source is displayed in Fig. A. 2-3.

Measurements on Solutions - The "Paramagnetic Correction"

In a transition-series atom a substantial hyperfine structure may be present, modifying the effect of the external magnetic field $\vec{H}_0$. In certain particularly simple cases, including those discussed here, the magnetic hfs may be represented by an internal magnetic field $\vec{H}_i$. Then we may write

$$\vec{H}_{eff} = \vec{H}_0 + \vec{H}_i \ . \qquad (1)$$

In each specific case some estimate must be made of the magnitude of the product $\omega_L \tau$, where τ is the electronic relaxation time. For $\omega_L \tau << 1$, Eq. (1) may be written in the form

$$\vec{H}_{eff} = \beta\, \vec{H}_0 \ , \qquad (2)$$

where β is the "paramagnetic correction factor." Here $\vec{H}_0$ is described as inducing a (collinear) internal field $(\beta-1)\,\vec{H}_0$ through polarization of electrons near the nucleus under study. For cases in which the hfs is a weak effect β is near unity. Strongly magnetic rare earths may have β's near 10 even at room temperature (and much larger below). These measurements on Ru^{99} constitute the first example of $\beta < 1$. Cases should exist (e.g., negative hyperfine fields at low temperatures: Fe^{3+} at 10° K) for which β is zero or negative.

Until now the "paramagnetic correction" has been formulated only for the weak crystal field case of rare-earth ions,[7] and discussions of β have been limited to this rather special series. Angular correlation precession g-factor measurements have been reported for many d-shell transition-series nuclei, all measured in aqueous solutions. In all these cases paramagnetic corrections either were simply ignored or were omitted on the basis of incorrect arguments. While in some cases accuracies of a few percent have been claimed for these g-factor measurements, these must, in light of arguments presented below, be regarded as expressions of precision only. Until the paramagnetic effects have been dealt with either empirically, as discussed below for Ru^{99}, or theoretically (an alternative for which there are presently not enough data available), the reported g factors must be regarded as being in doubt by approximately 5 to 10%.

In order to discuss properly the magnitude of the "paramagnetic correction" two data are essential:

(a) the oxidation state of the daughter atom during the lifetime of the nuclear state after the (usually beta or electron-capture) decay of the parent nuclear species, and

(b) the effect on the electronic state of the various interactions present, principally the ligand field.

With regard to the first problem, a survey of the available data[8] makes us pessimistic about the prospect of reliably predicting the oxidation states in question. In beta decay the Migdal effect[9, 10] can lead to higher oxidation states, and in electron capture decay the Auger effect plays the same role. Highly oxidized recoiling atoms can be reduced by water to the lowest stable states available to these atoms. Evidence for this effect was obtained by Burgus and Kennedy[11] in studies of the decay of $Mn^{51}O_4^-$ to $Cr^{51}O_4^{2-}$ and Cr^{3+}, wherein the latter two species were obtained in approximately equal abundances. Thus it is incorrect to assume that only a particular ionic species is present after decay.

Ruthenium can exist in the seven oxidation states II through VIII, with 0 to 6 4d electrons.[12] Both electron-capture and β^+ decay occur, and we can offer no unassailable arguments to eliminate any of the seven states. We therefore disagree with the assumption of Bodenstedt et al.[5] that Ru^{99} is present only as Ru^{3+} after the decay of Rh^{99} in $RhCl_6^{3-}$. The 2+ oxidation state is more likely on the basis that it is isoelectronic with the parent,[8,11,6] but it is probably only one of several species present.

In those cases for which the oxidation state is known one must next determine the effect on the electronic state of the various interactions present. We discuss this problem for Ru very briefly below.

The exact approach would be to make use of the ligand field theory, which is quite thoroughly worked out for the d shells.[13] Under cubic symmetry the d shell is split, in the strong-field case, into a high-lying doublet, e_g, and a lower triplet, t_{2g}, spaced by $10\,Dq \approx 2\times10^4\ cm^{-1}$. We need consider only t_{2g}. As a three-dimensional representation of the octahedral group t_{2g} is formally equivalent to a p shell. This equivalence may be employed in estimating hfs effects. For Ru(II) $4d^6 t_{2g}^6$, for example, we have a closed shell and diamagnetism, while for Ru(V) $4d^3 t_{2g}^3$, a half-filled shell leads to spin paramagnetism.

If one assumes Ru(III) $4d^5 t_{2g}^{-1}$ as the correct structure, one finds that $\vec{H}_{eff}$ differs from the applied field by about ±9%. We might expect the above estimate to represent an upper limit for the magnitude of the correction because several of the other oxidation states, which are probably also present, are diamagnetic or only weakly paramagnetic. This expectation is borne out, as discussed below.

Measurements in a Copper Lattice

Fortunately one may greatly diminish the uncertainties of paramagnetism for transition-series atoms by using metallic sources. The rigid solid lattice and the reducing action of conduction electrons combine to bring the daughter atom into chemical equilibrium in a very short time ($\ll 10^{-9}$ sec) following decay of the parent. The Pauli principle allows only a fraction $\approx kT/E_F$ (E_F is the energy at the Fermi surface) of conduction electrons to participate in paramagnetism, and the paramagnetic correction is accordingly reduced by this factor, which has a numerical value of $\approx 10^{-2}$. The resulting fractional shift, $(H_{eff} - H_0)/H_0$, of $\approx 10^{-4}$ to 10^{-3} is the same phenomenon that is responsible for the Knight shift for NMR in metals.

The cubic copper lattice was chosen for this experiment on Ru^{99} because the target Ru has a hexagonal lattice, which could create quadrupole interaction and complicate the measurement. The weighted-average result for a copper lattice,

$$g = -0.189(2),$$

includes statistical errors only, and is to be compared with the value

$$g = -0.181(2)\ ,$$

which also includes only statistical errors, determined for liquid sources. The comparison yields an empirical paramagnetic correction

$$\beta = 0.958(15).$$

This is the first case for which a β of less than 1 has been found. The $(4.2 \pm 1.5)\%$ correction agrees well with the previous estimates. This experiment demonstrates the feasibility of precession-correlation measurements in a cubic metallic lattice and at the same time indicates the existence of a substantial paramagnetic effect in solutions. We conclude that cubic metallic sources should be used whenever accuracy is sought in g-factor measurements.

Footnote and References

* Condensed version of Phys. Rev. 139, B532 (1965) (UCRL-11900).

1. O. C. Kistner, S. Monaro, and R. Segnan, Phys. Letters 5, 299 (1963).
2. O. C. Kistner and R. Segnan, Bull. Am. Phys. Soc. 9, 396 (1964), and private communication.
3. O. C. Kistner, S. Monaro, and A. Schwarzschild, Phys. Rev. 137, B23 (1965).
4. J. D. Kurbatov, C. W. Townley, B. Feigley, and M. H. Kurbatov, Bull. Am. Phys. Soc. 5, 240 (1960).
5. E. Bodenstedt, C. Günther, J. Radeloff, W. Engels, W. Delang, M. Forker, and H. Luig, Phys. Letters 13, 330 (1964).
6. E. Matthias, L. Boström, A. Maciel, M. Salomon, and T. Lindquist, Nucl. Phys. 40, 656 (1963).
7. C. Günther and I. Lindgren, "Paramagnetic Effects," in Perturbed Angular Correlations, eds. E. Karlsson, E. Matthias, and K. Siegbahn (North-Holland, Amsterdam, 1964), p. 357.
8. M. Haissinsky, Nuclear Chemistry and its Applications, translated by D. G. Tuck (Addison-Wesley, Reading, Mass., 1964).
9. E. L. Feinberg, J. Phys. USSR 4, 424 (1941).
10. A. Migdal, J. Phys. USSR 4, 449 (1941).
11. W. H. Burgus and J. N. Kennedy, J. Chem. Phys. 18, 97 (1950).
12. P. J. Durrant and B. Durrant, Introduction to Advanced Inorganic Chemistry (John Wiley and Sons, New York, 1962) p. 1032.
13. See, for example, Carl J. Ballhausen, Ligand Field Theory (McGraw-Hill, New York, 1962) for a clear discussion of the relevant ligand field theory.

Table A. 2-I. Summary of the results of all independent g-factor measurements performed with a liquid source. The amplitudes of the cosine waves are given to emphasize the consistency between the different runs, and no conclusions are drawn from the values of a. The external magnetic field was in all cases 41.6 ± 0.4 kG.

Run No.	Cascade	g	Δg statistical error	a Amplitude (%)
1	354–90 keV	-0.1851	0.0041	10.3 ± 0.5
2	"	-0.1810	0.0034	10.9 ± 0.4
3	"	-0.1775	0.0064	10.5 ± 0.6
4	"	-0.1770	0.0054	11.3 ± 0.6
5	"	-0.1791	0.0050	11.1 ± 0.6
6	529–90 keV	-0.1760	0.0033	13.7 ± 0.5
7	"	-0.1930	0.0055	12.8 ± 0.6
8	"	-0.1859	0.0051	13.2 ± 0.6
	Weighted average:	-0.181	0.002	

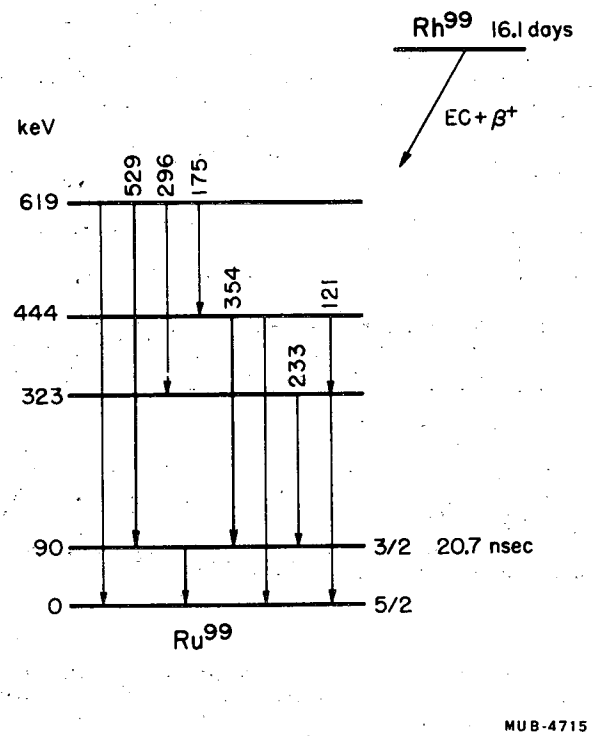

Fig. A. 2-1. Lowest part of the Ru^{99} decay scheme. The energies have been determined from Ge(Li) γ spectroscopy done by the authors.

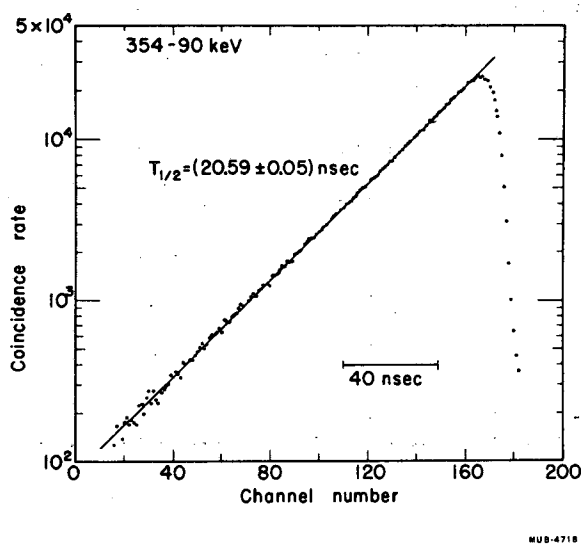

Fig. A. 2-2. Half-life measurements of the 90-keV level in Ru^{99}.

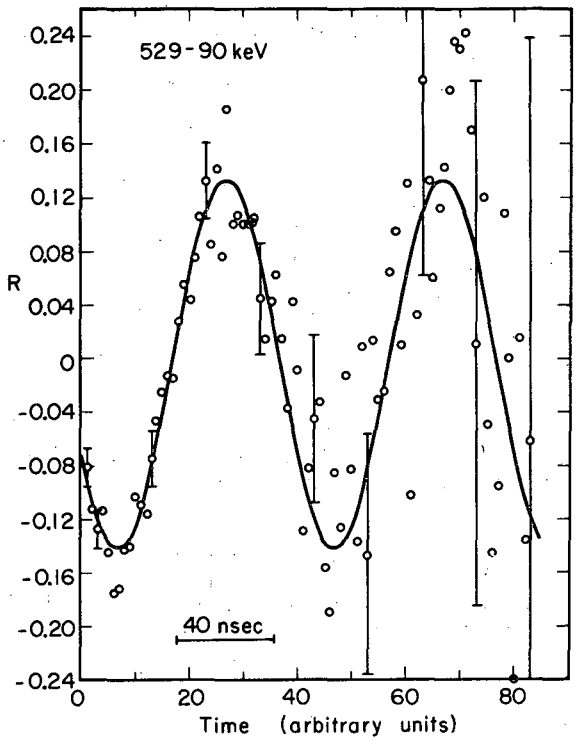

Fig. A. 2-3. Measurement of the time pattern of the angular correlation precessing in an external magnetic field of 41.6 kG, using a liquid source. The 529-keV γ rays were both detected with 1.5×1-in. NaI(Tl) crystals at a distance of 5 cm.

3. HALF LIFE AND g FACTOR OF THE 75-keV LEVEL IN Rh^{100} †

E. Matthias, D. A. Shirley, J. S. Evans, and R. A. Naumann

The decay of 4-day Pd^{100} has recently been investigated in detail by Evans and Naumann.[1] From a study of γ-ray and conversion-electron spectra the authors established a decay scheme in which there occurs a very intense 84–74.8-keV cascade. The intermediate state of this cascade was shown to have a half-life of $T_{1/2} = 180 \pm 20$ nsec.[1] The proposed spin sequence of this cascade makes one expect a large anisotropy in an angular correlation measurement, and a preliminary value of $A = +0.18 \pm 0.03$ was reported.[1] This large anisotropy and the long half life make the cascade very attractive for perturbed angular correlation measurements and promise a high accuracy for the determination of hyperfine interactions.

The 4-d Pd^{100} activity was produced by a (p, 4n) reaction on natural Rh^{103} by using a proton beam of about 20 μA-h and an energy of 45 MeV. For spectrum and half-life measurements the target material was used without further preparation. The g-factor measurements have been carried out both with a piece of the rhodium target and also with a source of rhodium in very dilute solution in copper. To prepare the latter source the Pd activity was chemically separated from the Rh target by a procedure described by Evans and Naumann.[1] The palladium was then electroplated carrier-free onto a copper foil. The foil carrying the activity was melted in an argon atmosphere at about 1200°C. The result was a shiny copper ball with a diameter of about 0.5 mm which was used for the angular correlation measurements.

All measurements were done exclusively with Ge(Li) detectors of 1×2 cm^2 and a 3-mm-deep drifted layer. Low-noise preamplifiers with an EC 1000 input stage as described by Goulding[2] were used in connection with the detectors. A typical γ spectrum obtained with our setup is shown in Fig. A.3-1. For calibration purpose the well-known γ rays of Co^{57} are indicated. The spectrum is in good agreement with the result of Evans and Naumann, and confirms the decay scheme shown in Fig. A.3-1. In addition we see clearly the two low-energy transitions at 32.7 and 42.1 keV.

For measuring coincidences of the 84.0–74.8-keV cascade as a function of time we used a time-to-height converter described by Wieber,[3] which was modified to give a linear time range of 1 μsec. The time calibration was performed with the delay trigger of a type-555 Tektronix dual beam oscilloscope, which in turn was calibrated with a 10-Mc crystal-stabilized frequency. The overall accuracy of the calibration is to within less than 1%. For the half-life measurements the Ge(Li) detectors were placed at 180 deg and as close as possible to the source. The result of a typical half-life measurement is shown in Fig. A.3-2. The final result,

$$T_{1/2} = 235 \pm 3 \text{ nsec},$$

is the weighted average of three independent determinations. Our value disagrees with the one reported in Ref. 1. It gives a hindrance factor of 9.3×10^5, using $\alpha = 0.3$ and the total transition intensities given in Ref. 1.

The nuclear g factor of the 74.8-keV level was measured by observing the Larmor precession of the angular correlation pattern in an external magnetic field.[4] The γ_2 detector was placed at an angle of 225 deg with respect to the γ_1 detector, counted clockwise from γ_1 toward γ_2. From the coincidence rate in channel i for a magnetic field pointing upward ($C_{i\uparrow}$) and downward ($C_{i\downarrow}$), the ratio

$$R_i = 2\,\frac{C_{i\downarrow} - C_{i\uparrow}}{C_{i\downarrow} + C_{i\uparrow}}$$

is formed, which can be expressed as a function of the Larmor frequency $\omega_L = -g\,H\,(\mu_N/\hbar)$:

$$R(t) = \frac{6A_2}{4 + A_2}\,\sin 2\omega_L t.$$

For the spin sequence of the 84–74.8-keV cascade the A_4 term in the angular correlation function vanishes.

In an earlier report on g-factor measurements in Ru^{99} the difficulty of a paramagnetic correction was discussed.[5] Following the conclusion of this work the g-factor measurements were performed with cubic metallic sources only; in this case we used as host lattices copper and rhodium. In Figs. A.3-3 and A.3-4 typical results obtained with the copper and rhodium source, respectively, are shown. It is obvious from these figures that in both cases there is not the slightest time-dependent attenuation present. This clearly indicates that the nuclear-lattice relaxation is still at least an order of magnitude longer compared with the measured range of 1 μsec. Also the quality of the fit in all cases rules out the presence of a quadrupole perturbation arising from a distortion of the cubic lattice.

A summary of all results obtained with the copper and the rhodium sources is given in Table A.3-I.

The external magnetic field is modified in metals essentially only by the Knight shift, $K = \Delta H/H$. NMR measurements by Seitchick et al.[6] on Rh^{103} provided the necessary Knight shift correction factor for Rh nuclei in Rh metal. These authors found at room temperature $K = +0.43\%$. Correcting our Rh-in-Rh results by this amount, we obtain, as a final value for the g factor of the 74.8-keV state,

$$g = +2.13 \pm 0.03.$$

The final error includes uncertainties of 1% for the time calibration, 1% for the magnetic field, and the statistical error quoted in Table A.3-I. The Rh-in-Cu data cannot be used to yield a g factor because the appropriate Knight shift correction is not independently known. We may, however, derive a value for this shift from the data in Table A.3-I

$$K\ (\text{Rh in Cu}) = +1.0 \pm 0.4\%.$$

Evans and Naumann[1] proposed for the 74.8-keV state two possible configurations: I, $[\pi(g_{9/2}^5)_{9/2}\ \nu(d_{5/2}^{5-n} s_{1/2}^n)_{5/2}]_{2+}$, and II, $[\pi(g_{9/2}^5)_{7/2}\ \nu(d_{5/2}^{5-n}\ s_{1/2}^n)_{3/2}]_{2+}$. To get an estimate for the expected g factor we choose for the proton configuration $g_\pi = +1.25$, interpolated from the values +1.37, +1.26, and +1.23 for the $g_{9/2}$ proton states in Nb^{93}, Tc^{99}, and $In^{109,111,113,115}$, respectively. From the systematic behavior of nine $d_{5/2}$ neutron states in this region we take an estimate of $g_\nu = -0.30$ for the g factor of the neutron configuration. When these two values are used, the expected g factors for configurations I and II come out as +2.54 and +2.03, respectively. The experimental result thus favors configuration II.

Footnote and References

† Shortened version of Phys. Rev. 140, B264 (1965) (UCRL-16069).

1. J. S. Evans and R. A. Naumann, Phys. Rev. 138, B1017 (1965).
2. F. S. Goulding, IEEE Trans. Nucl. Sci. 11, 177 (1964).
3. D. Wieber, Nucl. Instr. Methods 24, 269 (1963).
4. See, e.g., R. M. Steffen and H. Frauenfelder in Perturbed Angular Correlations, edited by E. Karlsson et. al. (North-Holland Publishing Company, Amsterdam, 1964).
5. E. Matthias, S. S. Rosenblum, and D. A. Shirley, Phys. Rev. 139, B532 (1965).
6. J. A. Seitchick, V. Jaccarino, and H. Wernick, Phys. Rev. 138, A148 (1965).

Table A. 3-I. Summary of g-factor measurements with copper and rhodium sources. In all cases the external magnetic field was 2.22 ± 0.02 kG. The amplitudes are given to emphasize the consistency of the different runs, but include no solid-angle correction. A separate time calibration has been done for each individual run.

Run No.	Source	Uncorrected g factor	Statistical error, Δg	Amplitude, a (%)
1	Rh in Cu	2.1598	0.0055	26.1 ± 0.5
2	Rh in Cu	2.1549	0.0087	25.6 ± 0.7
3	Rh in Cu	2.1359	0.0079	25.3 ± 0.7
	Weighted average:	2.1526	0.0071	
1	Rh in Rh	2.1360	0.0092	24.1 ± 0.7
2	Rh in Rh	2.1434	0.0074	23.8 ± 0.6
	Weighted average:	2.1405	0.0058	

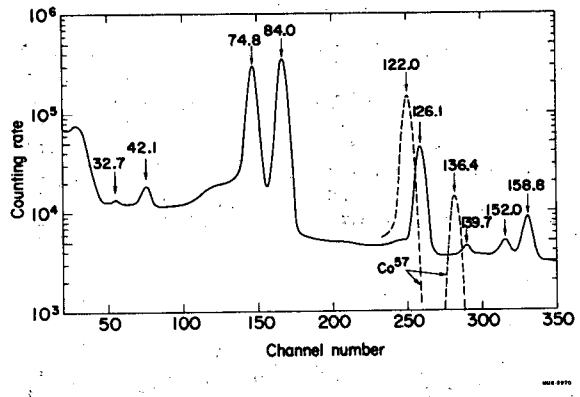

Fig. A.3-1. Typical γ spectrum of Pd^{100} obtained with a Ge(Li) detector of 3 mm depletion depth and an active surface of 1×2 cm^2. The Co^{57} calibration lines of 122.0 and 136.4 keV are shown.

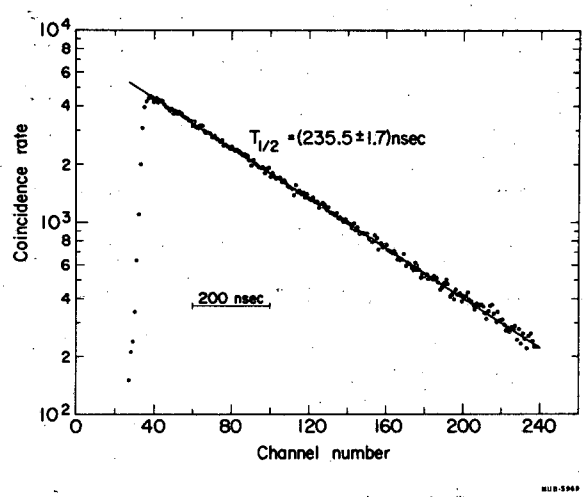

Fig. A.3-2. Half-life of the 74.8-keV level. The measurement shown is run No. 3 in Table A.3-I. The quoted error represents only the statistical uncertainty of this run.

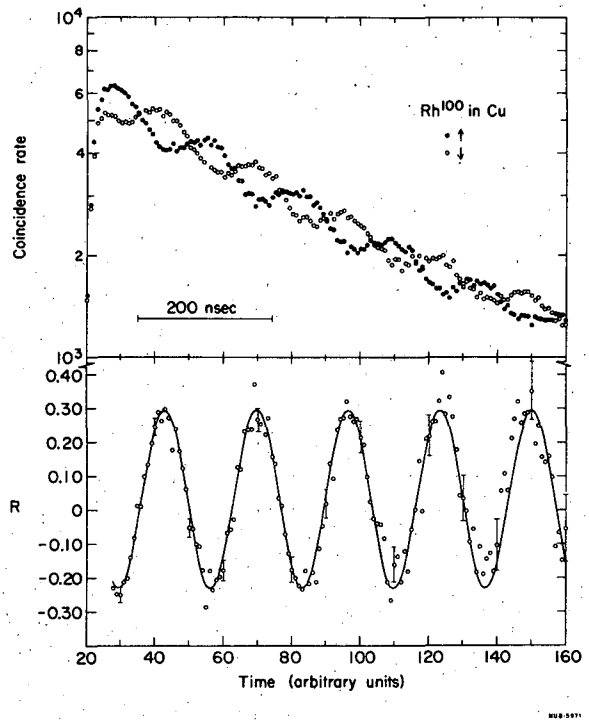

Fig. A. 3-3. Time-differential g-factor measurement with a source of Rh^{100} in copper in an external field of ± 2.22 kG. In the upper part of the figure the raw data of run No. 1 in Table A. 3-I are shown without any background correction. In the lower part the corresponding ratios R_i are displayed. The full line represents the weighted least-squares fit to the data.

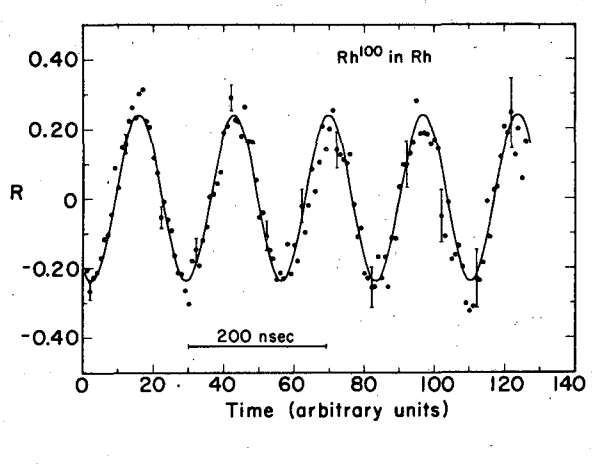

Fig. A. 3-4. Result of the g-factor measurement (run 2 of Table A. 3-I) with a source of Rh^{100} in Rh metal in an external magnetic field of ± 2.22 kG. The full line represents the weighted least-squares fit to the ratios R_i.

4. NUCLEAR SPIN AND MOMENT OF Ag^{110m} BY PARAMAGNETIC RESONANCE†

Warren Easley, Norman Edelstein, Melvin P. Klein,
D. A. Shirley, and H. Hollis Wickman

We have carried out electron paramagnetic resonance (EPR) experiments at 9.5 Gc/sec and room temperature with a superheterodyne spectrometer employing magnetic field modulation and synchronous detection, in order to measure the nuclear spin and nuclear magnetic dipole moment of 253-d Ag^{110m}. Paramagnetic Ag^{2+} is formed by treating dry $AgNO_3$ (or the metal) with a solution of benzene containing a large excess of tetraisopropyl thiuram disulfide.[1] The blue divalent Ag complex $[(iso\text{-}C_3H_7)_2NCS_2]_2Ag$ forms immediately. Measurements were carried out on solutions containing 0.02 atom % Ag^{110m} in a total of 2.3 mg of Ag^{107} and Ag^{109} and on solutions containing the enriched isotopes Ag^{107} (95.7%) and Ag^{109} (99.1%).

The spin Hamiltonian appropriate to Ag^{2+} in solution is

$$\mathcal{H} = g\,\beta\,\vec{H}\cdot\vec{S} + a\,\vec{I}\cdot\vec{S}, \qquad (1)$$

where g and a are the spectroscopic splitting factor and the hyperfine structure constant, respectively. The transition energies, including second-order terms, are given by

$$h\nu = g\beta H + aM_I - \frac{a^2}{2g\beta H}\left[I(I+1) - M_I^2\right], \qquad (2)$$

where $M_I = -I, -I+1, \cdots, I$.[1,2] For Ag^{110m}, a 13-line pattern was inferred from 11 observed lines, the remaining two being obscured by the hyperfine structure of the stable isotopes, and the spin value 6 was confirmed.[3] Positions of eight of the Ag^{110m} lines were measured accurately, and for Ag^{110m} we found $a_{110m} = 75.39 \pm 0.2$ gauss $(7.108 \pm 0.02)\times 10^{-3}$ cm^{-1}. In Table A.4-I the calculated and experimentally determined magnetic fields for the transitions are listed.

From the ratio of the hyperfine coupling constant of either stable isotope to that of Ag^{110m}, and the known nuclear moment of the stable isotope, the nuclear moment of Ag^{110m} can be calculated approximately. Since the hfs observed is due to the finite s-electron density at the nucleus,[1] the measured coupling constants include the effect of the hyperfine anomaly, and the nuclear moment obtained in this way will be uncorrected for this effect. Using the theory put forth by Bohr and Weisskopf[4] and Bohr,[5] and the tabulated coefficients of Eisinger and Jaccarino,[6] we estimate that the hyperfine anomaly, $\Delta_{109,110m}$, for Ag^{109}, Ag^{110m} is $-3.7 \pm 1\%$. Hence the uncorrected value of the moment (3.68 nm) is corrected to a final value of $\mu_{110m} = +3.55 \pm 0.04$ nm.[7]

The single-particle shell-model configuration for Ag^{110m} is $\pi(g_{9/2})^2\,\nu(d_{5/2})^5$. It is profitable, in estimating theoretical magnetic moments for odd-odd nuclei, to use empirical g factors of the nucleon configurations, obtained from neighboring odd-A nuclei. From Lindgren's tabulation[8] it is clear that the magnetic moments of $g_{9/2}$ proton ($d_{5/2}$ neutron) states vary systematically with proton (neutron) number. By interpolation we can estimate $g_p = +1.24$, $g_n = -0.32$ for the $g_{9/2}$ proton and $d_{5/2}$ neutron in Ag^{110m}. The moment is then calculated as

$$\mu_{110m} = +1.24(29/7) - 0.32(13/7) = +4.54 \text{ nm},$$

almost one unit too high. This difference is far outside what would be expected from the regularity of the empirical single-nucleon g factors. This method of estimating the moment should account for pairing and configuration-mixing effects in the configurations of the two types of nucleons.

An attractive explanation for the low moment is the coupling of the proton configuration to spin 7/2. The 6+ state would then be described as $|\pi(g_{9/2})^7\,7/2\,\nu(d_{5/2})^5\,5/2\rangle_6$. There are precedents for such higher-seniority coupling (for example in V^{51}). The calculated magnetic moment is then

$$\mu = +1.24(7/2) - 0.32(5/2) = +3.54 \text{ nm},$$

in good agreement with experiment.

Footnote and References

† Condensed from a paper in Phys. Rev. (in press).

1. R. Pettersson and T. Vänngård, Arkiv. Kemi 17, 249 (1961).
2. B. Bleaney, Phil. Mag. 42, 441 (1951).
3. W. B. Ewbank, W. A. Nierenberg, H. A. Shugart, and H. B. Silsbee, Phys. Rev. 110, 595 (1958).
4. A. Bohr and V. F. Weisskopf, Phys. Rev. 77, 94 (1950).
5. A. Bohr, Phys. Rev. 81, 331 (1951).
6. J. Eisinger and V. Jaccarino, Rev. Mod. Phys. 30, 530 (1958).
7. The positive sign assigned on the basis of nuclear polarization experiments, D. A. Shirley and G. A. Westenbarger, Phys. Rev. 138, 1A, A161 (1965).
8. I. Lindgren, "Table of Nuclear Spins and Moments," in Perturbed Angular Correlations, ed. by E. Karlsson, E. Matthias, and K. Siegbahn (North-Holland, Amsterdam, 1964), Appendix 1.

Table A. 4-I. Calculated and experimental hyperfine line positions of Ag^{110m}, a_{110m} = 75.39 ± .2 gauss. Lines are numbered arbitrarily: the highest field line is 1, the next highest is 2, etc.

Line	Calculated (gauss)	Experimental (gauss)
1	3752.2	3752.0
2	3667.4	3666.9
3	3584.2	3583.8
4	3502.8	3502.5
5	3423.2	
6	3345.2	
7	3268.9	
8	3194.4	3194.5
9	3121.6	3121.6
10	3050.5	3050.5
11	2981.1	2981.0
12	2913.5	
13	2847.5	

5. NUCLEAR MOMENTS OF AMERICIUM-241 AND 16-h AMERICIUM-242 AND ANALYSIS OF THE HYPERFINE FIELDS*

Lloyd Armstrong, Jr. and Richard Marrus

The nuclear moments of americium-241 and 16-h americium-242 have been directly measured by the method of triple resonance in an atomic beam. They are $\mu_I(Am^{241})$ = +1.58(3) nm and $\mu_I(Am^{242})$ = +0.3808(15) nm, including a correction for diamagnetic shielding. On the Nilsson model, $\mu_I(Am^{242})$ is a direct measure of the gyromagnetic ratio of the core (g_R); the measured

value of μ_I is in excellent agreement with the value $g_R = Z/A$. From these values of the magnetic moments and from previous measurements of the hyperfine constants, values are deduced for the magnetic fields at the nucleus. It is shown that breakdown of Russell-Saunders coupling including relativistic effects give magnetic-field contributions of the wrong sign. Arguments are given that show that the residual effect is most probably due to core polarization.

Footnote

* Abstract for the American Physical Society meeting, New York, January 26-29, 1966.

6. DIRECT MEASUREMENT OF THE MAGNETIC MOMENT OF PLUTONIUM-239†

John Faust, Richard Marrus, and William A. Nierenberg‡

The magnetic moment of Pu^{239} has been the subject of experimental work for about a decade. The original measurement was performed by Bleaney et al.[1] in 1954. They concluded, on the basis of paramagnetic resonance studies, that $\mu_I(239)$ equals $\pm 0.4(2)$ nm. An atomic-beam measurement by Hubbs et al.[2] of the hyperfine structure in the $^7F_1$ state of the free atom yielded $\mu_I(239) = \pm 0.02$ nm, with the assumption of pure Russell-Saunders coupling. Subsequently several determinations based on optical hyperfine structure were made, particularly by the Bellevue group (Refs. 3, 4). It should be emphasized that all these values of $\mu_I(239)$ are inferred from measurements of magnetic dipole hyperfine constants A according to the relation $\mu_I(239) = IJ\,(A/H_z)$, where H_z is the magnetic field at the nucleus, I is the nuclear spin and equals 1/2, and J is the electronic angular momentum. Hence all these determinations rest on assumptions concerning the magnetic field at the nucleus.

Recently, an analysis of the hyperfine structures (hfs) of the states arising from the ^7F level was undertaken by Bauche and Judd.[5] These authors showed that the A values of these states could be understood if contributions to H_z arising from core polarization and the breakdown of Russell-Saunders coupling were taken into account. The size of the Casimir correction factors indicated that relativistic effects are negligible. Bauche and Judd concluded that $\mu_I(239) = 0.17(0.04)$ nm. Armstrong's recent calculations of relativistic effects in the hyperfine structure of these states are based on a Hartree-Fock central field.[6] He shows that these effects may be the dominant contribution to the hfs. However, they have the same J dependence as the core polarization and would not interfere with the fit of Bauche and Judd. Only a measurement of the hyperfine anomaly could decide whether core polarization or relativistic effects are dominant.

In this note we report the result of a direct measurement of $\mu_I(239)$ by the method of triple resonance in an atomic beam.[7] The atomic-beam flop-in method was employed (it is described elsewhere[8]). For a hyperfine-structure system of I = 1/2, J = 1, the normal flop-in transition, which we denote as α, has the quantum numbers $F=3/2, m_F=1/2 \leftrightarrow F=3/2, m_F=-3/2$. The end hairpins were always set at the frequency corresponding to the center of the resonance line of α. The hyperfine constants determining these frequencies are taken from the data of Hubbs et al.[2] The two transitions that are sensitive to the nuclear moment we denote by a and b; they have the quantum numbers $F=3/2\ m_F=1/2 \leftrightarrow F=3/2\ m_F=3/2$ and $F=3/2\ m_F=-3/2 \leftrightarrow F=1/2\ m_F=-1/2$, respectively. These transitions are of the type $\Delta m_I = \pm 1$ and $\Delta m_J = 0$ in high field, and in the high-field limit the resonant frequencies are given by

$$\nu = \pm A + g_I\,\mu_0\,H\,,$$

where μ_0 is the Bohr magneton and H is the applied field. Therefore the field dependence of the resonant frequency is a precise, direct measure of the nuclear moment.

When the frequency applied to the center hairpin corresponds to the resonant frequency for either of these transitions, the detector registers an increase in signal.

The data were analyzed as follows: we combined the observed resonances of Hubbs et al. with our triple-resonance data, and on the IBM-7094 made a least-squares fit according to the Hamiltonian

$$\mathcal{H} = A(\underset{\sim}{I} \cdot \underset{\sim}{J}) - g_J \mu_0 \underset{\sim}{J} \cdot \underset{\sim}{H} - g_I \mu_0 \underset{\sim}{I} \cdot \underset{\sim}{H} \ .$$

The data of Hubbs et al. essentially determine the values of A and g_J, whereas our data fix the value of g_I. The value obtained in this way is

$$\mu_I(239) = +0.200(4) \text{ nm} \ ,$$

where a correction for diamagnetic shielding has been made. The results for the triple resonance only are given.

Our value of $\mu_I(239)$ is within the limits of error set by Bauche and Judd. We are currently trying to extend our measurements to the isotope Pu^{241}. If the hypothesis of large amounts of core polarization is correct, then a large hyperfine anomaly should exist in these isotopes.

The value of the $\mu_I(239)$ has also been calculated by Mottelson and Nilsson,[9] on the basis of the Nilsson model, to be -0.1 nm. Recently Rasmussen and Chiao[10] have recalculated this moment using "quenched" g factors and obtained -0.06 nm. Hence there is a discrepancy in sign between the theoretical and experimental values.

Footnotes and References

† Condensation of Phys. Letters 10, 71 (1965).
‡ Now at Scripps Institution of Oceanography, LaJolla, California.

1. B. Bleaney, P. M. Llewellyn, M. H. L. Pryce, and G. R. Hall, Phil. Mag. 45, 773 (1954).
2. J. C. Hubbs, R. Marrus, W. A. Nierenberg, and J. L. Worcester, Phys. Rev. 109, 390 (1938).
3. R.-J. Champeau and S. Gerstenkorn, Compt. Rend. 251, 352 (1960).
4. S. Gerstenkorn, Ann. Phys. (Paris) [13], 7, 367 (1962).
5. J. Bauche and B. R. Judd, Proc. Phys. Soc. (London) 83, 145 (1964).
6. Lloyd Armstrong, Jr. (Lawrence Radiation Laboratory, Berkeley), private communication, 1965.
7. P. G. H. Sandars and G. K. Woodgate, Nature 181, 1395 (1958); W. A. Nierenberg and G. O. Brink, J. Phys. Radium 19, 816 (1958).
8. W. A. Nierenberg, Ann. Rev. Nucl. Sci. 7, 349 (1957).
9. B. R. Mottelson and S. Nilsson, Kgl. Danske Videnskab. Selskab Mat.-Fys. Skrifter 1, No. 8 (1959).
10. J. O. Rasmussen and L. W. Chiao, in Proceedings of the International Conference on Nuclear Structure, Kingston, Canada, 1960, edited by D. A. Bromley and E. W. Vogt (University of Toronto Press, Toronto, 1960), 646.

7. HYPERFINE STRUCTURE AND NUCLEAR MOMENTS OF PROMETHIUM-148 AND ERBIUM-165†

Dolores Ali, Isaac Maleh,* and Richard Marrus

The hyperfine structure of the $^6H_{7/2}$ level in 5.3-d Pm^{148} and the $^3H_6$ level in 10-h Er^{165} have been measured by atomic-beam magnetic resonance. The spins of these isotopes have been verified to be $I(Pm^{148}) = 1$ and $I(Er^{165}) = 5/2$. The electronic g factor for the $^6H_{7/2}$ level in Pm^{148} is found to be $g_I = -0.8278(1)$. The hyperfine constants and inferred nuclear moments are for Pm^{148}: A = +1038(75) Mc/sec, B = -98(103) Mc/sec, μ_I = +2.07(21) nm, Q = +0.2(2) b; and for Er^{165}: $|A|$ = 195(6) Mc/sec, $|B|$ = 3502(115) Mc/sec, $B/A < 0$, $|\mu_I|$ = 0.65(3) nm, $|Q|$ = 2.2(1) b, $Q/\mu_I > 0$. The nuclear moments of Pm^{148} were calculated from the hyperfine constants and assumptions made concerning the electronic fields at the nucleus; these assumptions include a 2% correction for the breakdown of Russell-Saunders coupling, but do not include corrections for the Sternheimer effect. The stated errors include a 5% uncertainty for $\langle 1/r^3 \rangle$. The Fermi-Segrè formula and the direct measurement of the magnetic moment of Er^{167} were used to calculate the dipole moment of Er^{165}. The quadrupole moment of Er^{165} has not been corrected for the Sternheimer effect. The measurements indicate that Pm^{148} may be described by the shell model, but that Er^{165} is deformed and must be interpreted by the collective model.

Footnote

† Abstract from Phys. Rev. 138, B1356 (1965).

8. THE DECAY SCHEME OF Es^{254}

W. McHarris, F. S. Stephens, F. Asaro, and I. Perlman

We have studied the alpha, gamma, and electron radiations emitted in the alpha decay of long-lived Es^{254}. These data are summarized in Tables A.8-I, A.8-II, and A.8-III, respectively. The alpha spectrum was investigated with a magnetic spectrograph and with Si solid-state detectors. The γ rays were investigated with NaI detectors and high-resolution Ge detectors in a variety of singles and coincidence measurements. The electrons were measured with a high-resolution permanent-magnet spectrograph.

There are two known isomers of Es^{254} with half lives of 38.5 hours and $\approx$ 280 days. Closed-cycle calculations with our α-decay energy for the long-lived isomer indicate the long-lived isomer to be the ground state, and the 38.5-hour isomer to be an excited state with an energy of 101 ± 22 keV.

Most of our information has been used to characterize rather unambiguously four low-lying rotational bands as indicated in the decay scheme shown in Fig. A.8-1. The properties of these bands have been compared rather carefully with those predicted by considering the odd neutron and odd proton to move independently of each other. The agreement is surprisingly good, as illustrated in Table A.8-IV. We have compared experimental values with predicted energies, rotational constants, and approximate α-decay hindrance factors for the various expected Nilsson states. The rotational constants, $\hbar^2/2\mathfrak{J}$, were simply determined from the lowest-energy rotational spacings with the equation $\mathfrak{J}_{Bk^{250}} = \mathfrak{J}_{Bk^{249}} + \mathfrak{J}_{Fm^{255}} - \mathfrak{J}_{Fm^{254}}$. B is the corfficient of the $I^2(I+1)^2$ term in the energy expansion. The sign of B would be expected to be negative from the vibrational-rotational interaction except when large Coriolis interactions are present; e.g., for nuclei in this region with even-parity odd-proton states or odd-parity neutron states. The estimated α-decay hindrance factors are simply the product of the lowest hindrance factors for the α decay to the corresponding odd-neutron and odd-proton bands.

All the foregoing data and their various ramifications have been discussed.[1,2]

References

1. W. McHarris, F. S. Stephens, F. Asaro, and I. Perlman, The Deacy Scheme of Einsteinium-254, Phys. Rev. (to be published) (UCRL-11676, Oct. 1965).
2. William C. McHarris, Decay Schemes of Odd-Odd Einsteinium Isotopes (Ph. D. thesis), UCRL-11784, July 1965.

Table A. 8-I. Data from the alpha spectra obtained by magnetic analysis.

Alpha-particle energy (MeV)	Intensity (%)	Hindrance factor	Excited-state energy (keV)
6.52	≤0.005	$>1.3\times10^5$	0
6.486 ± 0.005	0.27	1.7×10^3	35.5
6.437 ± 0.005	93.0	2.9	85.5
6.424 ± 0.005	1.7	1.4×10^2	99
6.392 ± 0.005	0.13	1.3×10^3	131
6.367 ± 0.005	2.9	43	155.9
6.355 ± 0.005	0.74	1.5×10^2	169
6.331 ± 0.005	0.05	1.7×10^3	193
6.284 ± 0.005	0.16	3.1×10^2	241
6.276 ± 0.005	0.22	2.1×10^2	249
6.200 ± 0.010	~0.05[a]	$\sim3.4\times10^2$	~326
6.193 ± 0.010	~0.05	$\sim3.8\times10^2$	~333
6.113 ± 0.005	0.33	23	414
6.056 ± 0.005	0.16	25	472

[a]This intensity has been reduced 0.03% for a presumed contribution of $Cf^{249}\alpha_0$.

Table A. 8-II. Gamma rays from E^{254} decay.

E_γ (keV)	Intensity (%)
≈15 - 18 (L x rays)	230[a]
63	2.0
104 (K_{α_2})	0.40
108 (K_{α_1})	
≈123 (K_β's)	0.13
150	0.02
(233)	0.008
249	0.025
264	0.05
278	0.03
≈285	0.01
304	0.07
316	0.15
342	0.009
348	0.007
377	0.015
385	0.05

[a]This intensity was obtained by comparing the Es^{254} L x rays with those of E^{253}. The number represents L-electron vacancies rather than L x rays.

Table A.8-III. Electron lines from Es^{254}.

Electron energy (keV)	Subshell	Binding energy (keV)	Gamma-ray energy (keV)	Electron relative intensities[a]	Transition intensities (%)
9.18	L_I	25.23	34.41	VW	
10.04	L_{II}	24.34	34.38	M	
14.93	L_{III}	19.47	34.40	W	
27.81	M_I	6.56	34.37	W	
28.22	M_{II}	6.16	34.38	W	
masked	M_{III}	--	--	--	
32.74	N_I[b]	1.58	34.32	VVW	
33.20	N_{II}[b]	1.27	34.47	VVVW	
		Best value	34.4 M1-E2		≈30
10.24	L_I	25.23	35.47	M	
~10.87	L_{II}	24.34	≈35.2	VVW	
16.05	L_{III}	19.47	35.52	MS	
28.95	M_I	6.56	35.51	MS	
29.42	M_{II}	6.16	35.58	MW	
30.54	M_{III}	4.99	35.53	M	
33.80	N_I	1.77	35.57	W	
34.32	N_{III}	1.27	35.59	VW	
35.15	O_I, O_{II}, O_{III}	≈ 0.34	≈35.49	VVW	
		Best value	35.5 M2		≈70
17.36	L_I	25.23	42.59	VS	
18.19	L_{II}	24.34	42.53	MS-S	
23.18	L_{III}	19.47	42.65	MS	
36.17	M_I	6.56	42.73	VS	
36.55	M_{II}	6.16	42.71	MS	
37.61	M_{III}	4.99	42.60	S	
41.02	N_I[b]				
	N_{II}[b]	1.58	42.60	MS	
41.41	N_{III}	1.27	42.68	W-MW	
42.39	O_I, O_{II}, O_{III}	≈ 0.34	≈42.73	MW	
		Best value	42.6 M1-E2		100
≈44.5	L_I	25.23	≈69.7	VVVW	
≈45.4	L_{II}	24.34	≈69.7	VVW	
50.27	L_{III}	19.47	69.74	VW	
63.51	M_{II}	6.16	69.67	VVVW	
		Best value	69.7 (M1)-E2		≈1
45.15	L_I	25.23	70.38	W	
45.94	L_{II}	24.34	70.28	MW	
50.90	L_{III}	19.47	70.37	MW	
63.90	M_I	6.56	70.46	VVVW	
64.30	M_{II}	6.16	70.46	VW	
≈65.2	M_{III}	4.99	≈70.2	VVW	
		Best value	70.4 M1-E2		≈3
55.60	L_I	25.23	80.83	VVW	
56.45	L_{II}	24.34	80.79	VVW	
≈61.54	L_{III}	19.47	≈81.01	VVW	
		Best value	80.8 M1-E2		< 1
59.90	L_I	25.23	85.1	VVVW	
60.77	L_{II}	24.34	85.1	VVVW	
		Best value	85.1 (M1-E2)		<< 1

[a]W = weak, S = strong, V = very, M = moderately.
[b]The N_I and N_{II} lines were too close together to be resolved well; since the lines were read from the high-energy edge, the two lines were given the N_{II} position. Hence the N_{II} binding energy is used.

Table A. 8-IV. Properties of rotational bands in Bk^{250}.

Neutron states	Proton states: 7/2+[633↑]	Proton states: 3/2-[521↑]
	Predicted properties	
1/2+[620↑]	Kπ = 4+ (3+) E = 0 keV $\hbar^2/2\mathfrak{J}$ = 4.35 ± 0.14 B = positive HF = 750	Kπ = 2- (1-) E = 9 keV $\hbar^2/2\mathfrak{J}$ = 5.67 ± 0.24 B = negative HF = large
7/2+[613↑]	Kπ = 7+ (0+) E = 106 keV $\hbar^2/2\mathfrak{J}$ = 4.49 ± 0.01 keV B = positive HF = 2.0	Kπ = 5- (2-) E = 115 keV $\hbar^2/2\mathfrak{J}$ = 5.90 ± 0.02 keV B = negative HF = 90
	Experimental properties	
1/2+[620↑]	Kπ = 4+ E = 35.5 keV $\hbar^2/2\mathfrak{J}$ = 4.26 keV B = positive HF = 1300	Kπ = 2- E = 0 keV $\hbar^2/2\mathfrak{J}$ = 5.73 keV B = ? HF ≥ 1.3×10^5
7/2+[613↑]	Kπ = 7+ E = 85.5 keV $\hbar^2/2\mathfrak{J}$ = 4.40 keV B = positive HF = 2.89	Kπ = 5- E = 99 keV $\hbar^2/2\mathfrak{J}$ = 5.75 keV B = negative HF = 140

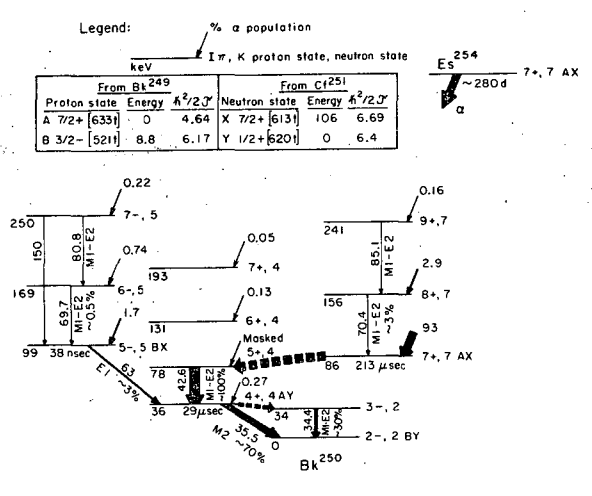

Fig. A.8-1. The decay scheme of Es^{254}.

9. ENERGY LEVELS OF Am^{239} AND Am^{241}

I. Ahmad, F. Asaro, and I. Perlman

The energy levels of Am^{239} and Am^{241} have been worked out by studying the α decay of Bk^{243} and Bk^{245}. The Bk isotopes were prepared by irradiating Am^{243} with 40- and 33-MeV α

particles at the 88-inch cyclotron for varying lengths of time, followed by intensive chemical separations to obtain pure Bk fractions. In the bombardment Bk^{243}(4.5 h), Bk^{244}(4.4 h), Bk^{245}(4.95 d), and Bk^{246}(1.8 d) were all made and their α or (and) γ radiations were observed in our experiments. In this report, however, we discuss only the radiations accompanying the α decay of Bk^{243} and Bk^{245}.

The Bk samples were analyzed for γ singles, α singles, and γ-α coincidences simultaneously in order to obtain maximum information in the shortest time. The γ rays were detected with a Li-drifted Ge crystal, and the α particles were detected with a 6-mm-diameter Au-Si surface-barrier detector (resolution 20 keV at 4% geometry).

Bk^{243} and Bk^{245} both have very low α branching ratios (0.15% and 0.1% respectively), which made the coincidence experiments with Ge(Li) crystals very difficult. The α-singles spectra of these isotopes are shown in Figs. A.9-1 and A.9-2. Their energies, intensities, and hindrance factors are listed in Tables A.9-I and A.9-II. We used Cm^{244} and Th^{226} α groups as energy standards, with the values given by Wapstra.[1] The hindrance factors were calculated by Michel[2] from the Preston[3] equations. The results of the coincidence experiments with a Ge(Li) crystal, in which the coincidence circuit was gated with specific α groups, are shown in Table A.9-III. Our proposed decay schemes are shown in Figs. A.9-3 and A.9-4.

The spin and parity assignment of the levels of Am^{239} and Am^{241} have been discussed by Stephens, Asaro, and Perlman,[4] and also by Nilsson and Mottelson.[5] We give here some of their arguments along with our new results.

Am^{241} has a measured spin of 5/2. From studies of its decay to Np^{237} it was concluded that this state must be 5/2 - [523↓]. The next three Am^{241} levels we observed fit well with the expected energies for the rotational members of this band. With the formula

$$E = E_0 + \frac{\hbar^2}{2\mathfrak{J}} I(I+1), \qquad (1)$$

the rotational constants $\frac{\hbar^2}{2\mathfrak{J}}$ have values of 5.96 keV for Bk^{245} and 5.81 keV for Bk^{243}. The level at 207.4 keV decays to the ground state and to the 41.7-keV level. As seen in Table A.9-III, comparison of the K-conversion coefficients of these γ rays with the theoretical values indicates that these radiations are either E1 or E2, and hence the 207.4-keV level has spin and parity 5/2+, 7/2+ or 3/2- → 9/2-. The only reasonable Nilsson state in this region is the 5/2+ [642↑] level, the ground state of Np^{237}. The relative intensities of the 165.3-keV and 207.4-keV radiations agree well with the theoretical expectations for fast E1 transitions between K = 5/2 rotational bands, as seen in Table A.9-IV. The next four levels, at 237, 274.5, 324.3, and 378.2 keV, are very likely the rotational members of this band. The α intensities to these levels agree fairly well with the theoretical calculations of Poggenburg.[6] The disturbed spacing between various members of this band is similar to that observed in other odd-proton nuclei, which have been interpreted in terms of Coriolis interaction with other even-parity states arising from the $i_{13/2}$ shell-model level.

The state at 474.5 keV is assigned 3/2- because the low value of the hindrance factor indicates favored α decay, and hence K and π of this state must be the same as that of Bk^{245} ground state, 3/2- [521↑]. The γ transition to the ground state is found to be M1 (with some E2 admixture), which has previously been noted[4] in the electron-capture decay of Cm^{241}.

The spectra associated with Bk^{243} α decay are very similar to those associated with Bk^{245}, as can be seen by a comparison of the decay schemes (Figs. A.9-3 and A.9-4). The quantum-number assignments for the Am^{239} levels are based on arguments which are nearly identical with those for the Am^{241} levels, and hence will not be repeated.

References

1. A. H. Wapstra, Nucl. Phys. 57, 48 (1964).
2. H. V. Michel (Lawrence Radiation Laboratory) to be published.
3. M. A. Preston, Phys. Rev. 71, 865 (1947).
4. F. S. Stephens, F. Asaro, and I. Perlman, Phys. Rev. 113, 212 (1959).
5. S. G. Nilsson and B. R. Mottelson, Kgl. Danske Videnskab. Selskab Mat. -Fys. Skrifter 1, No. 8 (1959).
6. John K. Poggenburg, Jr., Theoretical Alpha Decay Rates of Deformed Nuclei (Ph. D. Thesis), UCRL-16187, Aug. 1965.

Table A.9-I. Bk^{243} alpha data.

E_α (MeV)	Level (keV)	α intensity (%) Experimental	α intensity (%) Theoretical	Hindrance factor
6.758	0.0	15.4	14.1	1.14×10^3
6.718	40.7	12.5	14.7	9.46×10^2
6.666	93.6	≈1.2	2.8	5.83×10^3
6.605	155.6	≈ 0.7	2.0	5.37×10^3
6.574	187.1	25.6	20.8	1.07×10^2
6.542	219.6	19.4	15.1	1.01×10^2
6.502	260.3	6.9	8.7	1.87×10^2
6.446	317.3	0.7	0.5	1.01×10^3
6.394	370.1	0.3	0.1	1.35×10^3
6.210	558.2	13.6	17.0	3.8
6.182	586.6	3.9	2.9	9.7

Table A.9-II. Bk^{245} alpha data.

E_α (MeV)	Level (keV)	α intensity (%) Experimental	α intensity (%) Theoretical	Hindrance factor
6.358	0.0	16.5	15.2	7.17×10^2
6.317	41.7	15.0	14.2	5.03×10^2
6.265	94.9	1.4	2.7	3.00×10^3
6.200	160.6	1.4	1.7	1.47×10^3
6.153	207.4	18.9	14.1	64
6.124	237.0	14.7	10.1	59
6.087	274.5	5.6	5.8	1.01×10^2
6.038	324.3	0.6	0.3	5.27×10^2
5.985	378.2	0.2	0.1	9.89×10^2
5.889	474.5	21.8	29.7	2.4
5.858	505.5	4.0	4.5	9.3

Table A.9-III. Multipolarity determinations.

E_γ (keV)	Relative Intensity: Experimental	Theoretical: E1	E2	M1
Bk^{243} α				
187.1	5.0			
146.4	1.0	1.0	1.0	1.0
K x rays	1.1	0.67	1.0	40
Bk^{245} α				
207.4	4.4			
165.3	1.0	1.0	1.0	1.0
K x rays	0.64	0.46	0.79	18
Bk^{245} α				
474.5	1.0	1.0	1.0	1.0
K x rays	0.17	0.013	0.035	0.30

Table A.9-IV. Relative γ-ray intensities depopulating the $K\pi = 5/2+$ levels in Am^{239} and Am^{241}.

$$\left(\frac{B_1}{B_2}\right)_{exp} = \left(\frac{E_2}{E_1}\right)^{2\lambda+1} \cdot \frac{I_1}{I_2}$$

$$\left(\frac{B_1}{B_2}\right)_{theo.} = \left|\frac{\langle I_i\ \lambda\ K_i(K_f-K_i)\,|I_i\ \lambda\ I_f\ K_f\rangle}{\langle I_i\ \lambda\ K_i(K_f-K_i)\,|I_i\ \lambda\ I_f'\ K_f\rangle}\right|^2$$

$$K_i = K_f = 5/2$$

		Multipolarity	$(B_1/B_2)_{exp}$	$(B_1/B_2)_{theo}$
Bk^{243}	$B_{187.1}/B_{146.4}$	E_1	2.35	2.50
		E_2	1.41	0.75
Bk^{245}	$B_{207.4}/B_{165.3}$	E_1	2.30	2.50
		E_2	1.45	0.75

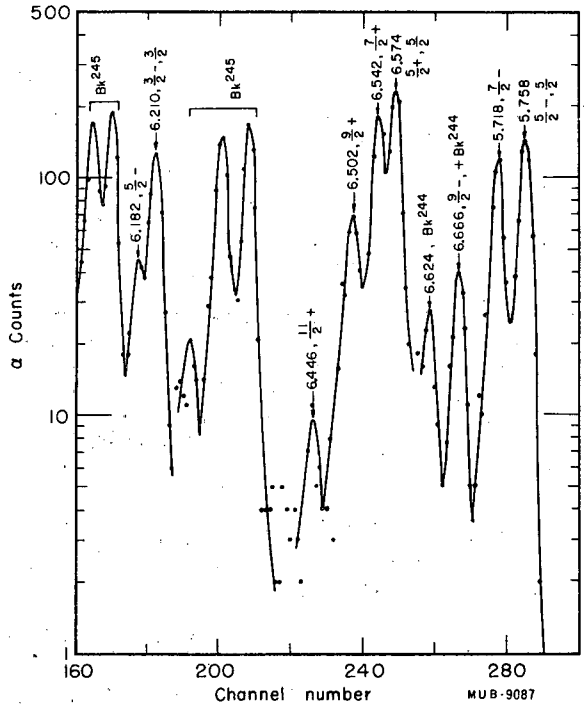

Fig. A.9-1. Bk^{243} and Bk^{244} α-particle spectra.

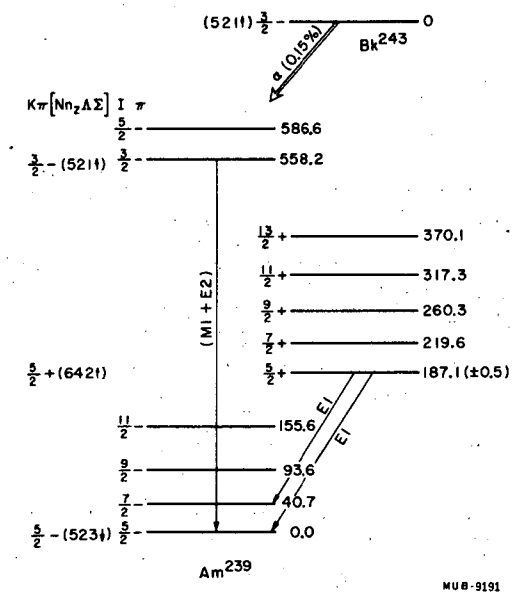

Fig. A.9-3. Alpha-decay scheme of Bk^{243}.

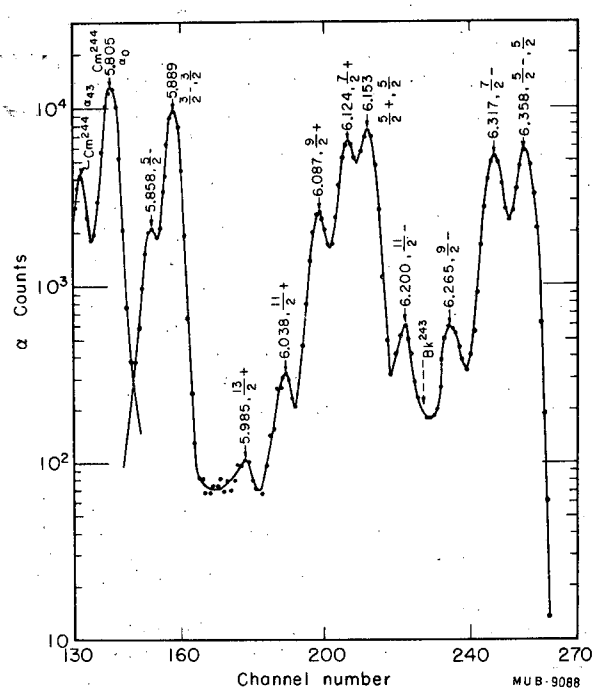

Fig. A.9-2. Bk^{245} α-particle spectra.

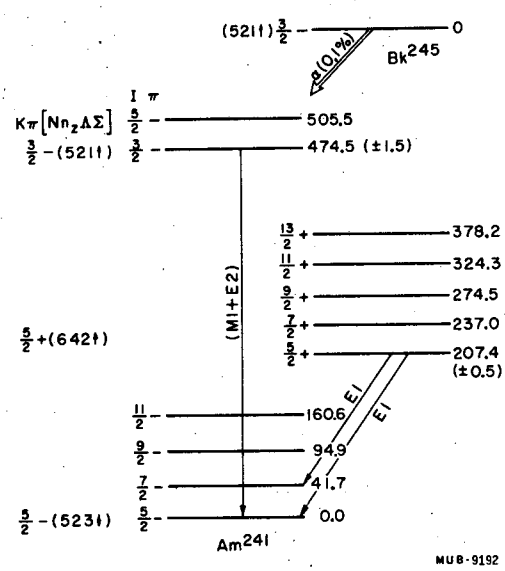

Fig. A.9-4. Alpha-decay scheme of Bk^{245}.

the occurrence of single transitions at energies around 1 MeV in even-even nuclei might serve to indicate such bands. Transitions fitting these requirements are known to occur in Cm^{244} (Bk^{244} decay)[11] and Cf^{250} (Es^{250} decay),[12] suggesting 2- levels in these nuclei at about 950 and 850 keV, respectively. Thus, collective 2- levels lying around 900 keV may be a systematic feature of nuclei in this region.

These K = 2- bands presumably correspond to octupole vibrations, similar to the well-known K = 0- bands in the Ra-Th-U region. In this regard it would be important to try to Coulomb-excite the 2- bands and show the enhanced B(E3) values (as has been done for the K = 0- bands).[13] It is not likely that a K = 0- band lies below the K = 2- band in Cm^{246}, and thus the lowest octupole band has probably changed between plutonium and curium from K = 0- to K = 2-. It is interesting that in just this same region the lowest quadrupole vibration changes from K = 0+ (beta) to K = 2+ (gamma). This must have to do with the general type of orbitals filling in these regions, and the calculations of Soloviev and Siklos bear out both of these cross-overs in a general way; although they have probably underestimated the collective nature of the K = 2- bands.

Footnote and References

†Condensed from Phys. Rev. Letters 15, 420 (1965).

1. D. Englekemeir, P. R. Fields, S. Fried, G. L. Pyle, C. M. Stevens, L. B. Asprey, C. I. Brown, H. Louise Smith, and R. W. Spence, J. Inorg. Nucl. Chem. 1, 345 (1955).
2. D. C. Hoffman and C. I. Brown, J. Inorg. Nucl. Chem. 2, 209 (1956).
3. H. L. Smith, C. I. Brown, D. C. Hoffman, J. P. Mize, and M. E. Bunker, J. Inorg. Nucl. Chem. 3. 93 (1956).
4. F. S. Stephens, Frank Asaro, Sherman Fried, and I. Perlman, Phys. Rev. Letters 15, 420 (1965).
5. S. G. Nilsson, Kgl. Danske Videnskab Selskab Mat-Fys. Medd. 29, no. 16 (1955).
6. B. R. Mottelson and S. G. Nilsson, Kgl. Danske Videnskab. Selskab Mat-Fys. Skrifter 1, no. 8 (1959); F. S. Stephens, F. Asaro, and I. Perlman, Phys. Rev. 113, 212 (1959).
7. V. G. Soloviev and T. Siklos, Nucl. Phys. 59, 145 (1964).
8. C. J. Gallagher and V. G. Soloviev, Kgl. Danske Videnskab. Selskab Mat-Fys. Skrifter 2, No. 2 (1962).
9. A. Bohr and B. R. Mottelson, Atomnia Energia (to be published). See Ref. 10.
10. O. Nathan and S. G. Nilsson, Chapt. X in Alpha-, Beta- and Gamma-Ray Spectroscopy, edited by K. Siegbahn (North-Holland Publishing Co., Amsterdam, 1965).
11. F. Asaro, A. Chetham-Strode, F. S. Stephens, and I. Perlman, unpublished data.
12. F. Asaro, B. G. Harvey, and I. Perlman, unpublished data.
13. R. M. Diamond, B. Elbek, G. Igo, and F. S. Stephens, in Proceedings of the International Conference on Nuclear Structure, edited by D. A. Bromley and E. W. Vogt (University of Toronto Press, Toronto, 1960) p.563.

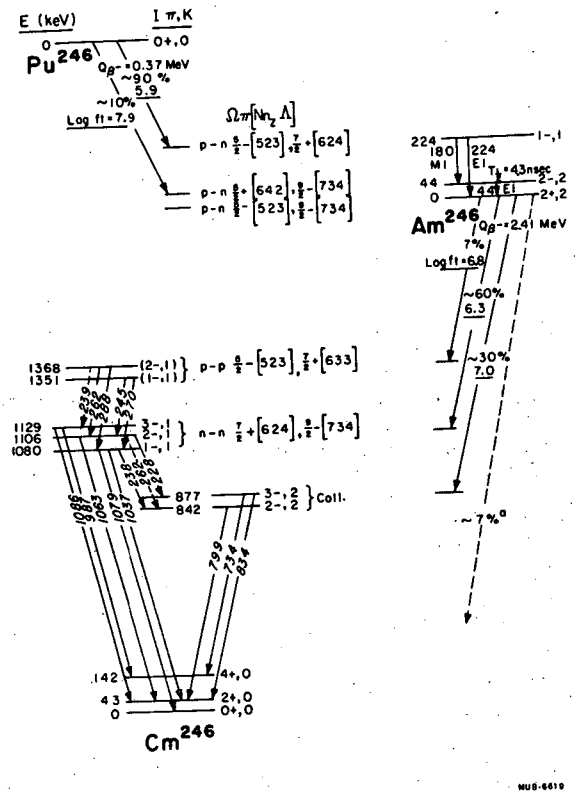

Fig. A.10-1. Decay schemes of Pu^{246} and AM^{246}. a, this intensity was measured by other workers (see Ref. 3).

11. A NEW PARTICLE-CONSERVING VARIATIONAL WAVE FUNCTION FOR THE NUCLEAR PAIRING-FORCE PROBLEM

Oliver Johns and J. O. Rasmussen

The nuclear pairing-force Hamiltonian

$$H = \sum_{j;m>0} \epsilon_j (c^+_{jm} c_{jm} + c^+_{j\bar{m}} c_{j\bar{m}}) - G \sum_{\substack{j;m>0 \\ j';m'>0}} c^+_{jm} c^+_{j\bar{m}} c_{j\bar{m}'} c_{jm'} \tag{1}$$

has a ground state which can be approximated, for $G > G_c$, by minimization of the energy, using a BCS trial wave function,

$$\psi_0 = \prod_{j;m>0} (U_j + V_j c^+_{jm} c^+_{j\bar{m}}) \,|\, 0), \tag{2}$$

where $U_j^2 + V_j^2 = 1$, and G_c is some critical value of G. For $G < G_c$, only trivial solutions with no configuration mixing are obtained. The G_c may be zero, but there are important cases in which it is nonzero. Furthermore, the ordinary BCS wave function has the defect that particle number is not conserved. If only the terms in ψ_0 containing the correct number of particles are retained and the energy based on such a trial function is then minimized, the critical behavior of solutions at $G = G_c$ disappears.[1] This is the FBCS method of Dietrich, Mang, and Pradal.[2]

The FBCS method was applied to the example of Ω pairs of nucleons in two levels of identical pair degeneracy Ω by Rho and Rasmussen.[3] The symmetry of the problem is such that the FBCS trial wave function becomes

$$\sum_{q=0}^{\Omega} \binom{\Omega}{q} X^q \, | a^{\Omega-q} b^q \rangle$$

where X is a variational parameter and $|a^{\Omega-q}b^q\rangle$ is a state with Ω-q pairs in the lower level and q pairs in the upper level. The correct ground-state wave function was found by exact diagonalization of H. It is of the form

$$\sum_{q=0}^{\Omega} C_q \, | a^{\Omega-q} b^q \rangle .$$

The FBCS solution was found to match well the correct coefficient ratio C_1/C_0, but the coefficient ratios C_q/C_0 for $q>1$ were not matched well when G was small. In fact, in the small-G limit, the coefficient ratios C_q/C_0 were underestimated by factors of q!. To remedy the underestimation of the coefficients of states with two or more pairs in the upper level, Mang, Rasmussen, and Rho[4] suggested a two-parameter trial function of the form

$$P_\Omega(1 + \beta A_a^+ A_b^+)\psi_0(X),$$

where A_p^+ creates two quasi particles in the pth level, coupled to J = 0. This function was found to improve somewhat the low G agreement with the coefficient ratio C_2/C_0, but it still underestimated the ratios C_q/C_0 for $q \geq 2$ in the small-G limit.

The success of the two-parameter trial function of Ref. 4 suggests the use of a trial function such as

$$\psi = P_\Omega \, e^{\beta A_a^+ A^+ b} \psi_0(X). \tag{3}$$

A similar form appears in the ground-state wave function by random-phase approximation, but has not been studied hitherto with projection of fixed particle number. In fact, the wave function

$$P_\Omega e^{-\frac{\Omega G}{2} A_a^+ A_b^+} \psi_0(0)$$

does exactly reproduce the correct coefficient ratios of all states in the small-G limit, and we know that the projected FBCS form with no exponential operator factor is exceedingly good in the limit of large G. Thus, we had hope that the two-parameter variational trial function of Eq. (3) might be quite good over the full range of G. The results of a search for an energy minimum at an intermediate pairing-force strength is shown in Fig. A.11-1, for G = 0.1 and Ω = 5. The energy is defined by

$$\langle\psi|H|\psi\rangle / \langle\psi|\psi\rangle = E(\beta, X). \tag{4}$$

A minimum is seen to exist for a small negative value of β. The FBCS solutions lie on the X axis for $\beta = 0$. The values of β and X which minimize the energy were calculated for several G values, by use of an electronic computer. The coefficient ratios obtained by this minimization are compared with the correct C_q/C_0 values for three q values in Figs. A.11-2, A.11-3, and A.11-4. It is seen that excellent agreement is obtained over a range from G = 0.01 to G = 1.0. Five coefficient ratios are very closely reproduced by a variational method using only the two parameters β and X. The minimum-energy β and X values as functions of G are shown in Fig. A.11-5. The behavior of β for large G (β is proportional to $1/G^2$) is consistent with the known result that the wave function ψ_0 is correct in the large G limit.

The trial function ψ is similar in form to the unprojected ground state for the symmetric two-level problem, derived by Högaasen-Feldman[5] using the quasiboson approximation. It is

$$e^{f(G)(A_a^+ - A_b^+)^2}\psi_0.$$

where f(G) is proportional to $1/G^2$ for large G. The functions f(G) and β are approximately proportional and of the same order of magnitude for $G > 0.5$. The exponent in the quasiboson ground state contains terms $(A_a^+)^2$ and $(A_b^+)^2$ not found in our trial function of Eq. (3), but since X is large only when β is small, and since the leading contribution from these terms in a projected wave function is one power of X smaller than that of the cross term $-2A_a^+A_b^+$, the squared terms may not be so important.

It would appear that the new fixed-particle-number variational form of Eq. (3) will not significantly lower the variational energy below the FBCS method, which already comes close to the exact eigenvalue over the whole range of G. However, the smaller amplitudes in the wave function may be greatly improved over FBCS in the range of pairing force strength encountered in real nuclei. It is hoped that the new variational expression can be generalized to cases of more than two orbitals.

References

1. H. J. Mang, J. K. Poggenburg, and J. O. Rasmussen, Nucl. Phys. 64, 353 (1965).
2. K. Dietrich, H. J. Mang, and J. H. Pradal, Phys. Rev. 135, B22 (1964).
3. M. Rho and J. O. Rasmussen, Phys. Rev. 135, B1295 (1965).
4. H. J. Mang, J. O. Rasmussen, and M. Rho, Comparisons of BCS Nuclear Wave Functions with Exact Solutions. II. Particle-Number-Conserving Method, Phys. Rev. (to be published) (UCRL-16550, Dec. 1965).
5. J. Högaasen-Feldman, Nucl. Phys. 28, 258 (1961).

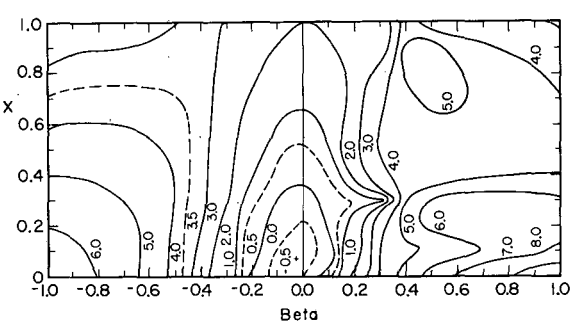

Fig. A.11-1. A contour plot shows the results of a search for a minimum of the function E(β, X) for an intermediate G value, G = 0.1. The function E(β, X) is defined in Eq. (4) (Ω = 5, $\epsilon_a = 0$, $\epsilon_b = 1$).

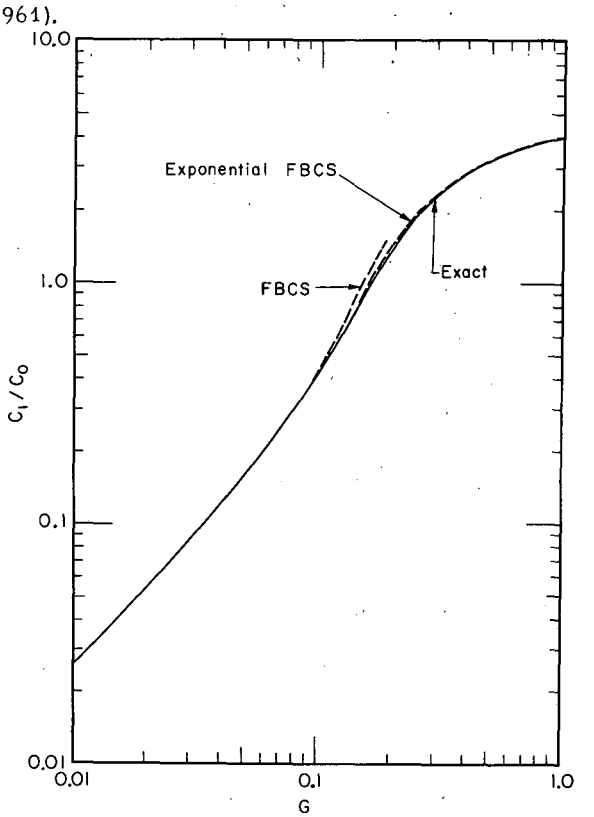

Fig. A.11-2. The coefficient ratio C_1/C_0 is plotted as a function of G. The curve marked "Exponential FBCS" was obtained by an energy-minimization procedure using the wave function defined in Eq. (3). The Exact and FBCS values are plotted for comparison (Ω = 5, $\epsilon_b - \epsilon_a = 1$).

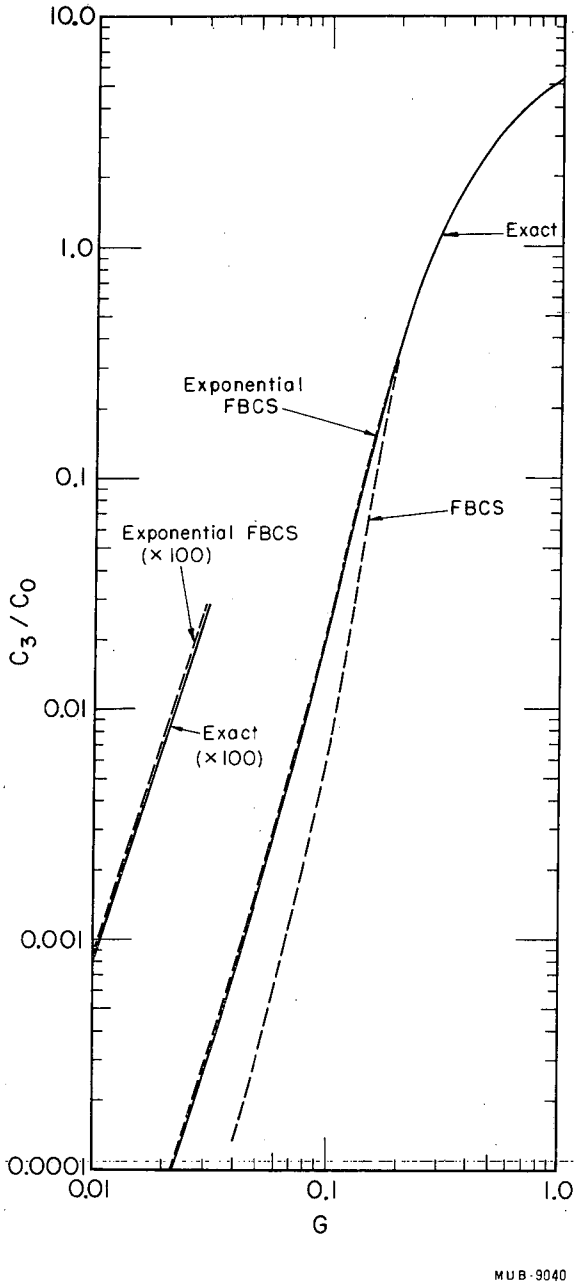

Fig. A.11-3. A plot of C_3/C_0 under the same conditions as in Fig. A.11-2.

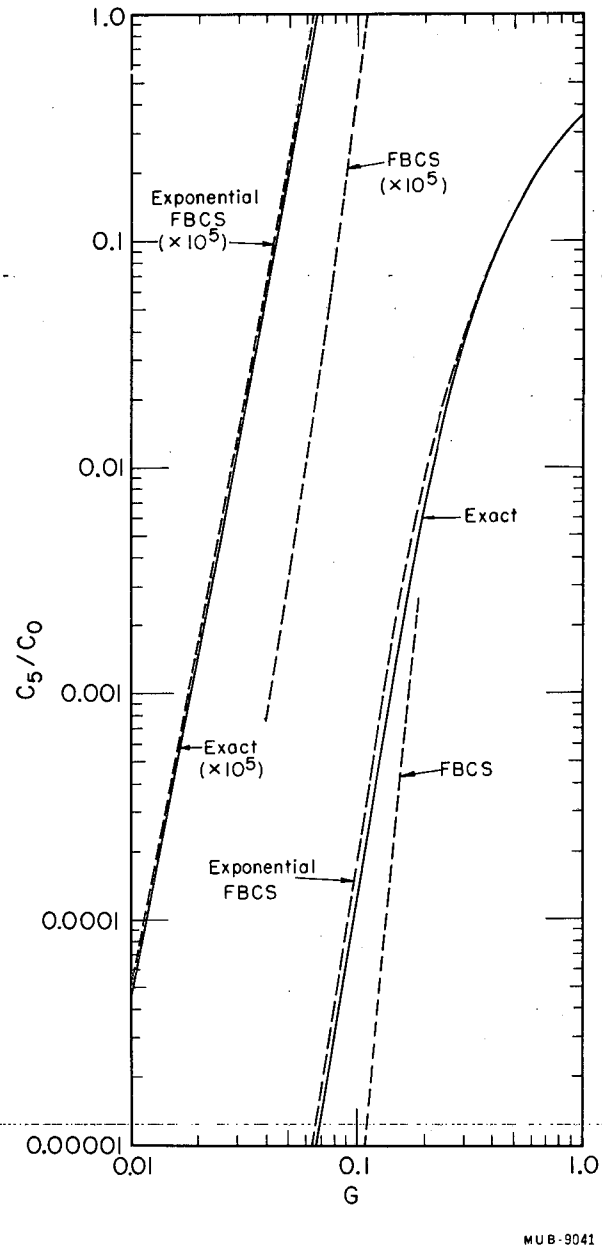

Fig. A.11-4. A plot of C_5/C_0 under the same conditions as in Fig. A.11-2.

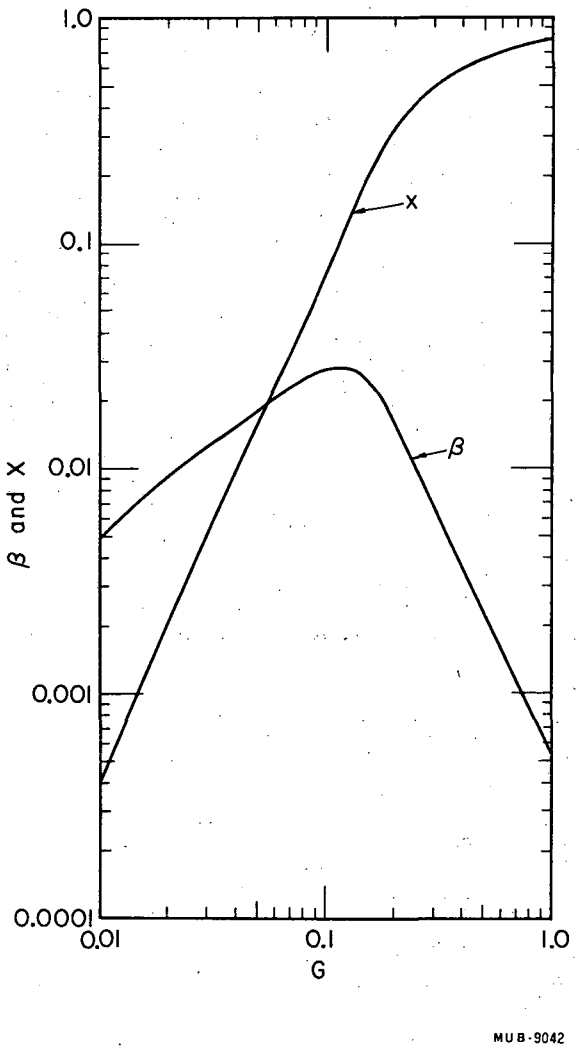

Fig. A.11-5. The values of β and X that minimize the function E(β, X) defined in Eq. (4) are plotted as functions of G ($\Omega = 5$, $\epsilon_b - \epsilon_a = 1$).

12. MEASUREMENT OF PAIR PRODUCTION CROSS SECTION NEAR THRESHOLD†

T. Yamazaki and J. M. Hollander

A determination has been made of the total pair production cross section near threshold in germanium (Z = 32) with use of lithium-drifted germanium γ-ray detectors. Figure A.12-1 shows an example of the pair spectra of Rb^{86} and Co^{60}, obtained with a triple coincidence pair spectrometer employing a Li-drifted germanium detector and two 3 × 3-in. NaI crystals. In the case of higher photon energies ($\gtrsim$ 1.3 MeV), the pair peaks ("double-escape" peaks) can be measured directly from the singles spectra obtained with Ge(Li) detectors. These measurements allowed us to deduce, after necessary corrections, the total pair-production cross sections (relative). In Table A.12-I the experimental values are compared with the Bethe-Heitler cross section.[1] A systematic deviation from the B-H value is illustrated in Fig. A.12-2. Since the Bethe-Heitler theory is based on the Born approximation, this deviation in the threshold region is reasonable. In fact the tendency seems in qualitative agreement with the calculation of Jaeger and Hulme,[2] which takes into account more realistically the interaction of the produced pairs with the nucleus.

Footnote and References

†Shortened version of paper published in Phys. Rev. 140, B630 (1965).

1. H. A. Bethe and W. Heitler, Proc. Roy. Soc. (London) 146A, 83 (1934).
2. J. C. Jaeger and R. H. Hulme, Proc. Roy Soc. (London) 153A, 443 (1936).

Table A.12-I. Experimental pair-production cross sections in comparison with the Bethe-Heitler cross sections.

Photon energy MeV	Photon energy k	Isotope	σ_{pair} (exp)	σ_{pair} (BH)	$\sigma_{pair}(exp)/\sigma_{pair}(BH)$
1.077	2.108	Rb^{86}	5.76 ± 0.50(-4)[a]	2.855(-4)[a]	2.02 ± 0.18
1.115	2.182	Zn^{65}	2.33 ± 0.17(-3)	1.243(-3)	1.82 ± 0.14
1.173	2.295	Co^{60}	7.86 ± 0.29(-3)	4.614(-3)	1.70 ± 0.07
1.278	2.500	Na^{22}	2.63 ± 0.08(-2)	1.781(-2)	1.48 ± 0.05
1.332	2.607	Co^{60}	4.18 ± 0.43(-2)	2.846(-2)	1.47 ± 0.05
1.368	2.677	Na^{24}	5.18 ± 0.16(-2)[c]	3.677(-2)	1.41 ± 0.04
1.407	2.753	Eu^{152}	6.36 ± 0.36(-2)	4.693(-2)	1.36 ± 0.08
1.477	2.890	Mo^{93m}	9.39 ± 0.43(-2)	6.804(-2)	1.38 ± 0.07
1.596	3.123	La^{140}	1.32 ± 0.07(-1)	1.112(-1)	1.19 ± 0.06
1.837	3.594	Y^{88}	2.58 ± 0.11(-1)	2.191(-1)	1.18 ± 0.05
2.185	4.276	Nb^{90}	4.43 ± 0.16(-1)	4.041(-1)	1.10 ± 0.04
2.318	4.536	Nb^{90}	4.78 ± 0.13(-1)	4.791(-1)	1.00 ± 0.03
2.754	5.389	Na^{24}	7.60 ± 0.23(-1)[b,c]	7.303(-1)	1.04 ± 0.03

a. 5.76 ± 0.50(-4) ≡ (5.76 ± 0.50) × 10^{-4}.
b. Normalized at 2.754 MeV to the JH value, which is 4% higher than the BH value.
c. These relative values were obtained from a pair spectrum of Na^{24}, being considered as most reliable.

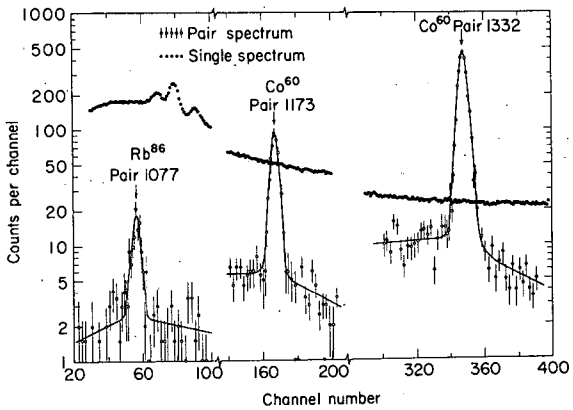

Fig. A.12-1. Some pair spectra taken with the pair spectrometer, showing also singles spectra from the same sources.

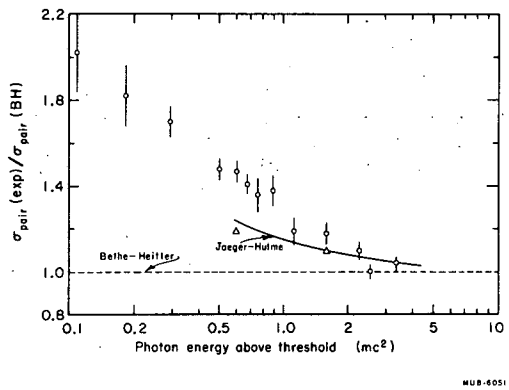

Fig. A.12-2. The ratio of $\sigma_{pair}(exp)/\sigma_{pair}(BH)$. The JH curve extrapolated from high-Z values is also shown. The triangles represent interpolated values from the experiments of Hahn et al. and of Dayton.

13. THE EFFECT OF THE CHEMICAL STATE ON THE LIFETIME OF THE 24-SECOND ISOMER OF Nb^{90} †

J. A. Cooper, J. M. Hollander, and J. O. Rasmussen

The rate of decay of a radioactive nucleus is generally unaffected by its chemical and physical environment. However, in 1947 Daudel[1] and Segrè[2] predicted that under certain conditions a dependence of the decay constant on the chemical and physical environment of the nucleus should be observable, and subsequently such a dependence was found experimentally in the K-capture decay of Be^7,[3] and in the internal-conversion decay of Tc^{99m}.[4-6] This report describes an experiment by which a large change in the decay constant of the 24-sec Nb^{90} isomer was observed following a change in the chemical state.

Recently Cooper et al.[7] proposed a partial decay scheme for Mo^{90} (Fig. A. 13-1) in which a very low-energy isomeric transition in Nb^{90} was postulated. The transition was not detected directly, but an upper limit of 3 keV was placed on its energy. It is thus of interest to obtain evidence of the existence of this isomeric transition.

Such evidence may be obtained, if the transition energy is sufficiently low, by changing the chemical environment of the nucleus and thus altering its decay constant. (As pointed out by Daudel[1], the change in isomeric decay constant arises from a change in electron density near the nucleus.) For the 2-keV isomeric transition in Tc^{99m}, Bainbridge, Goldhaber, and Wilson[4] observed a difference of 0.3% in the decay rate of Tc^{99m} in the compounds $KTcO_4$ and Tc_2S_7. In the case of the Nb^{90} isomer, the chemical bonding electrons are in the N and O shells of Nb, with binding energies $\lesssim$ 50 eV. If the decay energy should be less than 200 eV (binding energy of the M_V shell), internal conversion could take place only in the N and O shells and appreciable chemical effects might be expected.

In the case of a short-lived daughter activity in equilibrium with a long-lived parent, a sudden change in decay constant of the daughter caused by a chemical reaction will perturb the equilibrium, which will again be restored with the half-period of the daughter in its altered environment. (By "chemical reaction" is meant a change in chemical state of the daughter, not a chemical separation of daughter from parent.) Such a chemical effect on the liftetime of Nb^{90m1} has been demonstrated by an experiment in which an intensity change of the 122-keV E2 γ ray (in cascade with the low-energy isomeric transition) was observed following a rapid chemical reaction. About 200 Nb foils (0.02 in.^{2} × 0.0005 in.) were bombarded with 50-MeV protons, producing Mo^{90} by a p, 4n reaction. Each foil, which contained Nb^{90m1} in equilibrium with the Mo^{90}, was rapidly dissolved (1 to 2 sec) in a mixture of hot concentrated HNO_3 and HF, thus changing the chemical

environment of the metastable state from metallic to that of a fluoride complex.

Immediately after the chemical reaction, a growth in activity was noted. A four-point growth curve was obtained by recording four successive γ-ray spectra from a Ge(Li) detector for 18 sec in each of the four 100-channel blocks of a 400-channel pulse-height analyzer. This procedure was repeated about 200 times to insure the statistical reliability of the data. The entire experiment was repeated at a later date and a lower counting rate was used so as to improve the resolution. The resulting γ-ray spectra from the first block of 100 channels are shown in Fig. A.13-2.

The resolved growth curve of the 122-keV photopeak was obtained by assuming that the background under the photopeak is constant (as it is on both sides of the photopeak) and subtracting this background value from the total number of counts under the photopeak (Fig. A.13-3). A least-squares analysis of the four γ-ray spectra was made in order to obtain an average value of the background.

The expression for the intensity of the 122-keV γ ray after the reaction is obtained from the usual relationship for the growth and decay of a two component system,

$$N_{Nb^{90m_1}} = \frac{\lambda_{Mo^{90}} N^\circ_{Mo^{90}}}{\left[(\lambda_{Nb^{90m_1}} + \Delta\lambda) - \lambda_{Mo^{90}}\right]} \left\{ \exp(-\lambda_{Mo^{90}} t) - \exp\left[-(\lambda_{Nb^{90m_1}} + \Delta\lambda)t\right] \right\} + N^\circ_{Nb^{90m_1}} \exp\left[-(\lambda_{Nb^{90m_1}} + \Delta\lambda)t\right], \quad (1)$$

where $N^\circ_{Mo^{90}}$ and $N^\circ_{Nb^{90m_1}}$ are the number of nuclei present at the time of the chemical reaction and $\lambda_{Nb^{90m_1}} + \Delta\lambda$ is the decay constant for the isomer in the fluoride complex. By substituting $\lambda_{Nb^{90m_1}} N^\circ_{Nb^{90m_1}}$ for $\lambda_{Mo^{90}} N^\circ_{Mo^{90}}$ in Eq. (1)(equilibrium condition immediately before the reaction) and dropping $\lambda_{Mo^{90}}$ from the denominator, one obtains

$$N_{Nb^{90m_1}} (\lambda_{Nb^{90m_1}} + \Delta\lambda) = \lambda_{Nb^{90m_1}} N^\circ_{Nb^{90m_1}} \exp(-\lambda_{Mo^{90}} t) + \Delta\lambda\, N^\circ_{Nb^{90m_1}} \exp[-(\lambda_{Nb^{90m_1}} + \Delta\lambda)t] . \quad (2)$$

Thus the intensity of the 122-keV γ ray is given by either the sum or difference (depending on the sign of Δλ) of two exponentials,

$$I(t) = \alpha \exp\left[-\lambda_{Mo^{90}} t\right] + \beta \exp\left[-(\lambda_{Nb^{90m_1}} + \Delta\lambda)t\right] . \quad (3)$$

Thus, $\beta/\alpha = \Delta\lambda/\lambda_{Nb^{90m_1}}$, the fractional change in decay constant of the isomer.

The functional relationship of Eq. (3) was fitted to the four points of the growth curve by the method of least squares. The best solutions (Fig. A.13-3) were obtained with a Nb^{90m_1} half life of 21 sec, which is in good agreement with the 24 ± 3-sec value reported by Mathur and Hyde.[8] The results of the two experiments were compared (Fig. A.13-4) by normalizing the B results to the first point of the A results with a normalization factor of 2.865. The results of this analysis show that the decay constant of the metal is 3.6 ± 0.4% greater than the decay rate of the fluoride complex.

The size of the effect, an order of magnitude greater than that observed by Bainbridge et al.[4] with Tc^{99m} in Tc metal and $KTcO_4$, indicates that the transition depopulating the 24-sec isomeric state has a very low energy and decays by internal conversion in the outermost electron shells, where changes in the chemical state can be expected to affect most strongly the electron density at the nucleus. So far as we know, this 3.6% change is the largest alteration in half-life yet noted for a radioactive isotope.

Not only is the effect an order of magnitude greater than but it is also in the opposite direction from the effect observed in Tc^{99m}. Slater suggested that the faster decay rate observed for $KTcO_4$ is due to a greater squeezing of the Tc atom in the $KTcO_4$ (Tc-0 bond distance of 1.7 Å) than in the metal (Tc-Tc bond distance of 2.7 Å).[9] The same effect of smaller bond distance should also be present in the case of the solid Nb fluoride salt, $KNbF_7$, since it has a Nb-F bond distance of 2.0 Å,[10] compared with the Nb-Nb metal bond distance of 2.85 Å.[11] We have no knowledge of the Nb-F bond distance in the niobium fluoride complexes in the solution which was the final state in our experiment, but if it is also less than the Nb-Nb bond distance in the metal, another explanation must be sought for the direction of the observed effect. Possibly this could be attributed to the very high electronegativity of the fluorine atom. Since the Nb-F chemical bond involves essentially the 4d and 5s electrons, our results would then indicate that an appreciable fraction of the isomeric decay takes place by ejection of valence electrons, which would indeed indicate a very-low-energy transition.

Footnote and References

†Phys. Rev. Letters 15, 680 (1965).

1. R. Daudel, Rev. Sci. 85, 162 (1947).
2. E. Segrè, Phys. Rev. 71, 274 (1947).
3. R. F. Leininger, E. Segrè, and C. Wiegand, Phys. Rev. 76, 897 (1949); Erratum: Phys. Rev. 81, 280 (1951).
4. K. T. Bainbridge, M. Goldhaber, and E. Wilson, Phys. Rev. 90, 430 (1953).
5. D. H. Byers and R. Stump, Phys. Rev. 112, 77 (1958).
6. K. T. Bainbridge, unpublished results, 1952; see R. A. Porter and W. G. McMillan, Phys. Rev. 117, 795 (1960).
7. J. A. Cooper, J. M. Hollander, M. I. Kalkstein, and J. O. Rasmussen, Nucl. Phys. 72, 113 (1965).
8. H. Mathur and E. K. Hyde, Phys. Rev. 98, 79 (1955).
9. J. C. Slater, Phys. Rev. 85, 1261 (1951).
10. J. L. Hoard and W. J. Martin, J. Am. Chem. Soc. 63, 11 (1941).
11. J. Waser and L. Pauling, J. Chem. Phys. 18, 747 (1950).

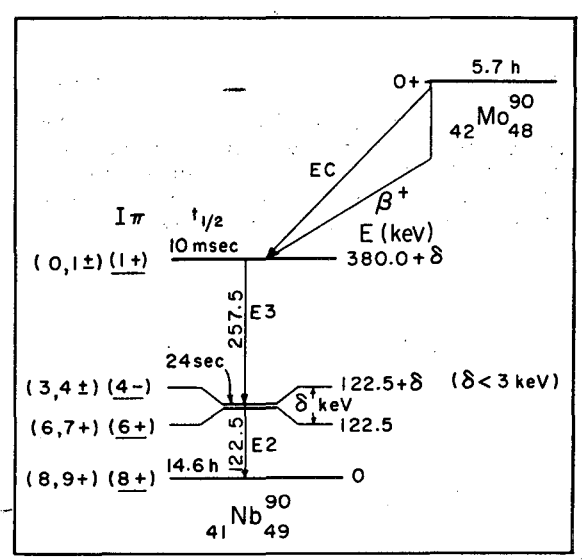

Fig.A.13-1. Partial decay scheme of Mo^{90} as proposed by Cooper et al.[5] The first metastable state (Nb^{90m1}) at 122.5+δ keV is indicated by m_1 and the second metastable state (Nb^{90m2}) at 380.0+δ keV is m_2.

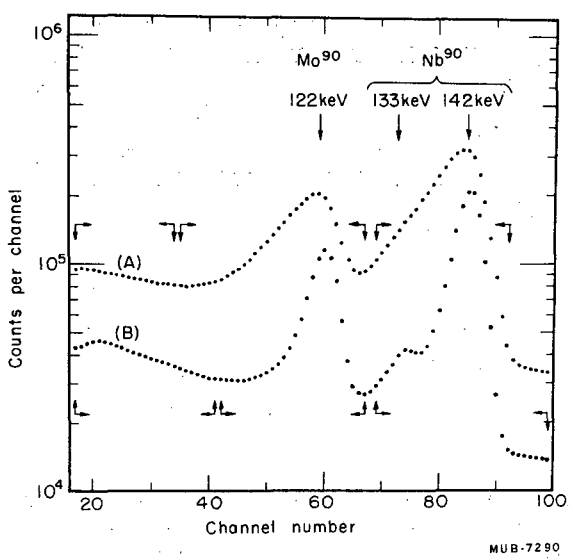

Fig. A.13-2. Accumulated γ-ray spectra from the first 18-sec counting interval after the chemical reaction, showing the 122-keV photopeak of Mo^{90} decay and the 133- and 142-keV photopeaks of Nb^{90} decay. Spectra A and B were taken at different counting rates.

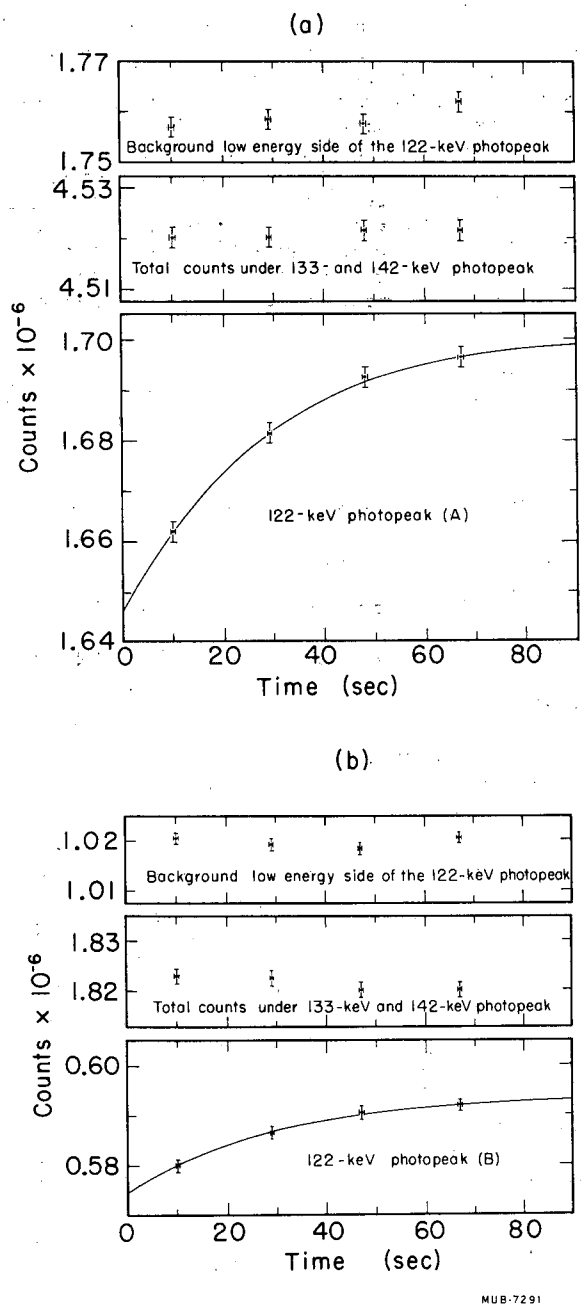

Fig. A.13-3. (a) Growth curve of the 122-keV photopeak A intensity and plot of the background at lower and higher energies. The solid line indicates the least-squares fit to the points. (b) Growth curve of the 122-keV photopeak B intensity and plot of the background at lower and higher energies. The solid line indicates the least-squares fit to the points.

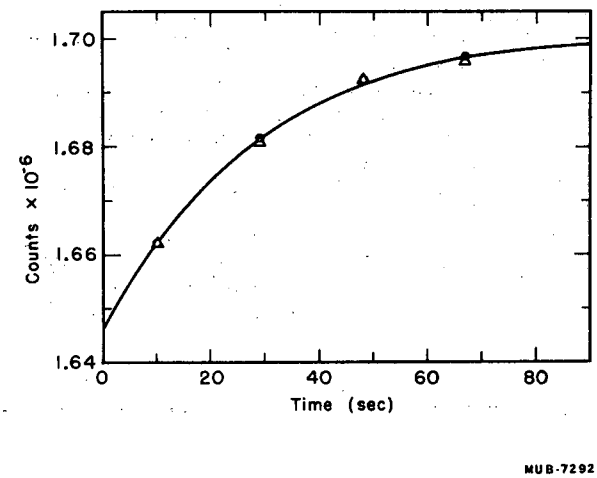

Fig. A.13-4. Comparison of the experimental growth curves obtained from spectrum A and spectrum B. The B results were normalized to the first point of the A results by multiplying all B points by 2.865. O: A series; Δ: B series.

14. NEW WEAK BETA TRANSITION FROM Y^{88}

M. Sakai, T. Yamazaki, and J. M. Hollander

We report here on the observation of a weak electron-capture branch from 105-day Y^{88} to the 3.24-MeV level of the sub-double-closed-shell nucleus Sr^{88}. A pair spectrometer[1] employing a 2 × 3-cm × 1-cm-deep Ge(Li) crystal was used for the detection of weak high-energy γ rays in the decay of Y^{88}. The results are summarized in Table A.14-I. A peak was found at 2.22 MeV in the pair spectrum, which corresponds to the γ ray of 3.24 MeV, previously unobserved from Y^{88}. In a study of the β decay of Rb^{88}, Lazar et al.[2] have established the existence of the 3.24-MeV level in Sr^{88}, deexcited by transitions of 3.24 and 1.39 MeV. The 1.39-MeV γ ray was not visible in our pair spectrum because of the very low pair peak efficiency at this energy. The new decay scheme of Y^{88} is shown in Fig. A.14-1.

The log f_0t value for electron-capture decay to the 3.24-MeV level was calculated to be 9.4, with use of Q_{EC}^0 = 3.62 MeV.[3] This value becomes log f_1t = 8.1 after shape-factor correction.[4] This value is compatible with interpretation of the transition as first-forbidden "unique," leading to a spin-parity assignment 2+ for the 3.24-MeV level. The alternative assigments 4+ and 3+ cannot be ruled out by f t arguments alone; however, 4+ is eliminated by the fact that the 3.24-MeV γ ray is a ground-state transition, and 3+ is considered very unlikely on the basis of the large relative transition probability observed by Lazar et al.[2] for the 3.24-MeV transition in Rb^{88} decay.

References

1. T. Yamazaki and J. M. Hollander, Phys. Rev. 140, B630 (1965).
2. N. H. Lazar, E. Eichler, and G. D. O'Kelley, Phys. Rev. 101, 727 (1956).
3. Nuclear Data Sheets, Nuclear Data Group (Oak Ridge National Laboratory).
4. J. P. Davidson, Jr., Phys. Rev. 82, 48 (1951).

Table A.14-I. Results of pair spectrum of γ rays from the decay of Y^{88}.

Energy of pair peak (MeV)	Transition energy (MeV)	Relative intensity of pair peak	Relative efficiency	Relative intensity
0.815	1.835	47248	4.3×10^{-3}	100
1.72	2.74	633	9.2×10^{-3}	0.63
2.22	3.24	14	1.35×10^{-1}	$(9.5\pm3)\times10^{-3}$

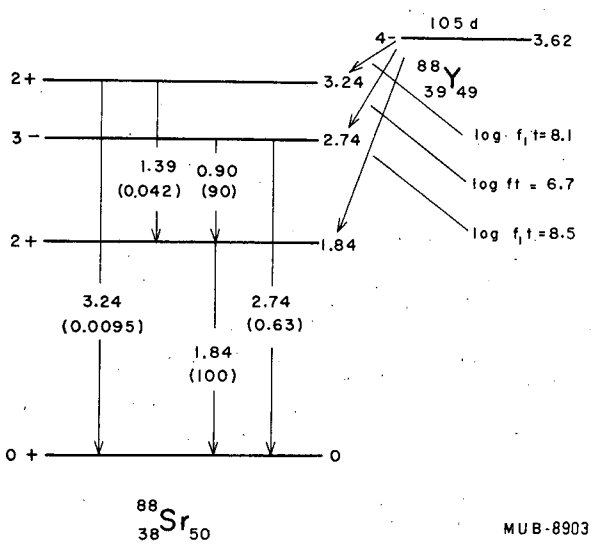

MUB-8903 Fig. A.14-1. Decay scheme of Y^{88}.

15. AN 8- ISOMARIC STATE IN THE 106-NEUTRON NUCLEI: W^{180}, Os^{182}, Pt^{184} †

J. Burde,* R. M. Diamond, and F. S. Stephens

In a continuing study of the γ-ray cascades following (heavy ion, Xn) reactions as described in the previous report for the light isotopes of Yb, Hf, and W,[1] prompt radiations from the neutron-deficient nuclei of Os and Pt were investigated. At the same time, a search was conducted for possible millisecond to minute isomers in these nuclei. Such isomers can very conveniently be studied between beam pulses at the Hilac, and Os^{182m} was observed,[2] as well as the new activity, Pt^{184m}, both with 106 neutrons. To complete the study, a third, partially characterized 106-neutron isomer,[2-4] W^{180m}, was also investigated.

Conversion-electron spectra from the targets were observed at 90 deg to the beam direction with a single-wedge-gap spectrometer. Gamma-ray spectra were detected with 5×5-cm NaI (Tl) crystals and with a lithium-drifted Ge detector. Gamma-gamma coincidence experiments and angular distribution measurements were made with 5×5-cm NaI(Tl) crystals.

The isomeric level in W^{180} was produced by the reaction $Hf^{178}(\alpha, 2n)W^{180}$ by irradiating a foil of natural Hf with 23-MeV He^4. An example of the conversion-electron spectrum obtained between the beam bursts and with the long-lived activity subtracted is shown in Fig. A.15-1. Five transitions were seen with a half life of 5.2 ± 0.2 msec. Determination of their conversion coefficients indicates that the transition of 390 keV is an E1 and the others are E2. All have about the same total intensity, and all are in coincidence. The γ-γ angular correlation experiments indicate an 8(1) 8(2) 6(2) 4(2) 2(2) 0 cascade, although a 4(1) 4(2) 6(2) 4(2) 2(2) 0 combination is not excluded. No cross-over transitions were observed, and we believe that the decay scheme is as shown in Fig. A.15-5.

The activity Os^{182m} was produced by the reaction $Lu^{175}(B^{11}, 4n)O^{182}$. A conversion electron spectrum observed between beam bursts is shown in Fig. A.15-2. Again there are five prominent transitions of comparable intensity, of which one, the 554-keV one, is an E1, and the others are E2. All five show the same half life, 0.78 ± 0.07 msec. The γ-γ angular distribution measurements again suggest an 8(1) 8(2) 6(2) 4(2) 2(2) 0 cascade, so that we believe a decay scheme very similar to that in W^{180m} is involved, as shown in Fig. A.15-5. But, in fact there seems to be a small increase in the intensity of the transitions on going down the cascade, and at least one weak additional transition, ≈ 1245 keV, has the 0.8-msec half life as the isomer. Both features suggest that a small side branch to the main cascade occurs, but this has not been worked out because of the weakness of the branch.

The last isomer, Pt^{184m}, was produced in a variety of ways: $Ta^{181}(B^{11}, 8n)Pt^{184}$; $Lu^{175}(N^{14}, 5n)Pt^{184}$; and $Tm^{169}(F^{19}, 4n)Pt^{184}$. A conversion electron spectrum of it is shown in Fig. A.15-3, and a γ-ray spectrum obtained with a lithium-drifted Ge detector is shown in Fig. A.15-4. As can be seen, the decay is more complicated than in the two previous cases, but again there are five prominent transitions tracing out the main cascade. They all have the half life 1.01 ± 0.05 msec. Conversion coefficients and K/L electron intensity ratios show that the 610-keV transition is an E1 and the other four are E2's. The γ-γ angular distribution measurements again suggest the 8(1) 8(2) 6(2) 4(2) 2(2) 0 sequence, although the 4(1) 4(2) 6(2) 4(2) 2(2) 0 sequence is not ruled out. The proposed scheme is shown in Fig. A.15-5. But this time there are a number of additional (weaker) transitions with the same half life that carry about one-half of the total intensity in branching γ decays. The multipolarity of some of these can be established from the value of their conversion coefficients, and by means of energy sums and γ-γ coincidence measurements most of these transitions, but not all, have been placed in the decay scheme.

It is interesting to compare the isomeric states and their mode of de-excitation in the three isotones. From the systematic appearance of the isomers it appears that the states have to be connected with an intrinsic configuration of the neutrons. In Table A.15-I are summarized the energies of the deexciting E1 transitions of the three isotones, and the retardation of their transition probabilities with respect to the single-particle value. The transition probabilities seem to be equal within a factor of 3. It is remarkable to note that there is no obvious trend for a relaxation in the K-forbiddenness in the transition probabilities in going from W^{180}, the best rotor, to Pt^{184m}, the poorest one and the, initially, least deformed nucleus. It might be expected that the effect of the K-forbiddenness would decrease in approaching the spherical nuclei as the validity of the K quantum number itself diminishes.

The excited states of a fourth isotone, Hf^{178}, are also known from previous work.[5-7] Two 8- states were found in this nucleus at energies of 1480 and 1148 keV, while in Hf^{180} and 8-

state has been observed at an energy of 1142 keV. The 1148-keV and the 1142-keV states are probably due to a two-proton configuration in the Hf^{178} and Hf^{180} isotopes, respectively. In fact, Gallagher and Nielsen[7] have so assigned them as the two-quasiparticle state formed from the Nilsson [404↓+514↑] proton orbitals. These authors have also assigned the 1480-keV level in Hf^{178} as a two-neutron state made up of the Nilsson [624↑+514↓] orbitals. Gallagher and Soloviev[8] found good agreement between the experimental energies and theoretical values calculated on the basis of a model which applies pairing correlations to nuclei with a deformed core.

Their neutron configuration assignment of the 1480-keV level in Hf^{178} is supported by the systematic occurrence of the 8- isomeric states in the three nuclei described in the present work; these other 106-neutron isotones have most probably the same [624↑+514↓] neutron configuration. It is interesting to note, as is apparent from Table A.15-I, that the transition probability of the deexciting transitions from the two-neutron state to the ground rotational band is at least four orders of magnitude larger than that from the two-proton state (in Hf^{180m}) to the ground band, despite the fact that both transitions have the same K forbiddenness.

Footnotes and References

†Brief version of UCRL-16163.

*Permanent address: Physics Department, The Hebrew University, Jerusalem, Israel.

1. F. S. Stephens, N. L. Lark, and R. M. Diamond, Phys. Rev. Letters 12, 225(1964); Nucl. Physics 63, 82 (1965).
2. N. L. Lark and H. Morinaga, Nucl. Phys. 63, 466 (1965).
3. S. D. Softky, Phys. Rev. 98, 736 (1955).
4. V. V. Remaev, Yu. S. Korda, and A. P. Klyucharev, Bull. Acad. Sci. U. S. S. R. (translation) 29, 133 (1963).
5. F. F. Felber, F. S. Stephens, and F. Asaro, J. Inorg. Nucl. Chem. 7, 153 (1958).
6. B. Harmatz, T. H. Handley, and J. W. Milelich, Phys. Rev. 119, 1345 (1960).
7. C. J. Gallagher, Jr., and H. L. Nielsen, Phys. Rev. 126, 1520 (1962).
8. C. J. Gallagher, Jr., and V. G. Soloviev, Kgl. Danske Videnskab. Selskab, Mat.-Fys. Skrifter 2, No. 2 (1962).

Table A.15-I. The energies, configurations, and E1 hindrance factors for the 8- levels.

	Pt^{184}	Os^{182}	W^{180}	Hf^{178a}	Hf^{178a}	Hf^{180a}
Level	1838	1832	1525	1480	1148	1172
Configuration	$[624\uparrow+514\downarrow]_{nn}$	$[624\uparrow+514\downarrow]_{nn}$	$[624\uparrow+514\downarrow]_{nn}$	$-A[404\downarrow+514\uparrow]_{pp}$ $+\sqrt{1-A^2}[624\uparrow+514\downarrow]_{nn}$	$\sqrt{1-A^2}[404\downarrow+514\uparrow]_{pp}$ $+A[624\uparrow+514\downarrow]_{nn}$	$[404\downarrow+514\uparrow]_{pp}$
Transition energy(keV)	610	554	390	(420)	88.8	57.6
% of decay	≈50	≈95	100		100	81
$T_{1/2}$(sec)	1.01×10^{-3}	7.8×10^{-4}	5.2×10^{-3}		4	1.98×10^{4}
$(1+\alpha)$	1.00	1.01	1.01		1.50	1.30
Hindrance over s.p.[a]	2.13×10^{12}	6.5×10^{11}	1.44×10^{12}		1.9×10^{13}	2.8×10^{16}

[a]Nuclear Data Sheets, Nuclear Data Group, Oak Ridge National Laboratory, Oak Ridge, Tennessee.

[b]The single-proton transition probability is calculated as $1.0\times10^{14} A^{2/3} E_\gamma^3 S$ when E_γ is in MeV and S is taken as unity. The expression is from S. A. Moszkowski, Theory of Multipole Radiation, in Alpha-, Beta-, and Gamma-Ray Spectroscopy, Vol. 2, K. Siegbahn, Ed. (North-Holland Publishing Co., Amsterdam, 1965), Chapter XV, p. 881.

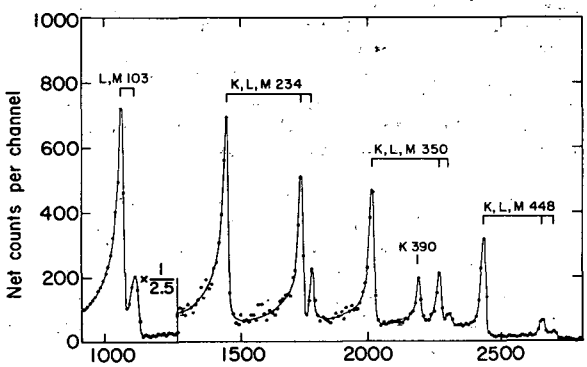

Fig. A.15-1. Conversion-electron spectrum of 5.2-msec W^{180m}.

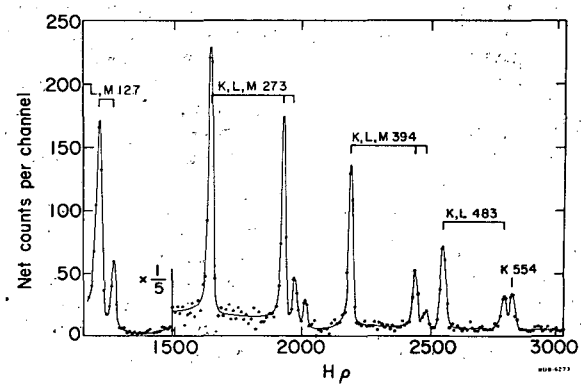

Fig. A.15-2. Conversion-electron spectrum of 0.8-msec Os^{182m}.

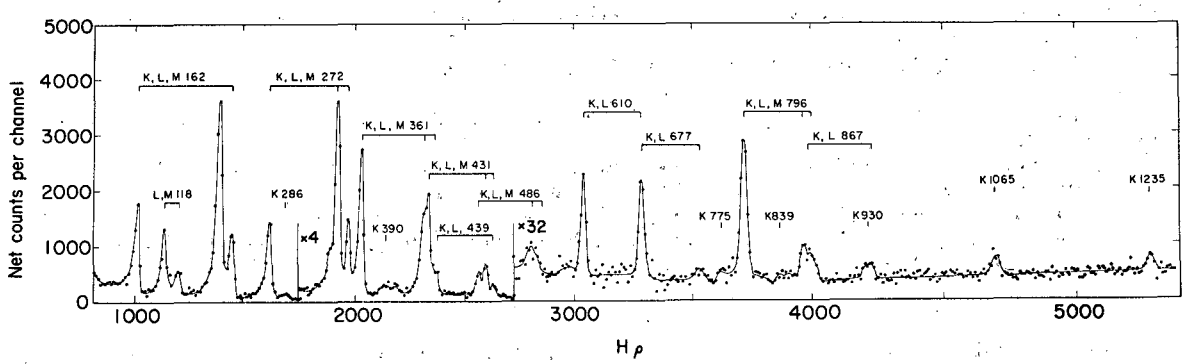

Fig. A.15-3. Conversion-electron spectrum of 1.0-msec Pt^{184m}.

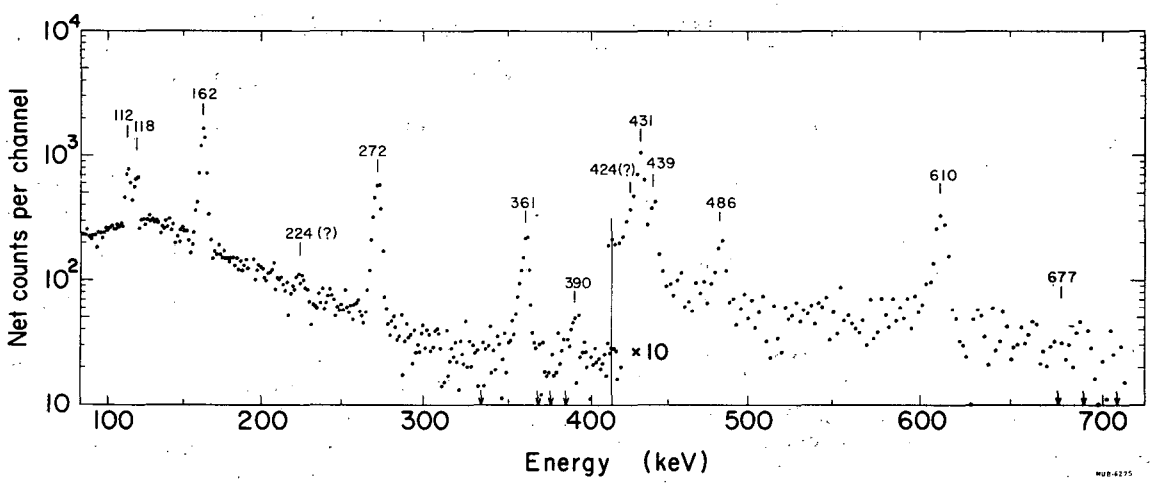

Fig. A.15-4. Gamma-ray spectrum of Pt^{184m} taken with a lithium-drifted Ge detector.

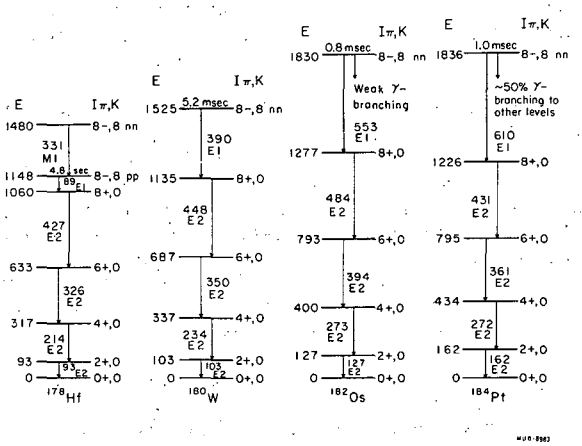

Fig. A.15-5. Partial decay schemes of the 106-neutron nuclei.

16. AN ISOMER OF SPIN $25/2^+$ IN Re^{183}†

M. J. Emmott, J. R. Leigh, J. O. Newton, and D. Ward

A 1-msec isomeric state of Re^{183} was discovered when Ta^{181} was bombarded with helium ions from the Manchester University heavy-ion linear accelerator. The internal conversion lines were studied at Manchester and the isotope was assigned to Re^{183} from the excitation function and the correspondence of the lowest-energy transitions with those already known from the decay of Os^{183} to Re^{183}.[1]

The investigation of this isomer was continued at Berkeley by observations of the γ radiation from its decay with a 6-cm^2 × 8-mm germanium detector at 27.5 MeV bombarding energy. A typical spectrum of the γ rays, taken in a 2-msec interval after the Hilac beam pulse, is shown in Fig. A.16-1.

The observed transitions can be placed in a decay scheme as shown in Fig. A.16-2. The two lowest states were already known from Os^{183} decay,[1] and the rest of the scheme depends on energy relations between the rather accurately measured energies. It appears that the decay takes place through the ground-state rotational band. The conversion coefficients, derived from a comparison of the electron and γ-ray data, are consistent with this interpretation, the cascade transitions being mainly M1 and the crossover transitions E2. The conversion coefficients were not measured absolutely, but they could be obtained by comparison with the L line of the 145-keV transition, which is known to be mainly M1. If the states are assumed to be part of the rotational band, then the M1, E2 mixing ratios of the cascade transitions can be calculated from the intensities of the crossover transitions.[2] When this is done it is found that the percentage of E2 component in the cascade transitions varies from about 3 for the 145-keV transition to about 1.7 for the 303-keV transition. These results are consistent with a constant ratio of B(E2) to B(M1) for the cascade transitions, as would be expected for an unperturbed rotational band.

The total transition intensities can be calculated if the mixing ratios and theoretical conversion coefficients[3] are assumed, the theoretical conversion coefficients being more accurate than our measured ones. These are shown in Fig. A.16-2, the errors being ±9%. The total feeding and decaying intensities so obtained for each level are equal within the errors. Therefore, it appears that the proposed decay scheme is internally self consistent and we feel that the evidence in favor of it is very strong.

The 193.8-keV transition has a K conversion coefficient of 0.2 ± 0.07, which is consistent only with an E2 transition.[3] The K/L ratio of this transition is also consistent with this interpretation. The fact that the isomeric state decays to the $21/2^+$ member of the rotational band by an E2 transition fixes its spin within the limits $17/2^+$ to $25/2^+$. However, if the spin were other than $25/2^+$, it would be expected to decay also to states of the band with spins less than $21/2^+$.

No evidence for such transitions is seen, and in particular the intensity of any possible transition to the $19/2^+$ member is less than 2% of that to the $21/2^+$ member. Since the transition to the $19/2^+$ state would be favored by a factor of a hundred over that to the $21/2^+$ state by the energy difference in the transitions, the evidence that the isomeric state is $25/2^+$ seems very strong.

The half life for a single proton, neglecting the statistical factor but including internal conversion, for a 193-keV E2 transition is 23 nsec. Thus the isomeric transition is hindered by a factor of about 4×10^4. Since the transition has a degree of K-forbiddenness of 8, a hindrance factor between 10^8 and 10^{16} might have been expected, therefore the observed hindrance factor seems rather low. In view of the fact that the E2 transitions in the rotational band are enhanced by a factor of order 100 over the single-proton values, an admixture of about 10^{-7} in intensity of the $I = 25/2^+$, $K = 5/2^+$ state into the $K = 25/2^+$ state could account for this discrepancy. Since these two states are expected to be separated in energy by only about 400 keV, and since, as will be seen below, the isomeric state probably differs from the ground state only in the excitation of a single particle, this very small admixture may perhaps not be unreasonable.

The spin of the isomeric state is much higher than can be accounted for, at this excitation energy, by the excitation of the odd proton in Re^{183} to another Nilsson orbit. It is likely, then, that the state arises from the promotion of a paired neutron or proton to another orbit, giving rise to a three-quasi-particle state. Such states will be expected to occur above an energy corresponding to the energy gap arising from the pairing interaction. Up to this time only three examples of three-quasi-particle states have been reported, all observed in the decay of Lu^{177m}. If the odd proton is left in its original state of $5/2^+$, a state of $25/2^+$ has to be constructed by coupling two protons or two neutrons to give angular momentum and parity 10^+. The arrangement which seems most likely to us to give a state of minimum energy is the two-neutron state, ν, $9/2^+(624)$, $11/2^+(615)$. Another possible arrangement is the two-proton state, π, $9/2^-(514)$, $11/2^-(505)$.

The properties of the rotational band are of some interest; we have already remarked on the constancy of the ratio of reduced transition probabilities in the cascade transitions. In Fig. A.16-3 is shown a plot of $(E_{I+1} - E_I)/(I+1)$ versus $(I+1)^2$. If the energies of the levels are given by a relation of the form

$$E_I = AI(I + 1) + BI^2(I + 1), \qquad (1)$$

then the plot would be a straight line. As can be seen, it is not; moreover, it is apparent that an alternating term is required for the higher spin states. Such a term is expected in fifth-order perturbation theory for the Coriolis operator, operating between the states K and -K.[7] If this is the only operator of importance the correction term to the energy has the form

$$\Delta E_I = (-)^{I+1/2}(I - 3/2)(I - 1/2)(I + 3/2)(I + 5/2)B_5 . \qquad (2)$$

It is possible to fit the observed energy values with the terms of Eqs. (1) and (2), together with a further term, $CI^3(I + 1)^3$. The values we obtained for the coefficients are $A = 16.625\pm0.02$ keV, $B = -12.0\pm1$ eV, $C = +(14\pm6)10^{-3}$ eV and $B_5 = +(3.5\pm1)10^{-3}$ eV. The B_5 term might be expected to be about an order of magnitude smaller than the C term,[7] so that the value we obtain appears reasonable.

Footnote and References

†Condensed from Phys. Letters (January 15, 1966).

1. J. O. Newton, Phys. Rev. 117, 1510 and 1520 (1960).
2. A. Bohr and B. R. Mottelson, Kgl. Danske Videnskab. Selskab Mat-Fys. Medd. 27, No. 1b (1953).
3. L. A. Sliv and I. M. Band, Gamma Rays, (Academy Science of the USSR, Moscow-Leningrad, 1961).
4. P. Alexander, F. Boehm, and E. Kankeleit, Phys. Rev. 133, B284 (1964).
5. M. Jorgensen, O. B. Neilsen, and G. Sidenius, Phys. Letters 1, 321 (1962).
6. L. Kristensen, M. Jorgensen, O. B. Nielsen, and G. Sidenius, Phys. Letters 8, 57 (1964).
7. A. Bohr and B. Mottelson, Atomnia Energia (to be published).

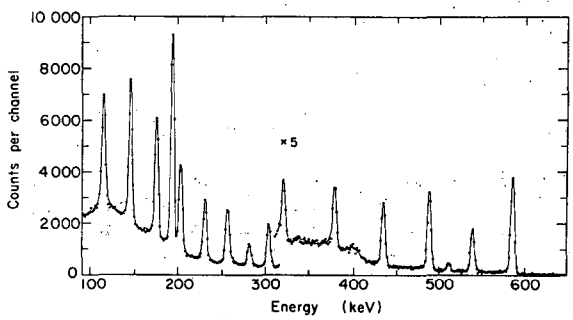

Fig. A.16-1. Typical spectrum of the γ rays taken in a 6-cm^2 × 8-mm Ge counter.

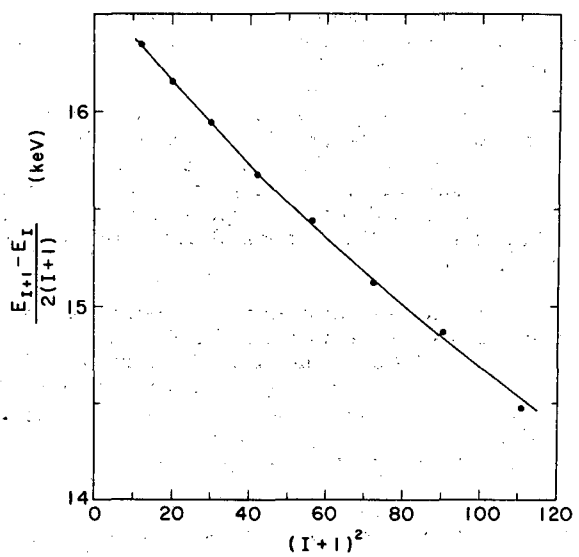

Fig. A.16-3. Energy spacings of the ground-state rotational band of Re^{183}. The experimental errors are smaller than the size of the points, being typically ± 0.01. The full line has no theoretical significance.

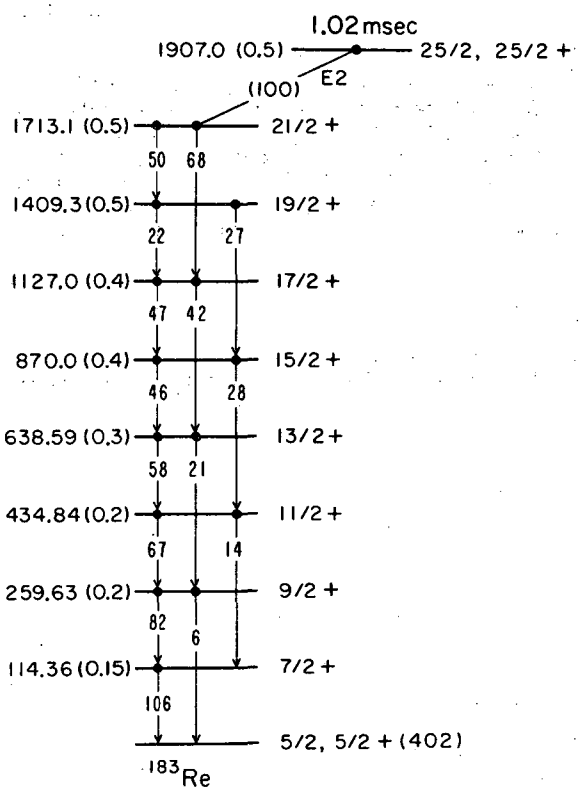

Fig. A.16-2. Decay scheme for the isomeric state. Only those levels of Re^{183} relevant to this decay are shown. The numbers in brackets following the energies show the estimated errors in keV of the energies. The number in the transition arrows are relative transition intensities.

MUB-8782

17. ANGULAR DISTRIBUTION OF γ RAYS IN $La^{139}(p, 2n)Ce^{138}$

Mitsuo Sakai, Toshimitsu Yamazaki, John R. Meriwether, and David L. Hendrie

This is a preliminary report on angular distribution of γ rays in $La^{139}(p, 2n)Ce^{138}$.

La^{139} was bombarded with 14-MeV protons from the Berkeley 88-inch cyclotron. The γ rays from highly excited Ce^{138} nucleus produced by the $La^{139}(p, 2n)Ce^{138}$ reaction were measured with a lithium-drifted germanium γ-ray spectrometer. Since the low-lying excited states in Ce^{138} are known from β-γ spectroscopy of La^{138},[1] as shown in Fig. A.17-1, we can expect to observe the 794-keV, 1044-keV, and 306-keV γ rays.

Figure A.17-2 shows a γ-ray spectrum taken with a 3×2-cm×10-mm deep germanium crystal and with a target of lanthanum oxide of thickness 5 mg/cm^2. Prominent peaks corresponding to the transitions mentioned above appeared with several other peaks some of which are due to contaminants. The angular distribution of these γ rays was measured at positions of 160, 135, 110, and 90 deg with respect to the direction of the incident proton beam. The result is shown in Fig. A.17-3. The errors attached to each point are only estimated from the statistics of the counting rates.

Beam current was monitored by a fixed germanium counter in case the thick target caused scattering loss of beam from the Faraday cup. The dead time of the multichannel analyzer was measured by the counting rate of monitor pulses which was introduced from a pulser into the preamplifier. Despite these precautions, we feel that some systematic instrumental error may be involved in this experiment. However, we clearly do not find any appreciable anisotropy in angular distribution of the γ rays in the reaction $La^{139}(p, 2n)Ce^{138}$. The same conclusions are obtained from similar runs on lanthanum metal targets of about the same thickness.

As far as the 794-keV and the 1044-keV γ rays are concerned, this conclusion is compatible with the preliminary results of angular anisotropy of conversion electrons in the same reaction obtained by one of the authors (M. S.) with his collaborators at INS in Tokyo.[2] However, the large anisotropy for the 306-keV transition obtained in the latter experiment is not consistent with the present results. Since the 2144-keV 7- state has a half-life of 9 msec, it is very natural to expect an isotropic angular distribution. Detailed measurements with conversion electrons are now in progress at INS. The present result is found to be consistent with a similar experiment performed in Tokyo by Ejiri et al.[3]

References

1. M. Fujioka, K. Hisatake, and K. Takahashi, Nucl. Phys. 60, 294 (1964).
2. H. Ejiri, M. Ishihara, M. Sakai, K. Katori, and T. Inamura, Phys. Letters 18, 314 (1965).
3. H. Ejiri, private communication, 1965.

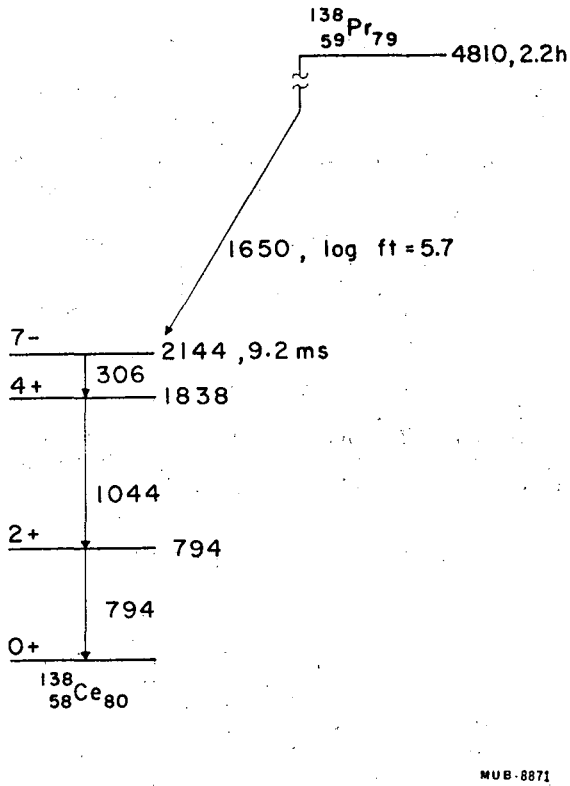

Fig. A.17-1. Decay scheme of La^{138}.

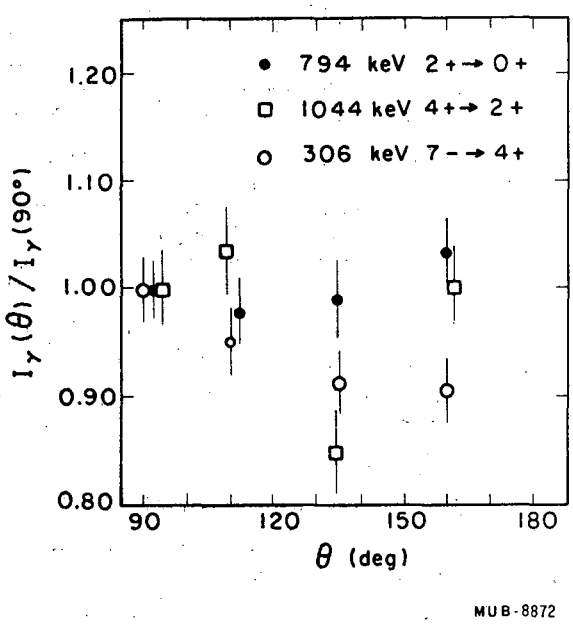

Fig. A.17-3. Angular distribution of the 1044-keV, the 794-keV, and the 306-keV γ rays.

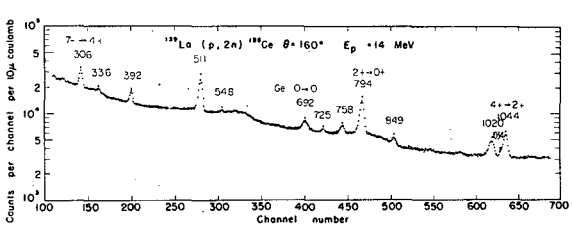

Fig. A.17-2. Gamma-ray spectrum taken with a lithium-drifted germanium γ-ray spectrometer in the reaction La^{139}(p, 2n) Ce^{138}.

18. SPIN AND PARITY OF Be^8 STATES AT 16.6 AND 16.9 MeV*

H. E. Conzett, P. Darriulat,† H. G. Pugh,‡ E. Shield, and R. J. Slobodrian

The 16.6- and 16.9-MeV states of Be^8 can decay via a particle mode only to two α particles, since the next lowest particle-channel threshold (Li^7+p) corresponds to an excitation of 17.3 MeV. Even though α-particle groups from the decay of these states have presumably been seen in the reaction[1] Li^7(d, n) Be^8, the direct excitation of these states in α-α scattering had not been observed. An α-α excitation function[2] taken at a scattering angle of 90 deg c.m. at energies E_α between 23 and 38 MeV ($E_{c.m.}$ = 11.5 to 19 MeV) exhibited no resonance behavior, but the beam spread was too large for these states to be observed or resolved. Because of their known α-decay mode, it follows that these levels should be excited by the inverse process. In the scattering of spin-zero identical particles we have $(J)^\pi = (l_{even})^+$, where l is the orbital angular momentum corresponding to the scattered partial waves, and therefore a clear assignment of spin and parity would be possible from a simple determination of the resonant partial wave.

Using the Berkeley 88-inch cyclotron, we have measured excitation functions for elastic α-α scattering between energies E_α of 23 and 55 MeV, with an energy resolution of 0.1%. During some 70 hours of data collection, the cyclotron energy was changed about 120 times. Measurements were made at c.m. angles of 90, 55.5, and 30.6 deg, the last two being approximately at zeros of $P_2(\cos\theta)$ and $P_4(\cos\theta)$ respectively. Since the nuclear scattering amplitude is given by

$$f_N(\theta, E) = \sum_{l_{even}} A_l(\delta_l)\, P_l(\cos\theta),$$

where $\delta_l = \delta_l(E)$ is the lth partial-wave nuclear phase shift, a resonant behavior of $\delta_{l=l'}$ would have no effect on the differential cross section at an angle $\theta=\theta'$ where $P_{l'}(\cos\theta') = 0$. At energies below E_α = 35 MeV only the l = 0, 2, 4 partial waves contribute appreciably to the scattering.[2,3]

Figure A.18-1 shows our measured excitation functions. The resonance structure near 34 MeV corresponds to the two states of Be^8 at excitations of 16.6 and 16.9 MeV. Here, data were taken at energy intervals as small as 40 keV. Since no resonant effect was observed at the c.m. angle of 55.5 deg, these states should be assigned spin 2 and even parity.

The energy region from 37 to 43 MeV has been examined in more detail through the measurement of nine angular distributions and their analysis in terms of complex phase shifts. Effects due to the opening of reaction channels seem to play a relevant role in the explanation of the differential cross sections.[4] The behavior of the excitation curves near E_α = 45 MeV suggests again the assignment of $J^\pi = 2^+$ to a resonance in that region.

Footnotes and References

*Results first reported by E. Shield et al., Bull. Am. Phys. Soc. 9, 703 (1964).
†Present address: C. E. N. Saclay, Gif sur Yvette, France.
‡Present address: Department of Physics, University of Maryland, College Park, Maryland.

1. P. Paul and D. Kohler, Phys. Rev. 129, 2698 (1963).
2. D. J. Bredin, W. E. Burcham, D. Evans, W. M. Gibson, J. S. C. McKee, D. J. Prowse, J. Rotblat, and J. N. Snyder, Proc. Roy. Soc. (London) A251, 143 (1959).
3. P. Darriulat, G. Igo, H. G. Pugh, and H. D. Holmgren, Phys. Letters 11, 326 (1964); Phys. Rev. 137, B315 (1965).
4. H. E. Conzett, E. Shield, R. J. Slobodrian, and S. Yamabe, Bull. Am. Phys. Soc. 9, 704 (1964), and Nuclear Chemistry Division Annual Report 1964 (UCRL-11828); R. J. Slobodrian, H. E. Conzett, E. Shield, and S. Yamabe, Bull. Am. Phys. Soc. 10, 693 (1965).

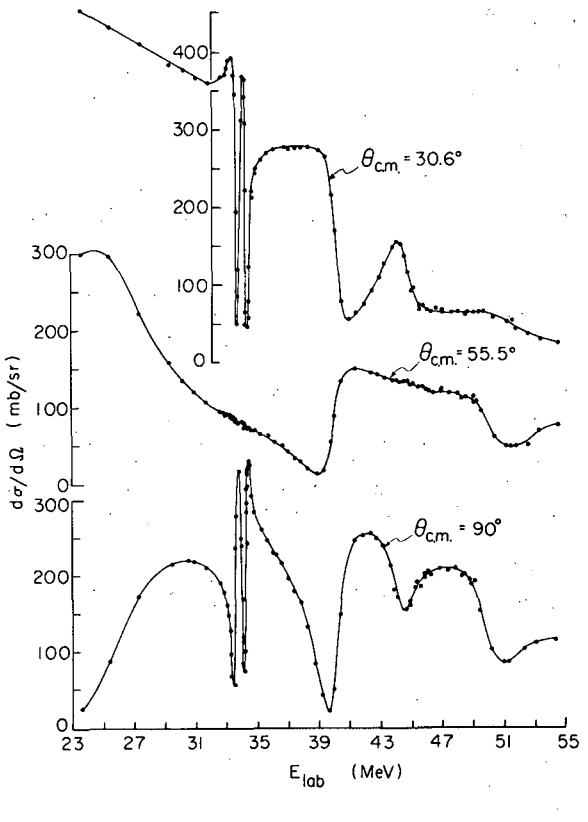

Fig. A.18-1. Excitation functions for elastic α-α scattering, measured at c.m. angles of 30.6, 55.5, and 90 deg.

19. (d, α) REACTIONS ON C^{12}, N^{14} AND O^{16} INDUCED BY 24 MeV DEUTERONS*

Richard H. Pehl, Joseph Cerny, Ernest Rivet,† and Bernard G. Harvey

Alpha-particle energy spectra from (d, α) reactions on C^{12}, N^{14}, and O^{16} have been obtained by use of 24-MeV deuterons. Marked variation in the relative cross sections of final states was observed in the energy spectra. The removal of two nucleons from the target nucleus in a direct reaction should favorably excite levels in the product nucleus whose configuration corresponds to two holes in the target. Thus, states not strongly excited in single-nucleon transfer reactions can be investigated. Although many (d, α) reactions in the light elements have been studied, most of them have involved the use of either single-counter systems or very low bombarding energies, and consequently the observable excitation in the residual nucleus was severely limited. The development of a semiconductor counter telescope system[1] has enabled us to investigate the formation of states of higher excitation.

These (d, α) reactions were induced by the 24-MeV deuteron beam of the late Crocker Laboratory 60-inch cyclotron. Particles were detected by a counter telescope that consisted of two semiconductor counters: A 2.7-mil phosphorus-diffused silicon transmission counter[1] backed by another phosphorus-diffused silicon counter,[2] which had a depletion thickness of 67 mg/cm^2 when a 240-V reverse bias was applied. In the study of reactions producing α particles having a range greater than 67 mg/cm^2 (23 MeV), lithium-drifted p-i-n junction silicon detectors[3] of various thicknesses were used. The reaction products were distinguished by an analog pulse multiplier. A multiplier spectrum with optimum He^3-He^4 separation is shown in Fig. A.19-1. Figure A.19-2 shows an α-particle energy spectrum from the $C^{12}(d, \alpha)B^{10}$ reaction.

Angular distributions of the α particles corresponding to formation of the B^{10} ground-state, 0.717-, 2.15-, 3.59-, 4.77-, 5.18-, and 6.04-MeV levels were obtained, but precise analysis of the energy spectra above an excitation of about 6 MeV is severely hampered by the α-particle continuum, and no angular distributions were obtained for levels above the 6.04-MeV level. Figure A.19-3 shows an α-particle energy spectrum from the $N^{14}(d,\alpha)C^{12}$ reaction. The angular distributions of the α particles corresponding to formation of the C^{12} ground-state, 4.43-, 7.66-, and 9.64-MeV levels are presented in Fig. A.19-4. Figure A.19-5 shows an α-particle energy spectrum from the $O^{16}(d,\alpha)N^{14}$ reaction. Since extensive theoretical studies of the N^{14} nucleus have been made[4, 5] the observed selectivity in the formation of the N^{14} levels is especially interesting.

The double closed-shell configuration of O^{16} could, by removal of two nucleons, produce the levels at 0, 3.95, and 7.03 MeV. But formation of the levels at 4.91, 5.10, 5.69, and 5.83 MeV would require raising one p nucleon into an s or d shell in addition to the removal of two nucleons, and formation of the levels at 6.21 and 6.44 MeV would require raising two p nucleons into the s or d shell (or both). These last six levels were observed, although in slightly reduced yield. All these levels could arise from an admixture of $[p^{-2}(s_{1/2})^2 + p^{-2}(s_{1/2}d_{5/2}) + p^{-2}(d_{5/2})^2]$ in the O^{16} ground state. These levels could also be formed by (a) a compound-nucleus mechanism; (b) knockout of an α particle from the $(p_{3/2})^8\,(p_{1/2})^4$ configuration and capture of one or both nucleons of the incident deuteron in the s or d shells. To eliminate compound-nucleus formation, this reaction could be studied at higher energies to see if the (sd) states are still strongly populated.

A DWBA analysis was made for several of the transitions; the outstanding characteristic of this analysis was the strong preference for L = 2 transitions over L = 0 transitions.

Footnotes and References

*Condensation of Phys. Rev. 140, B605 (1965).
†Present address: University of Montreal, Montreal, Quebec.

1. J. H. Elliott and R. H. Pehl, Rev. Sci. Instr. 33, 713 (1962).
2. These counters were developed by W. L. Hansen, Lawrence Radiation Laboratory, Berkeley, California.
3. J. H. Elliott, Nucl. Instr. Methods 12, 60 (1961).
4. E. K. Warburton and W. T. Pinkston, Phys. Rev. 118, 733 (1960).
5. W. W. True, Phys. Rev. 130, 1530 (1963).

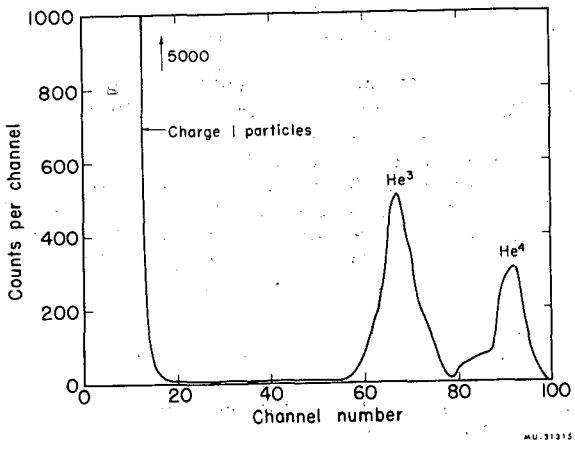

Fig. A.19-1. Multiplier spectrum at a scattering angle of 15 deg from bombardment of O^{16} with 24-MeV deuterons.

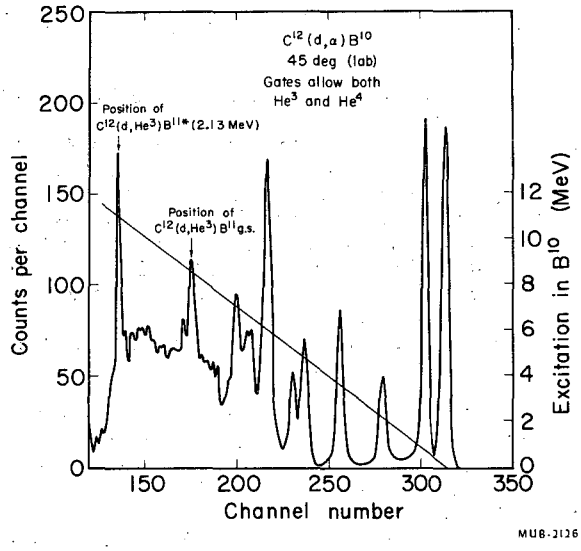

Fig. A.19-2. Alpha-particle energy spectrum from the $C^{12}(d,\alpha)B^{10}$ reaction.

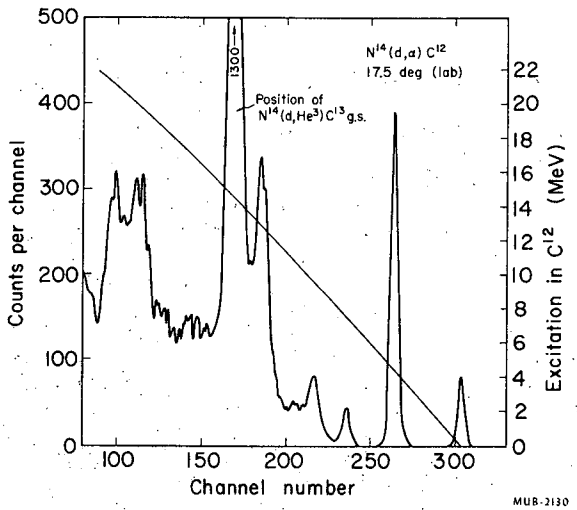

Fig. A.19-3. Alpha-particle energy spectrum from the $N^{14}(d, \alpha)C^{12}$ reaction.

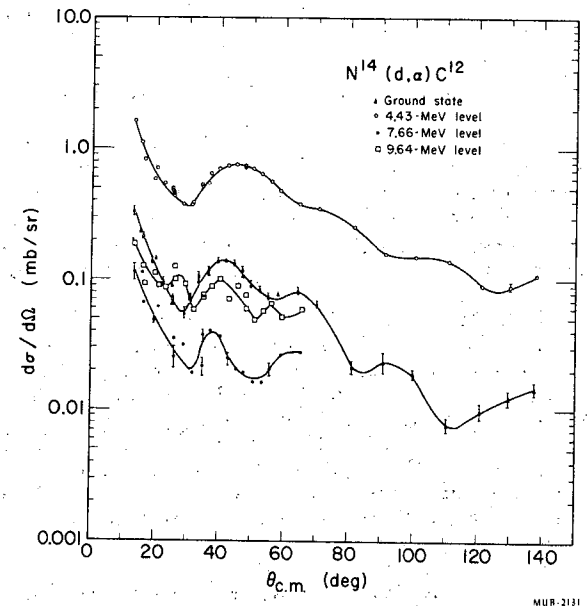

Fig. A.19-4. Angular distributions of α particles from formation of the ground-state, 4.43-, 7.66-, and 9.64-MeV levels of C^{12}.

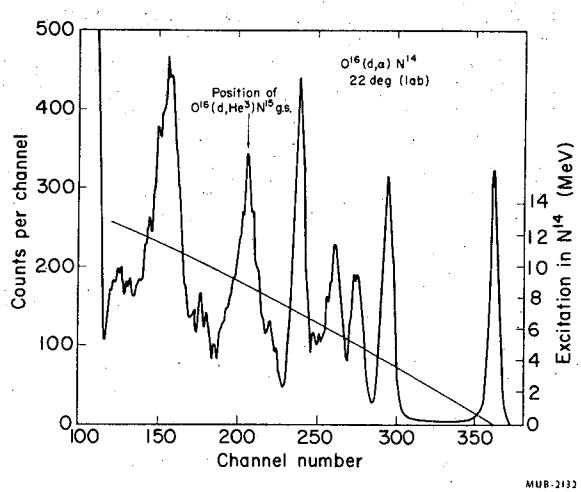

Fig. A.19-5. Alpha-particle energy spectrum from the $O^{16}(d, \alpha)N^{14}$ reaction.

20. INVESTIGATION OF HIGH SPIN LEVELS PREFERENTIALLY POPULATED BY THE (α, d) REACTION*

Richard H. Pehl, Ernest Rivet,† Joseph Cerny, and Bernard G. Harvey

The energy spectra of deuterons from the (α, d) reaction on C^{12}, N^{14}, N^{15}, O^{16}, Ne^{20}, Mg^{24}, Mg^{26}, Si^{28}, S^{32}, Ar^{40}, and Ca^{40} have been observed. These reactions were induced by α particles ranging in energy from 42 to 53 MeV. All the energy spectra were dominated by one or more preferentially populated levels. It is proposed that the levels preferentially populated are of a $[J_T + (j_p j_n)_{J'}]_J$ configuration, with the proton-neutron pair captured in the $d_{5/2}$ or $f_{7/2}$ shell, and that the maximum final spin (5, 6, or 7) is favored.

In a previous (α, d) investigation[1] on the target nuclei C^{12}, N^{14}, N^{15}, and O^{16}, the first evidence that all the strongly populated levels might be of the same $(d_{5/2})^2_5$ configuration was obtained when the Q values for their formation were plotted as a function of the mass number of the product nucleus. As Fig. A.20-1 illustrates, the (negative) Q values decrease in a regular way with increasing A. This relationship has now been extended to higher mass numbers by the addition of the 1.53-MeV level of Na^{22} and the ground state of Al^{26}. Figure A.20-1 also includes the Q values for the formation of the other preferentially populated levels observed. These points fall into what appear to be two groups, both of which resemble the behavior of the $(d_{5/2})^2_5$ points. This information was very useful in making the $(d_{5/2}f_{7/2})_6$ and $(f_{7/2})^2_7$ assignments given in this paper.

Describing the preferentially populated levels in terms of states of good J in deformed nuclei appears to be fairly well justified, since most of the strength goes to one level; no indication of a series of peaks built on a large peak was observed. Thus it appears that even in deformed nuclei the coupling between the two captured nucleons and the target core is relatively weak.

As Fig. A.20-2 illustrates, the angular distributions of the deuteron groups corresponding to the $(d_{5/2})^2_{5+}$ levels closely resemble one another, and they have therefore been used as an additional basis for the assignments of the preferentially populated levels. In no case is there any evidence for diffraction-like oscillations for the preferentially populated transitions, and the distributions are all strongly peaked in the forward direction. However, the angular distribution of the transition to the 5+ ground state of Al^{26}, which is not highly populated, exhibits a well-defined structure. The oscillatory angular distribution observed is not surprising, since the semiclassical explanations used for the other $(d_{5/2})^2_5$ levels may not be so applicable here because of the relatively low cross section.

Figure A.20-3 presents a plot of the summed cross sections of the $(d_{5/2})^2_{5+}$ levels, integrated over similar angular ranges (≈12.5 to 70 deg, c.m.) vs the mass number of the product nucleus. A constant cross section to these states is expected when the target nuclei all have completely empty $d_{5/2}$ shells; as the $d_{5/2}$ shell is filled, the cross section should decrease. The data are in good accord with this except for the transition to the $(d_{5/2})^2_{5+}$ level in the C^{12} (α, d) N^{14} reaction, which has a considerably smaller cross section than the other transitions to an empty $d_{5/2}$ shell.

Figure A.20-4 presents the angular distributions of the transitions to the tentative $(d_{5/2}\, f_{7/2})_{6-}$ and $(f_{7/2})^2_{7+}$ levels. These angular distributions again resemble one another, and also resemble the angular distributions of the $(d_{5/2})^2_{5+}$ levels. The structure shown by the angular distribution of the transition to the 0.60-MeV level of Sc^{42} probably arises because the observed peak corresponds to two levels, although the observed cross section should be attributed predominantly to the 7+ level.

Footnotes and References

*Condensation of Phys. Rev. ___, (1965).

†Present address: University of Montreal, Montreal, Quebec.

1. B. G. Harvey, J. Cerny, R. H. Pehl, and E. Rivet, Nucl. Phys. 39, 160 (1962).

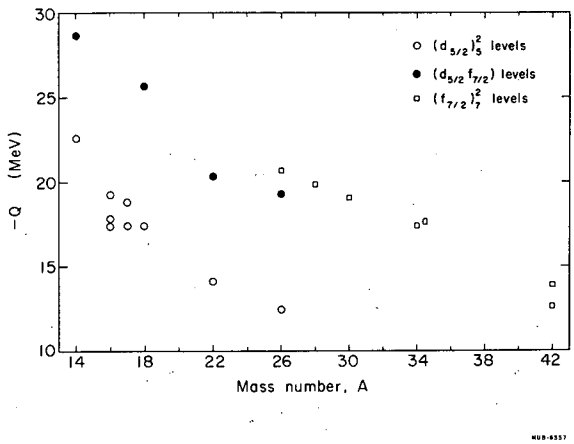

Fig. A.20-1. Relationship between the mass number A of the product nucleus and the Q value for the formation of the levels preferentially populated by the (α, d) reaction. [a]This point corresponds to a highly populated level at 5.2-MeV excitation that was observed during a brief investigation of the $S^{32}(\alpha, d)Cl^{34}$ reaction using 48-MeV α particles from the 60-inch cyclotron.

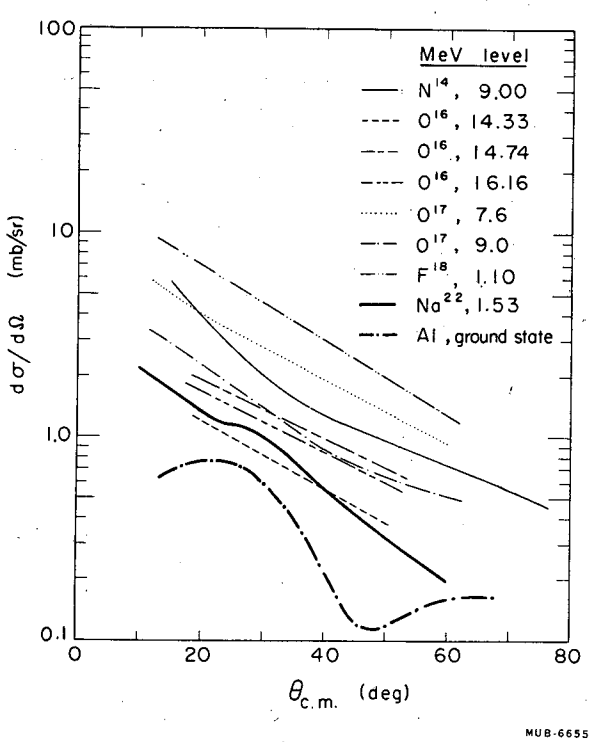

Fig. A.20-2. Angular distributions of the $(d_{5/2})^2_{5+}$ levels.

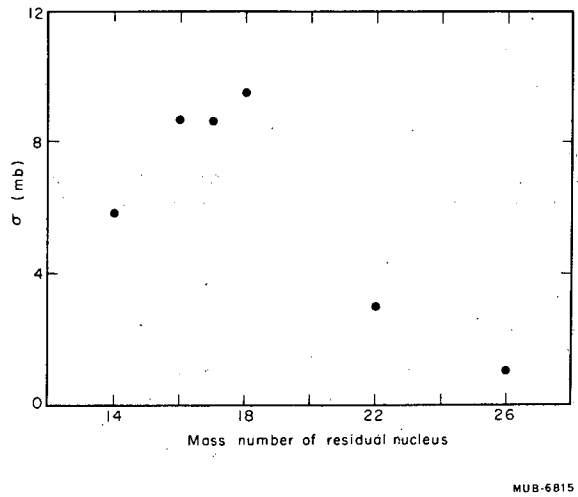

Fig. A.20-3. Integrated cross sections for the transitions to the $(d_{5/2})^2_5$ levels as a function of the mass number A of the product nucleus.

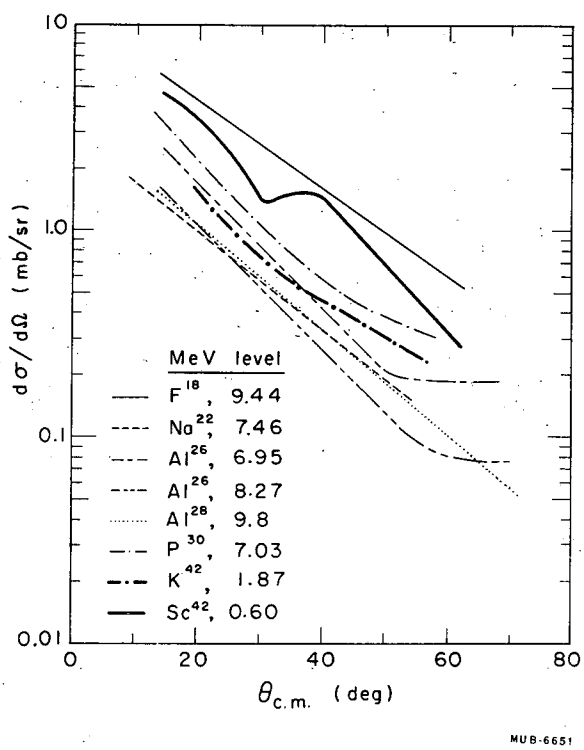

Fig. A.20-4. Angular distributions of the tentative $(d_{5/2}f_{7/2})_{6-}$ and $(f_{7/2})^2_{7+}$ levels.

21. ENERGY LEVELS OF O^{18} FROM SHELL THEORY

Martin G. Redlich

Recently, calculations for a Pb^{208} core plus two outer nucleons have been made on the basis of shell theory.[1] All two-neutron configurations of the $2g_{9/2}$, $1i_{11/2}$, $1j_{15/2}$, $3d_{5/2}$, $4s_{1/2}$, $2g_{7/2}$, $3d_{3/2}$ main shell were included, and the single-particle energies $\Delta(n\ell_j)$ were taken from the data for Pb^{209}. A singlet-even (SE) Gaussian interaction

$$V_{SE}(1, 2) = V_0 \exp(r/r_n)^2, \tag{1}$$

with parameters $V_0 = -31.61$ MeV and $r_n = 1.7765$ F, from low-energy p-p scattering and zero triplet-odd (TO) interaction V_{TO}, lead to good agreement with the data on Pb^{210} now available. Similarly, calculations for the two-hole nucleus Pb^{206} with single-hole energies from experimental data for Pb^{207} and including all configurations of the $1h_{9/2}$, $2f_{7/2}$, $1i_{13/2}$, $3p_{3/2}$, $2f_{5/2}$, $3p_{1/2}$ main shell, with the interaction (1) only, lead to excellent agreement with a large number of data on the excited states of this nucleus.[2]

The present investigation begins with similar calculations for an O^{16} core + two outer neutrons, with all configurations of the $1d_{5/2}$, $2s_{1/2}$, $1d_{3/2}$ main shell. The results for only interaction (1) between the outer nucleus are given in Fig. A.21-1(a). The harmonic-oscillator parameter is $\nu = 0.35041 F^{-2}$; it was determined by the O^{17}-F^{17} $1d_{5/2}$-state Coulomb-energy difference. States are labeled J x with x = a, b, c, ···. Here J a denotes the lowest state with J^+. Figure A.21-1(b) shows the corresponding experimental data. The lowest four states which are probably due predominantly to core excitation are drawn with dotted lines in Fig. A.21-1(b); the higher ones are not included. A comparison of Figs. A.21-1(a) and (b) shows only a rough correlation between the theoretical and experimental energies. Calculations with a Yukawa SE interaction also from low-energy p-p scattering, with zero TO interaction, or with central or central + tensor TO interactions do not lead to substantially improved agreement for a ν determined by the Coulomb energy.

This lack of good agreement suggests the possibility that the simple shell theory is far more accurate for isotopes of Pb than for isotopes of O. Further indication of this possibility is found in the fact that the energy of excitation of the first excited state of Pb^{208}, multiplied by a factor $(208/16)^{2/3}$, equals 14.46 MeV, as compared with the energy 6.05 MeV of the lowest excited state of O^{16}. Also, the energies of the four lowest core-excited states of O^{18}, given in Fig. A.21-1(b), differ substantially from those of probably approximately corresponding states of O^{16}. This again is in contrast with the situation for Pb^{206} and Pb^{208}. To obtain more information about the wave functions of O^{18}, it appears desirable to investigate the effect of admixtures of states of higher configurations. Here, primarily excitations of the type $2\hbar\omega$ will be examined. This means excitations to states which would have energy $2\hbar\omega$ above the ground state in a model of independent particles in a harmonic-oscillator well without spin-orbit coupling.

Matrix elements of a total Hamiltonian

$$H = \sum_{i=1}^{A} K_i + \sum_{i<j=2}^{A} V(i, j), \tag{2}$$

evaluated for states of A-particle configurations with harmonic-oscillator wave functions, will be considered. K_i is the kinetic energy operator for particle i. To estimate the effect of an excited state m upon the energy of a state 0 which does not include excitations of the $2\hbar\omega$ type, the formula

$$\Delta E_{0m} = |H_{0m}|^2/(E_0 - E_m) \approx -|H_{0m}|^2/2\hbar\omega \tag{3}$$

will be used. The denominator is estimated as $-2\hbar\omega$. For O^{16}, the state 0 will be taken as

$$(1s_{1/2})^4 \quad (1p_{3/2})^8 \quad (1p_{1/2})^4. \tag{4}$$

For O^{17} or O^{18}, corresponding states 0' which have the same configuration plus one or two states $n\ell_j$ in the $1d_{5/2}$, $2s_{1/2}$, $1d_{3/2}$ shell and a total Hamiltonian $\tilde{H}$ will be considered.

Corresponding to excitation m of 0, there will be excitations m' of 0'. For example, for the single-particle excitation $1s_{1/2} \rightarrow 2s_{1/2}$, m and m' are, for O^{16} and O^{17}:

$$m: [(1s_{1/2})^3\ 2s_{1/2}]\ (\bar{T},\bar{J}) = (0, 0), \tag{5}$$

$$m': [(1s_{1/2})^3\ 2s_{1/2}]\ (\bar{T},\bar{J}),\ n\ell_j,\ (T, J) = (1/2, j). \tag{6}$$

In (5) and (6) closed subshells have been omitted, but their effect is included in the calculations. It can be shown that for every excitation m of state 0 there exists one main corresponding excitation m' of O^{17} or O^{18}, except when such an excitation is prohibited by the exclusion principle. For (6), the main excitation has $(\bar{T}, \bar{J}) = (0, 0)$. It can be seen that a simple relation between matrix elements often exists. It will be written as

$$\tilde{H}_{0'm'} = c\, H_{0m}\,. \tag{7}$$

Here m' is the main excitation corresponding to m. For a two-particle excitation, c equals 1, unless the excitation is into a shell $n\ell_j$ which is already occupied in O^{17} or O^{18}. In the latter instance, c usually is not very much less than 1. For a one-particle excitation, c is also generally near 1. The effect of rearrangement excitations, such as (6) with $(\bar{T}, \bar{J}) \neq (0, 0)$, appears to be generally extremely small.

The effect of the exclusion principle in core excitation may be quite important in determining the Coulomb energy difference between the $n\ell_j = 2s_{1/2}$ states of F^{17} and O^{17}. This is seen when the excitation (6) is examined in a scheme without isotopic spin. The effect of the excitation (6) and other excitations of type $2\hbar\omega$ upon the Coulomb energy has been calculated for the $1d_{5/2}$ and $2s_{1/2}$ states of F^{17} and O^{17}. The results are, with $\Delta_B(n\ell_j)$ = binding energy difference between F^{17} and O^{17} in the $n\ell_j$ state:

	Exp't	Theory, with Coulomb interaction		
		Without core exc.	With core exc. $V_{TE} = V_{SE}$	With core exc. $V_{TE} = 1.5\ V_{SE}$
$\Delta_B(2s_{1/2}) - \Delta_B(1d_{5/2})$	371 keV	-179 keV	-18 keV	129 keV

In this calculation, V_{SE} is given by (1), and two triplet-even (TE) interactions have been assumed. The remaining interactions are: $V_{TO} = V_{SO} = 0$. Thus, the internal Coulomb energy could account for a part of the discrepancy between the energies of the $2s_{1/2}$ states of F^{17} and of O^{17}. Both of these states are bound, by 0.10 MeV and 4.14 MeV, respectively, with respect to nucleon emission. The remaining discrepancy could be accounted for by Coulomb wave-function distortion in the external region.[3]

Equations (3) and (7) suggest the possibility that the effect of core excitation upon the nuclear energies of states of O^{18} which are predominantly of outer-nucleon type may rather generally be roughly the same regardless of the outer-nucleon state

$$n\ell_j\ n'\ell'_{j'}\ (T, J). \tag{8}$$

A physical picture would be: The structure of the core may perhaps be roughly the same for O^{16} and for the low-lying outer-nucleon-type states of O^{17} and O^{18}. For O^{18} there are, however, excitations of type $2\hbar\omega$ which are not core excitations. These are excitations of only the outer nucleons, and their effect does vary with (T, J). Matrices of the Hamiltonian (2) for the states of the $1d_{5/2}$, $2s_{5/2}$, $1d_{3/2}$ shell and all such $2\hbar\omega$ configurations as well as those of type $3\hbar\omega$ (total excitation by three shells in a j-j coupling model) were diagonalized. The calculations were made for all states which are predominantly of outer-nucleon type, with outer nucleons in the $1d_{5/2}$, $2s_{1/2}$, $1d_{3/2}$ shell. Estimates were made for the energies of excitation of the higher single-particle states, which are:

$1f_{7/2}$, $2p_{3/2}$, $2p_{1/2}$, $1f_{5/2}$, $1g_{9/2}$, $2d_{5/2}$, $3s_{1/2}$, $1h_{11/2}$, $2d_{3/2}$, $1g_{7/2}$, $1i_{13/2}$.

These estimates range from 6.5 MeV for $1f_{7/2}$ to 30 MeV for $1i_{13/2}$. The estimate of the higher state of each doublet with given ℓ was based upon the empirical rule that the splitting is roughly proportional to $2\ell + 1$. Matrix elements for various interactions V(1, 2) were calculated on a computer with multiple-precision fixed-point arithmetic.[4] The results are given in part (c) of Fig. A.21-1 for the interaction of (1) and $V_{TO} = 0$, and in part (d) for the same V_{SE}, but with $V_{TO} = -0.5\ V_{SE}$. Level schemes (e), (f), and (g) of the figure 1 were obtained for three Yukawa interactions which were also used for Pb^{210}. The SE interaction is given by (4) of Ref. 1 for all three schemes. For (e), $V_{TO} = 0$; for (f), $V_{TO} = -0.5\ V_{SE}$(Yukawa). For (g), V_{TO} is -0.5 times the Feshbach-Schwinger central + tensor interaction of Ref. 1, (6). For Fig. A.21-1, (c) through (g), $\nu = 0.33930\ F^{-2}$; this is a reduction of about 3.2% from the value used for part (a), based upon an estimate of the effect of core excitation upon the Coulomb energy. Figure A.21-1 gives the results only up to 7.5 MeV; energies of higher states, not yet experimentally identified, were also calculated. The calculations were made for several sets of higher single-particle energies; the results do not depend very strongly upon these energies.

References

1. M. G. Redlich, Phys. Rev. 138, B544 (1965).
2. Reference 1, footnote 29 (extension of the work of True and Ford).
3. J. B. Ehrman, Phys. Rev. 81, 412 (1951); R. G. Thomas, Phys. Rev. 88, 1109 (1952).
4. R. M. Baer and M. G. Redlich, Communications Assoc. Computing Machinery 7, 657 (1964).

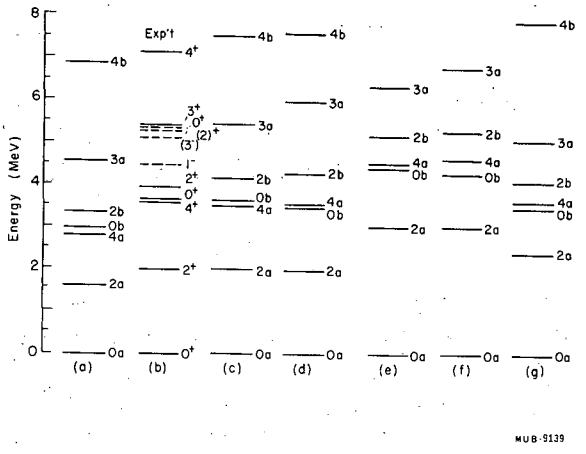

Fig. A.21-1. Energy levels of O^{18}. Part (b) gives all levels which have been experimentally identified as being probably of outer-nucleon type, and the lowest four levels which are probably due predominantly to core excitations. These four levels are drawn with dotted lines. Part (a) gives theoretical levels, calculated with single-particle states of the $1d_{5/2}$, $2s_{1/2}$, $1d_{3/2}$ shell only. The remaining schemes show the effect of all $2\hbar\omega$ and $3\hbar\omega$ outer-nucleon-type excitations. The states are labeled Jx, with x = a, b, c, ···. Here Ja is the lowest state with J^+. Schemes (a), (c), and (d) are for the Gaussian SE interaction (1), with $V_{TO} = 0$ for (a) and (c) and $-0.5\ V_{SE}$ for (d). Schemes (e), (f), and (g) are for a Yukawa SE interaction, with $V_{TO} = 0$ for (e), and $V_{TO} = -0.5\ V_{SE}$ (Yukawa) for (f), and a central + tensor V_{TO} for (g).

22. CORRECTED Na^{20} MASS AND LEVELS IN Na^{20} AND F^{16} USING THE (He^3, t) REACTION†

R. H. Pehl and J. Cerny

Indications that the presently accepted value[1] for the mass of Na^{20} is considerably in error[2, 3] have stimulated its remeasurement using the $Ne^{20}(He^3, t)Na^{20}$ reaction. Also, until very recently,[4] little has been accurately known about the levels in F^{16}.

These reactions were induced by an energy-analyzed 40.2-MeV He^3 beam from the Berkeley 88-inch cyclotron. A 50-mg/cm^2 transmission-360-mg/cm^2 stopping semiconductor counter telescope fed a new type of particle identifier.[5] Complete separation of the tritons from deuterons was obtained.

Figure A.22-1 shows an energy spectrum from the $O^{16}(He^3, t)F^{16}$ reaction, and Table A.22-I lists the easily observed low-lying levels of F^{16} with our tentative J^π assignments. The relative spacings of the first five levels are in excellent agreement with the results of a recent study of the $N^{14}(He^3, n)F^{16}$ reaction.[4] However, we believe that two of their tentative J^π assignments, which are based on level width arguments and are also given in Table A.22-I, should be reversed. One way to predict the level ordering of the low-lying quartet in F^{16} is to compare the observed $O^{16}(T = 1) - F^{16}$ level shifts with the predicted shift from a Coulomb energy calculation using mirror nuclei and with the systematics of the known $N^{16} - O^{16}(T = 1)$ shifts for the quartet. As illustrated in Table A.22-II, there is a marked downward shift of the 0^- and $1^-(T = 1)$ states in O^{16}, relative to their position in N^{16}, whereas the 2^- and 3^- states undergo only a minor shift. Since the first four states in N^{16} are bound, while the corresponding states in both O^{16} and F^{16} are unbound, this shift is probably due to the Thomas-Ehrman effect,[6] which would be most pronounced for the s-state proton. If our J^π assignments are correct, the 2^- and 3^- states are again shifted only a minor amount in F^{16} relative to O^{16}, while the 0^- and 1^- states undergo another downward shift. However, if the $1^- - 2^-$ assignments are reversed,[4] the level shifts become generally inconsistent.

The angular distributions of the 0.436- and 0.736-MeV levels closely parallel each other, exhibiting a smooth forward (< 18 deg c.m.) peaking pattern; the ground-state and 0.200-MeV level also parallel each other, but reach a maximum at ≈28 deg c.m. A comparison of the observed relative intensities also places the 0.436- and 0.736-MeV levels in one group, and the other two levels in a different group. From this information and the uncontroversial 3^- and 0^- assignments, one is tempted to associate the former group with transitions to the $[p_{1/2}^{-1}d_{5/2}]$ states, and the latter group with transitions to the $[p_{1/2}^{-1}s_{1/2}]$ states, which would also be in accord with our J^π assignments.

The energy calibration used to determine the mass of Na^{20} was based on the $C^{12}(He^3, t)N^{12}$ ground-state transition and $O^{16}(He^3, t)$ transitions to the 0.436- and 0.736-MeV levels of F^{16}, using mass excesses of 17.349[7] and 10.686 MeV[4] for N^{12} and F^{16}, respectively.

Figure A.22-2 shows an energy spectrum from the $Ne^{20}(He^3, t)Na^{20}$ reaction, and the observed levels of Na^{20} are listed in Table A.22-I. Since levels above 2 MeV could not be followed easily they have not been included. Our measured Q value for the $Ne^{20}(He^3, t)Na^{20}$ reaction is 14.04 ± 0.05 MeV (± 0.08 MeV including N^{12}, F^{16} errors), which corresponds to a mass excess for Na^{20} of 6.98 MeV. This is 1.30 MeV less than the currently accepted value[1] and in excellent agreement with the predicted Na^{20} mass.[2, 3]

Footnote and References

†Condensed from Phys. Letters 14, 137 (1965).

1. L. A. König, J. H. E. Mattauch, and A. H. Wapstra, Nucl. Phys. 31, 18 (1962).
2. G. T. Garvey, J. Cerny, and R. H. Pehl, Phys. Rev. Letters 13, 548 (1964).
3. V. I. Goldanskii, Nucl. Phys. 19, 482 (1960).
4. C. D. Zafiratos, F. Ajzenberg-Selove, and F. S. Dietrich, Phys. Rev. 137, B1479 (1965).
5. F. S. Goulding, D. Landis, J. Cerny, and R. H. Pehl, Nucl. Instr. Meth. 31, 1 (1964).
6. R. G. Thomas, Phys. Rev. 81, 148 (1951); S. B. Ehrman, Phys. Rev. 81, 412 (1951).
7. R. W. Kavanagh, Phys. Rev. 133, B1504 (1964).

Table A.22-I. F^{16} and Na^{20} levels observed.

F^{16}			Na^{20}	
E_x(MeV)[a]	J^{π}	J^{π}[b]	E_x(MeV)[c]	J^{π}
0	(0^-)	(0^-)	0	(2^+)
0.200	(1^-)	(2^-)	0.65[c]	
0.436	(2^-)	(1^-)	0.75	
0.736	(3^-)	(3^-)	0.85	
3.78			0.95	
4.25			1.27	
5.45			1.85	
5.9				
6.4				

a. All excitations accurate to ± 50 keV.
b. Tentative assignments given in Ref. 4.
c. There are four levels in this region, approximately equally spaced apart.

Table A.22-II. Comparison of the mass excesses (in MeV) of the low-lying levels of the mass-16 triad.[a]

J	N^{16}	Difference	O^{16}	Difference	F^{16} This paper	F^{16} Ref. 4
3^-	5.97	(2.55)	8.52	(2.90)	11.42	11.42
2^-	5.67	(2.56)	8.23	(2.89)	11.12	10.89
				(2.66)[4]		
1^-	6.07	(2.29)	8.36	(2.53)	10.89	11.12
				(2.76)[4]		
0^-	5.79	(2.26)	8.05	(2.64)	10.69	10.69
Coul. pred.		(2.68		(2.83)		

a. The mass table of König et al. (Ref. 1) has been used.

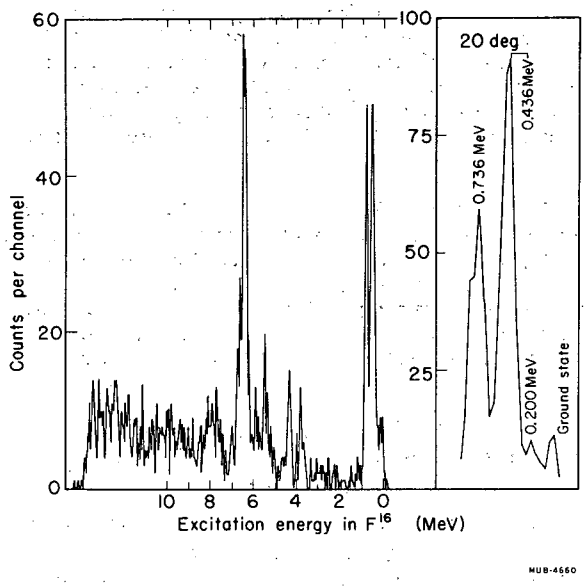

Fig. A.22-1. Triton energy spectra from the $O^{16}(He^3, t)F^{16}$ reaction. A gas target was used to obtain the more complete spectrum on the left (resolution 200 keV FWHM) while a Mylar target was used to improve the resolution (140 keV) of the low-lying levels shown on the right.

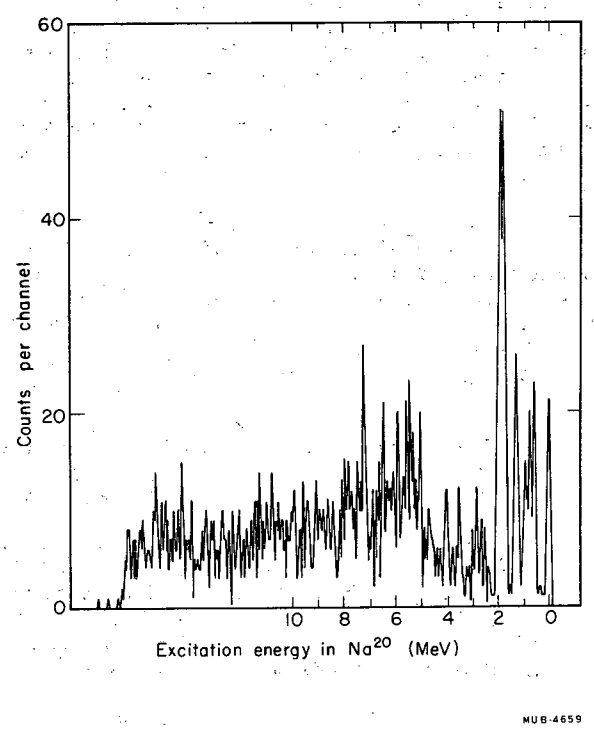

Fig. A.22-2. Triton energy spectrum at 15 deg from the $Ne^{20}(He^3, t)Na^{20}$ reaction.

23. OBSERVATION OF $T = \frac{3}{2}$ LEVELS IN Li^7-Be^7 AND THE UNCHARACTERIZED NUCLEI He^7, B^7, AND He^8 †

Claude Détraz,* Joseph Cerný, and Richard H. Pehl

The location and properties of the hitherto unestablished $T = \frac{3}{2}$ levels in the $T_Z = \pm \frac{1}{2}$ nuclei Li^7 and Be^7 are important nuclear structure information; in addition, the question of particle stability of the controversial nuclei He^7, B^7, and He^8 should be answerable by extrapolation from these $T = \frac{3}{2}$ states.

As has previously been shown,[1-3] (p, t) and (p, He^3) reactions can be a valuable spectroscopic tool for locating states of high isospin in the residual nuclei. To investigate these mass-7 nuclei, the reactions Be^9(p, t)Be^7 and Be^9(p, He^3)Li^7 were induced by 43.7-MeV protons from the Berkeley 88-inch cyclotron. Tritons and He^3 emitted from the 650-μg Be^9 target were detected by a (dE/dx)-E counter telescope which fed a particle identifier.[4] Figure A.23-1 shows two typical spectra obtained at 32.5 deg; the energy resolution averaged 170 keV for tritons and 200 keV for He^3.

One would, in general, expect the angular distributions of the $T = \frac{1}{2}$ mirror states of Be^7 and Li^7 formed in these reactions to differ both in shape and magnitude. This arises since the (p, t) transitions occur predominantly by ^1S, T = 1 pickup of two neutrons, while the (p, He^3) transitions can occur by pickup of a proton-neutron pair in a predominantly ^3S, T = 0 or ^1S, T = 1 configuration. Marked differences are in fact observed in the compared mirror angular distributions and are even apparent in Fig. A.23-1.

However, transitions to $T = \frac{3}{2}$ states in Li^7 and Be^7, assuming the charge independence of nuclear forces, proceed from identical initial to final states through only ^1S, T = 1 pickup of the two nucleons; as such, identical cross sections are expected for such transitions after phase-space and isospin-coupling corrections (here only 1.1%) are included (see Ref. 1). Indeed, Fig. A.23-2 shows that the transitions to the pair of previously unobserved "mirror" levels at 11.13±0.05 MeV in Li^7 and 10.79±0.04 MeV in Be^7 are identical, considering the background subtraction and statistical errors. Therefore, these two states can be assigned a $T = \frac{3}{2}$ isospin. Their excitation energies are close to the theoretical estimates for the lowest $T = \frac{3}{2}$ state[5,6] in Li^7—the first three $T = \frac{3}{2}$ states are predicted to be $\frac{3}{2}^-$ (10.9,[5] 10.1,[6]); $\frac{1}{2}^-$ (≈12.4,[5,6]), and $\frac{5}{2}^-$ (13.7,[5] 13.2,[6] MeV).

We note that the angular distributions in Fig. A.23-2 have the same shape as is standardly observed for known L=0 transitions at 43.7 MeV (see Fig. 3 of Ref. 3). Because of angular-momentum conservation, this also restricts our transitions to be to the $\frac{3}{2}^-$ states. These two $T=\frac{3}{2}$ states are therefore the lowest ones—analogs of the He^7 and B^7 ground states.

The difference between the two excitation energies in Li^7 and Be^7, which is about 340 keV, is qualitatively in accord with the variation of the Coulomb energy with excitation, as calculated by Fairbairn,[7] with the difference in pairing energies between the $T = \frac{1}{2}$ and $T = \frac{3}{2}$ states, estimated by Wilkinson[8] for the 1p shell, and with a probable Thomas-Ehrman shift.

These two $T = \frac{3}{2}$ levels are broad. Correcting for the experimental energy resolution, we find full widths at half maximum of 268 ± 30 keV for Li^{7*} and 298 ± 25 keV for Be^{7*}. These two widths are very similar, and both states can decay through three $T = \frac{3}{2}$ channels: He^6 + p, Li^{6*}(T = 1) + n, He^4 + p + 2n for Li^{7*}, and Be^6 + n, Li^{6*}(T = 1) + p, He^4 + 2p + n for Be^{7*}.

The mass of the He^7 nucleus can be obtained from the mass of $Li^{7*}(T=\frac{3}{2})$, if the neutron-hydrogen atom mass difference is taken into account and the Coulomb energy difference from the pair He^6—Li^{6*}(T=1) is calculated. We find for He^7 a mass excess of[9] 26.03 ± 0.15 MeV in the C^{12} system; therefore, He^7 is definitely unbound to neutron emission by about 360 keV. Assuming the first $T=\frac{3}{2}$ level of Li^7 to be lower than 10.81 MeV, Balashov[6] found that He^7 would be a β emitter with a half life of 30 to 100 msec. He^7 being unbound, the assignment of 50 μsec for its half-life, which appears in the Chart of the Nuclides,[10] presumably quoted from Ref. 6 through a misprint in its abstract,[11] should be dropped.

A similar calculation to that for He^7, but using the $T = \frac{3}{2}$ state in Be^7 and the Coulomb energy difference from the pair Be^{10}—B^{10*}(T = 1), indicates a mass excess of[9] 27.99±0.15 MeV for B^7. Though this value is smaller than the one predicted by Goldanskii[12] (29.4±0.5 MeV in C^{12} system), B^7 is still quite unstable for particle emission, decaying to Li^5 + 2p, Be^6 + p, and α + 3p.

To estimate the mass of He^8, we can use the arguments reported by Goldanskii,[13] namely that the difference between the binding energies of the fourth and third neutrons of the $1p_{3/2}$ shell, $B_n(He^8) - B_n(He^7)$, is smaller than for the second and first neutrons, $B_n(He^6) - B_n(He^5)$, but larger than $B_n(Li^9) - B_n(Li^8)$, where the extra proton disturbs, by a deuteron-like bond, the pairing between the two neutrons. Using the mass of He^7 as calculated above, we obtain the double inequality

$$31.6 \text{ MeV} < \text{mass excess } (He^8) < 32.4 \text{ MeV}.$$

Since the lightest particle-unstable channel is $He^6 + 2n$, the mass excess of which is 33.74 MeV, He^8 should be stable to neutron emission by at least 1.3 MeV.[14]

Footnotes and References

†Condensed from Phys. Rev. Letters 14, 708 (1965).

*CNRS and NATO fellow, visitor from Laboratoire Joliot-Curie de Physique Nucleaire, Orsay, France.

1. J. Cerny and R. H. Pehl, Phys. Rev. Letters 12, 619 (1964).
2. G. T. Garvey, J. Cerny, and R. H. Pehl, Phys. Rev. Letters 12, 726 (1964).
3. J. Cerny, R. H. Pehl, and G. T. Garvey, Phys. Letters 12, 234 (1964).
4. F. S. Goulding, D. A. Landis, J. Cerny, and R. H. Pehl, Nucl. Instr. Methods 31, 1 (1964).
5. S. Meshkov and C. W. Ufford, Phys. Rev. 101, 734 (1956).
6. V. V. Balashov, At. Energ. (USSR) 9, 48 (1960) [translation: Soviet J. At. Energy 9, 544 (1961)].
7. W. M. Fairbairn, Nucl. Phys. 45, 437 (1963).
8. D. H. Wilkinson, Phys. Rev. Letters 13, 571 (1964).
9. This error of 150 keV is considerably larger than the errors on the masses of the analog Li^{7*} and Be^{7*} states and is our estimate of the accuracy of a Coulomb energy correction in such light nuclei.
10. Knolls Atomic Power Laboratory, General Electric Company, Schenectady, New York, 1964, 7th ed.
11. Nucl. Sci. Abstr. 14, 2893 (1960).
12. V. I. Goldanskii, Nucl. Phys. 19, 482 (1960). See also A. I. Baz, V. I. Goldanskii, and Ya. B. Zeldovich, Usp. Fiz. Nauk 3, 211 (1961) [translation: Soviet Phys.-Usp. 3, 729 (1961)].
13. V. I. Goldanskii, Zh. Eksperim. i Teor. Fiz. 38, 1637 (1960) [translation: Soviet Phys.-JETP 11, 1179 (1960)].
14. Calculations in the mass-8, T = 2 system based on this He^8 mass give for C^8 a mass excess of 36.4±0.8 MeV, which agrees with the predictions of reference 12 (<38 MeV in the C^{12} system), and implies that C^8 is unbound.

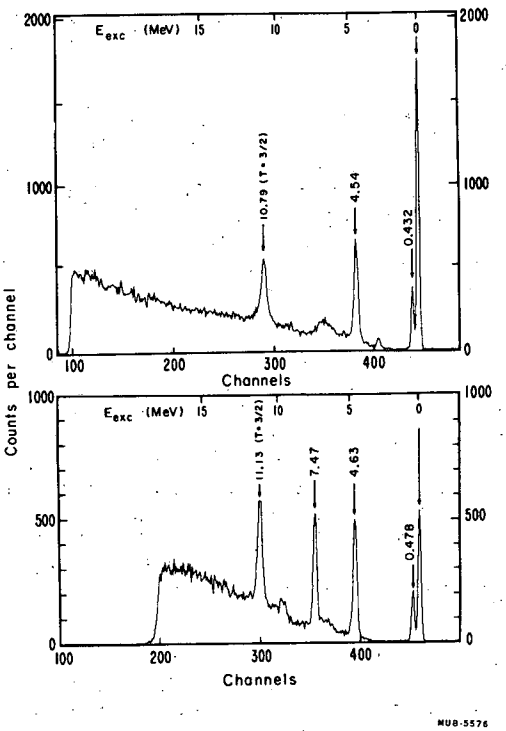

Fig. A.23-1. Energy spectra for the reactions (upper) $Be^9(p,t)Be^7$ and (lower) $Be^9(p,He^3)Li^7$ at 32.5 deg lab.

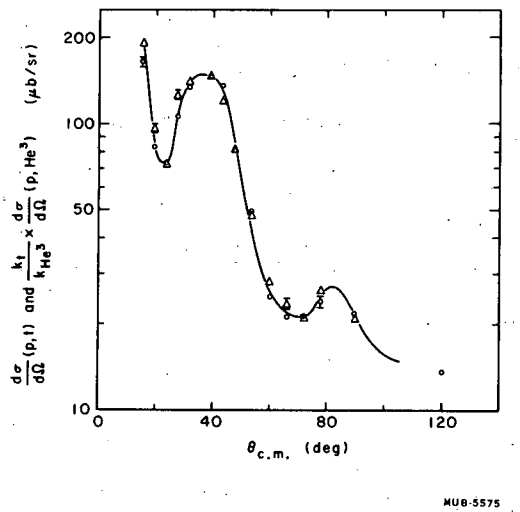

Fig. A.23-2. Angular distributions for the $T = \frac{3}{2}$ states from $Be^9(p,t)Be^7$ at 10.79 MeV in Be^7(o) and $Be^9(p,He^3)Li^7$ 11.13 MeV in Li^7(Δ). The cross sections for the Li^7 state have been corrected for phase space and isospin coupling by the factor of 0.989. The errors that appear on the figure are only statistical.

24. Li^4 AND THE EXCITED LEVELS OF He^4 †

Joseph Cerny, Claude Détraz, ‡ and Richard H. Pehl

There is continuing interest in a characterization of such nuclei as H^4 and Li^4; in addition, a determination of the mass of either should aid in locating the lowest T = 1 state of He^4, which is the subject of considerable current speculation. To accomplish this we have again[1] utilized the technique of simultaneous observation of (p, t) and (p, He^3) transitions to analog final states–here applied to the $Li^6(p,t)Li^4$ and $Li^6(p,He^3)He^{4*}$ (T = 1) reactions. The latter reaction and the $Li^7(p,\alpha)He^4$ reaction also allow the investigation of the T = 0 states of He^4.

Some of the recent data concerning the two lowest excited states of He^4 are summarized in Table A.24-I.[2-8] Since state I (≈20 MeV, probably 0^+, T = 0) lies just above the p+t threshold at 19.81 MeV excitation and state II (≈22 MeV, probably 1- or 2-, T = 0), above the n+He^3 threshold at 20.58 MeV, their exact nature is uncertain. Besides these two states, Vlasov and Samoilov suggest[9] the possibility that the lowest T = 1 state lies at 24 or 25 MeV. This would require Li^4 to be unbound by 4.5 to 5.5 MeV.

We have used 43.7-MeV protons from the Berkeley 88-inch cyclotron to induce (p, t) and (p, He^3) reactions on Li^6 and (p, α) reactions on Li^7. Targets of separated isotopes were used; the general experimental setup was as reported previously.[1]

Figure A.24-1 presents a $Li^6(p,t)Li^4$ spectrum at 15 deg. Such data, taken between 10 and 35 deg, show a broad state which is unbound by 2.9±0.3 MeV to He^3+ p decay. (Though we shall denote this peak as the Li^4 ground state throughout this report, it is probably not a single state.[10]) The width of the unbound Li^4 state is 5.0 ± 0.5 MeV at all angles. Using this Li^4 mass, a Coulomb calculation predicts that the T = 1 excited state of He^4 is located at approximately 22.5

MeV (± 0.3 MeV). Finally, one predicts that the analog H^4 nucleus is also unbound—by about 2.0 MeV.[11] These masses directly confirm the negative results of previous searches for the β decay of H^4 or Li^4 (see Imhof et al.[12]).

Figure A.24-2 presents spectra from the $Li^6(p, He^3)He^4$ and $Li^7(p, \alpha)He^4$ reactions. State I was observed in both these reactions, appearing at 20.10±0.15 MeV. If its 0^+ assignment is correct, the (p, He^3) transition to this level should correspond to an angular momentum transfer of L = 0 (or 2), while the (p, α) transition would require L = 1 transfer. The angular distributions of Fig. A.24-3a are in accord with these expectations and strongly support this 0^+ assignment. First, the (p, He^3) transition is essentially identical to the $Li^6(p, He^3)He^4$ g. s. transition, and both appear to be fairly pure L = 0, according to our two-nucleon transfer systematics in the light elements;[1] and, second, the limited (p, α) data are consistent with the $Li^7(p, \alpha)He^4$ g. s. transition, which must have L = 1 transfer.

It is apparent from Table A.24-I that there are large discrepancies in both the location and width of state II as reported from different experiments. These fluctuations and the above Li^4 results lead us to postulate that there are in fact at least two states near 22 MeV. We expect one to be a T = 0 state with a width of about 1 MeV, clearly apparent in the work of Parker et al.[2] at 21.2±0.2 MeV, and the other(s) to be the T = 1 state(s) predicted from our Li^4 mass to appear at 22.5±0.3 MeV. An analysis of the data using the width[13] given by Parket et al. for the prominent peak which appears at 21.4±0.25 MeV in the $Li^6(p, He^3)He^4$ spectra (Fig. A.24-2a) indicates the presence of an additional, somewhat smaller peak at 22.5±0.3 MeV. As expected, this new peak is broad; however, no width could be obtained because of the complexity of the spectra. This 22.5-MeV level can be postulated as the first T = 1 excited state of He^4—the analog of the Li^4 ground state.

Further confirmation of this assignment is presented in Fig. A.24-3b, where both analog transitions, $Li^6(p, t)Li^4$ g. s. and $Li^6(p, He^3)He^{4*}$(22.5 MeV, T = 1), are shown. The monotonically decreasing angular distributions to these T = 1 states over the observed angular range are similar to the $Li^6(p, He^3)He^{4*}$ (21.4 MeV, 1^- or 2^-, T = 0) angular distribution; all three transitions are consistent with the L = 1 angular momentum transfer that would be expected to 1^- or 2^- states. Finally—and most importantly—the relative cross sections to these two analog levels, after correction for isospin coupling and phase space,[14] are quite similar (within the large uncertainties of peak separation and background subtraction), as would be required for transitions proceeding from identical initial to final states through ^1S, T = 1 pickup of two nucleons.

To summarize, we have observed the unbound ground "state" of Li^4 and predict that H^4 must be unbound by 2 MeV. We have obtained angular distributions to the 20.1-MeV state of He^4 which are consistent with its 0^+ assignment, and have identified the lowest T = 1 "state" of He^4 at an excitation of 22.5±0.3 MeV.

Footnotes and References

†Phys. Rev. Letters 15, 300 (1965).
‡CNRS and NATO Fellow, visitor from Laboratoire Joliot-Curie de Physique Nucléaire, Orsay, France.

1. C. Détraz, J. Cerny, and R. H. Pehl, Phys. Rev. Letters 14, 708 (1965); and to be published.
2. D. Parker, P. F. Donovan, J. V. Kane, and J. F. Mollenauer, Phys. Rev. Letters 14, 15 (1965).
3. L. E. Williams, Inelastic Protons from He^4 (Ph. D. Thesis), University of Minnesota, June 1965.
4. P. G. Young and G. G. Ohlsen, Phys. Letters 8, 124 (1964).
5. S. Hayakawa, N. Horikawa, R. Kajikawa, K. Kikuchi, H. Kobayakawa, K. Natsuda, S. Nagata, and Y. Sumi, Phys. Letters 8, 333 (1964).
6. C. H. Poppe, Phys. Letters 2, 171 (1962).
7. N. A. Vlasov, in Proceedings of an International Conference on Neutron Interactions with the Nucleus (Columbia University, 1957), p. 236.
8. N. Jarmie, M. G. Silbert, D. B. Smith, and J. S. Loos, Phys. Rev. 130, 1987 (1963), analyzed by C. Werntz, Phys. Rev. 133, B19 (1964).
9. N. A. Vlasov and L. N. Samoilov, Atomic Energy 17, 3 (1964).
10. T. A. Tombrello, C. Miller Jones, G. C. Phillips, and J. L. Weil, Nucl. Phys. 39, 541 (1962); T. A. Tombrello, Phys. Rev. 138, B40 (1965).

11. Following Goldanskii's pairing energy systematics [JETP 11, 1179 (1960)], one can predict from this H^4 mass that H^5 is also unbound by at least 1.1 MeV.
12. W. L. Imhof, F. J. Vaughn, L. F. Chase, Jr., H. A. Grench, and M. Walt, Nucl. Phys. 59, 81 (1964).
13. The apparent width of a short-lived state can vary with the nuclear reaction employed to study it. [See, e.g., E. H. Berkowitz, Nucl. Phys. 60, 555 (1964).] However, the spectator particle velocity, which appears to be a relevant parameter influencing the width, is very similar in this experiment to that of Ref. 2.
14. J. Cerny and R. H. Pehl, Phys. Rev. Letters 12, 619 (1964).

Table A.24-I. Evidence for the first two excited levels of He^4.

Ref.	Reaction	Bombarding energy (MeV)	State I Position (MeV)	State I Width (MeV)	State II Position (MeV)	State II Width (MeV)
2	$d(He^3, p)He^4$	31.8	19.94±0.02	0.140±0.025	21.24±0.2	1.1±0.2
3	$He^4(p, p')He^4$	40	20.46±0.14	≈0.3	22.0 ±0.14	several MeV
4	$He^3(d, p)He^4$	6-10	20.08±0.5	0.2 ±0.05		
5	$He^4(p, p')He^4$	55			22.4 ±0.7	1.7±0.5
6	$T(d, n)He^4$	7.83	20.1	0.35 ±0.05		
7	$T(d, n)He^4$	19			22	
8	T(p, p)T	resonance	20.3 ±0.1			

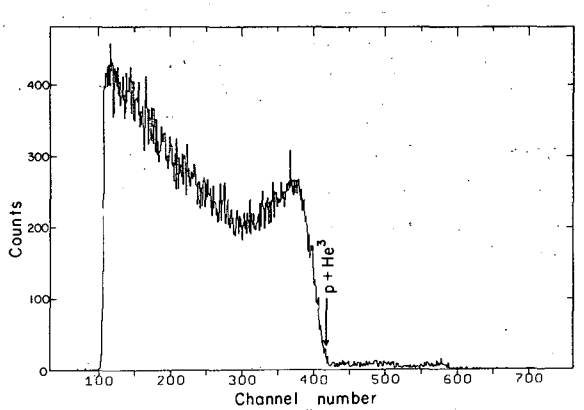

Fig. A.24-1. An energy spectrum of the $Li^6(p, t)Li^4$ reaction at 15 deg using 43.7-MeV protons. The counts above channel 420 arise from a slight deuteron breakthrough into the triton region of the identifier spectrum.

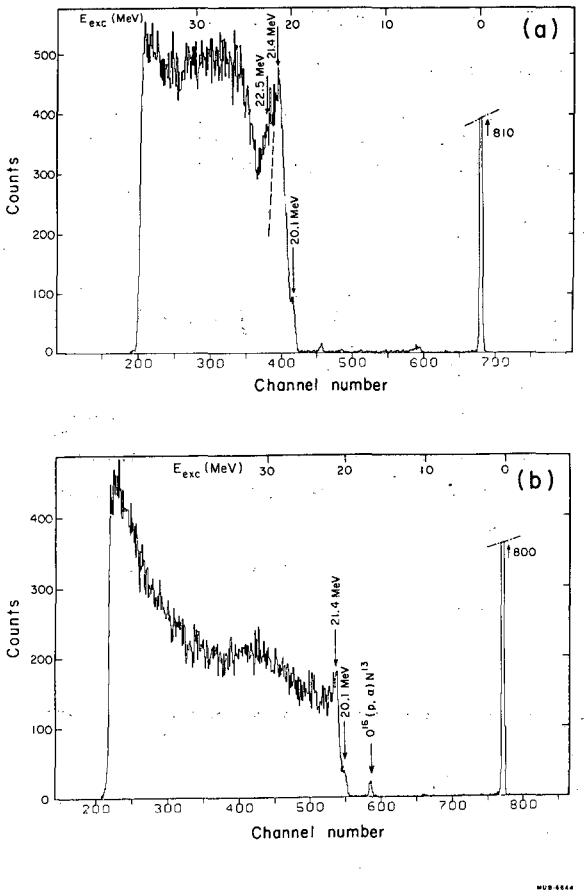

Fig. A.24-2. Typical energy spectra from (a) reactions the $Li^6(p, He^3)He^4$ at 15 deg and (b) the $Li^7(p, \alpha)He^4$ at 12 deg at 43.7 MeV. Part (a) exhibits the analysis of the prominent peak at 21.4 MeV using the width reported by Parker et al.[2]

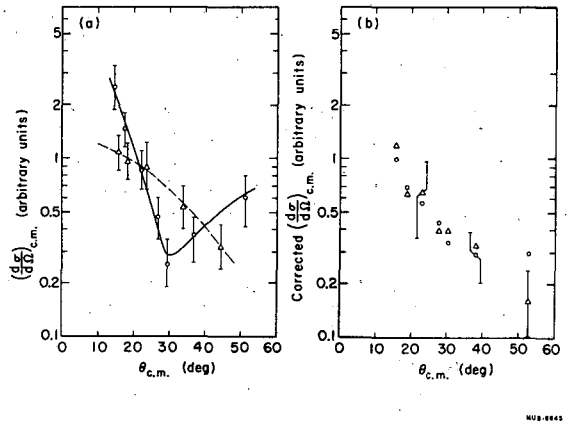

Fig. A.24-3. (a) Angular distributions to the 20.1-MeV excited state of He^4 for the two reactions $Li^6(p, He^3)He^{4*}(0)$ and $Li^7(p, \alpha)He^{4*}(\Delta)$. The arbitrary unit, common to both distributions, corresponds roughly to 15 to 20 μb/sr. (b) A comparison of the angular distributions of the analog reactions $Li^6(p, t)Li^4$ g. s. (0) and $Li^6(p, He^3)He^{4*}$ (T=1, 22.5 MeV)(Δ). The (p, He^3) cross sections have been multiplied by 1.99 to adjust for isospin coupling and phase-space factors. Because of the complexity of the spectra, the relative cross sections have been obtained from only the "corrected" peak heights, comparable widths being assumed for these analog states. Probable uncertainties introduced by this procedure are indicated.

25. He^3 AND He^4 SCATTERING ON B^{11}

D. L. Hendrie, Marc Chabre,* H. G. Pugh,† and E. Boschitz‡

In a recent $C^{12}(p, 2p)$ experiment,[1] the first four excited states of B^{11} (see Fig. A.25-1 for a level scheme) were made with comparable intensities, each about 20% of the ground-state intensity. In a one-step knock-out process, only states which have a parent in the ground state of the target nucleus can be made. C^{12} is known to contain an appreciable admixture of $(p_{1/2})^2(p_{3/2})^2$ configuration[2] in its ground state. However, admixture of contributions from higher shells is expected to be small.[3] Thus, although the $1/2^-$ and $3/2^-$ states might be reached by configuration impurities in the ground state of C^{12}, one feels another mechanism must be invoked to explain the appreciable excitation of the $5/2^-$ and $7/2^-$ states. Such a mechanism could be a double process involving excitation of the C^{12} core to its 2^+ first excited state at 4.43 MeV, which is known to be strongly excited by inelastic scattering at these energies.[4] Work at 155 MeV[5] has indicated large fractional parentage coefficients from the $5/2^-$ and $7/2^-$ states to the 2^+ state of C^{12}. If the $p_{3/2}$ proton hole is weakly coupled to the 2^+ state of C^{12}, several predictions can be made:[6]

(a) the center of gravity of the 4 states (5.26 MeV), should be equal to the C^{12} 2^+ state (4.43 MeV),
(b) the angular distributions of the 4 states should be similar,
(c) their cross sections should be in a ratio of 2J+1,
(d) the sum of their cross sections should equal that of the 2^+ state of C^{12}.

In order to check these predictions we scattered 42-MeV alphas and 40-MeV He^3 from B^{11}. A sample alpha spectrum is shown in Fig. A.25-1. The angular distributions obtained are shown for the alpha scattering in Fig. A.25-2 and He^3 scattering in Fig. A.25-3. Figure A.25-4 compares the elastic and sum of the 4 excited states with carbon data of Naqib[7] for 42-MeV alphas. Figure A.25-5 does the same for the He^3 work; the C^{12} data were taken during the same run. Systematic uncertainties of about 20% in the data probably limit the precision of the comparison in both cases.

In the He^3 results, we find quite good agreement with predictions (b) and (d), and fair agreement with prediction (c). In the alpha work, (b) and (c) are very badly met, and (d) seems to be significantly violated. These results are unexpected because the lack of spin and the sharper interaction radius[8] of the α particle should have made it a less ambiguous probe. It is possible that strong resonances in the N^{15} compound nucleus in this energy region cause effects which mask the direct reaction processes necessary for the validity of predictions (b) to (d). It is hard to see why properties of the B^{11} states themselves (such as configuration mixing between the ground state and $3/2^-$ excited state) should selectively perturb only the α-particle scattering.

Clegg et al.[9] have shown that the unified model can provide good fits to 155-MeV proton data. They find that a value of -4 for Nilsson's parameter, η, gives a good fit to their data and the energy levels. The overlap of the wave function with the wave function for $\eta = 0$ (the weak coupling limit) is 0.8, so that the weak coupling model would provide a good first approximation to B^{11}. The problem of why the He^3 results provide good agreement and alpha results yield such poor agreement remains to be solved.

Footnotes and References

*NATO Fellow on leave from CNRS, Institut Fourier, Grenoble, France.
†Now at University of Maryland, College Park, Maryland.
‡On leave from NASA-Lewis Research Center, Cleveland, Ohio.

1. H. G. Pugh, D. L. Hendrie, Marc Chabre, and E. Boschitz, Phys. Rev. Letters 14, 434 (1965).
2. D. Kurath (Argonne National Laboratory), private communication; D. Amit and A. Katz, Nucl. Phys. 58, 388 (1964).
3. A. Goswami and M. K. Pal, Nucl. Phys. 44, 294 (1963).
4. R. W. Peelle, Phys. Rev. 105, 1311 (1957); T. Stovall and N. M. Hintz, Phys. Rev. 135, B330 (1964).
5. S. M. Austin, G. L. Salmon, A. B. Clegg, K. J. Foley, and D. Newton, Proc. Phys. Soc. 80, 383 (1962).
6. A. de Shalit, Phys. Rev. 122, 1530 (1961).
7. I. M. Naqib, Ph. D. Thesis, University of Washington, 1962 (unpublished).
8. A. Springer, Marc Chabre, D. L. Hendrie, and H. G. Pugh (to be published).
9. A. B. Clegg, Nucl. Phys. 38, 353 (1962); D. Newton, A. B. Clegg, G. L. Salmon, and D. J. Rowe, Nucl. Phys. 53, 433 (1964).

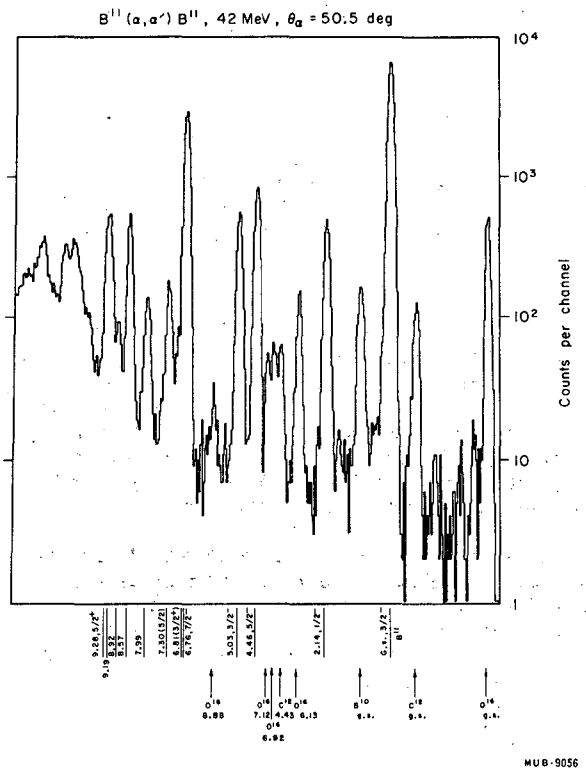

Fig. A.25-1. Typical spectrum of the B^{11} (α, α') reaction at 42 MeV. Resolution is about 100 keV. A level scheme for B^{11} is shown.

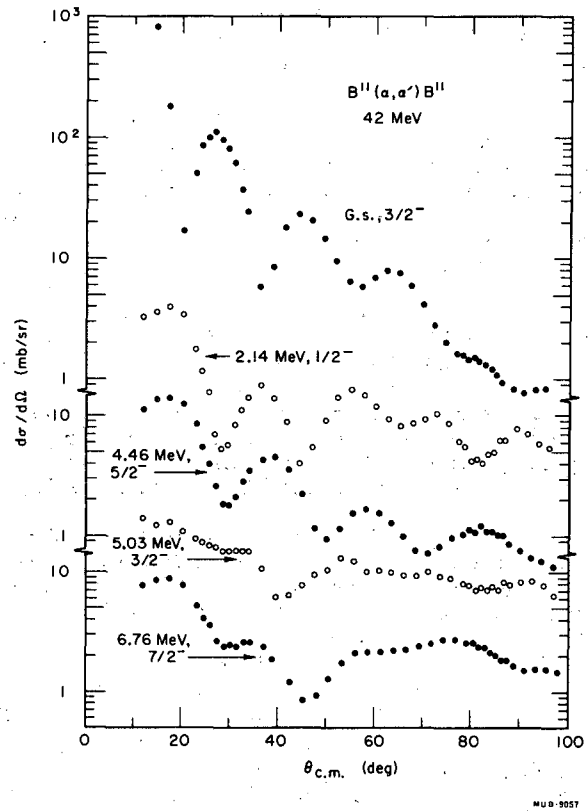

Fig. A.25-2. Angular distributions of the B^{11}(α, α') reaction at 43 MeV. Errors are of the order of the point size.

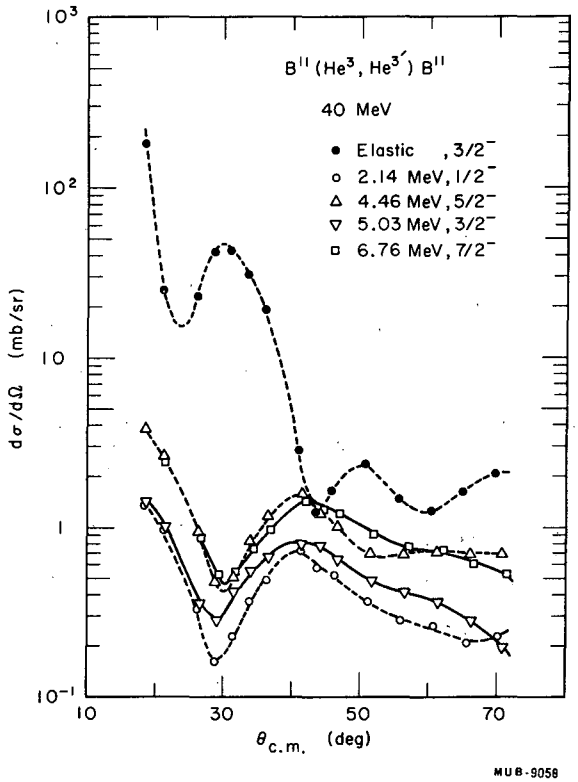

Fig. A.25-3. Angular distributions of the B^{11} $(He^3, He^{3'})$ reaction at 40 MeV. Errors are of the order of the point size.

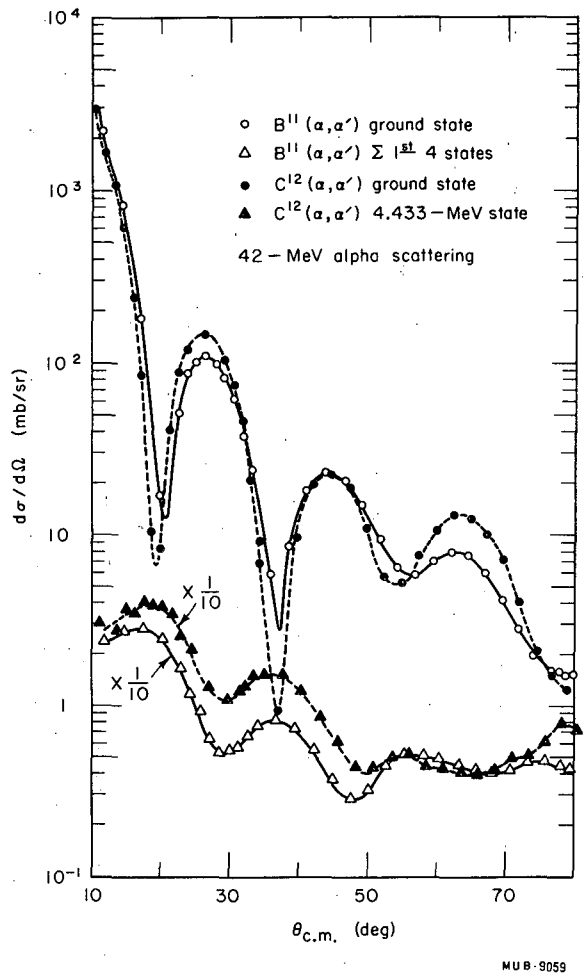

Fig. A.25-4. Comparison of the elastic and sum of the first four excited states of B^{11} for the (α, α') reaction with the C^{12} data of Ref. 7.

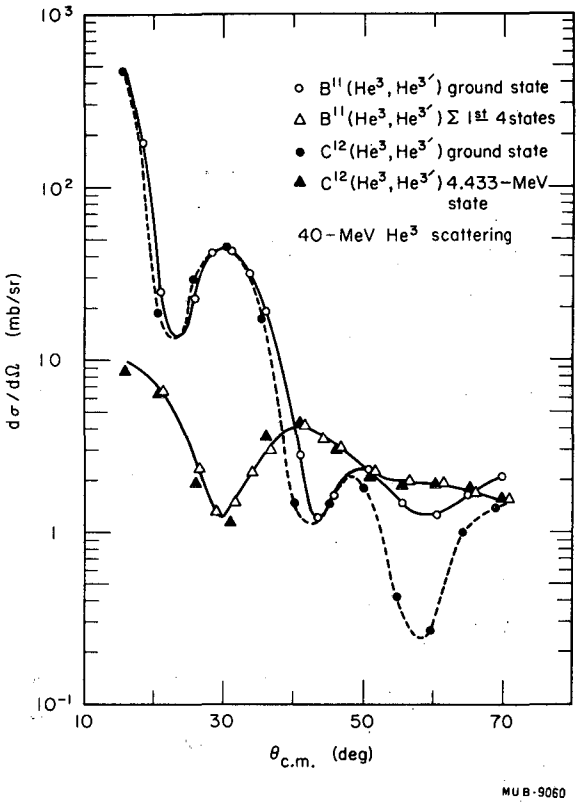

Fig. A.25-5. Comparison of the elastic and sum of the first four excited states of B^{11} for the (He^3, $He^{3'}$) reaction with the ground state and 2^+ state of C^{12}. The C^{12} data is normalized to the B^{11} for small angles in the elastic scattering.

26. THE $C^{12}(d, t)C^{11}$ AND $C^{12}(d, He^3)B^{11}$ REACTIONS

M. Chabre,* D. L. Hendrie, H. G. Pugh,† and C. Detraz‡

The $C^{12}(d, t)C^{11}$ and $C^{12}(d, He^3)B^{11}$ reactions were studied to investigate the excitation of the first $5/2^-$ and $7/2^-$ states in C^{11} and B^{11}. Those states had been found to be produced with large cross sections in the $C^{12}(p, 2p)B^{11}$ and $C^{12}(p, d)C^{11}$ reactions at 50 MeV.[1] As the ground state of C^{12} is a p 3/2 closed shell configuration, with some admixture of $(p\ 3/2)^{-2}$ $(p\ 1/2)^2$ but only a negligible amount of 1 f admixture, the $5/2^-$ and $7/2^-$ states should not be produced by a clean pickup or knockout reaction. In addition, identical angular distributions to states in both final nuclei provide direct evidence for mirror assignment.

The (d, t) and (d, He^3) reactions were chosen for the following reasons:

(a) The (d, He^3) reaction producing proton hole states is equivalent in this respect to the (p, 2p) reaction.

(b) The simultaneous study of the two reactions, using a Goulding-type identifier,[2] makes it possible to identify unambiguously the $7/2^-$ state at 6.76 MeV in B^{11}. This state cannot be separated from the next positive parity state at 6.81 MeV. But in C^{11} the mirror doublet is split by 140 keV, and therefore the contribution of the positive parity state can be measured.

The reactions were induced by a 50-MeV deuteron beam from the 88-inch cyclotron. Two solid-state counter telescopes were used, a 0.50-mm ΔE + 3 mm E combination at forward angles, and a 0.25-mm ΔE + 3 mm E combination at larger angles. Tritons and He^3 spectra were recorded simultaneously. The resolution was 100 keV for tritons and 160 keV for He^3. Figure A.26-1 shows two spectra on which 10 pairs of mirror states can be recognized. In C^{11} the positive parity state at 6.35 MeV was always less than 10% of the $7/2^-$ state close by, and most often barely seen.

Figure A.26-2 shows the angular distributions for the ground-state transitions and the first four negative-parity states. The similarities of the patterns are striking, although the (d, t) cross sections seem to be lower by a few percent than the corresponding (d, He^3) cross sections even after the correction is made for the difference in momentum transfers, due to the different Q values of the two reactions. The ground states, $1/2^-$, and $3/2^-$ states have characteristic l = 1 pickup patterns. Preliminary fits with a DWBA (distorted-wave Born approximation) program written by Glendenning[3] and using interpolated optical potential parameters are very satisfactory for the ground states, and in qualitative agreement with the $1/2^-$ and $3/2^-$ patterns at forward angles, although the agreement becomes poor at large angles where the experimental cross sections do not fall fast enough.

The cross sections for the $5/2^-$ and $7/2^-$ states are of the same order of magnitude as for the $1/2^-$ and $3/2^-$ states, but the angular distributions are very smooth, without any oscillations even at forward angles, and fall off very slowly at large angles. Trials were made, but no fits were found possible by DWBA, assuming l = 3 pickup. This suggests that those states are produced by a different and more complex mechanism than simple pickup mechanism, involving the core of C^{12}. Such processes are always neglected in DWBA calculations. One may assume that the C^{12} is inelastically excited to its 2+ level at 4.43 MeV, known to be strongly collective, and that the pickup takes place in this configuration, therefore allowing $1/2 \leq \Delta J \leq 7/2$ for a p 3/2 pickup. Calculations by Clegg[4] of the CFP (coefficient of fractional parentage) relating the first excited states of B^{11} to the C^{12} states, show that the $5/2^-$ and $7/2^-$ states of B^{11} have very large CFP with the 2+ states of C^{12}. This is in good agreement with our hypothesis, and shows the necessity of coupled-channel calculations to interpret the angular distributions of the $5/2^-$ and $7/2^-$ states. The CFP of the $1/2^-$ and $3/2^-$ excited states to the 2+ of C^{12} are also quite large, and contributions of the double stage process may also explain the filling of the minima and the slow fall of the cross section for those states at large angles.

For higher excited states, simple comparisons of angular distributions allow us to identify unambiguously the states at 6.90, 7.50, 8.10, and 8.43 MeV in C^{11} as being mirrors to the states at respectively 7.30, 7.99, 8.57, and 8.92 MeV in B^{11}, as seen on Fig. A.26-3.

Footnotes and References

*NATO Fellow on leave from CNRS Institut Fourier, Grenoble, France.
†Present address: University of Maryland, College Park, Maryland.
‡NATO Fellow, on leave from Laboratoire Joliot-Curie, Orsay, France.

1. H. G. Pugh, D. L. Hendrie, M. Chabre, and E. Boschitz, Phys. Rev. Letters 14, 536 (1965).
2. F. S. Goulding, D. A. Landis, J. Cerny, and R. H. Pehl, Nucl. Instr. Methods 31, 1 (1964).
3. N. K. Glendenning, Phys. Rev. 137, B102 (1965), and private communication.
4. A. B. Clegg, Nucl. Phys. 38, 353 (1962).

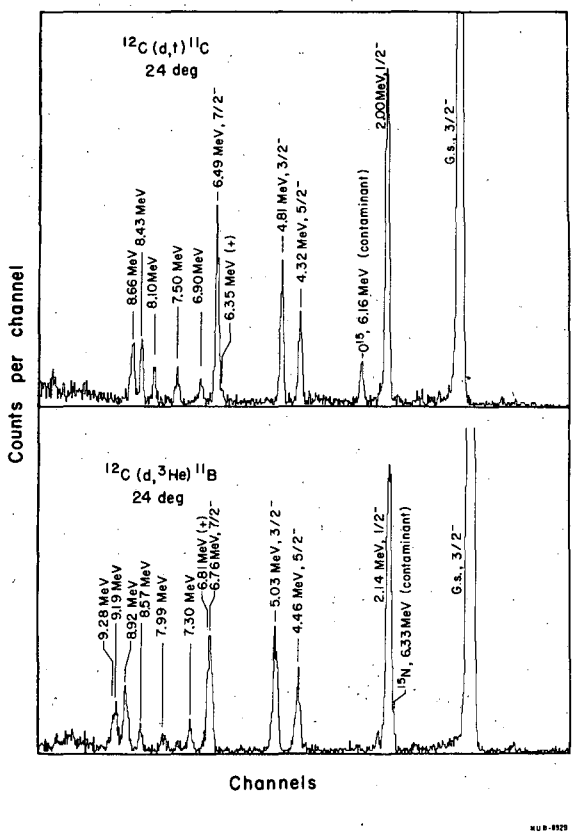

Fig. A.26-1. Tritons and He^3 spectra. The horizontal scales have been shifted to align the spectra.

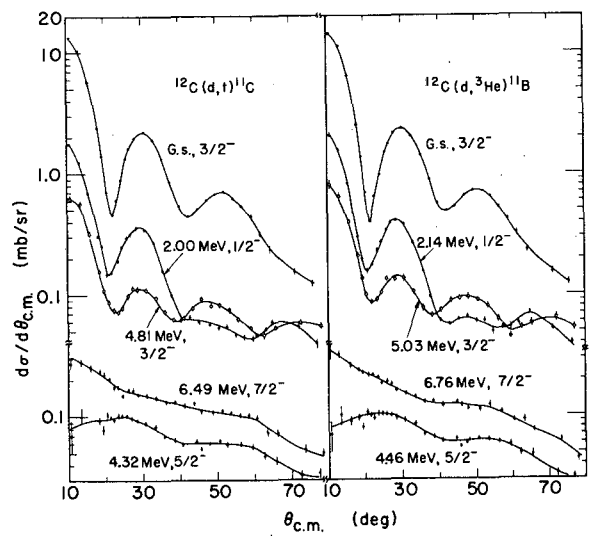

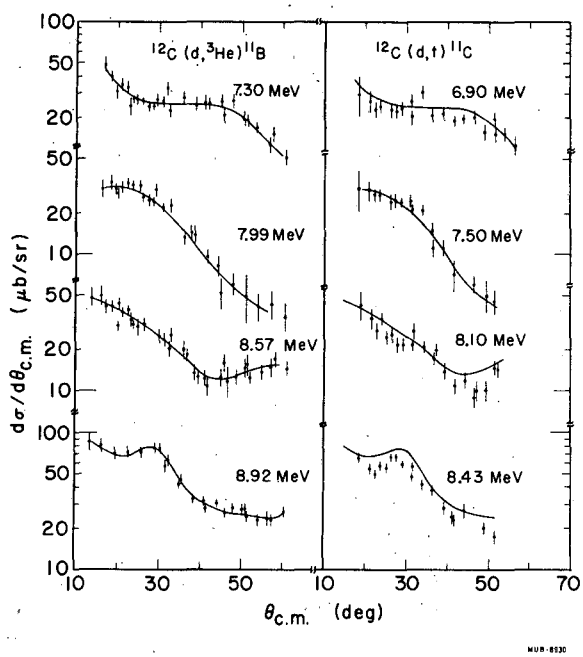

Fig. A.26-3. Angular distributions for mirror states in C^{11} and B^{11}. The same smooth line is drawn to the two sets of data points corresponding to two mirror states. Uncertainties are due mostly to background subtraction.

Fig. A.26-2. Angular distributions for the ground states and first four negative-parity excited states in B^{11} and C^{11}.

27. THE SCATTERING OF α PARTICLES BY Cr^{52}

John R. Meriwether, Italo Gabrielli, David L. Hendrie,
Jeannette Mahoney, and Bernard G. Harvey

The elastic and inelastic scattering of α particles by Cr^{52} has been studied with 23.5-, 33-, 50-, and 75-MeV α particles.

Figure A.27-1 shows the energy spectra, taken at a lab angle of 50 deg, obtained from the scattering of 50-MeV α particles from Cr^{52}. This angle was chosen because none of the alpha groups of interest is obscured by the group due to the impurities carbon and oxygen. The angular distributions for the principal alpha groups are shown in Figs. A.27-2 through A.27-5. The solid curves are those calculated from the Austern-Blair model.[1] The 2.97-MeV state, reported to be 2+ by van Patter,[2] is very weak at most angles, and no angular distribution could be obtained. The same is true for the 2.65-MeV, 0+ state. The angular distributions for the 3.45-, 4.10-, 4.73-, and 5.07-MeV states are very similar to those for the 4+ states at 2.37 and 2.77 MeV. An assignment of 4+ is thus indicated. The states at 6.16, 6.54, and 7.10 MeV appear to be negative parity, and probably are 3- states. This is in agreement with the electron scattering data of Bellicard, et al.[3] Several states between 4.9 and 7 MeV were too weakly excited for determination of the angular distribution. The 5.46-MeV group was strong but gave a featureless angular distribution. This group probably represents more than one state.

The reduced transition probabilities for a number of states were determined by comparison with the Austern-Blair model. These values are listed in Table A.27-I. It should be noted that the values are generally independent of energy, as they should be. The values we obtain are consistently lower, by a factor of two or more, than the electron-scattering data of Bellicard,[3] the Coulomb excitation work of McGowan,[4] or the Saclay group's[5] smooth-cutoff analysis of their alpha scattering data. We have reanalyzed the Saclay data, using the Austern-Blair model, and find a large reduction in the value of B(E2) obtained. These values along with Peterson's,[6] corroborating ours, are given in Table A.27-II. It would probably be erroneous to attribute the above discrepancies to failures of the Austern-Blair model, as there are many examples, in particular Ni^{62}, for which the agreement of this method with electromagnetic methods is excellent.

References

1. N. Austern and J. S. Blair, Ann. Phys. 33, 15 (1965).
2. D. M. van Patter, Bull. Am. Phys. Soc. 2, 47 (1961).
3. J. Bellicard, P. Barreau, and D. Blum, Nucl. Phys. 60, 319 (1964).
4. F. K. McGowan, P. H. Stelson, R. L. Robinson, W. T. Milmer, and J. L. C. Ford, Jr., in Gatlinburg Conference on Nuclear Spin-Parity Assignments, November 1965.
5. H. Faraggi (Saclay), private communication; A. Bussière de Nercy, J. C. Faivre, and G. Vallois, in Gatlinburg Conference on Nuclear Spin-Parity Assignments, November 1965.
6. R. J. Peterson, University of Washington Cyclotron Progress Report, 1965.

Table A.27-I. B(EI)↓ values obtained for Cr^{52}.

Level	J^{π}	E_{in} (MeV)	$\delta^2(I)$	$\frac{B(EI)\downarrow}{e^2}(F^{2I})$
1.434	2+	23.5	0.44	57.9
		33	0.41	53.9
		44.4	0.36	47.3[a]
		50	0.41	53.9
		75	0.34	46.0
3.16	2+	23.5	0.055	7.23
		33	0.036	4.73
		44.4	0.026	3.42
		50	0.042	5.52
3.78	2+	23.5	0.080	10.5
		33	0.090	11.8
		44.4	0.13	17.1
		50	0.12	15.8
4.59	3-	23.5	0.138	269
		33	0.153	298
		50	0.142	277
6.16	3-	50	0.034	64.7
6.54	3-	50	0.058	108.8
7.07	3-	50	0.058	108.5

a. Data from Ref. 5-analysis, this work.

Table A.27-II. Comparison of various B(E2)↓ values for the 1.434-MeV, 2+ state in Cr^{52}.

B(E2)↓	Determination	Analysis	Ref.
57.9	23.5-MeV(α, α')	A-B	a
53.9	33.0-MeV(α, α')	A-B	a
53.9	50.0-MeV(α, α')	A-B	a
46.0	75-MeV (α, α')	A-B	a
60.1	42-MeV(α, α')	A-B	6
102	44-MeV(α, α')	BSW	5
47.3	44-MeV(α, α')	A-B	5, a
103	150 to 180-MeV(e, e')		3
140	Coulomb excitation 33-MeV O^{16}		4

a. This work.

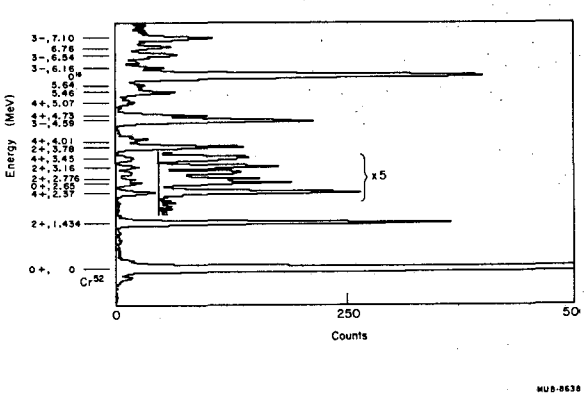

Fig. A.27-1. $Cr^{52}(\alpha, \alpha')Cr^{52}$ with 50-MeV α particle. The lab angle is 50 deg.

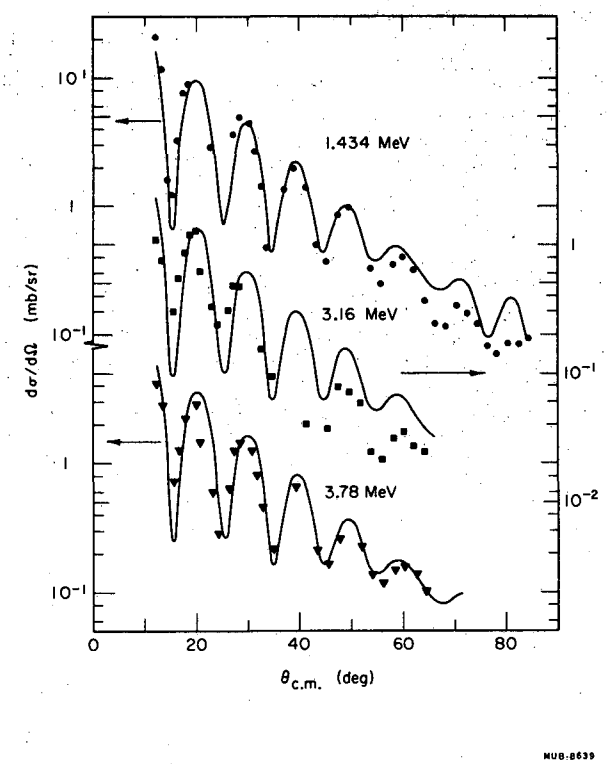

Fig. A.27-2. Angular distributions for the 1.434-, 3.16- and 3.78-MeV 2+ states in Cr^{52}. The solid curve is the Austern-Blair model calculation.

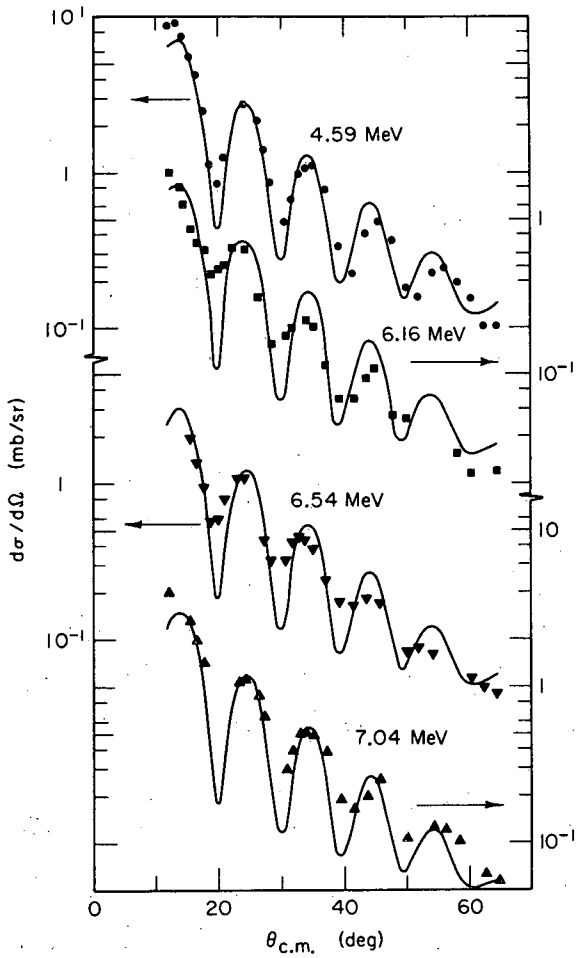

Fig. A.27-3. Angular distributions for the 4.59-, 6.16-, 6.54-, and 7.04-MeV 3- states of Cr^{52}. The solid curve is the Austern-Blair model calculation.

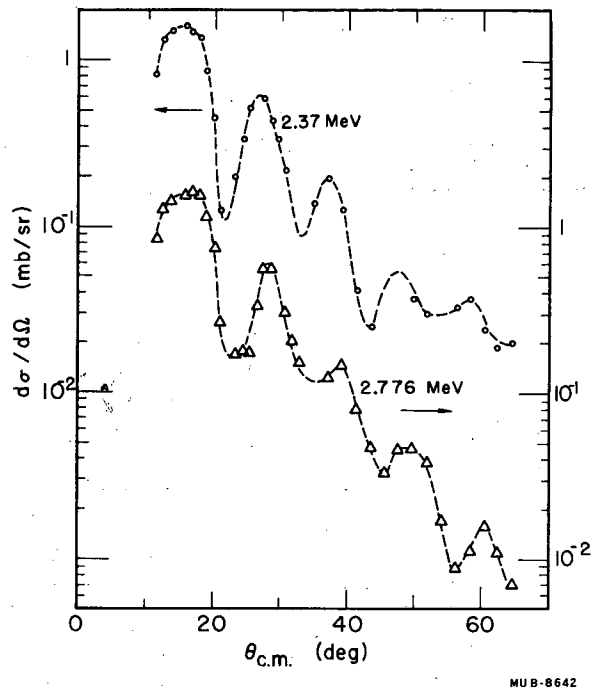

Fig. A.27-4. Angular distribution for the 2.37- and 2.776-MeV 4+ states in Cr^{52}.

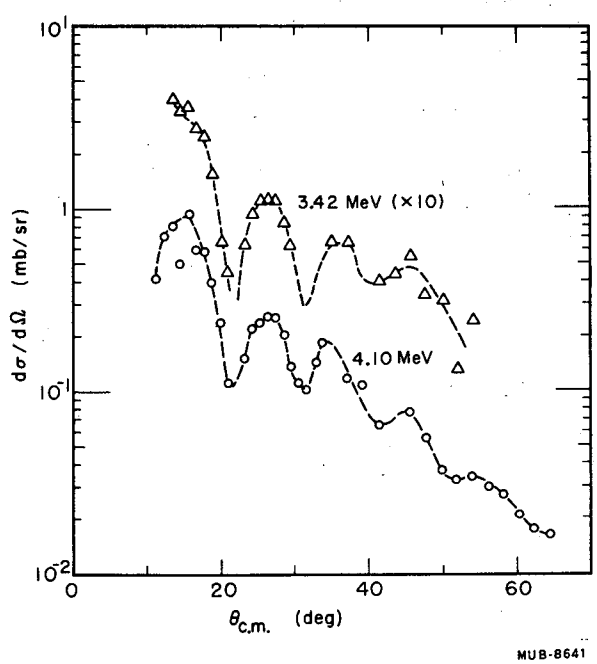

Fig. A.27-5. Angular distribution for the 3.42- and 4.10-MeV 4+ states in Cr^{52}.

28. CHARGE AND ENERGY DISTRIBUTIONS OF RECOILS FROM Th^{226} ALPHA DECAY*

K. Gunter, F. Asaro, and A. C. Helmholz

The charge and energy distributions of recoils from Th^{226} alpha decay were investigated with a high-resolution α-particle spectrograph. Th^{226} was chosen for investigation because its decay chain of three relatively short-lived alpha emitters makes conclusive identification of the recoils possible, because it has an appropriate complex alpha spectrum,[1] and because it can be prepared into an extremely thin source by electrostatic recoil collection.

The U^{230} was chemically prepared and purified from a previously purified Pa^{230} source which had been prepared by bombarding Th^{232} with 50-MeV deuterons. The U^{230} was then vaporized in vacuo onto a platinum plate. The resulting source was invisible. The 31-min Th^{226} daughter was electrostatically collected on a platinum plate from the thin U^{230} source under a uniformly applied negative potential of 225 V/cm in an air atmosphere.

Such Th^{226} samples were used as sources in a 180-deg double-focusing α-particle spectrograph[2] with photographic emulsions for detection. The α particles appear in the emulsion as nearly parallel tracks of approximately the same length. The recoils appear in the emulsion as two or three α tracks of varying length and direction coming from a common vertex on the surface of the emulsion (2- and 3-pronged events). These 2- and 3-pronged events represent only a portion of the total number of recoils striking the plate.

Figure A.28-1 shows that the +2 recoils struck the emulsion quite close to the position of the Th^{226} ground-state α group (α_0), as would be expected for a thin source. Charges +3 through +20 were each investigated separately by altering the magnetic field so that the recoils of a given charge followed approximately the same path in the spectrograph as had the α particles and +2 recoils. Charges +1 through -2 were obtained with the emulsions much closer to the source than they were for the other charges, which resulted in adequate charge separation but essentially no energy resolution.

Typical results for recoils of various charges are shown in Fig. A.28-1. Recoil peaks are identified by the notation Th^{226} R_E^{+n}, where n indicates the charge of the recoils and E indicates the energy in keV of the excited state of the recoil nucleus populated by the α decay of Th^{226}

The R_0^{+2} peak is separated from the α_0 peak by 0.17 keV, and was found to be much broader than the other R_0 peaks. The former effect could be the result of the recoils losing energy by collision in leaving the platinum backing plate. Such collisions could also involve a change in charge, and, in this case, a charge of +2 would be favored because it has a closed electronic configuration. The net effect would then be a selective broadening of the R^{+2} peaks. It was found that all the R_0^{+n} peaks except R_0^{+2} had approximately the same shape and half-width. This peak shape is indicated by the dashed line in Fig. A.28-1, and represents 64% of the total R_0^{+2} peak.

The R_{111}^{+n} peaks are composed of recoils of Th^{226} associated with the α group (α_{111}) that populates the 111-keV excited state (21.9%). These recoils can thus decay either by the emission of γ rays or conversion electrons. Those R_{111} recoils which decay by γ emission ($R_{111}\gamma$) should have the same charge distribution as the R_0 recoils, but they should have a slightly increased half-width because of the recoil energy associated with the γ rays. Those R_{111} recoils which decay by electron conversion ($R_{111}e$) should have a charge distribution that differs from that of the R_0 recoils because of the emission of Auger electrons associated with the conversion electrons. The half-width of the $R_{111}e$ recoil peaks should be considerably larger than that of the R_0 recoil peaks because of the recoil energy associated with the L and higher-order conversion electrons. As seen in Fig. A.28-1, the half-width of R_{111} is indeed appreciably larger than R_0. Also the spacing between the R_0^{+n} and R_{111}^{+n} peaks was equal to the spacing between the α_0 and α_{111} groups for all clearly resolved recoil peaks. This indicates that the increase in half-width of R_{111} must be roughly symmetrical, as would be expected from the foregoing explanation.

If one assumes that the recoils do not drift in the emulsion after their initial energy has been absorbed, then one should be able to calculate the counting efficiency of the recoils in the photographic emulsion, i.e., the intensity of the 2- and 3-prong events. The absolute intensity of 3-prong events, however, was greater than the calculated value by a factor of 2.5, possibly indicating unusual behavior of the recoils in the emulsions. The recoil counting efficiency was determined by setting the total intensity of the R_{111}^{+n} e groups equal to the known intensity of that portion of α_{111} which is followed by conversion electrons. The normalization factor so obtained was used

for all the experimental recoil intensities. This procedure is valid for charges +2 through +20 because these recoils struck the photographic emulsion at essentially the same angle. However, the intensities of charges +1, 0, -1, and -2 were obtained with the photographic emulsion in a different arrangement, and hence their corrected intensities can only be regarded as approximate.

The experimental intensities normalized in the above manner are presented in Table A.28-I. The errors in the table reflect 90% confidence limits, assuming no systematic errors are present.

For charge +3 the intensity of R_{111} is just the value one would expect from only $R_{111}^{+3}\gamma$ i.e., essentially all recoils followed by conversion electrons have higher charges. We assumed then that the 0, +1, and +2 recoils were composed of only R_0 and $R_{111}\gamma$, which was deduced from the known 111-keV γ-ray intensity (4.8%).

The resulting charge distributions of the R_0 recoils and the $R_{111}e$ recoils are plotted in Fig. A.28-2.

S. Szucs and J. M. Delfosse[3] studied Po^{216} recoils from Rn^{220} α decay and found the maximum in the charge distribution occurring at zero, in contrast to our results with Th^{226} R_0, for which the maximum intensity occurs at a charge of +1. The charge distribution of the Th^{226} $R_{111}e$ recoils is roughly similar to that found by A. H. Snell and F. Pleasanton[4] for Xe^{131}.

Footnote and References

*Submitted to Phys. Rev. Letters.

1. Frank Asaro and I. Perlman, Phys. Rev. 104, 91 (1956).
2. Carl P. Ruiz, UCRL-9511, April 1961.
3. S. Szucs and J. M. Delfosse, Phys. Rev. Letters 15, 163 (1965).
4. A. H. Snell and F. Pleasanton, Phys. Rev. 111, 1338 (1958).

Table A.28-I. Normalized experimental results.

n	(R_0^{+n}/α_0)	$(R_0^{+n} + R_{111}^{+n})/\alpha_0$	$R_{111}^{+n}/\alpha_{111}$
-2		<0.03%	
-1		<0.03%	
0		≈20%	
+1		≈50%	
+2		26.7±1.1%	
+3	7.06±0.50%		1.21±0.86%
+4	4.74±0.26%		1.06±0.52%
+5	4.55±0.39%		2.04±0.62%
+6	2.08±0.11%		1.91±0.24%
+7	0.651±0.065%		3.52±0.30%
+8	0.167±0.024%		6.67±0.40%
+9			8.07±0.52%
+10			10.03±0.62%
+11			9.64±0.65%
+12			9.38±0.67%
+13			9.26±0.67%
+14			5.25±0.40%
+15			5.10±0.32%
+16			3.38±0.27%
+17			2.67±0.27%
+18			1.57±0.22%
+19			0.80±0.19%
+20			0.44±0.0.11%

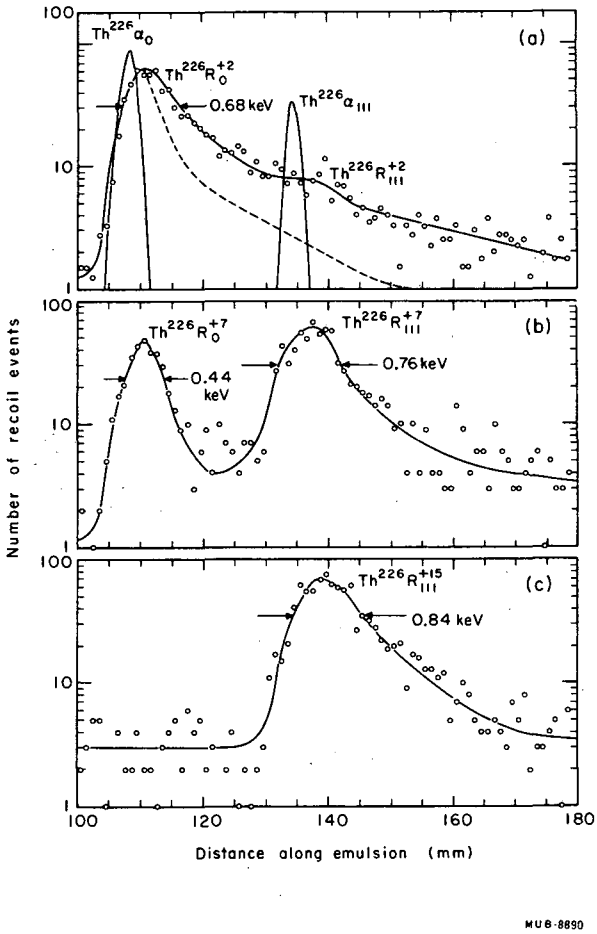

Fig. A.28-1. Experimental alpha and recoil spectra. (a) Partial Th^{226} α spectrum (shown on an arbitrary scale) and Th^{226} R^{+2} spectrum. The dashed line is the relative shape of all the R_0^{+n} peaks with a charge greater than +2. (b) Th^{226} R^{+7} spectrum. (c) Th^{226} R^{+15} spectrum.

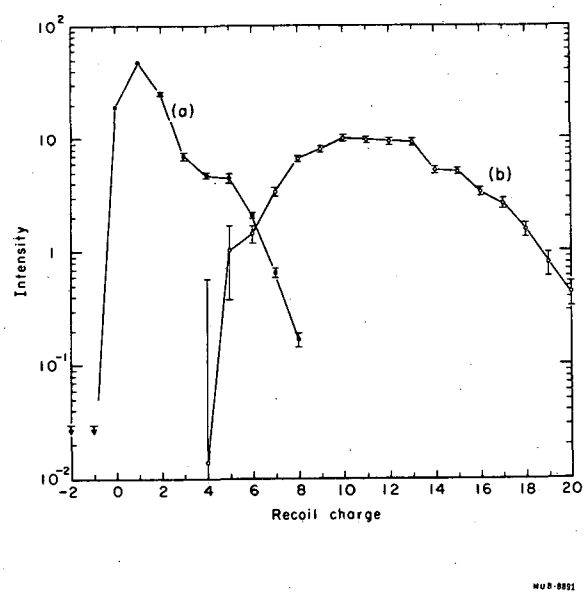

Fig. A.28-2. Charge distributions of recoils following Th^{226} α decay. (a) Charge distribution of R_0 recoils. (b) Charge distribution of $R_{111}e$ recoils (R_{111} recoils which decay by conversion electrons). Note: The sum of the charge intensities for any given recoil group (R_0 or R_{111}) is equal to 100%.

29. THE MASS 13 T = 3/2 QUARTET*

J. Cerny, R. H. Pehl, G. Butler, D. G. Fleming, C. Maples, and C. Détraz†

The completion of isobaric multiplets of four or more members permits an independent test of the isobaric multiplet mass equation,[1] which is based on the assumption of charge independence of nuclear forces. A first such study[2] completed the mass-9 T = 3/2 quartet through the determination of the mass of C^9. We would like to report measurements of the lowest T = 3/2 states in C^{13}, N^{13}, and O^{13}, thereby completing a second quartet.

It has been shown previously[3] that the (p, t) and (p, He^3) reactions are valuable spectroscopic tools in the study of high isospin states. We have used these reactions to locate the T = 3/2 levels in N^{13} and C^{13} via the N^{15}(p, t) and N^{15}(p, He^3) reactions. These experiments were performed with a 43.7-MeV proton beam from the Berkeley 88-inch cyclotron. Tritons and He^3 particles emitted from a pure N^{15} gas target were simultaneously detected by a (dE/dx)-E counter telescope which fed a particle identifier.[4] Figure A.29-1 shows energy spectra for both the

$N^{15}(p, t)N^{13}$ and $N^{15}(p, He^3)C^{13}$ reactions with typical resolutions (FWHM) of 150 keV.

The lowest $T = 3/2$ states in C^{13} and N^{13} are expected to lie near 15.3 MeV excitation, as calculated from the B^{13} mass after correction for Coulomb energy and neutron-hydrogen atom mass differences. As previously reported,[5] two new states near 15 MeV excitation are observed in these reactions–they are the presumed $T = 3/2$ ground-state analogs and lie at 15.065±0.037 and 15.103±0.045 MeV in N^{13} and C^{13}, respectively. These new analog states are sharp, with a resolution comparable to that of the respective ground-state transitions; this is consistent with a $T = 3/2$ assignment, since there are no $T = 3/2$ channels energetically available for decay.

The angular distributions confirm these assignments. To first order, the (p, He^3) reaction proceeds via the pickup of a ^1S, $T = 1$ or ^3S, $T = 0$ neutron-proton pair, whereas the (p, t) reaction is restricted to ^1S, $T = 1$ two-neutron pickup. Therefore, one might in general expect the angular distributions of the $T = 1/2$ mirror states of C^{13} and N^{13} formed in these reactions to differ in shape or magnitude or both. Marked differences are generally observed in such transitions, as exemplified by the ground-state transitions shown in Fig. A.29-2. However, assuming the charge independence of nuclear forces, transitions to the analog states proceed from identical initial states to identical final states through only ^1S, $T = 1$ pickup of the two nucleons. Since these $T = 3/2$ states, analogs of the known B^{13} ground state $(3/2-)$,[6] must also be $3/2^-$, conservation of angular momentum and parity restrict the transitions populating them to an $L = 2$ transfer. (Angular distributions to known states in N^{13} requiring solely $L = 0$ or $L = 2$ transfer are shown in Fig. A.29-2 for comparison.) Identical cross sections with $L = 2$ behavior are therefore expected for these analog transitions, after isospin coupling and phase-space corrections.[3] Indeed, Fig. A.29-2 shows that the angular distributions in question are essentially identical and that both distributions show the same structure as the known $L = 2$ transfer to the N^{13}(7.38 MeV, $5/2^-$) state.[7]

The (He^3, He^6) reaction has been used previously[2] to obtain the mass of C^9, and was employed here to measure the O^{13} ground-state mass, thus completing the quartet. A 65.3-MeV He^3 beam was focused on an O^{16} gas target from which emergent He^6 particles were separated by means of a particle identifier (general experimental details are given in Ref. 2). Typical resolutions (FWHM) were 250 keV. Simultaneous measurement of the Li^6 spectra, in conjunction with a He^6-Li^6 vs pulser calibration, permitted absolute energy measurements.

The particle stability of O^{13} has been predicted,[8] and O^{13} has been recently observed as a delayed proton emitter.[9] A mass excess of about 23.0 MeV on the C^{12} scale is expected. Figure A.29-3 presents typical $O^{16}(He^3, He^6)O^{13}$ and $O^{16}(He^3, Li^6)N^{13}$ energy spectra. Although there is a fairly high background, one can clearly see the sharp ground-state transition in the He^6 spectrum. The average cross section for measurements at four angles between 10 and 20 deg (lab) was only 1 μb/sr. The experimental mass excess of O^{13} was found to be 23.11±0.07 MeV.

Within the framework of charge independence of nuclear forces, the masses of the members of an isobaric multiplet are related by[1]

$$M = \underline{a} + \underline{b}T_z + \underline{c}T_z^2 .$$

This equation can now be tested by predicting the O^{13} mass from the masses of the other three members of the multiplet. By use of our experimental excitations (N^{13}, $T = 3/2$ at 15.065±0.037 and C^{13}, $T = 3/2$ at 15.103±0.045 MeV), and the ground-state mass excess of B^{13}(16.562±0.004 MeV,[10]), the mass excess of O^{13} is calculated to be 23.11±0.18 MeV. Though the agreement is excellent, the error on the predicted mass is large. Better error limits can be obtained by noting (a) a recent measurement of the $C^{14}(He^3, \alpha)C^{13}$ reaction,[11] which populated a sharp state at 15.108±0.014 MeV (which the above has shown to be the lowest $T = 3/2$ state), and (b) a measurement using the $B^{11}(He^3, n)N^{13}$ reaction,[12] observing a sharp state at 15.068±0.008 MeV. These data predict a mass excess for O^{13} of 23.10±0.05 MeV. Essentially complete agreement is also observed in the mass-9 quartet,[2] where a remeasurement of the C^9 mass excess gave 28.99±0.07 MeV instead of the earlier 28.95±0.15 MeV;[2] the prediction for C^9 using the mass equation is 29.00±0.05 MeV.

The above results comprise the most rigorous test of the isobaric multiplet mass equation to date; the data are sufficient to show that the coefficient of a possible term dT_z^3 in the mass equation is no greater than order $(Z\alpha)c$. (Unfortunately, no explicit theoretical estimate of the expected magnitude of d is available.) This accuracy is clearly sufficient to guide experimental searches for missing members of isobaric multiplets, such as, for example,[3] the $T = 2$ states in

F^{16} and Ne^{16}. However, as noted earlier,[2, 13] the best method of investigating a charge dependence of nuclear forces through use of the mass equation still remains a detailed study of the mass or isospin dependence or both of the b and c coefficients as more data become available.

Footnotes and References

*Submitted to Phys. Letters.

†CNRS and NATO Fellow, visitor from Laboratoire Joliot-Curie de Physique Nucleaire, Orsay, France.

1. D. A. Wilkinson, Phys. Letters 12, 348 (1964); E. P. Wigner and E. Feenberg, Rept. Progr. Phys. 8, 274 (1941); S. Weinberg and S. B. Treiman, Phys. Rev. 116, 465 (1959); E. P. Wigner, in Proceedings of the Robert A. Welch Foundation Conference on Chemical Research, Vol. I, Chapt. IV (1957), 86 (unpublished).
2. J. Cerny, R. H. Pehl, F. S. Goulding, and D. A. Landis, Phys. Rev. Letters 13, 726 (1964).
3. J. Cerny and R. H. Pehl, Phys. Rev. Letters 12, 619 (1964); J. Cerny, R. H. Pehl, and G. T. Garvey, Phys. Letters 12, 334 (1964).
4. F. S. Goulding, D. A. Landis, J. Cerny, and R. H. Pehl, Nucl. Instr. Methods 31, 1(1964).
5. J. Cerny, R. H. Pehl, D. G. Fleming, and C. C. Maples, Bull. Am. Phys. Soc. 9, 704 (1964).
6. A. Marques, A. J. P. L. Policorpo, and W. R. Phillips, Nucl. Phys. 36, 45 (1962).
7. F. C. Barker, G. D. Symons, N. W. Tanner, and P. B. Treacy, Nucl. Phys. 45, 449 (1963).
8. A. I. Baz, V. I. Goldanskii, and Ya. B. Zeldovich, Usp. Fiz. Nauk 3, 211 (1961) translated: Soviet Phys. Uspekhi 3, 729 (1961); J. Janecke, Nucl. Phys. 61, 326 (1965).
9. R. McPherson, R. A. Esterlund, A. M. Poskanzer, and P. L. Reeder, Phys. Rev. 140, B1513 (1965).
10. J. H. E. Mattauch, W. Thiele, and A. H. Wapstra, Nucl. Phys. 67, 1 (1965).
11. G. Ball and J. Cerny, article in preparation.
12. E. Adelberger and C. A. Barnes, Bull. Am. Phys. Soc. 10, 1195 (1965).
13. D. H. Wilkinson, Phys. Rev. Letters 13, 571 (1964).

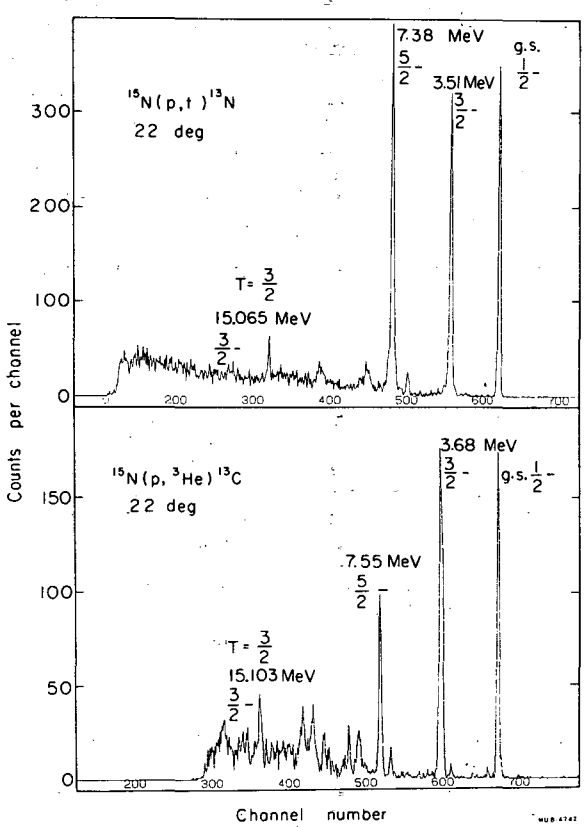

Fig. A.29-1. Energy spectra of the $N^{15}(p,t)N^{13}$ and $N^{15}(p,He^3)C^{13}$ reactions at 22 deg. The spectra have been adjusted to match the ground-state channels. There is a nonlinearity in the triton spectrum at the higher energies.

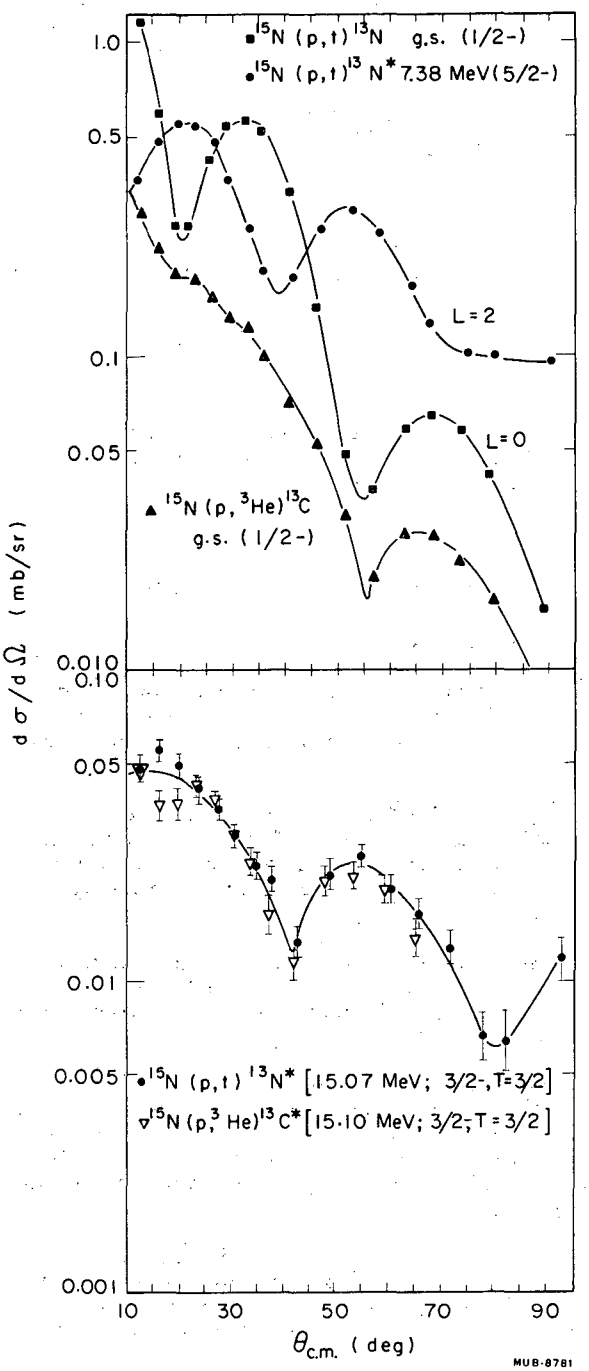

Fig. A.29-2. (a) Angular distributions of the $N^{15}(p,t)N^{13}$ transitions to the ground ($1/2^-$) and 7.38-MeV ($5/2^-$) levels and the angular distribution of the $N^{15}(p, He^3)C^{13}$ g. s. ($1/2^-$) transition. (b) Angular distributions for the T = 3/2 states at 15.065 MeV in N^{13} and at 15.103 MeV in C^{13}. The cross sections for the C^{13} transition have been corrected for phase-space and isospin coupling[3] by the factor of 0.924. The error bars are based on counting statistics only.

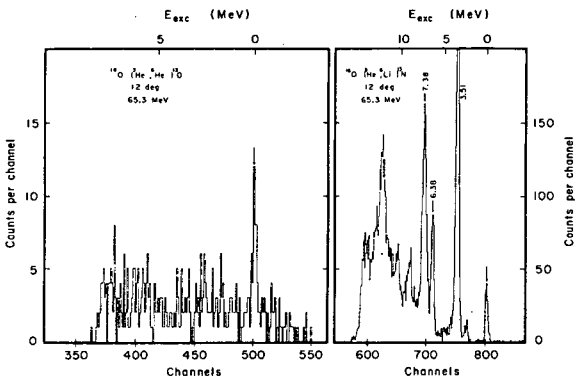

Fig. A.29-3. Energy spectra for the $O^{16}(He^3, He^6)O^{13}$ and $O^{16}(He^3, Li^6)N^{13}$ reactions at 12 deg.

30. NEW NEUTRON-DEFICIENT ISOTOPES OF EMANATION

Matti Nurmia, Kalevi Valli, and Earl K. Hyde

Heavy-ion beams were used to prepare a number of new isotopes of emanation by bombardment of targets of elements from erbium to lead. A variety of techniques was developed for the rapid removal of the gaseous element in a form suitable for measurement of α radiation with semiconductor diode counters.

The previously known isotopes Em^{208} to Em^{212}, with half-lives ranging from 23 min to 16 hr, were studied by irradiating a metallic target of thallium or lead. After bombardment the target was melted in an evacuated quartz chamber, and the emanation isotopes were affixed to small aluminum foils by the glow discharge technique of Momyer and Hyde.[1] The previously reported properties of those isotopes were confirmed.

For shorter-lived and lighter isotopes the emanation liberated from the melted target metal was allowed to expand into a small chamber, at the end of which was mounted a semiconductor diode. It was possible to start measurements of α-particle energies and half lives within 40 sec of the end of bombardment.

For the study of still shorter-lived isotopes the target for the bombardment consisted of the stearate compound of the appropriate target element (erbium, platinum, mercury, thallium, and lead). It is a well known property of the salts of stearic acid that they readily release from their open crystal lattices any gaseous emanation activity formed inside the crystals. Hence the isotopes of emanation produced in the bombardment quickly diffused out of the target and into an adjoining chamber containing the semiconductor counter.

Still another technique which proved useful for the study of very short-lived activities was the bombardment of a strip of a metallic target element (gold or platinum) mounted in such a way that an electric current could be passed through it during or immediately after the beam burst. The current served to heat the target foil and drive the emanation activity into an evacuated chamber.

A brief summary of new results is presented in Table A.30-I without the details of the experiments, which will be published later.

Reference

1. F. F. Momyer, Jr., and E. K. Hyde, J. Inorg. Nucl. Chem. 1, 274 (1955).

Table A.30-I. New data on emanation isotopes.

Isotope	Half-life	Alpha particle energy (MeV)
Em^{206}	~6 min	6.260 ± 0.003
Em^{205}	~1.5 min	6.260 ± 0.003
Em^{204}	75 ± 1 sec	6.416 ± 0.003
Em^{203}	45 ± 5 sec	6.497 ± 0.005
Em^{202}	28 ± 2 sec	6.547 ± 0.003
Em^{201}	13 ± 1 sec	6.636 ± 0.003
Em^{200}(?)	3 ± 1 sec	6.768 ± 0.005

31. DECAY PROPERTIES OF Zr^{86}†

E. K. Hyde, W. J. Treytl, A. Siivola, D. H. Sisson, and D. J. Horen

The radiations of 16.5-hour Zr^{86} were restudied with lithium-drifted germanium and silicon detectors and with a NaI crystal spectrometer. Besides x rays, there are γ rays of 28, 243, and 612 keV in relative intensity 21, 100, and 5.4. No other γ rays were detected. No annihilation radiation was present. There is no evidence for formation of 48-min Y^{86m} in the decay of Zr^{86}. The K-conversion coefficient of the 243-keV transition was found to be 0.035±0.003. The lifetime was measured as 29±3 nsec. These properties agree well with an E2 multipolarity. The lifetime and conversion coefficient of the 28-keV transition are < 10 nsec and 3.8±0.5, respectively, which corresponds to an E1 multipolarity. A decay scheme was constructed as shown in Fig. A.31-1. Reasonable shell-model assignments can be made to all levels except the 2- level of Y^{86}, whose character is uncertain.

Footnote

†Abstract of paper submitted to Phys. Rev.

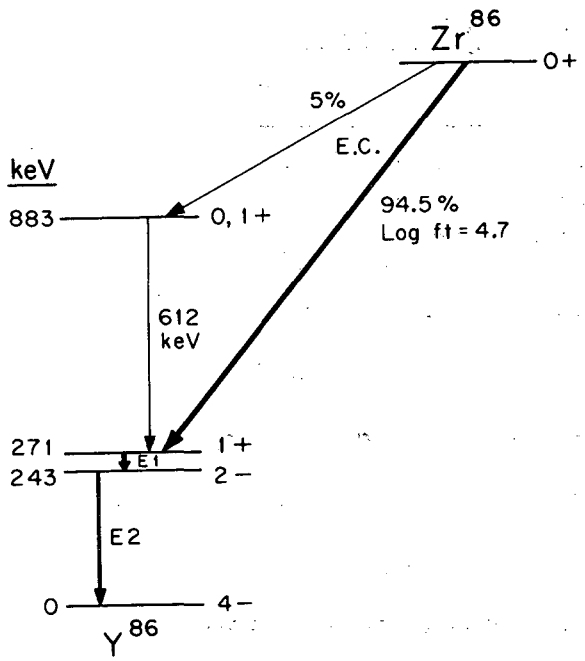

MUB-7881

Fig. A.31-1. Decay scheme of Zr^{86}.

32. SHELL-MODEL CALCULATION FOR Po^{212} †

Norman K. Glendenning and Kichinosuke Harada*

We have performed a shell-model calculation for the Po^{212} nucleus which involves the four nucleons beyond closed shells. Our technique for making this a tractable problem is discussed in the full paper. The calculated low-energy spectrum of low-spin states is compared in Fig. A.32-1 with the known levels. Higher-spin states in this region not yet found are mentioned in the figure captions.

Figure A.32-2 shows the lowest level of each spin plotted as a function of spin. The two arcs comprising the 0 to 10 group and the 12 to 18 group illustrate the tendency to isomerism at J = 10 and 18. The discovery[1] several years ago of a high-spin long-lived isomer inspired this and earlier work[2] on this nucleus. The lower, J = 10 state has not so far been observed. We calculate its lifetime against α decay to be of the order 10^{-5} or 10^{-6} second, so that it would not be seen by the technique used to find the long-lived isomer.

Alpha-reduced hindrance factors for a number of states were calculated and are listed in our paper. The influence of the correlations among nucleus on the α-decay probability and the role that several factors play is illustrated for the transition connecting ground states in Table A.32-I. Entry (a) shows that the probability is enhanced by a factor 30 over a pure configuration, because of the correlations built up by the residual interaction. Entry (b) shows that the p-n force adds only about 15% of the enhancement.

Gamma-transition probabilities were also calculated and several branching ratios compared with experiment.

Footnotes and References

†Shortened version of Nucl. Phys. 72, 481 (1965).
*Present address: Nuclear Physics Division, Japan Atomic Energy Research Institute, Japan.

1. I. Perlman, F. Asaro, A. Ghiorso, A. Larsh, and R. Latimer, Phys. Rev. 127, 917 (1962).
2. N. K. Glendenning, Phys. Rev. 127, 923 (1962).

Table A.32-I. Reduced width for ground-state α decay of Po^{212} in units of the reduced width of the dominant configuration $(h^2)_0(g^2)_0$. Results for the complete wave function are compared with various approximations to bring out the role of several features.

Description	$\gamma_\alpha^2/\gamma_\alpha^2(h^2g^2)$
(a) complete wave function	30
(b) p-n force absent	26
(c) higher seniority amplitudes < 1% neglected	22
(d) all amplitudes < 1% neglected	15
(e) p-n force absent but higher neutron configurations s, g, d added	43

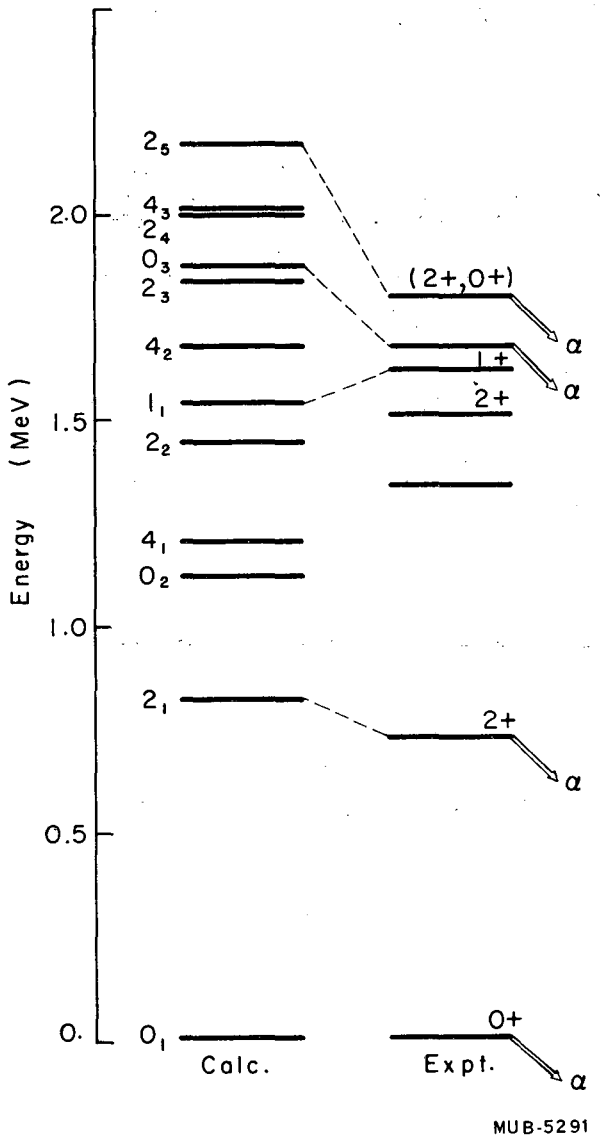

Fig. A.32-1. Calculated spectrum for Po^{212} is compared with experiment. Only the lower spins are shown. The dashed lines are correspondences inferred from the α-decay properties. In the same region covered by this figure the following levels are also calculated: 6+ at 1.36 MeV, 8+ at 1.41 MeV, and 10+ at 1.19 MeV. In addition around 2 MeV there may be a 3+, 5+, and 7+ level.

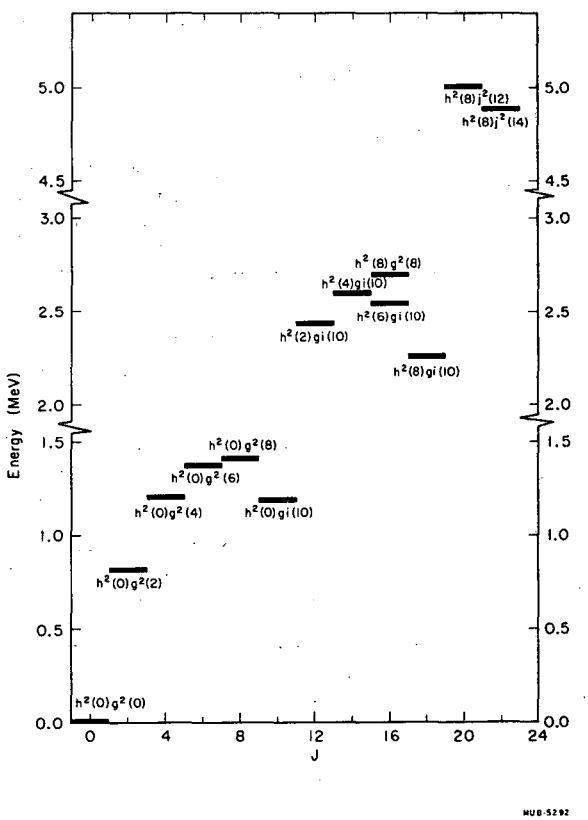

Fig. A.32-2. The lowest level of each even spin calculated for Po^{212} are shown. This figure illustrates the isomerism. The dominant configuration of each level is also shown.

33. RESTUDY OF ALPHA DECAY OF Fr^{212}

Kalevi Valli and Earl K. Hyde

The 19.3-minute activity, Fr^{212}, was identified many years ago by Hyde, Ghiorso, and Seaborg,[1] and in later publications[2,3] some features of its α spectrum were investigated by ionization chamber and magnetic spectrometer techniques. The alpha branching is reported to be 44%, and three α groups have been identified: 6.342 MeV (24%), 6.387 MeV (39%), and 6.411 MeV (37%).

Modern techniques of alpha spectroscopy with semiconductor detectors make it possible to restudy α radiation of short-lived nuclides with greater ease and good resolution. Hence in this work α decay of 19-min Fr^{212} was reinvestigated.

Samples were prepared by bombarding 3-mm-thick buttons of metallic thallium with 120-MeV C^{12} ions in the Berkeley heavy-ion linear accelerator. Immediately after bombardment the thallium was dissolved in nitric acid and heated to oxidize Tl^{+1} to Tl^{+3}. The solution was then chilled, diluted with concentrated hydrochloric acid, and saturated with HCl gas. A few drops of 0.4 M silicotungstic acid were added to precipitate white crystalline silicotungstic acid which served as a specific carrier for francium.[4] The precipitate was washed with 5 ml cold conc HCl, then dissolved in water to form a solution which was pipetted to the top of a 1-cm column of Dowex-50 resin. The silicotungstic acid passed through the column, while the Fr^{212} activity was adsorbed on the resin. Following this, the carrier-free francium was desorbed with a few drops of 6 M HCl and evaporated on the tantalum filament of a vacuum evaporator. The filament was heated by an electric current to volatilize the francium onto an aluminum collector foil. Weightless, evenly deposited samples were prepared in this fashion. The volatilization step removed Em^{212} activity and the α activity measured immediately after preparation of the sample was purely Fr^{212}.

Alpha energies were measured with surface-barrier semiconductor diodes of commercial manufacture (Nuclear Diodes Inc., Highland Park, Ill.). A direct alpha spectrum obtained with a detector of 25 mm^2 active area is shown in Fig. A.33-1. Alpha-particle energies and intensities are listed in Table A.33-I. These values were confirmed by several measurements taken on samples prepared in different bombardments.

The three α groups reported in the earlier work were confirmed, but at 4 kV lower energy. Five new groups with intensity 2% or less were identified. It is not surprising that these groups were not observed in the earlier studies. The major new feature uncovered in this work is that the most intense group in the α spectrum falls at 6.261 MeV. This peak had been observed previously but had been assigned to the K-capture daughter activity, Em^{212}, which is known to emit 6.264-MeV α particles.[2,3] However, in this work a 6.261-MeV peak was found immediately after the preparation of the samples, and several experiments demonstrated conclusively that this group belongs to the Fr^{212} spectrum.

Coincidence experiments were also performed. Figure A.33-2 shows an α spectrum obtained in coincidence with any electromagnetic radiation above a low threshold. The resolving time of the fast coincidence was 50 nsec. The ground-state transition at 6.407 MeV is absent, as expected, and the 6.383-MeV group is missing, presumably because of strong conversion of the low-energy γ transition. The presence of the 6.261-MeV group confirms its assignment to Fr^{212}, because the group of equal energy in the decay of Em^{212} is a ground-state transition.

Figure A.33-3 shows a γ spectrum taken in coincidence with α groups. The γ detector was a 3-mm-thick lithium-drifted germanium detector equipped with a cooled field-effect transistor (FET), used as the first stage of a charge-sensitive preamplifier. The energy resolution of this detector system was about 1.2 kV.[5] Our study of the γ radiations emitted by Fr^{212} is incomplete, and additional results will be reported later.

References

1. E. K. Hyde, A. Ghiorso, and G. T. Seaborg, Phys. Rev. 77, 765 (1950).
2. F. F. Momyer, Jr., and E. K. Hyde, J. Inorg. Nucl. Chem. 1, 274 (1955).
3. F. F. Momyer, Jr., F. Asaro, and E. K. Hyde, J. Inorg. Nucl. Chem. 1, 267 (1955).
4. E. K. Hyde, J. Am. Chem. Soc. 74, 4181 (1952).
5. Emanuel Elad, A Preamplifier with 0.7 keV Resolution for Semiconductor Radiation Detectors, Nucl. Instr. Methods 37, 327 (1965).

6. A. Rytz, Helv. Phys. Acta 34, 240 (1961).

Table A.33-I. Fr^{212} alpha energies and intensities.

Alpha energy (MeV)	Level energy in At^{208} (keV)	Alpha intensity (%)
6.407±0.003	0	20.7±2.0
6.383±0.003	24±3	23.3±2.0
6.338±0.003	70±3	12.3±1.0
6.261±0.003	147±3	40.0±4.0
6.179±0.003	232±3	2.1±0.3
6.127±0.003	285±3	1.0±0.2
6.077±0.005	336±5	0.4±0.2
5.983±0.005	432±5	0.1±0.05
5.828±0.008	590±8	0.05±0.03

RYTZ values (Ref.) for Bi^{211}(6.278 and 6.622 MeV), Bi^{212} (6.051 and 6.090 MeV), and Po^{210}(5.305 MeV) were used as calibration standards.

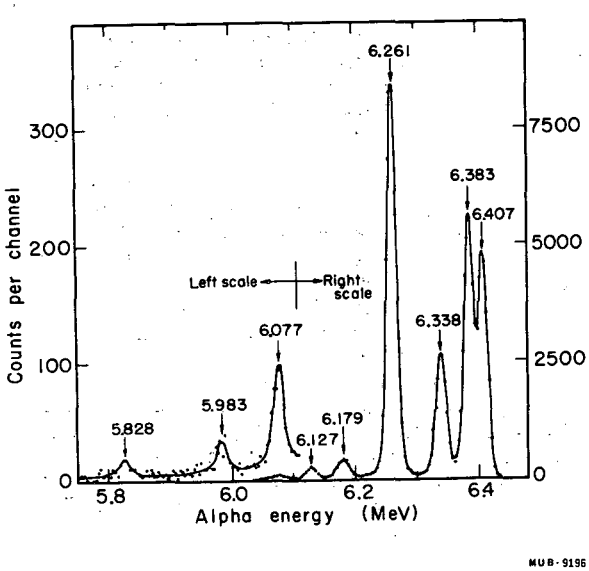

Fig. A.33-1. α Spectrum of Fr^{212} taken with surface-barrier semiconductor diode.

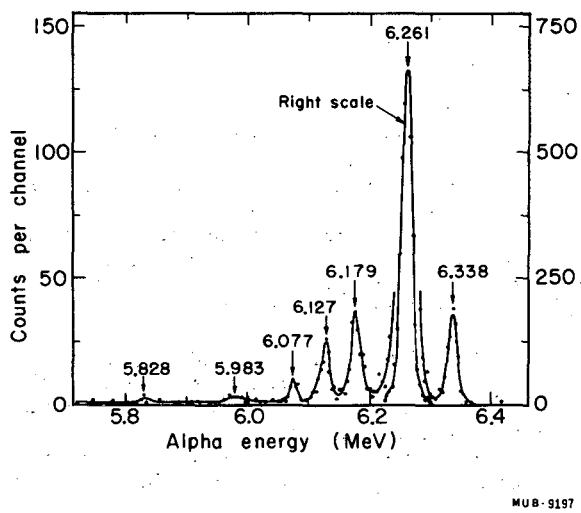

Fig. A.33-2. α Spectrum of Fr^{212} in coincidence with γ radiation. The 6.261-MeV peak is plotted on a different scale.

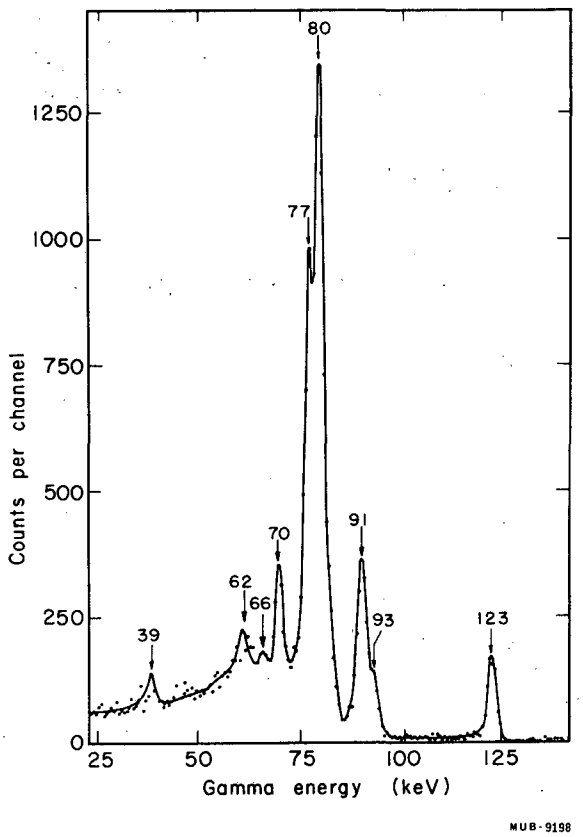

Fig. A.33-3. γ Spectrum of Fr^{212} taken with lithium-drifted germanium detector in coincidence with α particles.

34. RADIATIONS OF 14-MINUTE Nb^{88}

E. K. Hyde and J. M. Nitschke

The 15-minute isotope Nb^{88} was discovered by Korteling and Hyde[1, 2] in niobium targets bombarded with high-energy protons and in targets containing bromine which were bombarded with C^{12} ions. The mass number of the activity was proved, but very little was learned about the radiation. An independent discovery was made by Butement and Qaim,[3] who isolated the activity directly from niobium targets bombarded with protons and also from the molybdenum fraction of such targets. They reported that Mo^{88} decayed with a 28-minute half life to produce a 21-minute daughter, Nb^{88}. From the measurements made with a NaI crystal spectrometer they found evidence for γ rays of energy 200, 720, 970, and 420 keV emitted in the decay of Nb^{88}.

We have reinvestigated the γ spectrum of Nb^{88} with lithium-drifted germanium diodes. We prepared our samples by 20-minute bombardments of pressed tablets of sodium bromide with 120-MeV C^{12} ions. After bombardment the bromide target was dissolved, niobium carrier was added, and a brief radiochemical procedure was followed in order to isolate a pure niobium fraction.

The γ-ray spectrum emitted by the niobium sample about 30 minutes after the end of the bombardment is shown in Fig. A.34-1. Several γ rays belonging to 14-hr Nb^{90} are present, but in addition there are γ rays, with energy 76, 271.8, 399.2, 671, 1058, and 1083 keV, which decay with a 14-minute half life and which consequently can be assigned to Nb^{88}. The annihilation photons peak also had a 15-minute component, and there was uncertain evidence for a 503-keV γ peak. No evidence was found for the γ rays reported by Butement and Qaim.[3]

Investigations are being continued by $\gamma\gamma$- coincidence measurements. Preliminary evidence indicates that the 671-keV γ ray is a crossover transition in parallel with the 271.8- and 399.2-keV pair. With this exception all the γ rays appear to be in coincidence with each other, but the order of their occurrence is unknown. $\beta+\gamma$ experiments suggest that the level populated by positron decay has a measurable half life.

These γ rays provide information on the level scheme of Zr^{88}. This should be of interest because of the great theoretical interest in such nuclei as Zr^{90}.

References

1. Ralph G. Korteling, High-Energy Nuclear Reactions of Niobium with Incident Protons and Helium Ions (Ph. D. Thesis), UCRL-10461, Sept. 1962.
2. R. G. Korteling and E. K. Hyde, Phys. Rev. 136, B425 (1964).
3. F. D. S. Butement and S. M. Qaim, J. Inorg. Nucl. Chem. 26, 1481 (1964).

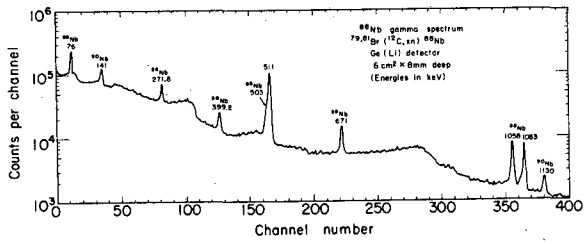

Fig. A.34-1. γ Spectrum of Nb^{88}.

35. THE RADIATIONS OF 1.9-HOUR Nb^{89}

E. K. Hyde and J. M. Nitschke

Isomeric forms of Nb^{89} were reported 10 years ago by Diamond[1] and by Mathur et al.[2] These isomers were prepared by proton bombardment of niobium, zirconium, yttrium, and silver targets and by carbon ion bombardment of sodium bromide. Radiochemical experiments proved the genetic relationship of an 0.8-hour and a 1.9-h activity to Zr^{89} daughter activity. The shorter-lived activity decays through the 4.4-min isomeric level of Zr^{89}, while the 1.9-h activity appeared to decay directly to the ground state. Both Nb^{89} isomers are positron emitters, whose spectra have end-point energies of about 3 MeV. More recent work by Butement and Qaim[3] confirms the earlier experimental work.

The simple shell model provides an explanation of the observed facts. The odd proton in Nb^{89} lies in the 40-50 subshell, where the lowest-lying states are $g_{9/2}$ and $s_{1/2}$. The spin difference of 4 accounts for the isomerism. Furthermore, the odd neutron in the daughter Zr^{89} also has its choice of $g_{9/2}$ and $s_{1/2}$ states, the former lying lower. Hence one expects the 0.8-h Nb^{89} to have spin 1/2 and to decay by an allowed transition to the 588-keV level in Zr^{89}. One also expects the 1.9-h activity to have spin 9/2 and to decay directly to the ground state of Zr^{89}.

Recent experimental work on the 1.9-h Nb^{89} in this Laboratory shows that the decay is more complex than the published work indicates. Measurements on intense sources carried out with lithium-drifted germanium detectors show that a large number of energetic γ rays, ranging in energy from 1.5 to 3.9 MeV, accompany the decay of the 1.9-h isomer.

Samples were prepared by bombarding pressed pellets of sodium bromide with 1-μA currents of C^{12} ions for periods of 30 min to 2 h. Niobium-89 is made by the reaction

$Br^{81}(C^{12}, 4n)Nb^{89}$.

After bombardment, the sodium bromide was dissolved, 5 mg each of niobium, yttrium, and zirconium carriers were added, and the niobium radioactivity was isolated by a radiochemical procedure which separated it cleanly from other radioelements. The final step was a precipitation of Nb_2O_5 from strongly acidic solution. The precipitate was centrifuged to the bottom of a small glass test tube which was placed in front of a germanium detector. Spectra were taken at intervals over a period of many hours. In the region below 1.5 MeV, the observed peaks were those of 14-h Nb^{90}, but a number of other peaks were found at higher energy which had half lives of approximately 2 h and which could be assigned to no nuclide other than 1.9-h Nb^{89}. A typical spectrum of the lower energies is shown in Fig. A.35-1, and of the higher energies in Fig. A.35-2.

For further confirmation of these peaks, spectra were taken with a pair spectrometer. This was similar to the one described by Yamazaki and Hollander,[4] and consisted of two 3×3-in. crystals of sodium iodide positioned at 180 deg and a third, lithium-drifted germanium counter. The counters were operated in triple coincidence in the usual manner for identification of pair production γ-absorption events with a typical time resolution of 40 nsec.

For use in the pair spectrometer measurements intense samples of 1.9-h Nb^{89} were prepared by bombarding niobium metal foils with 350-MeV protons in the internal beam of the 184-inch cyclotron. After bombardment, the niobium was dissolved and purified from molybdenum, zirconium, yttrium, and all other radioactive elements produced in the bombardment. Samples of niobium in the form of Nb_2O_5 were prepared in small glass tubes.

A typical result is shown in Fig. A.35-3. In the figure the energy labels on the peaks are those corresponding to the full energy of the incident photons; i.e., the rest energy (1.022 MeV) of the electron-positron pair has been added to the energy recorded in the germanium crystal. The agreement in energy of the peaks in the pair spectrum and those in the singles spectrum is strong confirmation of the existence of the γ rays. Spectra like that of Fig. A.35-3 were taken at intervals over a 24-h period in order to confirm the 2-h half life of the γ peaks. A list of γ rays identified in singles and pair spectra is given in Table A.35-I.[5]

There is little doubt that these γ rays belong to 1.9-h Nb^{89} as the half life corresponds to no other niobium isotope. They cannot be assigned to Nb^{87} or Nb^{86} because no evidence was found for the growth of Zr^{87} or Zr^{86} into the niobium fraction. On the other hand, the radiations of Zr^{89} were observed to grow into the niobium samples.

The total decay energy of Nb^{89} is 4.12 MeV according to Cameron,[6] and 4.0 MeV according to Yamada and Matumoto.[7] The presence of γ rays above 3 MeV means that electron capture must occur to high-lying levels, which then decay directly to ground. The positrons of 3 MeV observed by previous workers must represent direct decay to the ground state. The log ft for this decay is about 6. The electron-capture decay to the high-lying levels has a much lower log ft.

Further study is planned on this decay scheme because of the interest of Nb^{89} and Zr^{89} for the shell model. Zr^{89} is but one neutron removed from Zr^{90}, whose level scheme has been thoroughly investigated experimentally and theoretically.

References

1. R. M. Diamond, Phys. Rev. 95, 410 (1954).
2. H. B. Mathur, E. K. Hyde, C. A. Levine, and P. K. Kofstad, Phys. Rev. 97, 117 (1955).
3. F. D. S. Butement and S. M. Qaim, J. Inorg. Nucl. Chem. 26, 1481 (1964).
4. T. Yamazaki and J. M. Hollander, Phys. Rev. 140 B630 (1965).
5. We found it difficult to calibrate the energy scale in the pair spectra because not enough precise high-energy γ rays are known.
6. A. G. W. Cameron, report AECL-433 (1958).
7. T. Yamada and Z. Matumoto, J. Phys. Soc. Japan 16, 1497 (1961).

Table A.35-I. Observed γ rays and their half lives in the decay of 1.9-hour Nb^{89}.

Energy (keV)	Half life (min)
1510	122
1626	124
1713 (?)	
1832	132
1911 (?)	
2220	119
2572 ± 1	
2754 ± 1	≈ 120 (pair spectrometer)
2961 ± 1	110
3018 ± 1	
3093 ± 1	125
3282	
3333	
3513 ± 1	
3577 ± 1	≈ 120 } (pair spectrometer)
3838 ± 1	≈ 120 }
3908 ± 1	

Average half life : 120 ± 3 min

Note 1. Where error is not given it may be as large as 5 keV.
Note 2. More intense lines indicated by underlining.
Note 3. More recent spectra indicate additional weak γ rays between 2.5 and 3.9 MeV.

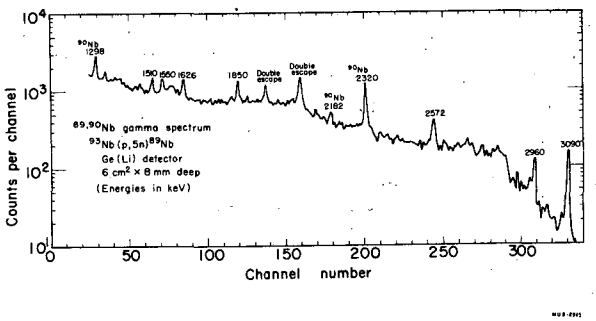

Fig. A.35-1. γ Rays of 1.9-h Nb^{89} in 1- to 3-MeV region.

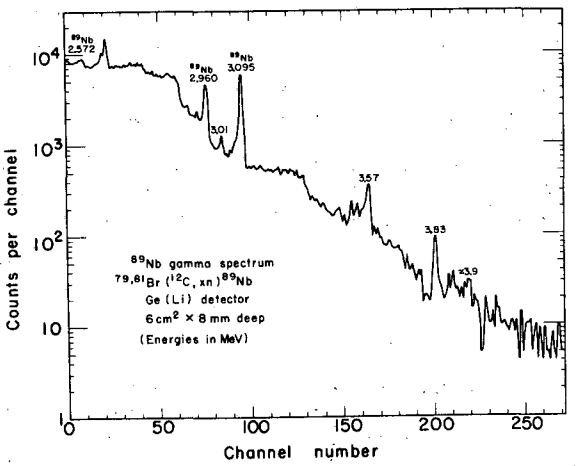

Fig. A.35-2. γ Rays of 1.9-h Nb^{89} in 2.5- to 4.0-MeV region.

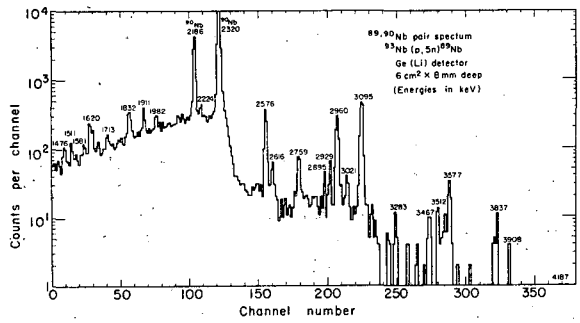

Fig. A.35-3. γ Rays of 1.9-h Nb^{89} as determined in pair spectrometer.

36. HIGH-RESOLUTION STUDY OF TRANSITIONS IN THE DECAY OF U^{237}

T. Yamazaki and J. M. Hollander

The internal conversion electron and γ-ray spectra from the decay of U^{237} have been studied with use of a high-resolution $\pi\sqrt{2}$ iron-free spectrometer and solid-state γ-ray spectrometers. In addition to the previously known transitions, several new lines were observed and fitted into the Np^{237} level scheme (see Fig. A.36-1). Absolute conversion coefficients for most of the transitions were determined. The presence of the previously undiscovered level at 281.35 keV, confirmed by the observation of a very strong 13.81-keV M1-E2 transition and a weak 220.8-keV cross-over transition, establishes that the 267.54-keV 3/2- level is the lowest member of a K = 1/2- band.

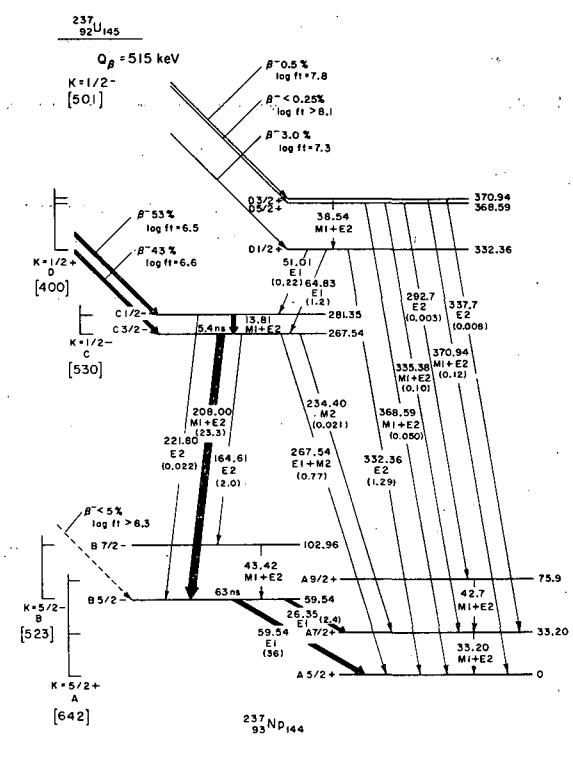

Fig. A.36-1. The decay scheme of U^{237}.

37. INTERNAL-CONVERSION COEFFICIENTS OF THE 381-keV AND 389-keV M4 TRANSITIONS FROM Y^{87m} AND Sr^{87m}

M. Sakai, T. Yamazaki, and J. M. Hollander

Internal-conversion spectra of the 381-keV M4 transition from Y^{87m} and the 389-keV M4 transition from Sr^{87m} (see the decay scheme in Fig. A.37-1) were measured with the Berkeley iron-free β-ray spectrometer, at 0.06% resolution. The electron spectra are shown in Figs. A.37-2a and b. Gamma-ray spectra of these transitions were also obtained with a Ge(Li) γ-ray spectrometer with 3.0-keV resolution, as shown in Fig. A.37-3. Electron intensities as well as γ-ray intensities were precisely determined by using the IBM 7094 computer.

The result on the K/L ratios is summarized in Table A.37-I. Although both K/L ratios are a few percent lower than the Sliv-Band theoretical value, there is no significant difference between these values.

Table A.37-II shows the result on the ratio $\alpha_K(381)/\alpha_K(389)$. The experimental ratio is 5% smaller than the theoretical one. The significance of this discrepancy depends on the estimate of experimental errors. The error analysis is still in progress.

Table A.37-I. Ratio of K line to L line.

Element	Transition energy (keV)	Reference	K-ICC	L-ICC	$(K/L)_{theo}$	$(K/L)_{exp}$	$\frac{(K/L)_{exp}-(K/L)_{theo}}{(K/L)_{theo}}$
Y^{87m}	381.1	Rose	0.2180	0.03239	6.730		-0.049 ± 0.017
						6.41 ± 0.11	
		Sliv-Band	0.2168	0.03286	6.597		-0.029 ± 0.017
Sr^{87m}	388.8	Rose	0.1815	0.02600	6.981		-0.024 ± 0.019
						6.82 ± 0.13	
		Sliv-Band	0.1816	0.02615	6.944		-0.018 ± 0.019

Table A.37-II. Ratio $\alpha_K(381)/\alpha_K(389)$.

Element	Transition energy (keV)	Relative intensity of K electrons (I_e)	Relative intensity of γ ray (I_γ)	Relative efficiency of γ-ray detector (η)	$I_e \cdot \eta / I_\gamma$ ($\propto \alpha K$)	$\alpha_K(381)/\alpha_K(389)$ Exp	Rose	Sliv-Band	exp/theo
Y^{87m}	381.1	203 758±732	22 822±210	1.054 ± 0.006	9.390				
						1.135 ± 0.019	1.201	1.194	0.95±0.02
Sr^{87m}	388.8	77 458±324	9 352±102	1.000	8.283				

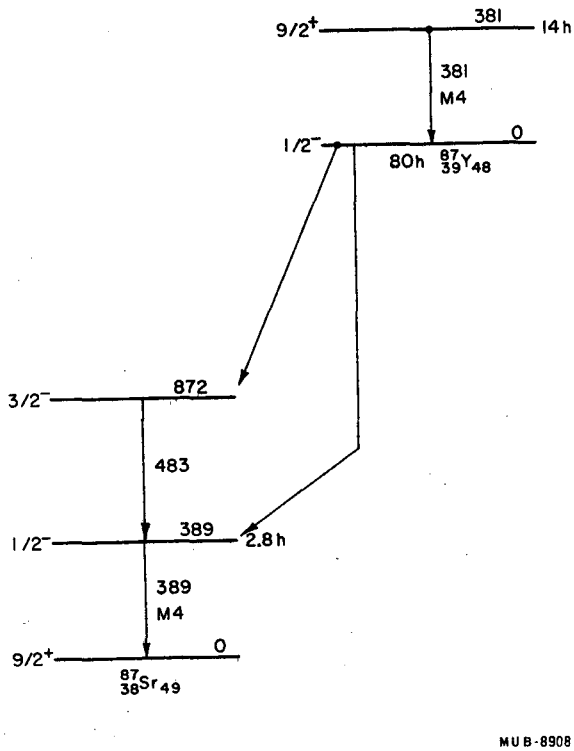

Fig. A.37-1. Decay scheme of Y^{87m}.

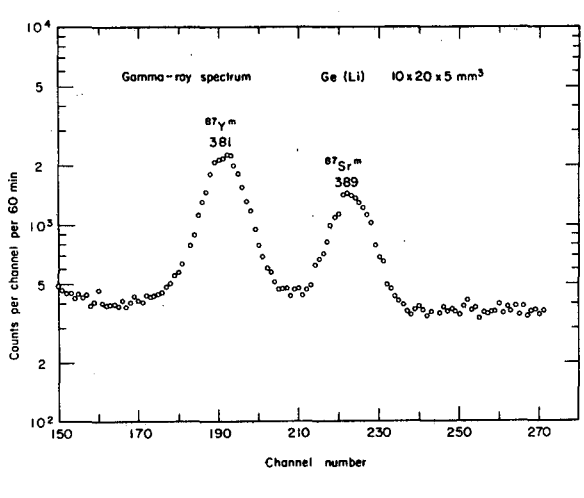

Fig. A.37-3. Gamma-ray spectrum of Y^{87m} and Sr^{87m} taken with a 10×20×5-mm^3 Ge(Li) detector.

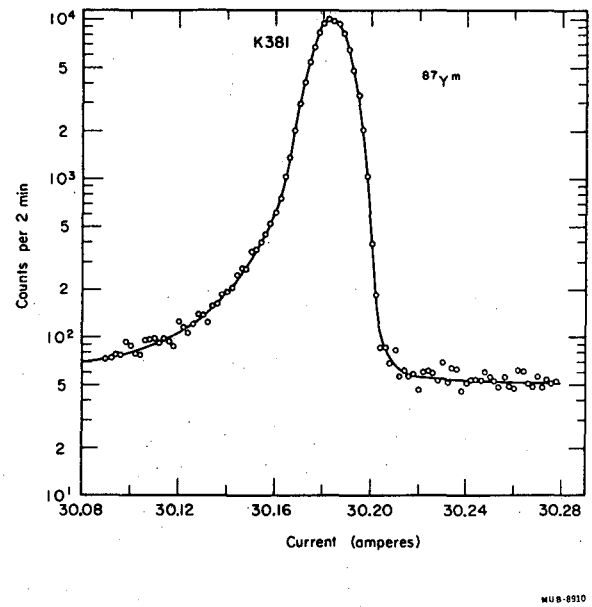

(a)

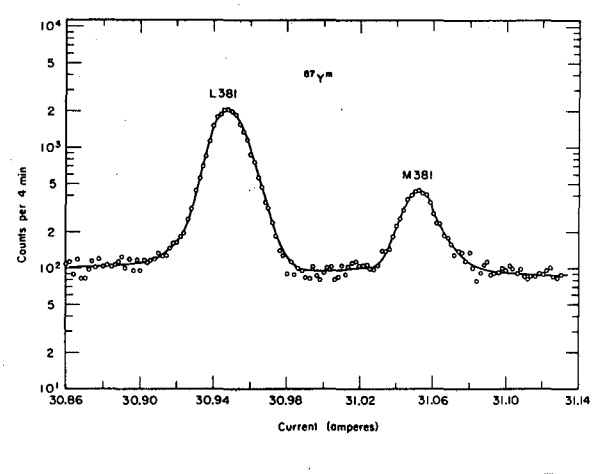

(b)

Fig. A.37-2 (a, b). Conversion-electron spectrum of the 381-keV transition from Y^{87m}.

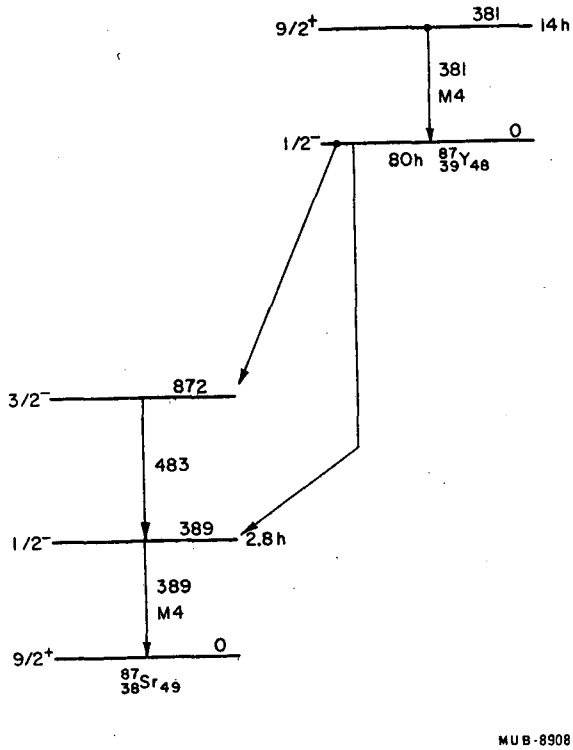

Fig. A.37-1. Decay scheme of Y^{87m}.

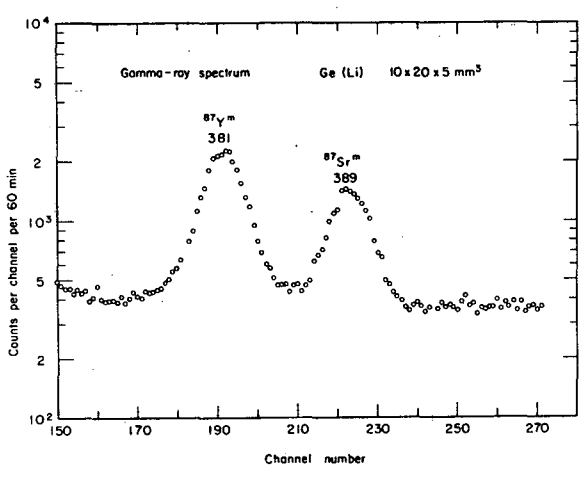

Fig. A.37-3. Gamma-ray spectrum of Y^{87m} and Sr^{87m} taken with a 10X20X5-mm^3 Ge(Li) detector.

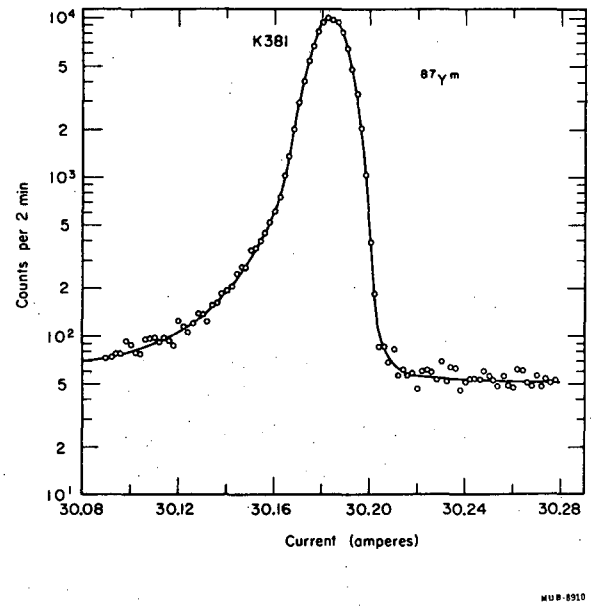

(a)

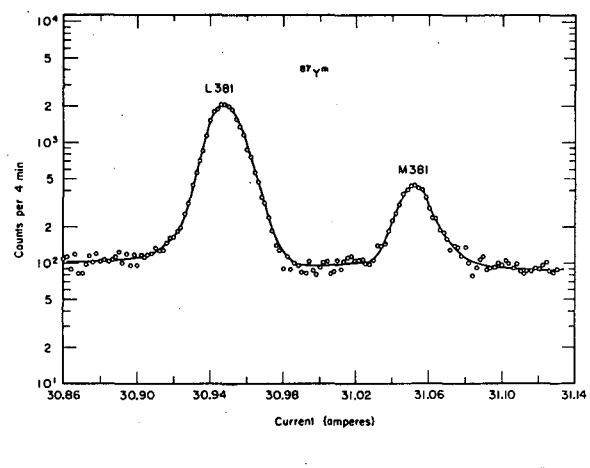

(b)

Fig. A.37-2 (a, b). Conversion-electron spectrum of the 381-keV transition from Y^{87m}.

B. FISSION

1. IDENTIFICATION OF HEAVY-ION REACTION PRODUCTS BY IN-BEAM x-RAY MEASUREMENT

H. R. Bowman and S. G. Thompson

x Rays emitted from heavy-ion reaction products have been observed directly from the target during the heavy-ion beam pulses by use of high-resolution x-ray detectors. In bombardments of lutetium with 92-MeV nitrogen ions, giving the compound nucleus Pt^{189}, we were able to identify not only the K x rays of platinum but also iridium K x rays from (N, pxn) reactions and osmium K x rays from the N, αxn reactions. In bombardments of gold with 83-MeV nitrogen ions, the K x rays of emanation were observed from the N, xn reactions.

These measurements were made with a lithium-drifted germanium detector 1×2×0.2 cm operated at liquid nitrogen temperatures. The first stage of the detector preamplifier consisted of a field-effect transistor (FET) which was also cooled to liquid nitrogen temperature. The germanium detector was placed 4 cm away from the target, and the reaction products were viewed through a 500-mg/cm^2 beryllium window.

Figure B.1-1 shows the x rays resulting from the reaction of nitrogen ions with the lutetium target. The major component in Fig. B.1-1 is the result of K x rays coming from the target material excited by the scattering of nitrogen ions. The reaction products are indicated by arrows as shown. Figure B.1-2 shows the results of bombarding gold with 83-MeV nitrogen ions and indicates that the N, xn reactions are the principal nuclear reactions at this bombarding energy. The prominent x rays are again the target x rays.

Experiments aimed at measuring the lifetimes of these reaction-product x rays were carried out by placing a beryllium catcher foil 3 cm beyond the target (downstream) and counting x rays from the catcher foil through a collimator slot. The impurities in the catcher foil have so far limited the usefulness of these experiments.

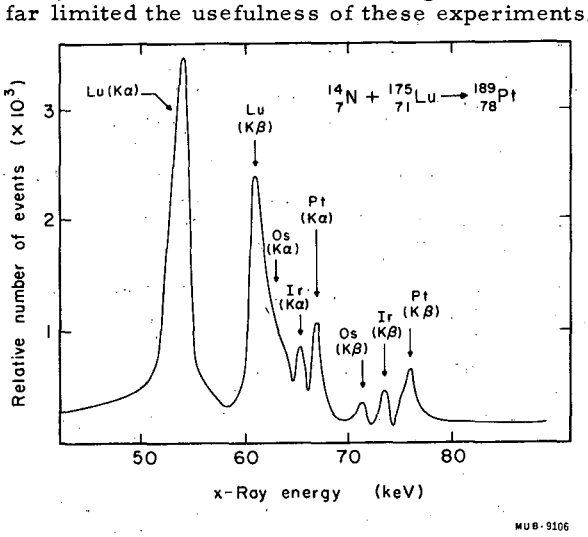

Fig. B.1-1. The K x rays emitted during the heavy-ion bombardment of lutetium with 92-MeV nitrogen ions. A silver absorber of 342 mg/cm^2 thickness was used.

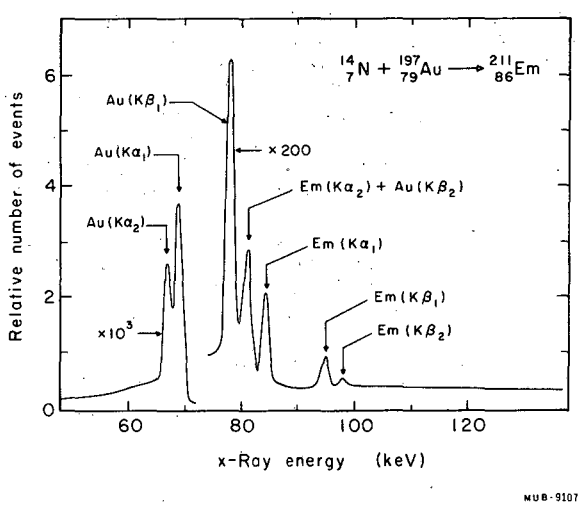

Fig. B.1-2. The K x rays emitted during the bombardment of gold with 83-MeV nitrogen ions.

2. GAMMA-RAY AND INTERNAL-CONVERSION ELECTRON STUDIES OF PRIMARY Cf^{252} FISSION FRAGMENTS

R. L. Watson, H. R. Bowman, S. G. Thompson, and J. O. Rasmussen

Recent studies[1-5] of the γ rays and internal-conversion electrons emitted in coincidence with the fission of Cf^{252} have yielded encouraging results concerning the possibility of obtaining nuclear spectroscopic information on the low-lying energy levels in the neutron-rich fragment nuclei. Moreover, these investigations are expected to provide a body of experimental data from which a number of general features of the fission process may be deduced.

The experimental method used in our studies consisted in simultaneously measuring, with semiconductor detectors, the kinetic energies of both fragments and the energies of the emitted γ rays or conversion electrons. These energies were then recorded individually and in sequence in a multidimensional pulse-height analyzer and recorded on magnetic tape. Subsequently, the magnetic tape, with the primary three (or more) dimensional information was sorted, event by event, on the IBM 7094 computer to obtain the energy spectra of the electrons and the γ rays for the cases of various fragment masses and total kinetic energies.

Study of the internal-conversion electrons emitted in coincidence with fission presents an experimentally difficult problem in that there is no straightforward means of isolating the electron detector from the direct radiation by fission fragments, α particles, and γ rays and still maintain a high collection geometry. In our experiments we have made use of a high-gradient magnetic field to provide a means of steering the electrons away from the source region and focusing them on a detector shielded from the other radiations. In this type of magnetic field, electrons leaving the source (on the symmetry plane) in any direction in the plane perpendicular to the magnetic lines of force will precess around the magnet at a constant radius (which is independent of the electron energy) in the same manner as particles are mirrored in the Van Allen belt about the earth. A photograph of the electron apparatus presently being used is shown in Fig. B.2-1.

The observed γ-ray spectra from these experiments show many discretely resolved peaks, and most of the peaks are found to be Doppler-shifted due to the motion of the fragments. These shifts have been used to ascertain which members of the pairs of fragments (heavy or light) emitted the γ rays as well as to deduce some information on the γ-ray lifetimes involved. As a typical case, Fig. B.2-2 shows the observed γ-ray spectra for the selected heavy fragment mass interval 143-145 and the complementary light fragment mass interval 103-105. The peaks are labeled alphabetically--the top spectrum with the heavy fragment moving toward the detector, the middle spectrum with the gamma rays emitted at 90 deg, and the bottom spectrum with the light fragment moving toward the γ-ray detector (heavy fragment away). On the basis of the observed Doppler shifts and relative intensities, it has been possible to identify the emitting fragment as either heavy or light for most of the observed γ peaks. In Fig. B.2-2 they are stipulated as such by the letter H or L, respectively, following their identification letter. Those peaks having components in the unshifted position (indicating γ emission after the fragment had stopped in the detector) are labeled with the letter U following their identification letter.

The most useful electron data to date have been obtained by placing the Cf^{252} source 1 cm off the median plane. In this configuration, the high magnetic field prevents those electrons leaving the immediate region of the source from reaching the electron detector, and only those electrons emitted along the portion of the flight path crossing the median plane of the apparatus will precess around to register in the electron detector. In this way, complete separation of the electrons emitted by single members of the pairs of fragments may be achieved. The delayed electron spectra (≈1 nsec after fission) for the same mass intervals as the γ spectra in Fig. B.2-2 (143-145 and 103-105) are shown in Fig. B.2-3.[6]

The electron peaks of Fig. B.2-3 have been used in conjunction with the γ-ray spectra of Fig. B.2-2 to determine the binding energies and hence the nuclear charges of the emitting nuclei. Use has also been made of most probable charge data[7] in reducing the experimental mass uncertainty. The tentative assignments resulting from these spectra are summarized in Table B.2-I.

It should be pointed out that in assigning charge numbers on the basis of binding energies, account must be taken of the increase in the binding energies due to the highly ionized state of the emitting nuclei (electronic charge ≈ +20 to 22). Detailed calculations of the binding energies of atoms spanning the region of Cf^{252} fission products as a function of electronic charge, using the Hartree-Fock self-consistent field method in the form developed by Roothaan,[8] are being carried

out at present. Preliminary results of these calculations indicate that the K binding energies in the region of interest are increased by about 1 keV on the average.

Further γ-ray and internal-conversion electron experiments are presently being conducted, utilizing the improved noise and resolution characteristics (≈1 keV FWHM for γ rays and ≈2.5 keV FWHM for electrons) afforded by the recent application of field-effect transistors to the preamplification of semiconductor detector signals.[9] It is expected that this work will yield data of considerable value for the determination of lifetimes and conversion coefficients, allowing the subsequent assignment of multipolarities.

Footnotes and References

1. H. R. Bowman, S. G. Thompson, and J. O. Rasmussen, Phys. Rev. Letters 12, 195 (1964).
2. R. L. Watson, H. R. Bowman, S. G. Thompson, and J. O. Rasmussen, Phys. Rev. Letters 14, 183 (1965).
3. H. R. Bowman, S. G. Thompson, R. L. Watson, S. S. Kapoor, and J. O. Rasmussen, in Proceedings of the International Symposium on the Physics and Chemistry of Fission, Salzburg, Austria, 1965 (IAEA, Austria, 1965), p. 125.
4. T. D. Thomas, R. A. Atneosen, W. M. Gibson, and M. L. Perlman, in Proceedings of the International Symposium on the Physics and Chemistry of Fission, Salzburg, Austria, 1965 (IAEA, Austria, 1965).
5. R. L. Watson, H. R. Bowman, S. G. Thompson, and J. O. Rasmussen, Internal Conversion Processes (Academic Press, New York, 1965), p. 423.
6. The energy values of the peaks shown in Fig. B.2-3 have been corrected for an experimental effect recently discovered (since the publication of Ref. 5).
7. S. S. Kapoor, H. R. Bowman, and S. G. Thompson, Phys. Rev. 140, B1310 (1965).
8. C. C. J. Roothaan, Rev. Mod. Phys. 32, 179 (1960).
9. E. Elad, submitted to Nucl. Instr. Methods (Lawrence Radiation Laboratory Report UCRL-16390, Sept. 1965).

Table B.2-I.

identification letter (see Fig. B.2-2)	Gamma-ray energy (keV)	K electron energy (keV) (see Fig. B.2-3)	Isotope assignment
A	95.5	73.0	^{105}Tc
C	112.7	74.0	^{144}Ba
K	170.0	149.0	^{105}Mo
N	191.5	170.5	^{105}Mo
O	198.0	161.0	^{143}Cs

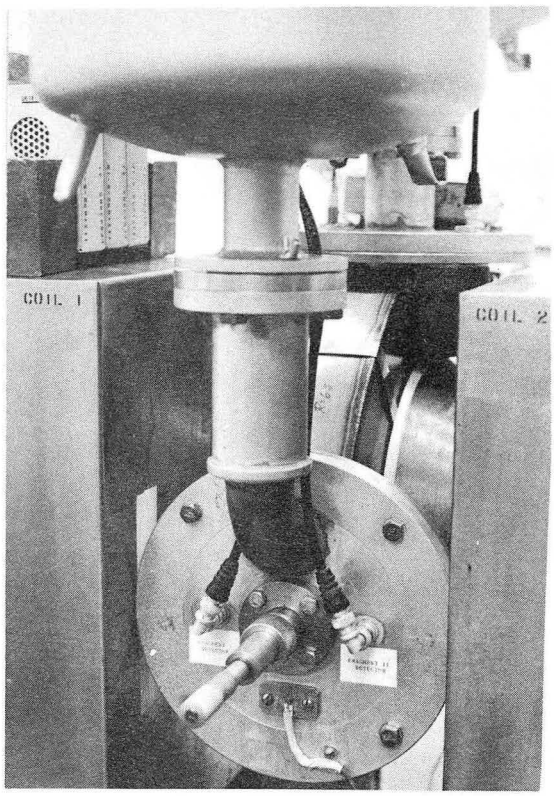

Fig. B.2-1. Photograph of the electron–fission-fragment detector apparatus.

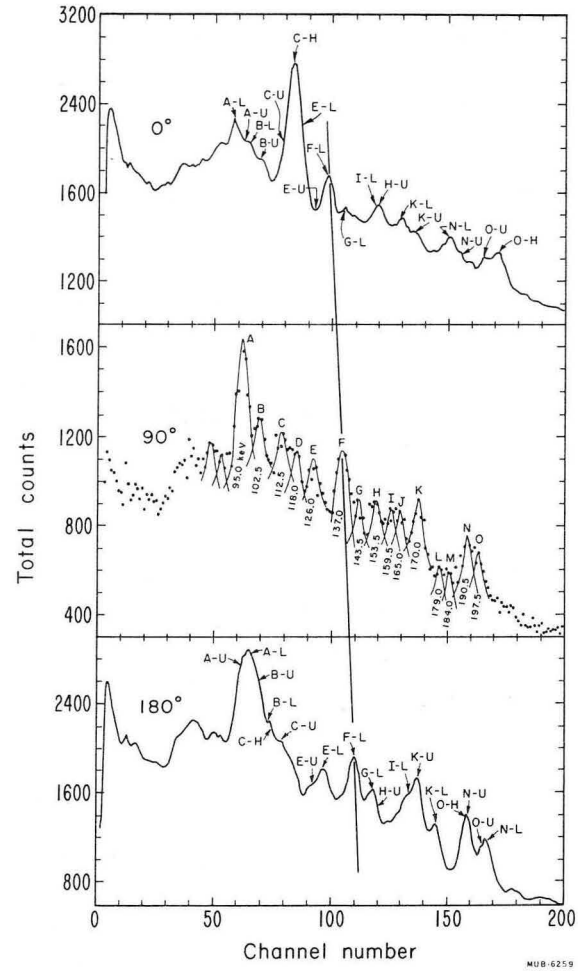

Fig. B.2-2. Gamma-ray spectra in coincidence with the mass 143-145—mass 103-105 fission fragment pair, with the heavy fragment moving toward (top), at 90 deg (center), and away from (bottom) the γ-ray detector. The γ-ray peaks are labeled alphabetically followed by the letter L, H, or U for peaks in a light-fragment Doppler-shifted position, a heavy-fragment Doppler-shifted position or an unshifted position, respectively.

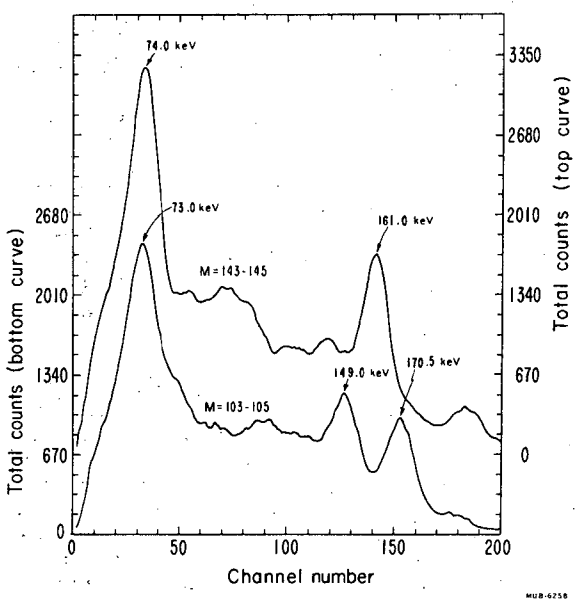

Fig. B.2-3. (Top curve). Delayed electron spectrum in coincidence with the mass 143-145 fission fragments (bottom curve). Delayed electron spectrum in coincidence with the complementary mass 103-105 fission fragments.

3. FRAGMENT ANGULAR DISTRIBUTION IN THE FISSION OF Bi^{209} AND U^{238} INDUCED BY α PARTICLES OF ENERGIES UP TO 115 MeV

Shyam S. Kapoor,* Hiroshi Baba,† and Stanley G. Thompson

In recent years, angular distributions of fragments have been intensively studied as a tool to investigate the properties of the highly stretched configuration of the fissioning nucleus represented by the saddle-point shape. The developments in this direction are primarily based on a model proposed by A. Bohr,[1] and further extended by Halpern and Strutinski[2] and Griffin.[3] On the basis of this theoretical frame, the angular distributions provide a measure of K_0^2 corresponding to the saddle-point configuration. Here K_0 is defined as the standard deviation of the distributions in the angular momentum projection on the nuclear symmetry axis, and according to the statistical theory, $K_0^2\hbar^2$ is equal to the product of the effective moment of inertia J_{eff} and nuclear temperature T for the saddle-point configuration. We have investigated the energy dependence of K_0^2 up to high excitation energies not studied before from the study of the fragment angular distributions.

Angular distributions of the fragments were measured in the fission of Bi^{209} and U^{238} induced by α particles of various energies (from 23 to 115 MeV) obtained from the 88-inch variable-energy cyclotron. The fragments were detected by semiconductor detectors placed on two movable arms located in the two halves of the vacuum chamber. The angular distributions were measured by changing the angle of one arm, carrying three detectors, while keeping the other arm, carrying the fourth detector, fixed at 90 deg in the other half of the chamber to serve as a monitor. The respective thin targets were mounted at 45 deg to the beam direction. By counting the fragments at 90 deg on both sides of the target, it was possible to correct the angular distribution for any small systematic error introduced by the possible noncentering of the beam position. The measured distributions were transformed to the center-of-mass system with the assumption of full momentum transfer of the α particles to the compound nucleus.

The observed angular distributions in the c.m. system in each case were fitted to the theoretical expressions to deduce the values of K_0^2. The transmission coefficients T_ℓ and the

mean square of the orbital angular momentum, $\langle \ell^2 \rangle$, required to deduce K_0^2 were obtained from the optical-model calculations using the Woods-Saxon parameters given by Huizenga and Igo.[4]

Figures B.3-1 and B.3-2 show plots of the deduced values of K_0^2 against the respective saddle-point excitation energy Ex^s. The values of Ex^s were calculated by taking into account the angular-momentum-dependent barrier energies as calculated by Swiatecki et al.[5] and the rotational energies. The shaded area in Fig. B.3-1 represents the values of K_0^2 given by statistical theory as obtained by normalizing the values of K_0^2 deduced from the measurements with 40-MeV α particles where essentially all the observed fissions take place with a single value of Ex^s corresponding to first-chance fission. For the sake of comparison with the present results, the values of K_0^2 obtained by Huizenga et al.[6] in the range of energy Ex^s between 4 and 16 MeV are also shown in Fig. B.3-1. The solid line in Fig. B.3-2 shows the values of K_0^2 calculated on the Fermi gas theory, using a_f equal to A/8 and J_{sph}/J_{eff} equal to 0.78, as deduced by Reising et al.[7] from their anisotropy measurements. It can be seen from Figs. B.3-1 and B.3-2 that the observed values of K_0^2 increase more rapidly with energy Ex^s than expected from the statistical theory, and thereby the observed values of K_0^2 are found to be larger than the theoretical values for higher values of Ex^s. If the effects of multichance fissions are taken into account, one instead expects the observed values of K_0^2 to be lower than given by theory, and consequently the deviations with the theory are more serious than apparent in these figures.

As a possible reason for the observed discrepancy with the theory, the presence of direct interactions and their effect on the deduced values of K_0^2 was then investigated. From the experimental measurements of the fragment-fragment angular correlations, it is found that in bombardment with 110-MeV α particles the fractions of fissions following direct interactions is 0% and 9% for the target nuclei of Bi^{209} and U^{238}, respectively. With the purpose of experimentally ascertaining the accuracy of the optical-model calculations and inferring the percentage of direct interactions not leading to fission, the fission cross section of U^{238} for α-particle energies up to 110 MeV were also measured. From this, it was found that in U^{238} the direct interactions not leading to fission are less than 15% of the total interactions. However, it was found that even after extreme corrections of the direct interaction effects are made, the values of K_0^2 are still higher than theory by about 16 to 34% for 110-MeV α bombardment of U^{238}. In 110-MeV α bombardment of Bi^{209}, there is good evidence from some measured (α, xn) cross sections that the expected percentage of direct interactions is too small (less than 10%) to account for the observed higher values of K_0^2. Assuming that as much as 15% of the events involve direct interactions, the observed values of K_0^2 will still be larger than theory by about the same fraction as for of U^{238}. On the assumption that the statistical approach is justified in calculating the angular distributions even for the high excitation energies involved in this work, one is led to the conclusion that the value of $J_{eff}/a_f^{1/2}$ increases with increasing α-particle energy. It is most reasonable to infer that the value of J_{eff} increases with the incident α-particle energy, as a result of the change in the saddle shape of the nucleus. This can come about, firstly, because of the dependence of the saddle-point shape on the angular momentum, and secondly, because of the increase in the amplitude of the wriggling and bending modes of oscillations with the nuclear temperature.

Footnotes and References

*On leave from the Atomic Energy Establishment, Trombay, India.

†Present address: Japan Atomic Energy Research Institute, Tokaimura, Ibaraki-ken, Japan.

1. A. Bohr, in Proceedings of the First United Nations International Conference on the Peaceful Uses of Atomic Energy, Geneva, 1955 (United Nations, New York, 1956), Vol. II, p. 151.
2. I. Halpern and F. M. Strutinski, in Proceedings of the Second United Nations International Conference on the Peaceful Uses of Atomic Energy, Geneva, 1958 (United Nations, New York, 1958), Vol. XV, p. 408.
3. J. J. Griffin, Phys. Rev. 116, 107 (1959).
4. J. R. Huizenga and G. Igo, Nucl. Phys. 29, 473 (1962).
5. Calculations on the rotating liquid drop carried out by W. J. Swiatecki and collaborators (unpublished).
6. R. Chaudhry, R. Vandenbosch, and J. R. Huizenga, Phys. Rev. 126, 220 (1962).
7. R. F. Reising, G. L. Bate, and J. R. Huizenga, Phys. Rev. (to be published).

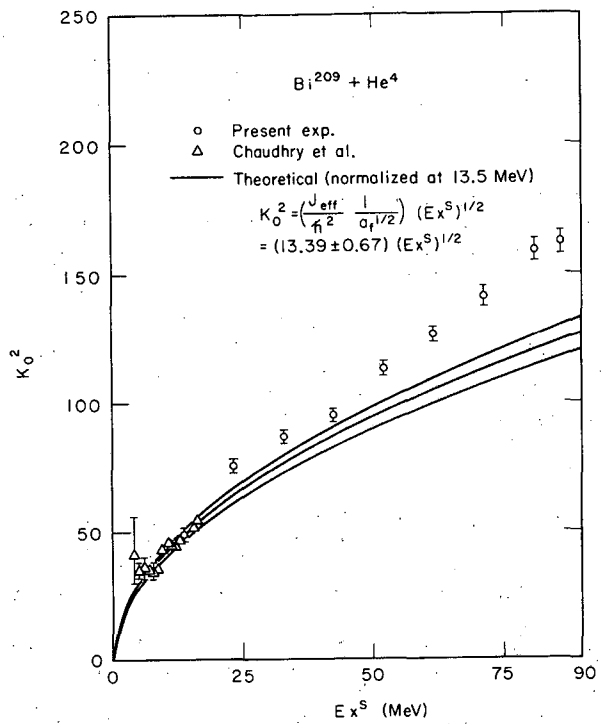

Fig. B.3-1. A plot of the deduced values of K_0^2 versus the saddle point excitation energy Ex^s in the case of fission of Bi^{209} by alpha particles of energies up to 115 MeV. The values of K_0^2 were obtained by the least square fit of the angular distributions to the theoretical expression given by Halpern and Strutinski. The shaded area shows the energy dependence of K_0^2 expected on the Fermi gas theory, obtained by normalization to the observed value of K_0^2 with 40 MeV alpha bombarding energy.

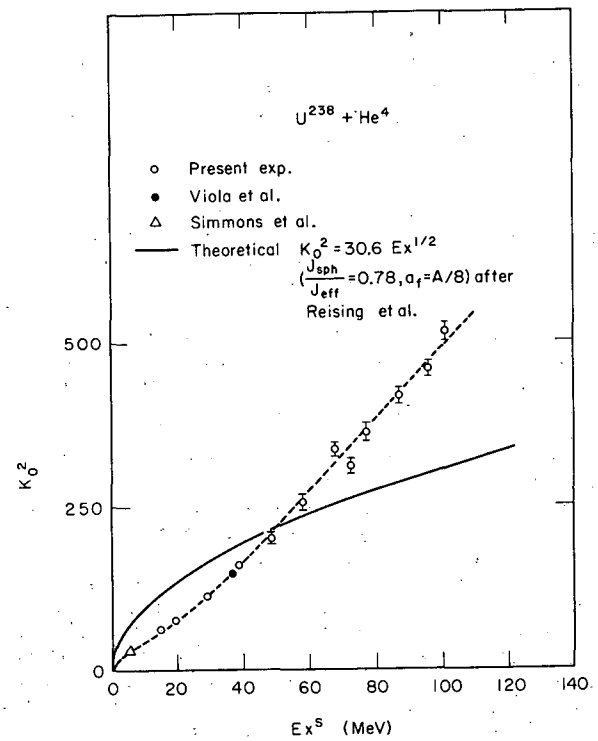

Fig. B.3-2. A plot of the deduced values of K_0^2 versus the saddle point excitation energy Ex^s in the case of fission of U^{238} by alpha particles of energies up to 115 MeV. The solid line curve shows the energy dependence of K_0^2 on the Fermi gas theory taking the values of J_{sph}/J_{eff} and a_f from Ref. 7.

4. FISSION PROPERTIES OF SOME ELEMENTS BELOW RADIUM

A. Khodai-Joopari, R. C. Gatti, and S. G. Thompson

Fission excitation functions were measured for several elements below radium with the primary objective of making accurate determinations of fission barriers. This work is a continuation of our work reported previously.[1] Mica was used for the detection of fission fragments, and the method is similar to that reported by Burnett et al.[2] Additional targets, namely enriched Pb^{206}, Pb^{207}, and Pb^{208} isotopes of desired purity, were obtained by careful partial vaporization of the metals in the same manner.[1]

The results of the measured fission cross sections, σ_f, for the reactions of helium ions with Bi^{209}, Pb^{206}, Pb^{207}, and Au^{197} (including the data of Ref. 1 for this target) are plotted against excitation energy in Fig. B.4-1. The data for the reactions of protons with the above targets (except Pb^{207}) are plotted in Fig. B. 4-2. Values of the total reaction cross section, σ_R, were obtained from optical-model calculations. In order to check the calculated values of σ_R at higher energies, some fission cross sections for the reaction of helium ions with U^{238} up to 110 MeV bombarding energy were measured, using solid-state counters. The agreement between the

measured and calculated results was found to be within 10%. The ratio σ_f/σ_R is plotted against excitation energy for the helium ion and proton bombardments in Figs. B.4-3 and B.4-4, respectively. In all figures smooth curves have been drawn through each set of data points for ease of identification. The solid symbols represent the experimental points measured by solid-state counters.

Analyses of these σ_f/σ_R data in terms of the theoretical expressions[2-4] for the competition between fission and neutron emission and the comparison of the determined fission barriers with the predictions[4-6] of the liquid drop model have been made. Some of the interesting results obtained from the analysis of the experimental data are as follows:

(a) The values of the fission barriers as determined from the low-energy data (up to 15 MeV above the lowest energy points), with a maximum standard deviation of 1.5 MeV, are given in Table B.4-I. Within the limits are included all values obtained with wide variations in choices of the level density parameter appropriate for fission, a_f, the residual nucleus, a_n, and values of the barrier-thickness parameter, $\hbar\omega$, ranging from 0 to 1.5 MeV. The ratio a_f/a_n is fairly constant, and greater than unity in each case. This can be explained by consideration of the effect of shell structure on the nuclear level densities. Table B.4-I also gives the values of B_f and the liquid-drop part of the fission barrier, B_f^{LD}, together with the shell correction term, Δm, obtained from the mass table of Myers and Swiatecki.[6]

(b) From the comparison of the measured values of the fission barriers with those calculated on the basis of two versions of the liquid-drop model which differ only in the use of a composition-dependent or -independent surface energy, the following conclusion is reached: The agreement between the calculated and measured values of the fission barriers is obtained <u>only</u> if a composition-dependent surface energy is used in the calculations.

(c) The expected increase in fission probability at higher energies and its decrease at energies close to the fission barrier as a result of increasing angular momentum is observed for the Po^{210} compound nucleus made in two different ways. However, it should be mentioned that the experimental errors are rather large and the magnitude of angular momentum involved is small compared with that obtained by heavy-ion bombardments.

(d) The effect of the shell term, Δm, on the values of the fission barriers can be seen qualitatively by comparison of the σ_f/σ_R data of Po^{210} and Po^{212}. The quantitative agreement can be seen in Table B.4-I.

(e) The slope and the order of σ_f/σ_R curves at higher energies reveals that the number of pre-fission neutrons is large. Even this qualitative result is of considerable interest for the interpretation of fission-fragment angular distributions and of fragment mass-energy distributions. Extension of the calculations of σ_f/σ_R to higher energies, using the parameters obtained from the best fits to low-energy data, showed a very large discrepancy with the experimental σ_f/σ_R data. It is impossible to account for this disagreement if it is assumed that the statistical treatment is valid and a_n does not change with energy. Quantitative analysis of higher-energy data requires better knowledge of nuclear level densities, more information on the cross section for charged-particle emission, and investigation of the validity of statistical theories at higher energies. In order to get some information about these, work is in progress to measure the cross sections and also mean ranges of the products of the (α, xn) reactions with Bi^{209} up to 120 MeV helium ion energy.

References

1. R. C. Gatti, A. Khodai-Joopari, and S. G. Thompson, in Nuclear Chemistry Division Annual Report, UCRL-11828, Jan. 1965, p. 81.
2. D. S. Burnett, R. C. Gatti, F. Plasil, P. B. Price, W. J. Swiatecki, and S. G. Thompson, Phys. Rev. 134, B952 (1964).
3. J. R. Huizenga, R. Chaudhry, and R. Vandenbosch, Phys. Rev. 126, 210 (1962).
4. Franz Plasil, Energy-Mass Distribution and Angular Momentum Effects in Heavy-Ion-Induced Fission (Ph. D. Thesis), UCRL-11193, Dec. 1963.
5. S. Cohen and W. J. Swiatecki, Ann. Phys. 22, 406 (1963).
6. William D. Myers and Wladyslaw J. Swiatecki, Nuclear Masses and Deformations, (to be published) in Nucl. Phys. (UCRL-11980, May 1965).

Table B.4-1. Measured and calculated[a] values of the fission barriers.

Compound nucleus	Calculated[b] B_f^{LD} (MeV)	Shell correction term,[b] Δm (MeV)	Calculated[b] fission barrier $B_f = B_f^{LD} - \Delta m$ (MeV)	Measured fission barrier B_f (MeV)
Hg^{198}	18.77	-3.43	22.20	21.6
Tl^{201}	17.44	-4.98	22.42	22.5
Bi^{207}	14.92	-7.22	22.15	21.5
Bi^{209}	15.37	-8.53	23.90	23.0
Po^{210}	13.76	-7.24	21.01	20.5
Po^{212}	14.17	-4.93	19.09	18.8
At^{213}	12.67	-3.57	16.24	16.8

[a] It should be noted that the mass formula of Myers and Swiatecki is normalized to the fission barrier of Tl^{201} as measured by Burnett et al. (Ref. 2).

[b] Ref. 6.

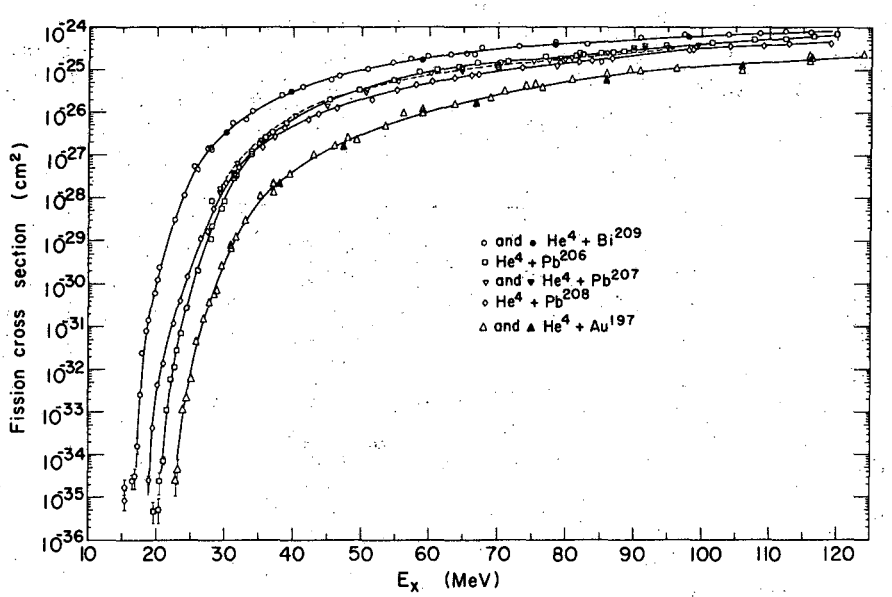

Fig. B.4-1. Measured fission cross sections as a function of excitation energy, E_x, of the compound nuclei formed in the bombardments of various targets with helium ions.

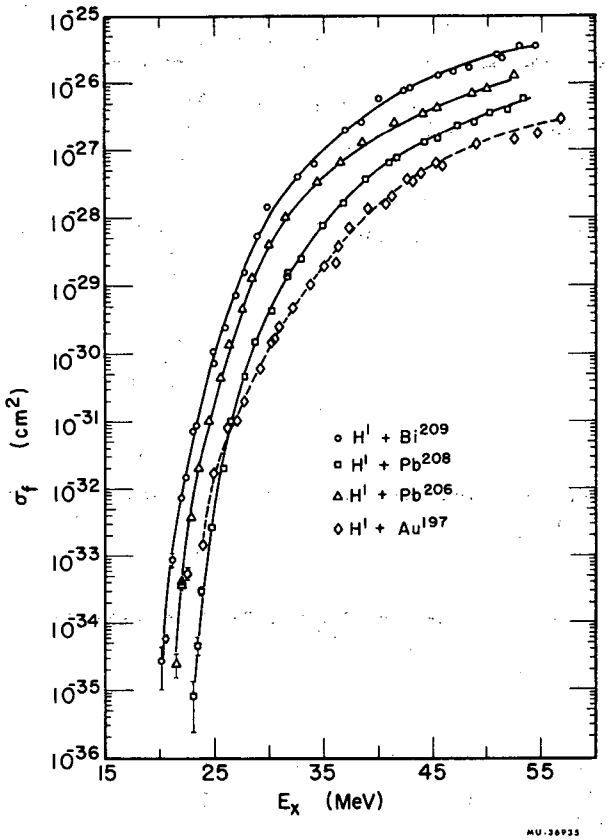

Fig. B.4-2. Measured fission cross sections as a function of excitation energy, E_x, of the compound nuclei formed in the bombardments of various targets with protons.

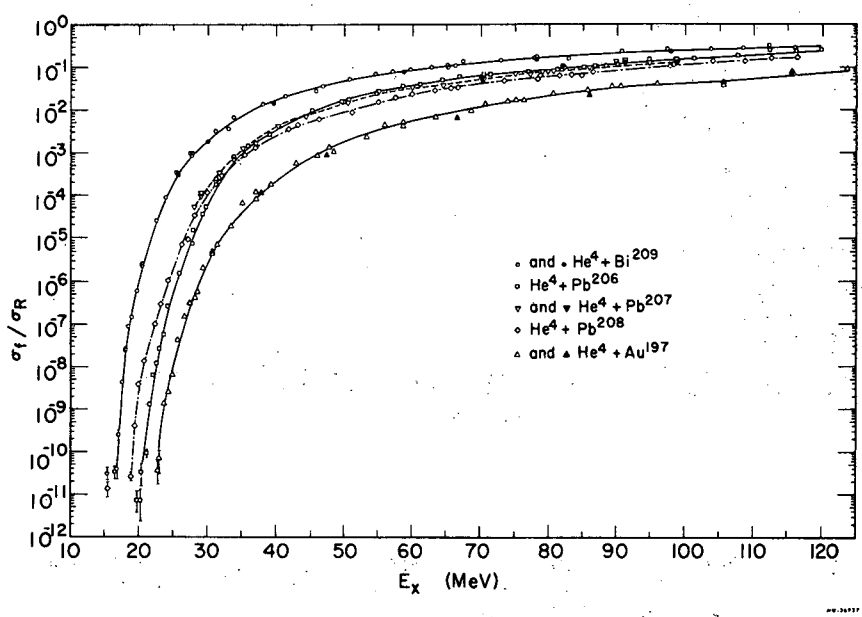

Fig. B.4-3. The ratio σ_f/σ_R as a function of excitation energy, E_x, of the compound nuclei formed in the bombardment of various targets with helium ions.

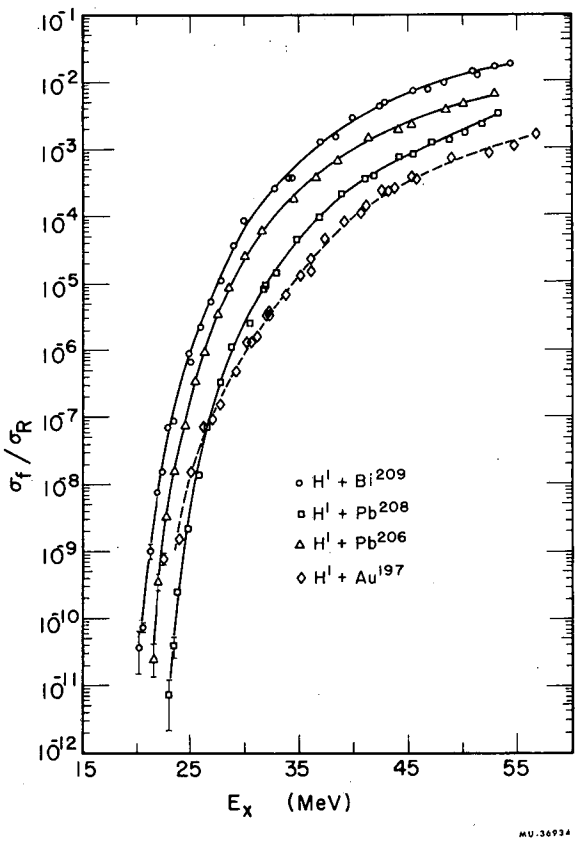

Fig. B.4-4. The ratio σ_f/σ_R as a function of excitation energy, E_x, of the compound nuclei formed in the bombardment of various targets with protons.

5. FISSION OF URANIUM-238 BY ARGON-40

Torbjørn Sikkeland

Using standard coincidence technique, we have measured fission cross sections, fragment-fragment angular correlation functions, and most probable kinetic energy release for binary fission in the interaction of U^{238} with Ar^{40}.

In Fig. B.5-1, experimental values for the total fission cross section are plotted versus the kinetic energy of Ar^{40}. The data have been corrected for energy resolution of the incident ions. In the same figure we have drawn the curve for the total interaction cross section. The latter was calculated by using the parabolic approximation to the real part of the optical potential with the parameter $V_0 = -70$ MeV, $r_0 = 1.26$ fermis, and $d = 0.440$ fermis.[1] The agreement is satisfactory, although there appear to be systematic differences near the barrier.

The angular correlation functions at the highest energies show two peaks with widely different widths. The narrower one consists of fragments from fissioning nuclei that are formed in a complete fusion (CF) of ion and target nuclei. From the angular relationship at this peak and the law of conservation of momentum, it is estimated that the most probable c. m. kinetic energy release in the fission of the nucleus 110^{278} is 221±3 MeV. The excitation energy of this nucleus formed in the interaction with 415-MeV Ar^{40} is about 220 MeV.

By comparing the c. m. energy of 221 MeV with the most probable final kinetic energy of the fragments, as seen by a detector, it is concluded that, on the average, about 25 neutrons are emitted from the two fragments.

The second peak in the correlation function corresponds to fission following an incomplete fusion (ICF) process. The ratio between the cross section for ICF to that of CF is found to be about 1.0, 0.85, and 0.33 at 415, 348, and 272 MeV, respectively.

At lower ion energy, the two peaks could not be separated.

Reference

1. For a description of these calculations see, e.g., V. E. Viola, Jr., and T. Sikkeland, Phys. Rev. 128, 767 (1962).

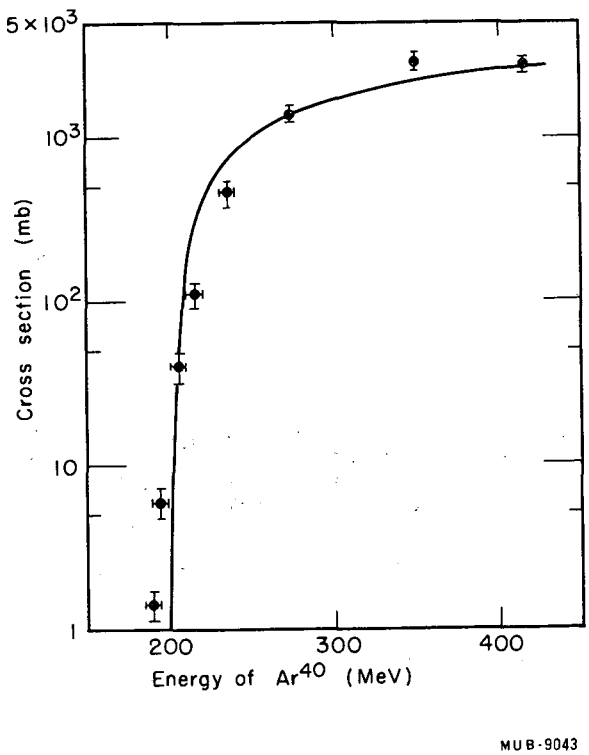

Fig. B.5-1. Comparison of experimental values of the total fission cross section with the curve calculated for the total interaction cross section.

C. NUCLEAR REACTIONS AND SCATTERING

1. CORRELATIONS AS REVEALED BY THE (p, t) REACTION†

Norman K. Glendenning

Nuclear physics has reached the point in its development where considerable work is being done to derive the properties of finite nuclei from a more or less basic starting point. Much of this activity centers around trying to reproduce the energy-level systematics and electromagnetic transition rates in spherical nuclei, some of whose states exhibit collective properties. The energy level systematics is of course the easiest part of such a program because the Hamiltonian is stationary at its eigenstates. Electromagnetic transition, inelastic scattering, and several-nucleon transfer probabilities all depend upon certain correlations among the nucleons. As a result transition rates can vary from strongly enhanced to strongly hindered when compared with the rate calculated for an uncorrelated state. These wide variations put a structure calculation to quite a severe test, much more so than the energy-level systematics. Moreover reactions, since the kinematics are at the disposal of the experimenter, in principle provide a more versatile tool than electromagnetic transitions in studying nuclear structure.

The subject of this note is the use of the two-nucleon transfer reaction in the above role. The theory for the reaction has been given elsewhere.[1]

The only systematic two-nucleon transfer experiments in a region where structure calculations have also been done are those of Hintz and collaborators in the nickel and tin regions.[2] In these experiments he measured the differential cross section of the (p, t) reaction connecting the ground states of the even isotopes, Sn^{A+2} (p, t) Sn^{A}. One is here probing certain ground-state correlations. The experimenters attempted to test the Kisslinger-Sorenson and Arvieu-Barranger-Veneroni calculations. They concluded that the structure calculations yield predictions for the reaction that are about orthogonal to the experiments. However, that analysis was based on a more approximate version of the two-nucleon transfer calculation than derived by me.[1] The approximation which I believe does the most damage to the extraction of nuclear information is the assumption that the triton can be treated as a point. The triton structure projects out the part of the motions in the nucleus of the transferred nucleons that can contribute to the reaction, and so plays an important role.

The effect of the point triton assumption on the overlap integrals Ω_ν is compared in the table with the values that correspond to a triton of the size indicated by electron scattering and a nucleus of the size generally accepted in structure calculations. The two results are in sharp contrast. Consequently the above two assumptions lead to quite different weights to the various terms, appearing coherently in the cross-section, and hence to quite different cross-sections.

Figure C.1-1 shows the experimental data together with the results of the point triton analysis used by the authors of the experiment. The third curve corresponds to a calculation based on the theory of Ref. 1. The parentage factors β were computed by use of the wave functions of Kisslinger and Sorenson. The overlap Ω_ν was computed using a finite-size triton, and the transfer amplitude B was computed in distorted wave approximation using a optical-model parameters for elastic scattering of proton and triton as nearly corresponding to the relavant situations as I could obtain from the literature. The triton optical-model parameters are in fact not very well known, and the calculation should be regarded as qualitative. There is one peculiar aspect of the experiment. The angular distribution is peaked at a very small angle corresponding to a very large scattering object, Fig. C.1-2. To reproduce this I had to suppress the contributions from the first five partial waves.

At this point it was necessary to determine if the elastic cross section, which determines the optical-model parameters for the reaction calculations, would allow this freedom. I therefore recomputed the elastic cross section for the triton but now setting to zero the amplitudes of the outgoing part of the first five partial waves. This did not introduce any detectable change in the cross section over the range of angles typically measured in experiments. Therefore elastic scattering, as regards the lower partial waves, only tells us that these waves are absorbed. The corresponding wave functions are accordingly highly ambiguous: only their asymptotic behavior is specified by the elastic scattering, although for the reactions we must have them at all points

inside the nucleus. Therefore my procedure in calculating the reaction is not inconsistent with the determination of the optical-model parameters from elastic scattering. Parenthetically I might add that the reaction may be useful in reducing the ambiguities in the optic parameters.

To conclude, this calculation suggests that the Kisslinger-Sorenson calculations, to the extent that they are tested by these experiments, are consistent with the experiments. This conclusion is contrary to that reached by the experimenters who used, however, fairly severe approximations, most notable of which concerns the incorrect projection on the nuclear wave function that is made by a point triton.

Footnote and References

†Contributed paper to APS meeting in Honolulu, Sept. 1965.

1. N. K. Glendenning, Phys. Rev. 137, B102 (1965).
2. G. Bassani, Norton M. Hintz, C. D. Kavaloski, J. R. Maxwell, and Glenn M. Reynolds, Phys. Rev. 139, B830 (1965).

Table C.1-I. Relative values of the overlap integrals Ω_ν which correspond to a point and finite-size triton.

ν	point	finite
1	1.	1.
2	1.2	0.3
3	1.4	0.1
4	1.5	0.03
5	1.6	0.008

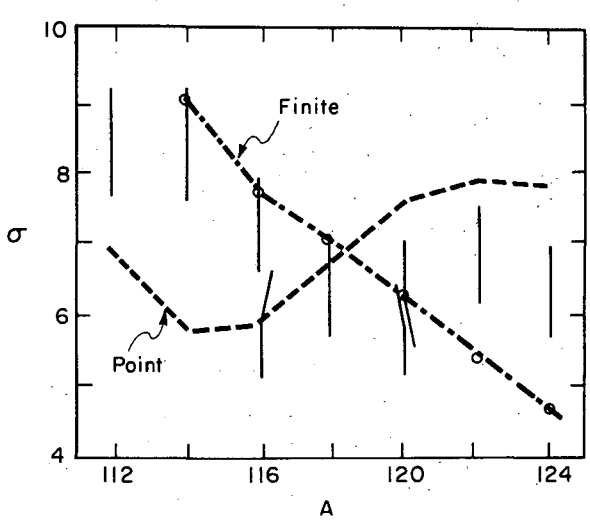

MUB-9394

Fig. C.1-1. Cross section for (p, t) connecting ground states of even tin isotopes. Experimental points shown by error bars. Dashed line marked "point" corresponds to experimenter's analysis based on various approximations including "point triton." Dashed line marked "finite" corresponds to analysis based on this author's theory of the reaction.

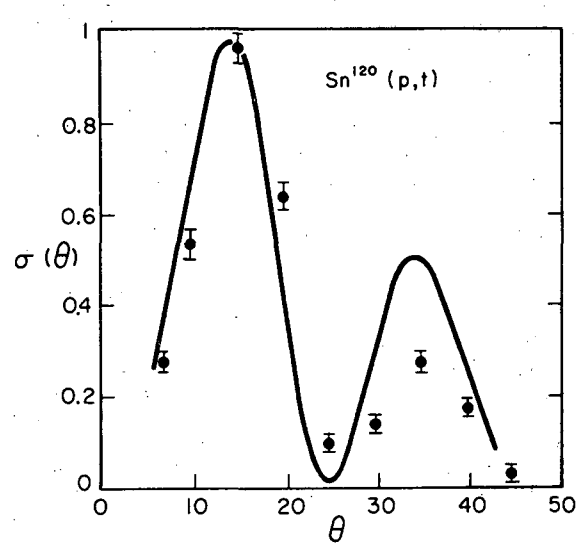

MUB-9395

Fig. C.1-2. Angular distribution for $Sn^{120}(p, t)$ with $E_p = 40$ MeV. Solid line is calculation based on theory of Ref. 1.

2. INELASTIC SCATTERING BASED ON A MICROSCOPIC DESCRIPTION OF NUCLEI*

Norman K. Glendenning and Marcel Veneroni†

In both experimental and theoretical work on inelastic scattering, attention has been focussed during the last 5 years on the strongly excited collective states. Information from the experiments has been extracted by assuming that the nucleus can be described by macroscopic parameters. The incident particle is pictured as interacting through an optical potential in which several collective degrees of freedom of the nucleus are included as deformation parameters for quadrupole and octupole shapes. The information content of the model is minimal and consequently (under appropriate circumstances) little more can be learned about the nucleus than the spin, parity, and deformation parameter of several of its states. A complete theory of the nucleus must describe all states, including but not solely the collective ones in terms of the underlying nucleon motions. Some progress in this direction has been made. It is important to subject these detailed structure calculations to the penetrating tests of which certain reactions are capable. Two-nucleon transfer and inelastic cross sections both depend upon nucleon correlations in the nucleus and are therefore appropriate.

We have formulated the calculation of inelastic cross sections in terms of a two-nucleon interaction and detailed microscopic wave functions of the nucleus.[1] The interaction between an incident nuclide and a nucleus is the sum of two-body potentials. Since each term contains only one nuclear nucleon, it is a one-body operator as far as the nucleus is concerned. Therefore it can connect only components in the wave functions of initial and final nuclear states that differ in at most the coordinates of one nucleon. In other words the direct excitation process involves at most a superposition of simple one-nucleon excitations. The form of the superposition depends of course on the wave functions. The probability of such a single-nucleon transition involves the matrix element of its interaction with the scattered particle, taken between its initial and final states in the nucleus, say "a" and "b". The interaction is expanded in multipoles to isolate the terms corresponding to transfer of specific units of orbital, spin, and total angular momenta (L, S, J). If the terms in the expansion that refer to the nucleus are denoted by $\mathfrak{F}_{LSJ}$, the above matrix element has the form

$$F^{ab}_{LSJ}(r) = \langle \phi_a \| \mathfrak{F}_{LSJ} \| \phi_b \rangle \quad ,$$

which is a function of the radial coordinate, r, of the scattered particle. Some single-particle form factors, F(r), appropriate to the nickel region are shown in Fig. C.2-1. In the limit of a zero-range force these form factors are just proportional to the product of the radial functions, $u_a\, u_b$, and the general character of F can be guessed in this way.

Any nuclear state in general involves the admixture of many single-particle configurations, and its form factor, according to the discussion above, will be a superposition of form factors corresponding to the various single-particle transitions by which its components are connected to the ground. The relevant single-particle form factors are shown in Fig. C.2-2 with signs and phases appropriate to the collective 2^+ state in Ni^{60}, showing how they add to give a large single-peaked scalar form factor, in rough analogy with the macroscopic model. That all contributions to the scalar form factor are coherent reflects the fact that the correlations in the low-lying collective states are built up by the spin-independent part of the force. In contrast the vector form factor for the same state is smaller by a factor five. The higher 2^+ states cannot be coherent in the same sense as the lowest one. As an example the scalar form factor for the 2^+_2 state is shown in Fig. C.2-3. It is of course made up from the same single-particle transitions, but they are not coherent. It is entirely possible, however, that a new type of collective state built up by the spin-dependent part of the force may exist at higher excitation energies. We found some evidence in our calculations for a trend to such correlations.

In the full report on this work we compared the neighboring nuclei Ni^{60} and Ni^{62} as being typical of the phenomena that occur for the nickel isotopes. It was found, for example, that the second and third 2^+ states can interchange their character in neighboring nuclei. Moreover, the shapes and magnitudes of the form factors exhibit a much greater variety than the macroscopic model with its strict selection rules. The variety is reflected in the cross sections as calculated for 11- and 40-MeV protons, which means that the details of the structure of these states is accessible to investigation by precision experiments (see Fig. 4). In contrast, strongly absorbed particles are quite insensitive to the nuclear interior, which makes them useful in measuring spins and parities but not as a probe of nuclear structure.

Footnotes and References

*Shortened version of paper (UCRL-16428, 1965) to be published in Phys. Rev.

†Summer visitor during 1964 and 1965. Permanent address: Laboratoire de Physique Théorique, Orsay (S. O.), France.

1. N. K. Glendenning and M. Veneroni, Phys. Letters 14, 228 (1965).

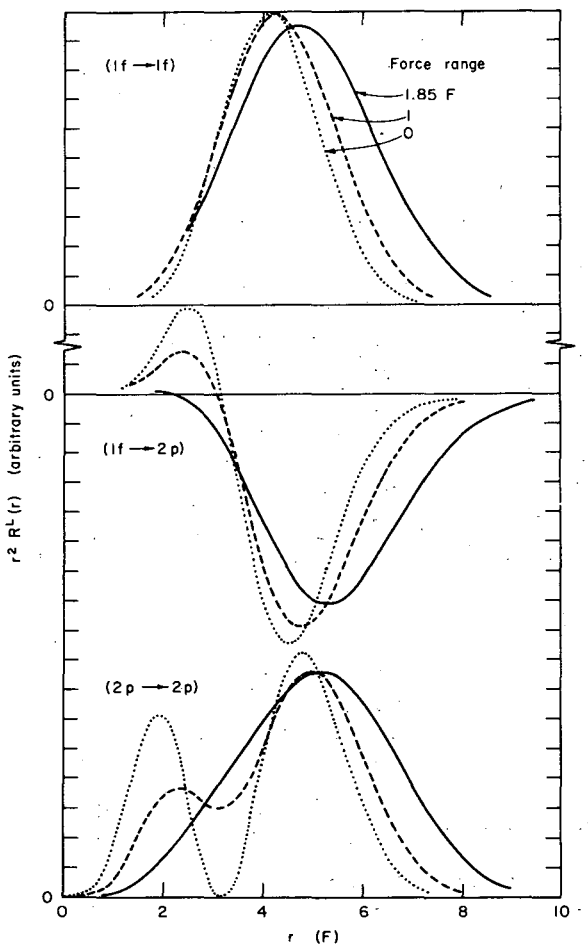

Fig. C.2-1. Shapes of quadrupole single-particle form factors for several transitions are shown for three values of the force range. The oscillator parameter $\nu = m\omega/\hbar$ has the value $0.25\,F^{-2}$ for the nickel isotopes.

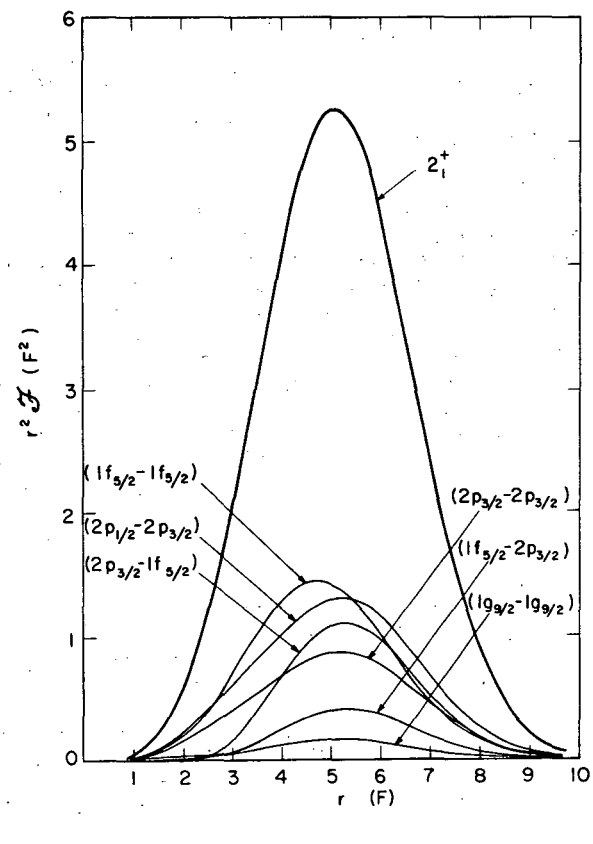

Fig. C.2-2. The quadrupole single-particle form factors that contribute to the 2^+ states of Ni^{60} are shown with the magnitudes and signs appropriate to the collective state showing how they all contribute constructively to the collective form factor.

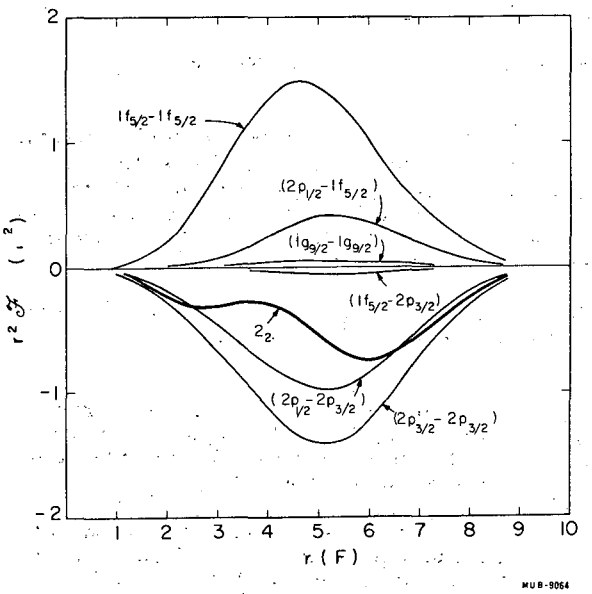

Fig. 2-3. The quadrupole single-particle form factors that contribute to the 2^+ states of Ni^{60} are shown with magnitudes and signs appropriate to the second excited (noncoherent) 2^+ state. The resultant small nuclear form factor is shown in contrast with Fig. C.2-2.

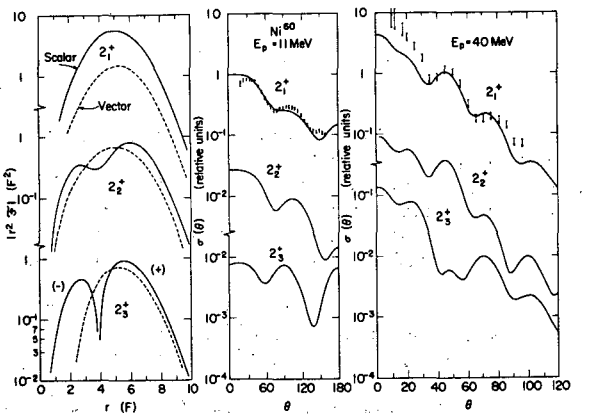

Fig. C.2-4. The form factors for three 2^+ states in Ni^{60} together with the corresponding cross sections for 11- and 40-MeV protons. Scalar form factors are shown by solid lines and vector form factors by dashed lines. Changes in sign are indicated by (-), since the absolute values of form factors are plotted.

3. INELASTIC SCATTERING OF 40.5-MeV ALPHA PARTICLES BY C^{12}, C^{13}, N^{14}, N^{15}, O^{16}, AND O^{18}

B. G. Harvey, J. R. Meriwether, J. Mahoney, A. Bussière de Nercy,*
and D. H. Horen†

The inelastic scattering of α-particles is a useful method for studying the surface shapes of medium-mass nuclei.[1] The levels most strongly excited are the 2+, 4+, and 3- collective states. It is therefore for the excitation of such levels that most of the angular distributions of scattered particles have been measured. The shapes of the angular distributions are determined almost entirely by the angular momentum transfer L, whereas the absolute value of the differential cross section depends upon the collective strength of the level excited.

The light nuclei present many opportunities for studying inelastic scattering of α-particles from targets for which the structure of the initial and final nuclear states is well understood. In many cases, collective effects are weak or absent.

In the experiment described here, 40.5-MeV α-particles from the 88-inch cyclotron were scattered from targets of C^{12}, C^{13}, N^{14}, N^{15}, O^{16}, and O^{18}. About 40 angular distributions were measured; many other excited states were observed but were too weakly populated (or too close to other states) to permit good angular distributions to be obtained.

In many cases the shape of an angular distribution was found to depend on the particular single-particle transition involved as well as on the angular momentum transfer. Figure C.3-1 shows the differential cross sections for excitation of the following levels: C^{12} 4.43 MeV 2+; C^{13} 3.68 MeV 3/2- and 7.55 MeV 5/2 -; N^{14} 3.945 MeV 1+ and 7.03 MeV 2+; N^{15} 6.33 MeV 3/2 -; O^{16} 6.916 MeV 2+; O^{18} 1.980 MeV 2+ and 3.92 MeV 2+. The abscissa is the function $kR\theta = 1/2\,(k_i + k_f)(1.3A^{1/3} + 1.2)\,\theta_{c.m.}$ in radians, where k_i and k_f are the center-of-mass wave numbers of the incident and outgoing particle at 0 deg, and A is the target nucleus mass number.

The first six angular distributions show a strong resemblance, especially in the systematic appearance of the first maximum at a value of $kR\theta$ of just under 6. In four cases the known wave functions of the initial and final states correspond predominantly to the promotion of a single nucleon from the $p_{3/2}$ to the $p_{1/2}$ shell, involving a change of 2 units of orbital angular momentum. The three oxygen L = 2 excitations (O^{16} 6.92 MeV 2+, O^{18} 1.98 MeV 2+, and 3.92 MeV 2+) gave angular distributions different from those of the $p_{3/2} \rightarrow p_{1/2}$ promotion. In O^{16} and O^{18} the $p_{1/2}$ shell is already filled.

Seven octupole transitions believed to be due predominantly to the single-particle promotion $p_{1/2} \rightarrow d_{5/2}$ were observed. The levels are: N^{14} 5.10 MeV 2- and 5.83 MeV 3-; N^{15} 5.276 MeV 5/2+ and 7.57 MeV 7/2+, O^{16} 6.131 MeV 3- and 8.870 MeV 2-; and O^{18} 5.09 MeV 3-. Excitation of the C^{12} 9.64 MeV 3- level gave an angular distribution clearly different from the other seven. Since C^{12} has no $p_{1/2}$ nucleons, the promotion $p_{1/2} \rightarrow d_{5/2}$ is obviously forbidden.

Figure C.3-2 shows the angular distributions for excitation of six levels by L = 1 transitions. The levels are: C^{13} 3.085 MeV 1/2+; N^{14} 4.91 MeV 0- and 5.69 MeV 1-; N^{15} 7.31 MeV 3/2+; O^{16} 7.115 MeV 1-; and O^{18} 4.45 MeV 1-. The corresponding single-particle transition is believed to be $p_{1/2} \rightarrow 2s_{1/2}$. The six angular distributions are remarkably alike.

Whereas the strengths of quadrupole and octupole inelastic excitations are expected to be proportional respectively to the reduced quadrupole and octupole electric transition probabilities B(E2) and B(E3),[2] there should be no similar relationship between dipole inelastic scattering and the corresponding B(E1) value. Since the two isospin states of the nucleon interact differently with an electromagnetic field, the Hamiltonian describing the interaction of a nucleus with a field can be separated into an isospin scalar and an isospin vector part. On making a multipole expansion, it is found that only the isospin vector part of the Hamiltonian contributes to the electric dipole (E1) transition amplitude, provided that the wave number of the photon is such that $kr \ll 1$.[3]

Since the interaction of α-particles through the nuclear forces is not isospin-dependent, there is no isospin vector component of the interaction Hamiltonian. The (scalar) Hamiltonian leads to no dipole excitation provided that the incident and scattered particles can be represented as plane waves and provided that $QR \ll 1$ (where Q is the momentum transfer $\underset{\sim}{k}_i - \underset{\sim}{k}_f$). The

observation of rather strong dipole excitations in this experiment shows that these assumptions are not valid. Probably the excitation is due mainly to failure of the plane wave assumption. Multiple excitations (as, previously reported for excitation of a 1- level in Ne^{20}) may also contribute.

Footnotes and References

*Laboratoire de Physique Nucleaire, Orsay (S.et. O.), France.

†Naval Radiological Defense Laboratory, San Francisco, California.

1. J. S. Blair, Phys. Rev. 115, 928 (1959).
2. W. T. Pinkston and G. R. Satchler, Nucl. Phys. 27, 270 (1961).
3. H. A. Bethe, Rev. Mod. Phys. 9, 69 (1937).
4. A. Springer and B. G. Harvey, Phys. Rev. Letters 14, 316 (1965).

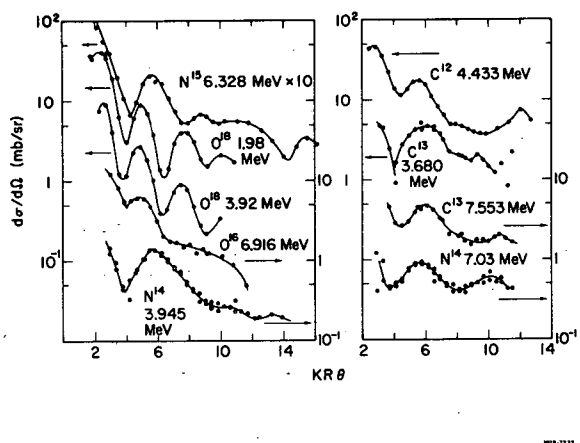

Fig. C.3-1. Angular distributions corresponding to the quadrupole excitation $P_{3/2} \rightarrow P_{1/2}$.

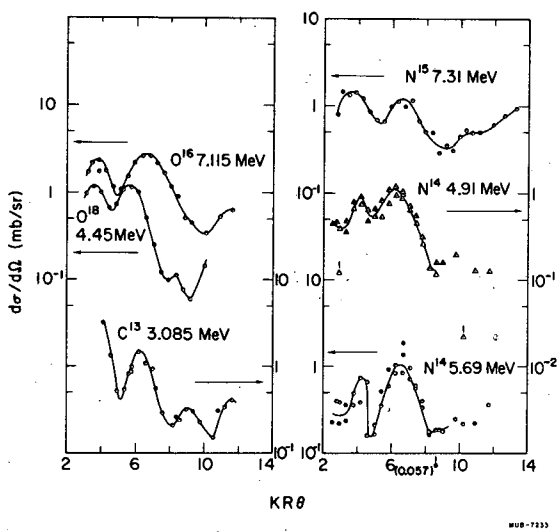

Fig. C.3-2. Angular distributions corresponding to the dipole excitation $P_{1/2} \rightarrow 2s_{1/2}$.

4. COMPARISON BETWEEN PHASE SHIFT AND COMPLEX POTENTIAL DESCRIPTIONS OF ELASTIC SCATTERING†

Jonas Alster‡ and H. E. Conzett

We want to emphasize the equivalence between parameterized phase-shift (PPS) and complex-potential model (CPM) analyses of the elastic scattering of strongly absorbed[1] "particles," such as deuterons, He^3, α particles, and heavier ions. We make specific comparisons, using analyses of α-particle scattering data. Then we point out several advantages of the PPS method, which encompasses all analyses[2-6] in which the partial-wave (complex) phase shifts are explicitly parameterized in the calculation and are not adjusted through an intermediary complex potential.

The differential cross section for elastic scattering is

$$\sigma(\theta) = |f(\theta)|^2,$$

with the scattering amplitude, in the absence of spin-dependent interactions, given by

$$f(\theta) = f_c(\theta) + \frac{i}{2k} \sum_{l=0}^{\infty} (2l+1)\, e^{2i\sigma_l} (1-\eta_l)\, P_l(\cos\theta), \tag{1}$$

where $f_c(\theta)$ is the Coulomb scattering amplitude, $k = (1/\hbar)(2\mu E)^{1/2}$, $\sigma_l = \arg\Gamma(1+l+in)$, with $n = z_1 z_2 e^2/\hbar v$. One can write

$$\eta_l = A_l \exp(2i\delta_l), \tag{2}$$

so that A_l, the amplitude of the outgoing lth partial wave, and δ_l, its nuclear phase-shift, are real. Thus, $0 \leq A_l \leq 1$, with $A_l = 1$ corresponding to no absorption and $A_l = 0$, to complete absorption of that partial wave. McIntyre et al.[2] introduced the (arbitrary) parameterization

$$A_l = 1 - \left[1 + \exp\left(\frac{l - l_A}{\Delta l_A}\right)\right]^{-1}, \quad \delta_l = \delta\left[1 + \exp\left(\frac{l - l_\delta}{\Delta l_\delta}\right)\right]^{-1} \tag{3}$$

as an improvement over the "sharp cut-off" model. This form for A_l has been justified by Elton,[5] whereas a form of δ_l suggested by Conzett et al.[3] as having qualitative theoretical justification differs from that of Eq. (3), particularly for $l < l_\delta$. However, we shall see for those cases examined here that the scattering amplitude is not seriously affected, because in the region of l values for which Eq. (3) is incorrect, $A_l \to 0$. This would not be the case for less strongly absorbed particles, and thus a theoretically proper form of δ_l would be required.

The CPM analysis determines A_l and δ_l by solving the equation satisfied by the radial wave function, $f_l(r)$:

$$\left[\frac{d^2}{dr^2} - \frac{l(l+1)}{r^2} + k^2 - \frac{2\mu}{\hbar^2} U(r)\right] f_l(r) = 0, \tag{4}$$

where $U(r) = V_c(r) + V_N(r)$, the Coulomb plus the nuclear potential. In order to provide a description of both the elastic scattering and absorptive processes, the latter is taken to be complex: $V_N(r) = -[V(r) + iW(r)]$. Comparison at $r = \infty$ of $f_l(r)$ with the solution of Eq. (4) for $V_N(r) = 0$ then gives A_l and δ_l. Strongly absorbed particles sample only the surface region of the nucleus, so one is justified in questioning the significance of using a parameterized complex potential to describe the scattering. The PPS analysis parameterizes the A_l and δ_l directly, so it is clear that the two analyses can be equivalent.

For purposes of comparison, one can make the correspondence between l and r, the distance of closest approach for a particle of orbital angular momentum $[l(l+1)]^{1/2}\hbar$, through the relation

$$kr = n + [n^2 + l(l+1)]^{1/2}. \tag{5}$$

We indicate this correspondence between coordinate (r) space and orbital angular-momentum (l) space by writing $A_l(r)$. The value of $r = R_a$ for which $A_l(r) = 1/2$ should not be expected to

agree with the value of $r = R$ for which $V(R) = V(0)/2$ in the CPM. Similarly, t, the interval Δl_A converted to coordinate space via Eq. (5), would not necessarily agree with the analogous complex-potential surface-thickness parameter a. These points have been developed previously.[4]

In order to demonstrate these considerations more explicitly, we have made PPS analyses of some existing data on the elastic scattering of α particles from A, Cu, and Pb at 18, 40, and 48 MeV, respectively.[7-9] These data had previously been used for a CPM analysis.[10] Figures C.4-1 shows one comparison between experimental and calculated angular distributions for both PPS and CPM analysis. The values of the parameters resulting from these analyses are compiled in Table C.4-I, together with those resulting from PPS[2] and CPM[11] analyses of data on the scattering of 22- and 40-MeV α particles from Ag. The expected differences between the complex-potential parameters, R and a, and the PPS parameters, R_a and t, are seen. If one now looks at the actual scattering amplitude parameters describing the l dependence of A_l and δ_l, the equivalence of the two analyses is seen. That is, the l_A and Δl_A values determined from the separate analyses are in excellent agreement, and the differences in the coordinate space parameters, R_0 and a vs R_a and t, clearly result from their different physical definition.

In summary, PPS and CPM analyses of the elastic scattering of strongly absorbed particles are seen to be equivalent. Some advantages of the PPS treatment are the following:

1. The calculation is simpler than for the CPM, since the numerical solution of Eq. (4) is bypassed. This is particularly advantageous whenever large numbers of partial waves contribute to the scattering.

2. The form of $A_l(r)$ gives a clear physical interpretation of the absorption of the incident particles, and we believe that for strong-absorption scattering the determined $A_l(r)$ curve is essentially unique. On the other hand, the CPM varies the parameters of $V_N(r)$ to produce this $A_l(r)$ curve, and ambiguities in the potentials describing, for example, α-particle[12] and deuteron[13] scattering result from the fact that different potentials can give essentially the same $A_l(r)$ and $\delta_l(r)$ values. Clearly the value of $V_N(r)$ for $r < r'$, where $A_l(r) = 0$ for $r < r'$, can have no effect on the scattering.

3. Equation (1) for the scattering amplitude is valid, also, in the relativistic region insofar as spin effects are unimportant.

Footnotes and References

†Shortened version of Phys. Rev. 139, B50 (1965).

‡Present address: Physics Department, Northeastern University, Boston, Massachusetts.

1. As used here, absorption encompasses all transitions out of the entrance channel.
2. For α-particle scattering: J. S. Blair, Phys. Rev. 95, 1218 (1954), "sharp cutoff" model; J. A. McIntyre, K. H. Wang, and L. C. Becker, Phys. Rev. 117, 1337 (1960), modified "sharp cutoff" model.
3. For heavy-ion scattering: J. Alster and H. E. Conzett, in Proceedings of the Second Conference on Reactions between Complex Nuclei, edited by A. Zucker, E. C. Halbert, and F. T. Howard (John Wiley and Sons, Inc., New York 1960), p. 175; J. Alster, Heavy-Ion Elastic Scattering (Ph. D. Thesis), UCRL-9650, 1961 (unpublished); J. A. McIntyre, S. D. Baker, and K. H. Wang, Phys. Rev. 125, 584 (1962); H. E. Conzett, A. Isoya, and E. Hadjimichael, in Proceedings of the Third Conference on Reactions between Complex Nuclei, edited by A. Ghiorso, R. M. Diamond, and H. E. Conzett (University of California Press, Berkeley, 1963).
4. J. Alster and H. E. Conzett, Phys. Rev. 136, B1024 (1964).
5. Applications to high energy nucleon scattering have been developed by K. R. Greider and A. E. Glassgold, Ann. Phys. (N. Y.) 10, 100 (1960) and L. R. B. Elton, Nucl. Phys. 23, 681 (1961).
6. For a very complete analytical development of PPS analyses of elastic scattering of strongly absorbed particles see W. E. Frahn and R. H. Venter, Ann. Phys. (N. Y.) 24, 243 (1963); R. H. Venter, Ann. Phys. (N. Y.) 25, 405 (1963).
7. L. Seidlitz, E. Bleuler, and D. J. Tendam, Phys. Rev. 110, 682 (1958).
8. G. Igo, H. E. Wegner, and R. M. Eisberg, Phys. Rev. 101, 1508 (1956).
9. R. E. Ellis and L. Schecter, Phys. Rev. 101, 636 (1956).

10. G. Igo, Phys. Rev. 115, 1665 (1959).
11. W. B. Cheston and A. E. Glassgold, Phys. Rev. 106, 1215 (1957); A. E. Glassgold, Progress in Nuclear Physics, edited by O. R. Frisch (Pergamon Press, London, 1959), Vol. 7, p. 123.
12. G. Igo, Phys. Rev. Letters 1, 72 (1958).
13. C. M. Perey and F. G. Perey, Phys. Rev. 122, 755 (1963); E. C. Halbert, Nucl. Phys. 50, 353 (1964).

Table C.4-I. Comparison of parameters resulting from PPS and CPM analyses of alpha-particle scattering data.

Data		CPM Analysis						PPS Analysis			
		parameters									
	MeV	V	W	R	a	l_A	Δl_A	l_A	Δl_A	R_a	t
$A + He^4$	18	100	15	5.4	0.6	9.7[a]	0.6	7.5[a]	0.6	6.67	0.33
$Cu + He^4$	40	49.3	11	6.8	0.5	17.8	0.8	17.0	0.8	7.92	0.30
$Pb + He^4$	48	25	15	8.1	0.6	21.1	1.3	21.0	1.3	10.16	0.41
$Ag + He^4$ [b]	22	50	20	7.5	0.6	10.5	1.5	10.8	0.75[c]	9.74	0.33
		150	20	7.5	0.6	11.3	1.3	10.8	0.75	9.74	0.33
$Ag + He^4$ [b]	40	50	20	7.1	0.6	19.3	1.2	19.0	1.1	9.27	0.40
		150	20	7.1	0.6	19.8	1.1	19.0	1.1	9.27	0.40

a. The disagreement in l_A values in this case arises from the difference in fits to the experimental data.
b. From references 2 (McIntyre et al.) and 11.
c. This Δl_A value resulted from an analysis in which δ_l was zero. This may account for its being appreciably lower than the value determined from the CPM analysis.

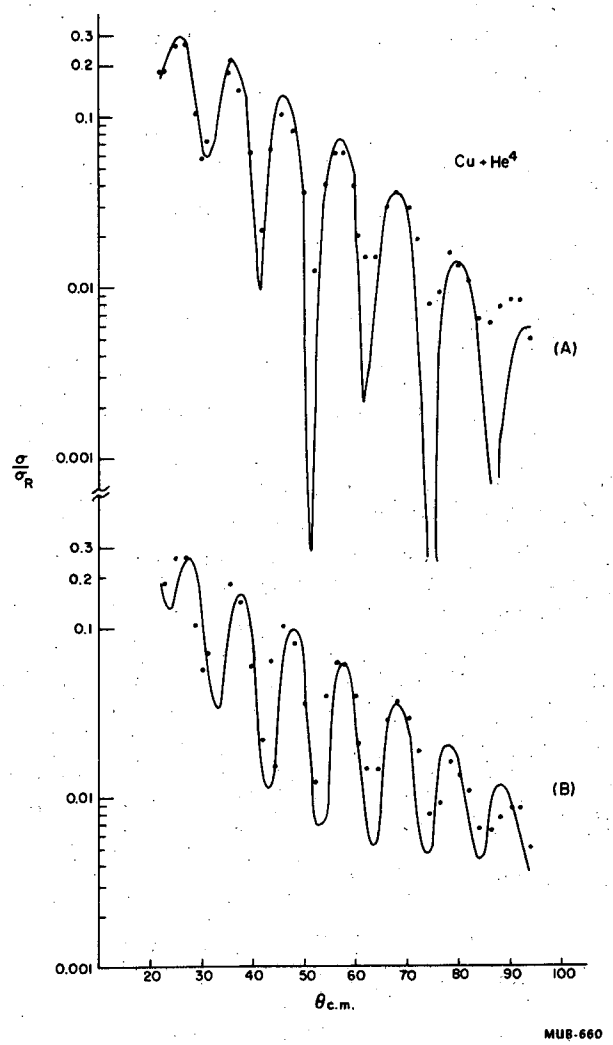

Fig. C.4-1. (A). The solid line is the CPM fit to the elastic scattering of He^4 from Cu (Ref. 10). The parameters are $V = -49.3$, $W_0 = -11$, $R = 1.14A^{1/3} + 2.24$, $a = 0.5$.

(B). The solid line gives the PPS fit to the same data. The parameters are: $l_A = 17$, $\Delta l_A = 0.8$, $\delta = 0.7$, $l_\delta = 17$, $\Delta l_\delta = 1.0$.

5. ENERGY DEPENDENCE OF THE POLARIZATION IN p-O^{16} ELASTIC SCATTERING BETWEEN 21 AND 53 MeV†

E. T. Boschitz,‡ M. Chabre,§ H. E. Conzett, and R. J. Slobodrian

It is clear that the cross sections and polarizations of medium-energy protons scattered by the heavier nuclei are well described by the optical model; however, its applicability to light nuclei is less certain. An extensive analysis[1] of p-C^{12} and p-O^{16} differential cross-section data between 10 and 20 MeV has indicated that the optical model is surprisingly successful in accounting for the p-C^{12} data, but less so for p-O^{16}, where the parameters vary severely as a function of energy.

In order to study the validity of the optical model for light nuclei at higher energies, in particular, to investigate the energy dependence of the spin-orbit potential, we have determined the polarization in the p-O^{16} elastic scattering at seven energies between 21 and 53 MeV. The source of polarized protons is the alpha-hydrogen scattering utilizing the variable-energy feature of the Berkeley 88-inch cyclotron. In the data presented in Fig. C.5-1 (the lines are visual aids and have no theoretical significance), a drastic change in the polarization pattern is found between 21 and 25 MeV. Above this energy the polarization distribution varies slowly with energy. We have also measured the differential cross section at 42.1 and 52.5 MeV to supplement the available data at 30.3 MeV (Rutherford Laboratory).

The optical model analysis was performed in Berkeley with SCAT 4 and at NASA with a modified version of SCAT 4 employing the Argonne search routine.[2] In this preliminary analysis, we have considered only the polarization data in the less energy-dependent region, and have limited the search to the conventional seven-parameter potential consisting of a real central potential of the Saxon-Woods type (V, a, R_0), a surface peaked imaginary potential with a derivative Saxon-Woods form factor (W, a_I, R_I), and a spin-orbit potential of the Thomas type (V_s, a, R_0). Keeping R_0 fixed at 1.25 ± 0.05 fermis and gridding on a, a_I, and R_I, we have searched for the best parameters V, W, V_s, to give good fits to both polarization and cross-section data. For the search at 32.8 MeV we have used the 30.3-MeV cross-section data from the Rutherford Laboratory; at 36.7 MeV interpolated cross sections served as a guide to the search routine. The "best fits" were selected by visual inspection under the constraint that the parameters were reasonable and compromising over this energy range. The results of the analysis are shown in Fig. C.5-2. The solid lines present the optical-model predictions with the parameters from Table C.5-I. Except at the highest energy, quite satisfactory fits to polarization and cross-section data can be obtained up to 120 deg c.m.

At present, we conclude that the optical model is reasonably applicable to the p-O^{16} elastic scattering at these energies, although there are some fluctuations in the parameters.

Footnotes and References

†Article in Proceedings of International Conference on Polarization Phenomena of Nucleons, Karlsruhe, Sept, 1965.

‡Permanent address: NASA-Lewis Research Center, Cleveland, Ohio.

§NATO fellow on leave from CNRS, Institut Fourier, Grenoble, France.

1. J. S. Nodvik, C. B. Duke, and M. A. Melkanoff, Phys. Rev. 125, 975 (1962); C. B. Duke, Phys. Rev. 129, 681 (1963).

2. We would like to thank Dr. H. Volkin and Dr. C. Giamati of the Lewis Research Center for the use of their optical-model program.

Table C.5-I. Parameters used for optical-model predictions.

E	V	W	V_s	a	a_I	R_0	R_I
32.8	41.0	5.4	7.5	0.65	0.50	1.25	1.35
36.7	41.3	6.3	8.1	0.67	0.50	1.25	1.30
42.0	36.0	3.5	8.1	0.75	0.76	1.20	1.30
52.5	31.4	3.6	5.7	0.70	0.44	1.20	1.25

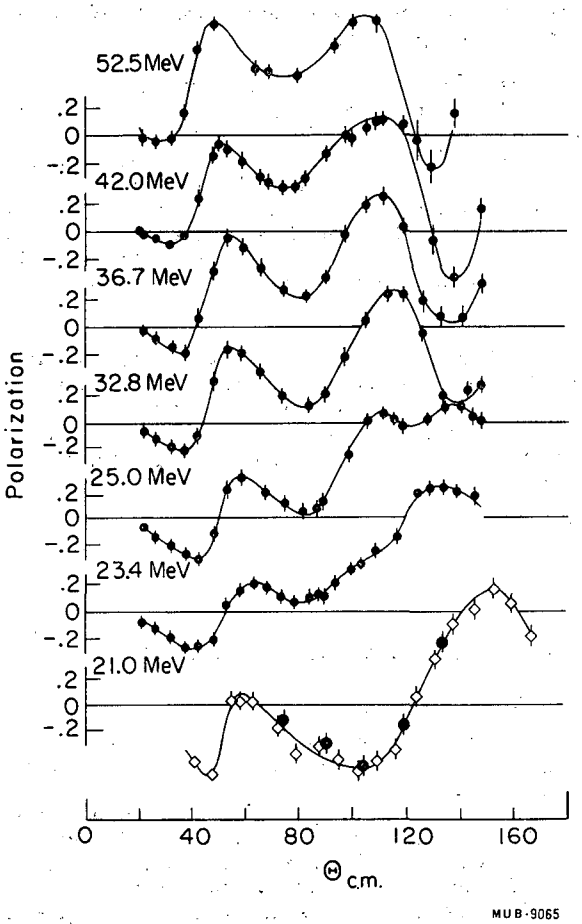

Fig. C.5-1. Energy dependence of the p-O^{16} polarization.

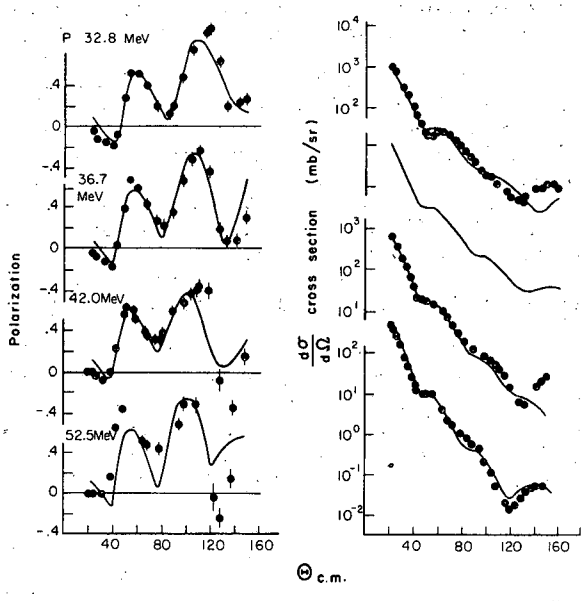

Fig. C.5-2. Optical-model predictions to the polarization and cross-section data, using the parameters of Table C.5-I.

6. POLARIZATION IN p-He^4 SCATTERING BETWEEN 27 AND 63 MeV†

E. T. Boschitz*, M. Chabre‡, H. E. Conzett, E. Shield, and R. J. Slobodrian

Using the polarized-proton facility at the Berkeley 88-inch cyclotron, we have measured the asymmetries in the elastic scattering of polarized protons from He^4 at energies of 26.8, 34.2, 44.1, 54.8, and 63.3 MeV. These energies were selected so that experimental results would then be available at approximately 5-MeV intervals over the region 10 to 63 MeV, the latter being the maximum energy available at this facility. With the beam polarization P_1 known from experimental results, we then determined from the measured asymmetries $\epsilon(E, \theta)$ the polarizations $P(E, \theta) = \epsilon(E, \theta)/P_1$. A phase-shift analysis of these and other data available throughout this energy range has been started, and we report here preliminary results of this analysis.

Figure C.6-1 shows our data along with those from the Rutherford Laboratory at 29, 40, and 48 MeV[1] and 21-MeV data from Berkeley.[2] The polarizations calculated from the phase-shift solutions are also shown. Available or interpolated differential cross-section data[3,4] were included in the analysis at all energies, although such data at 66 MeV were limited to c. m. angles forward of 60 deg. The 55-MeV polarization results show a continuation of the trend established with the lower-energy data, and they are in substantial disagreement with the polarization calculated by Kanada and Horikawa[5] from phase shifts derived from analysis of 55-MeV differential cross-section data.[4] Their calculated $P(\theta)$ has three maxima, of values approximately +0.37, -0.77, and +0.93 near c. m. angles of 50, 95, and 125 deg, respectively.

Figure C.6-2 shows our preliminary phase-shift results. We use the notation $\eta_l^{\pm}\exp(2i\delta_l^{\pm})$ for the (complex) amplitude of the outgoing lth partial wave, so that η^+ and δ_l^+, the absorption parameter and nuclear phase shift for the $j = l + 1/2$ state, and η_l^- and δ_l^- for the $j = l - 1/2$ state, are real. The smooth curves show the general energy dependence of the $\delta_l^{\pm}$, although the actual preliminary values show some scatter about these curves. Until further more complete searches are made, we do not ascribe physical significance to the slightly oscillatory behavior of δ_1^- and δ_2^- near and above 40 MeV. As is seen in the table listing the values of $n_l^{\pm}$, there are accompanying variations in these parameters in the same energy region. This behavior is not to be expected, because all possible reaction thresholds occur at lower energies, and a smoother behavior would be more plausible.

The arrows at 22.9 and 35.2 MeV in Fig. C.6-2 mark the threshold for the first reaction channel, going to d+^{3}He, and the energy at which all channels are open, the last being the 3p+2n five-body channel. In this energy interval the absorption appears to be strongest in the $l = 2$ ($j = 5/2$) partial wave, with appreciable absorption also taking place in the $l = 1$ ($j = 1/2$) and $l = 3$ ($j = 7/2$) waves. We see no evidence of threshold effects, but data more closely spaced in energy would be required in order to study such questions.

Footnotes and References

†Article in Proceedings of International Conference on Polarization Phenomena of Nucleons, Karlsruhe, September 1965.

*Permanent address: NASA-Lewis Research Center, Cleveland, Ohio.

‡NATO fellow on leave from CNRS, Institut Fourier, Grenoble, France.

1. M. K. Craddock, R. C. Hanna, L. P. Robertson, and B. W. Davies, Phys. Letters 5, 335 (1963); P. L. A. Progress Report, NIRL/R/60, 44, 1963.
2. H. E. Conzett, G. Igo, and A. Nir (Lawrence Radiation Laboratory), private communication.
3. P. W. Allison, Thesis, University of Colorado, 1964; S. M. Bunch, H. H. Forster, and C. C. Kim, Nucl. Phys. 53, 241 (1964); M. K. Brussel and J. Williams, Phys. Rev. 89, 422 (1953); B. W. Davies, M. K. Craddock, R. C. Hanna, L. P. Robertson, and R. E. Shamu, P. L. A. Progress Report, NIRL/R/81, 69, 1964; A. M. Cormock, J. N. Palmieri, N. F. Ramsey, and Richard Wilson, Phys. Rev. 115, 599 (1959).
4. S. Hayakawa, N. Horikawa, R. Kajikawa, K. Kikuchi, H. Kobayakawa, K. Matsuda, S. Nagata, and Y. Sumi, J. Phys. Soc. Japan 19, 2004 (1964).
5. H. Kanada and N. Horikawa, Nagoya University, Physics Department Report T-5, March 1965.

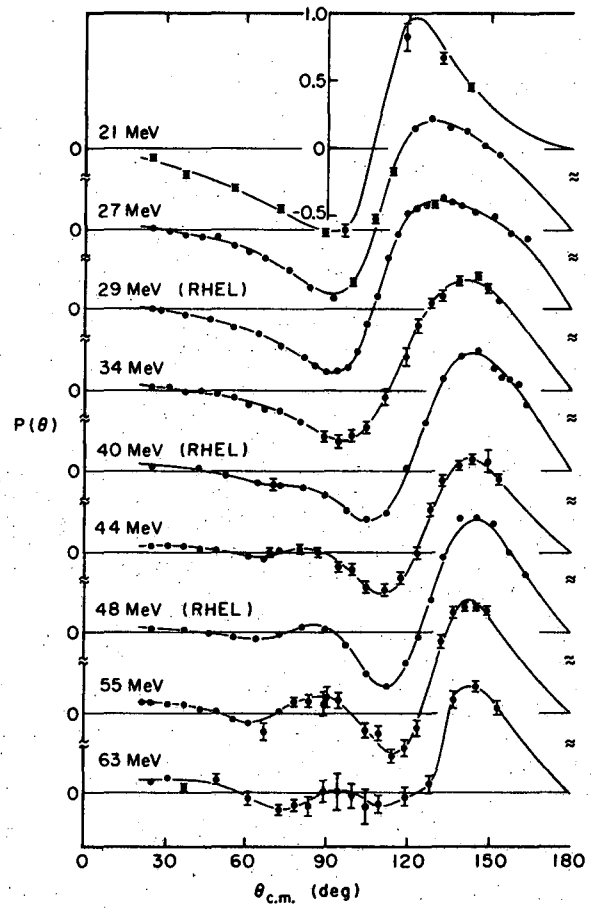

MUB-7490

Fig. C.6-1. Polarization P(θ) in p-He^4 elastic scattering. The dots are the experimental data (references in text). The curves represent values calculated in this analysis.

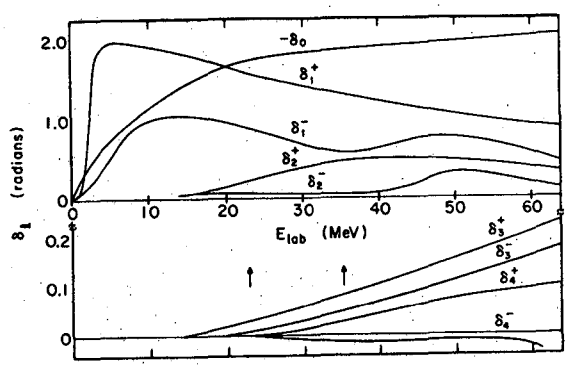

	E (MeV)	27	30	34	40	44	48	55	63
	η_0	1.00	1.00	1.00	0.92	0.99	0.94	1.00	0.96
	η_1^+	1.00	0.99	1.00	0.99	0.77	0.95	0.75	0.97
Absorption	η_1^-	0.92	0.94	0.97	0.90	0.84	0.92	0.84	0.81
parameters	η_2^+	0.81	0.85	0.82	0.77	0.85	0.97	1.00	0.88
	η_2^-	1.00	1.00	1.00	0.80	0.78	0.85	0.86	0.92
	η_3^+	0.98	0.94	0.72	0.84	0.71	0.71	0.77	0.78
	η_3^-	1.00	1.00	0.97	0.92	0.83	0.92	0.85	0.67
	η_4^+	0.93	0.96	1.00	0.96	0.99	0.99	0.99	0.99
	η_4^-	1.00	0.98	0.98	1.00	0.89	0.93	0.98	0.98

MUB-7491

Fig. C.6-2. Phase-shift parameters from preliminary analysis of the data. The symbols are defined in the text.

7. PROTON POLARIZATION IN SMALL-ANGLE p-He^4 SCATTERING AT 38.7 MeV†

E. Boschitz*, M. Chabre‡, H. E. Conzett, E. Shield, and R. J. Slobodrian

In the last two years different phase-shift analyses[1,2] of the p-He^4 cross section and polarization data[3,4] around 38 MeV have been published. Recently Giamati and Thaler[5] have discussed the possibility of determining a unique phase-shift solution by means of further double or triple scattering experiments. They point out that sufficient information can be obtained by a double scattering experiment, obviously more easy and precise than a triple scattering experiment, carried out in the region of interference between the Coulomb and the nuclear scattering amplitude. In this region, significantly different polarizations (about 0.20) are calculated from the different sets of phase shifts. Therefore small-angle polarization measurements with an absolute precision of about ±0.03 should allow one to decide between them. Recently the rotation of the polarization has been measured at 48 MeV.[6] The results are more consistent with the GMT or GMT-B type of solution,[5] but the energy at which the measurement was made differs appreciably from the energy of the phase-shift solutions.

We have measured the polarization at small angles with a standard double scattering technique. The experimental setup was basically the same as was described in an earlier paper.[7] The polarized protons were produced as recoils from a hydrogen target bombarded by a beam of α particles at approximately 80 MeV. The proton polarization was taken to be $P_1 = +0.83 \pm 0.03$, with the probable error arising principally from counting statistics.[8] The protons were scattered from the He-gas target at a mean energy of 38.7 ± 0.6 MeV. The intensity distribution and location of the beam at the gas target center, as well as its alignment with respect to the precision scattering table, were determined by beam profile measurements. For this purpose an ionization chamber with a tantalum slit 0.16 cm wide was used as a scanner. Beam radiographs on x-ray film were also obtained in order to get information on the actual beam shape. The beam width was 0.9 cm at the target center, and its divergence in the horizontal plane was ±0.10 deg. The maximum angular error in positioning the detectors was ±0.12 deg; this corresponds in first order to an instrumental asymmetry $\epsilon \leq \pm 0.003$ calculated from the known data for the cross section in the small-angle region.

Four CsI detectors mounted on DuMond 6363 phototubes were used. Two of them were fitted with collimation systems, designed especially for small-angle measurements, which provided an angular resolution of ±0.3 deg. The two remaining ones were used for check measurements at larger angles with the usual angular resolution (±1.5 deg).

In making the measurements, instrumental asymmetries were minimized by interchanging detector assemblies (and associated electronics). The smallest angle at which measurements were taken was 8 deg lab, and checks were carried out to insure that no scattering from the target window was detected. At smaller angles a large background counting rate produced results with a large uncertainty. The background was determined by reducing the pressure of the He gas from the operating pressure of 8 atmospheres down to 1 atmosphere, and obtaining spectra for equal charge collected in the monitoring system, and, alternatively, by inserting brass absorbers in front of the CsI crystals.

Figure C.7-1 shows our results along with larger-angle data from reference 4. Our measurements at 63.4 and 99.4 deg c.m. served as check points. With the exception of the polarization value at 10 deg c.m. all small-angle data favor the SY-A phase-shift solution.[1,5] However, the 10-deg c.m. data point, which is closest to the Coulomb interference minimum in the differential cross section, suggests that an intermediate phase shift set between SY-A and GMT-B might be found to better represent the experimental data to date. Also, in view of the data points between 50 and 90 deg c.m., it is interesting to notice that the SY solution, containing partial waves only up to $l = 3$, behaves too smoothly in this angular region, while the GMT($l_{max} = 5$) solution provides oscillations of larger amplitude than are present in the data. The SY-A solution does not include g waves, which could be contributing to the scattering at this energy ($kR \approx 4.25$). This possibility is supported by the Harwell polarization data[9] at 29, 40, and 48 MeV. While the 29-MeV data behave quite smoothly around 70 deg c.m. a "kink" appears at 40 MeV and finally develops into a new oscillation at 48 MeV. Thus, we feel that a complex phase-shift analysis of the 38-MeV data should definitely include at least $l = 4$ partial waves, and we expect that the small-angle values of the polarization will help to establish a unique solution.

Footnotes and References

†Shortened version of Phys. Letters 15, 325 (1965).

*Permanent address: NASA-Lewis Research Center, Cleveland, Ohio.

‡NATO Fellow on leave from CNRS, Institut Fourier, Grenoble, France.

1. S. Suwa and A. Yokosawa, Phys. Letters 5, 351 (1963).
2. C. C. Giamati, V. A. Madsen, and R. M. Thaler, Phys. Rev. Letters 11, 163 (1963).
3. M. K. Brussel and J. H. Williams, Phys. Rev. 106, 286 (1957).
4. C. F. Hwang, D. H. Nordby, S. Suwa, and J. H. Williams, Phys. Rev. Letters 9, 104 (1962).
5. C. C. Giamati and R. M. Thaler, Nucl. Phys. 59, 159 (1964).
6. T. H. Griffith, D. C. Imrie, G. J. Lush, and L. A. Robbins, Congrès International de Physique Nucléaire, Paris, July 1964, Abstract No. 1 bis/C 80, p. 19; also private communication.
7. H. E. Conzett, H. S. Goldberg, E. Shield, R. J. Slobodrian, and S. Yamabe, Phys. Letters 11, 68 (1964).
8. An additional uncertainty of 5 to 10% in P_1 will be resolved in a future measurement, but this uncertainty does not affect the conclusions stated here.
9. M. K. Craddock, R. C. Hanna, L. P. Robertson, and B. W. Davies, Phys. Letters 5, 335 (1963).

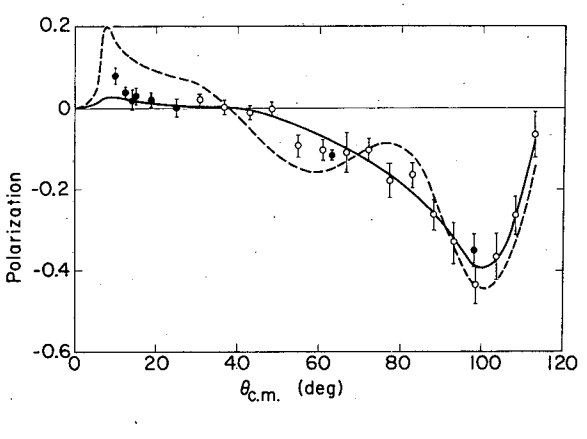

Fig. C.7-1. Polarization P as function of c. m. scattering angle. The open circles shown are the data taken from Ref. 4, the full circles are the result of this investigation. The curves are taken from Ref. 5. The solid curve is the prediction of the SY-A phase shift solution, the dashed line corresponds to the GMT-B solution.

8. THE REAL PART OF THE SCATTERING AMPLITUDE AT HIGH ENERGIES†

Homer E. Conzett

Analyses of p-p elastic scattering data[1-8] in the region 3 to 23 GeV/c and $\pi^{\pm}$-p data[7] near 10 GeV/c have provided strong evidence for the existence of a repulsive real part of the (spin-independent) nuclear forward scattering amplitude at these momenta. In both instances the ratio of real to imaginary parts of the forward amplitude, $\alpha(0) = \mathrm{Re}A_n(0)/\mathrm{Im}A_n(0)$, is approximately -0.25. The possiblity of spin dependence in the p-p case provides an alternative explanation,[2] but the π-p result has no such alternative explanation since the spin-flip amplitude goes to zero in the forward direction.[9]

Spin-independent models proposed[10, 11] to describe the data have employed the basic assumption that the elastic scattering is produced by the strongly absorptive processes at high energy, resulting in a scattering amplitude that is either completely imaginary or has, at least, a much larger imaginary than real part. A recent treatment[12] develops an impact-parameter expansion for the amplitude and assumes, for p-p scattering, a repulsive real contribution from small impact parameters. Support for this claim is provided by dispersion-relations calculations,[13, 14] which have given the proper magnitude and sign of $\alpha(0)$. In neither case, however, is suggestion made as to the origin of the $\mathrm{Re}A_n$ with a sign corresponding to a repulsive potential.

The purpose of this note is to point out that both the necessity for and the sign of the $\mathrm{Re}A_n$ can result from purely absorptive processes. Consider the partial-wave expansion for the nuclear scattering amplitude,[15]

$$A_n(\theta) = \sum_l (2l+1) \frac{(\eta_l - 1)}{2ik} P_l(\theta), \tag{1}$$

so that

$$\frac{\mathrm{Re}A_n(0)}{\mathrm{Im}A_n(0)} = \alpha(0) = \frac{\sum_l (2l+1)\, \mathrm{Im}\eta_l}{\sum_l (2l+1)(1-\mathrm{Re}\eta_l)} \; ; \tag{2}$$

we write

$$\eta_l = |\eta_l| \exp(2i\delta_l), \tag{3}$$

so that $|\eta_l|$, the (absolute) amplitude of the outgoing lth partial wave, and δ_l, the phase shift, are real quantities. Since $0 \leq |\eta_l| \leq 1$, with $|\eta_l| = 1$ corresponding to no absorption and $|\eta_l| = 0$ to complete absorption of that partial wave, it follows that $\mathrm{Im}A_n(0) \geq 0$. Thus $\alpha(0) < 0$ can result only from the condition that $\mathrm{Re}A_n(0) < 0$, which from (2) and (3) requires that

$$-\frac{\pi}{2} \leq \delta_l \leq 0 \tag{4}$$

for a sufficient number of partial waves. In particular, one expects (4) to be necessary for values of l near $L = kR$, with R defined as the absorption radius,[16, 17] because of the (2l+1) weighting factor in (2). Also, in instances of strong absorption $|\eta_l|$ may approach zero for $l < (L - \Delta l/2)$ with $\Delta l << L$, where Δl is the interval in l-space over which the transition from no absorption to maximum absorption takes place. Condition (4) has been met in cases involving the scattering from nuclei of strongly absorbed "particles" such as deuterons, α particles, and heavier ions at nonrelativistic energies, and we see no apparent reason for the explanation of this result not to apply in the relativistic region. The "repulsive" effect of absorption can be seen by examining complex-potential model (CPM) analyses[18, 19] of elastic scattering data; and this concept has been developed qualitatively for application in parameterized phase-shift (PPS) analyses[16] of such data. Specifically, in CPM analyses numerical solution of the (radial) Schrödinger equation, with the nuclear interaction represented by a complex potential

$$V_n(r) = -[V(r) + i\,W(r)],$$

has shown, beside the obvious absorptive result that $|\eta_l| \leq 1$, that $\delta_l < 0$ for strongly absorbed partial waves. Since this occurs even in the presence of the attractive real potential, which alone would result in $\delta_l > 0$, the absorptive repulsion is clearly indicated. Recent analyses[20-22] of 11- to 12- and 15-MeV elastic deuteron scattering data provide interesting examples of cases

for which $\alpha(0) < 0$. Figure C.8-1 shows $|\eta_l|$ and δ_l resulting from CPM analysis[20] of data for 11.8-MeV d+Sn. Substitution of these values into Eq. (2) results in

$$\alpha(0) \approx -0.20.$$

One can make phenomenological PPS analyses of the high-energy data, employing a parameterization of δ_l that gives an l dependence of the form indicated in Fig. C.8-1. Such analyses could provide useful descriptions of the energy dependence of such quantities as absorption radii, surface thicknesses, and opacities.

Footnote and References

†Shortened version of Phys. Letters 16, 189 (1965).

1. V. G. Grishin, in Proceedings of the International Conference on Nuclear Structure, edited by R. Hofstadter and L. Schiff (Stanford University Press, Stanford, 1964), p. 206.
2. K. J. Foley, S. J. Lindenbaum, W. A. Love, S. Ozaki, J. J. Russell, and L. C. L. Yuan, Phys. Rev. Letters 11, 425 (1963).
3. L. F. Kirillova, V. A. Nikitin, A. A. Nomofilov, V. A. Sviridov, L. N. Strunov, and M. G. Shafranova, in Proceedings of the Sienna International Conference on Elementary Particles, edited by G. Bernardini and G. P. Puppi (Societá Italiana de Física, Bologna 1963), p. 593.
4. E. Lohrman, H. Meyer, and H. Winzeler, Phys. Letters 13, 78 (1964).
5. L. Kirillova, L. Khristov, V. Nikitin, M. Shafranova, L. Strunov, V. Sviridov, Z. Korbel, L. Rob, P. Markov, Kh. Tchernev, T. Jodorov, and A. Zlateva, Phys. Letters 13, 93 (1964).
6. A. E. Taylor, A. Ashmore, W. S. Chapman, D. F. Falla, W. H. Range, D. B. Scott, A. Astbury, F. Capocci, and T. G. Walker, Phys. Letters 14, 54 (1965).
7. K. J. Foley, R. S. Jones, R. S. Gilmore, S. J. Lindenbaum, W. A. Love, S. Ozaki, E. H. Williams, R. Yamada, and L. C. L. Yuan, Phys. Rev. Letters 14, 74 (1965).
8. G. Bellettini, G. Cocconi, A. N. Diddens, E. Lillethun, F. Pahl, J. P. Scanlon, J. Walters, A. M. Wetherell, and P. Zanella, in Proceedings of the International Conference on High Energy Physics, Dubna, 1964 (to be published).
9. S. J. Lindenbaum, Rapporteur's Review, in Proceedings of the International Conference on High Energy Physics, Dubna, 1964 (to be published).
10. R. Serber, Phys. Rev. Letters 10, 357 (1963); Rev. Mod. Phys. 36, 649 (1964).
11. L. Van Hove, Rev. Mod. Phys. 36, 655 (1964).
12. W. N. Cottingham and Ronald F. Peirls, Phys. Rev. 137, B147 (1965).
13. P. Söding, Phys. Letters 8, 285 (1964).
14. I. I. Levintov and G. M. Adelson-Velsky, Phys. Letters 13, 185 (1964).
15. Effects of particle identity and the Coulomb field are not important in this discussion.
16. H. E. Conzett, E. Hadjimichael, and A. Isoya, in Proceedings of the Third Conference on Reactions between Complex Nuclei, edited by A. Ghiorso, R. M. Diamond and H. E. Conzett (University of California Press, Berkeley, 1963), p. 26.
17. J. Alster and H. E. Conzett, Phys. Rev. 136, B1023 (1964).
18. C. E. Porter, Phys. Rev. 112, 1722 (1958). To my knowledge, this reference contains the first remark (attributed to K. W. Ford) concerning the effect of absorption on the real phase shift
19. R. M. Eisberg and C. E. Porter, Rev. Mod. Phys. 33, 190 (1961).
20. E. C. Halbert, Nucl. Phys. 50, 353 (1964).
21. C. M. Perey and F. G. Perey, Phys. Rev. 132, 755 (1963).
22. W. E. Frahn and L. P. C. Jansen, Nucl. Phys. 59, 641 (1964).

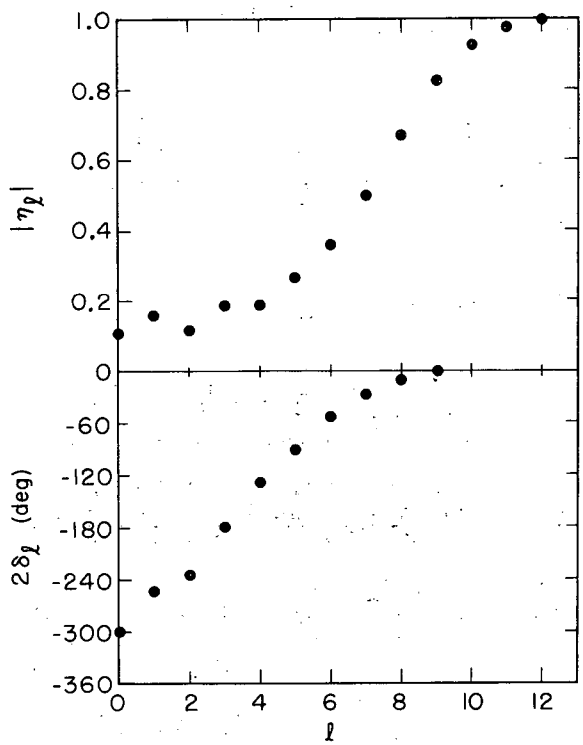

MUB-5306

Fig. C.8-1. The l dependence of $|\eta_l|$ and δ_l from CPM analysis of 11.8-MeV d + Sn elastic scattering data, Ref. 20.

9. STUDY OF THE $He^4(p,d)He^3$ REACTION WITH POLARIZED PROTONS AT 55 AND 63 MeV†

E. T. Boschitz*, M. Chabre‡, H. E. Conzett, and R. J. Slobodrian

The $He^4(p,d)He^3$ reaction, and the inverse stripping reaction $He^3(d,p)He^4$, are not yet well understood. Distorted-wave Born-approximation (DWBA) fits on intermediate-energy data are not very convincing, whereas a simple diffraction approach seems to be more successful.[1-3] Studies with polarized particles may help to elucidate the reaction mechanism. We have measured the asymmetry in the $He^4(p,d)He^3$ cross section with polarized protons, at 55 MeV where data are available for the cross section[4] and at 63 MeV.

We have used the polarized proton beam of the Berkeley 88-inch cyclotron, produced by alpha-proton scattering. At forward angles the deuterons were detected and identified by two large (4 cm^2) E-ΔE solid-state detector pairs. At backward angles the deuteron energies were too low for the deuterons to penetrate the ΔE detectors. Therefore, we counted instead the He^3 recoils at forward angles with CsI crystals of thickness sufficient to stop only the He^3. For those measurements, the main uncertainty is due to the subtraction of a continuous background, while for the deuteron measurements the peaks are very clean and the precision is limited almost purely by statistics. Figure C.9-1 shows the observed asymmetries, with P_1 being the polarization of the incident proton beams.

The asymmetry in a pickup reaction induced by polarized protons is related to the deuteron polarization by the formula[5]

$$\left(\frac{d\sigma}{d\Omega}\right)_{\text{polarized}} = \left(1 + \frac{1}{2}\,\underset{\sim}{P}_p \cdot \underset{\sim}{P}_d\right)\left(\frac{d\sigma}{d\Omega}\right)_{\text{unpolarized}}$$

Therefore we measure the component of the deuteron polarization parallel to the proton polarization. In an l = 0 nucleon pickup reaction, the deuteron polarization is due to spin-orbit distortion. In such a case a derivative rule analogous to the one for elastic scattering has been suggested.[6] However, comparing our data with the cross-section data at 55 MeV, we find that the asymmetry changes sign near the minima of the cross section, which occur near 30, 95, and 150 deg, but no zero of the asymmetry can be associated with maxima of the cross section. It may be that here, also, another approach, such as a diffraction model, could be more successful than the DWBA treatment in describing our results.

One knows that the asymmetry in a reaction induced by polarized particles is connected to the polarization occurring in the inverse reaction induced by unpolarized particles.[7,8] Our measurements of asymmetries are therefore equivalent to the measurement of the proton polarization in the stripping reaction $He^3(d,p)He^4$ at the corresponding energies 43 and 54 MeV.

Footnotes and References

†In Proceedings of International Conference on Polarization Phenomena of Nucleons, Karlsruhe, September 1965.

*Permanent address: NASA-Lewis Research Center, Cleveland, Ohio.

‡NATO Fellow, on leave from CNRS, Institut Fourier, Grenoble, France.

1. W. Tobocman, in Proceedings of the Rutherford Jubilee International Conference, Manchester, 1961 (Heywood and Company, Ltd., London, 1961), p. 465.
2. O. M. Bilaniuk and R. J. Slobodrian, Phys. Letters 4, 209 (1963).
3. A. Dar, Nucl. Phys. 55, 305 (1964).
4. S. Hayakawa et al., Phys. Letters 8, 330 (1964).
5. Vysotskii and A. G. Sitenko, Soviet Phys. JETP 36, 812 (1959).
6. L. C. Biedenharn and G. R. Satchler, Suppl. Helv. Phys. Acta 6, 372 (1961).
7. G. R. Satchler, Nucl. Phys. 8, 65 (1958).
8. L. C. Biedenharn, Nucl. Phys. 10, 620 (1959).

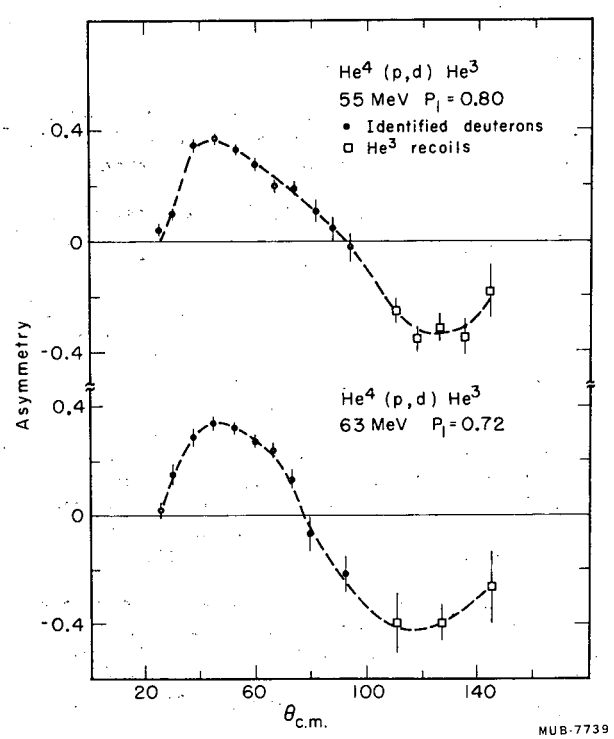

Fig. C. 9-1. Deuteron asymmetries from the $He^4(p,d)He^3$ reaction induced by polarized protons at 55 and 63 MeV.

10. ON THE DETERMINATION OF THE PROTON-PROTON $^1S_0$ SHAPE PARAMETER*

R. J. Slobodrian

In a recent letter[1] a determination of the $^1S_0$ shape parameter P for proton-proton scattering was produced through fits to very accurate phase shifts, as obtained from experimental data at five energies between 0.3825 and 3.037 MeV in the laboratory system.[2,3] The main conclusion was that best agreement with the data was achieved by the Coulomb-corrected partial-wave dispersion relation (PWDR). The boundary condition model (BC) was ruled out because it gave the wrong sign for the shape parameter.[1]

Breit has expressed some doubts about such determination of the shape parameter,[4] and this note presents some evidence against the certainty of our knowledge of P, based on shape-dependent (SD) fits to the five experimental points today available with high accuracy, without and with the vacuum polarization correction[5] (from now on called VPC), and also fits to the experimental points, excluding the points at 1.397 and 0.3825 MeV, again with and without the VPC. The reason for doing this may be found in the paper by Foldy and Eriksen[5] concerning the VPC, where they discuss at length the implications of their choice of the parameter C, as calculated by Jackson and Blatt[6] for the Yukawa well, in the expression

$$K = A + BE + CE^2, \tag{1}$$

where E is the laboratory-system energy in MeV.

The function K is related to the function F defined below through the equality K = RF (F is currently used nowadays in the representation of low energy p-p scattering):[7]

$$F = C^2 k \cot \delta_0 + \frac{1}{R} h(\eta) = -\frac{1}{a_p} + \frac{1}{2} r_e k^2 - P r_e^3 k^4, \tag{2}$$

where

$$C^2 = \frac{2\pi\eta}{e^{2\pi\eta}-1}, \quad k^2 = \frac{M_p E}{2\hbar^2}, \quad R = \frac{\hbar^2}{M_p e^2},$$

$$h(\eta) = \mathrm{Re}\,\frac{\Gamma'(-i\eta)}{\Gamma(-i\eta)} - \ln\eta,$$

a_p is the proton-proton scattering length, E is the lab energy, M_p is the proton mass, $\eta = e^2/\hbar v_{lab}$ (e is the proton charge, $\hbar$ is Planck's constant divided by 2π, v_{lab} is the relative velocity), η is usually called Coulomb parameter, r_e is the effective range, and P is the shape parameter.

Table C.10-I summarizes the results of the least-squares fit to the data as described previously. One learns from the table that, excluding the points at 0.3825 and at 1.397 MeV lab, the effect of the VPC is simply to turn the SD fit more shape-independent, whereas the sign of P remains negative. Including the point at 1.397 MeV, the effect of the VPC is to reverse the sign of the shape parameter p, although with or without VPC, P can be considered consistent with zero because of the experimental error of ±0.014 (see Ref. 1 and Table C.10-I). Finally, including the point at 0.3825 MeV, there is again a reversal of sign when one includes the VPC, and P becomes much larger. This certainly means that the VPC is dominating the parameter. There is also a basic contradiction with the meaning of the shape parameter P because of the algebraic structure of Eq. 2 or its equivalent C in Eq. 1. The parameter C is the coefficient of the quadratic term of expansion 1, and therefore it should be determined by the higher-energy points. The function 1 should be very well approximated by a straight line at low energies if C is small, and deviate at higher energies. A large-scale plot of the function K easily reveals that the vacuum polarization corrected point at 0.3825 MeV lab is too low with respect to the almost straight line defined by the remaining four points, and this forces the increase in the parameter.

The conclusions seem simple: the existing very accurate data do not seem to confirm yet the validity of the VPC. In the author's opinion a reiteration of the old measurements at 0.3 and 0.2 MeV lab with high accuracy is necessary to settle the question of the VPC as it stands now; lower-energy measurements, if possible, would also be desirable. Additional measurements between 0.3825 and 1.397 MeV should help to confirm the measurement at 0.3825 MeV.

Finally, the algebraic structure of Eq. 2 implies that the shape parameter P should be determined preferably by the context of the higher-energy points. If the context of the very-low-energy points forces a shape parameter in disagreement with the higher-energy points (the latter being more sensitive to it), the result should be viewed with suspicion. Lastly, and this refers to the remaining scattering parameters also, a reexamination of the electromagnetic corrections to the p-p scattering parameters is desirable on a different basis than the approach of Schneider and Thaler,[8] in view of the accuracy of present data and experimental possiblities. The author of this paper has explored the effect of the extended electromagnetic structure of the proton with positive results.[9]

If all the above-mentioned questions and problems are favorably solved, more meaningful and accurate scattering parameters will be obtained, and the sign and value of the shape parameter will perhaps be definitely settled, permitting thereby a choice between existing models for the nuclear interaction, or a readjustment of their parameters, or both.

Footnote and References

*Short version of paper to be published in Nuovo cimento.

1. H. Pierre Noyes, Phys. Rev. Letters 12, 171 (1964).
2. D. J. Knecht, S. Messelt, E. D. Berners, and L. C. Northcliffe, Phys. Rev. 114, 550 (1959), and P. F. Dahl, D. J. Knecht, and S. Messelt (University of Wisconsin), private communication to H. Pierre Noyes.
3. J. E. Brolley, J. D. Seagrave, and J. G. Berry, Bull. Am. Phys. Soc. 8, 604 (1963).
4. G. Breit, as quoted by D. Amati, Rapporteur on Nuclear Forces in Comptes Rendus du Congrès International de Physique Nucléaire, Paris 1964, Vol. I, p. 60.
5. Leslie L. Foldy and Erik Eriksen, Phys. Rev. 98, 775 (1955).
6. J. D. Jackson and J. M. Blatt, Rev. Mod. Phys. 22, 77 (1950).
7. It is pertinent to note that M. L. Gursky and L. Heller, Phys. Rev. 136, B, 1693 (1964), have stated that around 3 MeV lab energy some models predict an additional term k^6 in Expression (2), or, correspondingly, a term DE^3 in Eq. (1) comparable to CE^2. It can be shown that such a cubic term is not warranted by the experimental data.
8. R. E. Schneider and R. M. Thaler, Phys. Rev. 137, 874 (1965).
9. R. J. Slobodrian, Extended Electromagnetic Structure Effects on Low-Energy Proton-Proton Scattering, UCRL-16322 Rev., Aug. 1965, to be submitted for publication.

Table C.10-I. Comparison of the SD fit to the experimental data without and with VPC, at 5, 4, and 3 energies, excluding successively the lower energy points; SD: shape-dependent fit, SI: shape-independent fit.

	A	B (MeV^{-1})	C (MeV^{-2})	$-a_p$ (F)	r_e (F)	P
SD[a]				7.8284±0.0080	2.794±0.026	0.026±0.014
SI[a]				7.8163±0.0048	2.746±0.014	0
Five experimental points[b]						
SD (no VPC)	3.73380	0.45644	0.003367	7.7189	2.6303	-0.0443
SD (with VPC)[c]	3.67934	0.48690	-0.002767	7.8332	2.8062	0.0277
Four experimental points[d]						
SD (no VPC)	3.71969	0.46967	0.0005888	7.7482	2.7069	-0.00711
SD (with VPC)	3.68698	0.479713	-0.001189	7.8170	2.7648	0.0133
Three experimental points[e]						
SD (noVPC)	3.74955	0.44521	0.005330	7.6865	2.5659	-0.0755
SD (with VPC)	3.72181	0.46042	0.001039	7.7438	2.6536	-0.0133

a. Values taken from Ref. 1.
b. At 0.3825, 1.397, 1.855, 2.425, and 3.037 MeV lab.
c. The slight discrepancy with the values of Ref. 1 is well within experimental error and has no effect on the arguments presented in this paper.
d. At 1.397, 1.855, 2.425, and 3.037 MeV lab.
e. At 1.855, 2.425, and 3.037 MeV lab.

11. THE $C^{12}(p, 2p)B^{11}$ REACTION AT 50 MeV†

H. G. Pugh,* D. L. Hendrie, Marc Chabre,‡ and E. Boschitz§

The (p, 2p) reaction has been extensively used at energies above 150 MeV to investigate shell-model structure and momentum distributions of nuclear protons.[1] Two major experimental limitations have hitherto been encountered.

(a) Poor energy resolution has not permited investigation of any but gross shell-model states or groups of states.

(b) The low duty factor of the accelerators at these energies has limited precision and has caused loss of information by necessary electronic integrations over large energy ranges of the outgoing particles.

The high duty factor of the 88-inch cyclotron and improved electronic and counting devices have allowed us to perform the $C^{12}(p, 2p)$ experiment without the previous limitations.

Two ΔE-E counter telescopes, able to detect protons in the range 9 to 25 MeV, were used to detect the outgoing protons. A fourfold fast coincidence was required, and only those events were selected by electronic particle identifiers in which both particles were protons. The resulting pulses were fed into a 4096-channel two-dimensional analyzer; one axis was proportional to the sum of the energies of the two protons, E1+E2, the other axis was proportional to their difference, E1 - E2. A sample E1+E2 spectrum is shown in Fig. C.11-1, showing energy resolution of better than 250 keV and permitting us to identify individual states in the residual B^{11} nucleus.

Several different experimental arrangements were used during the experiment. Figure C.11-2 shows the angular correlation obtained when both counters were moved so that they made equal coplanar angles on opposite sides of the incident beam. Figure C.11-3 gives the correlation when one counter was held fixed at 30 deg and the second counter was moved in the scattering plane. The way in which the two protons share their energy is indicated in Fig. C.11-4 for several of the symmetrical runs. The angular correlations have all been integrated over an energy range $|E1 - E2| < 5$ MeV, as shown by the dotted lines in Fig. C.11-4. The dotted line in Fig. C.11-1 is an estimate made from the E1 - E2 spectra to correct for the integration over E1 - E2.

Noteworthy in the angular correlations are the large rise in cross section at small angles, and the oscillatory nature of the distribution at larger angles. Further runs were made with both counters on the same side of the beam to see if final-state interactions between the two outgoing protons when their relative momentum was small would account for the large forward cross section; results were negative. The most probable explanation of the small-angle cross section is the large increase in the free p-p scattering cross section at low energies. This is most easily seen in the quasi-free-scattering approximation, where the angular correlation is determined by the momentum of the struck proton. The diffraction-like angular distribution might indicate a surface interaction, reflecting the short nuclear mean free path of protons of these energies.

Because of the good energy resolution, we were able to obtain angular distributions for the first four excited states of B^{11}, seen in Fig. C.11-5. In a clean knockout process, excitation of these states could arise only from configuration mixing in the ground state of C^{12}, which is mainly $p_{3/2}$. Since it is quite unlikely that enough $f_{7/2}$ and $f_{5/2}$ configurations are admixed,[2] it is likely that the excitation mechanism goes by a double process, coupling the $3/2^-$ proton hole to the excitation of the 2^+ state of the C^{12} core. Work at higher energies has made such configurations for the four first excited states of B^{11} quite plausible.

Footnotes and References

†Shortened version of Phys. Rev. Letters 14, 434 (1965).

*Present address: University of Maryland, College Park, Maryland.

‡NATO Fellow on leave from CNRS, Institut Fourier, Grenoble, France.

§On leave from NASA-Lewis Research Center, Cleveland, Ohio.

1. For a recent review, see M. Riou, Rev. Mod. Phys. 37, 375 (1965).
2. A. Goswami and M. K. Pal, Nucl. Phys. 44, 294 (1963).
3. S. M. Austin, G. L. Salmon, A. B. Clegg, K. J. Foley, and D. Newton, Proc. Phys. Soc. (London) 80, 383 (1962).

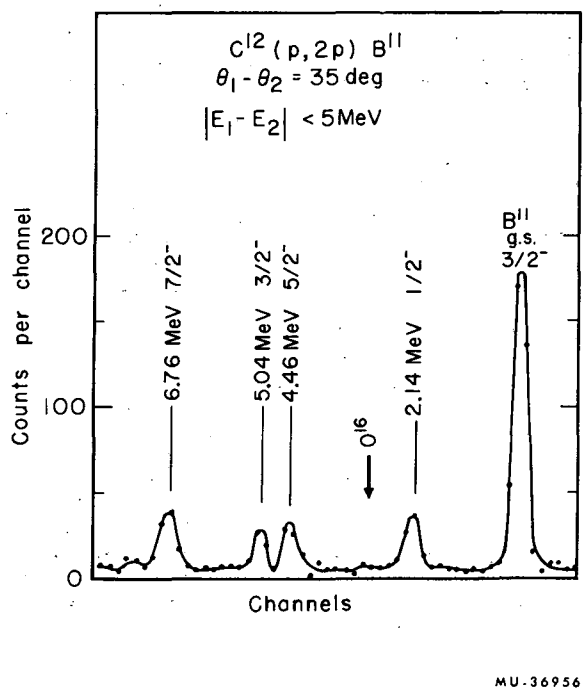

Fig. C.11-1. A summed energy spectrum (E_1+E_2) for $C^{12}(p, 2p)B^{11}$ at 50 MeV. The positions of low-lying states of B^{11} are indicated.

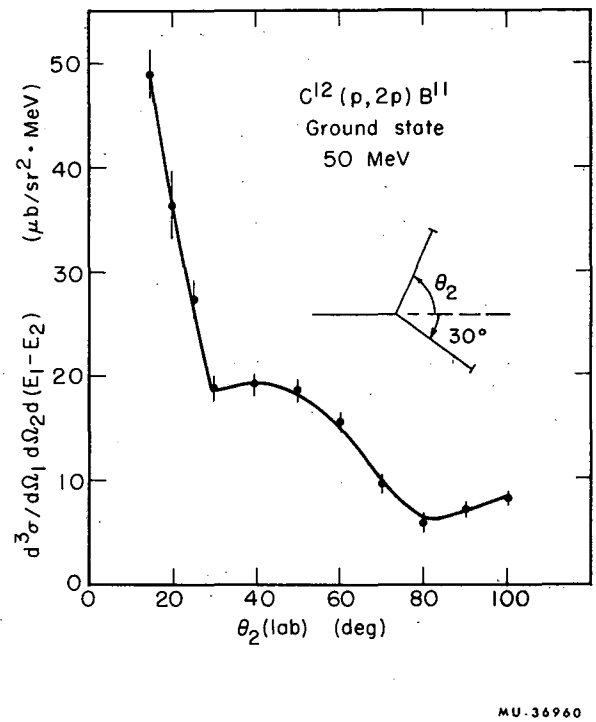

Fig. C.11-3. The angular correlation for the $C^{12}(p, 2p)B^{11}$ (g. s.) reaction in which one counter is held fixed at 30 deg.

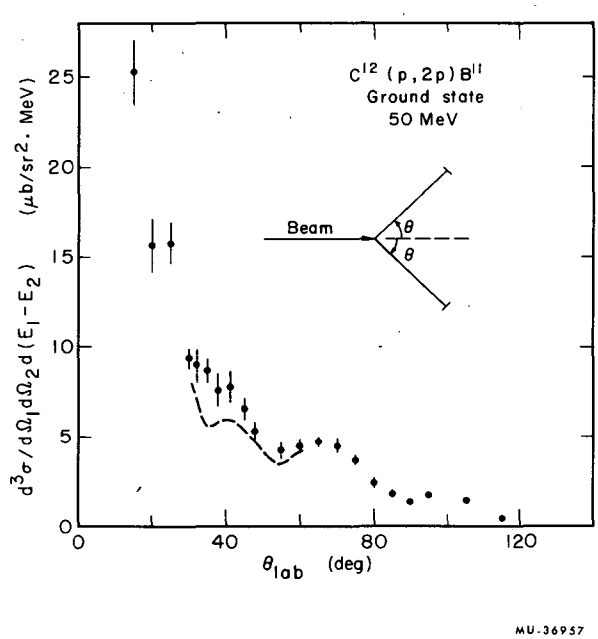

Fig. C.11-2. The angular correlation for the symmetric $C^{12}(p, 2p)B^{11}$ (g. s.) work, integrated over $|E1 - E2| < 5$ MeV. The dotted line indicates an estimate of the cross section for E1=E2.

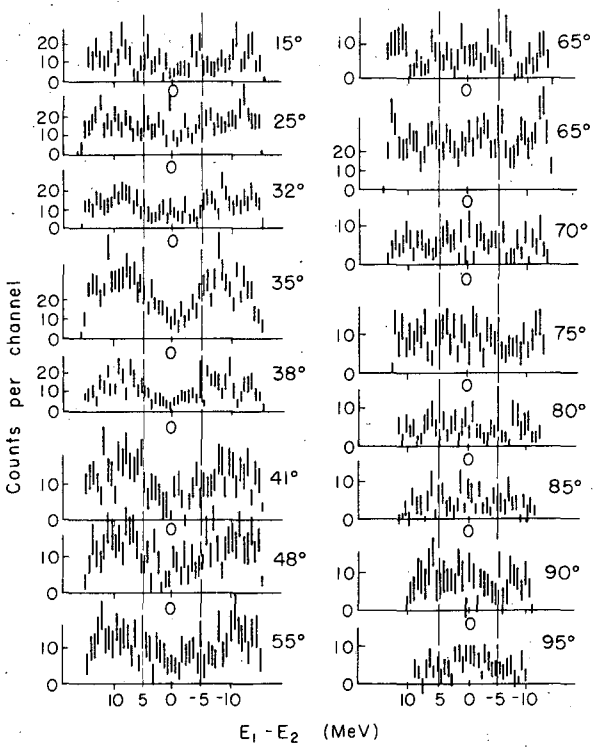

Fig. C.11-4. Energy-sharing spectra (E1-E2) for the symmetric $C^{12}(p, 2p)B^{11}$ (g. s.) work. The dashed lines indicate the region included to obtain angular cancelations.

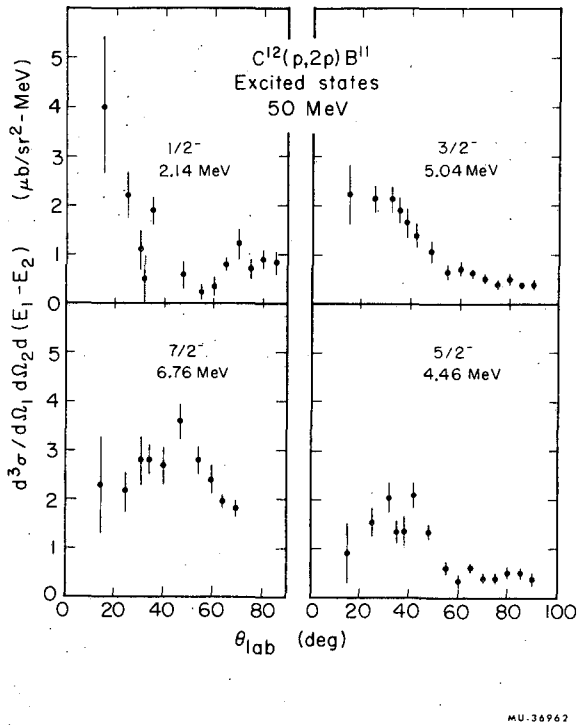

Fig. C.11-5. The angular correlation for the first four excited state of B^{11} obtained in the symmetric $C^{12}(p, 2p)B^{11}$ work.

12. INELASTIC SCATTERING OF α PARTICLES ON Fe^{56}

J. Valentin,† I. Gabrielli,‡ B. G. Harvey, D. L. Hendrie, J. Mahoney, and J. R. Meriwether

Because of their short nuclear mean free path, α particles of cyclotron energies (18 to 130 MeV) have proven valuable probes for inspection of collective states of the nuclear surface. Angular distributions from such states and the ground state show a diffraction-like structure at forward angles (less than ≈ 60 deg) the envelope of which gradually decreases with increasing angle. Parity assignments of the excited states are made by the Blair phase rule,[1] which predicts that odd-parity states have diffraction maxima in phase with the elastic maxima; even-parity states are out of phase. The discovery by workers at Saclay[2] of a known 4^+ state at 2.97 MeV in Fe^{56} has instigated experimental and theoretical reevaluation of the phase rule. The theoretical approach[3] has attributed the reversed phase to a double-excitation process of two phonon levels. Further experimental[4] work has uncovered other cases of reversed phase in 4^+ and 2^+ levels, but has found normal phases in cases in which double excitation might be expected. Work at this Laboratory has shown that the phases of some expected two-phonon levels change as a function of bombarding energy,[5] which has been attributed to mixing of the two-phonon with neighboring one-phonon states. In order to verify the interpretation of these results, we repeated the $Fe^{56}(\alpha, \alpha')$ work over a range of energies.

The experiment consisted of bombarding thin Fe^{56} foils with α particles of 23.5, 33, and 50 MeV. (The original Saclay work was at 44 MeV.) Four movable solid-state detectors were used to obtain the angular distributions. Angular distributions for several excited states obtained at 50 MeV are shown in Figs. C.12-1 and C.12-2. The levels at 0.845 and 2.66 MeV are known 2^+ states. The similarity of the angular distributions permits us to assign spin and parity of 2^+ to the 3.85-MeV (previously assigned to have $J^\pi = 3^+$ [6]) and the 4.74 MeV levels. Comparison of the phases of the 2.08-MeV (4^+) and 2.97-MeV (2^+) levels with those of the elastic and 4.54-MeV (3^-) levels indicates the double excitation process is invoked. The more gradual decrease of cross section with increasing angle shown by the 2.08- and 2.97-MeV levels is an additional feature expected for the double-excitation process.

Figure C.12-3 shows the angular distributions of the 2.08-MeV state at the three incident energies plotted as a function of $kR\theta_{c.m.}$ to remove the energy dependence. Here k is the wave number of the incident α particle and R, the interaction radius, was determined by fitting the 0.845-MeV level with the Blair diffraction model.[1] We see no variation of phase with angle. Similar results were obtained for the 2.97-MeV level. This is in complete contrast to the results obtained on nickel isotopes for the corresponding "two-phonon" levels. Recent calculations using microscopic wave functions have cast some doubt on the validity of the two-phonon description for the nickel isotopes.[7]

Footnotes and References

†On leave from the University of Grenoble, Grenoble, France.

‡NATO Fellow on leave from Istituto de Física dell' Universitá, Trieste, Italy.

1. J. S. Blair, Phys. Rev. 115, 928 (1959).
2. M. Barloutaud-Crut, G. Bruge, J. C. Faivre, H. Faraggi, and J. Saudinos, Phys. Letters 6, 222 (1963).
3. N. Austern and J. S. Blair, Ann. Phys. 33, 15 (1965).
4. H. Faraggi and J. Saudinos, Paper C-7, ANL-6848 (1964).
5. D. J. Horen, J. R. Meriwether, B. G. Harvey, A. Bussière de Nercy, and J. Mahoney, Nucl. Phys. 72, 97 (1965).
6. H. Appel and W. Mayer, Nucl. Phys. 43, 393 (1963).
7. R. Arvieu, E. Salusti, and M. Veneroni, Phys. Letters 8, 334 (1964).

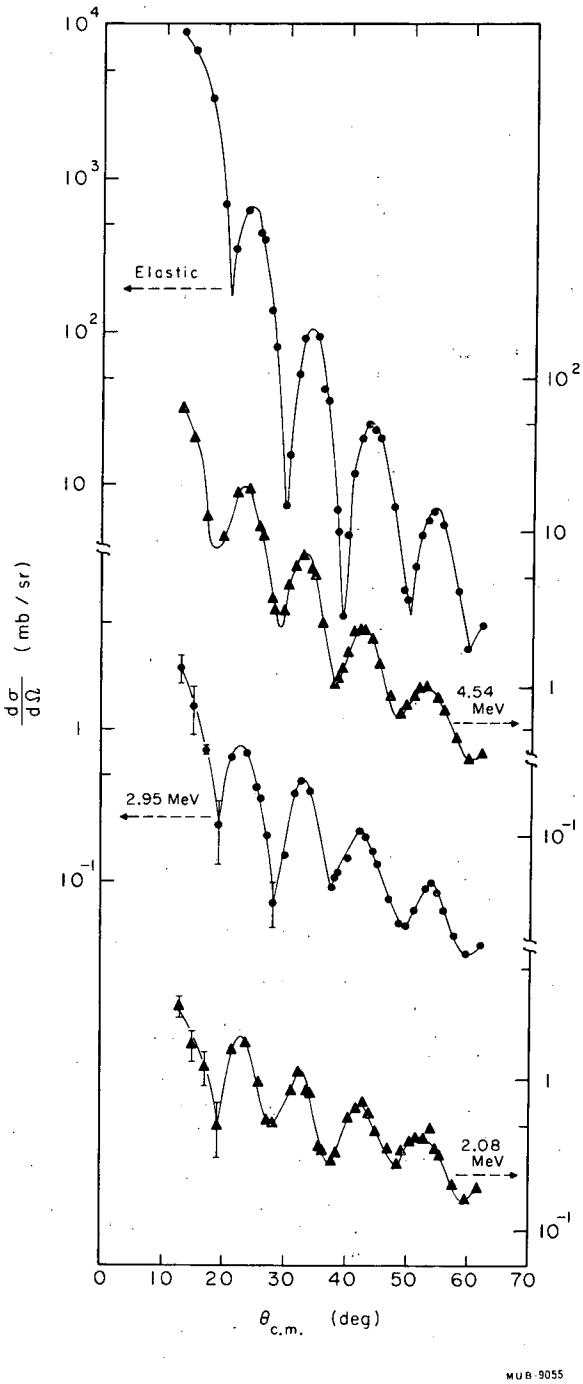

Fig. C.12-1. Angular distributions for levels in phase with the ground state for the 50-MeV $Fe^{56}(\alpha, \alpha')$ reaction

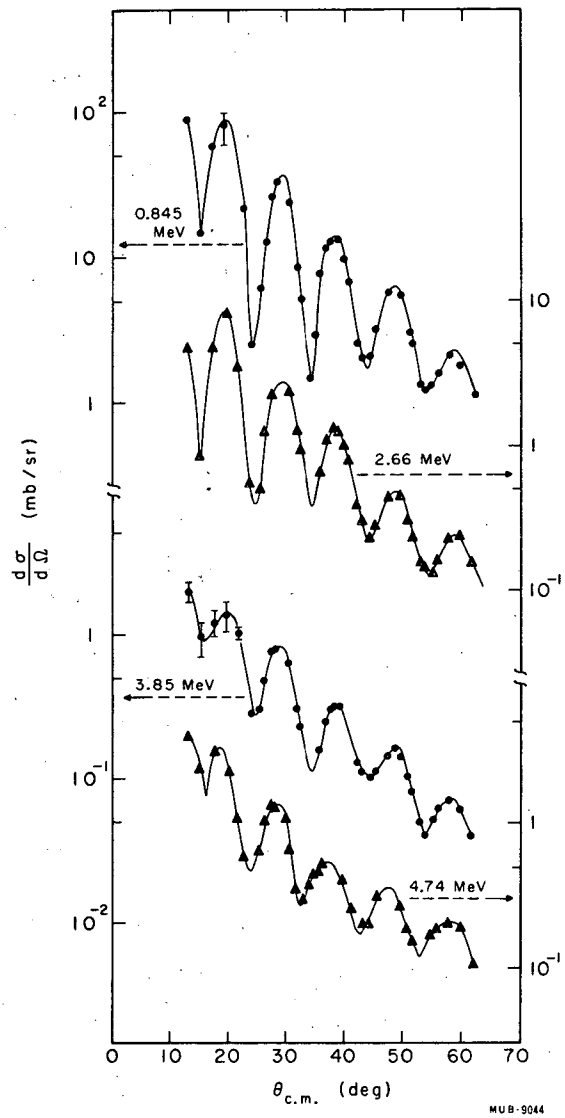

Fig. C.12-2. Angular distributions for prominent 2^+ levels in the 50-MeV $Fe^{56}(\alpha, \alpha')$ reaction.

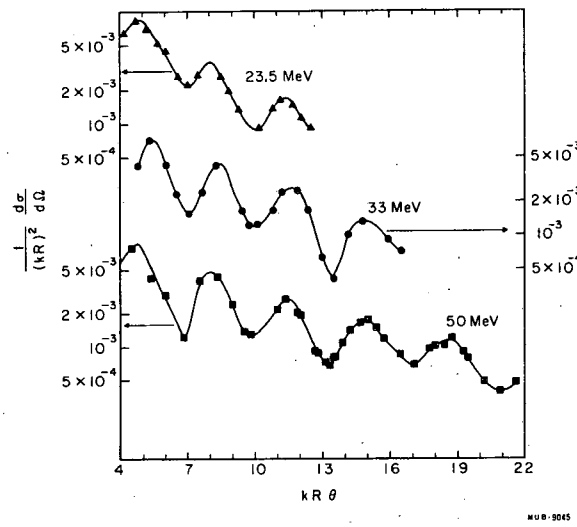

Fig. C.12-3. Angular distributions for the 2.09-MeV 4^+ level of Fe^{56} at three incident alpha energies. The cross sections are divided by k^2, and the center-of-mass scattering angle is multiplied by kR in order to remove the energy dependence of the distributions.

13. COMPARISON OF THE ELASTIC SCATTERING OF He^3 AND He^4 BY Ca^{40}

A. Springer,† Marc Chabre,* D. L. Hendrie, and H. G. Pugh‡

The scattering of medium-energy He^4 ions has been extensively used in the last several years for investigating nuclear properties. The characteristic feature of the scattering is the oscillatory angular distribution, originally explained by using a semiclassical diffraction model in which the α-particle waves were assumed not to penetrate inside a well-defined interaction radius near the nuclear surface.[1] As the experiments have become more refined it has become necessary to introduce new parameters to allow for a lack of definition, or a "diffuseness," of the interaction radius. We have attempted to bring direct evidence to bear on this diffusness by comparing the scattering of He^3 and He^4 from the same nucleus under carefully chosen conditions. Accurate angular distributions showing a characteristic diffraction pattern were already available[2] for the scattering of 50.9-MeV He^4 by Ca^{40}, so the He^3 energy was chosen as 65.3 MeV, since this yields the same relative momentum in the center-of-mass system as for 50.9-MeV He^4. Thus in the absence of the Coulomb interaction the diffraction model would give the same angular distribution in both cases.

We bombarded a 1.02-mg/cm^2 natural calcium target with 65.3-MeV He^3 ions from the Berkeley 88-inch cyclotron and used a solid-state counter telescope and particle identification to measure the elastic scattering angular distribution between 9 and 64 deg in the c.m. system, with an effective angular resolution of 0.6 deg. The results for both 50.9-MeV He^4 and 65.3-MeV He^3 are shown in Fig. C.13-1, where the absolute normalization of each set of measurements is independently known to ±10%. Both projectiles yield a diffraction-like pattern. The major difference is that the He^3 cross section is generally smaller and drops off more quickly as a function of angle. The anomalously large maximum in the He^3 data at 60 deg in the region of low cross-section may be due to more complex processes. The lower cross section for He^3 at small angles is explained by the difference in Coulomb scattering.

The more significant feature is that the He^3 differential cross section falls more rapidly as a function of angle than the He^4 cross section. To explain this we analyze in terms of the usual partial-wave expansion,[3]

$$\frac{d\sigma}{d\Omega} = \frac{1}{4k^2}\left|\sum_l (2l+1)[1-\eta_l \exp(2i\sigma_l)]P_l(\cos\theta)\right|^2,$$

where η_l is the scattering amplitude, σ_l is the Coulomb phase shift, $P_l(\cos\theta)$ is a Legendre polynomial, and k is the wave number of an incident particle in the c.m. system. To simplify the analysis we have restricted the variations of the η_l according to the notation

$$\eta_l = \epsilon + a\frac{\partial\epsilon}{\partial l} + i\left(b\frac{\partial\epsilon}{\partial l} + c\frac{\partial^2\epsilon}{\partial l^2}\right)$$

where

$$\epsilon = \{1 + \exp[(l - l_0)/\Delta]\}^{-1}.$$

The real and imaginary parts of the scattering amplitudes η_l as determined by a least-squares fit to the data are shown in Fig. C.13-2. The important difference between the two projectiles is that for He^3 the change in η_l takes place over a larger range of l than for He^4. By making the usual classical connection between impact parameter and angular momentum $l = kr$, we conclude that the diffuseness of the interaction surface is greater for He^3 than for He^4 by a factor ≈ 1.5. The possibility that the effect may be due to a spin-orbit interaction has been ruled out by tests using the optical-model program SCAT-4. The negative dip in the He^4 curve is not significant, since it comes in the region of $l < 16$, which we can show may be changed without affecting the fit to the data. This seems to be in contradiction with the statement[4] that nuclei appear "blacker" to He^3 than to He^4. However, similar results have been seen by Venter and Frahn,[5] using an equivalent method with a three-parameter fit to the η_l's.

We have recently been informed by Dr. R. H. Bassel that he has independently observed the same phenomenon in comparing optical-model-derived phase shifts from He^3 and He^4 scattering at a number of lower energies, for a variety of nuclei.

Footnotes and References

†Present address: University of California, Davis, California.

*NATO Fellow on Leave from C. N. R. S., Institut Fourier, Grenoble, France.

‡Present address: University of Maryland, College Park, Maryland.

1. J. S. Blair, Phys. Rev. 115, 928 (1959).
2. A. Springer and B. G. Harvey, Phys. Letters 14, 116 (1965).
3. J. M. Blatt and V. F. Weisskopf, Theoretical Nuclear Physics (John Wiley and Sons, New York, 1952), p. 321.
4. P. E. Hodgson, in Comptes Rendus du Congres International Physique Nucleaire, Paris, 1964, p. 257; V. Z. Goldberg, V. P. Rudakov, and I. N. Serikov, Soviet Physics JETP 20, 381 (1965).
5. R. H. Venter and W. E. Frahn, Ann. Phys. 27, (1964) 401.

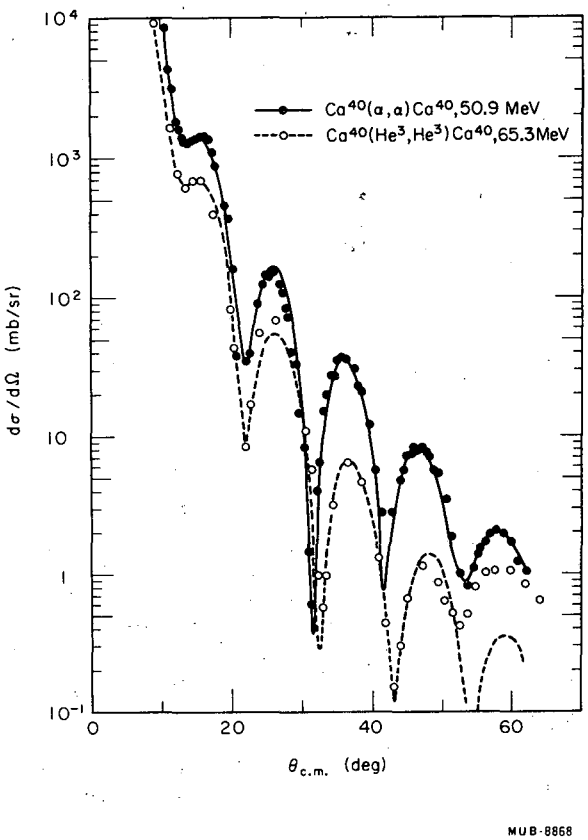

Fig. C.13-1. Elastic scattering differential cross sections for 50.9-MeV α particles and 65.3-MeV He^3's on Ca^{40}. The curves are the results of parameterized phase-shift fits described in the text.

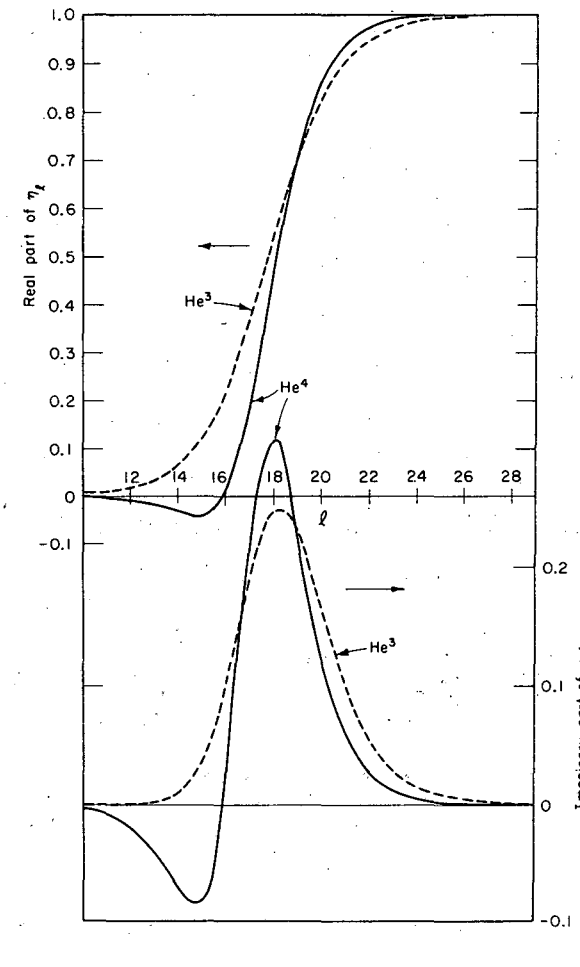

Fig. C.13-2. The real and imaginary parts of the scattering amplitudes which fit the elastic cross sections. The steep α-particle curves are related to a less diffuse interaction region for α particles than for He^3.

14. HIGH-ENERGY DEUTERON CROSS SECTIONS†

V. Franco and R. J. Glauber*

A theoretical analysis of the collisions of particles with deuterons is carried out in the high-energy approximation. This approximation, which corresponds to a generalized form of diffraction theory, takes explicit account of double collision processes as well as single ones. It is used to express the amplitudes for elastic and inelastic scattering by deuterons in terms of the elastic scattering amplitudes of the neutron and proton and the deuteron wave functions. The resulting expressions are used to evaluate the differential cross section for elastic scattering and the angular distribution of the inelastic scattering (i.e., the differential cross section for deuteron breakup integrated over final energies of the incident particle). The contributions to these cross sections of the various single and double scattering processes and the terms which represent their interference are exhibited individually. Expressions are derived for the total cross section of the deuteron and for its elastic and inelastic total scattering and absorption cross sections. The difference between the various types of deuteron cross sections and the sum of the corresponding cross sections for the free neutron and proton is explained in some detail. Spin-dependent interactions are treated, and for incident particles of spin 1/2 an expression is given for the deuteron total cross section in terms of the general spin-dependent scattering amplitudes of the neutron and proton.

The theory is applied to antiproton-deuteron collisions in the energy range from 100 MeV to 17 BeV. If a total cross-section defect $\delta\sigma$ is defined in terms of the deuteron, free proton, and free neutron total cross sections, σ_d, σ_p, and σ_n, respectively, by

$$\sigma_d = \sigma_n + \sigma_p - \delta\sigma ,$$

then $\delta\sigma$ is given by

$$\delta\sigma = -\frac{2}{k^2}\int S(\vec{q})\ \mathrm{Re}\,[f_n(\vec{q})\,f_p(-\vec{q})]\ d^{(2)}\vec{q} ,$$

where $\hbar\vec{k}$ is the incident momentum, $\hbar\vec{q} = \hbar(\vec{k} - \vec{k}')$ is the momentum transferred to the deuteron, $S(\vec{q})$ is the form factor for the deuteron ground state, f_n and f_p are the free neutron and proton elastic scattering amplitudes, and the integration is over a plane tangent to the shell $\vec{k}' = k$ at the forward direction. If we assume that at high energies $f_n = f_p$ and that these amplitudes are purely imaginary near the forward direction and Gaussian in form, we may write

$$\delta\sigma = \frac{\sigma_N^2}{4\pi}\int_0^\infty e^{-a^2q^2}\ S(q)\,q\ dq,$$

where σ_N is the antiproton-proton total cross section and a^2 is a parameter related to the antiproton-proton elastic scattering angular distribution. We show in Fig. C.14-1 the way in which the actual cross section of the deuteron differs, as a function of energy, from the sum of the cross sections of the two nucleons. As input data in the calculations for this graph we have used the curves labeled σ_N and σ_{Nel}, which have been drawn to fit the measured values of the total and elastic proton cross sections. The deuteron wave function used was "Approximation II" of Moravcsik.[1] We observe that the cross-section defect decreases quite slowly with increasing energy. The graph shows quite clearly the importance of $\delta\sigma$ in calculating the cross section of the deuteron.

Calculations of the absorption cross section of the deuteron (i.e., total minus the sum of elastic plus inelastic scattering cross sections) have been carried out for the energy range 100 MeV to 2.5 BeV. The influence of double interactions on the absorption cross section is shown as a function of energy in Fig. C.14-2. The absorption cross sections predicted by taking double interactions into account (σ_{abs}) agree much more closely with the experimental values of the absorption cross section of the deuteron than those which neglect them ($2\sigma_N - 2\sigma_{Nel}$).

Footnotes and Reference

†Material condensed from Phys. Rev. (in press).

*Harvard University, Cambridge, Massachusetts.

1. M. J. Moravcsik, Nucl. Phys. 7, 113 (1958).

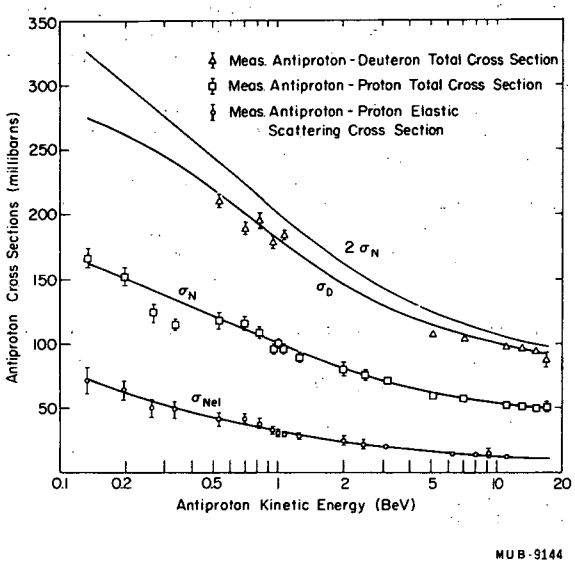

Fig. C.14-1. The theoretical total cross section for antiproton-deuteron collisions as a function of the incident antiproton laboratory kinetic energy (measured values, ⊥). The two lower curves are smoothed representations of the indicated measurements of the total (⊥) and elastic (Φ) antiproton-proton cross sections. The deuteron total cross sections calculated from the smoothed data are given by the curve labeled σ_D. The uppermost curve represents twice the antiproton-proton cross section. The total cross-section defect is the difference of the ordinates of the two uppermost curves.

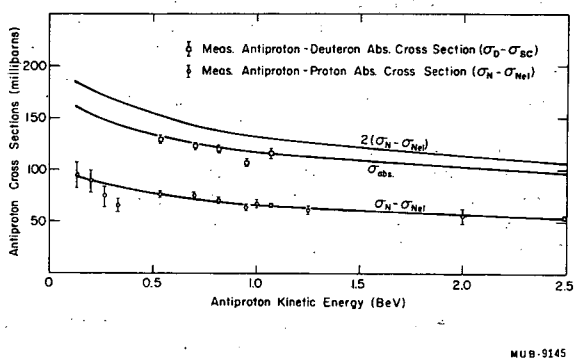

Fig. C.14-2. The theoretical absorption cross section for antiproton-deuteron collisions as a function of the incident antiproton laboratory kinetic energy (measured values, ⊥). The lowest curve is an approximate fit to the values of the antiproton-proton absorption cross section (Φ) i.e., the difference between the measured values of the total and elastic scattering cross sections. The calculated deuteron absorption cross section is given by the curve labeled σ_{abs}. The uppermost curve represents twice the antiproton-proton absorption cross section. The cross-section defect for absorption is given by the difference of the ordinates of the two uppermost curves.

15. QUALITATIVE ASPECTS OF NEUTRON-NUCLEAR INTERACTIONS AND THE OPTICAL MODEL†

V. Franco

The appearance of broad maxima and minima in the energy dependence of neutron-nuclear total and scattering cross sections at less than 100 MeV is given a simple explanation. Within the framework of the Glauber diffraction approximation, the general conditions for the occurrence of the maxima and minima are obtained in terms of an integral, over impact parameters involving a phase shift function. A modification of the approximation is employed so that the formalism may be applied below 100 MeV. The assumption that the average phase difference between that portion of the neutron wave which traverses the nucleus and that which does not is equal to an integral multiple of π at cross-section maxima and minima is shown to be incorrect.

The approximations are illustrated with some optical-model calculations which indicate that the positions of the maxima and minima shift to higher energies with increasing target mass number. Some numerical calculations using the Schrödinger equation with square-well and Woods-Saxon potentials are compared with cross sections calculated from the approximation. Near regions of maxima appreciable contributions come from a number of partial cross sections. The appearance of these maxima implies neither a resonance in any single partial wave nor a maximum in any single partial cross section. A brief consideration of the energy dependence of the total, absorption, and scattering cross sections separately reveals that the principal qualitative features of the total cross section are manifest in the scattering cross section.

The neutron-nuclear total cross section may be written in the Glauber diffraction approximation[1] as

$$\sigma = 2 \int [1 - \mathrm{Re}\, e^{i\chi(\underset{\sim}{b})}]\, d^{(2)} \underset{\sim}{b} ,$$

where $\underset{\sim}{b}$ is the inpact parameter vector and lies in a plane perpendicular to the direction of the incident beam, and the integration is over this plane. The phase shift function $\chi(\underset{\sim}{b})$ is complex and may be expressed in terms of an optical potential $V(\underset{\sim}{b}, z)$ by

$$\chi(\underset{\sim}{b}) = k \int_{-\infty}^{\infty} \left\{ \left[1 - \frac{2V(\underset{\sim}{b}, z)}{\hbar k v} \left(1 - \frac{1}{2} \frac{V(\underset{\sim}{b}, z)}{E} \right) \right]^{1/2} - 1 \right\} dz , \qquad (1)$$

where $\hbar k$ is the incident momentum, v is the relative velocity, and E is the total energy of the incident neutron. The direction of the incident beam is taken to be along the z axis.

In the application of Eq. (1) to nuclei, we have considered both a real square well and a complex square well whose real and imaginary parts are both negative, with magnitudes given by the solid curves in Fig. C.15-1. In Fig. C. 15-2 we show the calculated loci of points for the incident neutron kinetic energies at which the maxima and minima in the total cross section are found for the range of mass number $1 \leq A < 250$. The experimental maxima and minima are shown as points. The calculations yield the result, in agreement with measurements, that neutron-nuclear total cross sections possess broad maxima and minima when plotted against incident energy, with the lighter nuclei having only one maximum and the heavy nuclei having three maxima and three minima. A partial-wave analysis shows that these maxima are not caused by resonances of any partial wave and that no one partial cross section contributes such a great amount to the total cross section that the other partial cross sections may be neglected. The broad cross-section maxima are caused by a joint effort on the part of many phase shifts to contribute a large share to the total cross section.

Footnote and Reference

†Material condensed from Phys. Rev. 140, B 1501 (1965).

1. R. J. Glauber, Lectures in Theoretical Physics, Vol. I (Interscience Publishers Inc., New York, 1959), p. 315.

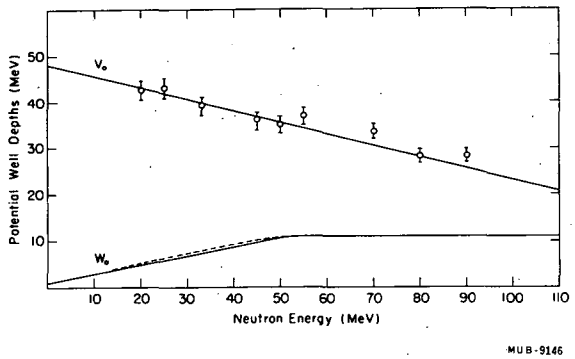

Fig. C.15-1. The depths used for the real and imaginary parts of the potential wells as a function of neutron kinetic energy. The values obtained by P. H. Bowen et al., Nucl. Phys. 22, 640 (1961), for the real part V_0 are shown as points with ±5% error bars. The broken curve is the imaginary part W_0 used by Bowen et al., and was obtained from neutron absorption cross sections. The solid curves represent assumed analytical forms for the well depths used in the present calculations. For energies greater than 55 MeV the broken and solid curves are identical.

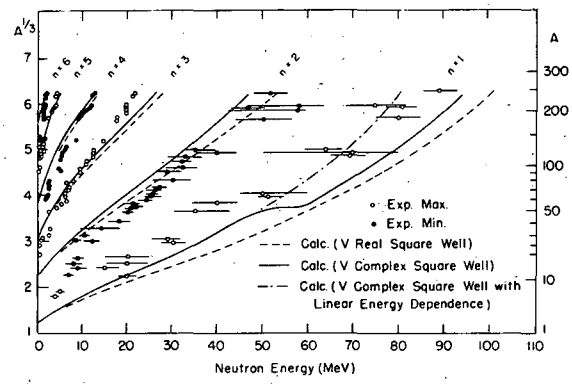

Fig. C. 15-2. Plot showing the calculated loci of maxima and minima (curves), together with the observed values (points). The broken curves are obtained by using a real square-well potential, and the solid curves by using a complex square-well potential. The well depths are shown in Fig. C.15-1. The dot-dashed curve for the n=1 locus is calculated with W_0 given in Fig. C.15-1 for T < 40 MeV and with the linear extrapolation of that segment of the curve for kinetic energies greater than 40 MeV.

16. EXTENDED CHARGE EFFECTS ON LOW-ENERGY PROTON-PROTON SCATTERING*

R. J. Slobodrian

The accuracy of the measurements of proton-proton scattering in the low-energy region (between 0 and 5 MeV, laboratory system) has called for refined calculations of departures from the simple Coulomb potential energy term $V_C = e^2/r$, like the vacuum polarization contribution,[1,2] or the magnetic dipole interaction effects,[3] the latter proven finally to be unimportant.[4] Several recent letters[5] and papers have dealt with comparisons of the reputedly very accurate experimental results with different models for the p-p interaction, and best agreement was found with the Coulomb-corrected partial-wave dispersion relation (PWDR). The boundary-condition model (BC) was ruled out because it gave the wrong sign for the shape parameter P.[5]

If one believes in a quantum-mechanical Hamiltonian formulation of the proton-proton interaction, it should be describable in terms of a potential

$$V_{pp} = V_N + V_{ES} + \sum_i V_i \,, \tag{1}$$

where V_N is attributed to nuclear effects, V_{ES} is the energy due to the electrostatic interaction, and $\sum_i V_i$ is the contribution, if any, of other interactions that may be present. It is usually assumed that $\sum_i V_i$ is very small compared with the two remaining terms, and it is safe to ignore it. The S-wave scattering is described by the well-known amplitude

$$f(\theta) = f_c + \frac{1}{2ik}\, e^{2i\zeta_0}(e^{2i\delta_0}-1) \,, \tag{2}$$

where $\zeta_0 = \mathrm{Arg}\,\Gamma(1+i\eta)$, η is the Coulomb parameter, $\eta = e^2/\hbar v_{lab}$ ($\hbar$ is Planck's constant divided by 2π, e is the charge of the proton, and v_{lab} is the relative velocity), δ_0 is the S-wave "nuclear" phase shift, and f_c is the Coulomb scattering amplitude. Of course(2) has to be adequately symmetrized. Here again the accuracy of the experimental information has forced the consideration of P waves and also relativistic corrections to η.[6] Conventionally it is assumed that $V_{ES} = V_C$, and the nuclear field is parameterized in order to obtain the phase shift δ_0 extracted from the experimental data. This step, as is well known, is relevant for the comparison with n-p $^1S_0$ potentials,[7] and in the near future with n-n potentials, in view of the increasing accuracy and reliability of n-n scattering parameters,[8] in order to settle the old questions of charge independence and charge symmetry of the nucleon-nucleon interaction.

Hofstadter's experiments[9,10] have proven beyond doubt that there is a positive extended charge in the proton with an rms radius of 0.8 F. This report presents some calculations concerning the influence, on low-energy S-wave p-p scattering parameters, of the extended charge of the proton, using the same first-order perturbation technique employed earlier by Foldy and Eriksen to correct for vacuum polarization effects. We assume that the charge distributions overlap at short distances without appreciable distortion. If we imagine the protons as uniformly charged spheres of radius R (equal to the rms radius of the charge) the potential energy is given by the well-known expressions

$$V_i(r) = \frac{e^2}{R^4}\left(\frac{6}{5}R^3 - \frac{1}{2}Rr^2 + \frac{3}{16}r^3 - \frac{1}{160}\frac{1}{R^2}r^5\right), \quad \text{for } 0 \leq r \leq 2R, \tag{3}$$

$$V_0(r) = \frac{e^2}{r}, \quad \text{for } r \geq 2R, \tag{4}$$

where r is the distance between the centers of the spheres and e is the electric charge of each sphere. As will be seen, the assumption of a uniform charge distribution with a sharp cutoff at a radius equal to the rms radius of Hofstadter's charge distribution yields results which do not differ appreciably from a more realistic calculation using a charge density of exponential form $\rho = ke^{-\alpha r}$. The potential function of such a charge distribution is given by

$$U(r) = e\left[\frac{1}{r} - e^{-\alpha r}\left(\frac{1}{r} + \alpha/2\right)\right]. \tag{5}$$

The expression for the potential energy of two such overlapping charge densities is too lengthy to be presented here, but Fig. C.16-1 summarizes the results. It also includes the potential energy of a point charge in the field given by (5). Presently it is customary to use, for the low-energy p-p scattering,[11] the representation

$$F = C^2 k \cot\delta_0 + \frac{1}{R}h(\eta) = -\frac{1}{a_p} + \frac{1}{2}r_e k^2 - Pr_e^3 k^4, \tag{6}$$

where
$$C^2 = \frac{2\pi\eta}{e^{2\pi\eta}-1}, \quad k^2 = \frac{M_p E}{2\hbar^2},$$

$$R = \frac{\hbar^2}{M_p e^2}, \quad h(\eta) = \mathrm{Re}\,\frac{\Gamma'(-i\eta)}{\Gamma(-i\eta)} - \ln\eta$$

(E is the laboratory energy, M_p is the proton mass), η is again the Coulomb parameter, r_e is usually called effective range, and P shape parameter. Foldy and Eriksen[1,2] use instead the function

$$K = RF = A + BE + CE^2, \tag{7}$$

where E is the laboratory-system energy of the protons. It is clear that if the electrostatic energy within some range is not given by e^2/r, but rather by functions like those of Fig. C.16-1, the electrostatic energy has been overestimated. Consequently what is conventionally attributed to "nuclear" interaction contains in part effects of the excess of electrostatic energy,

$$V_d = V_c - V_{ES}, \tag{8}$$

where V_d can be classified as a short-range perturbation. To correct this we can calculate the change induced in the function K by a potential energy change $\Delta V = -V_d$. As long as the quadratic term of (7) is small we can make use of first-order perturbation theory and calculate ΔK ($\Delta K = B\Delta E$) as

$$\Delta K = \frac{M_p C^2 R}{\hbar^2} \int_0^{R_f} \Delta V(r)\, U^2(r)\, dr, \tag{9}$$

where

$$U(r) = [F(r) \cot \delta_0 + G(r)]\ (1 - e^{-\beta r}), \tag{10}$$

and F(r) and G(r) are the regular and irregular Coulomb wave functions adequately normalized.[12] The parameter β was taken the same as indicated by Foldy and Eriksen.[1] The integration was carried out numerically up to $R = 1.6$ F, with sufficient accuracy even for the cases with extended charges without cutoff.

A least-squares fit to $K' = K - \Delta K$ was calculated; K was obtained from the very accurate phase shifts quoted by H. Pierre Noyes[5] and due to several experimental groups.[13-15] Table C.16-I summarizes the results. It can be appreciated that the change in a_p is quite small, about 0.4% when V_{ES} is changed from the exponential case to the uniform charge distribution with sharp cutoff (about 20% change).

Schneider and Thaler[16] have calculated recently the effect of electromagnetic corrections to low-energy nucleon-nucleon scattering, using a hard core of 0.388 F, from another viewpoint, i.e., with the purpose of changing the parameters of the potential in order to obtain the empirical values of a_p and subsequently produce values for a_n. Table C.16-I contains calculations of the corrections for a model with a core of 0.4 F and also for a soft core as corresponding to the Gartenhaus model[17]; the values excluding the point at 0.3825 MeV are also presented on grounds that such measurement may be questionable,[18] and the shape parameter P depends critically on it.

The conclusions are that a nonnegligible correction to the p-p scattering parameters arises from the consideration of the extended charge distribution of the proton, far beyond the errors quoted in the recent literature.

Footnote and References

*Modified version of paper submitted to Phys. Rev.

1. Leslie L. Foldy and Erik Eriksen, Phys. Rev. 98, 775 (1955).
2. Erik Eriksen and Leslie L. Foldy, Phys. Rev. 103, 781 (1956).
3. J. S. Schwinger, Phys. Rev. 78, 135 (1950).
4. E. E. Salpeter, Phys. Rev. 91, 994 (1953).
5. H. Pierre Noyes, Phys. Rev. Letters 12, 528 (1964), and references therein.
6. David J. Knecht, S. Messelt, E. D. Berners, and L. C. Northcliffe, Phys. Rev. 114, 550 (1959), and references therein.
7. H. Pierre Noyes, Phys. Rev. 130, 2025 (1963).
8. R. P. Haddock, R. M. Salter, Jr., M. Zeller, J. B. Czirr, and D. R. Nygren, Phys. Rev. Letters, 14, 318 (1965).
9. R. Hofstadter, F. Bumiller, and M. R. Yearian, Rev. Mod. Phys. 30, 482 (1958).
10. R. Hofstadter and R. Herman, Phys. Rev. Letters 6, 293 (1961).
11. M. A. Preston, Physics of the Nucleus (Addison-Wesley Publishing Company, Inc., Reading, Massachusetts, 1962).
12. The choice of U(r) as given by Eq. (10) is consistent with a model for the nucleon-nucleon interaction as given by A. M. Green, Nucl. Phys. 33, 218 (1962), with a velocity-dependent potential that generates a repulsive core dynamically. Therefore at low energies the core is negligible. Of course, hard-core models will produce a much smaller ΔK, although presently they are discredited and instead soft-core models are more popular. However, even with a hard-core model (core radius ≈ 0.4 F) the corrections to p-p scattering parameters are nonnegligible.
13. J. E. Brolley, J. D. Seagrave, and J. G. Berry, Bull. Am. Phys. Soc. 8, 604 (1963) and Ref. 5.
14. M. L. Gursky and L. Heller, Bull. Am. Phys. Soc. 8, 605 (1963).
15. P. F. Dahl, D. J. Knecht, and S. Messelt, University of Wisconsin, private communication to H. Pierre Noyes, Ref. 5.

16. R. E. Schneider and R. M. Thaler. Phys. Rev. 137, B874 (1965).
17. S. Gartenhaus, Phys. Rev. 100, 900 (1955).
18. R. J. Slobodrian, On the Determination of the Proton-Proton $^1S_0$ Parameter UCRL-16408, Sept. 1965, Nuovo Cimento (to be published).

Table C.16-I. Calculated scattering parameters for a least-squares fit to the corrected values K'. For comparison the parameters obtained from the point-charge assumption are transcribed, together with the predictions of the BC and PWDR models.[a] The lines numbered 1, 2, 3, correspond respectively to a point charge in the field of an exponential distribution, to two uniformly charged spheres, and to two exponential distributions; the last should be considered the most realistic picture because it is consistent with the electron-scattering results of Hofstadter. (Refs. 9, 10). The lines labeled 5 correspond to fit with five experimental points, and those labeled 6 correspond to four experimental points excluding the point 0.3825 MeV.

Parameter		A	B	C	$-a_p$	r_e	P
Model			MeV^{-1}	MeV^{-2}	F	F	
Extended charge							
	1	3.77431	0.48619	-0.0023968	7.6354	2.8021	0.02607
SD	2	3.78856	0.48610	-0.0023522	7.6067	2.8016	0.02560
	3	3.80377	0.48607	-0.0023015	7.5770	2.8014	0.02506
	1	3.77920	0.47806	0	7.6265	2.7552	0
SI	2	3.79341	0.47810	0	7.5980	2.7555	0
	3	3.80847	0.47826	0	7.5679	2.7568	0
Hard core	5	3.69602	0.48602	-0.0025336	7.7978	2.8011	0.02759
r_c = 0.4 F	6	3.70237	0.48005	-0.0012301	7.7845	2.7667	0.01390
Soft core	5	3.71893	0.48379	-0.0019897	7.7498	2.7882	0.02197
Gartenhaus[17]	6	3.72461	0.47848	-0.0008342	7.7380	2.7576	0.01003
POINT CHARGE							
SD (a)				7.8284 ± 0.0080	2.794 ± 0.026	0.026 ± 0.014	
SI (a)				7.8163 ± 0.0048	2.745 ± 0.014	0	
BC (a)				7.8009	2.687	-0.036	
PWDR (a)				7.8259	2.786	0.024	

(a) See Ref. 5.

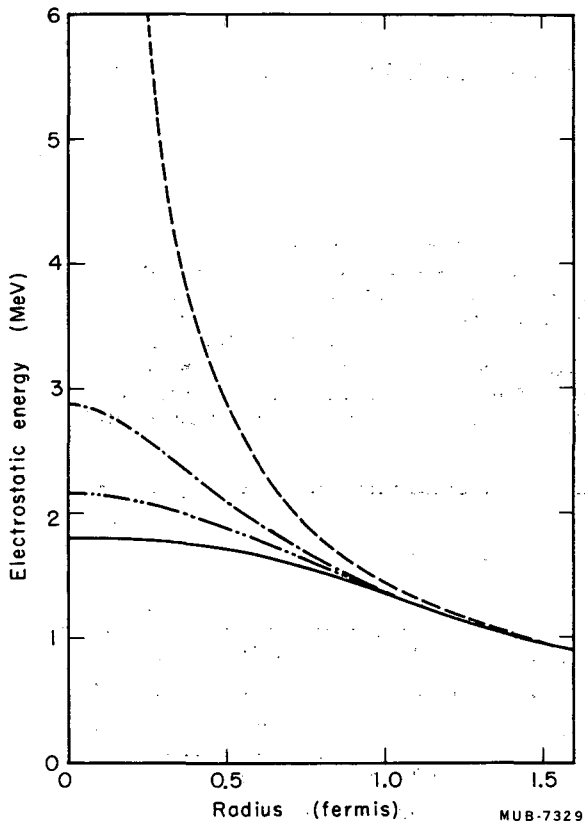

Fig. C.16-1. Electrostatic potential energy. — — —, point-charge model; — · — · —, a point charge in the field of an exponential charge density $\rho = ke^{-\alpha r}$; — · · — · · —, two uniformly charged spheres; and ———, two exponential charge distributions consistent with the results of the Hofstadter group.

17. THE Li^6 (p, pd) He^4 AND Li^7 (p, pt) He^4 REACTIONS AT 55 MeV

D. L. Hendrie, Marc Chabre,* and H. G. Pugh†

Several experiments have shown that the (p, pd) reaction proceeds with high probability in nuclear reactions induced by medium- or high-energy protons incident on Li^6 targets.[1] The angular correlations between the scattered proton and outgoing deuteron show a large peak at angles corresponding to free p-d scattering. This has been interpreted to mean that the incoming proton has interacted with and ejected a preformed deuteron from the nucleus. Cluster-model calculations select Li^6 to be a good example of a nucleus that contains such preformed deuterons.[2] Evidence indicates that competing mechanisms such as indirect pickup and sequential processes are less important. Much of the analysis has been done in terms of the quasi-free scattering approximation, in which distortion of the incoming and outgoing particle waves is neglected, as is the binding energy of the deuteron to the core. The shape of the angular correlation is then determined by the momentum distribution of the deuteron in the nucleus. The cross section in the quasi-free approximation[1] is

$$\frac{d^3\sigma}{d\Omega_p\, d\Omega_d\, dE_d} = \frac{9}{2}\,\frac{k_0 k_p k_d}{E_0}\,\frac{d\sigma}{d\Omega}\bigg|_{p-d} P(d)\,|\psi_L(Q)|^2 ,$$

where k_0, k_p, k_d are the wave numbers of the incident and outgoing particles; $\frac{d\sigma}{d\Omega}\big|_{p-d}$ is the free p-d scattering cross section, P(d) is the probability of finding a deuteron cluster in the nucleus, and $\psi_L(Q)$ is the wave function of the deuteron cluster with momentum Q and angular momentum L. This separation can be valid only if the amount of clustering is large (i.e., $P(d) \approx 1$) and more complex effects, such as exchange and contributions from the core, are neglected.

We have looked at the Li^6(p, pd) He^4 reaction, using the 88-inch cyclotron to provide the 55-MeV protons. The outgoing particles were detected in two ΔE-E solid-state counter

telescopes. A fast coincidence was required and the particles were electronically identified and summed before being fed into a 4096-channel two-dimensional analyzer. The two axes of the analyzer were fed with summed energy pulses ($E_p + E_d$) and deuteron energy pulses (E_d) respectively. The correlations were obtained by maintaining the proton counter at fixed angles and moving the deuteron counter in the scattering plane.

An angular correlation obtained at a proton angle of 60 deg is seen in Fig. C.17-1. The peak in the correlation occurs at $\theta_d = 46$ deg, where the momentum transfer to the recoiling nucleus (-Q) is zero, or just the angle at which the deuterons would appear from protons scattered from free deuterons at rest. The half width of the peak, corresponding to a variation in Q of 64 MeV/c, can be compared with the momentum distribution of 60.6 MeV/c expected for a deuteron bound by 1.47 MeV. Similarly, Fig. C.17-2 shows the correlation obtained for fixed angles ($\theta_p = 60$ deg, $\theta_d = 46$ deg) and varied deuteron energy. One again obtains a peak with a half-width corresponding to a variation in Q of 64 MeV/c. The dotted lines in Figs. C.17-1 and C.17-2 indicate the fit obtained by using harmonic oscillator wave functions for $\psi_L(Q)$ with the range parameter equal to 37.6 MeV/c and L = 0. With these values we obtain a probability of ≈ 15% of finding a deuteron in Li^6. Similar results obtain at other proton angles.

These results and the low binding energy of a triton in Li^7 (2.47 MeV) encouraged us to try the $Li^7(p, pt)He^4$ reaction, although clustering may be less significant in Li^7.[3] Figures C.17-3 and C. 17-4 show the resulting angular correlation for $\theta_p = 75$ deg, and energy correlation for $\theta_p = 75$ deg, $\theta_t = 41$ deg. Again we find results equivalent to quasi-free scattering, but with non-zero angular momentum transfer. The dotted line in Fig. C.17-3 is an attempt to fit the data with harmonic oscillator wave functions with L = 1 and the range parameter equal to 55.6 MeV/c. Clearly, we would have better fits if we had chosen wave functions that arise from wells with a longer range than the harmonic oscillator well. Since the free p-t scattering cross section is not known at this energy, no probability of clustering can be obtained.

Although we have used the theory in its very crudest form, quasi-free scattering seems to fully account for our $Li^6(p, pd)He^4$ results. However, it is expected that the deuteron clustering probability would change markedly with improved theoretical handling. Since experimental conditions are little changed from the $Li^6(p, pd)$ to the $Li^7(p, pt)$ reaction, quasi-free scattering should occur in this case, if P(t) is not negligible. That this is, in fact, the case indicates that triton clustering in Li^7 may be about as important[4] as deuteron clustering in Li^6. Conversely, further results not shown here indicate that triton clusters in Li^6 and deuteron clusters in Li^7 are less important by 1 to 2 orders of magnitude.

Footnotes and References

*NATO Fellow on leave from CNRS, Institut Fourier, Grenoble, France.

†Present address: University of Maryland, College Park, Maryland.

1. See, for example, M. Riou, Rev. Mod. Phys. 37, 375 (1965); D. W. Devins, Bruce L. Scott, and H. H. Forster, Rev. Mod. Phys. 37, 396 (1965).
2. Y. C. Tang, K. Wildermuth, and L. Pearlstein, Phys. Rev. 123, 548 (1961).
3. D. R. Inglis, Rev. Mod. Phys. 34, 165 (1962).
4. R. K. Sheline and K. Wildermuth, Nucl. Phys. 21, 196 (1960).

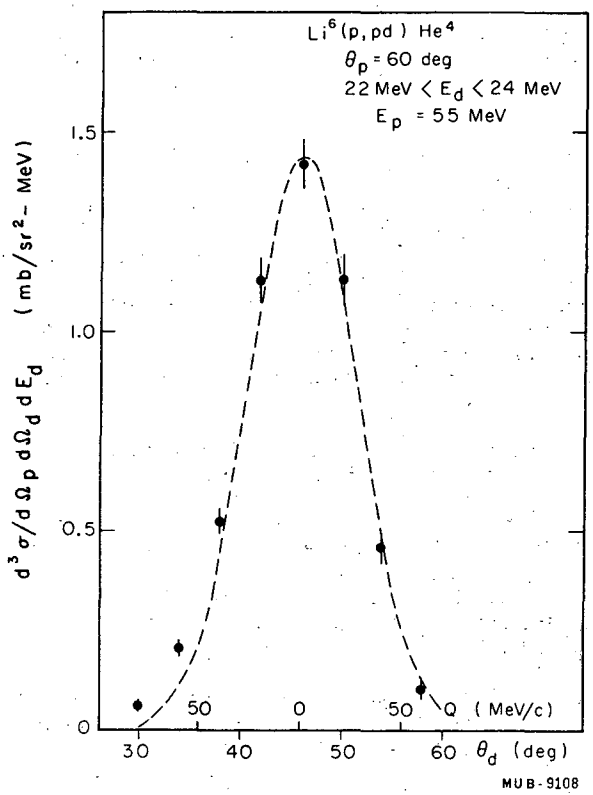

Fig. C.17-1. Angular correlation for the $Li^6(p, pd)He^4$ reaction. The dashed line is a fit with harmonic oscillator wave functions with L = 0.

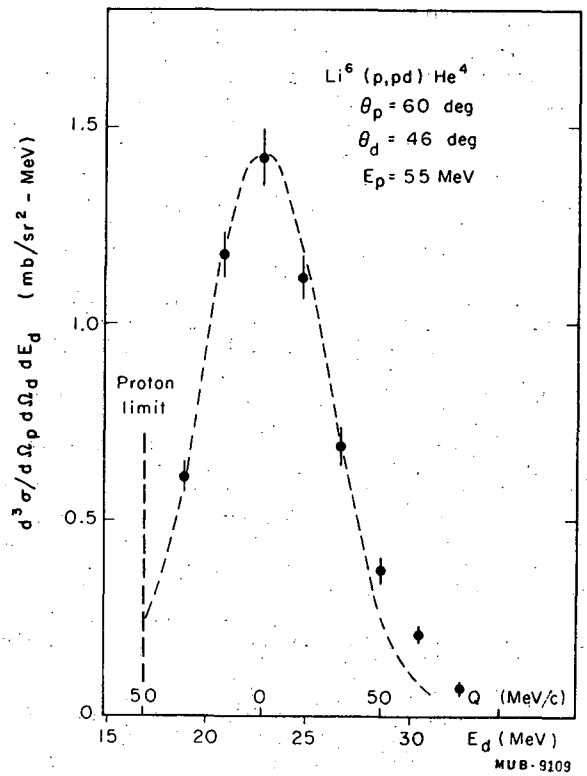

Fig. C.17-2. Energy correlation for the $Li^6(p, pd)He^4$ reactions. The dashed line is a fit with harmonic oscillator wave functions. The proton limit was imposed by the proton counter thickness.

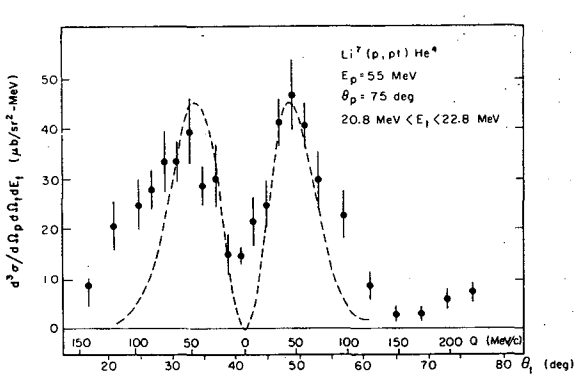

Fig. C.17-3. Angular correlation for the $Li^7(p, pt)He^4$ reaction. The dashed line is a fit with harmonic oscillator wave functions with L = 1.

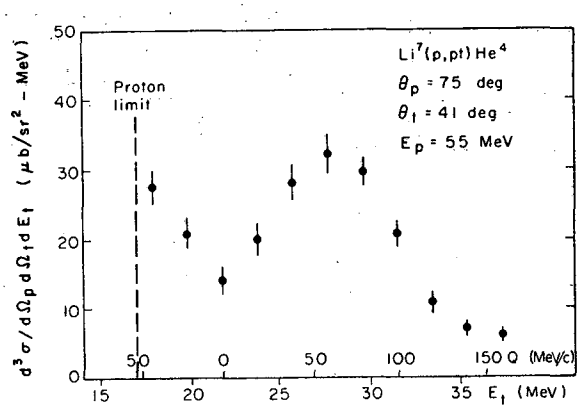

Fig. C.17-4. Energy correlation for the $Li^7(p, pt)He^4$ reaction. The proton limit was imposed by the proton counter thickness.

D. CHEMISTRY

1. SYSTEMATIC VARIATION OF QUADRUPOLE CRYSTAL-FIELD SHIELDING IN RARE-EARTH ETHYLSULFATES

Johan Blok and D. A. Shirley

It has long been clear that application of group-theoretical methods to rare-earth ions in crystals gave a quantitatively correct description of stark levels only if the crystalline field terms could be parameterized into the actual components of the crystalline field A_L^M and multiplicative correction factors, $(1-\sigma_L)$, which account for shielding of the 4f electrons by other electron orbitals on the central ion. By comparing measured quadrupole coupling constants with optical data we have been able to evaluate σ_2, the leading-term shielding parameter, in rare-earth ethylsulfates.[1]

In the crystal-field model the Coulombic interaction of the 4f electron level with the crystal field may be written

$$\mathcal{H} = \sum_k \sum_{L,M} \left\{ A_L^M [r_k^L + S_L(r_k)] + T_L^M(r_k) \right\} \Phi_L^M(\theta_k, \phi_k). \tag{1}$$

Here r_k, θ_k, and ϕ_k are the coordinates of the kth 4f electron, Φ_L^M is a linear combination of spherical harmonics Y_L^M and Y_L^{-M}, A_L^M is a multiplicative factor giving the strength of the crystal field, and S_L is the linear shielding term arising from deformation of closed electronic shells. Nonlinear shielding[2] is described by T_L^M, which depends on several A_L^M. Experimentally, optical data are fitted with crystal-field parameters $V_L^M = A_L^M(1-\sigma_L)\langle r^L\rangle_{4f}$. This may be regarded as the defining equation for σ_L. It is important to note that both linear and nonlinear shielding terms are contained in σ_L in a completely empirical way. Thus σ_2 is not independent of A_2^0.

Interaction of the rare-earth ion with the crystal field sets up field gradients at the nucleus through a variety of mechanisms. Experimentally one finds that the nuclear spin Hamiltonian has a term of the form

$$\mathcal{H} = P[I_z^2 - \tfrac{1}{3} I(I+1)]. \tag{2}$$

We refer to the directly measurable quantity P as the quadrupole coupling constant. P may be a linear combination of several terms,

$$P = \sum P_i = P_{4f}^{(1)} + P_{pq} + P_{Lat} + P_{4f}^{(2)} + \cdots . \tag{3}$$

Here $P_{4f}^{(j)}$ arises from the 4f configuration in jth-order perturbation theory. While $P_{4f}^{(1)}$ is most common, $P_{4f}^{(2)}$ is very important in Eu^{3+} in the $^7F_0$ ground state. The antishielded lattice contribution is given by

$$P_{Lat} = -\left[\frac{3Q}{I(2I-1)}\right](1-\gamma_\infty)A_2^0, \tag{4}$$

and the first-order 4f term by[3]

$$P_{4f}^{(1)} = -\frac{3e^2Q}{4I(2I-1)}(1-R_Q)[3J_z^2 - J(J+1)]\langle r^{-3}\rangle_{4f}\langle J \| \alpha \| J\rangle . \tag{5}$$

Here γ_∞ is the Sternheimer factor for the lattice and R_Q is the "atomic Sternheimer factor." The quantity $\langle J \| \alpha \| J\rangle$ arises in application of the Wigner-Eckart theorem to evaluation of the crystal-field interaction by the "operator equivalent" technique,[3] and $\langle r^{-3}\rangle_{4f}$ is the actual expectation value of r^{-3} for 4f electrons in the ion. The effective $\langle r^{-3}\rangle_Q$ for quadrupole interactions is given by[4]

$$\langle r^{-3} \rangle_Q = (1 - R_Q) \langle r^{-3} \rangle_{4f} . \tag{6}$$

With sufficient knowledge of the behavior of a given ion in a crystal along with the values of P, P_{4f} where necessary, Q, and I for a specific isotope, it is possible to obtain the quantity $(1 - \gamma_\infty)A_2^0$. We have derived this quantity for several ions in the ethylsulfate lattice from P values obtained by nuclear orientation, Mössbauer spectroscopy, and nuclear magnetic resonance.[1] Comparison with the calculated value[5] $\gamma_\infty = -80$ yields A_2^0 in each case. Comparison of these "directly measured" crystal-field parameters with the V_2^0's determined from optical spectroscopy yields the shielding factors $1-\sigma_2$. In Figs. D.1-1, D.1-2, and D.1-3 are shown the variations of V_2^0, $(1-\gamma_\infty)A_2^0$, and $1-\sigma_2$ with atomic number throughout the rare earth series. Values are summarized in Table I. The value of $\sigma_2 \approx 0.6$ for heavy rare earths is roughly what is expected theoretically, but the much larger σ_2's in light rare earths is surprising.

References

1. An account of the nuclear orientation data used in this study, involving orientation of La^{140}, En^{154}, Gd^{159}, Lu^{177}, and Lu^{177m}, is given in Lawrence Radiation Laboratory Report UCRL-16328. A more extensive account of the work described herein is given in UCRL-16318.
2. A. J. Freeman and R. E. Watson, Phys. Rev. 127, 2058 (1962).
3. R. J. Elliott and K. W. H. Stevens, Proc. Roy. Soc. (London) A218, 553 (1953).
4. A. J. Freeman and R. E. Watson, Phys. Rev. 132, 706 (1963).
5. R. E. Watson and A. J. Freeman, Phys. Rev. 135, A1209 (1964).

Table I. Crystal-field data for the rare-earth ethylsulfates

n in $4f^n$	ion	isotope	method[a]	P_{Lat} ($\times 10^{-5}$ cm^{-1})[b]	Q(barns)	$(1-\gamma_\infty)A_2^0$ (10^4 cm^{-1} a_0^{-2})	A_2^0(cm^{-1} a_0^{-2})[m]	$A_2^0(r^2)$ (cm^{-1})[n]	$A_2^0(r^2)$ (cm^{-1})[o]	$(1-\sigma_2)A_2^0$ (cm^{-1})[q]	σ_2[as]	σ_{theory}	references
0	La^{3+}	139	NMR	1.98[c]	+0.27(1)[h]	1.43(6)	177			(-40)	1.23		12, 31
		140	NA	-1.42(12)[d]	+0.13(2)[i]								this work
1	Ce^{3+}									-13(8)[r]	(1.1)	0.68[cc]	
2	Pr^{3+}								616[p]	14.1[s]	(1.0)	0.52[dd] 0.59[ee]	
3	Nd^{3+}									58.4[t]	(0.9)		
4	Pm^{3+}									(73)	(0.8)		
5	Sm^{3+}									87[u]	(0.75)		
6	Eu^{3+}	154	NA	-78(4)[d,e] p=41.7(28)	+3.75(37)[i]	+2.9(3)	362	317		96[v]	0.73		this work
7	Gd^{3+}	159	NA	-144(5)[d]	(+1.56)[j]	+2.54(26)	314	246		(121)	0.61		this work
8	Tb^{3+}									146[w]	(0.65)		
9	Dy^{3+}	161	M	-120(6)[e,f]	+2.6[k]	+4.29(22)	530	385		171[x]	0.68		15
10	Ho^{3+}									180[w]	(0.6)		
11	Er^{3+}								313, [p]406	188[y]	(0.6)		
12	Tm^{3+}	169	M	g	+1.5[l]	+5.10	630	403		204[z]	0.68[bb]	0.50[cc]	14
13	Yb^{3+}									(220)	(0.6)		
14	Lu^{3+}	175	NMR	108.64(20)[c]	+3.6[j]	+5.9	730			(236)	0.68		31
		177	NA	-67(2)[d]	+3.6[j]	+3.65(12)	450				0.48		this work

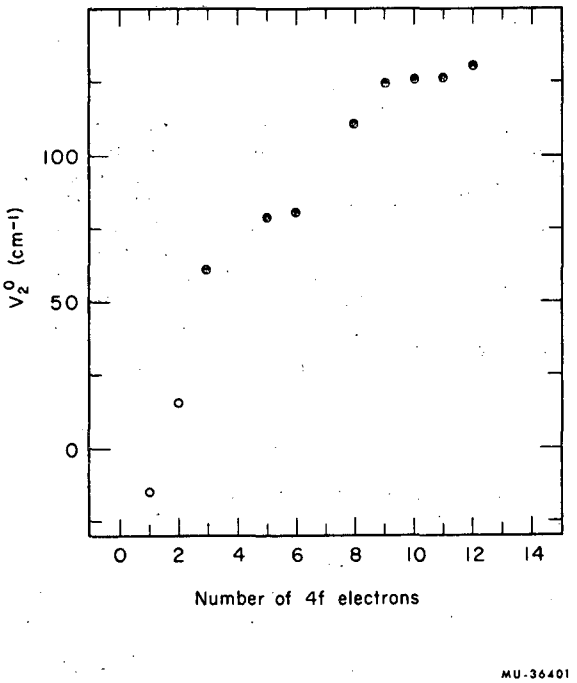

Fig. D.1-1. Experimental values of $V_2{}^0 = A_2{}^0 (1 - \sigma_2) \langle r^2 \rangle_{4f}$, for trivalent rare-earth ions in the ethylsulfate lattice, obtained from optical and paramagnetic resonance data. Values are also given in Table I. $V_2{}^0$ seems to change sign in the very light rare earths.

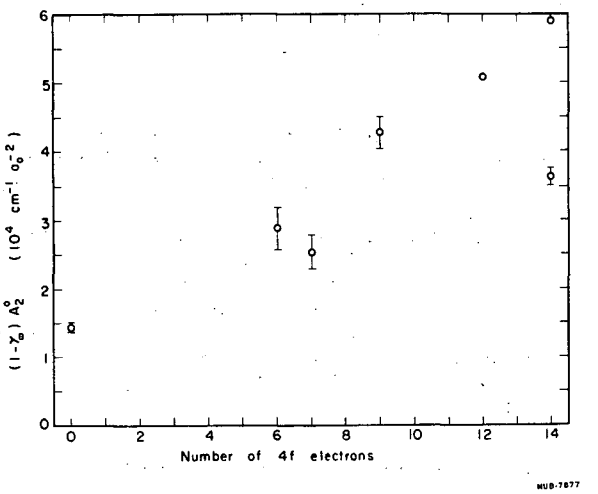

Fig. D.1-2. Antishielded crystal-field gradient, $(1-\gamma_\infty) A_2{}^0$, derived from quadrupole coupling constants, for several trivalent rare-earth ions in the ethylsulfate lattice. A definite upward trend is evident.

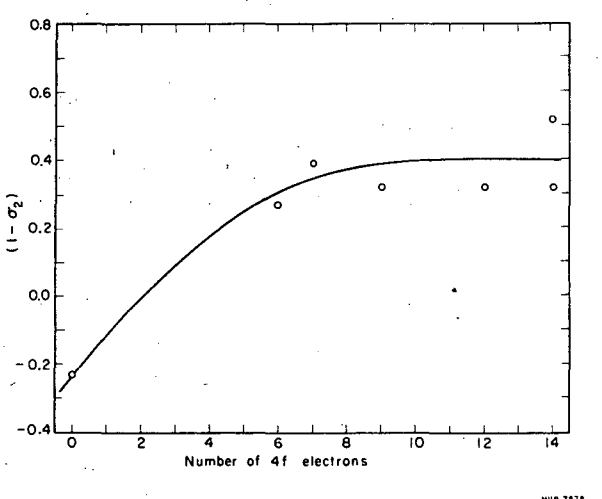

Fig. D.1-3. Derived values of $(1-\sigma_2)$ for trivalent rare-earth ions in the ethylsulfate lattice, obtained by combining points shown in Figs. 1 and 2, using $\gamma_\infty = -80$, and neglecting any possible variation of ions' properties with host. After this work was completed S. Hüfner (Munich) informed us of his recently determined value $\sigma_2 = 61$ for Ho($4f^{10}$); this falls right on the curve.

2. SYSTEMATIC VARIATION OF HYPERFINE FIELDS AT NUCLEI OF SOLUTES IN FERROMAGNETIC LATTICES

D. A. Shirley

For some time we have conducted a long-range program to characterize the hyperfine fields induced at nuclei of atoms dissolved in ferromagnetic lattices. The original purpose of this work was to assess, for the various elements, the "universal" method of nuclear orientation introduced by B. N. Samoilov and co-workers.[1] This was to be accomplished by determining experimentally enough of those fields that trends throughout the periodic table could be established. At this time this original objective is near completion. With the help of two completely new techniques - Mössbauer spectroscopy and time-differential angular correlation - and substantial improvement in the nuclear polarization method, as well as further application of the NMR and heat-capacity methods, various workers throughout the world have accumulated sufficient data on induced fields to allow several trends to be observed. Although a few gaps remain, we have a rather complete systematic (albeit empirical) picture of induced fields. The various trends are described below.

1. Proportionality to lattice magnetization.

For solute atoms of normally "magnetic" elements there is some tendency to take a certain hyperfine interaction into the host lattice. This field may be essentially constant, as is the case for rare earth, in which the fields arise from orbital, as well as spin, magnetism, and in which the moments are patently localized. Of course this hyperfine interaction, $A\vec{I} \cdot \vec{J}$ may be manifest as various values of hyperfine field in different crystal-field environments, but these fields can be treated theoretically to give A, the hyperfine-structure constant.

A second class of solutes comprises atoms of elements that are normally "magnetic" at low temperatures. Manganese and iron are good examples of this class. Although the behavior of these atoms as solutes in ferromagnetic hosts is by no means well understood, there is some evidence that "localized moments" are formed, with the solute atom largely bringing its own magnetism into the lattice.

The third class of elements is far more important for nuclear orientation purposes. It consists of those atoms that are normally not magnetic in the elemental form. Hyperfine fields in these solutes are induced by the ferromagnetic hosts. Near the center of the 4f, 5d, and 6p series these induced fields tend to follow the host magnetization. The major conclusion to be drawn from the above discussion is that for orienting nuclei of nominally "nonmagnetic" elements one should choose a lattice with maximum magnetization. For most purposes iron is the optimum choice.

2. Regular variation of induced fields with atomic number.

Distinct regularities have been discovered[2,3] in the variation of induced fields with atomic number in both Fe and Ni hosts. These are illustrated for 3d, 4d, and 5d solutes in Fe in Fig. D.4-1, and for the 4d-5p series in Fe and Ni in Fig. D.4-2.

For the noble metals, presumably for the alkalies, and less certainly for the alkaline earths and II-B metals, the dominant contribution to the hyperfine field arises via polarization of conduction (s) electrons. Near the center of the d shell, however, core polarization apparently takes over, creating a pronounced maximum in this region (Fe-Co, Ru-Pd, Os-Pt). The p shells apparently produce the same kind of trends, but with positive, rather than negative, induced fields.

3. Prospects for the "universal" method of nuclear orientation.

With the detailed knowledge that is presently available, we can now predict to which elements the "universal" method may be applicable. Since laboratory magnetic fields of 10^5 gauss are available, we shall use as a criterion the existence of fields, in suitable lattices, in excess of this figure. To date all together 39 elements have had nuclei oriented by all equilibrium methods. The "universal" method should extend this list to at least 22 additional elements -Ni, Ga, Ge, Se, Zr, Mo, Tc, Ru, Rf, Pd, Cd, Te, Hf, Ta, W, Os, Pt, Hg, Tl, Pb, Bi, and Po.

References

1. B. N. Samoilov, V. V. Sklyarevskii, and E. P. Stepanov, Soviet Physics JETP 11, 261 (1960).
2. R. B. Frankel et al., Phys. Letters 15, 163 (1965).
3. D. A. Shirley and G. A. Westenbarger, Phys. Rev. 138, A170 (1965).

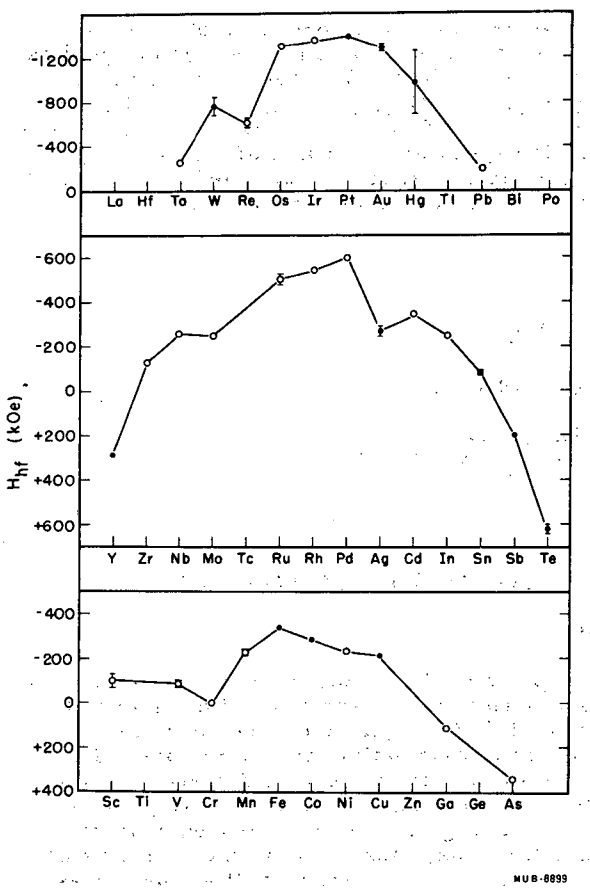

Fig. D.2-1. Induced hyperfine magnetic fields, in an iron lattice, for several elements in the 3d, 4d, and 5d series.

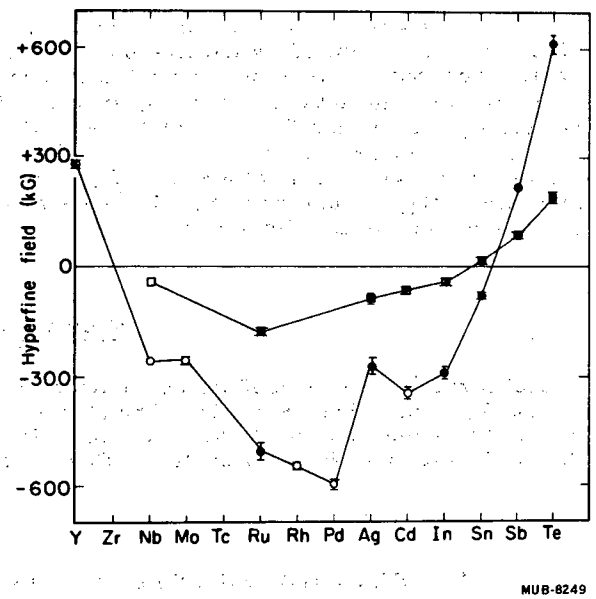

Fig. D.2-2. Induced fields for the 4d-5p in iron (circles) and nickel (squares). Filled points are those for which the signs have been determined.

3. HYPERSENSITIVE TRANSITIONS IN RARE-EARTH IONS†

B. R. Judd

A few years ago, it was noticed that the intensities of some absorption lines in the solution spectra of rare-earth ions are peculiarly sensitive to the solvent.[1] The source of the hypersensitivity was later examined in detail, and it was concluded that it owed its existence to the inhomogeneous polarizability of the solvent, which was visualized as enhancing the variation of the electric vector of the electromagnetic radiation across a rare-earth ion, thereby greatly increasing the intensities of quadrupole transitions.[2]

An additional source for the hypersensitivity can arise from the presence of constant electric fields produced by the ligands. These distort the f shells, and mix in states of opposite parity such that the net electric field at a rare-earth nucleus is zero. The point symmetry can be at the very highest one of the sequence C_s, C_1, C_2, C_{2v}, C_3, C_{3v}, C_4, C_{4v}, C_6, or C_{6v}. It is thus significant that the lines at 17·300 cm^{-1} and 19 320 cm^{-1} of Nd^{3+}, already classed as hypersensitive,[1] appear to be the most intense in the absorption spectrum of $Nd_2Mg_3(NO_3)_{12} \cdot 24H_2O$, for which the Nd^{3+} ion is at a site of C_{3v} symmetry. Furthermore, it is to be noted that for Sm^{2+} at a site of C_{4v} symmetry in BaClF, there appears to be strong evidence for constant electric-field terms in the Hamiltonian.[3]

Footnote and References

†Brief form of UCRL-16380 (to be published in J. Chem. Phys.).

1. B. R. Judd, Phys. Rev. 127, 750 (1962).
2. C. K. Jørgensen and B. R. Judd, Mol. Phys. 8, 281 (1964).
3. Z. J. Kiss and W. A. Weakleim, Phys. Rev. Letters 15, 457 (1965).

4. SECOND QUANTIZATION AND ATOMIC SPECTROSCOPY†

B. R. Judd

The method of using annihilation and creation operators in the theory of atomic spectroscopy has been examined in detail. Basic formulae have been derived, and several examples of the effect of configuration interaction on the configuration $(n\ell)^N$ of equivalent electrons are discussed. These include corrections to the hyperfine structure originating from core polarization, and also displacements of terms. The results of Rajnak and Wybourne[1] can be derived in a particularly transparent way, and a number of errors thereby removed. Illustrations are provided by drawing out the Feynman graphs and interpreting them through the topologically equivalent angular-momentum graphs of Jucys.[2] Complete calculations may thus be carried out graphically, the final combinations of 3-j, 6-j, or 9-j symbols being specified in detail as well as their phase and associated factors.

A large field for further study opens up when the tensorial character of the creation and annihilation operators is examined. The reduced matrix element of a creation operator is simply related to the fractional parentage coefficient $(\psi\{|\bar{\Psi})$, and this permits a rapid derivation of a number of formulae involving such coefficients. In particular, the undetermined normalizing factor N in Redmond's formula[3] for $(\psi\{|\bar{\Psi})$ is given an explicit form.

Further applications become possible when a creation and an annihilation operator are regarded as the two components $(m_q = \pm 1/2)$ of a tensor of rank 1/2 with respect to quasispin $\underset{\sim}{Q}$. It turns out that for a state ψ of seniority v,

$$Q = (2\ell + 1 - v)/2, \qquad M_Q = -(2\ell + 1 - N)/2.$$

Hence questions of seniority reduce to problems of quasi angular-momentum. Triple tensors are introduced, their three ranks specifying their rank with result to quasispin, spin, and orbital angular momentum. Conjugation, the operation that connects hole states to particle states, corresponds to $M_Q \rightarrow -M_Q$, and is thus analogous to time reversal, for which $M_S \rightarrow -M_S$ and

$M_L \rightarrow -M_L$. The frequent vanishing of matrix elements for half-filled shells is related to the vanishing of 3-j symbols in which quasispin quantum numbers appear in the top row and zeros in the bottom.

The curious connection between states $(v_1 S_1)$ and $(v_2 S_2)$ for which $v_1 + 2S_2 = v_2 + 2S_1 = 2\ell + 1$, which was noted some years ago by Racah,[4] is found to correspond to the interchange of spin and quasispin. This has an important application in allowing matrix elements of double tensors, such as are required in hyperfine-structure calculations, to be related to those of single-rank tensors that have already been tabulated.

Among many results obtained in the study of groups, it may be mentioned that the entire atomic f shell spans the simplest spin representation (of dimension 16384) of R_{29}, the rotation group in 29 dimensions.

Footnote and References

†Brief form of UCRL-16098.

1. K. Rajnak and B. G. Wybourne, Phys. Rev. 132, 280 (1963).
2. See, for example, A. Jucys, J. Levinsonas, and V. Vanagas, Mathematical Apparatus of the Theory of Angular Momentum (in Russian) (Vilna, 1960).
3. P. J. Redmond, Proc. Roy. Soc. (London) A222, 84 (1954).
4. G. Racah, Phys. Rev. 76, 1352 (1949).

5. THREE-PARTICLE OPERATORS FOR EQUIVALENT ELECTRONS†

B. R. Judd

Interaction between the electronic configurations $(n\ell)^N$ and $(n\ell)^{N\pm1}(n'\ell')^{\mp1}$ can be represented for $(n\ell)^N$ by the addition of effective three-particle operators to the Hamiltonian, the effective two-particle parts being absorbed by operators already present in the elementary linear theory of configuration interaction. For f electrons, the three-particle operators are decomposed into nine operators t_i that are labeled by irreducible representations W and U of the groups R_7 and G_2 respectively. We find WU≡ (000)(00), (220)(22), (222)(00), (222)(40), (400)(40), (420)(22), (420)(40), (420)(42), (600)(60), for $i = 1, 2, \cdots, 9$. The matrix elements of t_9 are always zero, while those for t_5 are proportional to the two-particle operator e_2 of Racah,[1] which is already included in the total Hamiltonian. Furthermore, t_1 can be absorbed by e_0 and e_1. Hence for f electrons, only six parameters are required to completely reproduce the effective three-particle operators. For the d shell the situation is even simpler; Feneuille[2] has shown that two additional parameters suffice. Complete tables of the matrix elements of the t_i for f^3 have been constructed.

The dependence on N of matrix elements between states of given seniorities is studied by breaking the t_i down into parts characterized by well-defined quasispin. To do this, the decompositions of a number of representations of R_{28} are required. The analysis, incidentally, reveals why Racah achieved such success by writing $e_3 = (e_3 + \Omega) - \Omega$ and then evaluating the matrix elements of $e_3 + \Omega$ and Ω separately to find those for e_3. It turns out that $e_3 + \Omega$ and Ω correspond to quasispins $K = 2$ and 0 respectively, and consequently possess the striking properties expected when quasispin is a good quantum number. The six t_i $(i = 2, 3, 4, 6, 7, 8)$ break down into parts corresponding to $K = 1$ or 3. For a half-filled shell, operators with odd K can be shown to vanish between states of seniorities v and v' for which $v - v' \equiv 0 \pmod 4$; whereas the ordinary two-particle operators e_i correspond to even K and are nonvanishing only when this condition is fulfilled. It follows that the effect of the three-particle operators vanishes for a half-filled shell such as Gd^{3+} $4f^7$ in the limit of Russell-Saunders coupling.

Footnote and References

†Brief form of UCRL-16321 (to be published in Phys. Rev.)

1. G. Racah, Phys. Rev. 76, 1352 (1949).
2. S. Feneuille, Opérateurs à trois particules pour des électrons d équivalents, submitted to Comptes Rendus.

6. ZEEMAN EFFECT AS A PROTOTYPE FOR INTRA-ATOMIC INTERACTIONS†

B. R. Judd

When an atom is placed in a unit magnetic field, the energies of the components of a level J are given in units of the Bohr magneton by gM_J, where g is the Landé factor and M_J is the quantum number of the projection J_z of the total angular momentum J. That gM_J should be a simple product is a consequence of the Wigner-Eckart theorem, applied to the group R_3 of rotations in ordinary three-dimensional space. Since intra-atomic interactions are all scalars in R_3, a similar application of the Wigner-Eckart theorem to these cases does not give useful results. However, if our eigenfunctions are described by the representations of higher groups, such as R_5 for d electrons, the theorem can again be applied when the interactions have been broken down into parts having well-defined properties with respect to these groups.

The method is illustrated in detail for the spin-spin and spin-other-orbit interactions, and applied to the d shell. It is found that the spin-spin interaction H_{ss} can be decomposed into two parts h_1 and h_2, corresponding to the respective classifications (22000)(20) $^5D_0$ and (22000)(22) $^5D_0$. Here (22000) stands for a representation of the symplectic group Sp_{10}; (20) and (22) are representations of R_5; and the spin and orbital characteristics are described by the familiar spectroscopic symbols. The spin-other-orbit interaction is more complicated, and for d electrons five components are needed. Their representations of Sp_{10} and R_5 are (11000)(11), (11110)(21), (22000)(11), (22000)(21), and (22000)(31); they all correspond to $^3P_0$.

These decompositions make apparent a number of striking properties that spin-spin and spin-other-orbit interactions possess, and also point the way to a treatment of the f shell.

Footnote

†Brief form of UCRL-16273 (paper presented at the Zeeman Centennial Conference in Amsterdam, September 1965) (to be published in Physica).

7. THE HYPERFINE MAGNETIC FIELDS AT NUCLEI OF INDIUM IN IRON AND NICKEL†

R. J. Holliday, D. A. Shirley, and N. J. Stone‡

The decay scheme in In^{114m} is shown in Fig. D.7-1. This isotope was one of the first used by Samoilov et al.[1] to demonstrate the existence of large hyperfine magnetic fields at the nuclei of diamagnetic atoms dissolved in ferromagnetic lattices. They found a lower limit of H_{hf}(In in Fe) $\geq$175 kG for the field for In in iron. Later this value was changed to 250 kG and an attempt was made to measure H_{hf}(In in Ni), but no anisotropy was observed.[2] The sign of H_{hf}(In in Fe) was subsequently determined as negative (i.e., opposite to the polarizing field) by Kogan et al.[3] Westenbarger independently confirmed this result.[4] Thus before the present work was undertaken the hyperfine field for In in Fe was known to be approximately - 250 kG.

Recent activity in this area of research has yielded rather accurate values for several hyperfine fields at nuclei of elements between Y (Z=39) and Te (Z=52) in Fe and Ni lattices,

determined by the techniques of perturbed angular correlations, nuclear polarization, Mössbauer spectroscopy, and NMR. Frankel et al.[5] have found a strikingly regular variation of H_{hf} in Fe and Ni lattices with solute atomic number; accurate experimental values for the fields at In nuclei in Fe and Ni have thereby acquired a new significance. Accordingly we have made accurate determinations of these fields, using a Co^{57} γ-ray thermometer.

The apparatus described by Westenbarger and Shirley[6] was used in these experiments. Those authors also described the portion of the theory of nuclear orientation that is relevant to this work. The recently developed Ge(Li) γ-ray detectors enabled us to resolve the 122.0- and 136.4-keV γ rays of Co^{57} very well, and we used the 136.4-keV γ ray as a nuclear thermometer. The decay scheme and γ-ray spectrum of Co^{57} are shown in Fig. D.7-2. Table D.7-I gives the calculated intensity of the 136.4-keV γ ray vs temperature, for Co^{57} oriented in Fe and in Ni. These calculated values are based on the nuclear moment of 4.6 nm for Co^{57} and hyperfine fields of -286 kG and -120 kG in Fe and Ni, respectively. The Co^{57} anisotropies have been shown to obey the calculated relationship by comparison with a Co^{60} thermometer.[7] For many experiments Co^{57} should prove a more convenient thermometer because of the low intensity of potentially interfering high-energy radiations.

The alloys were prepared and soldered to a copper fin assembly which was embedded in a chrome alum-glycerine slurry and adiabatically demagnetized from 1.0° K to ≈ 0.01° K. The anisotropy of the Co^{57} γ rays was used to measure the alloy temperature. The samples were polarized by a magnetic field of 2 kG trapped during demagnetization in a short tube of pure niobium, which is superconducting under the experimental conditions.

The In^{114m} $(5+ \xrightarrow{E4} 1+)$ and Co^{57} γ-ray intensities were measured along the axis of magnetization, by use of a Ge(Li) detector for Co^{57}, and both Ge(Li) and NaI(Tl) detectors for In^{114m}. The In^{114} $\beta^-(1+ \rightarrow 0+)$ spectrum was taken with the second Ni-In alloy, both at 0 and at 180 deg, with a silicon surface-barrier detector mounted inside the cryostat. Intensities were measured with the alloy "cold" and were normalized to the 1° K (isotropic) values.

The data were corrected for background and solid angle, and $W(\theta)$ was calculated for each case [$W(\theta)$ = cold intensity/warm intensity at angle θ]. This was compared (Figs. D.7-3 and D.7-4) with theoretical curves calculated for different values of the hyperfine fields (H_{hf}), based on the known[8,9] magnetic moment μ_{114m} = +4.75(10) nm, yielding

$$|H_{hf}| = 295 \pm 5 \text{ kG (In in Fe)},$$

$$|H_{hf}| = 42 \pm 3 \text{ kG (In in Ni)}.$$

The above statistical errors are the root-mean-square values. They should be doubled in both cases to include miscellaneous systematic errors.

For the In^{114} β^- measurements we found that $W(0) > 1$ and $W(\pi) < 1$, implying $\mu H_{hf} < 0$ (In in Ni). At $1/T = 25° K^{-1}$ the approximate magnitudes were $W(0) - 1 \cong 1 - W(\pi) \cong 0.03$. This number is uncorrected for scattering and solid angle, and the magnitude is thus of doubtful accuracy, but the sign of the asymmetry is certain. For In^{114m} in Fe, $\mu H_{hf} < 0$ was also found.[3,4]

To deduce the sign of H_{hf} from the above data we must know the sign of the relevant nuclear moment μ. Kogan et al.[3] assumed that reorientation takes place in the 72-sec ground state of In^{114}, and that the magnetic moment of this state, μ_{114}, is therefore the one in question. If this is correct we can estimate the moment theoretically as +3.4 nm, using the nuclear shell-model single-particle states $g_{9/2}$ (proton) and $g_{7/2}$ (neutron). This estimate is based upon Schmidt-limit values for the single-particle moments, and more sophisticated methods of calculation would reduce its magnitude somewhat, but if the proton has mainly $g_{9/2}$ character a positive sign for μ is inescapable. This interpretation yields the result: both H_{hf}(In in Fe) and H_{hf}(In in Ni) are negative.

In Table D.7-II are listed the best values to date for H_{hf} at nuclei of elements between Y and Te dissolved in Fe and Ni. These values are plotted in Fig. D.7-5. There now is very good evidence that this open 4d shell contributes (probably via core polarization) heavily to the negative hyperfine fields above the middle of the shell. This conclusion is supported by recent measurements on local moments for Ru in Ni by Matthias et al.[10] The continuing large negative H_{hf} in Ag and Cd may be understood as arising from polarization of 5s "conduction" electrons.[11]

No convincing explanation exists as yet for the systematic sign change of H_{hf} in the 5p shell. This experiment underscores the regularity of this trend. Possibly the positive Y-in-Fe point is another manifestation of this phenomenon. Certainly a successful quantitative explanation of these fields will have to account for both the regularity exhibited in Fig. D.7-5 and for the pronounced trends.

Footnotes and References

†Paper to be published in Phys. Rev.

‡Present address: Clarendon Laboratory, University of Oxford, Oxford, England.

1. B. N. Samoilov, V. V. Sklyarevskii, and E. P. Stepanov, Zh. Eksperim. i Teoret. Fiz. 38, 359 (1960) [English transl; Soviet Phys. JETP 11, 261 (1960)].
2. B. N. Samoilov, V. V. Sklyarevskii, and E. P. Stepanov, in Proceedings of the VIIth International Conference on Low Temperature Physics, ed. by G. M. Graham and A. C. Hollis Hallett (University of Toronto Press, Toronto, 1961), p. 171.
3. A. V. Kogan, V. D. Kul'kov, L. P. Nikitin, N. M. Reinov, M. F. Stelmakh, and S. Schott, Zh. Eksperim. i Teoret. Fiz. 43, 828 (1962) [English transl., Soviet Phys. JETP 16, 586 (1963)].
4. G. A. Westenbarger , private communication, 1963.
5. R. B. Frankel, J. Huntzicker, E. Matthias, S. S. Rosenblum, D. A. Shirley, and N. J. Stone, Phys. Letters 15, 163 (1965).
6. G. A. Westenbarger and D. A. Shirley, Phys. Rev. 138, A161 (1965).
7. N. J. Stone, unpublished data, 1964.
8. L. S. Goodman and S. Wexler, Phys. Rev. 108, 1524 (1957).
9. I. Lindgren, in Perturbed Angular Correlations, ed. by E. Karlsson, E. Matthias, and K. Siegbahn (North-Holland Publishing Company, Amsterdam, 1964), p. 379.
10. E. Matthias, S. S. Rosenblum, and D. A. Shirley, Phys. Rev. 139, B532 (1965).
11. D. A. Shirley and G. A. Westenbarger, Phys. Rev. 138, A170 (1965).

Table D.7-I. $W(\theta)$ vs $1/T$ for the Co^{57} γ-ray thermometers.

1/T	Fe lattice		Ni lattice	
($°K^{-1}$)	W(0)	W(π/2)	W(0)	W(π/2)
10	0.980	1.010	0.995	1.002
20	0.927	1.036	0.986	1.007
30	0.851	1.070	0.968	1.016
40	0.767	1.106	0.947	1.026
50	0.682	1.138	0.920	1.039
60	0.602	1.165	0.890	1.053
70	0.531	1.185	0.856	1.068
80	0.465	1.202	0.822	1.083
90	0.404	1.216	0.786	1.098
100	0.353	1.225	0.750	1.113

Table D.7-II. The known values of H_{hf} for Y-Te in Fe and Ni. Errors are given parenthetically.

Element	T (°K)	H_{hf} in Fe	T (°K)	H_{hf} in Ni	Reference[a]
Y	< 1	+205			b
	4.2	286(5)			c
Nb		258	1.4	39	d, e
Mo	4.2	256(5)			b
Ru		-505(20)	300	-178(7)	b, f
Rh	4.2	545(8)			c
Pd	4.2	600(10)			c
Ag	< 1	-272(19)		-84(5)	b
Cd	300	348(10)	300	-65.3(1.6)	b
In	< 1	-295(10)	< 1	-42(6)	
Sn	100	-81(4)	100	+18.5(1.0)	b
Sb		193(3)			b
	< 1	+205			b
	< 1	170(8)			b
		230	4.2	+88(5)	c, e
Te	4.2	+620(20)	4.2	+195(10)	b

a. Signs of hyperfine fields are given where known. Error limits are stated parenthetically for some cases. Original references should be consulted.
b. D. A. Shirley and G. A. Westenbarger, Phys. Rev. 138, A170 (1965).
c. M. Kontani, K. Asayama, and J. Itoh, J. Phys. Soc. Japan 20, 1737 (1965).
d. K. Asayama, M. Kontani, and J. Itoh, J. Phys. Soc. Japan 19, 1984 (1964).
e. Y. Koi et al. private communication, quoted in Ref. c.
f. O. C. Kistner private communication, 1965.

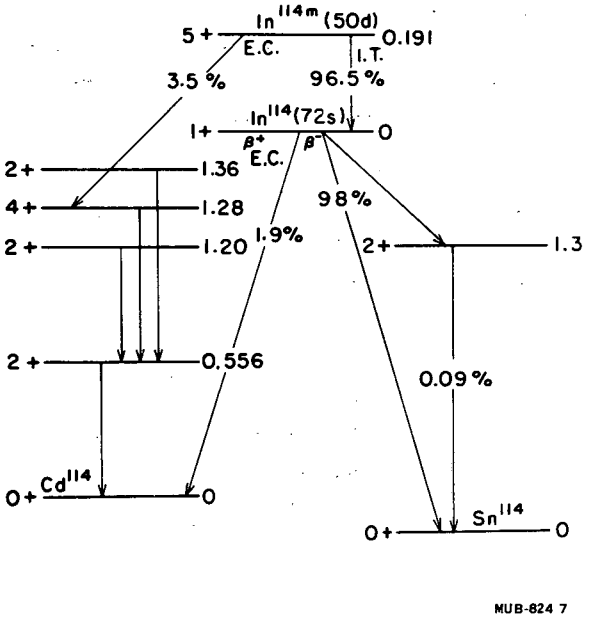

Fig. D.7-1. Decay scheme in In^{114m}.

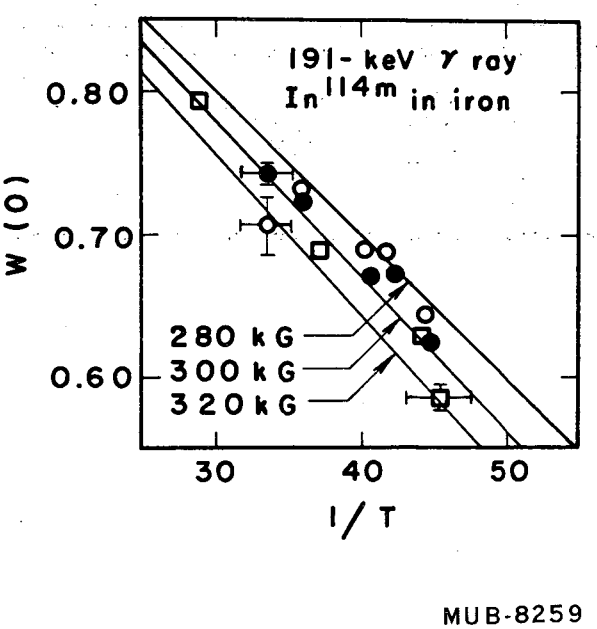

Fig. D.7-3. W(0) for 191-keV γ ray from In^{114m} in Fe as a function of temperature. Each point represents one demagnetization. Curves are for various values of the hyperfine field. □, source 1 [NaI(Tl)]; 0, source 2 [Ge(Li)]; ●, source 2 [NaI(Tl)].

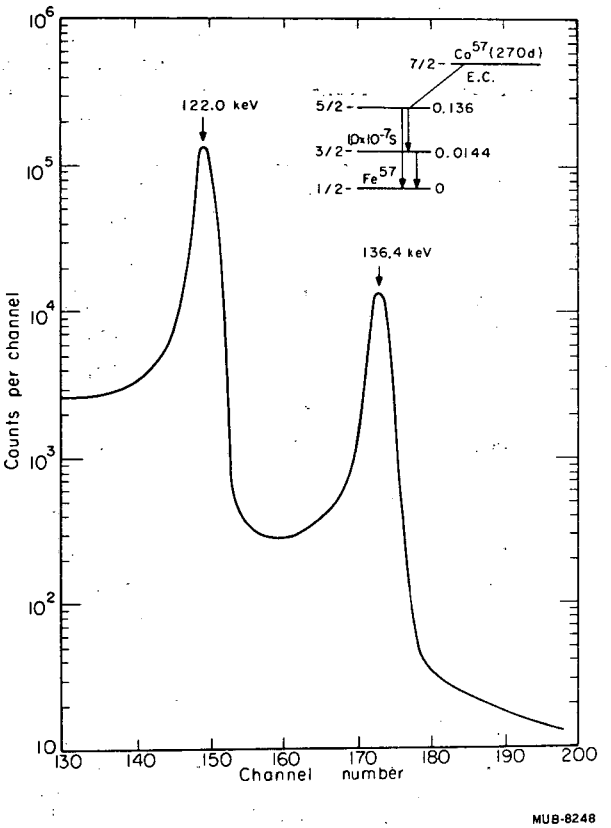

Fig. D.7-2. Gamma-ray spectrum of Co^{57} as recorded with a Ge(Li) detector. The decay scheme of Co^{57} is also shown.

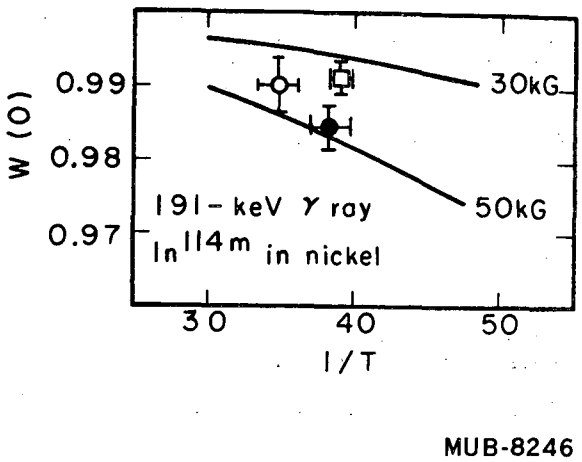

Fig. D.7-4. W(0) for 191-keV γ ray from In^{114m} in Ni as a function of temperature. Each point represents the average of several demagnetizations. Curves are for various values of the hyperfine field. □, source 1 [Ge(Li)]; ○, source 2 [Ge(Li)]; ●, source 2 [NaI(Tl)].

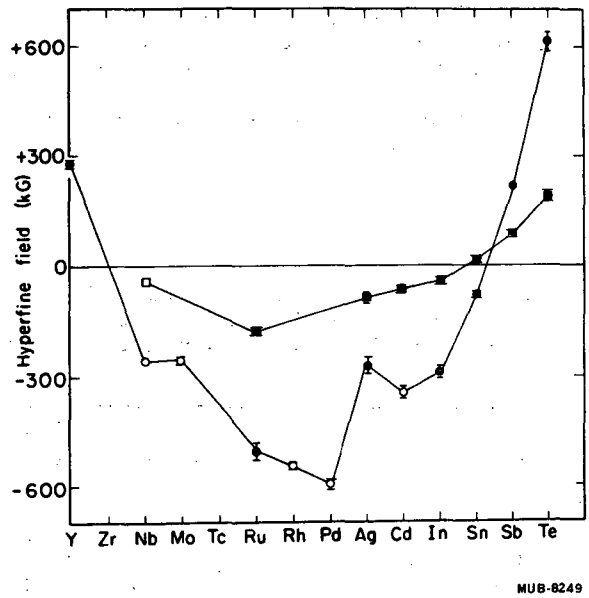

Fig. D.7-5. Hyperfine fields at nuclei of atoms (Z = 39 to 52) dissolved in Fe (circles) and Ni (squares) hosts. Cases for which the sign is known are shown as filled points.

8. THE TEMPERATURE SCALE FOR NEODYMIUM ETHYLSULFATE BELOW 1° K

Johan Blok, D. A. Shirley, and N. J. Stone

High-precision nuclear orientation studies of several isotopes in the neodymium ethylsulfate (NES) lattice have shown a reproducible systematic discrepancy between experimental data and theoretical curves. The discrepancy was independent of the particular Hamiltonian governing orientation of the nuclear spin system. The only real contact among the several experiments was that a temperature scale based on measurements made by Meyer[1] was used throughout. Two cases in which this discrepancy is especially plain are Ce^{137m} [2] and Lu^{177} (Fig. D.8-1). Because of the importance of NES as a coolant, we have restudied the temperature scale. In practice this involves relating the absolute temperature, T, to the entropy, S, of the electronic spin system.

Two methods were used. The first is the classic thermodynamic method of γ-ray heating, by which one relates the entropy and temperature to a measurable "magnetic" temperature, T^*, obtained from the susceptibility and from Curie's Law. Determination of the magnetic heat capacity, $C^* = dQ/dT^*$, and the T^*-S relation allows the calculation of

$$T = dQ/dS = C^*/(dS/dT^*).$$

A typical heat-capacity run is depicted in Fig. D. 8-2. While the heat leaks during the fore drift and after-drift periods were large, they were also linear and essentially equal. Accurate measurement of T^* thus made reliable corrections possible. Still at temperatures below 1/60 °K the S^*-T curve became very steep, and the necessity of differentiating the data to obtain dS/dT^* rendered the result uselessly inaccurate. Fortunately the statistical mechanical method of nuclear orientation[3] could be used in this range. This method is based on the fact that for a given orientation Hamiltonian there is a unique 1 to 1 relationship between the absolute temperature and

each of several statistical tensors, B_k, describing orientation of the nuclear spin system. We chose Ce^{137m} to establish the T-S relation for NES, shown parametrically in Fig. D.8-3 (by this we mean that S is uniquely related to the ratio $(H/T)_i$ the initial field and temperature from which the salt is cooled). Values obtained by both methods are shown. They join satisfactorily.

Confirmation of the new temperature scale is demonstrated in Fig. D.8-4, in which the Lu^{177} data are shown to fit a theoretical curve based on the new scale.

References

1. Horst Meyer, Phil. Mag. 2, 521 (1957).
2. R. B. Frankel, D. A. Shirley, and N. J. Stone, Phys. Rev. 136, B577 (1964).
3. R. B. Frankel, D. A. Shirley, and N. J. Stone, Phys. Rev. 140, A1020 (1965).

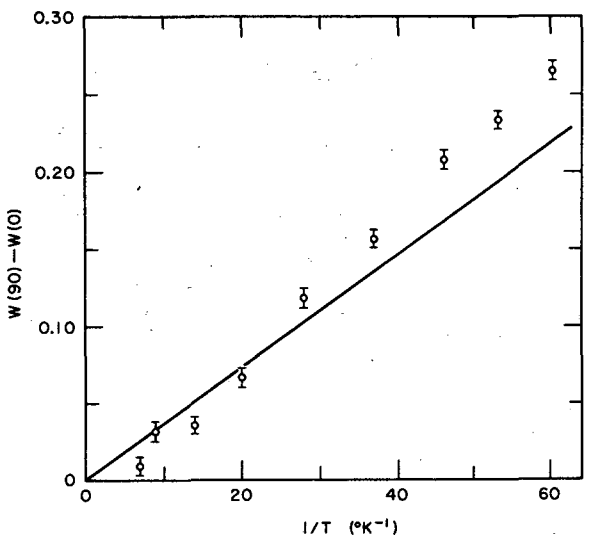

MUB-7976

Fig. D.8-1. Temperature dependence of a nuclear orientation function for the 208-keV γ ray in Hf^{177}, following the decay of Lu^{177} oriented in NES and using the temperature scale given by Meyer. Discrepancy between the experimental points and theoretical curve is obvious.

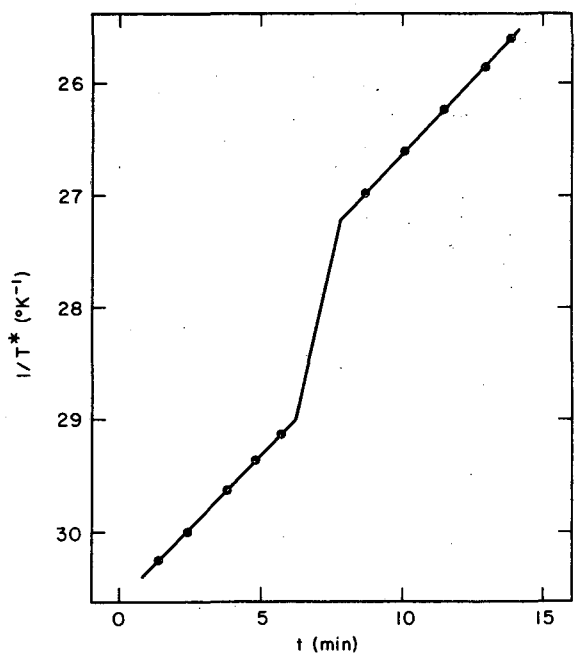

MU-36420

Fig. D.8-2. Heating curve, showing fore-drifts and afterdrifts, for a typical heat-capacity run.

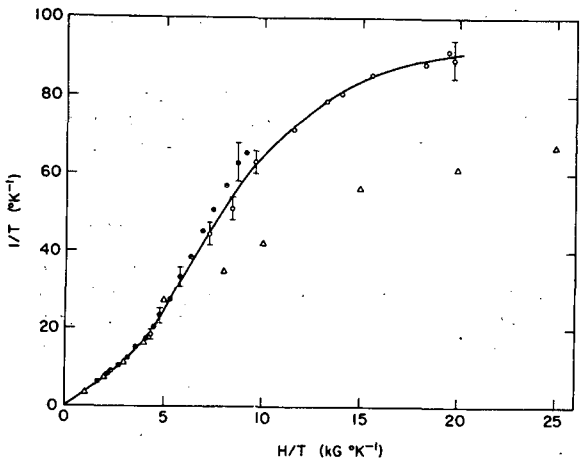

Fig. D.8-3. Reciprocal temperature reached on demagnetization versus initial H/T, for NES. Open circles represent data obtained by nuclear orientation, filled circles those obtained by the older heating method. Meyer's results are indicated by triangles.

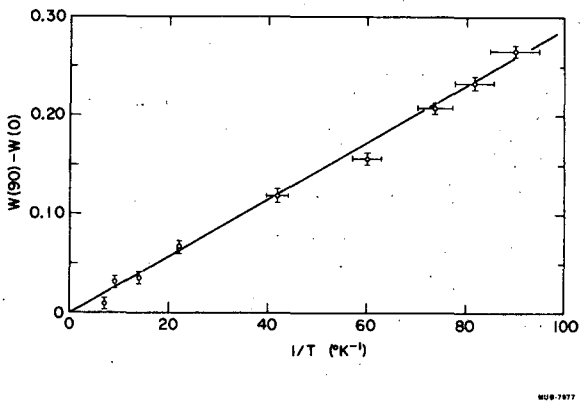

Fig. D.8-4. Data for Lu^{177} plotted against 1/T, using new scale. Excellent agreement with theoretical curve is evident.

9. CRYSTAL STRUCTURE AND LATTICE PARAMETERS OF CURIUM TRICHLORIDE†

J. C. Wallmann,‡ J. Fuger,* J. R. Peterson, and J. L. Green

The lattice parameters of curium trichloride reported by Asprey, Keenan, and Kruse[1] disagree substantially with the lattice parameters for curium trichloride calculated from data obtained in this laboratory. We describe in some detail below the derivation of our experimental data, and the methods of calculation used to arrive at the lattice parameters.

X-ray diffraction data were obtained on two samples of curium trichloride, derived from separate curium stock solutions which had been subjected to different purification procedures.

Diffraction lines from these preparations were recorded on Films 1500 A and 2069 A, respectively.

The diffraction equipment consisted of a Model 80-000 Jarrel-Ash Microfocus x-ray source and a 114-mm-diameter Norelco Precision Powder Camera, manufactured by the Philips Electronics Instrument Company.

Line positions on Film 1500 A were read twice and averaged; those on 2069 A were read once.

Following indexing, the data were transferred to cards for 7094 computer determination of the most probable lattice parameter values, according to a least-squares fit of the differences between experimental $\sin^2\theta$ values and those calculated from the assigned indices. Two computational programs were used: the LCR-2 program developed by Williams[2] and the MET-124 program of Mueller and Heaton.[3]

Lattice parameters calculated from the same set of data by the two programs were the same to within less than 0.001 Å.

Line intensities were calculated theoretically, on the basis of the assumed UCl_3-type hexagonal structure, by using the POWD program developed by Smith.[4]

Lines were indexed on the basis of the hexagonal UCl_3 structure type up to $\sin^2\theta = 0.97$ for both samples. With the exception of two extremely faint lines at $\sin^2\theta = 0.5498$ and 0.5566, which could not be indexed, the greatest difference between an observed and a calculated $\sin^2\theta$ was 0.0012.

There were no significant discrepancies between observed and calculated intensities.

From film 2069A the lattice parameters were calculated to be $a = 7.3803 \pm 0.0002$ Å and $c = 4.1862 \pm 0.0002$ Å. From film 1500A the calculated parameters were: $a = 7.3793 \pm 0.0003$ Å, $c = 4.1847 \pm 0.0002$ Å. The above error limits are standard deviations for the individual patterns computed by use of the LCR-2 program.

Footnotes and References

†A brief version of UCRL-16476.

‡Deceased.

*Present address: Université de Liège, Laboratoire de Chimie Nucléaire, 2 Rue A. Stévart, Liège, Belgium.

1. L. B. Asprey, T. K. Keenan, and F. H. Kruse, Inorg. Chem. 4, 985 (1965).
2. D. E. Williams, Ames Laboratory Report IS-1052, 1964.
3. M. H. Mueller and L. Heaton, ANL-6176, 1961.
4. D. K. Smith, UCRL-7196, 1963.

10. THE HEAT OF SOLUTION OF CURIUM METAL AND THE HEATS OF FORMATION OF $Cm^{+3}_{(aq)}$ AND $CmCl_{3(c)}$ †

J. C. Wallman,‡ J. Fuger,* Hermann Haug,†† Sayed A. Marei,** and Brij M. Bansal†††

A number of samples of curium metal were prepared essentially according to the method of Cunningham and Wallmann.[1] The heat of solution in 1 M HCl was determined in a microcalorimeter, described previously.[2,3]

All the samples of curium metal exhibited the double hexagonal structure, $a = 3.496 \pm 0.003$ Å, $c = 11.331 \pm 0.005$ Å, as reported previously.[1] This structure is believed to be the stable crystalline form at room temperature, and hence to represent the standard state for the metal at the temperature of the calorimeter runs.

Pieces of metal weighing from 100 to 600 micrograms were used for the heat measurements; these were dissolved in about 8 ml of standardized 1 M HCl.

The results of the calorimetric measurements are given in Table D.12-I. The observed heat corresponds to the reaction

$$Cm_{(c)} + (3000 \text{ to } 16000)\,[HCl \cdot 54.2\,H_2O] \longrightarrow$$

$$\{CmCl_3 \text{ in } (3000\text{-}3 \text{ to } 16000\text{-}3)\,[HCl \cdot 54.2\,H_2O]\} + 3/2\,H_{2(g)}\,.$$

We neglect the slight change in composition of the HCl solution resulting from reaction with the metal, take the relative heat content of HCl in $HCl \cdot 54.2\,H_2O$ to be -39.6 kcal mol^{-1}, and calculate -259.0 ± 1 kcal mol^{-1} for the heat of formation of $CmCl_3$ dissolved in (3000 to 16000) $HCl \cdot 54.2\,H_2O$.

Westrum and Robinson[4] measured the heat of solution of $PuCl_{3(c)}$ in various concentrations of hydrochloric acid, obtaining -22.15 ± 0.1, -29.5 ± 0.1, and -31.76 ± 0.1 kcal mol^{-1} in 6 M, 1.5 M, and 0.1 M acid, respectively.

Fuger and Cunningham[2] found -31.60 ± 0.35 kcal mol^{-1} for the heat of solution of $PuCl_{3(c)}$ in 0.001 M $HClO_4$, 0.099 M NH_4ClO_4. They also reported -30.60 ± 0.2 and -33.36 ± 0.25 kcal mol^{-1} for the heat of solution of $AmCl_{3(c)}$ in 1.5 and 0.001 M HCl, respectively.

We may use the data given above to arrive at an estimate for the heat of formation of $CmCl_{3(c)}$ and $Cm^{+3}_{(aq)}$.

The heat of solution of $AmCl_{3(c)}$ in 1.5 M HCl is more negative than that of $PuCl_{3(c)}$ in acid of the same concentration by 1.1 ± 0.3 kcal. For (HCl) $\leq$ 0.1 M to 0.001 M, the corresponding difference is 1.4 ± 0.3 kcal.

By extrapolating the above heat of solution data to $CmCl_{3(c)}$ we predict the heat of solution of $CmCl_{3(c)}$ in dilute HCl of a specified concentration to be more negative by 1.2 ± 0.4 kcal than that of $AmCl_{3(c)}$ in acid of the same concentration.

Thus our predicted heat of solution of $CmCl_{3(c)}$ in 1.5 M HCl is -31.8 ± 0.5 kcal mol^{-1}.

From a plot of the $PuCl_3$ heat-of-solution data of Westrum and Robinson[4] against HCl concentration, the interpolated difference between 1.5 M and 1 M HCl is -0.8 kcal mol^{-1}.

Applying this same correction to $CmCl_{3(c)}$, one can predict the heat of solution in 1.0 M HCl to be -32.6 ± 0.5 kcal mol^{-1}. Accordingly, the heat of formation of $CmCl_{3(c)}$ = $(-259.0 \pm 1) - (-32.6 \pm 0.5)$ -226.4 ± 1.2 kcal mol^{-1}.

The estimated heat of solution of $CmCl_{3(c)}$ in infinitely dilute HCl is -34.6 ± 0.4 kcal mol^{-1}, whence

$$\Delta H^0 f_{Cm^{+3}(aq)} = -226.4 + 3(40.02) - 34.6 - 140.9 \pm 1.3 \text{ kcal mol}^{-1}.$$

Although americium and curium metals have similar crystal structures and similar lattice parameters,[1] the heat of formation of $Cm^{+3}_{(aq)}$ is some 20 kcal less negative than that of $Am^{+3}_{(aq)}$.[2] A contributing factor to this difference may be the larger heat of vaporization of curium.

Footnotes and References

†A brief version of UCRL-16468.

‡Deceased.

*Present address: Universite de Liège, Laboratoire de Chimie Nucléaire, 2 rue A. Stévart, Liège, Belgium.

††Present address: Chemistry Division, Argonne National Laboratory, Argonne, Illinois.

**Present address: Department of Chemistry, University of Pittsburg, Pittsburg, Pennsylvania.

†††Part of the work described here represents research carried on by Brij Bansal in partial satisfaction of the requirements for the degree of Doctor of Philosophy.

1. B. B. Cunningham and J. C. Wallmann, J. Inorg. Nucl. Chem. 27, 271 (1964).
2. J. Fuger and B. B. Cunningham, J. Inorg. Nucl. Chem. 25, 1423 (1963).
3. John L. Burnett, The Thermochemistry of Di- and Tri-valent Europium (Ph. D. Thesis), UCRL-11850, December 18, 1964.
4. E. F. Westrum, Jr., and H. P. Robinson, in Radiochemical Studies: The Transuranium Elements (Edited by G. T. Seaborg, J. J. Katz and W. M. Manning) Plutonium Project Record NNES, Div. IV (McGraw-Hill Book Co., Inc., New York, 1949), Vol. 14-B, p. 922.

Table D.10-I. Heat of solution of curium metal in 1 M HCl at 298.4 ± 0.2° K.

Sample no.	Weight (μg)	Micromoles of Cm	Heat (cal)	ΔH Soln* (kcal mol^{-1})
1	265.5	1.088	0.1540	141.5 ± 1
2	605.1	2.480	0.3465	139.7 ± 1
3	118.3	0.4848	0.0677	139.6 ± 0.5
4	192.0	0.7869	0.1101	139.9 ± 0.5
		Average		140.2 ± 1

*Corrected for: (a) the heat of vaporization of the water required to saturate the dry nitrogen in the sample bulb, (b) the heat of vaporization of water required to saturate the hydrogen evolved, and (c) the heat of bulb breakage ($[6\pm3]\times10^{-4}$ cal bulb^{-1}).

11. THE ABSORPTION SPECTRUM OF Cf^{+3} AND CRYSTALLOGRAPHY OF CALIFORNIUM SESQUIOXIDE AND CALIFORNIUM TRICHLORIDE

J. L. Green and B. B. Cunningham

Californium has recently become available in quantities sufficient to allow initiation of studies on its bulk chemical and physical properties. The material available for this study was 6 μg of Cf^{249}, which was derived from the decay of Bk^{249}. This amount of material was adequate for the proposed studies; however, several major problems are associated with procedures applicable to purifications on this scale. Even when microtechniques are used, wet chemical operations involve rather dilute solutions, e.g., 10^{-5} to 10^{-4} M in californium. This results in marked sensitivity to recontamination during processing, particularly with respect to cations with low atomic weight. Such "background" contamination was avoided as much as possible by first minimizing the availability of contaminants--i.e., operating in very clean systems and using very pure reagents--and second by maximizing the concentration of the californium by volumetrically scaling down the operations. Except for changes necessitated by these problems, the purification operations were essentially those which have become standard in actinide chemistry.

Because of the considerable difficulties involved in the purification techniques, it was considered essential that analytical procedures be developed to evaluate the purity of the preparations prior to their use. By use of mass analysis techniques, the Nd content was determined to be 0.32 atom %, and total rare earths were estimated at approximately 1.5 atom %. By use of alpha pulse-height analysis, Cm^{244} was estimated at < 1 atom % and Am < 1 atom %, and although it is not possible to set a quantitative limit for Pu, it is felt that chemical and spectroscopic evidence indicated its absence. The single-bead assay technique indicated that other materials are potentially present as contaminants. Chemical and relative-abundance arguments lead to the tentative identification of the most probable contaminants as Al and Ca.

Absorption spectrum data were recorded for Cf^{+3} absorbed on single beads of cation-exchange resin (Table D.13-I) and as hydrated californium chloride. It is suggested that these data should closely approximate the solution spectrum of Cf^{+3}. By comparison of the Cf^{+3} bead spectra with the spectrum of Pr^{+3} taken under identical conditions, the molar extinction coefficients of Cf^{+3} in solution were estimated to be between 1 and 10 for the transitions observed. Room-temperature absorption data were also recorded by use of a crystal of $CfCl_3$ containing ≈ 150 to 200 mg of Cf (Table D.13-II). Preliminary calculations were carried out by Dr. K. Rajnak, fitting these data to a theoretical energy level scheme. The least-squares fits obtained appear to be satisfactory; however, it will not be possible to be certain about J-level assignments until low-temperature data are available. This should clearly be an early objective for future studies.

Samples of Cf_2O_3 were prepared and characterized crystallographically by use of x-ray powder techniques. This compound was found to exhibit the monoclinic Sm_2O_3 structure with $a = 14.124 \pm 0.020$ Å, $b = 3.591 \pm 0.003$ Å, $c = 8.809 \pm 0.013$ Å, and $\beta = 100.31 \pm 0.02$ deg. It is suggested that this structure crystalized during the final stages of the air ignition of the bead. This implies that the air-ignited oxide of californium approximates the sesquioxide stoichiometry. This is in direct contrast to the behavior of the lighter actinides, which form higher oxides under similar treatment. Samples of $CfCl_3$ were also prepared and characterized. This compound was found to exhibit the hexagonal UCl_3 structure with $a = 7.393 \pm 0.040$ Å and $c = 4.090 \pm 0.060$ Å. The ionic radius for Cf^{+3} computed from the chloride data is 0.98 Å. This indicates an actinide contraction of 0.01 Å between Cm^{+3} and Cf^{+3}.

Table D.11-I. The absorption spectrum of Cf^{+3} observed on Dowex-50 cation—exchange resin.

Peak position (mμ)	Estimated molar extraction coefficients	Qualitative description
473 ± 2	5-10	Strong
491 ± 2	1-2	Weak and relatively sharp
591 ± 2 595 ± 2	2-4	Visual observation indicated two lines; however, photographically often only one moderately strong line at 593 μm was apparent
605 ± 2	2-4	Weak to moderate
620 ± 3	—	Very weak-existence uncertain
645 ± 3	1-2	Weak
675 ± 3	2-4	Moderate
720 - 760	5-10	Strong

Table D.11-II. Absorption spectrum of a single crystal of anhydrous $CfCl_3$ photographed by use of a grating spectrograph.

Peak position (Å)	Error limits (Å)	Description of components	Relative intensity of band
4304	5	major peak	moderate-broad
4383	5	small shoulder	
4505	5	small shoulder	
4579	5	small shoulder	
4828	5	major peak	strong-moderately broad
5005	5	major peak	weak-sharp
5837[a]	5	trace	trace-very sharp
6148	5	major peak	moderate-broad
6237	10	minor shoulder	
6295	10	medium shoulder	
6678	5	large shoulder	weak-broad
6872	5	major peak	
7539	5	major peak	strong-moderately broad
7764	5	major peak	strong-broad
8043[a]	5	trace	trace-very sharp
8546[b]	5	major peak	weak-broad
8734[b]	10	minor shoulder	
8907[b]	10	minor shoulder	

a. Lines ascribed to Nd impurity.
b. Only one useful exposure available; therefore, the measurements of peak positions were not done in duplicate.

12. HYPERFINE FIELDS IN GOLD-MANGANESE COMPOUNDS

M. O. Faltens and D. A. Shirley

Much interest has been shown in the gold-manganese system because of its magnetic and structural characteristics. Several ordered crystallographic phases have been discovered which represent the intermetallic compounds of gold and manganese: AuMn, Au_2Mn, Au_3Mn, Au_4Mn and $AuMn_3$. The structures of the ordered phases have been studied by many investigators and some have been reported as follows:

- AuMn has the distorted CsCl structure with tetragonal symmetry, [1]
- Au_2Mn has a tetragonal sublattice.[2]
- Au_3Mn resembles Cu_3Pd, being face-centered orthorhombic[3] or tetragonal with antiphase structure, [4]
- Au_4Mn is isomorphous to Ni_4Mo,[5] having a face-centered tetragonal unit cell,
- $AuMn_3$ appears to have a face-centered or body-centered sublattice. [2]

These compounds are found to be magnetically ordered as well, with AuMn, [1] Au_3Mn,[6] and $AuMn_3$ being antiferromagnetic, Au_2Mn metamagnetic[7] with helicoidal magnetic arrangement[8] (Meyer initially reported Au_3Mn as being metamagnetic also), and Au_4Mn ferromagnetic.[5, 9]

We have done Mössbauer experiments on the compounds in the gold-rich region of the system to determine the magnetic hyperfine fields, H, at the gold nuclei and elucidate the correlation between such fields and the corresponding magnetic and structural properties. All experiments were performed at 4.2° K. The γ-ray source was the 77-keV isomeric state of Au^{197}, which is populated in the decay of Pt^{197}. The latter is produced in the reaction (65% enriched) $Pt^{196}(n, \gamma)$.

Care is required in the preparation of the compounds due to the high volatility and reactivity of manganese and the complexity of the gold-manganese phase diagram. To help reduce the high vapor pressure of manganese, a large ingot of approximately 50 atomic % each of electrolytic manganese and gold foil was first made from which the stoichiometric compounds were in turn prepared. Since manganese reacts with both quartz and alumina, a high-purity graphite crucible served as the refractory vessel. Evaporation and oxidation of manganese were prevented by melting and annealing each sample in the graphite crucible, which was enclosed in a quartz-tube housing. The tube was evacuated to less than 10^{-5} mm Hg, then filled with spectroscopically pure argon to just under 1 atmosphere at room temperature. The samples were melted by heating to about 1360° C in an induction furnace for about 15 minutes.

This initial melting was followed by annealing in a resistance furnace for 2 to 3 weeks each. In view of the long annealing periods, the above precautions were taken to eliminate oxygen from the annealing system. AuMn was annealed at 950° C and the others at 700° C. A surface of each ingot was prepared for microscopic inspection by the usual metallurgical techniques; then they were either chemically etched with a (I_2-C_2H_5OH: KI-H_2O) solution or electropolished in HCl. The specimens were then carefully inspected for homogeneity and given further heat treatment where indicated. See micrographs, Fig. D.12-1.

The microscopically homogeneous specimens were prepared for Mössbauer experiments by filing: the iron from the filing treatment was removed by a magnet. Chemical analysis showed that this effectively removed the iron to within less than 0.01%. The little detected is probably in the form of free iron chips and not incorporated in the gold-manganese lattice sites. This filing treatment was followed by further annealing for 2 to 4 days to remove cold-work deformations.

Hyperfine structure was observed for the three gold-rich compounds. The Mössbauer spectra were least-square fitted with six Lorentz curves by incorporating the known magnetic moments μ of the ground state [0.14485(1) nm] [10] and of the 77-keV isomeric state (0.402 ± .025nm)[11] and the relative transition intensities (1: 2 :3: 3: 2: 1).

The hyperfine fields were calculated from the energy separation of the levels given by

$$\Delta E_H = g\, m_I H.$$

ΔE_H is the Doppler velocity separation observed, g is the nuclear g factor (= μ/I), and m_I = 0, ±1 from transition selection rules. The details of the hyperfine level scheme are given in Fig. D.12-2. The results are shown in Table D.12-I.

From the difference between the results of the annealed and unannealed samples, it is evident that the magnetic ordering is highly sensitive to the heat treatment of the specimens. The

absence of a magnetic hyperfine field for AuMn can be explained from the symmetry properties of the CsCl structure and the antiferromagnetic ordering of the ferromagnetic planes.[1] The effective field at each gold nucleus would be expected to exactly cancel.

Pending completion of additional work, interpretation of the results of the remaining compounds will not be made at this time. Recently, L. D. Roberts[12] has done experiments on an Au_2Mn sample and has obtained a larger hyperfine field. His samples were not filed but were sliced instead. We are currently preparing thin plates of samples at more nearly stoichiometric composition for further investigations.

Acknowledgment

We thank R. Busch for his help in the preparation of the samples.

References

1. G. E. Bacon, Proc. Phys. Soc. 79, 938 (1962).
2. A. Raub, U. Zwicker, and H. Bauer, Z. Metallk. 44, 312 (1953).
3. D. Watanabe, J. Phys. Soc. Japan 15, 1030 (1960).
4. H. Morris, G. Davis, and J. L. Hughes, Acta Cryst. 17, 209 (1964).
5. D. Watanabe, J. Phys. Soc. Japan 15, 1260 (1960).
6. K. Sato, T. Hirone, H. Watanabe, S. Maeda, and K. Adachi, J. Phys. Soc. Japan, Vol. I, Supp. B-I, 1962; Proceedings of International Conference on Magnetism and Crystallography, 1961, Vol. I.
7. A. J. Meyer and P. J. Tagland, J. Phys. Radium 17, 457 (1956).
8. A. Herpin, P. Meriel, and J. Villain, Compt. rend. 249, 1334 (1959).
9. A. Kussman and E. Raub, Z. Matallk. 47, 9 (1956).
10. H. H. Woodbury and G. W. Ludwig, Phys. Rev. 117, 1287 (1960).
11. Dietrich Seyboth, E. F. Obenshain, L. D. Roberts, and J. O. Thomson, J. Am. Phys. Soc. 10, 444 (1965).
12. L. D. Roberts (Oak Ridge National Laboratory), private communications.

Table I. Parentheses indicate estimation of the next place. Brackets indicate best estimate. The calculations are based on the recent value of 1.066 cm/sec for the splitting of the outer lines of Fe^{57}. This value was obtained by Ronald Zane from laser calibrations done (at room temperature) at the Lawrence Radiation Laboratory (unpublished work).

Compound	Absorber thickness (mg/cm^2)	Line width, Γ (mm/sec) ± ~ (.08)	Isomer shift (mm/sec) ± ~(.08)	H (k Oe)
Unannealed filings				
$Au_{1.000}Mn_{1.00(0)}$ [a]	< 200	3.40	3.41	—
$Au_{2.000}Mn_{0.98(1)}$	188	5.61	1.13	462 ± 12
$Au_{2.000}Mn_{0.9(5)}$	164	4.37	0.91	452 ± 6
$Au_{3.000}Mn_{0.95(8)}$	132	3.57	0.48	480 ± 5
$Au_{3.000}Mn_{0.99(9)}$	543	4.72	0.53	515 ± 8
$Au_{4.000}Mn_{1.00(7)}$	166	3.82	0.32	442 ± 6
$Au_{4.000}Mn_{1.02(2)}$	190	3.73	0.14	425 ± 16
Annealed filings				
$Au_1Mn_{[0.96]}$	185	4.09	2.90	—
$Au_{1.00}Mn_{0.99(4)}$ [a]	125	2.66	3.32	—
$Au_{2.000}Mn_{0.90(2)}$ [a]	145	3.05	0.68	747 ± 18
$Au_2Mn_{[0.91]}$	154	3.34	0.56	597 ± 6
$Au_{3.000}Mn_{0.96(0)}$ [a]	< 200	3.26	0.58	614 ± 6
$Au_{4.000}Mn_{0.99(6)}$ [a]	< 200	3.68	0.26	573 ± 6

a. Analysis done at Anamet Laboratories, Berkeley, Calif; all others analyzed at Lawrence Radiation Laboratory.

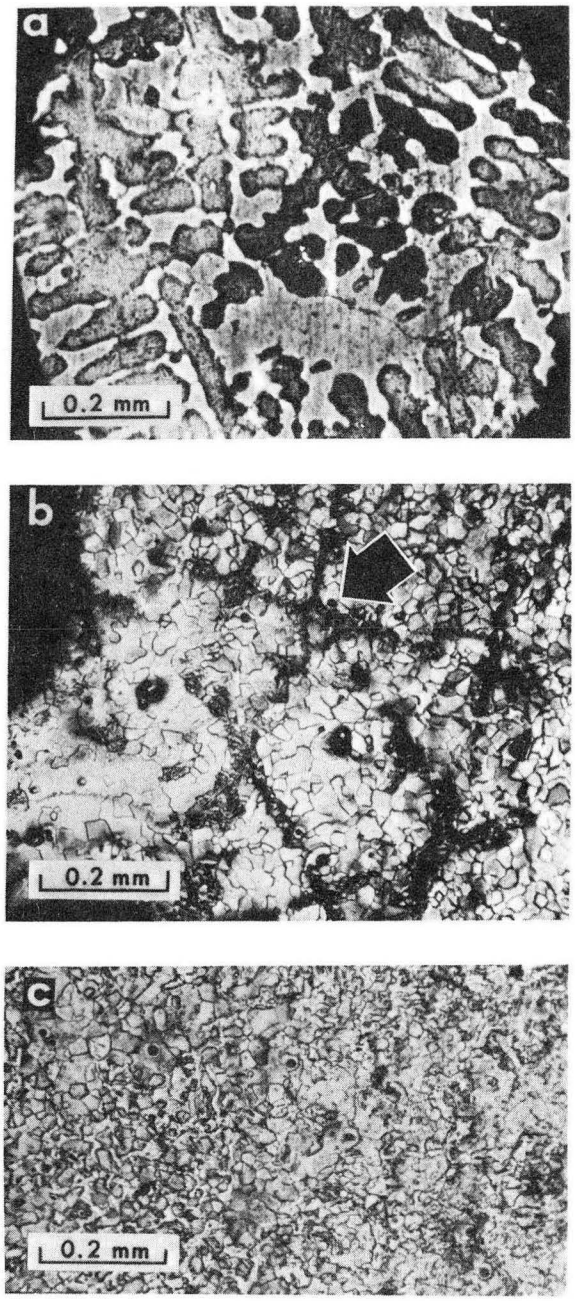

Fig. D.12-1. Micrographs of Au_2Mn annealing process.
a. Au_2Mn as cast. The dendritic (tree-like) structure is formed during solidification.
b. Au_2Mn ingot annealed at 700° C. Residual dendrites indicate inadequate annealing.
c. A second sample of Au_2Mn homogenized after three weeks of annealing at 700° C.

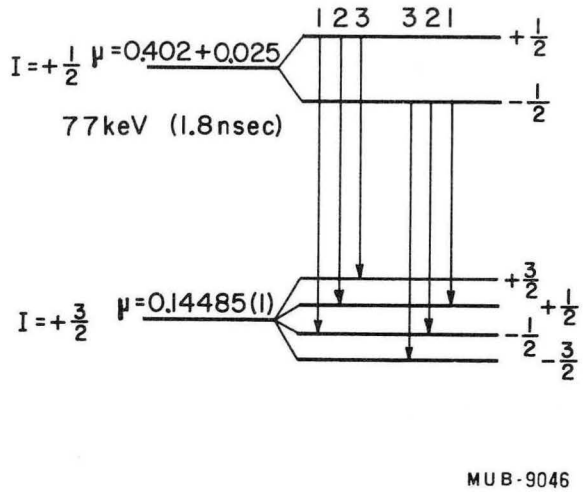

Fig. D.12-2. Hyperfine level scheme for Au-197.

13. ATOMIC-BEAM METHOD FOR THE STUDY OF ISOTOPE SHIFTS*

Richard Marrus and Douglas McColm

A new method for the study of isotope shifts is based on the atomic beam technique; it has the considerable advantage over optical techniques that it can be applied to radioactive nuclei in the presence of large amounts of stable carrier. Therefore, it will make possible an extension of our knowledge of isotope shifts to the large class of radioactive nuclei which cannot be practicably studied by any currently existing techniques. As a demonstration we report here the application of this method to a measurement of the Cs^{133}- Cs^{134m}(2.9 h) isotope shift in the $6^2P_{1/2}$-$6^2S_{1/2}$ transition (D_1 line).

The basic apparatus employed is a conventional atomic beam apparatus with flop-in magnet geometry.[1] However, the C region consists of a pair of electric field plates capable of sustaining very large electric fields. The region between the plates is illuminated with D_1 radiation from a filtered lamp of stable Cs^{133}. The lamp employed is a Varian X49-609 spectral lamp. The output of this lamp is a resolved doublet separated by approximately the ground-state hyperfine structure (hfs). The excited-state hfs is about 10% of the ground-state hfs.[2] (It makes no essential difference in the following discussion and is ignored.) The energy levels giving rise to the doublet are shown schematically in Fig. D.13-1.

Consider now the action of a Cs^{133} atom in the atomic beam irradiated by the reasonance radiation at zero electric field. Under this condition, the absorption lines of the beam atom coincide with the centers of the emission lines of the lamp. Consequently, resonance absorption of photons takes place. In the subsequent decay, the spin-flip of half the cesium atoms occurs and a large flop-in signal is observed at the detector. As the electric field is turned on, the Stark effect shifts the center of the absorption lines to lower frequencies until resonant absorption no longer occurs, and the flop-in signal goes to zero. However, when the shift is equal to the ground-state hyperfine structure a new overlap of the absorption line with the emission line of the lamp occurs (see Fig. D.13-1), and another flop-in signal is observed. In this way the Stark effect can be measured for the D_1 line; if the V^2 dependence characteristic of the Stark effect is assumed, a calibration of frequency shift vs applied voltage is obtained.

These same principles can be directly applied to the measurement of isotope shifts. Consider now a beam atom of some other cesium isotope. Because of the different ground-state hyperfine structure and the isotope shift there is, in general, no signal at zero field. However, if the energy of the absorption lines is displaced to the high-energy side of either of the emission lines of the lamp, then the application of a suitable voltage brings the absorption lines into coincidence with the emission lines and a signal is observed at the detector. If the hyperfine splitting is large compared with the emission width of the lamp ($\approx$ 1500 Mc),[3] then the hyperfine structure can be determined. The use of radioactive detection, which has been employed so successfully in the study of spins and moments, makes it possible to study rare radioactive isotopes.[4]

The spacing of the electric field plates used in our apparatus is sufficiently narrow (plate separation = 0.10 cm) that only the transition for which $m_J = -1/2$ in the A magnet and $m_J = +1/2$ in the B magnet is refocused. This precludes signals from the upper hyperfine level. Only signals resulting from atoms in the F = 3 state of Cs^{133} and F = 15/2 state of Cs^{134m} (I=8) can be observed.

The flop-in signal for a Cs^{133} beam as a function of applied voltage squared (V^2) is shown in Fig. D.13-2. The signals at zero electric field and at 25 000 volts correspond to the absorption of the F = 3 and F = 4 hyperfine lines in the lamp by atoms in the F = 3 state in the beam. The separation between the peaks corresponds to the known hyperfine structure 9192 Mc. The half width of the peaks is about 1500 Mc, which agrees well with an independent measurement of the half width of the lamp emission line.[3]

Figure D.13-3 is a graph of signal vs V^2 for a beam of Cs^{134m} atoms. The presence of a single peak at 24.1 kilovolts establishes the zero-field positions of the Cs^{134m} hyperfine levels to be as shown in Fig. D.13-1 relative to the Cs^{133} hfs. The energy of the D_1 transition in Cs^{134m} is smaller than that in Cs^{133} by 900(350) Mc or 0.030(.012) cm^{-1}, where the difference is taken between the centers of gravity of the hyperfine levels.

In this experiment we have chosen to use an electric field to "tune" the absorption lines of beam atoms. Similar optical resonance experiments have been performed which utilize

magnetic fields for line tuning.[5] Electric fields have the advantage that to second order all the hyperfine components of a J = 1/2 level are shifted together; i. e., there is a displacement of only the center of gravity. Relative shifts of the hyperfine levels[6] and of their Zeeman components[7] are much smaller, and for the purpose of this experiment are entirely negligible. This makes for easily interpretable signals which are much larger in intensity than those which would be obtained with magnetic tuning. However, the Stark effect shifts the energy in one direction only, whereas magnetic tuning increases the energy of some transitions and decreases the energy of others. For some isotopes, therefore, only magnetic tuning will make possible isotope-shift measurements.

Footnote and References

*Phys. Rev. Letters 15, 813 (1965).

1. J. R. Zacharias, Phys. Rev. 61, 270 (1942).
2. H. Kleiman, J. Opt. Soc. Am. 52, 441 (1962).
3. We thank Dr. R. McLaughlin of the Lawrence Radiation Laboratory for providing us with a lamp profile obtained from a densitometer trace.
4. For a review, see W. A. Nierenberg, Ann. Rev. Nucl. Sci. 7, 349 (1957).
5. O. Buhl, Z. Physik 109, 180 (1938) and 110, 395 (1938); F. Bitter, S. P. Davis, B. Richter, and J. Young, Phys. Rev. 96, 1531 (1954).
6. R. D. Haun, Jr., and J. R. Zacharias, Phys. Rev. 107, 107 (1957).
7. P. G. H. Sandars and E. Lipworth, Phys. Rev. Letters 13, 716 (1964).

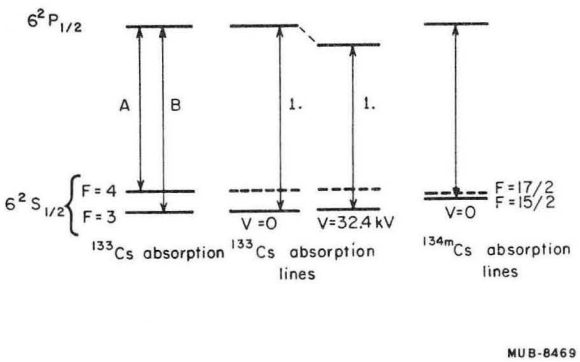

Fig. D.13-1. Energy level diagram. The lines labeled A and B are both present in the lamp. At zero applied voltage, the energy of the transition labeled 1 is in resonance with the emission line B and a flop-in signal is observed. At 32 kV, transition 1 now resonates with the emission line A. Our apparatus geometry precludes the observation of signals from the F = 4 state.

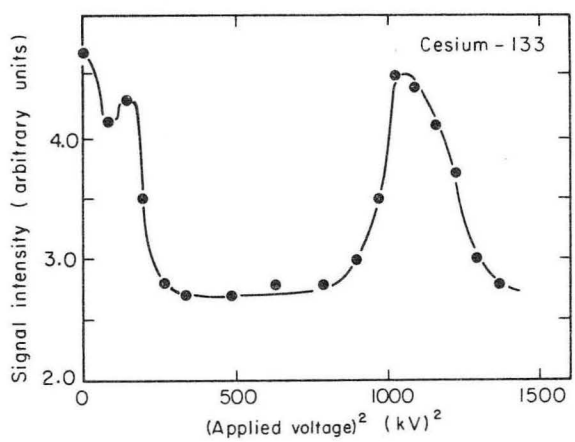

Fig. D.13-2. Observed signal vs (applied voltage)^2 for a cesium-133 beam.

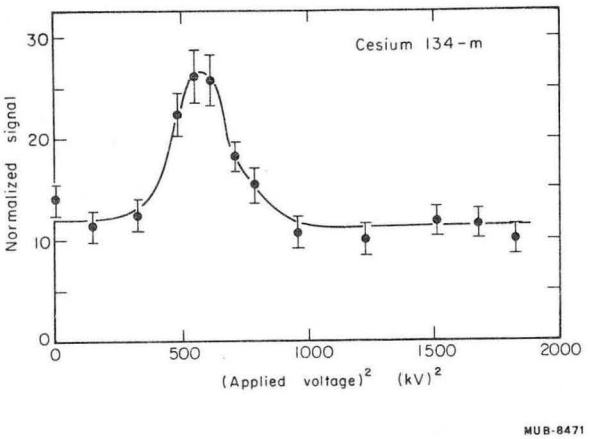

Fig. D.13-3. Observed signal vs (applied voltage)^2 for a cesium-134m beam.

14. MEASUREMENTS OF THE FANO FACTOR AND THE ENERGY PER HOLE-ELECTRON PAIR IN GERMANIUM*

Sven O. W. Antman, Donald A. Landis, and Richard H. Pehl

For a rough estimate of the statistical fluctuation Δn in the number of hole-electron pairs created in a detector by an incident particle with energy E, the equation

$$\Delta n = (E/\epsilon)^{1/2} \tag{1}$$

can be used, where ϵ is the average energy per hole-electron pair. Experimentally, however, the statistical fluctuation is less than that calculated from Eq. (1). The magnitude of this discrepancy is given by the Fano factor F, defined by

$$(\Delta n)^2_{exp} = F\,(\Delta n)^2, \tag{2}$$

where $(\Delta n)_{exp}$ is the experimental statistical fluctuation.

Fano[1] treated the statistical fluctuation in the number of ions produced by radiation in gases and predicted a factor of approximately 1/3 to 1/2, and recently Van Roosbroeck[2] did a detailed calculation of yield and Fano factor for hole-electron pairs generated in semiconductors. From Eq. (2) it can be seen that a Fano factor of 1 would correspond to the Poisson distribution that applies when the events in the ionization process are independent. But the energy-loss mechanisms in the semiconductor are not independent, and therefore a Fano factor between 0 and 1 would be expected.

Energetic particles incident on a semiconductor can lose energy in two fundamentally different ways:

(a) Creation of a hole-electron pair. The available energy (primary electron energy minus band-gap energy loss) is randomly shared by the degraded primary electron and the pair. The electron and the hole are assumed to share equally the energy given to the pair.

(b) Phonon losses to the crystal lattice. These phonons arise from electrons having energies both above and below the band-gap energy.

For a mathematical description of the creation of hole-electron pairs in semiconductors, the following parameters are introduced. The relative yield Y is defined by the ionization threshold energy E_{th} divided by the average energy per hole-electron pair ϵ:

$$Y = E_{th}/\epsilon\ . \tag{3}$$

The statistical behavior of the energy-loss process is determined mainly at the end of the branching process, where most of the secondaries having an energy of just a few ionization-threshold

units are generated. The yield and Fano factor, and therefore the average energy per hole-electron pair, are essentially independent of the type of incident particle.

Figure D.14-1 illustrates the dependence of yield and Fano factor on the ratio of energy losses to phonons and to ionization.[2] For the application of this theory to a germanium detector, an estimate of the relative yield is necessary. This estimate requires knowledge of the threshold energy and the average energy per hole-electron pair. The average energy per hole-electron pair has been determined to be 2.98 ± 0.01 eV. Although the threshold energy for germanium at 77° K is not accurately known, $E_{th} \approx E_g$ (where E_g is the energy gap) is a good approximation.[2] Since $E_g = 0.74$ eV, the relative yield can then be calculated by means of Eq. (3):

$$Y = 0.74/2.98 = 0.25.$$

From Fig. D.14-1 a corresponding theoretical Fano factor of 0.32 is determined.

A lithium-drifted germanium detector with a 0.5-cm depletion region and a rectangular 1×1.5-cm area was used in these experiments. In the measurements, an addition in quadrature of the electronic noise and the statistical fluctuation in the detector will correspond to the observed FWHM of the peak:

$$(\mathrm{FWHM})^2_{\mathrm{observed}} = (\mathrm{FWHM})^2_{\mathrm{electronic}} + 2.35^2\, FE\epsilon, \tag{4}$$

where the last term represents the statistical fluctuation obtained from Eq. (2), converted to energy units by multiplication by ϵ, and to FWHM of a Gaussian distribution by the factor 2.35.

The observed resolutions are plotted in Fig. D.14-2, where lines calculated from Eq. (4) are drawn. The linearity of the plot indicates that very little charge trapping occurs in this detector. On the basis of the lines drawn in, we estimate a Fano factor of $F = 0.30 \pm 0.03$, which is in excellent agreement with the value predicted. It is noteworthy that this factor remained constant throughout the energy region investigated. Using Fig. D.14-1 and the experimental value of the Fano factor, one can determine that the value of the threshold energy is $E_{th} = 0.80$ eV, a value only 6% higher than the energy gap and thus consistent with the assumption $E_{th} \approx E_g$.

Knowledge of the Fano factor and ϵ enables one to determine the theoretical limitation of the energy resolution. Figures D.14-3 and D.14-4 show these limiting values as a function of the energy loss in the detector for different electronic (pulser) resolutions.

Footnotes and References

*Short version of Nucl. Instr. Methods (to be published).

†Present address: Institute of Physics, University of Uppsala, Uppsala, Sweden.

1. U. Fano, Phys. Rev. 72, 26 (1947).
2. W. Van Roosbroeck, Phys. Rev. 139, A1702 (1965).

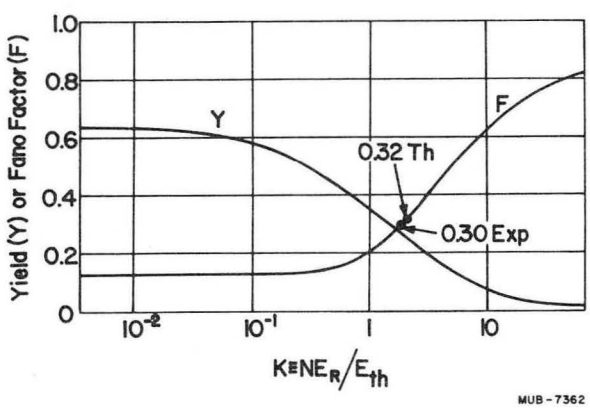

Fig. D.14-1. Dependence of yield and Fano factor on the ratio of energy losses to phonons and to ionization. The theoretical and experimental Fano factors are shown.

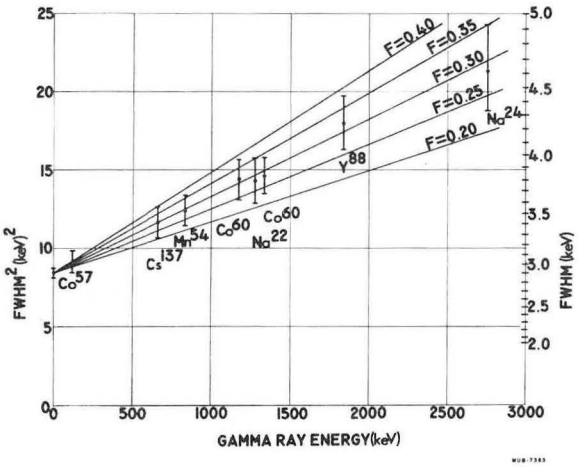

Fig. D.14-2. Plot of the resolution of the germanium detector versus γ-ray energy. Lines representing Fano factors calculated on the basis of the value of $\epsilon = 2.98$ eV are shown.

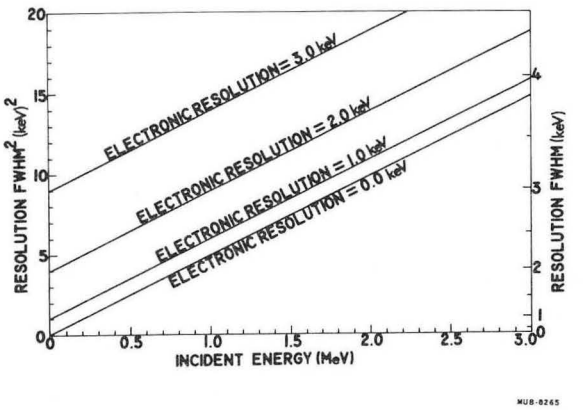

Fig. D.14-3. Total energy resolution as a function of the energy loss in the detector (up to 3 MeV) for different electronic (pulser) resolutions.

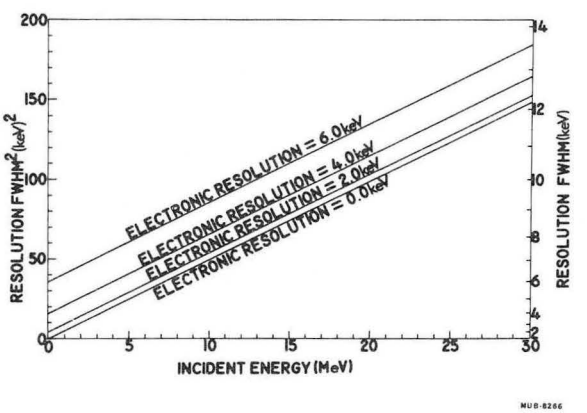

Fig. D.14-4. Total energy resolution as a function of the energy loss in the detector (up to 30 MeV) for different electronic (pulser) resolutions.

15. THE PRODUCTION AND CHARACTERIZATION OF Am^{+2} IN CaF_2 CRYSTALS

N. Edelstein, W. Easley, and R. McLaughlin

One of the properties that the lanthanide series of the periodic table has exhibited is the ability of a large number of the elements to form a stable +2 oxidation state in various crystal matrices. In the actinide series there has been until now no clear evidence of a stable +2 oxidation state. We report herein the production, stabilization, and identification of Am^{+2} in crystals of CaF_2.

Single crystals of CaF_2 containing 0.1 to 0.2 weight % of Am^{243} were grown by the Bridgman-Stockbarger technique. When first removed from the furnace these crystals had the characteristic light pink color of Am^{+3}, and the optical spectrum showed the characteristic absorption bands around 500 mμ. The crystals showed considerable darkening to a brownish color in 3 to 4 weeks. Absorption spectra indicated the growth of some new broad bands, the most intense of which was at 430 mμ. The appearance of these bands is similar to f-d transitions observed from +2 lanthanides in CaF_2.[1] The doped CaF_2 crystals were electrolytically reduced[2] at approximately 600° C, and a deep reddish brown color developed which formed first at the cathode and then spread towards the anode. These crystals showed the same absorption spectrum as the aged CaF_2 crystals described earlier except that the spectrum was much more intense.

Paramagnetic resonance was performed on electrolytically reduced crystals and on aged crystals, and six resonance lines were seen at 4° K and 1° K which could be fitted to the parameters of the spin Hamiltonian

$$\mathcal{H} = gB\vec{H}\cdot\vec{S} + A\vec{I}\cdot\vec{S}$$

(for Am^{243}, $I = 5/2$). We find $g = 4.490 \pm 0.002$ and $A_{Am^{243}} = 86.9 \pm 0.2$ gauss, $(1.823 \pm 0.003)\times 10^{-2}$ cm^{-1}. Am^{+3}, f^6, $^7F_0$ has no paramagnetic resonance spectrum, so we assign the spectrum to the cubic Γ_6 crystal field state of Am^{+2}, f^7, $^8S_{7/2}$. A calculation with the wave function of Lea, Leask, and Wolf[3] gives g for this state as 4.517. The small difference between the calculated and experimental value may be ascribed to the effect of covalent bonding.[4]

We conclude from the above observations that initially Am^{+3} is present in the CaF_2 lattice but that because of the radiation from the Am decay, free electrons are formed in the lattice and some of the Am^{+3} ions are reduced to Am^{+2}. We can also do the reduction electrolytically and more efficiently. When the radiation-damaged crystals are heated to about 500° C a green glow is emitted, the spectrum of which shows it to consist mainly of four sharp bands around 500 mμ characteristic of Am^{+3}. Fluorescence of the +3 ion is also observed when CaF_2 containing +2 lanthanides is heated.[1] After approximately 1 hour of heating at 500° C the absorption spectrum shows only bands characteristic of Am^{+3}.

Further experiments are being planned to study in detail the phenomena described above.

References

1. Z. J. Kiss and P. N. Yocum, J. Chem. Phys. 41, 1511 (1964), and references therein.
2. F. K. Fong, J. Chem Phys. 41, 2291 (1964).
3. K. R. Lea, M. J. M. Leask, and W. P. Wolf, J. Phys. Chem. Solids 23, 1381 (1962).
4. I. Fidone, and K. W. H. Stevens, Proc. Phys. Soc. (London) 73, 116 (1959).

16. OPTICAL PUMPING TRANSIENTS IN Rb^{87} AND APPLICATION TO DISORIENTATION CROSS SECTIONS*

Richard Marrus and Joseph Yellin

Detailed studies have been made of the light transmitted through Rb^{87} vapor during the optical pumping process, both with and without buffer gas present. The observed transients are single exponentials with no buffer gas present, and double exponentials with buffer gas present over a wide range of pumping intensities and relaxation times. These results are in excellent

agreement with the predictions based on phenomenological equations in which nuclear spin is included and a single relaxation time is assumed. From a study of the amplitudes of the two exponential components of the optical-pumping transient, an effective cross section σ_{eff} is deduced for the disorientation of Rb^{87} within the $5^2P_{1/2}$ state as a result of its collision with a buffer-gas atom. It is shown that $\sigma_{eff} = \sigma_{1/2} + \sigma_{3/2}$, where $\sigma_{1/2}$ is the cross section for disorientation within the $5^2P_{1/2}$ level, and $\sigma_{3/2}$ is the cross section for transfer from the $5^2P_{1/2}$ level to the $5^2P_{3/2}$ level by means of collisions with the buffer gas. On the basis of recently measured values for $\sigma_{3/2}$, values are deduced for $\sigma_{1/2}$. The cross sections are $\sigma_{1/2}(\text{Rb-He}) = 1.5(0.8)\times 10^{-17}$ cm^2,

$$\sigma_{1/2}(\text{Rb-Ne}) = 4.4(2.2)\times 10^{-17}\ cm^2,$$

and

$$\sigma_{1/2}(\text{Rb-Ar}) = 3.5(1.8)\times 10^{-16}\ cm^2.$$

These cross sections are deduced from a model in which the probabilities for Rb^{87} to relax from any hyperfine level to any other are all equal. This model gives a better fit with the observed transients than the assumption that the electron spin only is randomized in the $P_{1/2}$ state with the nuclear spin unaffected.

We show that accurate relaxation -time measurements can be made by measuring the time constants associated with the double exponentials as a function of light intensity, and extrapolating them to zero light intensity. Moreover, since no shutter is required, relaxation times $< 10^{-3}$ sec can be easily observed. From a study of the relaxation times as a function of buffer-gas pressure, disorientation cross sections ($\sigma_{G.S.}$) have been obtained in the ground state ($5^2S_{1/2}$). The measured cross sections are

$$\sigma_{G.S.}(\text{Rb-Ar}) = 3.3(1.0)\times 10^{-22}\ cm^2,$$
$$\sigma_{G.S.}(\text{Rb-Ne}) = 1.0(0.3)\times 10^{-22}\ cm^2,$$
$$\sigma_{G.S.}(\text{Rb-Xe}) = 1.8(0.3)\times 10^{-19}\ cm^2,$$
$$\sigma_{G.S.}(\text{Rb-Kr}) = 3.0(0.5)\times 10^{-20}\ cm^2.$$

The cross sections for krypton and xenon were measured directly. These cross sections are compared with those obtained by other methods.

Footnote

*Abstract of Phys. Rev. (to be published).

17. CRYSTAL AND MOLECULAR STRUCTURE OF A DOUBLE COMPLEX OF MANGANESE WITH PHTHALOCYANATO AND PYRIDINE LIGANDS*

Lester H. Vogt, Jr.,† Allan Zalkin, and David H. Templeton

One approach to understanding the chemistry involved in complicated biological processes has been to study the physical and chemical properties of compounds which are related to, but less complex and more stable than, those which occur in nature. The chemistry of phthalocyanatomanganese (II)[1,2] is of interest because of (a) the similarities between the structures of phthalocyanine and porphyrin rings, (b) the implication of manganese (possibly as a porphyrin complex) in biological oxidative processes, and (c) the report by Elvidge and Lever[1] that in pyridine solution the complex may reversibly combine with oxygen. Englesma, Yamamoto, Markham, and Calvin[2] did not detect oxygen evolution accompanying the reverse reaction. The absorption of oxygen takes place in two steps,[2] ending in the formation of a complex which can be isolated as short opaque purple crystals with a metallic luster. Elvidge and Lever formulated this complex as $Mn^{IV}PcPyO$ (Pc = phthalocyanato, Py = pyridine). Because of the low solubility of the complex neither the molecular weight nor the magnetic susceptibility in solution was measured.[2] Magnetic susceptibility measurements[2] on the solid indicated 0.71 B. M. instead of the

expected 3.87 B. M. for Mn(IV). This fact suggested a different oxidation state or electronic interactions between Mn atoms in the solid.

By x-ray diffraction methods we have determined the structure of these crystals and have shown the molecules to be a novel double complex of manganese(III): $(Mn^{III}PcPy)_2O$. This complex (Fig. D.17-1) consists of two approximately flat and parallel phthalocyanine ring systems, each with manganese at its center. These rings are bridged by the oxygen atom, which is midway between the manganese atoms. Each manganese also has a pyridine molecule coordinated opposite its oxygen atom. The crystals consist of these complex molecules together with other molecules of pyridine of crystallization, which are not bonded in any direct way to the complex molecules.

We failed to get good diffraction patterns with crystals dried in air. To prevent loss of pyridine we grew crystals from pyridine solution and kept them in an atmosphere saturated with pyridine. We sealed a crystal of dimensions $0.15 \times 0.15 \times 0.30$ mm in a thin-walled glass capillary with a drop of pyridine in the other end. We measured lattice dimensions and diffraction intensities with a General Electric XRD-5 diffractometer equipped with a goniostat and scintillation counter, with copper radiation, $\lambda(K\alpha_1) = 1.54051$ Å. We measured intensities of 3156 independent reflections by the stationary-crystal stationary-counter technique. Absorption was neglected ($\mu R \approx 1$).

The crystals are orthorhombic with cell dimensions

$a = 22.635 \pm 0.005$,
$b = 23.850 \pm 0.005$,
$c = 12.808 \pm 0.003$ Å.

The space group is $P2_12_12_1$ with each cell containing four asymmetric units consisting of $(MnPcPy)_2O \cdot 2Py$ or $C_{84}H_{52}Mn_2N_{20}O$ (molecular weight 1467.3, 107 atoms excluding hydrogen). The molecular weight from the volume of the asymmetric unit and density measured by flotation (1.41 g/ml at 25°) is 1470.

The structure determination was surprisingly straightforward and presented no special difficulty except excessive arithmetic. We guessed the two Mn positions correctly from the Patterson function. A sequence of least-squares and three-dimensional Fourier calculations, coupled with the assumption that the phthalocyanine rings would have essentially the same shape as determined by Robertson[3] in other crystals, led to the structure. To refine the 107 atoms required 439 parameters including a scale factor, coordinates, anisotropic thermal parameters for each manganese atom, and individual isotropic thermal parameters for the other atoms. The least-squares program on our IBM-7044 (32K memory) computer can handle 160 parameters in a full-matrix calculation. We started the refinement procedure with this program, refining about a third of the structure at a time. At 2 hours per run, this procedure required 6 hours to shift each parameter at least once. We modified the program to neglect off-diagonal elements of the matrix. This change permitted all parameters to be shifted in 1 hour, and more refinement per hour of computer time was realized. The function $R = \Sigma \, ||F_0| - |F_c|| / \Sigma |F_0|$, which was 0.48 for the two Mn atoms, was reduced to 0.084 for 107 atoms. The anomalous dispersion effect of Mn was included in the calculations and was sufficient to establish the absolute configuration of the structure.[4]

Most atoms shifted less than 0.002 Å in the last cycle. We estimate the standard deviations of individual bond distances to be about 0.04 Å on the basis of the differences between bonds that are chemically equivalent and a comparison with the known dimensions of benzene rings. These estimates do not apply to the pyridine of crystallization, which appears to have very large and anisotropic thermal motion ($B \approx 15$ to 20 Å^2) and which may have some kind of disorder. Average values of the lengths and angles of some chemically equivalent bonds are given in Fig. D.17-2. We expect these average distances to have standard deviations of the order of 0.01 Å. They are in agreement with previous results on other phthalocyanines.[3]

Each terminal pyridine (Figs. D.17-1 and D.17-2) is oriented so that its plane bisects two of the N—Mn—N angles of the adjacent phthalocyanato complex. One phthalocyanine ring is rotated 41 deg with respect to the other about the Mn–O–Mn axis, so that its benzene rings are approximately between the benzene rings of the other. Except for the benzene rings the atoms of each ring system lie in a plane with the respective manganese atom. The benzene rings bend inward toward the empty spaces of the opposite half of the molecule by from 0.1 to 0.6 Å. We consider this bending to be the result of molecular packing forces in the crystal, and assume it to have no chemical significance except as a reflection of the flexibility of such a large molecule.

The Mn–O distance of 1.71 ± 0.01 Å is shorter than we would have predicted for a single covalent bond. We expect that an explanation of the magnetic properties will involve electronic coupling between manganese atoms through this bond system.

The mechanisms proposed for the formation of this complex[1,2] need to be reexamined in the light of this new formulation.

Footnotes and References

*Science (to be published).

†Present address: General Electric Research and Development Center, K-1, P. O. Box 8, Schenectady, N. Y. 12301.

1. J. A. Elvidge and A. B. P. Lever, Proc. Chem. Soc. 195 (1959).
2. G. Englesma, A. Yamamoto, E. Markham, and M. Calvin, J. Phys. Chem. 66, 2517 (1962).
3. J. M. Robertson, J. Chem. Soc. 1195 (1936); J. M. Robertson and I. Woodward, ibid. 219 (1937), 36 (1940).
4. All molecules in one crystal are of the same handedness, but another crystal from the same preparation is as likely to be right-handed as left-handed. Thus there is no general significance to the absolute configuration which we found.
5. One of us (L. H. V.) was National Institutes of Health Postdoctoral Fellow under the sponsorship of Prof. Melvin Calvin. We thank Prof. Calvin for bringing this very interesting substance to our attention. This work was done in part under the auspices of the U. S. Atomic Energy Commission.

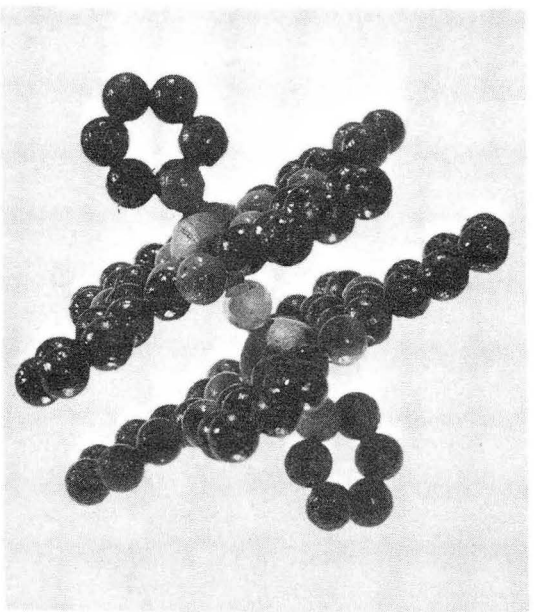

Fig. D.17-1. Photograph of a cork-ball model of the $(MnPcPy)_2O$ molecule. Hydrogen atoms are omitted.

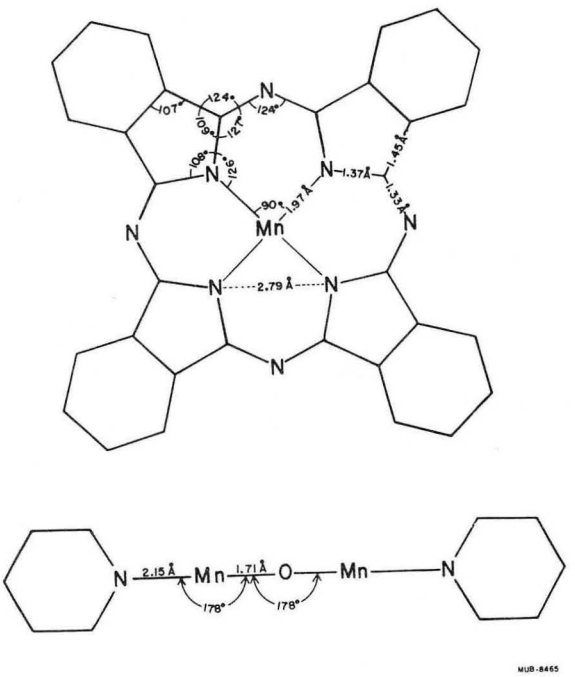

Fig. D.17-2. Average bond distances and angles.

18. THE CRYSTAL AND MOLECULAR STRUCTURE OF $C_5H_5FeB_9C_2H_{11}$

Allan Zalkin, David H. Templeton, and Ted E. Hopkins†

A compound designated π-cyclopentadienyl π-(1)-2,3-dicarbollyl iron (III) was synthesized by Hawthorne and Pilling.[1] We determined its crystal structure by x-ray diffraction and found a "sandwich" type of molecular structure, as predicted by Hawthorne. This work is the first x-ray crystallographic confirmation of the structure of the $B_9C_2H_{11}^{-2}$ ion, and it gives support for the structures suggested previously for several other derivatives.[2,3]

Crystals of $C_5H_5FeB_9C_2H_{11}$ were received from Hawthorne and Pilling[1] as tiny flat plates. They are monoclinic, space group $P2_1/c$, with unit cell dimensions a = 11.470, b = 6.629, c = 16.808 Å, β = 99.86 deg. With four molecules in the unit cell the density is calculated as 1.34 g/ml. We measured the intensities of 1639 independent reflections by the stationary-crystal technique, using MoKα radiation (λ = 0.71069 Å) and a scintillation detector. The Patterson function revealed the iron atom location, and a Fourier calculation phased by the iron atom showed all the boron and carbon atoms. Carbon and boron atoms in the carborane were distinguished by the behavior of their thermal parameters when scattering factors were interchanged in least-squares calculations. The assignment was confirmed by the bond distances which resulted, which correspond to smaller bond radius for carbon than for boron. After some refinement by least squares, a difference function showed evidence for all the hydrogen atoms. In the final refinement, isotropic thermal parameters were used for hydrogen, and anisotropic parameters for all other atoms. The function $R = \Sigma \, | \, |F_{obs}| - |F_{cal}| \, | / \Sigma |F_{obs}|$ was reduced to 0.074. In Table D.18-I are listed the final coordinates of the heavy atoms. The standard deviations of these coordinates correspond to about 0.001 Å for Fe and 0.01 Å for the other atoms. These estimates of precision make no provision for systematic errors.

The thermal motion is large and anisotropic. In the cyclopentadienyl ring the largest amplitudes are tangential to the ring, and the atoms are very poorly resolved in Fourier sections. This evidence for torsional motion or internal rotation is very similar to that reported in ferrocene.[4] In the carborane part of the molecule the amplitudes are less, the bond distances are greater, and the atomic resolution is very much better. We have found no simple way of describing the thermal anisotropy of this part of the molecule.

Average bond distances are listed in Table D.18-II, without any correction for thermal motion. This correction may be as much as 0.05 Å for some of the bonds, but we cannot estimate it with confidence. In each case the correction will increase the bond distance. Each distance in a group (except bonds to H) is within 0.03 Å of the average value. Because of the large and uncertain thermal corrections, we give no significance to the deviations within each group.

The skeleton of the molecule is shown in Fig. D.18-1. The atoms of the carborane part are at 11 of the 12 corners of an icosahedron which is approximately regular. The iron atom is at the twelfth corner, but somewhat further away. Within the experimental accuracy of about 0.2 Å, each hydrogen atom is on the line passing through its neighbor and the opposite atom of the icosahedron. The hydrogen atom positions on the cyclopentadienyl ring are more poorly determined, but within the large experimental uncertainty they are in the expected locations in the plane of the ring.

The iron atom is almost equidistant from the carbon atoms in the ring and the five neighbors in the icosahedron. The configuration is almost exactly eclipsed, rather than staggered as in the ferrocene crystal.[4] We tested the staggered structure in the least-squares calculations, but got significantly worse agreement. Because of the large twisting motion, the configuration in the crystal may have little chemical significance.

Footnote and References

†J. Am. Chem. Soc. 87, 3988 (1965).

1. M. F. Hawthorne and R. L. Pilling, J. Am. Chem. Soc.
2. M. F. Hawthorne, D. C. Young, and P. A. Wegner, ibid. 87, 1818 (1965).
3. M. F. Hawthorne and T. D. Andrews, ibid., in press.
4. J. D. Dunitz, L. E. Orgel, and A. Rich, Acta Cryst. 9, 373 (1956).

Table D.18-I. Atomic coordinates and rms amplitudes.

Atom	x	y	z
Fe	0.2244	-0.0331	0.1897
C(1R)[a]	0.0917	-0.0331	0.0909
C(2R)	0.1817	0.0862	0.0767
C(3R)	0.2779	-0.0361	0.0780
C(4R)	0.2433	-0.2285	0.0942
C(5R)	0.1278	-0.2228	0.1026
C(2)	0.3345	-0.1476	0.2871
C(3)	0.2008	-0.1537	0.2978
B(4)	0.1354	0.0749	0.2794
B(5)	0.2502	0.2337	0.2580
B(6)	0.3764	0.0795	0.2621
B(7)	0.3035	-0.1630	0.3822
B(8)	0.1786	-0.0172	0.3790
B(9)	0.2127	0.2301	0.3555
B(10)	0.3607	0.2328	0.3447
B(11)	0.4159	-0.0112	0.3609
B(12)	0.3173	0.0825	0.4194

a. R indicates an atom in the cyclopentadienyl ring.

Table D.18-II. Average bond distances.

Atoms	Distance (Å)
Fe-B (3)[a]	2.09
Fe-C (2)	2.04
Fe-C (5)[b]	2.07
B-B (18)	1.75
B-C (6)	1.68
C-C (1)	1.58
C-C (5)[b]	1.36
B-H (9)	0.9
C-H (2)	0.8
C-H (5)[b]	0.7

a. Number of bonds in molecule.
b. Cyclopentadienyl distances.

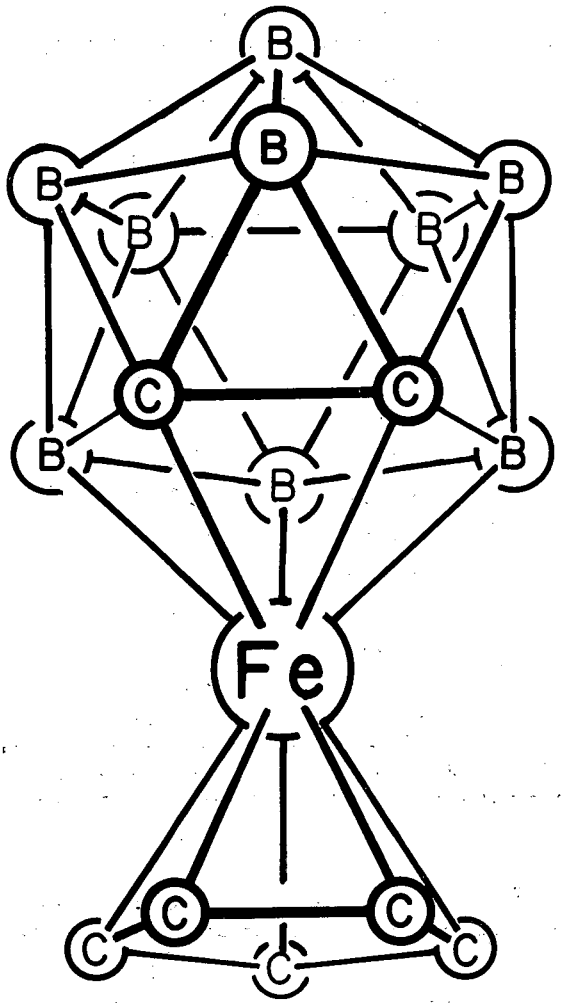

MUB-6096

Fig. D.18-1. Skeleton of the $C_5H_5FeB_9C_2H_{11}$ molecule.

19. CRYSTAL STRUCTURE OF THORIUM NITRATE PENTAHYDRATE BY X-RAY DIFFRACTION*

Tatzuo Ueki, Allan Zalkin, and David H. Templeton

Thorium nitrate crystallizes readily from aqueous nitric acid solutions as the pentahydrate, $Th(NO_3)_4 \cdot 5H_2O$. The earlier literature is confused and contradictory concerning its composition, and it is often found in chemical storerooms labeled as $Th(NO_3)_4 \cdot 4H_2O$. Ferraro, Katzin, and Gibson made a definitive study of the phase diagram and showed that the tetrahydrate crystallizes only when the nitric acid concentration is very high.[1]

An earlier x-ray study of the pentahydrate, then referred to as the hexahydrate, revealed the unit cell, space group, and thorium atom positions.[2] No attempt was made at that time to determine the rest of the structure. With the advantage of electronic computers and better methods for x-ray intensity measurement, we recently solved the structure as reported here. An independent analysis by neutron diffraction, with results in good agreement with ours, is described by Taylor, Mueller, and Hitterman.[3] These studies confirm the composition, show an interesting coordination geometry for the thorium ions, and reveal an intricate structure of hydrogen bonds.

A bottle from Allied Chemical, General Chemical Division, New York, and labeled $Th(NO_3)_4 \cdot 4H_2O$, contained large clear colorless crystals and white powder. Our x-ray diffraction data were obtained from a fragment with dimensions $0.22 \times 0.08 \times 0.08$ mm, cut from one of the clear crystals. It was sealed in a silica-glass capillary (wall thickness 0.01 mm) to prevent deliquescence. Cell dimensions and intensities were measured by means of molybdenum radiation. Intensities were measured of 1036 independent reflections (121 recorded as zero).

$Th(NO_3)_4 \cdot 5H_2O$ crystals are orthorhombic, space group Fdd2, with eight formula units in the cell:

$$a = 11.182 \pm 0.003 \text{ Å} (11.191 \pm 0.005 \text{ Å}),$$
$$b = 22.873 \pm 0.005 \text{ Å} (22.889 \pm 0.010 \text{ Å}),$$
$$c = 10.573 \pm 0.003 \text{ Å} (10.579 \pm 0.005 \text{ Å}).$$

The dimensions found by Taylor, Mueller, and Hitterman[3] are given in parentheses. The discrepancy of 6 to 8 parts in 10,000 is only slightly more than one would expect from the estimated accuracies. The density calculated from our data, 2.800 ± 0.002 g/cm^3, is between the density measured by flotation in this Laboratory, 2.84, and that reported by Staritzky,[4] 2.787. Our measurements were made at about 21° C.

Crystal data for the isomorphous cerium and plutonium compounds are given by Staritzky.[4] These crystals are expected to have very nearly the same atomic arrangement. $R = \Sigma \, ||F_0| - |F_c|| / \Sigma |F_0|$, and refinement with anisotropic thermal parameters for all atoms (hydrogen excluded) reduced R to 0.034.

We had proceeded with the assumption that the water content was in doubt. To check for additional water molecules, we calculated a Fourier synthesis of $(F_0 - F_c)$, deleting reflections with zero intensity. The largest peaks in this function were about 0.28 electron Å^{-3}, in the neighborhood of the thorium atom. No evidence was found of further water molecules. Five peaks were selected as hydrogen atoms, but were not refined.

The calculations to this point had neglected the out-of-phase component $\Delta f''$ of thorium. Because of the polar nature of the space group Fdd2, two orientations of the structure must be considered, one of which is the reflection of the other in (001). Further calculations with $\Delta f''$ included and the correct orientation reduced R to 0.033. With the reverse structure R could not be reduced below 0.035, and the weighted sum of squares was 15% larger. The final coordinates are given in Table D.19-I. The anisotropic thermal parameters, Table D.19-II, are listed in the units of the isotropic Debye B, Zalkin, Forrester, and Templeton,[5] and Cruickshank.[6]

Inclusion of the thorium phase shift in the calculations gives enough change in some of the structure-factor magnitudes to establish the polarity of the structure; though the change in R is hardly dramatic, it causes a significant change in the structure. With the origin defined by the thorium atom, all other atoms were shifted about 0.05 Å in the positive z direction when the correction was included. A similar shift of the reverse structure causes the two structures, after refinement, to differ by about 0.10 Å. This behavior is explained by the fact that all the calculations were made with reflections with positive values of l. The effect of the phase shift

(which is an advance of phase) is to make the thorium atom appear to be closer to the x-ray source and detector than it really is. The symmetry of the space group gives a cancellation of the effect on x and y coordinates, but there is a systematic biasing of the z components of interatomic vectors between thorium and the rest of the structure.

This kind of shift will be a general feature of polar structures that are refined with such incomplete data, unless one of several obvious steps is taken to prevent it.

The two structures of opposite polarity are not different in the sense of right and left handedness, but only with respect to their orientation in a specimen. We have not made a correlation of the polarity with respect to morphology or other physical property.

The neutron diffraction study by Taylor, Mueller, and Hitterman[3] gives us a chance to check the accuracy of the x-ray method in a case in which the heavy atom dominates the data. The agreement of the coordinates is excellent, and it confirms that the estimated standard deviations are the correct magnitude. Of 31 independent coordinates, 17 are within 1 standard deviation, and none is as much as 3 standard deviations from the corresponding neutron result. The atomic positions in the two structures differ by 0.026 Å on the average, and by 0.045 Å in the most extreme case.

The structure obtained before correction for the thorium phase shift is in significantly poorer agreement with the neutron results; the average distance between atomic location is 0.065 Å.

Each hydrogen location determined by x rays is in the correct neighborhood, but indicates errors of 0.2 to 0.5 Å from the correct position determined by neutrons. Some interatomic distances are listed in Table D.19-III. The thorium atom has its 11 oxygen neighbors arranged in a highly unsymmetrical way with respect to the polar direction (Fig. D.19-1). These oxygen atoms are two each from four nitrate groups and three from water molecules, with all the water on one side. This polar arrangement is probably related to the large pyroelectric effect observed when the crystals are dipped in liquid nitrogen. One expects about eight oxygen neighbors for thorium if the oxygen atoms are not bonded to each other. Two oxygen atoms in nitrate are closer than normal for atoms from separate molecules, and thus the coordination can be as high as 12 if the atoms are from six nitrate groups as in $MgTh(NO_3)_6 \cdot 8H_2O$.[7] Thus to have 11 neighbors is reasonable if 8 of them are from nitrate ions.

In each nitrate ion the noncoordinated oxygen atom is significantly closer to nitrogen than are the other two. A similar effect is observed in several other nitrate crystals as listed by Taylor, Mueller, and Hitterman,[3] as well as in $Ce(NO_3)_3 \cdot 6H_2O$ and $Ce(NH_4)_2(NO_3)_6$.[8] The terminal oxygen atom, in each case we have studied, has higher thermal parameters than the other two. Thus a correction of bond distance for thermal motion removes some of the difference, but this correction seems to be inadequate to explain as much as half of the effect. In the present case, the thermal effect is estimated to account for about 0.01 Å of the difference.

We thank J. C. Taylor, M. H. Mueller, and R. L. Hitterman for sending us their manuscript prior to submission for publication.

Footnote and References

*Condensed from Acta Crystallographica (to be published).

1. J. R. Ferraro, L. I. Katzin, and G. Gibson, J. Am. Chem. Soc. 76, 909 (1954).
2. D. H. Templeton and C. H. Dauben, unpublished report abstracted in Struct. Reps. 15, 278 (1950).
3. J. C. Taylor, M. H. Mueller, and R. L. Hitterman, Acta Cryst. (to be published).
4. E. Staritzky, Annal. Chem. 28, 2021, 2022 (1956).
5. A. Zalkin, J. D. Forrester and D. H. Templeton, Acta Cryst. 17, 1408 (1964).
6. D. W. J. Cruickshank, Acta Cryst. 19, 153 (1965).
7. S. Ščavničar and B. Prodić, Acta Cryst. 18, 698 (1965).
8. Tatzuo Ueki, Allan Zalkin, and David H. Templeton, unpublished data.

Table C.19-I. Atomic coordinates and estimated standard deviations. All values have been multiplied by 10^4.

Atom	x	y	z
Th	0	0	0
O(1)	0	0	2277(17)
O(2)	-0042(11)	1041(4)	0656(11)
O(3)	4543(11)	-0892(5)	-1066(12)
N(1)	2651(10)	0046(6)	0508(12)
O(11)	2094(9)	-0381(4)	0025(15)
O(12)	1970(10)	0453(5)	0915(13)
O(13)	3733(8)	0093(5)	0538(13)
N(2)	0471(12)	0772(5)	-2259(17)
O(21)	1318(9)	0551(5)	-1619(12)
O(22)	0579(9)	-0631(4)	-1924(12)
O(23)	0677(12)	1066(6)	-3213(12)

Table C.19-II. Anisotropic thermal parameters. T. F. = $\exp(-\beta_{11}h^2 - 2\beta_{12}hk - \cdots)$; $4\beta_{12}=B_{12}a^*b^*$, etc. Standard deviations estimated by least squares are less than 0.05 for Th and from 0.3 to 0.8 for the other atoms.

Atom	B_{11}	B_{22}	B_{33}	B_{12}	B_{13}	B_{23}
Th	1.2	1.4	2.1	0.0	---	---
O(1)	4.5	2.0	3.7	0.9	---	---
O(2)	2.1	2.0	4.3	-0.3	0.0	-0.5
O(3)	2.4	2.6	3.3	0.1	-0.6	-0.2
N(1)	1.5	2.0	2.9	0.5	-0.5	-0.5
O(11)	2.2	1.4	3.8	0.8	-0.6	-0.7
O(12)	2.3	2.5	3.7	0.3	-0.2	-0.5
O(13)	1.0	2.8	5.2	-0.1	-0.5	0.0
N(2)	2.1	2.0	4.4	-0.9	0.3	0.2
O(21)	1.3	2.9	3.9	0.2	-0.3	0.9
O(22)	1.7	1.7	3.8	-0.2	0.4	-0.1
O(23)	3.5	3.6	3.0	-0.2	1.1	1.5

Table D.19-III. Bond lengths in Å, uncorrected for thermal motion. Values found by Taylor, Mueller, and Hitterman are given in parentheses.

	Th-O (nitrate)	
Th-O(11)	2.50 ± 0.01	(2.528)
Th-O(12)	2.62 ± 0.01	(2.618)
Th-O(21)	2.59 ± 0.01	(2.573)
Th-O(22)	2.58 ± 0.01	(2.554)
	Th-O (water)	
Th-O(1)	2.41 ± 0.02	(2.438)
Th-O(2)	2.48 ± 0.01	(2.473)
	Nitrate groups	
N(1)-O(11)	1.27 ± 0.02	(1.270)
N(1)-O(12)	1.28 ± 0.02	(1.250)
N(1)-O(13)	1.21 ± 0.01	(1.202)
N(2)-O(21)	1.27 ± 0.02	(1.264)
N(2)-O(22)	1.27 ± 0.02	(1.275)
N(2)-O(23)	1.24 ± 0.02	(1.206)
	Hydrogen bonds	
O(1)-O(3)	2.74 ± 0.02	(2.698)
O(2)-O(3)	2.71 ± 0.02	(2.697)
O(2)-O(22)	2.90 ± 0.02	(2.953)
O(3)-O(23)	2.86 ± 0.02	(2.901)
O(3)-O(13)	2.96 ± 0.02	(2.946)

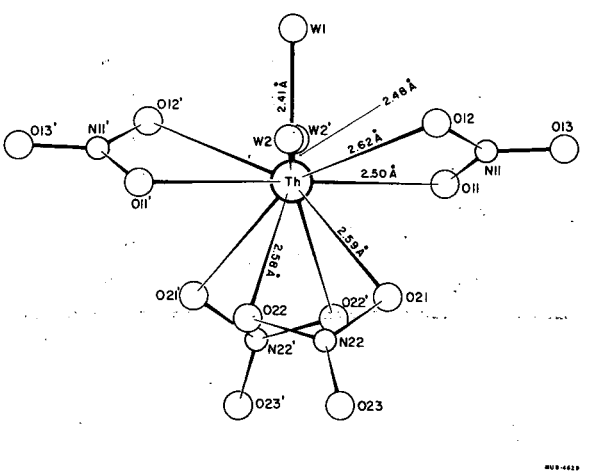

Fig. D.19-1. Neighbors of the thorium atom in $Th(NO_3)_4 \cdot 5H_2O$.

20. THE STRUCTURE OF CYCLOALLIIN HYDROCHLORIDE MONOHYDRATE*

K. J. Palmer† and Kay Sue Lee‡

There is considerable interest in the stereochemistry of sulfur, since it can function as an asymmetric center; some isomeric forms have been shown to exhibit different biological activity. The first determination of the absolute configuration of a sulfur atom was made by Hine,[1] who determined the crystal structure of (+)-S-methyl-L-cysteine sulfoxide. The absolute configuration of (-)-menthyl-p-iodobenzenesulfinate has also been established[2] by determining its crystal structure and utilizing the known configuration of the (-)menthyl group. Recently the absolute configuration of a sulfoxide mustard oil was established by a determination of the crystal structure of a crystalline product formed with thiourea.[3]

To our knowledge the absolute configuration of a cyclic sulfoxide has not previously been determined. For this reason and because cyclic sulfoxide L-5-methyl 1,4-thiazane-3-carboxylic acid-1-oxide (cycloalliin) is obtained from and is related to the aroma of onions,[4] we decided to determine the crystal structure of cycloalliin hydrochloride monohydrate ($C_6H_{11}NO_3S \cdot HCl \cdot H_2O$). The structure of cycloalliin and the numbering system used in this investigation are shown in Fig. D.20-1.

The isolation and identification of cycloalliin was first reported in 1959.[4] Crystals of this material in the form of the hydrochloride monohydrate were grown from an acetone-water mixture acidified with hydrochloric acid. The crystals belong to the monoclinic sphenoidal class, and usually occur as trapezoidal plates or tablets. The optical and crystallographic properties have been described elsewhere.[5]

Weissenberg photographs established that the crystals are monoclinic with the probable space group $P2_1$-C^2_2. The cell dimensions are:
$a = 5.292 \pm 0.004$ Å, $b = 12.375 \pm 0.008$ Å, $c = 8.447 \pm 0.006$ Å, $\beta = 107.45 \pm 0.02°$; $Z = 2$,
$\rho = 1.456$ g/cm^3, ρcalc. $= 1.447$ g/cm^3.

Intensities were obtained by means of a Picker scintillation counter and solid-state detector coupled with a General Electric XRD-5 diffractometer equipped with goniostat. A total of 1219 intensities was measured, of which 38 were assigned a zero intensity.

Complete intensity data were obtained on two crystals because it was thought that the first crystal might have undergone radiation damage. The intensity data for the second crystal were obtained after installation of a magnetic shutter on the x-ray collimater which cut off the incident x-ray beam except when aligning the crystal and for the 10 second interval used to record an intensity. The second crystal thus received much less total irradiation than the first crystal. No obvious trends in the two sets of intensity data could be established, however; consequently for the final stages of least-squares refinement the two sets of intensities were summed in order to decrease the effect of random errors.

Calculations were made with an IBM 7044 computer using a full matrix least-squares refinement program written by Gantzell, Sparks, and Trueblood[6] with modifications by Zalkin. The electron density and distance programs were written by Zalkin.

A three-dimensional Patterson function was calculated by using all the data from which the positions of three atoms were readily deduced. The parameters for these three atoms, assumed to be chlorine, sulfur, and oxygen, were refined by least-squares. The conventional unreliability factor R, defined as $\Sigma \, |F_0| - |F_c| \, | \, / \, \Sigma |F_0|$, decreased from 0.71 to 0.35 after four cycles, and after three additional cycles, to 0.337.

The values obtained for the parameters of these three atoms were then used to calculate a three-dimensional electron-density map. With the aid of a model of the molecule it was possible to locate two additional oxygen and five carbon atoms.

Additional refinement and further Fourier maps permitted the rest of the carbon, nitrogen, and oxygen atoms to be found. Further refinement was undertaken by giving sulfur, chlorine, four oxygens, and one carbon atom anisotropic temperature factors of the form $\exp(\beta_{11}h^2 - \beta_{22}k^2 - \beta_{33}l^2 - 2\beta_{12}hk - 2\beta_{13}hl - 2\beta_{23}kl)$. After four cycles of least-squares refinement

R became 0.0577. At this stage all 13 atoms were given anisotropic temperature factors and the parameters refined by two cycles of least squares. This reduced R to 0.0554.

A three-dimensional electron-density difference function with all atoms subtracted out except hydrogen was calculated with use of the results of the last anisotropic refinement. This allowed the positions of all 14 hydrogens to be readily located. Four cycles of least-squares refinement were calculated with isotropic temperature factors of the form $\exp(-B\lambda^{-2}\sin^{-2}\theta)$ for the hydrogens and anisotropic temperature factors for the 13 heavy atoms. This reduced R to 0.0461. As a final step the intensity data for the two crystals were summed and these data used for four additional cycles of least-squares refinement. This resulted in the final value for R of 0.0390.

The molecular configuration of cycloalliin is shown in Fig. D.20-1. The absolute configuration of the molecule was derived with the knowledge that the configuration about C(3) is L, since this amino acid is from a natural source.

The six-membered ring has the chair conformation. The ring conformation, bond angles, and distances are in good agreement with those found by Shearer[7] for the α modification of 1:4-dithian-1:4-dioxide.

A point of particular interest is the configuration of the methyl group, sulfoxide oxygen, and carboxyl group with respect to the ring. The oxygen atom occupies the axial position, in agreement with that found for many other sulfoxides[7-10]. The S-O bond distance of 1.492 Å is also in good agreement with the value found for those sulfoxides where sulfur is bonded to two carbons and one oxygen.[7,11] The two C-S-O angles are both slightly less than tetrahedral, as was found to be the case in both diethyl and dibenzyl sulfoxides[11] and in dithian disulfoxide.[7]

The molecules in the crystal are held together by a network of hydrogen bonds as shown in Fig. D.20-2. The water molecule is hydrogen-bonded to one carboxyl group and two chloride ions. The N – O(7) distance of 2.692 Å and the N – O(10) distance of 2.687 Å are nearly the same, but apparently only O(7) forms a hydrogen bond with N. This is evident from the fact that H(5) is 2.0 Å from O(7), but is 2.6 Å from O(10). Any attraction that exists between N and O(10) must result from the formal positive charge on N and the negative charge on O(10) which results from resonance in the carboxyl group.

The O(9)–H---O(aq.) distance of 2.541 Å is indicative of a strong hydrogen bond. The O(aq.)–H---Cl distances (3.156 and 3.140 Å) and the N–H---Cl distance (3.108 Å) are those to be expected for hydrogen bonding between chloride ion and oxygen and nitrogen, respectively.

Although the accuracy of the hydrogen parameters is considerably less than for the heavier atoms the C-H distances cluster around the values reported for this bond. The N–H(4) distance of 0.93 Å indicates unequivocally that H(4) is covalently bonded to nitrogen and that chlorine occurs in the structure as the negative ion.

Footnotes and References

*Brief form from Acta Crystallographica (to be published).

†Visiting scientist, 1964-1965.

‡Western Regional Research Laboratory, Western Utilization Research and Development Division, Agricultural Research Service, U. S. Department of Agriculture, Albany, California 94710.

1. R. Hine, Acta Cryst. 15, 635 (1962).
2. E. B. Fleischer, M. Axelrod, M. Green, and K. Mislow, J. Am. Chem. Soc. 86, 3395 (1964).
3. K. K. Cheung, A. Kjaer, and G. A. Sim, Chem. Comm. No. 6, 100 (1965).
4. A. I. Virtanen and E. J. Matikkala, Acta Chem. Scand. 13, 623 (1959).
5. F. T. Jones, K. S. Lee, D. R. Black, and K. J. Palmer, Microscope and Crystal Front 14, 379 (1965).
6. P. K. Gantzel, R. A. Sparks, and K. N. Trueblood, private communication with A. Zalkin, 1961.
7. H. M. M. Shearer, J. Chem. Soc. 1394 (1959).
8. C. R. Johnson and D. McCants, Jr., J. Am. Chem. Soc. 86, 2935 (1964).
9. J. C. Martin and J. J. Uebel, J. Am. Chem. Soc. 86, 2936 (1964).

10. T. Cairns, G. Eglington, and D. C. Gibson, Spectrochim. Acta 20, 159 (1964).
11. S. C. Abrahams, Quart. Rev. (London) 10, 407 (1956).

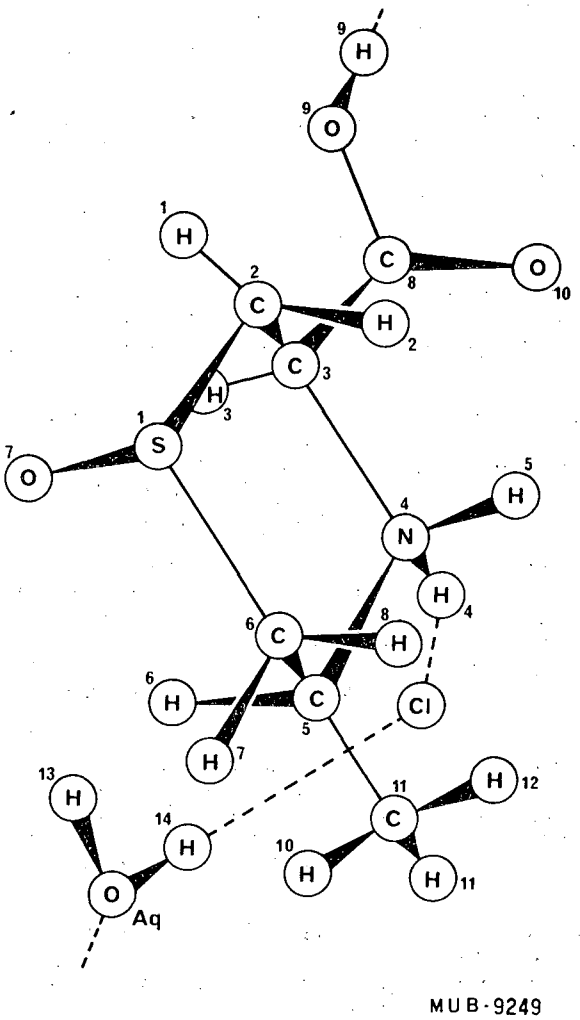

Fig. D.20-1. Molecular configuration of cycloalliin HCl · H_2O and the numbering system used in this investigation.

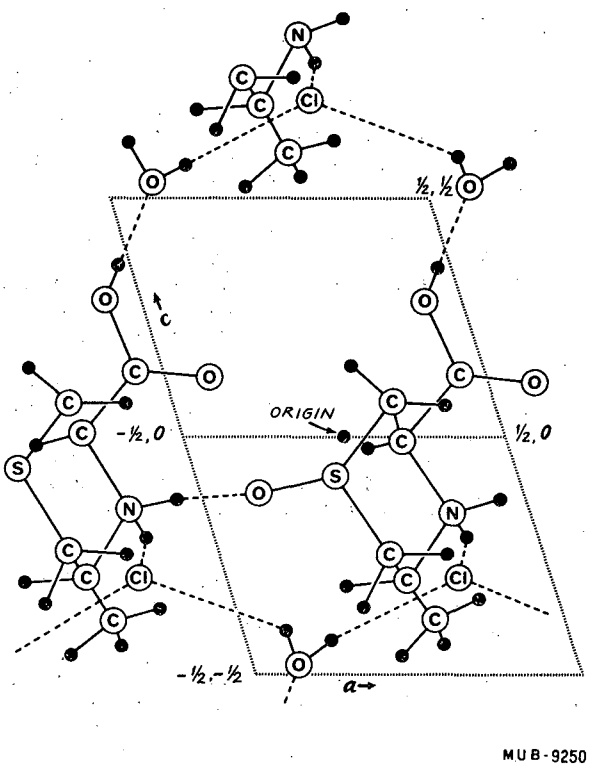

Fig. D.20-2. The hydrogen bond network in crystalline cycloalliin hydrochloride monohydrate.

21. MASS SPECTROSCOPY. THE DETERMINATION OF FIRST IONIZATION POTENTIALS BY SURFACE IONIZATION METHODS

F. L. Reynolds

The determination of the first ionization potentials of the actinide elements by optical spectroscopic means is a difficult experiment because of the complexity of the spectra. A value of americium has so far been the only published determination in the series.[1] The possible determination of these data by mass spectroscopic surface ionization (SI) techniques is the subject of this report.

In order to study the possibilities for the accurate determination of first ionization potentials by this method a series of experiments has been conducted, using elements whose first ionization values are well known. In a recent publication,[2] the elements Sr and Ca were studied on single-crystal tungsten surfaces and present data concern similar studies of La and Sr on single-crystal tungsten, specifically on the (110) and (100) crystal planes of the metal.

Other authors have studied the SI technique, and found certain results inconsistent with predicted values. Werning[3] looked at Nd using SI, and found a value of 5.10 eV for the ionization potential of this element. In comparison Hassen[4] found 5.62 or 5.46 eV, the ambiguity having to do with the identification of the series limit in the Nd optical spectra, while Ionov and Mittsev[5] by SI methods obtained 5.51 ± 0.02 eV.

Dresser[6] studied the SI of Gd, Er, and Yb on polycrystalline tungsten. Upon heating, his filaments recrystallized, mostly with a (113) surface orientation having (112) plateaus as facets to the surface plane. His results indicate values for the first ionization potential of these elements to be Gd 6.70, Er 6.20, and Yb 6.66 eV. Moore's summary[7] gives 6.16 eV for Gd, and 6.22 eV for Yb, Er at 6.08 eV is tentative, and is a SI value. Gd and Yb are optical values.

Previous experimental attempts[8] to find agreement with the optical spectroscopic value of La (5.61 eV) resulted in a SI value some 0.46 eV low. There was some speculation that an excited level of La was impinging on the surface. In the above experiment a single polycrystalline tungsten filament was used, and also a single effusion oven supplying a La neutral beam to this surface. Subsequent design has evolved an ion source employing two effusion ovens and a triple filament arrangement so that comparisons can be made with other elements or with other than one single surface.

The data so far presented fail to make this comparison in a single experiment. We have not succeeded in getting the two ovens to track or to emit simultaneously in one given sample loading. However, data are available for La and for Sr using the summation of values obtained from the various surfaces independently. Since La and Sr have very nearly the same ionization potential--La = 5.61 eV and Sr = 5.69 eV--their slopes, when the ion current is plotted against the reciprocal temperature for each filament surface should be similar.

Table D.21-I lumps the entire data from several separate oven charges, but from the same set of filaments, having crystal planes (100),(110) and (113 or 112) surfaces. Delta (in eV) is the average slope obtained from Saha-Langmuir equation plots of the indicated number of determinations. The delta deviation is an index of the spread of these slope values. The average ϕ (surface work function) is obtained from the known ionization potential of the impinging beam and the average delta.

If one assumed that the value of ϕ for the (100) and the (110) surface obtained from the Sr data alone is correct, namely 4.59 eV for (100) and 5.56 eV for (110), this would give an ionization potential for La of 5.62 and 5.56 eV respectively on the two different planes. Unfortunately there were no data available for La on the polycrystalline (113-112) surface. The agreement with the spectroscopic value seems to be quite reasonable. Further attempts to get both the La and Sr atomic beams working on a single run will be made.

In discussing the experimental method briefly, one can only conclude that one of the main reasons for a lack of agreement between the results of the SI method with the optical methods lies with the extreme surface sensitivity to foreign impurities, coming mostly from the hot metal filament. The surface does not seem to be very sensitive to residual gases present within the ultra-high-vacuum system of the mass spectrometer. Several techniques in taking the data indicate that the most reliable procedure is to flash the filament at high temperature with the beam shutter

closed, then quickly adjust to the desired temperature range before opening the shutter. Pretreatment of the filament for long periods at elevated temperatures is apparently necessary.

Initially there is also a vast difference between the type of plot obtained from a (100) oriented surface and a (110) oriented surface. While almost all surfaces give consistently straight-line Saha-Langmuir plots at temperatures between 2300 and 2800 °K, the range between 1700 and 2300 °K may for many days give a distinct plateau to the curve with the (100) oriented filament while the (110) orientation is a straight-line semilog plot. After many hours of heating this plateau slowly diminishes. Both filaments were cut from the same single crystal. This seems to point out that perhaps the rate of impurity migration is considerably different for the two orientations. It must, however, be pointed out that in the case of the (110) tungsten surface, the high work function of this surface also makes it less sensitive to slope changes with metals such as La or Sr.

It also may be quite important for long outgassing or aging of filaments to heat them during this period with ac supplies. The dc-heated filaments do show some surface structure change which can be detected optically, and to some extent by a slight fuzziness of the Laue x-ray spots from back-reflected exposures. The basic (100) or (110) structure has not changed after many hours of heating at high temperatures.

On the matter of surface structure we have looked at a (100) oriented filament using low-energy electron diffraction techniques. The conclusion was that the surface was a true (100) surface with essentially no faceting from other crystal planes. This was ascertained on a new filament, whose heat treatment consisted of flashing and heating for a period of 24 hours in the LEED equipment to temperatures of 2500 to 2800° K.

References

1. M. Fred and F. S. Tomkins, J. Opt. Soc. Am. 47, 1076 (1957).
2. F. L. Reynolds, J. Chem. Phys. 39, 1107 (1963).
3. Joseph R. Werning, Thermal Ionization at Hot Metal Surfaces. (Thesis), UCRL-8455, Sept. 1958.
4. G. E. M. A. Hassan, Physica 29, 1119 (1963).
5. N. I. Ionov and M. A. Mittsev, Soviet Phys. JETP (English Transl.) 11, 972 (1960).
6. M. J. Dresser and D. E. Hudson, Phys. Rev. 137, A673 (1965).
7. Charlotte E. Moore, Appl. Optics 2, 665 (1963).
8. F. L. Reynolds and M. C. Michel, unpublished data.

Table D.21-I. Data from several oven charges but same set of filaments.

Number of determinations	Filament surface plane	Atomic beam	I. P. values (optical)	Average Δ (eV)	Δ Dev. (eV)	φ (eV) (I. P.-Δ)	I. P. La (eV) ($\phi_{Sr}+\Delta_{La}$)
25	(100)	Sr	5.69	1.10	+.12 -.08	4.59	
13	(110)	Sr	5.69	.13	+.05 -.04	5.56	
18	close to (113)-(112)	Sr	5.69	1.09	+.05 -.04	4.60	
11	(100)	La	5.61	1.03	+.01	4.58	5.62
5	(110)	La	5.61	0.0[a]	—	5.61	5.56

a. Within the limits of the determination the slope was essentially zero.

22. METASTABLE PEAKS IN THE MASS SPECTRA OF N_2O AND NO_2*

Amos S. Newton and A. F. Sciamanna

Begun and Landau[1, 2] reported the existence of a metastable peak at M/q = 20.45 in the mass spectrum of nitrous oxide, which they ascribed to the metastable dissociation

$$N_2O^+ \xrightarrow{(m)} NO^+ + N. \tag{1}$$

Friedman and Irsa[3] questioned this conclusion and showed data indicating that the peak observed by Begun and Landau was due to a collision-induced dissociation. Friedman and Irsa further stated that evidence for metastable electronically excited states of small molecules has been extremely rare. It has recently been shown that a metastable state of CO_2^{+2} exists,[4, 5] and Dibeler and Rosenstock have studied three metastable ions in the mass spectrum of H_2S.[6] To clarify this point, N_2O and other small molecules have been studied further. The work presented here shows not only that the metastable peak in N_2O is the result of a unimolecular dissociation, but also that there are two metastable states in NO_2^+, each with its own half life for dissociation and each leading to different kinetic energies of the fragments NO^+ and O.

The peaks resulting from metastable dissociations in N_2O and NO_2 are shown in Fig. D. 22-1. The peaks appear at apparent masses of 20.45 and 19.57 respectively, but are quite broad owing to kinetic energy given the fragments in the dissociation process.

N_2O Studies

The half life of the metastable state dissociating to yield the M/q = 20.45 peak when investigated by the method of Hipple[7] and Coggeshall[8] was found to be $\geq 0.2 \times 10^{-6}$ second. In Fig. D.22-2, the peak heights of M/q = 20.45, 30, and 44 are plotted against inlet system pressure. The metastable peak height increases at a rate greater than linear, but certainly not as the square of the pressure, as would be demanded by a purely collision-induced process. The ratio of M/q = 20.45 peak height to the height of either mass 30 or 44 peak increases with pressure, but extrapolates to a real value at zero pressure. (The exact extrapolated values are arbitrary, as they are dependent on experimental parameters: V_A, V_R, and collector slit width.) There is no doubt that the nonzero ratio at zero pressure represents a unimolecular dissociation, and the increase with pressure the collision-induced contribution to the dissociation.

The total kinetic energy, T, given the fragments NO^+ and N in the dissociation has been estimated in three ways.

(a) The width, d, of the peak in mass units for the dissociation

$$M_0^+ \xrightarrow{(m)} M_1^+ + M_2 \tag{2}$$

which is related to the kinetic energy, T, and the accelerating voltage, V_A, by the equation[7]

$$d = 4 \frac{M_1^2}{M_0} \sqrt{\frac{M_2}{M_1} \frac{T}{eV_A}} . \tag{3}$$

The problem is to decide where to measure the peak width. Beynon[7] used the width of the top of the peak, while Fuchs and Taubert[5] measured both the top width and 50% peak height widths and compared these results with those found by the deflection method, the top giving too low an energy and the 50% width too high an energy. In Table D.22-I, the width measurements at top and 70% peak height are compared with the results by methods 2 and 3 below, and the 70% peak height values are found to agree with the other.

(b) The difference in peak width at high and low accelerating voltages. As a first approximation these differences should be independent of the method of measurement if the peak shapes are constant.

(c) The voltage spread of the metastable suppressor voltage (ΔV_{mss}) required to suppress the peak, which is related to T by the relation[7]

$$\Delta V_{mss} = \frac{4M_1 V_A}{M_0} \cdot \sqrt{\frac{M_2}{M_1} \frac{T}{eV_A}} . \tag{4}$$

The metastable cutoff curve for M/q = 20.45 peak in N_2O is shown in Fig. D.22-3. The kinetic energies found are summarized in Table D.22-I, and a best value of T in the metastable dissociation of N_2O was 1.05 ± 0.05 eV.

NO_2 Studies

From the shape of the M/q = 19.57 peak from NO_2 (Fig. D.22-1) it is apparent there are two components with different kinetic energies. A half-life study on these components shows the metastable NO_2^+ ions dissociating to give NO^+ ions, comprising the base peak, to have a half life of $0.7 \pm 0.1 \times 10^{-6}$ sec, while those dissociating to the narrower peak superimposed on the base peak have a half life of $2.5 \pm 0.5 \times 10^{-6}$ sec.

At a given accelerating voltage, the peak pattern--i.e., the relative peak heights at the shoulders, tops, and middle--are constant, independent of pressure. The behavior with pressure is shown in Fig. D.22-4. It is seen that the metastable peak rises essentially linearly with pressure, and the ratio of the metastable peak height to either the NO^+ on NO_2^+ peak height is almost independent of pressure. Therefore this is a unimolecular dissociation process.

The kinetic energies of the fragments from the two dissociation processes are given in Table D.22-II, as evaluated by the same three methods as given for N_2O. The metastable suppressor cutoff curve for this peak, shown in Fig. D.22-5, shows the two components fairly well on the low-voltage side, but less distinctly on the high-voltage side. It was possible to get a value for T of the high-energy component, but only a limit can be set on the energy of the low-energy component. The results show the two components to have dissociation energies of 1.12 ± 0.10 eV for the base peak and 0.51 ± 0.1 eV for the center peak.

Both N_2O^+ and NO_2^+ have been shown to possess excited states which are metastable, and which on dissociation give fragments of high kinetic energy. The NO_2^+ has been shown to possess two such excited states, each with its own half life and its own kinetic energy release to the dissociation fragments.

Footnote and References

*Short version of an article to be submitted to the Journal of Chemical Physics.

1. G. M. Begun and L. Landau, J. Chem. Phys. 35, 547 (1961).
2. G. M. Begun and L. Landau, J. Chem. Phys. 36, 1083 (1962).
3. L. Friedman and A. P. Irsa, J. Chem. Phys. 36, 1082 (1962).
4. A. S. Newton and A. F. Sciamanna, J. Chem. Phys. 40, 718 (1964).
5. R. Fuchs and R. Taubert, Z. Naturforsch. 20a, 823 (1965).
6. V. H. Dibeler and H. M. Rosenstock, J. Chem. Phys. 39, 3106 (1963).
7. J. H. Beynon, R. A. Saunders, and A. E. Williams, Z. Naturforsch. 20a, 180 (1965).
8. J. A. Hipple, Phys. Rev. 71, 594 (1947).
9. N. D. Coggeshall, J. Chem. Phys. 37, 2167 (1962).

Table D.22-I. Kinetic energy of fragments in the metastable dissociation of N_2O^+.

V_A	d (top)	T^a (eV)	d (70% peak height)	T^a (eV)
1010	1.67	[0.90]	1.80	[1.05]
3850	0.81	[0.86]	0.94	[1.09]
	Δd		Δd	
ΔV_A(1010-3850)	0.86	1.03	0.86	1.03
Metastable suppressor cutoff				1.09
			T (average)	1.05 ± 0.05

a. Figures in brackets not included in the average.

Table D.22-II. Kinetic energy given to fragments in the metastable dissociation of NO_2^+.

Main Peak V_A	d (top)	T^a (eV)	d (70% peak height)	T^a (eV)
581 V	1.61	[0.46]	1.69	[0.51]
2328 V	0.77	[0.42]	0.85	[0.51]
	Δd		Δd	
ΔV_A(581-2328)	0.84	0.51	0.84	0.51
Metastable suppressor cutoff				[≤ 0.65]
			T (average)	0.51 ± 0.10
Base Peak				
581	2.44	[1.06]	2.56	[1.17]
2328	1.22	[1.05]	1.20	[1.19]
	Δd		Δd	
ΔV_A(581-2328)	1.22	1.07	1.26	1.14
Metastable suppressor cutoff				1.16
			T (average)	1.12 ± 0.10

a. Figures in brackets not included in the average.

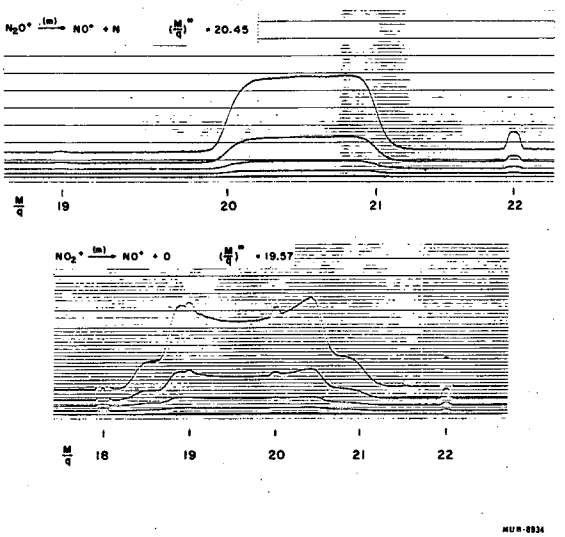

Fig. D.22-1. Metastable peaks in the mass spectrum of N_2O and NO_2. N_2O peak-Magnetic scan: V_A=3838 V, average repellers=75 V, V_I=95 V , inlet pressure=400μ.
NO_2 peak - Voltage scan: MV_A=11 336, repellers=1% V_A, V_I=70 V, inlet pressure=300 μ.

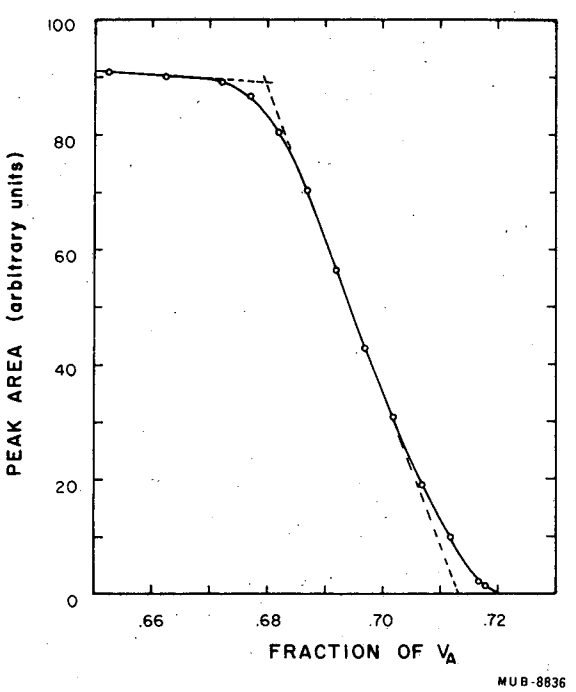

Fig. D.22-3. Metastable suppressor cutoff curve of M/q=20.45 in N_2O. MV_A=69 700, V_R= 1.8% V_A, inlet pressure = 400 μ.

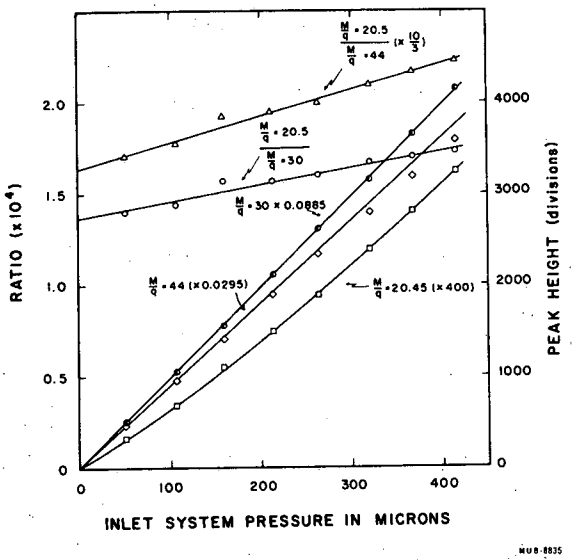

Fig. D.22-2. Variation with inlet system pressure of peak heights and ratios of M/q=20.45 to M/q=30 and M/q=44 in N_2O. MV_A= 45 100, V_R=1.2% V_A.

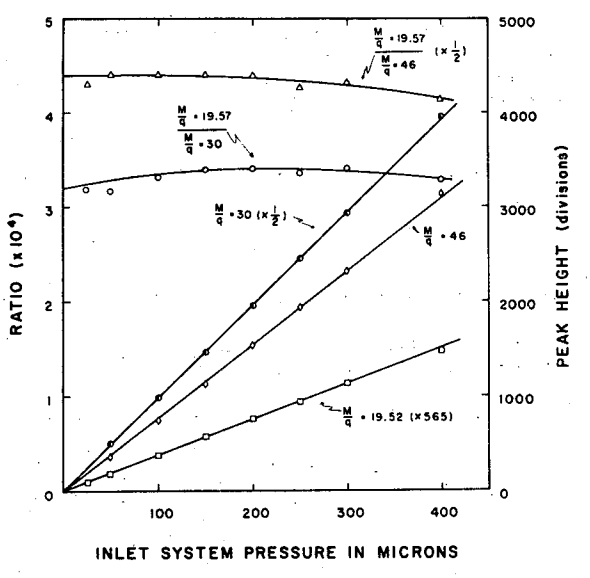

Fig. D.22-4. Variation with inlet system pressure of peak heights and ratios of M/q=19.57 and M/q=30 and M/q=46 in NO_2. M/q=19.57 scanned at MV_A=11 300, V_R=1.2% V_A. M/q=30 and 46 scanned at MV_A=45 200, V_R=1.2% V_A.

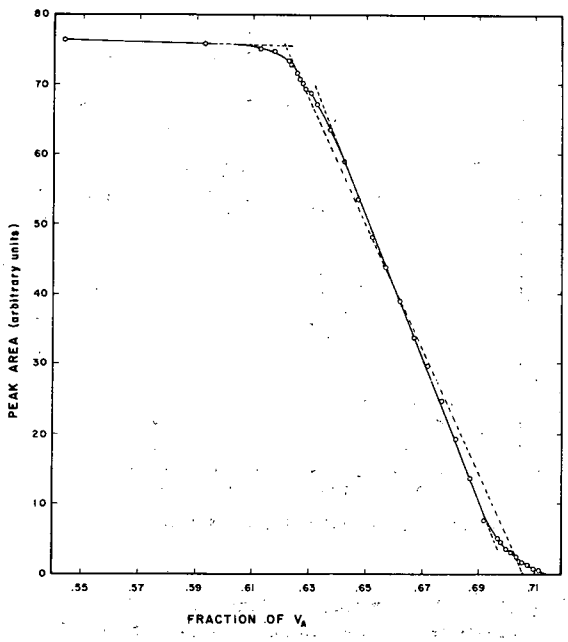

Fig. D.22-5. Metastable suppressor cutoff curve for $M/q = 19.57$ in NO_2. $MV_A = 11\,300$, $V_R = 1.2\%\ V_A$, inlet pressure = 300 μ.

23. METASTABLE ION PEAK SHAPES IN DEMPSTER-TYPE MASS SPECTROMETERS*

Amos S. Newton

Hipple[1] has shown why metastable ions should appear in a Dempster-type mass spectrometer, but when Coggeshall[2] investigated the question of peak shape, he predicted a sharp cutoff on the low-mass side of such peaks with tailing toward the high-mass side. Experimentally most such peaks are broad fairly symmetrical peaks which appear in the mass spectrum at an apparent mass, M^*.

The peak shape of the $M^*/q = 31.88$ peak in n-butane arising from the metastable transition

$$n\text{-}C_4H_{10}^+ \xrightarrow{(m)} C_3H_7^+ + CH_3 \qquad (1)$$

has been studied with a CEC-Model 21-103B mass spectrometer. The profiles of $M^*/q = 31.88$ in butane at three accelerating voltages are shown in Fig. D.23-1, and a comparison profile of a normal zero-kinetic-energy peak, O_2^+, is shown in Fig. D.23-2. The estimated error in the mass scale is ± 0.01 mass unit.

Some features of metastable peaks as exemplified by the peak in Fig. D.23-1 are:

(a) the half width is abnormal and increases as the accelerating voltage is decreased,
(b) the peaks have rounded tops whereas the O_2^+ peak has a flat top,
(c) the center of the peak is displaced about 0.08 mass unit from the calculated value of 31.88, and
(d) the peak height varies as the square root of the accelerating voltage.

It is reasonable to assume that the increased widths of the metastable peak over normal peaks is caused by velocity components added from the dissociation process. Beynon, Saunders, and Williams[3] have derived the relation of peak width, d, with accelerating voltage, V_A, and kinetic energy, T, released in the fragmentation,

$$d = 4\ \frac{M_0^{\,2}}{M_1}\left(\frac{M_2}{M_1}\ \frac{T}{eV_A}\right)^{1/2}. \qquad (2)$$

If the widths of the peaks in Fig. D.23-1 at various fractions of the peak height are plotted against $V_A^{-1/2}$, Fig. D.23-3, a series of straight lines results, the slope of which is a measure of the kinetic energy release. In Fig. D.23-4 the apparent kinetic energy release for the dissociation is plotted as a function of fraction of peak height measured, and it is seen that the apparent kinetic energy must lie between 0.001 and 0.04 eV.

Coggeshall[2] has analyzed the ion optics of metastable dissociations in a Dempster-type mass spectrometer, and shown that there is an increase of apparent mass with distance beyond the ion source at which dissociation occurs. Three contributing half lives to M/q = 31.88 from n-C_4H_{10} were also found by Coggeshall.

Because of added velocity from dissociation, the beam width of ions resulting from a metastable dissociation is increased over that for a normal peak such as oxygen. The peak shape for those butane ions decomposing just at the exit slit of the ion source can then be represented by a trapezoid with a top width of beam width minus the slit width, and a bottom width of beam width plus slit width. The beam width assumed is the normal O_2^+ beam width plus the width calculated from Eq. (2). The observed peak will be the sum of a manifold of such trapezoids, with increasing mass centers as the butane ion travels further from the exit slit before dissociation. At the same time, the height of these trapezoids must decrease according to the time of travel to the dissociation point and the half life of the metastable butane ion. Cutoff occurs after 17 deg of travel, when the trajectories of the fragment ions strike the analyzer tube.

To obtain an integrated peak shape, the time of travel of the butane ion from the exit slit to the cutoff point was divided into 10 equal time intervals. A trapezoid of width determined by the assumed energy was constructed for each interval, and on the mass center corresponding to the center of the interval, as shown in Fig. D.23-5. Summing the contribution from each trapezoid at each mass point yields the final peak shape.

Calculations of peak shape have been made using only one adjustable parameter, the kinetic energy, T, of the dissociation. Half lives of 0.61×10^{-6} and 2.7×10^{-6} sec were assumed for the metastable $C_4H_{10}^+$ ion as reported by Coggeshall,[2] and it was assumed that the same kinetic energy was associated with each half life. The results, shown in Fig. D.23-6, show that T = 0.015 eV yields a fair representation of the observed metastable peak shapes at V_A = 1550 V and 582 V respectively. At 582 V the top of the calculated peak is skewed to the high-mass side, indicating there is some parameter still not included in the peak representation.

Footnote and References

*Short version of paper submitted to J. Chem. Phys.

1. J. H. Hipple, Phys. Rev. 71, 594 (1947).
2. N. D. Coggeshall, J. Chem. Phys. 37, 2167 (1962).
3. J. H. Beynon, R. A. Saunders, and A. E. Williams, Z. Naturforsch. 20a, 180 (1965).

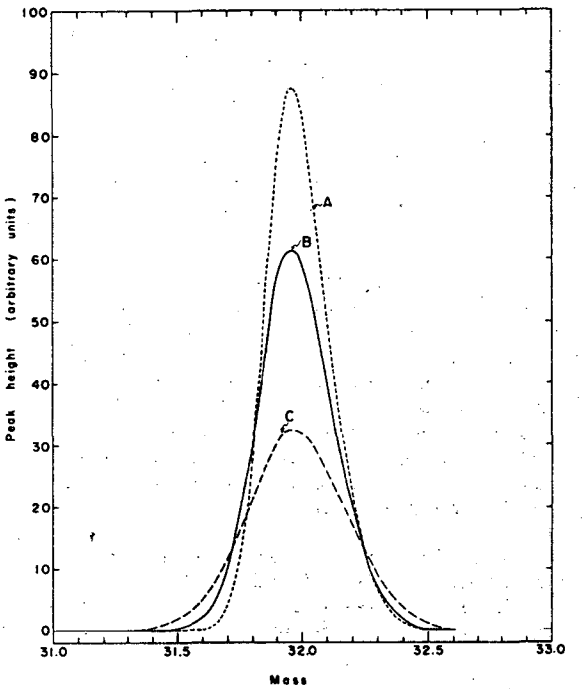

Fig. D.23-1. Profiles of $M/q = 31.88$ peak from the metastable dissociation $n\text{-}C_4H_{10}^+ \rightarrow C_3H_7^+ + CH_3$. Curve A at accelerating voltage, $V_A = 3100$ V; curve B, $V_A = 1550$ V; and curve C, $V_A = 582$ V. Mass scale assumes $M/q = 28\,(C_2H_4^+) = 28.00$.

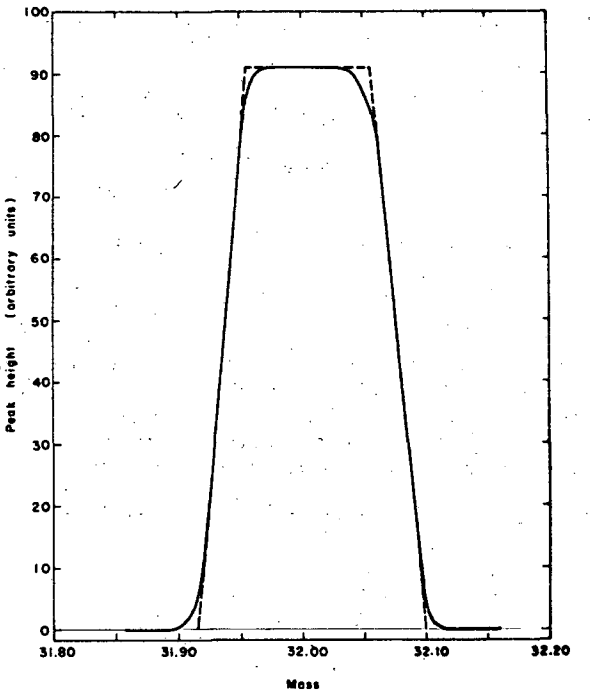

Fig. D.23-2. Profile of O_2^+ peak of oxygen at $V_A = 3100$ V. Solid line - Observed profile. Dashed line - Trapezoidal representation of peak.

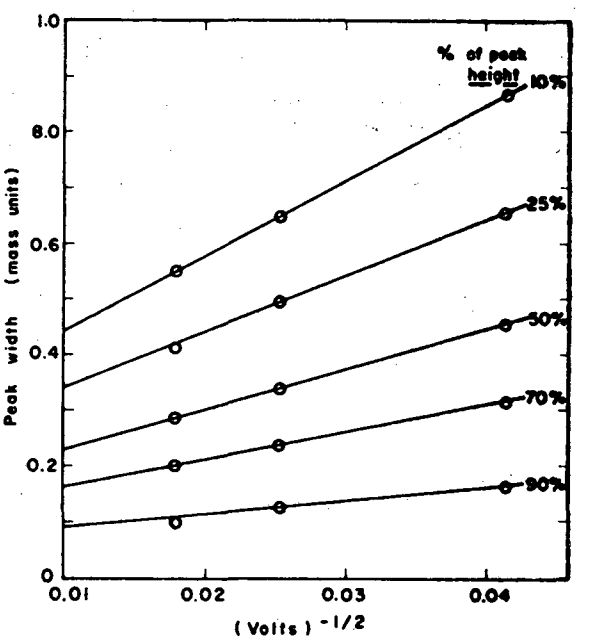

Fig. D.23-3. Peak widths in mass units of the $M/q = 31.88$ peak in $n\text{-}C_4H_{10}$ at various percentages of the total peak height plotted against the inverse square root of accelerating voltage.

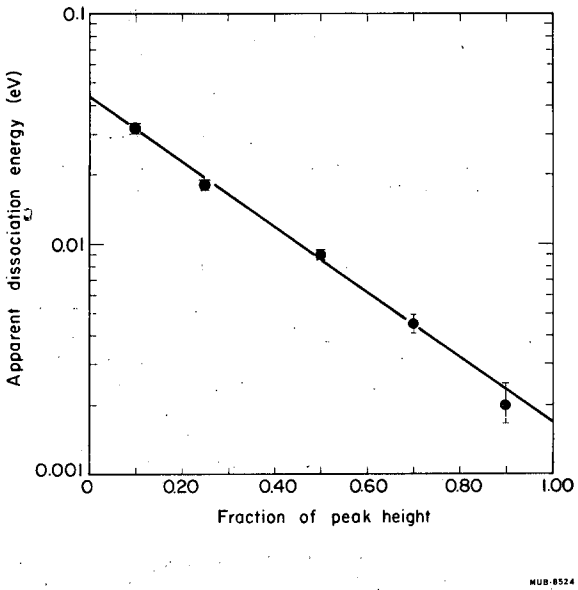

Fig. D.23-4. Apparent dissociation energy of metastable $C_4H_{10}^+ \rightarrow C_3H_7^+ + CH_3$ as measured by the change in peak width with accelerating voltage plotted as a function of percentage of peak height at which widths were measured.

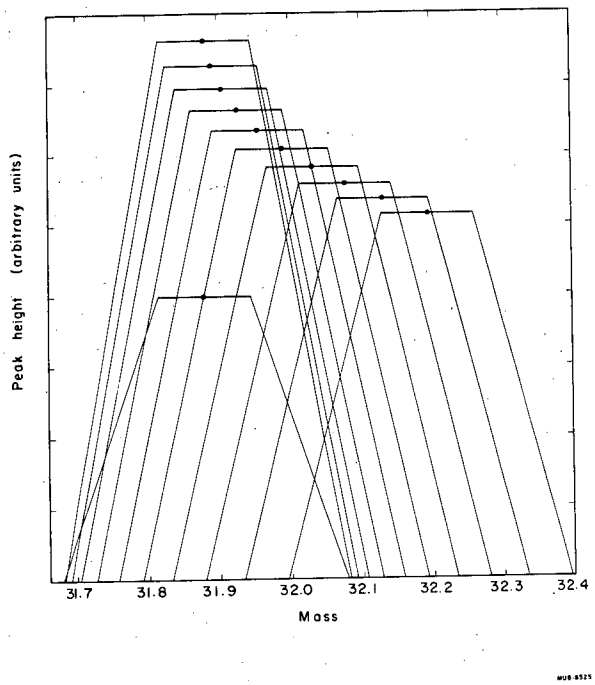

Fig. D.23-5. Schema for integrating mass peak M* = 31.88 in mass spectrum of n-C_4H_{10}. V_A = 1550 V. The zero point is counted at 1/2 value because dissociations before slit S_2 do not contribute, so the time interval is 1/2 the other time intervals. Peak shapes assume T = 0.015 eV. Peak heights assume equal parts 0.61-μsec and 2.7-μsec half lives present at emergence of beam from S_2.

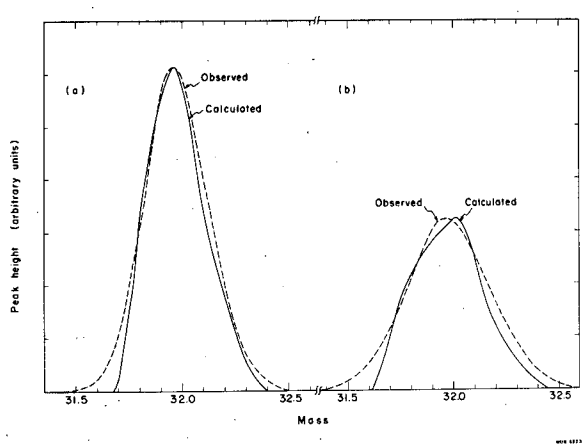

Fig. D.23-6. Comparison of the calculated against the observed peak shape for M/q = 31.88 peak in n-C_4H_{10}.
(a) V_A = 1550 V.
(b) V_A = 582 V.

24. APPLICATION OF HIGH-RESOLUTION SEMICONDUCTOR DETECTORS IN x-RAY EMISSION SPECTROGRAPHY*

H. R. Bowman, E. K. Hyde, S. G. Thompson, and R. C. Jared

A new system for the chemical analysis of materials by x-ray emission spectrography has been conceived and tested. The new system makes use of semiconductor diode detectors to analyze the energy spectrum of characteristic x rays excited in a specimen by γ rays from a radioactive isotope. Figure D.24-1 is a schematic outline of the system.

A γ-ray source of moderate strength (e.g., 10^9 dpm) is placed near the analytical specimen. For analysis of lighter elements Am^{241} is a suitable source because the neptunium L x rays and the 60-keV γ ray emitted by Am^{241} are effective in exciting the K x rays of elements up to erbium. For the heavier elements Co^{57}, which emits 122-keV and 137-keV γ rays, is a suitable choice. The γ-ray source is shielded from the semiconductor counter. The characteristic x rays excited in the specimen impinge on the semiconductor diode detector and produce electrical pulses which are linearly amplified and fed to a multichannel analyzer. After a period of data collection the contents of the memory of the pulse-height analyzer are printed or plotted out. The result is an energy spectrum of the characteristic x rays. The energy of the x rays identifies the elements, and the integrated counts are proportional to the amount of each element present in the sample.

Such a system is possible only because of numerous improvements in the manufacture of semiconductor detectors and associated electronic circuitry.[1] In particular the work reported here was stimulated by the advances made by Nakamura and Elad[2,3] These workers used a field effect transistor (FET) as the first stage of a charge-sensitive preamplifier, and found that by mounting this part immediately behind the semiconductor diode and cooling it to liquid nitrogen temperature they could achieve a great overall improvement in energy resolution. For γ-ray photons of 20 to 100 keV impinging on the detector, the resolution, expressed as full width at half maximum, was 1.1 keV. Subsequent changes reduced the figure below 1 keV. This number is to be compared with 2.5 keV for the best systems previously in use.

The implication of this resolution improvement for x-ray analysis is that x rays of neighboring elements can be distinguished.

The performance of the new system of x-ray emission spectrography is demonstrated here in a series of figures.

Figures D.24-2 through D.24-4 show results obtained with metallic foil samples irradiated with photons emitted by Am^{241} ($\approx 10^8$ dpm). The semiconductor detector was a lithium-drifted silicon diode with a sensitive depth of 2.5 mm and overall diameter of 1.4 cm. It was placed in a vacuum chamber covered by a Be window.

Figure D.24-2 represents data collection for 2 minutes. In the region of Ti-Cu an unresolved K peak is obtained with slight separation of peaks of neighboring elements. In the Zr-Mo group there is a separation of K_α and K_β groups and the clearer separation of neighboring elements. L x rays of heavy elements can also be excited by Am^{241} radiations, as shown in the insert.

Analysis of silver ions in solution and of common materials like phosphor bronze and solder is shown in Figs. D.24-3 and D.24-4.

For heavier elements it is necessary to use more energetic exciting radiation. Co^{57} is a good choice. Also it is preferable to use a lithium-drifted germanium diode. In these experiments a 1×3 cm diode with a 3-mm-deep sensitive layer was used. Figures D.24-5 through D.24-7 show the performance of the system in 2-min analyses of characteristic γ rays emitted by metallic foils struck by the Co^{57} primary radiations. A characteristic pattern of $K\alpha_2$, $K\alpha_1$, $K\beta_1$, and $K\beta_2$ is observed for each element, and there is little difficulty in resolving the x-ray peaks of neighboring elements.

It is believed that this new system has many advantages over the conventional x-ray spectrograph based on Bragg reflection of x rays from crystal lattices. The overall simplicity and the capability of rapid simultaneous analysis of all constituent elements are outstanding advantages. The efficiency of measurement when all intrinsic and geometrical factors are considered

is orders of magnitude greater. No x-ray tube and no complex power supply is necessary, nor is a goniometer required. The K x rays of the heavy elements can be excited and measured as easily as the x rays of the lighter elements.

The simplicity of the system, particularly the fact that the essential "head end" of the system can be made quite small, also opens up the possibility of attractive applications in analysis of chemical plant process streams, in analysis of minerals in test holes in mines, in analysis of materials on ion-exchange columns, etc.

A further discussion of this x-ray emission spectrograph is given in the report (UCRL-16485, Nov. 1965) of which this is a condensation.

Footnote and References

*Short version of paper submitted to Science.

1. Fred S. Goulding, Semiconductor Detectors for Nuclear Spectrometry, UCRL-16231, July 1965, lectures given at Herceg-Novi, Summer School for Physicists, August 1965.
2. Emanuel Elad, A Preamplifier with 0.7 keV Resolution for Semiconductor Radiation Detectors (UCRL-16390, Sept. 1965), Nucl. Instr. Methods 37 327 (1965). E. Elad and M. Nakamura, High-Resolution x-Ray and Electron Spectrometer (UCRL-16515, Nov. 1965), to be submitted to Nucl. Instr. Methods.

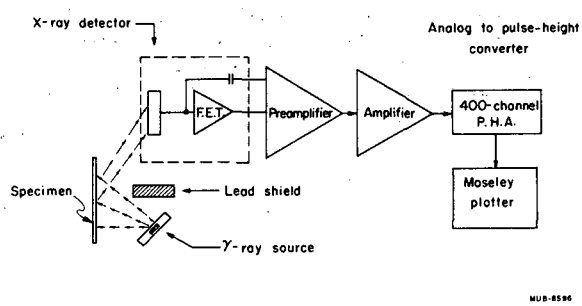

Fig. D.24-1. Schematic arrangement of apparatus for excitation and measurement of characteristic x radiation of an analytical sample. That part of the apparatus outlined in dashed lines is maintained at low temperature.

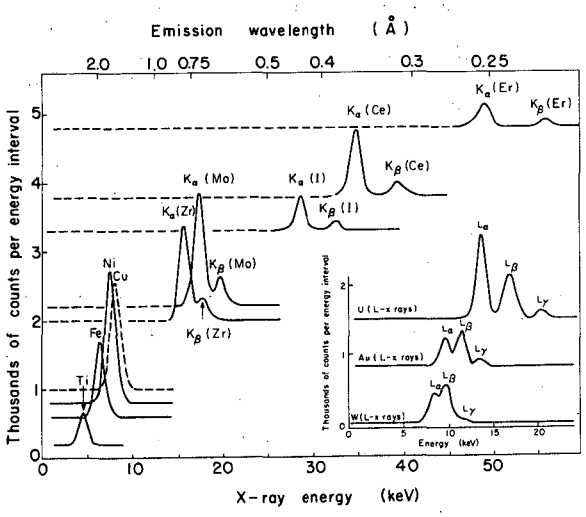

Fig. D.24-2. K x-ray spectra of several elements taken with lithium-drifted silicon detector. Americium-241 source used to excite characteristic x rays. Each spectrum represents a separate experiment with a metallic or oxide sample of the element. Counting period was 2 min. Vertical scale is linear in the number of counts but the zero of the scale lies at a different level for each element. The insert shows L x radiation excited in heavy elements by Am^{241} radiation, data collection for 2 min; vertical scale identical to main figure.

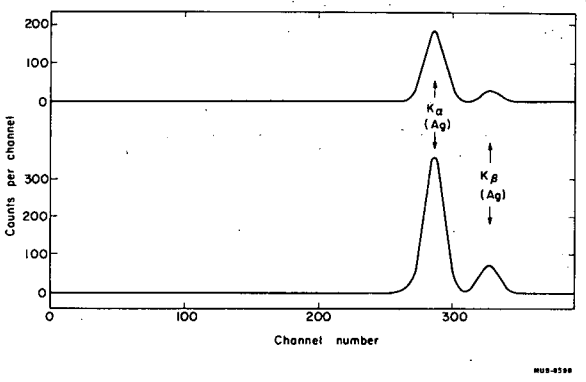

Fig. D.24-3. Characteristic K x rays of silver excited in dilute solutions of $AgNO_3$ by 60-keV γ ray of Am^{241}. Americium-241 source strength--10^8 dpm. Lower curve 0.5 g silver in 5 ml water held in cellulose nitrate tube. Data-collection time 2 min. Upper curve 10 mg silver in 1 ml water. Data-collection time 7 min plus 7 min background subtraction with sample replaced with 1 ml pure water. Lithium-drifted silicon detector.

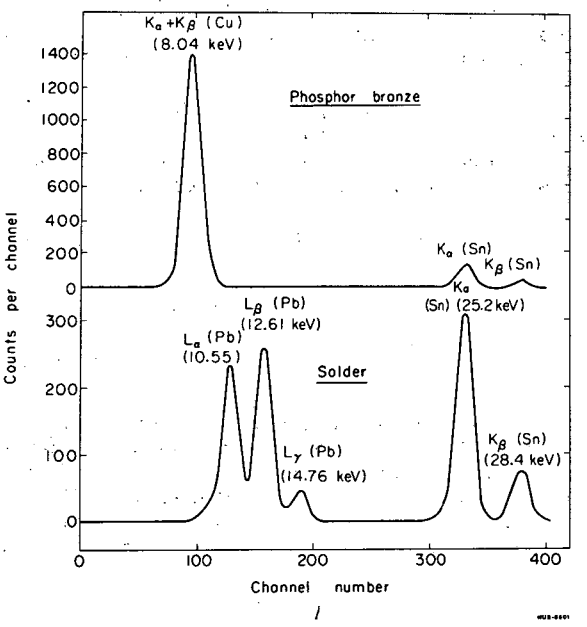

Fig. D.24-4. Analysis of samples of solder and phosphor bronze. Figures show x rays excited in sample by Am^{241} source and analyzed by lithium-drifted silicon detector. Counting time 2 min.

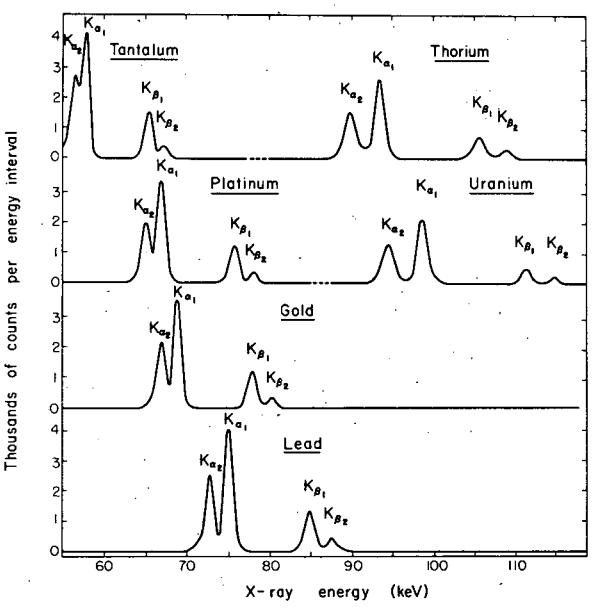

Fig. D.24-5. K x-ray spectra of tantalum, platinum, gold, lead, thorium, and uranium recorded by lithium-drifted germanium semiconductor. The x radiation was excited in metallic foils of these elements by γ radiation of Co^{57}. Counting times were 2 min. Data across range of figures taken with 400-channel analyzer.

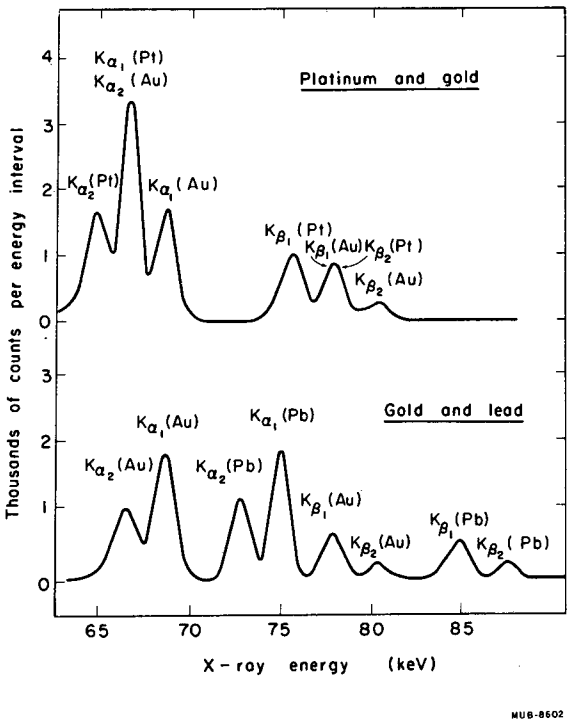

Fig. D.24-6. K x-rays of platinum and gold (upper spectrum) and gold and lead (lower spectrum) as recorded by lithium-drifted germanium detector. Counting time 2 min. x Rays excited in metallic foils by γ radiation of Co^{57}. Central peak of Kα group in upper spectrum shows superposition of platinum $K\alpha_2$ on gold $K\alpha_1$. In lower spectrum Kα group of lead falls between Kα and Kβ groups of gold.

Fig. D.24-7. Analysis of x radiation emitted by aqueous solutions containing tungsten (element 74) and gold (element 79). Bottom curve--1 ml solution of silicotungstic acid containing 350 mg W. Center curve--1 ml solution of silicotungstic acid containing 35 mg W. Top curve--2 ml solution of silicotungstic acid containing 17 mg W and 220 mg Au. Characteristic x radiation excited by Co^{57}. Counting times 2 min plus 2 min background subtraction with pure water solutions in sample position. Lithium-drifted germanium detector used in all cases.

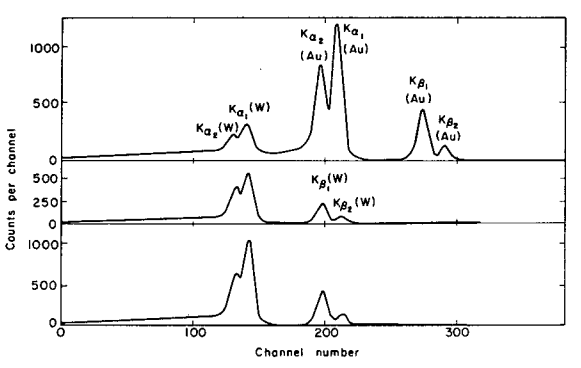

E. RADIATION CHEMISTRY

1. REACTIVITY OF THE HYDRATED ELECTRON WITH ORGANO-NITROGEN COMPOUNDS †

Rodney L. S. Willix and Warren M. Garrison

Radiolysis of water leads to formation of reducing and oxidizing species,

$$H_2O \rightsquigarrow H_2O_2,\ H_2,\ OH,\ H,\ e^-_{aq},\ H^+ ,$$

where e^-_{aq} represents the hydrated electron. With γ rays the 100-eV yields of these decomposition products correspond[1] to $G_{H_2} = 0.45$, $G_{H_2O_2} = 0.7$, $G_{OH} = 2.9$, $G_H = 0.55$, $G_{e^-_{aq}} = 2.8$.

Recent studies of the radiation chemistry of the simpler α-amino acids, viz., alanine and glycine, in oxygen-free solution have shown that the hydrated electron reacts with both the zwitterion and cation forms of these amino acids via reductive deamination.[2] In this work we measure the velocity constants for reaction of e^-_{aq} with a number of α-amino acids, β-amino acids, N-acylamino acids and certain simple peptides at pH 7 and at pH 3. The experimental approach is based on a study of competition kinetics involving the organo-nitrogen compound at a fixed concentration (0.3 M),

$$R_3N + e^-_{aq} \rightarrow \text{products}, \tag{1}$$

and a second solute, chloroacetic acid, in increasing concentration over the range ≈ 0.001 M to ≈ 0.1 M. The latter reacts with e^-_{aq}, according to the stoichiometry[3]

$$RCl + e^-_{aq} \rightarrow R + Cl^-, \tag{2}$$

to give chloride ion, which product is followed analytically.

Chemicals were of research grade. The organo-nitrogen compounds were recrystallized from distilled water. The chloroacetic acid was redistilled in vacuo. Chloride ion was determined by the method of Luce et al.[4] following Hayon and Allen.[3] Methods used in water purification, in solution preparation, and in irradiation all have been described.[5] The irradiations were made with Co^{60} γ rays at a dose rate of 1.6×10^{18} eV/g/min for a total dose of 1×10^{19} eV/g.

All the compounds studied have pK values such that at pH 7 each solute exists almost exclusively as a single species, i.e., the zwitterion form of the α-amino acids, β-amino acids, and dipeptides, the cation form of the simple amines, and the anion forms of the acetylamino acids and the chloroacetic acid. For simplicity we distinguish these proton-deficient species in terms of $\overline{R_3N}$ and $\overline{RCl}$ as defined by the equilibria

$$(\overline{R_3N})(H^+)/(R_3N) = K_{R_3N}$$

$$(\overline{RCl})(H^+)/(RCl) = K_{RCl}$$

The reactions in neutral solution then are written

$$\overline{R_3N} + e^-_{aq} \rightarrow \text{products}, \tag{$\bar{1}$}$$

$$\overline{RCl} + e^-_{aq} \rightarrow \bar{R} + Cl^-, \tag{$\bar{2}$}$$

to distinguish from the corresponding reaction of the acid forms given by Eqs. 1 and 2. For simple competition in these two solute systems at pH 7 we may derive the expression

$$\frac{1}{G(Cl^-)} = \frac{1}{G_{e^-_{aq}}} + \frac{1}{G_{e^-_{aq}}}\left(\frac{\bar{k}_1}{\bar{k}_2}\right)\left(\frac{\overline{R_3N}}{\overline{RCl}}\right), \tag{3}$$

where $G(Cl^-)$ represents the experimentally observed chloride yield, $(\overline{R_3N})$ and $(\overline{RCl})$ the concentration of the two solutes species in neutral solution, and $\bar{k}_1$ and $\bar{k}_2$ the respective velocity constants for reaction with e^-_{aq}. A plot of the reciprocal of the chloride yield as a function of $(\overline{R_3N})/(\overline{RCl})$ gives a straight line as shown in Fig. E. 1-1 with slope $\frac{1}{G_{e^-_{aq}}}(\bar{k}_1/\bar{k}_2)$.

The intercept value $1/G(Cl^-) = 0.36$ gives $G_{e^-_{aq}} \approx 2.8$, in good agreement with published values Taking $\bar{k}_2 = 1.2\times10^9\ M^{-1}sec^{-1}$ as determined by Anbar and Hart[6] in pulse radiolysis studies, we obtain the values of $\bar{k}_1$ given in Table E. 1-I.

A parallel series of experiments was run at pH 3 to obtain rate constants for reactions of e^-_{aq} with these organo-nitrogen compounds in the protonated form. Results are obtained in terms of the rate constant for reaction of e^-_{aq} with the undissociated chloroacetic acid molecule. Corrections must be included for removal of e^-_{aq} by

$$H^+ + e^-_{aq} \rightarrow H, \tag{4}$$

with $k_4 = 2\times10^{10}\ M^{-1}S^{-1}$ and for the competition by $\overline{R_3N}$ and $\overline{RCl}$ at the concentrations determined by the equilibrium constants K_{R_3N}, K_{RCl}. It can be shown that Eq. 3 then takes the more complicated form

$$\frac{1}{G(Cl^-)} = \frac{1}{G_{e^-_{aq}}} + \frac{1}{G_{e^-_{aq}}}\left\{\frac{k_1(H^+) + \bar{k}_1 K_{R_3N} + k_4(H^+)^2/(R_3N)}{k_2(H^+) + \bar{k}_2 K_{RCl}}\right\}\left(\frac{R_3N}{RCl}\right). \tag{5}$$

Here again a plot of the reciprocal chloride ion yield versus $(R_3N)/(RCl)$ should give a straight line with intercept equal to $1/G_{e^-_{aq}}$. From the slopes given by

$$\frac{1}{G_{e^-_{aq}}}\left[\frac{k_1(H^+) + \bar{k}_1 K_{R_3N} + k_4(H^+)^2/(R_3N)}{k_2(H^+) + \bar{k}_2 K_{RCl}}\right]$$

we may calculate the respective values of k_1, assuming $k_2 = 6.6\times10^9\ M^{-1}sec^{-1}$ as derived from the work of Hayon and Allen.[3] Values of k_1 so obtained are listed in Table E. 1-I.

We note that all the plots of $1/G(Cl^-)$ in Fig. E. 1-1 show a linear dependence on chloroacetate concentration over the range 10^{-3} M to 10^{-1} M. Although kinetic salt effects are observed in the reactions of e^-_{aq} with ionic species,[7,8] the magnitude of this effect over the indicated chloroacetate concentration range is within the experimental error of the present work, $10^{\pm0.1}$. Effects of ionic strength and also of dielectric constant on the reactivity of e^-_{aq} towards organo-nitrogen compounds have been observed.[9]

Footnotes and References

†Condensed version of paper to be submitted to Radiation Research.

1. A. O. Allen, Radiation Res. Suppl. 4 54 (1964); J. T. Allan, J. Phys. Chem. 68, 2697 (1964).
2. B. M. Weeks, S. A. Cole, and W. M. Garrison, J. Phys. Chem., in press.
3. E. Hayon and A. O. Allen, J. Phys. Chem. 65, 2181 (1961).
4. E. N. Luce, E. C. Denice, and F. E. Akerlund, Ind. Eng. Chem. 15, 365 (1943).
5. R. L. S. Willix and W. M. Garrison, J. Phys. Chem. 69, 1579 (1965).
6. M. Anbar and E. J. Hart, J. Phys. Chem. 69, 271 (1965).
7. G. Czapski and H. Schwarz, J. Phys. Chem. 66, 471 (1962).
8. P. J. Coyle, F. S. Dainton, and S. R. Logan, Proc. Chem. Soc., 219 (1964).
9. R. L. S. Willix and W. M. Garrison, to be published.

Table E. 1-I. Rate constants for reaction of organo-nitrogen compounds with the hydrated electron.

Compound	$k_1 (M^{-1} sec^{-1})$	$\bar{k}_1 (M^{-1} sec^{-1})$
α-alanine	3.1×10^9	2.0×10^7
β-alanine	3.3×10^8	1.3×10^7
2-methyl alanine	$< 0.5 \times 10^8$	5.2×10^6
N-acetyl alanine	2.3×10^8	5.7×10^6
glycine	4.5×10^8	1.3×10^7
glycl glycine	8.9×10^8	1.9×10^8
glycyl glycyl glycine	----	7.2×10^8
proline	----	2.4×10^7
N-ethyl acetamide	5.7×10^6	----
ethylamine	$\approx 1 \times 10^6$	----

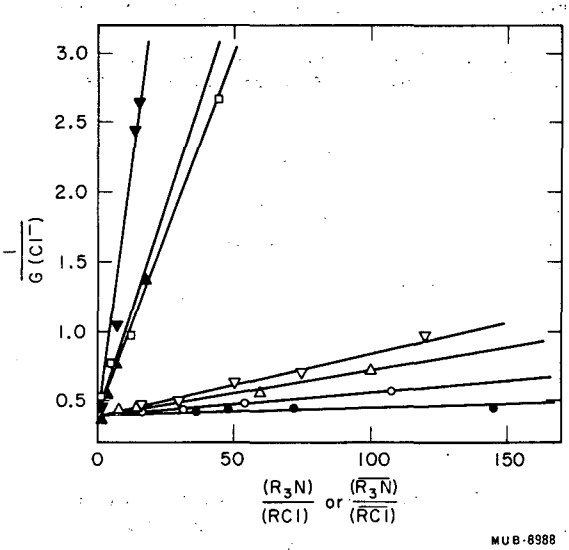

Fig. E. 1-1. Typical plots of the reciprocal chloride yield as a function of $(R_3N)/(RCl)$ or $(\overline{R_3N})/(\overline{RCl})$: α-alanine (▼ cation, ▽ zwitterion), glycine (▲ cation, △ zwitterion), glycyl glycine (zwitterion □), N-ethylacetamide (O), ethylamine cation (●).

2. FORMATION OF UNSATURATED PRODUCTS IN THE RADIOLYSIS OF PEPTIDES IN THE SOLID STATE†

Mathilde Kland-English and Warren M. Garrison

Among the chemical changes observed on radiolysis of peptides, polypeptides, and proteins[1-3] are those associated with the production of unsaturated derivatives through dehydrogenation,

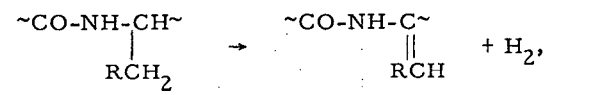

(1)

and in the case of the serine and threonine residues through dehydration,

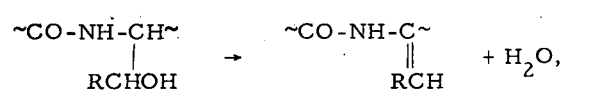

(2)

where Reactions 1 and 2 express only the formal stoichiometric requirements. Compounds containing the ~CONH-C(=CHR)~ function have been designated dehydropeptides by Greenstein.[4] These unsaturated peptide derivatives are stable in neutral solution at room temperature but are readily hydrolyzed to yield ammonia and keto acid on mild hydrolysis in dilute mineral acid, ~CONH-C(=CHR)~ + H_2O → ~COOH + NH_3 + RCO~. The chemical evidence for dehydropeptide production in peptide radiolysis has been based largely on studies of these hydrolysis products.[2,3]

The α-amino acid anhydrides (2,5-diketopiperazines) are of particular interest from the radiation chemical standpoint in that the dehydropeptide derivatives of these cyclic dipeptides (I) are isomeric with the

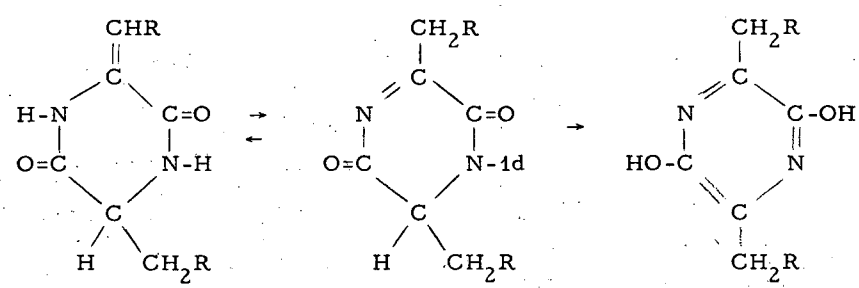

(I) (II)

corresponding 2,5-dihydroxypyrazine structure (II). The dihydroxypyrazine nucleus exhibits strong optical absorption in the visible and near-ultraviolet region (300 to 400 mμ),[5] and is readily determined spectrophotometrically at concentrations down to 10^{-5} M.

Preliminary experimental evidence has been given[6] for the production of the 2,5-dihydroxypyrazine nucleus through rearrangement in alkaline solution of dehydropeptides formed in the Co^{60} γ irradiation of amino acid anhydrides derived from glycine and alanine. We report here spectrophotometric evidence for formation of unsaturated product species in the γ radiolysis of a series of cyclic dipeptides containing glycine, alanine, serine, and phenylalanine residues in various combinations.

Glycyl alanine (gly-ala)[7] and glycyl serine (gly-ser) anhydrides were synthesized.[8,9] The symmetrical anhydrides of glycine and alanine, (gly-gly), (ala-ala), were obtained from Nutritional Biochemical Corp. The other cyclic dipeptides--viz., (ala-ser), (phen-ser), (phen-ala), and (phen-gly)--were obtained from Calbiochem; those which were not chromatographically pure, were fractionally recrystallized three times from water. The microcrystalline powders were evacuated on the vacuum line in Pyrex ampoules for a minimum period of 48 hours. After irradiation with Co^{60} γ rays (1.6×10^{18} eV/g/min) the ampoules were opened to the atmosphere and the contents were dissolved in neutral water under nitrogen aeration. At this point the solutions show no appreciable absorption at wavelengths above

≈300 mμ when read differentially against corresponding solutions of the unirradiated anhydride. Addition of sodium hydroxide (0.02 M) then leads in each case to a rapid increase in optical density in the 300- to 400-mμ range.

With the irradiated dipeptides of the aliphatic series, (gly-gly), (gly-ala), (ala-ala), (gly-ser), and (ala-ser), a characteristic absorption maximum is observed at ≈370 mμ. The authentic cyclic dehydropeptide, 3-methylene-2,5-diketopiperazine prepared after Bergmann and Miekely,[9] develops identical spectrophotometric properties on standing in oxygen-free 0.02 N sodium hydroxide. Typical examples of the fully developed spectra are compared in Fig. D.15-1 with the spectrum of authentic 2,5-dihydroxypyrazine (3,6-dimethyl) prepared after the method of Karmas and Spoerri.[10] All these chromophores are rapidly destroyed on exposure of the solutions to the atmosphere: the dihydroxypyrazine nucleus in alkaline solution is extremely labile towards molecular oxygen.[10]

The aromatic dipeptides (phen-gly) and (phen-ala) give somewhat different results on dissolution of the irradiated samples in 0.02 N sodium hydroxide. The rapid increase in optical density is observed but the wavelength of maximum absorption appears at 325 mμ (Fig. E.2-2) rather than at the 370-mμ value obtained with the aliphatic series. The unsaturated derivative 3-benzylidine-2,5-diketopiperazine, which is one of the expected irradiation products from (phen-gly), was prepared[5, 11] and found to rearrange in dilute base to give the 325-mμ absorption band. Apparently, resonance between the benzylidene double bond and the benzene ring is sufficient to prevent a shift of the double bond into the heterocyclic ring, and as a result full isomerization to the 2,5-dihydroxypyrozine nucleus is not observed. Growth of the 325-mμ band would then be related in terms of simple enolization, e.g.

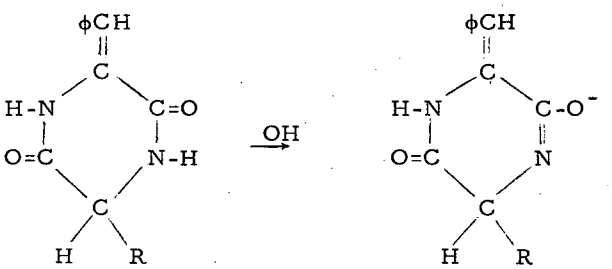

We note also that the presence of the phenylalanine residue in a cyclic dipeptide does not invariably result in the formation of the benzylidene derivative. For example, irradiated (phen-ser) on base treatment yields a 373-mμ absorption maximum with negligible absorption at 325 mμ. The evidence is that in (phen-ser) the unsaturation arises almost exclusively through dehydration of the serine residue to give the methylene derivative, which then undergoes the normal pyrazine rearrangement in alkaline solution.

From these studies we conclude that the cyclic dipeptides represent a unique class of compounds for studies of mechanism in peptide radiolysis. The identification of irradiation products which on dissolution in basic solution develop characteristic absorption maxima in the visible and near ultraviolet makes possible the direct spectrophotometric study of specific radiation chemical change.

Footnotes and References

†Brief version of paper to be submitted to Radiation Research.

1. M. E. Jayko and W. M. Garrison, J. Chem. Phys. 25, 1084 (1956).
2. A. Caputo and K. Dose, Z. Naturforschung 12b, 172 (1957).
3. W. M. Garrison and B. M. Weeks, Radiation Res. 17, 341 (1962).
4. J. P. Greenstein and M. Winitz, Chemistry of the Amino Acids (John Wiley and Sons, Inc., New York, 1961).
5. H. Sorkin, Isomerization of Methylene Diketopiperazines (Ph. D. Dissertation), Cornell University, 1960.
6. M. Kland-English and W. M. Garrison, Nature 197, 895 (1963).

7. We adopt here the informal notation of H. J. Svec and G. A. Junk, J. Am. Chem. Soc. 86, 2278 (1964).
8. E. Fischer and H. Scheibler, Ann. Chem 363, 136 (1908).
9. M. Bergmann and A. Miekely, Z. Physiol. Chem. 140, 128 (1924).
10. G. Karmas and R. E. Spoerri, J. Am. Chem. Soc. 79, 680 (1957).
11. T. Sasaki and T. Hashimoto, Berichte 54, 169 (1929).

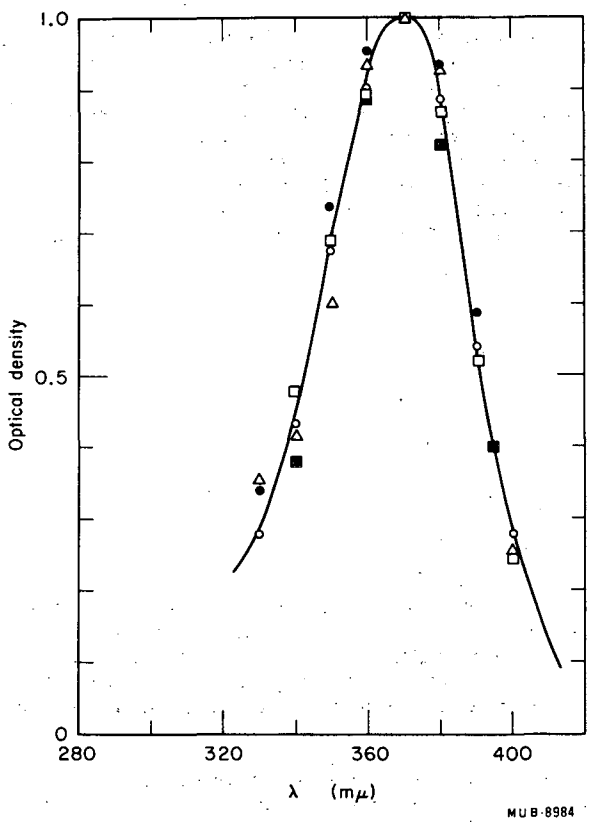

Fig. E.2-1. Absorption spectra of irradiated (gly-gly), (●); (gly-ser), (△); (ala-ser), (□); and the authentic compounds: 3-methylene-2,5-diketopiperazine (O) and 2.5-dihydroxy-3,6-dimethylpyrazine, all in 0.02 N sodium hydroxide.

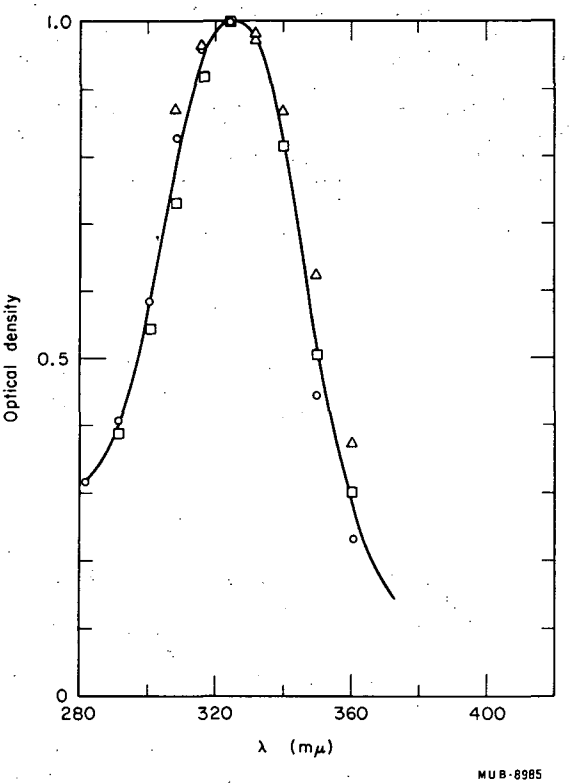

Fig. E.2-2. Absorption spectra of irradiated (phen-gly), (O); (phen-ala), (□); and authentic 3-benzylidene-2, 5-diketopiperazine (△); all in 0.02 N sodium hydrozide.

F. INORGANIC CHEMISTRY

1. THE EXTRACTION OF PERCHLORIC ACID BY TRILAURYLAMINE. I. AROMATIC DILUENTS†

J. J. Bucher and R. M. Diamond

Among the prominent organic extractants, the trialkylamines are the most basic and, hence, the best extractants for acids. In such systems, consisting of an acid in an aqueous phase and an organic extractant in a solvent medium, the extraction or distribution can be considered a competition among the organic extractant, water, diluent, and anion for coordinating or solvating the proton. The basic amine can take the proton away from the water to form an ammonium ion,

$$H_3O^+ + R_3N_{(o)} \rightleftarrows R_3NH^+_{(0)} + H_2O,$$

and it might be expected that such a system would be relatively simple in its behavior. However, the possibility of electrostatic ion aggregation in the low-dielectric-constant organic phase, and the effect of the co-extracted anion and of the organic diluent must also be considered, as well as the possibility of extracting excess acid.

In this paper we are interested in discussing the role the organic diluent plays in the extraction, and how its chemical (basic) and its dielectric (Coulombic) properties influence the extraction. Only aromatic diluents and a related π-electron-containing solvent, tetrachloroethylene, were employed. To minimize the effect of the anion, the large anions, ClO_4^- and ReO_4^-, were used, and to prevent extraction of excess acid, aqueous acid concentrations less than 0.2 M were employed.

Figures F.1-1, F.1-2, and F.1-3 show the results obtained for the extraction (actually the back-extraction) of $HReO_4$ tracer in $HClO_4$ by trilaurylamine, TLA, in anisole, benzene, 1, 3, 5-trimethylbenzene, 1, 3, 5-triethylbenzene, o-dichlorobenzene, chlorobenzene, tetrachloroethylene, and nitrobenzene. For Figs. F.1-1 and F.1-2 the logarithmic plots are of the organic alkylammonium salt concentration vs the product of the concentrations of the organic amine, aqueous hydrogen ion, and aqueous perchlorate ion. Concentrations of TLA$\cdot HClO_4$ in the organic and aqueous phases were determined by counting the ReO_4^- tracer in an aliquot and comparing with a standard sample. The dotted lines for each of the curves in Figs. F.1-1 and F.1-2 are the results of determining the aqueous-phase acid concentrations by titration. This direct determination, instead of using the ReO_4^- tracer data, is necessary in the more concentrated ammonium salt region where the difference in extraction between $HReO_4$ and $HClO_4$ becomes greatly exaggerated because of organic-phase aggregation. Figure F.1-3 has a log-log plot of the mean alkylammonium salt activity, as well as of the organic-phase ammonium ion concentration, vs the product $[H^+][ClO_4^-][R_3N]_{(o)}$.

The organic diluent influences the extraction in two main ways. It can interact with the extracted salt through the effect of its dielectric properties on the charged ions, and it can interact directly with the amine and the ammonium salt by short-range chemical forces. The first effect is easy to understand. As can be seen by applying the Born charging expression to the transfer of a pair of ions from water to the organic phase, there is a relatively large, positive electrostatic free energy which opposes the transfer. But the higher the dielectric constant of the organic phase, the better the extraction of a particular acid to form an amine salt. Thus, in this study, it has been found that the extraction of $HClO_4$ and $HReO_4$ is greater into nitrobenzene ($\epsilon = 34.8$) solutions of TLA than into any other solvent system observed (all $\epsilon < 35$). Furthermore, it is shown that in nitrobenzene the extracted ammonium salt occurs as dissociated ions, and this is confirmed by cryoscopic measurements.

All the rest of the diluents extract the ammonium salt as an ion pair at low concentrations in the organic phase,

$$R_3N_{(o)} + H_3O^+ + ClO_4^- \rightleftarrows R_3NH^+ClO_4^-{}_{(o)} + H_2O.$$

Aggregation beyond the ion pair occurs with most diluents at higher concentrations. Table F.1-I shows that the order of increasing K_1; the overall constant for the extraction of TLA$\cdot HClO_4$

as an ion pair, parallels roughly the order of increasing dielectric constant.

On the other hand, the parallelism in the order is not exact. For example, anisole with a dielectric constant of 4.33 has a larger K_1 than chlorobenzene with a dielectric constant of 5.62. Thus, at least one other factor is involved. Besides "electrostatic" solvation of the ions--that is, the effects of the long-range Coulomb field of the ions--there is also a "chemical" solvation, a short-range interaction. By this is meant the direct coordination of the ions with the solvent molecules. The perchlorate anion is a very weak base and as such is not expected to take much part in interactions with the weakly basic solvent molecules used in this study, but the acidic R_3NH^+ cation can do so via its hydrogen. This hydrogen, which is most likely the site of the cationic charge, would like to surround itself with negative charge (i.e., the anion), with the negative end of solvent dipoles, or with any unbonded electron pairs that are available. The π electrons of the aromatic molecules used as diluents in this study come under this classification, as do the basic electron-donating oxygen atoms of the ether, ester, keto, and nitro groups. The stronger the interaction of the ammonium cation with the π electrons or the basic groups, the greater is the reduction in free energy of the species in the organic phase, and the greater its extraction.

A similar argument holds for the order of the organic-phase TLA·$HClO_4$ concentrations at which the salt aggregates beyond the ion pair in the different solvents. The order goes roughly as the dielectric constant, but with the same abnormalities. Again these can be explained by the same hypothesis that the stronger the complexing of the ammonium cation by the basic solvent molecules (either through π electrons or more strongly through basic oxygen-containing groups), the less need the ions have to lower their free energy by ion aggregation. Another way of looking at this is that the stronger the complexing of the ammonium cation by the solvent molecules, the larger the dynamic size of that (solvated) cation, and hence the smaller the degree of aggregation.

Finally, the appearance of steric hindrance in the cation complexing by trimethyl and triethylbenzene supports the suggested ammonium-cation solvent interaction, and the particular hypothesis of the π-electron, ammonium-cation interaction would explain the observed fact that the ion aggregation in aromatic solvents is less than that in aliphatic or saturated cyclic solvents.

Footnote

†Brief form of J. Phys. Chem. 69, 1565 (1965) (UCRL-11616 Rev.).

Table F.1-I. Comparison of order of extraction constants and dielectric constants.

Solvent	K_1	Dielectric constants
Triethylbenzene	2.4×10^4	2.26
Tetrachloroethylene	3.3×10^4	2.30
Trimethylbenzene	1.8×10^5	2.28
Benzene	3.7×10^6	2.28
Chlorobenzene	4.2×10^7	5.62
Anisole	1.2×10^8	4.33
o-dichlorobenzene	1.5×10^8	9.93

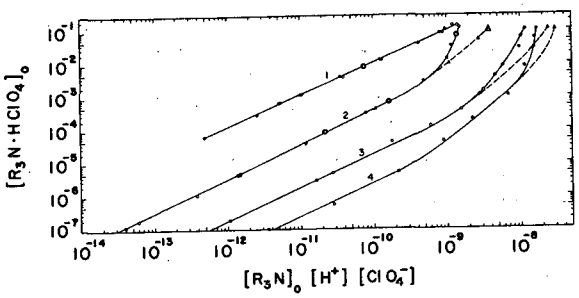

Fig. F. 1-1. Plot of organic-phase alkylammonium salt molarity vs the product of free amine and aqueous hydrogen and perchlorate ions concentrations, for the organic diluents (1) anisole, (2) benzene, (3) mesitylene, and (4) triethylbenzene. O, data from ReO_4^- tracer; Δ, data from acid titration; ∇, data from acid and amine dependencies in benzene.

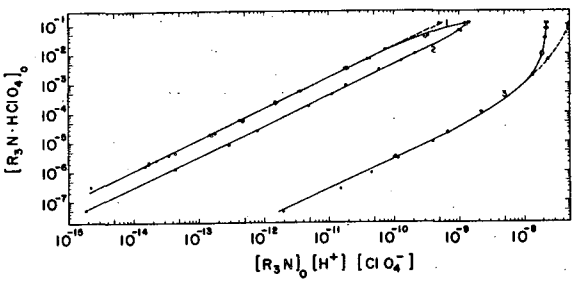

Fig. F. 1-2. Plot of organic-phase alkylammonium salt molarity vs the product $[R_3N]_{(o)}[H^+][ClO_4^-]$, for the organic diluents (1) o-dichlorobenzene, (2) chlorobenzene, and (3) tetrachloroethylene. O and ●, data from ReO_4^- tracer; Δ, data from acid titration.

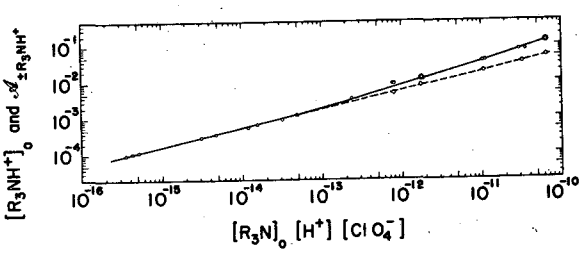

Fig. F. 1-3. Plot of organic-phase alkylammonium salt molarity O, and mean ion activity ◇, in nitrobenzene vs the product $[R_3N]_{(o)}[H^+][ClO_4^-]$.

2. SPECTROPHOTOMETRIC DETERMINATION OF GOLD WITH AZIDE†

Ray G. Clem and E. H. Huffman

A spectrophotometric method for the determination of gold has been based on measuring the absorbance of the complex formed when gold(III) reacts with azide. Gold alone, in the optimum range from 38 to 127 μg, may be determined by measuring the absorbance at 325 mμ in aqueous solution buffered at pH 6.00. Gold in the presence of the tolerated platinum metals is determined by extraction of the complex into n-butyl alcohol and measuring the absorbance in the organic phase at 330 mμ. From 1.5 to 5.3 ppm of gold give absorbances in the optimum range, although Beer's law is followed well beyond these limits. Figure F. 2-1 shows the spectral scans in the near ultraviolet region of the gold azide complex in water and in n-butyl alcohol, taken against appropriate blanks.

Gold is easily separated, by reduction to the metal, from gross amounts of most metal impurities. Because of the ease of this separation, an extensive list of diverse ions was not studied. The metal ions which might be used for the separation, or which follow gold, are tellurium, mercury, silver, palladium, platinum, and rhodium. None of these elements, in 1-mg quantities, causes an error in excess of 2.8% in the determination of 39.4 μg of gold by the recommended procedure.

Mole ratio plots show sharp breaks at a ratio of 4 N_3^- to 1 Au^{-3}, as shown in Fig. F.2-2. These results could be interpreted to indicate either of the reactions

$$AuCl_4^- + 4\,N_3^- = Au(N_3)_4^- + 4\,Cl^-$$

or

$$AuCl_4^- + 4\,N_3^- = Au(N_3)_2^- + 4\,Cl^- + 3\,N_2^-,$$

although no nitrogen evolution was noted. The addition of azide to gold(III) has been reported to form explosive orange-colored crystals upon careful evaporation of the solution.[1] No analysis was reported for the product, but is has been referred to as AuN_3.[2] A similar product, prepared for this study, was analyzed for azide. The results indicated negligible oxidation of azide, hence, negligible reduction of the gold(III). The product, when redissolved in water, again had an absorption maximum at 325 mμ, indicating no change on evaporation. It appears that the earlier preparations gave sodium and potassium tetraazidogold(III) salts rather than gold(I) azide, and that the $Au(N_3)_4^-$ species is the absorbing ion used herein.

Footnote and References

†Brief version of Anal. Chem. 37, 1155 (1965).

1. T. Curtius and J. Rissom, Prakt. Chem. 58, 304 (1898).
2. J. W. Laist, in Comprehensive Inorganic Chemistry, M. C. Sneed, J. L. Maynard, and R. C. Brasted, Eds. (Van Nostrand, New York, 1954), Vol. 2, p. 237.

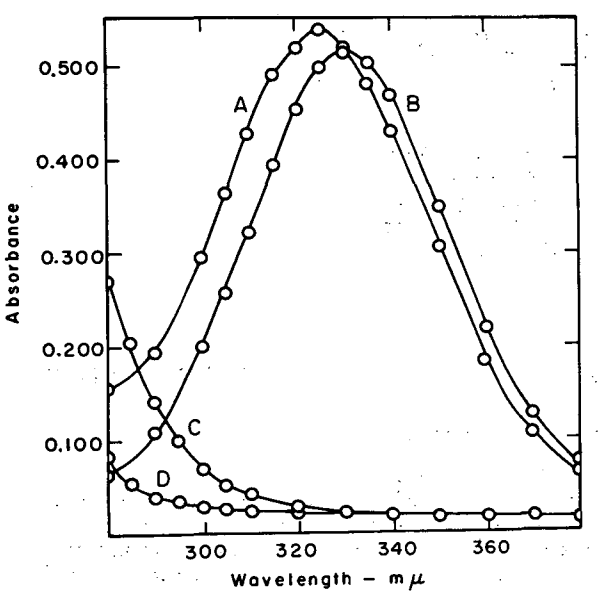

MUB-5224

Fig. F.2-1. Absorption spectra of analytical species and blanks
(A) 2×10^{-5} M Au^{+3} in water; 0.10 M N_3^-; 0.50 M PO_4^{-3}; pH 6.00; readings vs (D);
(B) n-butyl alcohol extract of solution as for (A) except 0.20 M N_3^-; readings vs (C);
(C) n-butyl alcohol extract as for (B) without Au^{+3}; readings vs solvent;
(D) solution as for (A) without Au^{+3}; readings vs water.
All with 1.00-cm cell.

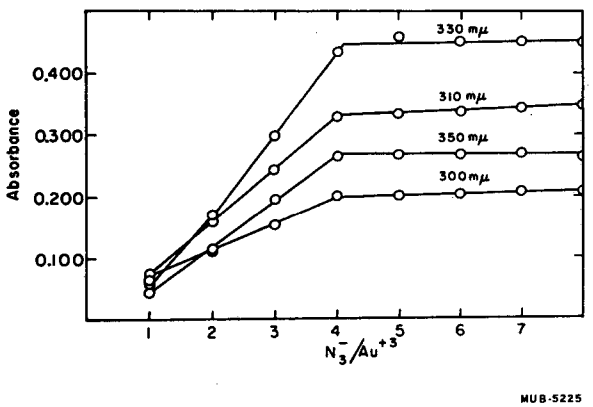

Fig. F.2-2. Mole ratio plots.
2×10^{-4} M Au^{+3}.
2 to 16×10^{-4} M N_3^-.
Ionic strength 1.00.
pH 4.07 ± 0.10.
0.10-cm cell.

G. INSTRUMENTATION

1. 88-INCH CYCLOTRON RESEARCH AND DEVELOPMENT

David J. Clark, Elon Close, and Hogil Kim

This report briefly summarizes the research and development work completed in the past year. The following people have been responsible for this work. H. Conzett is head of operations. The mechanical design group is under D. Elo. P. Pellissier is the electrical project engineer. General coordination is under A. Hartwig. Development and general machine improvement studies have been done by D. Clark, H. Kim, E. Close, and R. Burger. The crew supervisor is John Bowen and the accelerator technician supervisor is John Meneghetti.

Operation

The machine runs three 8-hour shifts per day, 7 days a week. The distribution of time among various users is as follows: Nuclear reactions and scattering, 54%; isotope production, 22%; biomedical research, 4%; beam development, 10%; maintenance, 10%.

Improvements in Internal Beam Region

A remote gas-feed system was put into operation. This will allow the ion source gas to be changed remotely from the control room. Gases can also be mixed for best ion source operation. The dummy-dee test was completed. It showed that the center region will have to be readjusted when the dummy dee is used. It was removed to improve the contact design, and will be reinstalled when axial injection is ready for testing. Tests were made on deflector power handling. The most difficult problem with this type of deflector is the construction of the thin septum which divides the internal and external beams. About 1/3 of the internal beam is dumped on the leading portion during deflection. It was found that 0.010-in. -thick tungsten, radiation cooled, with a carefully shaped slot gave better power handling than water-cooled copper. External beams of up to 3 kW are available at most energies. The use of TV viewing of the septum and a jack for remotely raising and lowering it have helped greatly in this work. The new deflection system is discussed separately.

The electrical improvements in this region include new trim-coil supplies, now being installed. This increases the number from 11 to 17, so that each of the 17 trim coils will have its own supply, allowing more flexibility in trimming the magnetic field. The dee voltage ripple was reduced with the installation of a filter in the oscillator power supply. A new dee voltage-pickup plate was installed at the dee edge. This gives a frequency-independent signal and displays the accelerating voltage waveform.

Improvements in External Beam Region

The beam line which brings the deflected beam to the switching magnet has been greatly improved. An exit probe has been installed where the beam leaves the tank. This monitors beam which formerly hit the tank walls. A new box placed outside the tank contains a new steering magnet for aligning all beams to the beam pipe,[1] a new x collimator which reads beam current, a new blank plate for measuring the total extracted beam current, a new slotted plate for increased precision in measuring horizontal beam emittance, and a remote quartz plate which can be viewed with TV. The first quadrupole magnet on this line has a new elliptical beam pipe 6 in. horizontally by 3 in. vertically to match the beam shape better than the previous 4-in. -diameter beam pipe. An improved support frame was made for this quadrupole. An unequal distribution of current to its poles is being provided to steer the beam vertically, when required.[2]

A large box with many ports has replaced the "staging" beam line from the first quadrupole to the switching magnet. Most of the old probes have been transferred into this new box, with some improvements. A new analyzing slit has been built for installation in this box. This can be used to align the beam with the beam pipe, or to define the radial source for the switching magnet when it is used for energy analysis in Cave 1 or 2. A new slotted plate has been made to be installed in this box. It will be used for vertical emittance measurements.

Tests are being made on an NMR probe for stabilizing the magnetic field of the switching magnet. This will improve the energy stability of beams in Caves 1 and 2. A beam sweeper has been built. It consists of vertical and horizontal sweeping magnets, which will spread the beam over an area 8 by 8 in. for biomedical irradiations.

Beam Development

Development of new beams has continued during the past year. Energies now available are: protons from 10 to 55 MeV, α particles from 15 to 130 MeV (D at half these energies), and He^3 from 10 to 145 MeV. To develop a new beam we calculate trim-coil settings from the desired isochronous magnetic field, and estimate center-region and deflector settings. We then optimize the external beam with trim coils, center region, deflector, dee frequency, dee voltage, and possibly harmonic coils. Third harmonic acceleration must be used on α particles at less than 24 MeV and on He^3 at less than 18 MeV. In this mode the dee frequency is three times the particle frequency, making acceleration less efficient in the first few particle revolutions. Beam intensities are about half those for normal first-harmonic operation. Some time was spent improving older beams. Future work will include developing He^3 energies up to about 160 MeV, as required.

Studies have been made of the external beam quality and extraction efficiency. Measurements were made on the best operation of the old deflection system before it was removed from the machine, as a reference for comparison with the new system. The best deflector transmission obtained was 60% on a 65-MeV α beam, and 70% on a 120-MeV α beam. In overall transmission from internal to external beam, up to 10% loss occurs at a coupling resonance just before extraction, and a 10 to 30% loss occurs near the tank exit because the beam is more than 4 in. wide horizontally. Emittance measurements gave a value of about 50 mm-mr horizontally, the same as measured previously.

Line 4 in the cyclotron vault was used for studies of energy spread and phase width of the external beam. This line is the continuation of the staging line straight through the switching magnet, and is useful to study the "raw" beam from the machine. On this line a phase probe and a scattering foil with a solid-state counter have been installed. An x collimator has also been put in this line to study the energy dispersion of the deflection system.

Studies have been continued from last year on the effects of machine parameters on the energy and phase of the external beam. The beam is sensitive to dee voltage and frequency variations. This is because the present precession method of extraction is very sensitive to the number of particle revolutions in the machine. The dee voltage should be regulated to 0.1% and the frequency to 0.002% for stable operation with this type of extraction system. It is believed that the new deflector will be less sensitive to these parameters. With careful tuning the energy spread of the extracted beam could be as small as 0.2% FWHM with normal extraction efficiency, for a 65-MeV α beam. This percentage is rather independent of particle energy. The phase width is about 45 degrees FWHM.

Computer studies have been continuing on beam dynamics. The tabulation of the equilibrium properties of various internal beams is in progress, using the equilibrium orbit code. These help to understand various problems of injection, acceleration, and extraction of beams. One interesting result is that the cyclotron could accelerate protons to 75 MeV if the dee frequency went higher. At present this limit is 60 MeV. A center-region code is being debugged. This will serve as a guide in improving internal beam quality and designing the axial injection system. Studies have also been made with the general orbit and extraction codes in designing the new deflection system. Some studies have also been done by computer and hand calculation on the gap-crossing resonance near the center of the cyclotron. This resonance moves the beam centers about 0.4 in. in this region. This must be compensated either by ion source offset or by the first harmonic coil. Studies indicate that it is preferable to use the harmonic coil for best beam quality, and this will be tested in the cyclotron.

Special Projects

The largest project during the past year has been the design and construction of a new deflection system. The principal change in the system has been the addition of an electrostatic regenerator to give controlled turn separation at the entrance to the deflector, as described in last year's report. The regenerator is an electrode, 24 in. long, with positive voltage up to 60 kV. The deflector itself is similar to the old design, but with three sections instead of two, for more flexibility (see Fig. G. 1-1). The mechanical and electrical design of the new system includes

support and face plates, electrodes with two additional power supplies, electrode position drives, and readouts. A new 10-in. diffusion pump was added to the dee tank to improve the vacuum for regenerator voltage stability. The deflection channel shape was designed from computer studies for a 130-MeV α beam, the most difficult case. The best settings were also predicted from computer runs for a 65-MeV α beam. The expected improvements are better extraction efficiency, beam quality, and stability. The new system was installed during November 1965. After 3 days of testing with beam, there were six energies of α beams developed, from 23 MeV to 130 MeV. The deflector transparency varied from 25% to 60%. The energy spread could be tuned consistently to 0.3% FWHM. The stability of the external beam quality is better than with the old system. It is expected that the operation can be improved considerably with more beam development.

Work on the design of an axial injection system started this year. A full-scale model bench test was set up, including an ion source, 5-ft pipe with focusing lenses, and probes for studying the beam characteristics. This model will guide the final design of a system for injecting ions from an external source down a hole through the center of the magnet pole. There it will be inflected into the normal first revolution of the acceleration cycle. This system will be useful for accelerating polarized protons and deuterons.

An automation system is being designed to provide greater speed and reliability for the setting and monitoring of machine parameters.[3] The input will be on IBM cards, punched with the machine parameters of standard beams.

References

1. J. Burnside, Radial Beam Steering Magnet, LRL Engineering Note EET-1080, Nov. 1965.
2. Designed by R. Cox; to be described in a later report.
3. David R. Struthers, Automatic-Control-System Design for the Berkeley 88-Inch Cyclotron. UCRL-16210, June 1965.

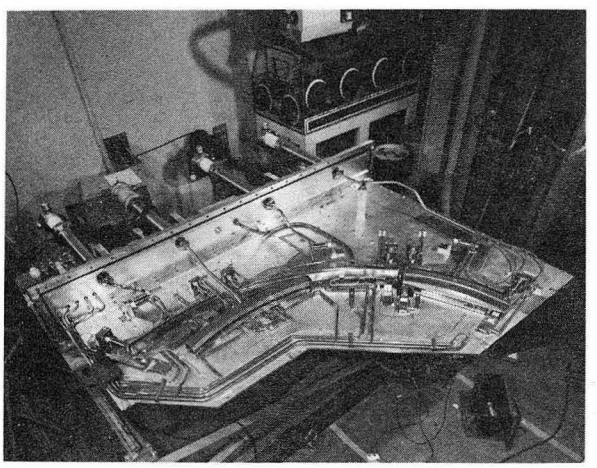

Fig. G. 1-1. -New deflection system, showing the electrostatic regenerator and the three-section electrostatic deflector. It was installed in November 1965.

2. ENERGY LEVELS OF Pu^{+3} ON $LaCl_3$.†

John G. Conway and K. Rajnak

Recent studies of configuration interaction effects in the rare earth ions have prompted our interest in this problem to determine values of the configuration interaction parameters for the actinides. At present Pu^{+3} is the only trivalent actinide on which there are sufficient data for such a calculation. Previous calculations using hydrogenic assumptions give a rms deviation of 500 cm^{-1}. The addition of two configuration interaction parameters, α and β, reduces this rms deviation to 103 cm^{-1}. These calculations used 12 levels below 20 000 cm^{-1}. The good fits prompted an extention of the measurements, using the original plates of Lämmermann, to the limit of the observations at about 32 000 cm^{-1}. A strong absorption sets in at this point. An additional 13 levels were obtained, and these together with the original 12 were fitted to a rms deviation of 100 cm^{-1}.

The values of the parameters for the 25-level fit are E_0 = 14 930.5, E^1 = 3726.0, E^2 = 14.99, E^3 = 350.18, ζ = 2260.2, α = 36.50, β = -1171.

Footnote

† Short form of J. Chem. Phys., Jan. 1966 (UCRL-16292, July 1965).

3. A PREAMPLIFIER WITH 0.5 keV RESOLUTION FOR SEMICONDUCTOR RADIATION DETECTORS.†

E. Elad and M. Nakamura

The high resolution of semiconductor radiation detectors put stringent demands on the performance of the preamplifier unit. In order to exploit fully the capabilities of these detectors further development in preamplifiers was needed. The inherent low noise of the field-effect transistor (FET) made it an attractive candidate for the input stage of high-resolution preamplifiers. The FET preamplifier described has pulse generator resolution of 0.5 keV FWHM, and it allowed measurement of γ-ray and electron spectra with 1.1 keV and 1.5 keV resolution, respectively. Low-energy x rays were measured with resolution as good as 0.95 keV.

The approach followed in the design of the preamplifier was based on the optimization of the signal-to-noise ratio. The main effort made was to minimize the input capacitance and to find the best device for the input stage and the configuration in which it will be employed. The actions taken were as follows: The input stage of the unit, which uses the FET as its active device, was inserted into the chamber containing the detector, thus minimizing the stray input capacitance and simplifying the cooling of the FET. The best performance of the FET was obtained at -180°C, and this temperature was achieved by mounting the FET directly on the cold finger. Several types of transistors were checked, and the best units were found among the Texas Instrument 2N3823 type. The semiconductor detector was electrically insulated from ground by a good heat conductor such as sapphire. This feature allowed direct coupling between the detector and the FET stage, eliminating the strays of the coupling capacitance.

The block diagram of the preamplifier described is given in Fig. G. 3-1. The charge delivered by the detector is applied to a charge-sensitive amplifier composed of a common-source FET stage, an integrator and amplifier 1. In addition to optimization of the input stage, further improvement of the signal-to-noise ratio was achieved by filtering the output of the FET stage, with low-pass filters. The output signal of the charge-sensitive section is amplified by feedback amplifier 2 in order to diminish the influence of low-frequency pickup by the cables between the preamplifier and the main amplifier.

A large variety of lithium-drifted germanium and silicon detectors was operated in conjunction with the preamplifier. The best resolution was obtained with low-capacitance detectors, LRL-Berkeley and Livermore type. For a 2-pF germanium detector, 1.1 keV resolution was obtained for Co^{57} γ rays. With a smaller silicon detector (5 mm diameter and 3 mm thick), 0.95

keV resolution was obtained for the 14.36-keV x rays of Co^{57} and 1.5 keV for U^{237} conversion electrons.

The potential capabilities of the described low-noise preamplifier can be deduced from the spectrum of platinum x rays given in Fig. G. 3-2, where the K_α and K_β groups are clearly separated. The preamplifier was used successfully by many experimenters in our Laboratory, and among their achievements one has to mention the development of a novel technique for chemical analysis of material samples.[1]

Footnote and Reference

† Short version of reports UCRL-16390, Sept. 1965 and UCRL-16515, Dec. 1965, submitted to Nucl. Instr. Methods.

1. H. R. Bowman, E. K. Hyde, and S. G. Thompson, UCRL-16485, to be published.

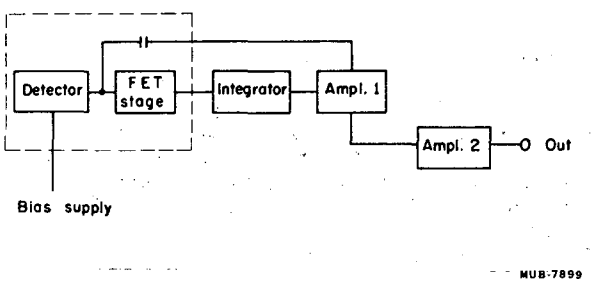

Fig. G. 3-1. Block diagram of the preamplifier.

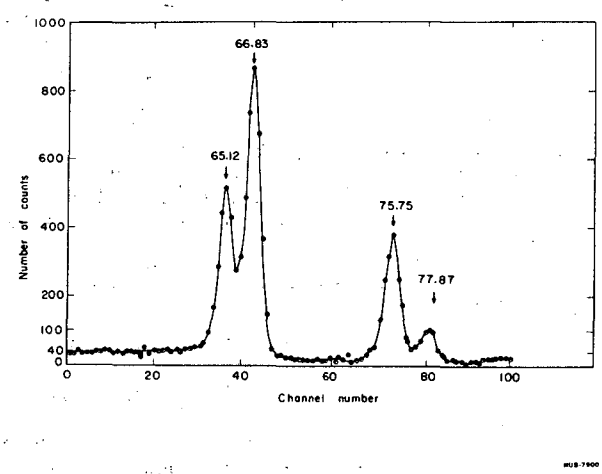

Fig. G. 3-2. K_α and K_β groups of platinum x rays.

4. NUCLEAR INSTRUMENTS

William Goldsworthy

Two separate programs have been undertaken in the design of new instruments. One of these has been associated with the design of a high-pulse-rate single-channel analyzer. The other has to do with the design of a pulse area sensitive device that allows pulses to be compared and analyzed on a strictly pulse area basis.

In the further studies into linear amplifier circuitry, a new method of pulse shaping has also been developed which displays certain advantages over presently employed methods.

Single-Channel Pulse-Height Analyzer

This analyzer has been developed to handle extreme pulse rates with a minimum of resolution degradation and to provide either timed, trailing-edge, or crossover readout programming.

In order to reduce the spread in resolution resulting from high counting rates, this analyzer can provide a completely d. c. logic system following the input. Readout from the analyzer

can be programmed to occur at the trailing edge of the input pulse, at any time from 0.4 μsec to 10 μsec after the arrival of the input pulse, or at a time determined by an externally connected device such as a crossover detector. Particular care was taken in the design so that the operation would not be sporadic even under the most extreme conditions. This instrument is being evaluated by the Chemistry Electronics group.

Integrating Window Amplifier

Evaluations are presently being made to determine the feasibility of employing measurements of pulse area rather than of pulse amplitude in the energy analysis of nuclear-produced reactions. Improvements in resolution and linearity are anticipated by the employment of this technique.

An instrument with the capability of converting pulse-area information into pulse-amplitude information is now being evaluated, and a second improved version of this type of instrument is presently being fabricated.

If this technique of pulse-area analysis proves successful, the whole concept of analyzing nuclear-energy-produced pulses may have to be modified.

Symmetrical Pulse Shaping

A new technique has been developed to symmetrically shape pulses in amplifier systems. This technique, which employs one rather than two delay lines, is described in detail in the December 1965 Review of Scientific Instruments, as well as in UCRL-16006, March 1965. Advantages gained by the use of this single line symmetrical shaper are more accurate control at the crossover time, reduced loss in amplifier gain, and considerable circuit simplification.

5. A 4096-CHANNEL ANALOG-TO-DIGITAL CONVERTER

F. S. Goulding, L. B. Robinson, and F. Gin

The advent of computers used on-line for nuclear spectroscopy and the high-resolution performance of germanium x-ray detector systems have resulted in a demand for improved and more adaptable analog-to-digital converters. In particular, larger numbers of channels, high speed, and the ability to connect to a computer are requirements. We have developed a 4096-channel ADC meeting these needs. It employs a binary approximation technique and uses the scheme proposed by Gatti[1] to improve differential linearity. The conversion time is 24 μsec (later to be changed to 12 μsec). Integrated circuits are used for all logic circuits.

A number of these ADC's will be multiplexed to a PDP-7 computer system for γ-ray spectroscopy. In order to accomplish this a multiplexer unit is being developed which will service the ADC's in either a priority or random order as counts occur in the ADC's.

One version of the ADC is to be used for multiparameter analysis. Eight pulse inputs drive stretcher circuits and the ADC encodes each of the stretcher inputs and presents the digital codes to the computer for immediate analysis and storage. This unit is presently being used as a part of the particle identificator system for rare events in the 88-inch cyclotron installation, but its design is suitable for other multiparameter applications.

Reference

1. E. Gatti, in Karlsruhe Conference on Automatic Acquisition of Nuclear Data, EANDC, July 1964, p. 261.

6. INSTRUMENTS DEVELOPED FOR THE NEW AEC MODULAR SYSTEM

F. S. Goulding, S. Wright, D. Schurr, and D. Landis

A brief description of several instruments developed during the past year and packaged in the new AEC 8-3/4-inch modular bin is given below.

Standard Amplitude Negative Pulse Generator

11X3281P-1: Size 3 Module

This generator provides negative pulses with a decay time of 120 μsec. The amplitude of the output is stable with time and temperature. The amplitude variation with temperature is less than 0.005%/°C.

The generator is well suited to check the resolution of preamplifiers and pulse amplifier systems. The output is adjustable by helipot (100 mV to 1.1 V), to correspond to a given energy range—this makes possible direct energy calibration of preamplifiers.

The generator can either free-run with adjustable periods from 10 sec to 2 msec, or be triggered externally up to a rate of 500 cps. A synchronizing output is provided for oscilloscope triggering.

Pulse Generator

11X3341: Size 3 Module

This is a general-purpose pulse generator. The free-running oscillation period is adjustable from 0.2 μsec to 100 msec. It may be triggered externally by a positive or negative input or manually pulsed.

The output can be delayed from 100 nsec to 10 msec, and its width is adjustable from 100 nsec to 10 msec. Positive or negative output is available with an amplitude adjustable from 1 to 10 volts, using a helipot. Attenuators of 10 and 100 are also provided. The output can be integrated with time constants of 0.1, 0.2, or 0.5 μsec. The nonintegrated rise time is 10 nsec. A synchronizing pulse is available for oscilloscope triggering.

Count Ratemeter

11X3871P-1: Size 3 Module

The diode-pump scheme is used to achieve a ratemeter providing six linear ranges (1 to 10^6 cps) and three three-decade logarithmic ranges (1 to 10^5 cps) with an accuracy within 2%. Switches provide for the handling of positive and negative input pulses, meter-range changing, and meter time-constant shortening for low count rates. An input discriminator is provided. A simplified block diagram is given in Fig. G. 6-1.

Scale-Down Unit

11X3580P-1: Size 2 Module

The scale-down unit has two different input modes. One is coupled directly into the scale-down unit and the other goes through a special anticoincidence circuit. The input level must be at least 2 V positive and at a rate no greater than 2 mc.

The second input can be used when a spectrum is desired from the singles count in a coincidence system. The anticoincidence circuit rejects the counts that have a coincidence pulse and allows the scale-down to reduce the singles count to a rate equal to or below the coincidence rate. The output of the scale-down can be used to open a linear gate to allow the spectrum to be analyzed in a pulse-height analyzer.

The scale-down ratio is switched from 1 to 100 in steps of 1, 2, 5, 10, 20, 50, and 100. The timing is not affected by different ratios of scale-down. The output signal is a positive 5-V pulse equal in width to the input pulse. A block diagram of the unit is shown in Fig. G. 6-2.

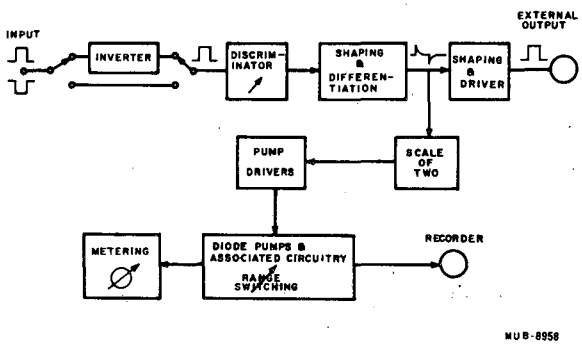

Fig. G.6-1. Count Ratemeter 11X3871P-1.

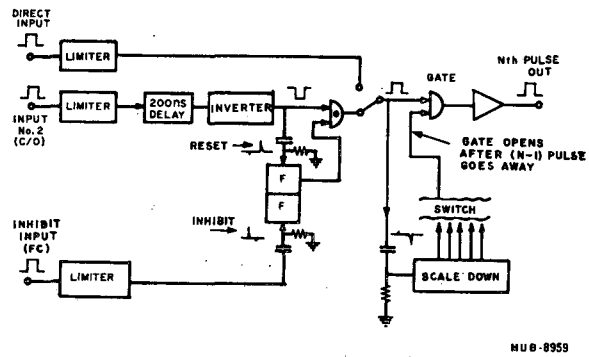

Fig. G.6-2. Scale-Down 11X3580P-1.

7. GERMANIUM GAMMA RAY DETECTOR DEVELOPMENT

W. L. Hansen and B. V. Jarrett

Progress in the development of germanium detectors has been greatly retarded in the past six months due to the inability to obtain good quality germanium crystals. Most germanium used for detectors has come from a single source whose crystal quality deteriorated in the middle of 1965. At this time, detectors with sensitive depths greater than 6 mm can rarely be made, and even less than 6 mm only with considerable difficulty.

Aside from the germanium problem, significant progress has been made in producing thin entrance windows and in energy resolution. Given reasonable quality germanium, detectors with window thickness comparable to silicon surface barriers can be made routinely. These detectors have a cross-sectional geometry as shown in the figure.

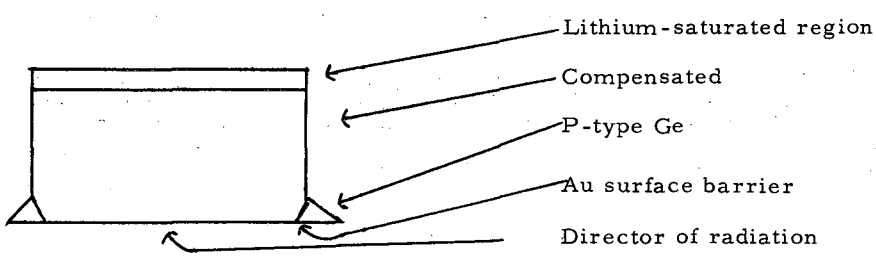

Coupled with the newly developed FET preamplifier these detectors give about 1 keV energy resolution and almost 100% efficiency in the range 5 to 100 keV. These detectors also have the prospect of giving very good energy resolution for charged particles with more penetration than can be used with silicon detectors. The present limit on stopping power for particles entering normal to the gold surface is 5 g/cm^2.

8. NITRIDE AND OXIDE BANDS OF MOLYBDENUM

John C. Howard* and John G. Conway

The only electronic band spectrum of molybdenum recorded in the literature has been assigned to MoO. The most complete listing is for some 16 bands in the atlas of oxide bands by Gatterer, Jenkins and Salpeter for the region 5760-8880 Å. Of the many sources tried the most satisfactory was a commercially available plasma jet.

A Pyrex glass envelope was placed around the plasma jet to permit operation with a controlled atmosphere. A study was made of the appearance of the bands with different gases, including O^{16}, O^{18}, N^{14}, N^{15}, H_2, and water vapor. Isotope shift using N^{14}-N^{15} shows that 11 of the 16 bands are due to nitride. A 50-50% mixture shows that only one nitrogen is involved in the bands.

Some very weak bands not previously reported are due to the oxide as a result of the oxygen isotope experiments. The red band around 6500 Å could not be excited in the plasma jet but appears in the d.c. arc spectrum. These are most likely due to a higher oxide such as MoO_2.

Footnote

* Livermore - LRL

9. BEAM CURRENT INTEGRATOR SYSTEM WITH BUILT-IN PRESET DUMP SCALER AND CONTROL CIRCUITRY

D. A. Landis and F. S. Goulding

Development has been completed on the beam integrator (Drawing No. 11X4140P-1) described in last year's annual report. The unit is contained in a bin with its own power supply and occupies 7 inches of panel space. The system consists of a feedback integrator reset by a diode pump that removes an accurate amount of charge from the feedback capacitor, and a count rate meter circuit that measures the resetting or dump rate of the integrator, thereby indicating the current. The dumps are recorded in a seven-decade integrated-circuit scaler with Nixie display. A preset dump circuit operates control functions in the integrator system and external equipment.

The charge measurement by the integrator (even down to currents of 5×10^{-10} A) is within 1% of the true value over long periods. Ranges from 1 μC per dump to 10^{-4} μC per dump are available. Each range is accurately adjustable with preset controls. The current-measuring (dump rate) circuit operates a meter calibrated to read the amount of current fed to the integrator. This circuit can also drive an external 100-μA meter for current indication at a remote location. The current-indicating meter ranges from 10^{-9} to 5×10^{-4} A full scale, the indication being within ±3% of the true value. A test current can be connected to the input of the integrator and is adjustable from 2×10^{-9} to 10^{-4} A in steps of 1, 2, 5, and 10.

The integrated circuit scaler and preset dump circuitry are interrelated in such a way that only the required number of decades is used. If the number of preset dumps is less than 10 only one decade is needed, but if the number is greater than 1000 more than three are needed. The preset dump total can be from one dump to 9.999×10^6 dumps, and is fixed by setting the four most significant digits and then setting the power of ten. The scaler has Nixie display on only the last four decades, which correspond to the four most significant digits set in the preset circuit (providing a reading error less than 0.1%). The seven-decade scaler provides for almost 6 hours of running time at the highest dump rate (500 per second).

When the final dump occurs, the scaler is gated off, and both visual and audible alarms are operated. Six outputs are also provided to control scalers and pulse-height analyzers. The control circuitry can be operated with push buttons on the front panel or by external signals. Outputs are provided to read out the total charge from the integrator to a computer.

10. IMPLEMENTING AUTOMATIC DATA HANDLING

Richard Leres

Spectrum stripping of data that have been accumulated on two or more gated pulse-height analyzers must usually be accomplished by hand. By use of a new approach, spectrum stripping is being routinely performed automatically on data accumulated by four analyzers.

The term spectrum stripping, as used here, refers to automatic data handling techniques such as subtracting background data from spectra and adding or subtracting, in discrete amounts or percentages, short-lived activity spectra from long-lived ones. When two analog-to-digital converters (ADC) are used in obtaining data, the inherent differential and integral linearity inequalities between the two prevent absolute correlation of energy to channel number. Since the analyzers mentioned are sequentially gated on between beam bursts, only one time-shared ADC is required to furnish digital information to the memory-storage sections of the four analyzers.

A unit has been designed and constructed which, when connected to the analyzers, allows an experimenter to use any one of the four ADC's to accumulate data in all four memories. This unit provides the switching and buffering needed to connect all the reset, store, and count train lines to one chosen ADC. Because only one ADC with its input gating intact is used, the other analyzers must be gated in the memory cycle of data storage. Since the ommission of the "add one" pulse logically prevents storage, and inhibit "add one" gate for each memory is employed.

Existing analyzer connectors are used with this setup and no modifications were required other than an ADC disconnect switch on the rear apron of each analyzer.

11. SILICON RADIATION DETECTORS

R. P. Lothrop, M. D. Roach, H. E. Smith, and B. V. Jarrett

A. Diffused Detectors

1. Avalanche diodes

Huth has shown[1] that very high voltage diodes may be prepared by surface contouring. This device will give very large pulses on all events including minimum-ionizing, and may have application in very fast timing experiments.

Preliminary experiments with quartz passivated structures on 57 ohm-cm, p-type material show promise. Figure G. 11-1 shows the reverse voltage vs leakage current for such a device. The field at breakdown is approximately 80 kV/cm, and charge multiplication with α particles is obvious at voltage just below breakdown. It should be noted that conventional planar structures on silicon of this type and resitivity typically exhibit breakdown voltages below about 100 volts.

2. dE/dx detectors

Techniques have been adopted which permit the fabrication of dE/dx detectors having thicknesses down to approximately 10 μ. Previously, dE/dx detectors were limited to a few mils by mechanical breakage during etching. The addition of planar etching[2] to the process now makes it possible to produce these devices in thicknesses well below 1 mil.

These detectors are used in particle identification systems. The availability of thinner detectors has significantly increased the range of usefulness of these systems.

B. Lithium-Drifted Detectors

1. Double Drifting

A number of contoured, grooved, and double-drifted structures were fabricated in an effort to improve the high-voltage characteristics of lithium-drifted silicon radiation detectors. Of the structures tested, the double-drifted one has shown the best characteristics.

The double-drifted structure is fabricated as follows: A wafer is lithium-diffused over one entire face. A large-area intrinsic region is drifted to a depth of about 0.5 mm. A 5-mm-diameter mesa is etched on the lithium-diffused face and the device is drifted through. A thin gold entrance window and surface protection complete the device.

The finished device has the advantages of a long surface leakage path (about twice the device thickness), as well as a region of high electric field perpendicular to the n-type surface channels.

Figure G. 11-2 shows the curve for reverse voltage vs leakage current for such a device. Resolution at 300 V bias and about -150° C was better than 1 keV FWHM on low-energy x rays and 1.5 keV FWHM on 90-keV electrons.

References

1. Gerald C. Huth, Study of the Noise Characteristics and Energy Resolution of Contoured Semiconductor Radiation Detectors, USAEC Report NYO-3246-1.
2. T. C. Madden and W. M. Gibson, Uniform and Stable dE/dx P-N Juntion Particle Detectors, Bell Telephone Labs., Inc., Murray Hill, N. J.

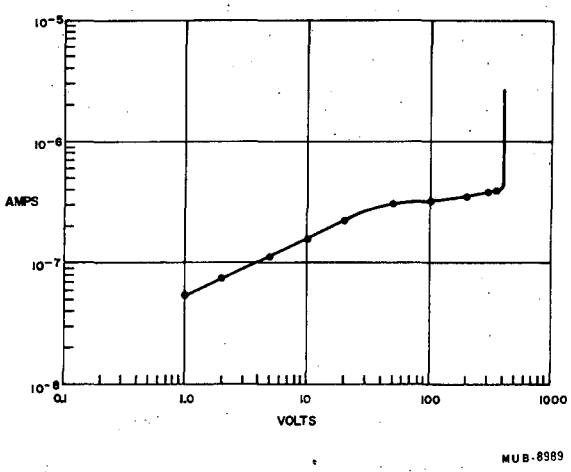

Fig. G. 11-1. Leakage current of avalanche diode.

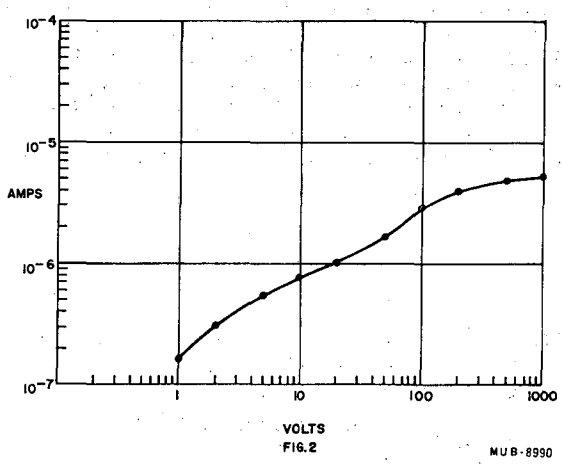

Fig. G. 11-2. Leakage current for improved lithium-drifted silicon detector.

12. DETECTION OF 30- AND 40-MeV PROTONS BY A THIN-WINDOW LITHIUM-DRIFTED GERMANIUM COUNTER*

Richard H. Pehl, Donald A. Landis, Fred S. Goulding, and Blair V. Jarrett

Since the use of Li-drifted silicon counters for the detection of charged particles having a range greater than ≈3 mm is severely hampered by the inability to collect all the charge within a reasonable period of time, it is of considerable interest to evaluate the ability of Li-drifted germanium counters to detect long-range charged particles. Recent developments in producing thin-window Li-drifted germanium counters[1] have enabled us to investigate the response of such counters to 30- and 40-meV protons. Although the effective window thickness has not been accurately measured, the window is certainly less than 5 μ, and is probably about 0.5 μ.

The depletion region of the detector is about 1×1×0.5 cm. This small size was chosen to reduce the γ-ray background. To further reduce the background the beam was stopped about

4.5 m behind the target, and the counter was shielded by lead from the Faraday cup and beam pipe. The Berkeley 88-inch variable-energy cyclotron was used for these experiments; the protons were scattered from either a gold or carbon foil–both of which were about 200 $\mu g/cm^2$ thick. All measurements were made at a fixed scattering angle of 19.7 deg, and with the detector, preceded by a 2.5×5-mm collimator, approximately 65 cm from the target. To protect the germanium detector from the relatively dirty scattering-chamber vacuum system, a 2.5-μ Havar window separated the counter holder from the system. The counter was operated at 77° K in a vacuum of 10^{-5} mm Hg.

Resolutions of 41 and 52 keV (FWHM) were obtained when 30- and 40-MeV protons, respectively, were scattered off gold. To determine the contribution from the germanium counter itself one must correct for the energy spread introduced by (a) the spread of the beam energy, assumed to be 0.08%, and thus 24 and 32 keV for the two energies used; (b) the thin window, calculated[2] to cause a FWHM of 12.3 and 9.5 keV for 30- and 40-MeV protons, respectively; (c) electronic noise, determined by observation of many pulser peaks to be 23 and 26 keV for the system adjusted for 30 and 40 MeV, respectively. (No correction for the angular resolution contribution is necessary because with the geometry used such a correction is less than 1 keV.) After these contributions have been subtracted the remaining spread is 21 keV for 30-MeV protons and 30 keV for 40-MeV protons.

Knowledge of the Fano factor F and the average energy-per-hole-electron pair, ϵ, enables one to determine the theoretical limitation of the energy resolution. Figure G.12-1 presents this limitation as a function of the energy deposited in a germanium crystal for different nondetector contributions. This calculation was based on $F = 0.30$ and $\epsilon = 2.98$ eV.[3] For 30 and 40 MeV the theoretical limit is 12.2 and 14.0 keV, respectively. Thus our results are somewhat worse than the theoretical limit. However, the detector used was rather poor–it would not operate at more than 400 V bias, and exhibited a relatively broad satellite peak of slightly lower energy than the main peak. Nevertheless, the use of Li-drifted germanium counters for the detection of long-range charged particles appears very promising.

Footnote and References

*Condensed from Phys. Letters 19, 495 (1965).

1. F. S. Goulding and B. V. Jarrett, A Method of Making Thin-Window Germanium Detectors, UCRL-16480, Nov. 1965.
2. B. Rossi, High-Energy Particles (Prentice-Hall, Inc., Englewood Cliffs, New Jersey, 1952), chap. 2.
3. S. O. W. Antman, D. A. Landis, and R. H. Pehl, Measurements of the Fano Factor and the Energy per Hole-Electron Pair in Germanium, Nucl. Instr. Methods (to be published).

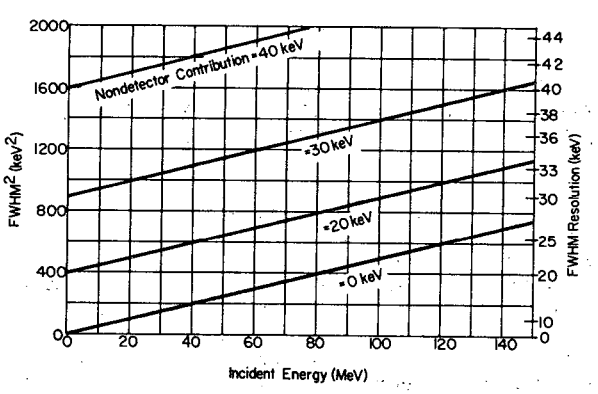

Fig. G.12-1. Energy resolution as a function of the energy loss in the detector for different nondetector contributions.

13. COMPUTER SYSTEM FOR NUCLEAR SPECTROSCOPY PROGRAM

L. Robinson, M. Myers, J. Meng, and H. Cingolani

A PDP-7 computer has recently been delivered for use in nuclear spectroscopy studies. The machine's circuitry is being augmented and special programs are being prepared to allow simultaneous on-line use by several independent experimenters. A number of analog-to-digital converters will use parts of the 8192-word memory as storage for pulse-height analysis, while other parts of the memory will be used for computation and preliminary data analysis, and for CRT display, graph plotting on a digital plotter, and permanent storage of data on magnetic tape.

Hardware has been developed that will allow protection of each experimenter's data from programs operated by other users. A monitor program will aid in the assignment of memory to various users and automatically load specific analysis programs to the required area in memory when needed. Only a single memory-cycle time of 1.75 μsec is required to add a count to a word or "channel" during pulse-height analysis, so that eight connected pulse-height converters, each with a count rate of 10^4 counts per second, would still leave more than 80% of the computer's time for computation.

Since most experiments using this system will last for many hours, it is expected that the more expensive items of hardware such as the magnetic tape units, the typewriter, and the digital graph plotter will be shared by all users. A CRT display and a simple control console will be provided at the location of each connected experimental setup.

14. COMPUTER SYSTEM AT THE 88-INCH CYCLOTRON

L. Robinson, T. Schaeffer, and J. Mahoney

A PDP-5 computer is now used routinely for CRT display, graph plotting, storage, and preliminary analysis of data taken by the 4096-channel nuclear data pulse-height analyzer at the 88-inch cyclotron. The PDP-5 has an 8192-word magnetic core memory with 12 bits per word. The pulse-height analyzer is electrically connected to the PDP-5, allowing the computer to control the operation of the analyzer and to transfer data back and forth between the magnetic core memories of the two machines. (Two 12-bit computer words are used to store each channel of data from the analyzer.)

Data are automatically transferred from the analyzer to the computer at the end of each run, and stored on magnetic tape together with special information such as run number, reaction name, integrated beam current, etc. The analyzer is free to start the next run after a delay that can be made as short as a few seconds.

Several data handling programs are used. A typical program can recall data from the magnetic tape when the run number is typed, and allows simultaneous CRT display, graph plotting on a Cal Comp digital plotter, data typeout, and punching of data on paper tape. The speed of the system is such that the computer can generate a flicker-free 1000-channel display and operate all these output devices simultaneously. A "light pen" is used to select particular groups of channels for typeout, and to determine the typeout format, which may be channel by channel or the sum of selected channels with and without background subtraction. (A light pen is a photodiode which sends a pulse to the computer when it detects a bright spot on the CRT.)

The ability to do this preliminary data analysis during the course of an experiment is very advantageous because it enables the experimenter to choose the optimum conditions for the experiment and to compensate for unexpected effects. When more detailed analysis is required, data are stored on IBM compatible magnetic tape and dealt with at the LRL Computer Center.

A unique feature developed for the computer system at the 88-inch cyclotron allows the experimenter to load one of a number of selected programs by merely setting a 12-position rotary switch and pushing a button. The loader uses special electronic circuits to load an initial "bootstrap" program, so that the program loader will work even after the computer memory has been completely erased. This feature is particularly valuable when the machine is being used by people who are unfamiliar with the computer.

Although most programs for this computer are written in symbolic machine language, a PDP-5 Fortran system is also available. The normal PDP-5 Fortran has been modified to use fast multiply-divide hardware and also to allow calculations to proceed while data are being read in or out on the typewriter. The Fortran compiler has also been modified to use the PDP-5 magnetic "micro-tape" system without recourse to punched paper tape.

A typical Fortran program used by experimenters on this system calculates relativistic kinematics to a first approximation and types out a table of values giving the particle's center-of-mass angle, its energy in the laboratory system, and the Jacobian, for specified lab angles.

15. AN ADVANCED MULTISCALER

A. A. Wydler

Commonly multichannel pulse-height analyzers are employed for use as scalers, hence the term "multiscaler mode." Although this is a convenient function, it suffers from a serious limitation, notably, the necessity of timed serial storage and lack of any indication of status of stored data.

MARVA, memory access random Victoreen accessory, is the result of an attempt to improve this situation. It allows semirandom access to the analyzer's memory and also provides visual indication of the state of all data both current and past. Although it is intended for use with a Victoreen "M" series analyzer, there is no fundamental reason why it cannot be adapted to other analyzers.

The pulse-height analyzer, in readout-display mode, is systematically presenting to its oscilloscope the data contained in each memory channel. These data are returned to the memory unaltered, therefore the constant visual presentation. MARVA causes the pulse-height analyzer to scale while in this mode by adding to the data before their return to the memory. As shown in the block diagram (Fig. G.15-1) the rate generator continuously advances the address or channel number of the analyzer. This address is displayed on the "X" axis of the oscilloscope while its scaler value is being displayed vertically. The address is coded in the BCD to 100-line converter and, simultaneously with its display, developes a "reset" pulse for the corresponding count storage flip-flop. Had an input acceptable to the threshold discriminator previously "set" this same flip-flop, then a "carry" would be produced. Therefore, the act of resetting this flip-flop generates an add-1 pulse to increase the value of the displayed data and make the circuit available to accept another input. These data, when returned to the memory, would have now been increased by one. One hundred inputs are available and a like number of flip-flops provide temporary storage for the random data. At present there is a 65-μsec-per-channel time resolution, limited by the address rate generator frequency of 15 kilocycles. The ultimate limit is 12 μsec per channel, the memory cycle time of the analyzer. This represents the design rate and is usable; however, visual presentation is lost at this rate, as the oscilloscope unblanking circuit will not operate beyond about 18 kilocycles. There is no adjacent channel time resolution loss, since all inputs may be loaded simultaneously at the 15-kilocycle rate. An external gate is provided for control use, such as blocking flip-flop storage during accelerator beam pulses.

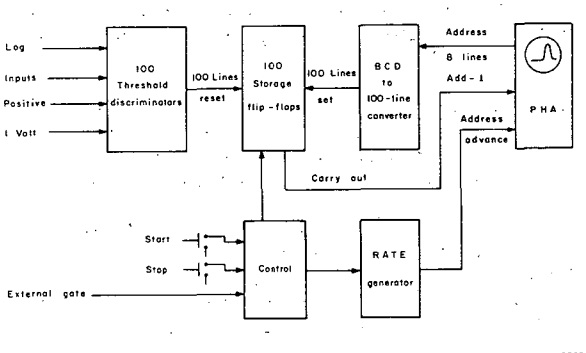

Fig. G.15-1. Advanced multiscaler.

16. IMPROVED ACCURACY IN MEASUREMENT OF LOW GAS FLOW RATES WITH A BUBBLE METER*

Amos S. Newton and G. W. Kilian

One of the major factors determining the sensitivity of a gas chromatographic apparatus utilizing thermal conductivity detectors is the flow rate of the carrier gas. As the sensitivity is inversely proportional to carrier-gas flow rate, a 1% change in flow rate is reflected in a 1% change in sensitivity in the opposite direction. If control of sensitivity of a gas chromatograph to ± 0.1% is to be achieved, the gas-flow rate must be measured to within less than 0.1%.

Recently Noble, Abel, and Cook have described an electromechanical device for absolute measurement of low flow rates,[1] but the usual method of determining low flow rates is by use of a bubble flowmeter and a stopwatch. Levy has discussed the experimental parameters of the bubble method and analyzed the errors inherent in each parameter.[2]

The experimental variables in the bubble meter are (a) the time of rise of the bubble between two fixed marks, (b) the volume between the marks, (c) the temperature of the gas, (d) the pressure of the gas, and (e) the degree of saturation of the gas with water vapor. As analyzed by Levy, by careful design of the apparatus, close control of temperature, accurate measurement of the pressure, and presaturation of the gas, each of these variables except time can be reduced to an uncertainty of less than 0.02% to 0.04%.

The measurement of time is the most difficult to control. By use of a stopwatch, reproducibility to ± 0.2 sec with one observer is good, and with different observers it varies as much as ± 0.4 sec. These errors were cut in half when an electric timer[3] having a 1-sec sweep hand and controlled by an external microswitch was substituted for the stopwatch. The basic problem appears to be in making reproducible decisions as to when the bubble crosses the index mark and in achieving reproducible reaction times.

For gas chromatographic use, the time interval of interest is usually between 10 and 120 sec for displacement of a volume of 50 ml. Thus the error in time varies from 1 to 2% for the short interval to 0.1 to 0.2% for the longer interval. Most of the work we have encountered involves flow rates of 40 to 120 ml/min, where the timing errors are 0.3% to 0.8%.

In order to reduce timing errors to less than 0.02%, an electronic timer has been devised which operates on the principle that the fixed marks on the gas burette are replaced by two light beams 0.25 mm (10 mil) in diameter across the burette. Interruption of the lower light beam by a bubble turns on a scaler which counts pulses from a 100-kc generator, and interruption of the top beam turns off the scaling circuit. Thus times can be measured to ± 0.00001 sec (or ± 1 count of the 100-kc frequency). Operator bias is also removed, since the decision as to when the bubble crosses the index mark is determined by scattering of the light beam by the bubble, and is hence made in a reproducible manner at both the top and bottom index marks.

A block diagram of the apparatus is shown in Fig. G.16-1. The gas entered the thermostated flowmeter (± 0.01°) through a thermostated presaturator. A bubble is formed in the usual way by means of a rubber bulb, containing a bubble-forming liquid. "Snoop" was used as the bubble forming liquid,[4] as it gave very uniform bubbles which retained the same degree of flatness as they progressed up the tube. At the lower detector, the bubble interrupted the light beam, reducing the output of the 2N 2175 photocell. This change in photocell output was amplified and fed to a trigger-forming circuit which generated a start pulse. This start pulse activated the electronic switch and gated on the decade scaling circuit. The scaling circuit then counted the pulses coming from a crystal-controlled 100-kc pulse generator.

The bubble traveled up the tube and passed the upper light beam. This generated a stop pulse in the same manner as the start pulse was generated. The electronic switch gated the scaler off. The time for the bubble to travel between the two light beams was then read directly off the scaler.

The volume between the light beams was calibrated by (a) filling with water and weighing the water collected between the interruption of the upper light beam and interruption of the lower light beam, and (b) filling with mercury and weighing the mercury collected in the same manner. The water collection was run as a function of drainage time. For a volume of 44.50 ml, the difference between water and mercury calibrations was 0.10 ml (1 min water drainage), and the

water volume increased with increase in drainage time. Thus for ultimate accuracy, the volume must be calibrated to take account of the liquid film thickness on the gas burette at various rise times of the bubble, this amounting to approximately a 0.05-ml difference between the volume collected in drainage times of respectively 1 minute and 3 minutes, i.e., about 0.01% difference.

Typical results for a very fast flow, a medium flow, and a low flow are shown in Table G.16-I. The fast flow was regulated by the flow from a helium tank fitted with a two-stage pressure regulator at 40 psig, a ballast tank, and a temperature-insulated Nupro double pattern metering valve.[4] The medium and low flow rates were through a Moore flow regulator[5] (temperature insulated) with the pressure drop controlled by the same type of Nupro valve as above. The room was thermostatically controlled to 25 ± 0.5°.

The results in Table G.16-I show that over most of the range from 20 to 500 ml/min the reproducibility is better than 0.01%. The break to greater deviations (≈ 0.1%) comes at about 30 ml/min, and this may be a failure in operation of the flow regulator rather than in the bubble flowmeter.

This flowmeter has been used, not as a working measurer of the flow rate, but rather as a primary standard to calibrate the working meters, Hastings Flowmeters Model LF-100.[6] With suitable precautions regarding bias and zero settings, the output of these latter flowmeters, when measured on a sensitive potentiometer, was found to be reproducible to ± 0.10% between flow rates of 30 and 250 ml/min, and the calibration has held for a period of 6 months.

Footnote and References

*Paper to be submitted to Analytical Chemistry.

1. F. W. Noble, K. Abel, and P. W. Cook, Anal. Chem. 37, 1631 (1965).
2. A. Levy, J. Sci. Instr. 41, 449 (1964).
3. Standard Electric Time Co., Springfield, Massachusetts.
4. Nuclear Products Co., Cleveland, Ohio.
5. Moore Products Co., Philadelphia, Pennsylvania.
6. Hastings-Raydist, Inc., Hampton, Virginia.

Table G.16-I. Reproducibility of bubble meter measurements using electronic timing.

	Nominal flow-520 ml/min[a]		Nominal flow-62 ml/min[a]		Nominal flow-22 ml/min[a]	
	sec/44.50 ml	Δ from average	sec/44.50 ml	Δ from average	sec/44.50 ml	Δ from average
	5.12399	0.00077	42.9710	0.0028	118.8041	0.2269
	5.12340	0.00018	42.9652	0.0030	119.0687	0.0023
	5.12372	0.00050	42.9693	0.0011	119.2625	0.1915
	5.12381	0.00059	42.9610	0.0072	119.2847	0.2138
	5.12344	0.00022	42.9650	0.0032	119.1149	0.0439
	5.12296	0.00036	42.9664	0.0018	118.9133	0.1577
	5.12305	0.00017	42.9732	0.0050	118.8973	0.1737
	5.12240	0.00082	42.9729	0.0047	119.0092	0.0618
	5.12260	0.00062	42.9705	0.0023	119.1758	0.1048
	5.12283	0.00039	42.9677	0.0005	119.1793	0.1083
Average	5.12322	0.00045	42.9682	0.0032	119.0710	0.1324
% Average deviation		0.0088		0.0074		0.110
% Maximum deviation		0.016		0.017		0.224
Flow calculated	521.157 ± 0.046		62.139 ± 0.005		22.444 ± 0.025	
Flow STP (dry)	450.131 ± 0.040		53.670 ± 0.004		19.368 ± 0.022	

a. Ten consecutive measurements at nominal flow.

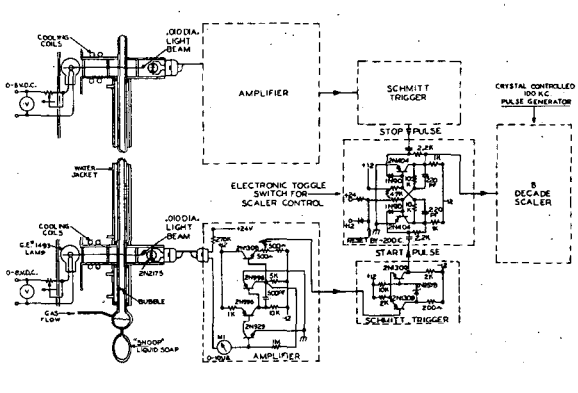

Fig. G.16-1. Schematic diagram of apparatus for electronically measuring displacement time in a bubble flowmeter.

17. ELECTRON-GAMMA ANGULAR CORRELATION APPARATUS USING SEMICONDUCTOR DETECTORS

T. Yamazaki, D. A. Landis, R. S. Stone and J. M. Hollander

An apparatus, consisting of a fixed Ge(Li) γ-ray spectrometer, a fixed Si(Li) electron spectrometer, and a movable NaI(Tl) γ-ray spectrometer, has been developed for angular correlation experiments involving conversion electrons. A schematic view is shown in Fig. G. 17-1. With this system, γ-γ and γ-e angular correlations can be measured simultaneously. Both semiconductor detectors have sufficient resolution to discriminate from any others those gamma and electron lines of interest. In particular, the 5×3-mm thick Si(Li) crystal coupled to a FET preamplifier exhibits resolution (FWHM) as good as 1.4 keV for electrons below 100 keV, and 1.0, 1.2, and 1.3 keV for 14-, 59-, and 101-keV γ rays, respectively. A spectrum of U^{237} obtained with this detector is shown in Fig. G. 17-2. The L_{III}-59 line is completely separated from the L_I, L_{II} - 59 doublet. This resolution is comparable to that of a lens-type magnetic spectrometer even in the 50-keV region, and to that of sector-type magnetic spectrometers in the 200-keV region. When higher resolution is required, for example, in order to resolve each L subshell line, the Si(Li) detector can be replaced by the Berkeley 50-cm-radius iron-free spectrometer.

The electronic system consists of eight units: three linear amplifier systems (11X1981P-1), two 10-input single-channel analyzer units (11X3520P-1), a coincidence control unit (11X3670P-1), a motor control unit (15X5662P-1), and a 400-channel Packard pulse-height analyzer capable of random-access addressing. A block diagram of the system is shown in Fig. G. 17-3.

The linear amplifier systems amplify and shape the detector output signals, as well as provide timing signals from the three detectors. Fast coincidence circuits incorporated in two of the linear amplifier systems are used. The resolving times are set at about 50 nsec. The output of the movable counter (NaI) is taken in coincidence with both the fixed gamma counter (Ge) and the electron counter (Si). The ungated linear, timing, and coincidence pulses from the amplifier systems are connected to the coincidence control unit. Scale-down circuits select every tenth or hundredth singles count from the timing pulses provided by the three detectors. Matrix boards inside the control unit connect the appropriate signal to the two 10-input single-channel analyzer units, which select peaks from the spectra of the three detectors. The output of any one of the single-channel circuits can be selected by switches on the control unit and used to gate the correct linear amplifier system in order to facilitate the accurate adjustment of the discriminator windows of the analyzers.

The outputs of the single-channel analyzer units are gated by the coincidence or scaled-down pulses, and the resulting signal addresses a single channel in one of four 100-address subgroups in the pulse-height analyzer. The correct subgroup is determined by the position of the movable (NaI) counter. The number in the correct address is then incremented by one. Time signals are also recorded in each subgroup to allow normalization of the data for each position. Inhibit circuits prevent the analyzer from storing any signal when more than one address is selected should multiple coincidences occur at the same time. A typical format for the stored data is shown in Fig. G. 17-4. The format can be changed by changing connections on the matrix boards which supply the signals to the single-channel analyzer units.

The motor control unit automatically causes the NaI counter to move to a new position after one prescribed time interval; also the analyzer can be programed to read out the stored information on paper tape after another set time interval.

It is planned to replace the movable NaI detector by a set of four fixed Ge detectors. Circuits in the coincidence control unit will then be used to combine the signals from these four detectors and provide timing pulses, which will indicate the counter in which the γ ray was recorded.

Figure G. 17-5 illustrates some preliminary results obtained from electron-gamma angular correlation measurements with Au^{196}. Figure G. 17-6 shows more recent results obtained for the e-γ correlations with a source of Bi^{207}. The energy levels involved in the correlation experiments are shown in the figures. Although at this time the preliminary results are too rough to allow quantitative interpretation, they do illustrate clearly the versatility and convenience of this apparatus for e-γ angular correlation studies.

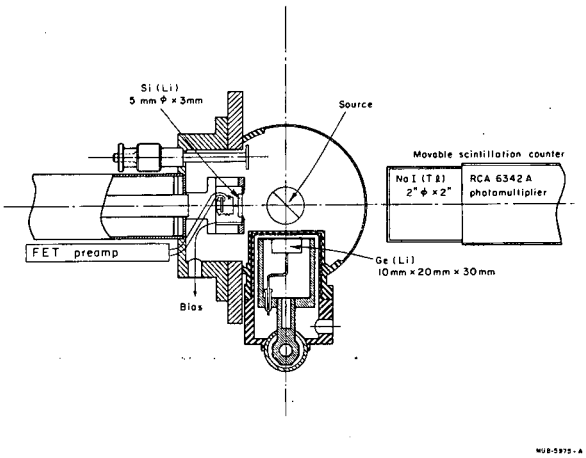

Fig. G. 17-1. Schematic drawing of angular correlation apparatus showing Si(Li) conversion electron detector with FET.

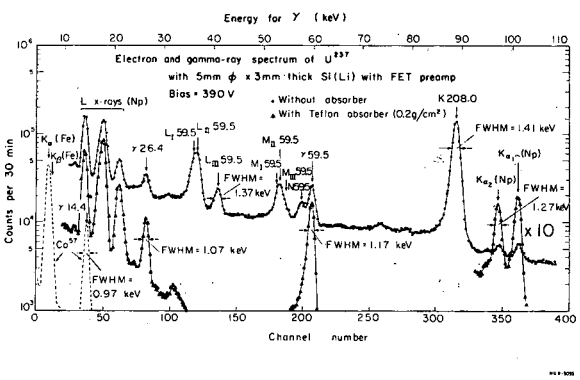

Fig. G. 17-2. Electron spectrum of U^{237} taken with the Si(Li) detector with FET preamplifier.

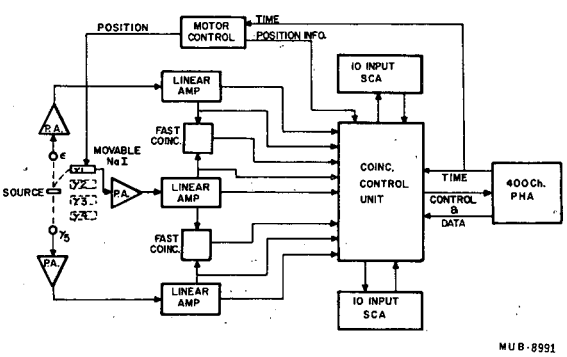

Fig. G. 17-3. Block diagram of angular correlation system.

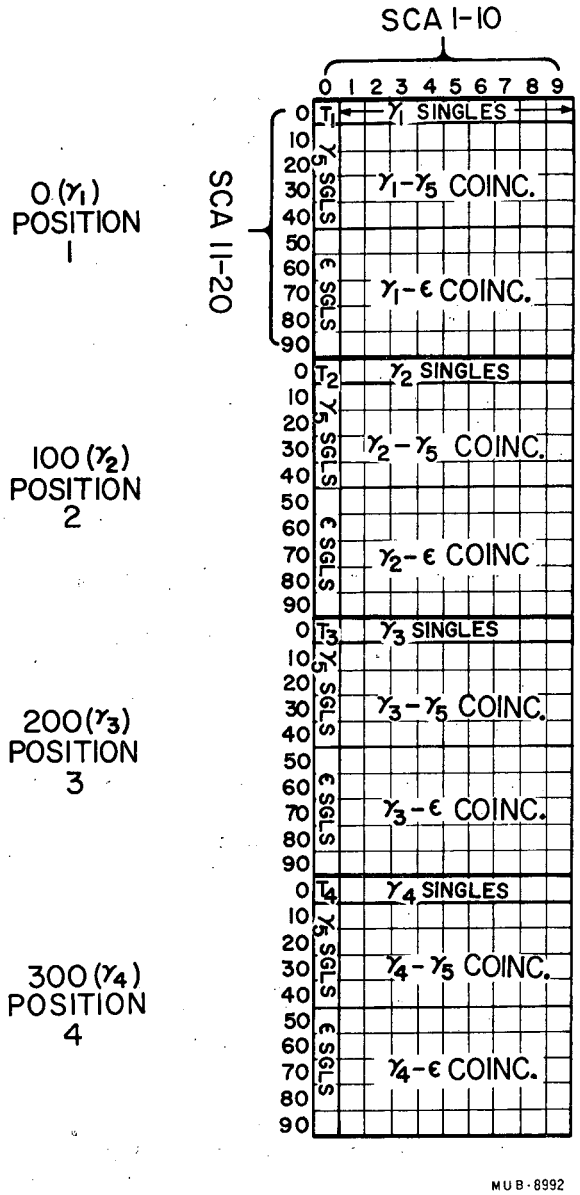

Fig. G. 17-4. A typical format of data stored in the 400-channel analyzer.
T_1 through T_4 are for time signals.
γ_1 through γ_4 are the four positions of the movable NaI detector.
γ_5 is the fixed Ge detector.
ϵ is the fixed Si detector.

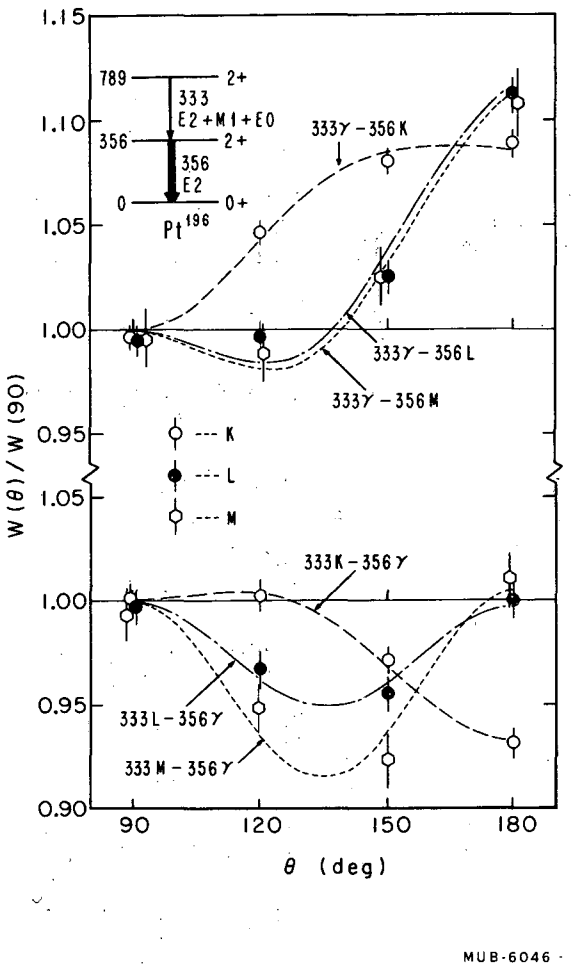

Fig. G. 17-5. Preliminary results on the γ-γ and e⁻-γ angular correlations in Pt^{196}.

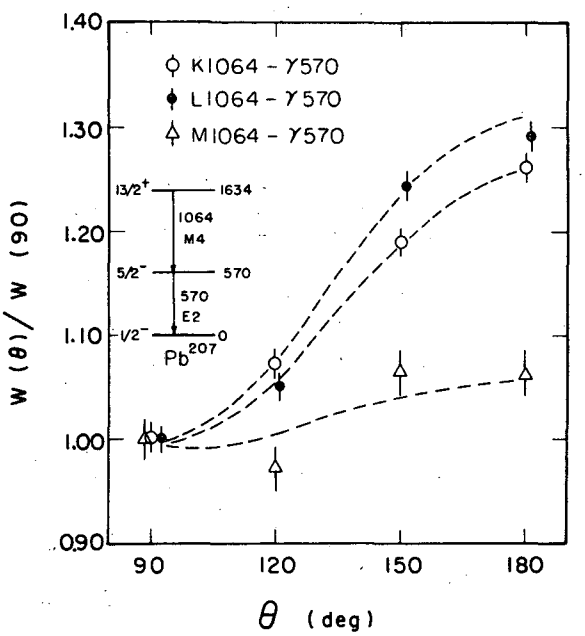

Fig. G.17-6. e^--γ correlation results obtained with a source of Bi^{207}.

18. A THREE-COUNTER PARTICLE IDENTIFIER FOR STUDIES OF LOW-YIELD NUCLEAR REACTIONS

F. S. Goulding, D. A. Landis, J. Cerny, and R. H. Pehl

Studies of low-yield nuclear reactions such as (He^3, He^6) or (He^4, He^8) require the identification of very small numbers (≈10 to 100) of the interesting reaction product particles in the presence of very large numbers (≈10^7 to 10^8) of other types of other reaction products. Conventional ΔE, E identifier systems are of limited value in these experiments, as a small fraction of the abundant reaction particles produces ΔE signals which deviate considerably from their normal value. The resulting false identification signals cause a general background in the identifier output spectrum which interferes with the peak due to the interesting particles. In the improved identifier two ΔE detectors are employed and, each time a particle passes through the counter telescope, two identifications are made, each using one of the ΔE signals. If they do not agree with each other within prescribed limits (due to deviation from normal of one of the ΔE signals) the event is completely rejected. Fast coincidence techniques are used to reduce the effects of chance coincidences between unrelated detector signals, and a fourth counter is used to reject high-energy particles, which pass completely through the telescope.

The performance of the system is illustrated in Figs. G. 18-1, G. 18-2, and G. 18-3. Figure G. 18-1 shows the energy spectrum obtained in a $C^{12}(He^3, He^6)C^9$ experiment with the older dual-counter identifier system, with the analyzer gated by a single-channel analyzer set to the region of the He^6 peak in the identifier. The ground-state peak is seen to be superimposed on a general background due to leak-through of He^3 and He^4 particles into the He^6 region. In Fig. G. 18-2 the same energy spectrum is shown taken with the triple-counter identifier. The background is seen to be much improved. Figure G. 18-3 shows the typical performance of the three-counter particle identifier in separating He and Li isotopes produced in a reaction experiment.

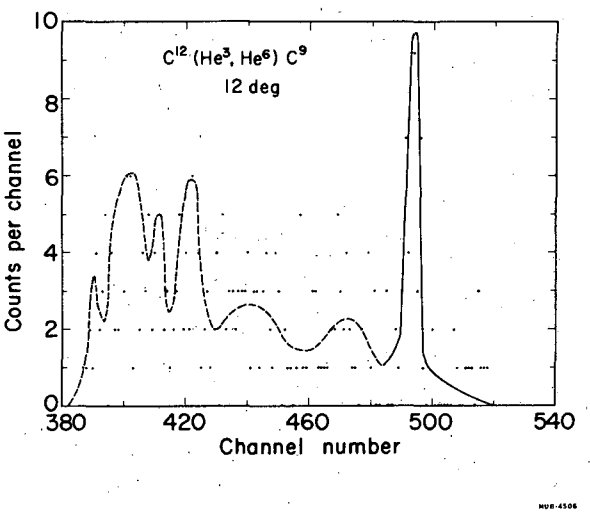

Fig. G. 18-1. Energy spectrum from the $C^{12}(He^3, He^6)C^9$ reaction.

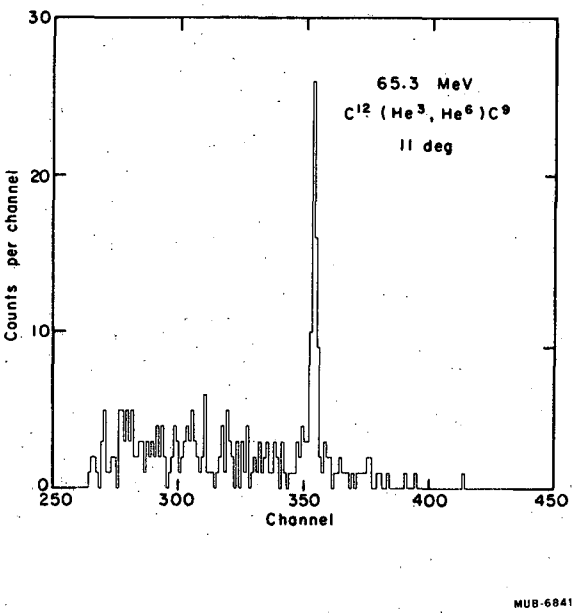

Fig. G. 18-2. Same as in Fig. G. 18-1 when the three-counter particle identifier is used.

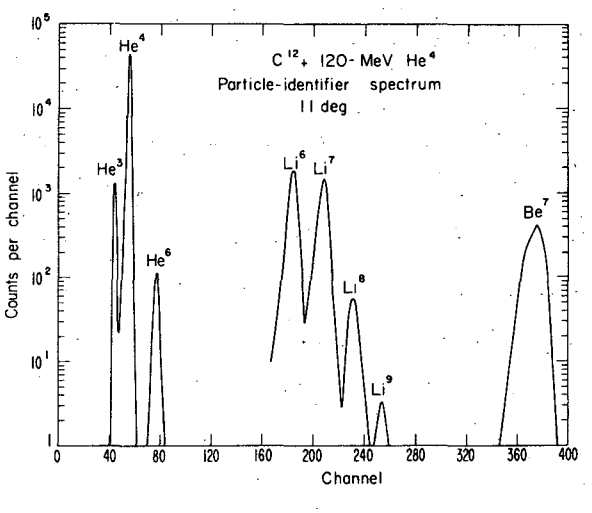

Fig. G. 18-3. A three-counter particle identifier spectrum from C^{12} plus 120-MeV He^4.

19. APPLICATION OF LITHIUM-DRIFTED GERMANIUM γ-RAY DETECTORS TO NEUTRON ACTIVATION ANALYSIS: NONDESTRUCTIVE ANALYSIS OF A SULFIDE ORE

J. Lamb, S. G. Prussin, J. A. Harris, and J. M. Hollander

The applicability of lithium-drifted germanium γ-ray detectors to nondestructive activation analysis has been demonstrated by Prussin, Harris, and Hollander[1] and by Girardi, Guzzi, and Pauly,[2] for samples in which the activation of major constituents is small and does not interfere with the determination of trace and minor components. However, when the major constituents of a sample contribute appreciably to the gamma activity, the sensitivity of analysis for a given component may be severely limited by the complexity of the γ-ray spectrum and by the masking effect of the radiations from the major constituents. The latter problem is of particular concern in the application of available Ge(Li) detectors, since the ratio of Compton-to-photopeak efficiencies is considerably larger than for the commonly used 3×3-in. (diam) sodium iodide scintillators.

To explore the applicability of Ge(Li) detectors for analysis of samples containing major constituents with appreciable activation cross sections, we have analyzed samples of a sulfide ore by neutron activation. Samples of ore were irradiated for periods of 2 to 72 hours in a neutron flux of approximately 5×10^{12} n/cm^2-sec. The γ-ray spectra of the activated samples were obtained with two Ge(Li) detectors of dimensions 2 cm$^2\times$7 mm (active thickness) and 6 cm$^2\times$10 mm (active thickness), respectively, and with a very good 3×3-in. (diam) NaI(Tl) scintillator. Qualitative analysis was performed by measurements of the energies and half-lives of photopeaks and by comparison of the experimental γ-ray relative intensities with literature values for isotopes yielding more than one photon in their spectra. These data are given in Table G. 19-I. Quantitative analyses were performed by comparison of the photopeak intensities in sample spectra with corresponding intensities in standard samples irradiated simultaneously with the test samples. The quantitative data for In, Mn, Zn, Sb, Na, Au, Ga, and Fe are given in Table G. 19-II, and cover a concentration range of 1.8×10^5 ppm (Fe) to 2.0 ppm (Au).

References and Bibliography

1. S. G. Prussin, J. A. Harris, and J. M. Hollander, Anal. Chem. 37, 1127 (1965).
2. F. Girardi, G. Guzzi, and J. Pauly, Radiochim Acta 4 [2] 109 (1965).
3. G. T. Ewan and A. J. Tavendale, Can. J. Phys. 42, 2286 (1964).
4. Fred S. Goulding, A Survey of the Application and Limitations of Various Types of Detectors in Radiation Energy Measurements, UCRL-11302, Feb. 1964.
5. Fred S. Goulding and W. L. Hansen, An Automatic Lithium-Drifting Apparatus for Silicon and Germanium Detectors, UCRL-11261, Feb. 1964
6. William L. Hansen and Blair V. Jarrett, Techniques for the Fabrication of Lithium-Drifted Germanium Gamma Detectors, UCRL-11589, Aug. 1964.
7. Gene Miner, Mountings and Housings for Lithium-Drifted Silicon and Germanium Detectors, UCRL-11946, Feb. 1965.
8. F. S. Goulding and D. Landis, in Proceedings of Conference on Instrumentation Techniques in Nuclear Pulse Analysis, Monterey, April 1963, NAS-NRC publication 1184, p. 61-4.
9. R. L. Heath, Scintillation Spectrometry Gamma-Ray Spectrum Catalogue, Vol. I (IDO-16880-1).
10. Nuclear Data Sheets, Nuclear Data Group, Oak Ridge National Laboratory, Oak Ridge, Tennessee.
11. W. S. Lyon, Guide to Activation Analysis (D. Van Nostrand, Inc., Princeton, New Jersey, 1964).
12. R. C. Hawkings, W. J. Edwards, and E. M. McLeod, Tables of Gamma Rays from the Decay of Radionuclides (Atomic Energy of Canada Limited, Chalk River, Ontario, 1961, Publication CRDC-1007).

Table G. 19-I. Isotope assignments for nondestructive activation analysis of a sulfide ore with use of lithium-drifted germanium detector.

	Experimental			Literature[a]		
Isotope	$T_{1/2}$	E_γ (keV)	Relative Intensity	$T_{1/2}$	E_γ (keV)	Relative Intensity
In^{116m}	54 m	137	14.2	54 m	135	12
		416	100[b]		406	100
		819	39.1		820	--
		1100	233		1085	216
		1300	320		1270	300
Mn^{56}	2.65 h	845		2.58 h	845	
Cu^{64}	12.5 h	1345		12.8 h	1340	
		511 (annihilation)				
Zn^{69m}	14 h	438		13.8 h	439	
Ga^{72}	14.4 h	835		14.3 h	835	
Na^{24}	15.5 h	1369		15 h	1368	
As^{76}	26 h	559	100[b]	26.3 h	559	100[b]
		657	14.6		657	14.6
		1216	--		1216	9.7
Sb^{122}	≈ 60 h	563		67.2 h	566	
		686			686	
Au^{198}	≈ 60 h	411		64.8 h	411	
Fe^{59}	--	1095		45 d	1100	
		1292			1290	

a. Nuclear data sheets.
b. Relative intensities normalized to this value.

Table G. 19-II. Nondestructive analysis of a sulfide ore by neutron activation with use of lithium-drifted germanium detector.

Element	Amount present (μg)	Sample wt (mg)	Irradiation time (hours)	E_γ (keV)	ppm[a]
Mn	6.0	62.9	2	845 (Mn^{56})	95 ± 7
In	7.6	62.9	2	1300 (In^{116m})	120 ± 5
Ga	3.8	62.0	2	835 (Ga^{72})	61 ± 16
Zn	3020	24.5	24	438 (Zn^{69m})	$(1.2 \pm 0.009) \times 10^5$
As	60	19.0	72	559 (As^{76})	$(3.1 \pm 0.04) \times 10^3$
Sb	8.2	19.0	72	563 (Sb^{122})	430 ± 6
Cu	1240	19.0	72	511 (Cu^{64})[b]	$(6.5 \pm 0.01) \times 10^4$
Na	16	19.0	72	1369 (Na^{24})	840 ± 25
Fe	3370	19.0	72	1095 (Fe^{59})	$(1.78 \pm 0.01) \times 10^5$
Au	0.038	19.0	72	411 (Au^{198})	2.0 ± 0.2

a. Error shown represents statistical counting error only.
b. Copper concentration corrected for contribution to 511-keV photopeak from decay of Zn^{69} and Na^{24}.

20. A MICA TRACK SCANNER

R. LaPierre, M. Nakamura, and K. Ward

An instrument for displaying and counting the number of tracks on a mica slide is being developed. The apparatus is to be used in fission-fragment angular correlation studies and fission-fragment scattering cross-section studies.

The system includes a microscope, a Vidicon scanning and display system, and associated digital and analog circuitry for detecting tracks.

The microscope has a trinocular body with a prism beam splitter. Eighty percent of the light source is directed to the Vidicon camera lens and the remaining light goes to the visual lenses.

The resultant video signals from the Vidicon camera tube are amplified and applied to the cathode input of a standard laboratory oscilloscope which is used as a monitor camera.

The detection of actual tracks from background tracks and scratches is enhanced by imposing minimum and maximum criteria on the associated video signals. The operator selects the proper criteria by observing the average height and width of the tracks on the monitor camera. The video signals associated with a particular track are sorted by use of standard analog and digital circuitry, and if the established conditions are met a counter is advanced by one to indicate the presence of a track.

21. MODIFICATION OF INTERNAL CONVERSION COEFFICIENT SPECTROMETER

A. J. Haverfield and J. M. Hollander

Recently, the application of semiconductor detectors to the measurement of absolute internal conversion coefficients has been reported,[1,2] with the use of a device that permitted the simultaneous measurement of conversion electron and γ-ray spectra with lithium-drifted silicon and germanium detectors, respectively. Figure G. 21-1 is a photograph of the original design of the conversion-coefficient spectrometer, and Fig. G. 21-2 presents a scale drawing of the component parts. The device was essentially a small vacuum chamber in which the silicon and germanium detectors were mounted at 180 deg fixed geometry, and into which active sources could be inserted through a conventional spectrometer air lock.

In this apparatus, however, the unprotected surface layer of germanium was susceptible to damage from the intrusion of water vapor or oil into the system. The design has now been changed so that the germanium crystal is enclosed in a separate conventional vacuum chamber. This germanium detector assembly fits reproducibly into a "well," machined into the vacuum chamber of the silicon detector system. The modified design is shown in Figs. G. 21-3 and G. 21-4.

A field-effect transistor (FET) preamplifier of the type described by Elad[3] has recently been incorporated into the silicon detector system. The first stage of this preamplifier is contained within the vacuum chamber and the FET is cooled to liquid-nitrogen temperature. Examples of the resolution obtained with the silicon detector are shown in Figs. G. 21-5 and G. 21-6. Here the resolution of the silver K_α x ray is 1.4 keV and that of the K-conversion line of the 87.5-keV transition in Ag^{109} is 2.5 keV. The latter figure seems to be limited by source thickness. The resolution of the K-conversion line of the 569.7-keV transition in Pb^{207} is shown to be 3.3 keV.

The modified spectrometer is presently being calibrated for internal conversion coefficient measurements, by the procedure described earlier.[1] The isotopes having sufficiently well-known conversion coefficients to be used as standards for this calibration are listed in Table G. 21-I.

References

1. H. T. Easterday, A. J. Haverfield, and J. M. Hollander, Nucl. Instr. Methods 32, 333 (1965).
2. J. M. Hollander, UCRL-16307, 1965.
3. E. Elad, UCRL-16390, Sept. 1965, submitted to Nucl. Instr. Methods; E. Elad and M. Nakamura, UCRL-16515, Nov. 1965, to be submitted to Nucl. Instr. Methods.
4. J. H. Hamilton, Internal Conversion Processes, Ed. J. H. Hamilton (Academic Press, Inc., New York, 1965).
5. J. H. Hamilton, S. R. Amtey, B. vanNooijen, A. V. Ramayya, and J. J. Pinajian, to be published in Proceedings of Bases of Spin-Parity Assignment, Ed. F. K. McGowan, 1965.

Table G. 21. I. "Standard" internal-conversion coefficients used for calibration of the e-γ spectrometer.

Isotope	Transition energy (keV)	Electron energy (keV)	ϵ_K	References
Cd^{109}	87.9 ± 0.2	62.4	11.0 ± 0.3	4
Ce^{141}	145.5 ± 0.3	103.5	0.379 ± 0.004	4
Ce^{139}	165.84 ± 0.03	126.9	0.2148 ± 0.0012	4
Hg^{203}	279.16 ± 0.02	193.6	0.163 ± 0.002	4
Sn^{113}	393.0 ± 1.0	365.1	0.440 ± 0.008	4
Au^{198}	411.80 ± 0.01	328.7	0.0302 ± 0.0003	4
Cs^{137}	661.60 ± 0.08	624.2	0.0894 ± 0.001	4
Co^{58}	810.5 ± 0.1	803.4	0.0295 ± 0.001	4
Mn^{54}	835.0 ± 0.3	829.0	0.000224 ± 0.00001	5
Y^{88}	898.2 ± 0.3	882.1	0.000301 ± 0.00002	5
Zn^{65}	1115.4 ± 0.4	1106.4	0.000166 ± 0.000007	5

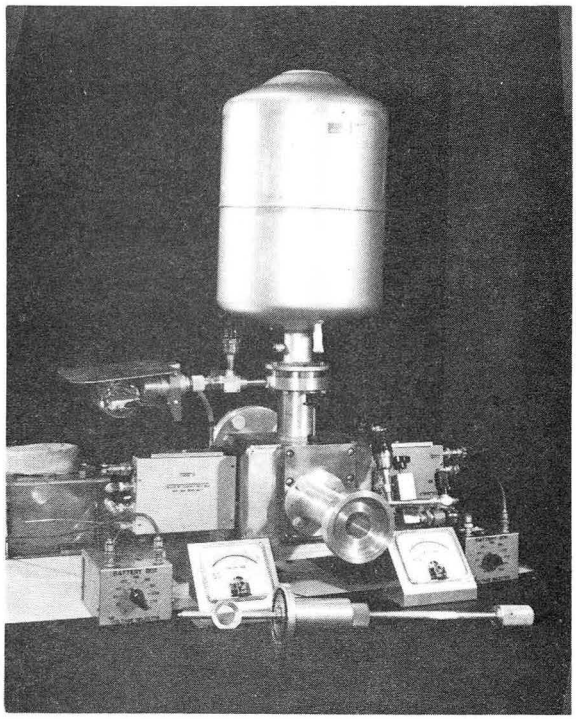

Fig. G. 21-1. The first conversion-coefficient spectrometer.

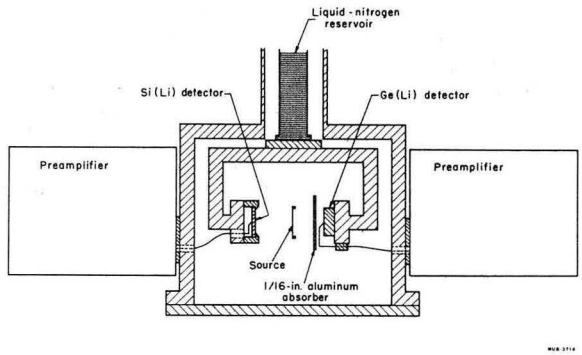

Fig. G. 21-2. The spectrometer of Fig. G. 21-1.

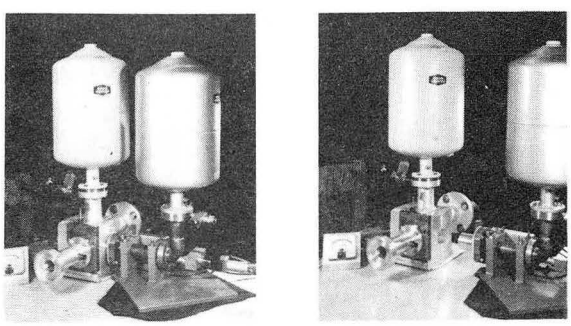

Fig. G. 21-3. Modified version of conversion-coefficient spectrometer.

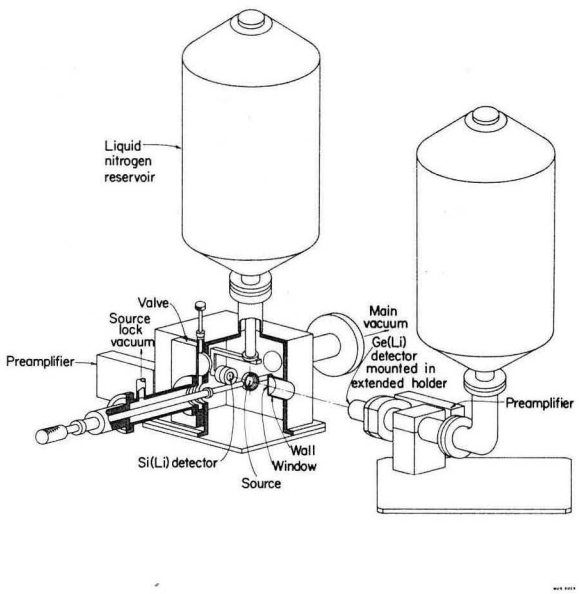

Fig. G. 21-4. The modified spectrometer of Fig. G. 21-3.

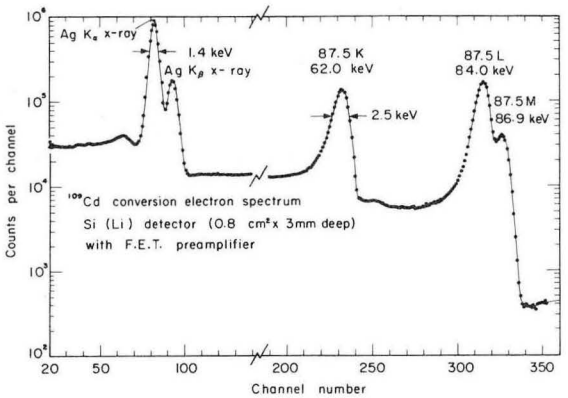

Fig. G. 21-5. Cd^{109} electron and x-ray spectrum taken on Si(Li) detector with FET preamplifier.

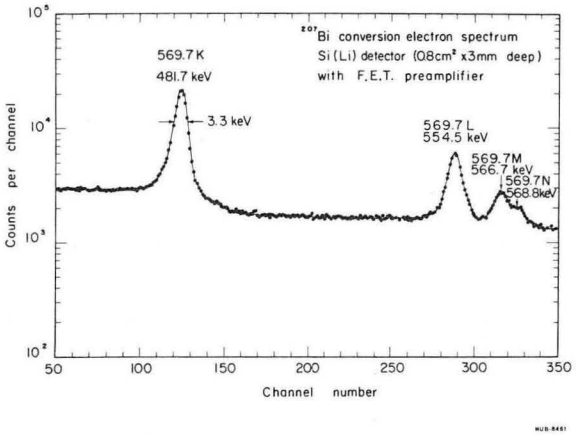

Fig. G. 21-6. Portion of Bi^{207} conversion-electron spectrum taken with Si(Li) detector with FET preamplifier.

22. PHENOMENOLOGICAL CORRECTION OF THE FIELD SHAPE OF THE BERKELEY IRON-FREE $\pi\sqrt{2}\,\beta$ SPECTROMETER†

Karl-Erik Bergkvist* and J. M. Hollander

A magnetic field-correction system has been introduced in the Berkeley iron-free $\pi\sqrt{2}$ β spectrometer in order to bring its performance closer to that theoretically inherent in the $\pi\sqrt{2}$ type of design. In the practical execution of such a design one is always left with imperfections of more-or-less significant magnitudes in the magnetic field shape. An up-down asymmetry of unknown origin in the field of the Berkeley iron-free spectrometer has been known to be present and has limited its performance, especially at high resolution. Such an asymmetry in general requires for its accurate description quite a number of field parameters and, correspondingly, for its complete removal makes necessary a rather involved system of correction coils. In the type of field correction described here we have been content with a field symmetry which is not complete, but which, with respect to the radial aberrations and hence the resolution, is essentially equivalent to that of the theoretically assumed field. It has been possible to achieve this limited symmetry with a fairly simple system of correction coils.

In order to understand the kind of symmetry achieved, consider first Fig. G. 22-1 (a), which represents the perfectly symmetric, ideal case. The ordinate represents the radial aberration ρ in the detector plane for different values of the radial and axial aperture angles ϕ_r and ϕ_z respectively. The aberration pattern shown is that described by the second-order aberration terms; higher orders modify the pattern towards larger magnitudes of ϕ_r and ϕ_z. In the so-called tall-aperture case, which corresponds to a value $a_2 = 3/8$ in the field expansion $B_z = B_0\,[1 - (1/2)\,\frac{r - r_0}{r_0} + a_2\,(\frac{r - r_0}{r_0})^2 + \cdots]$, the aberration parabolas coincide for all values of the axial aperture parameter ϕ_z. The favorable performance of this case at high resolution relies on the possibility of working--over an appreciable range of ϕ_r and ϕ_z--on the flat and coinciding vertex regions of the aberration parabolas.

When an asymmetry is present in the magnetic field, the aberration parabolas become distorted and displaced relative to each other in a way exemplified in Fig. G. 22-1(b). To combine an appreciable range in ϕ_r with a small radial aberration, i. e., a small interval in ρ, one must necessarily use intervals of ϕ_r around a vertex point. Since the vertices for different ϕ_z are now spread out along the ρ axis, it is now impossible to satisfy this requirement within a small range in ρ (i. e., small radial aberration) for any reasonable range in ϕ_z. Hence the solid angle suffers at high resolution.

The complete remedy for the situation of Fig. G. 22-1(b) would be to move, by means of a correction field, the vertices of the aberration parabolas for $\phi_z \neq 0$ along both the ρ axis and the ϕ_r axis until the conditions of Fig. G. 22-1(a) are obtained. In this work, however, only the less demanding condition of moving the vertices to the same position in the ρ direction has been attempted (dotted curves of Fig. G. 22-1b). The ϕ_r position for the vertices then still varies with ϕ_z and the field retains a certain asymmetry. However, by shaping the entrance aperture suitably one can still arrange that, for each ϕ_z, the midpoint of the ϕ_r interval selected by the aperture coincides with the ϕ_r value for the corresponding vertex. The basic requirements for efficient high-resolution performance then become fulfilled.

For the experimental study of the aberration pattern of the spectrometer an electron gun was mounted at the normal source position and the detector replaced by a fluorescent screen that could be observed through a telescope with an eye-piece scale. The gun provided a narrow beam of electrons of about 2.5 keV for any desired pair of aperture parameters ϕ_r, ϕ_z within the aperture. Five identical coils C_1, C_2, C_3, C_4, and C_5 were first wound around the outer tank wall, symmetrically around the midplane of the spectrometer at 8.5-cm intervals. The spectrometer current was adjusted in such a way that the vertex position for $\phi_z = 0$ fell at $\rho = 0$ when the currents $I_1, I_2, \cdots, I_5$ through the extra coils were zero. In this case the relative positions of the vertices for different values of ϕ_z are those shown in Fig. G. 22-2(a). The asymmetry in the pattern clearly appears. Let ρ_N be the radial vertex position for the Nth ϕ_z value. The derivatives $\partial\rho_N/\partial I\mu$ were experimentally determined and used to solve the currents $\Delta I\mu$ from the linear equation system

$$-\rho_N = \sum_{\mu} \frac{\partial \rho_N}{\partial I\mu} \Delta I\mu \quad (\text{for } N = 1, 2, \cdots, 5).$$

It turned out that the initial five-coil set led to unreasonable magnitudes of the currents $\Delta I\mu$, and a sixth coil was added for that reason and the procedure repeated. The solutions $\Delta I\mu$ were used as starting points for a trial-and-error final adjustment of the currents. Figure G. 22-2(b) shows the relative radial vertex positions with the adjustment currents on. Comparison with Fig. G. 22-2(a) gives an indication of the improvement. Finally, the adjustment coils were replaced by coils of different numbers of turns in such a way that the proper number of ampere-turns was obtained with the same magnitude of current through each adjustment coil. The adjustment coils are powered by a separate current supply automatically controlled from the main current supply. Table G. 22-I gives some data for the adjustment coils.

Figure G. 22-3 shows some entrance aperture shapes for two different maximum radial aberrations (expressed in momentum resolution) within the respective apertures. Within the axial aperture $|\phi_z| \leq 0.15$ the performance of the instrument is now essentially equal to that theoretically possible with the $\pi\sqrt{2}$ design. At 0.05% resolution the adjustment has involved an improvement by a factor of about two in solid angle.

A minor disadvantage of the residual asymmetry present with the kind of correction described here is that the axial aberrations are larger than is inherently the case in the proper $\pi\sqrt{2}$ field.

Footnotes

†To be submitted to Nucl. Instr. Methods.
*On leave from the Research Institute for Physics, Stockholm, Sweden.

Table G. 22-I. Some data for the correcting coils (wound around the outermost spectrometer tank). The correcting-coil current amounts to 0.022 of the main spectrometer current. A negative sign at the number of turns means that the coil so designated gives a field opposite that of the spectrometer field.

Coil position (cm relative to spectrometer midplane)	Number of turns
17	2 (-)
8.5	1 (-)
0	18
- 4.3	48 (-)
- 8.5	6
- 17	15

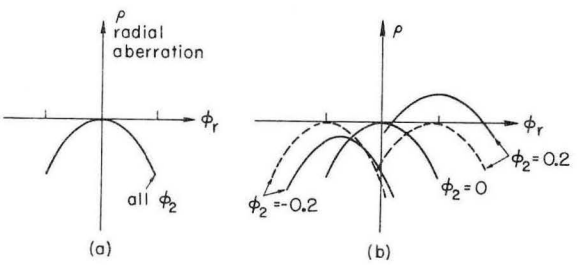

MUB-9308

Fig. G. 22-1. (a) Qualitative pattern for radial aberrations in ideal $\pi\sqrt{2}$ field with $a_2 = 3/8$. (b) Example of pattern of radial aberrations in the same $\pi\sqrt{2}$ field with certain asymmetries present. Solid lines indicate situation in the Berkeley spectrometer before correction, dotted lines after correction as described in this work.

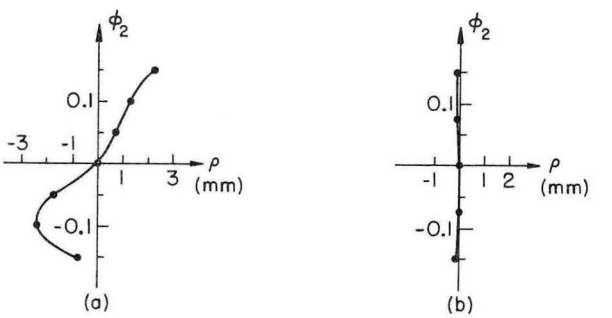

MUB-9309

Fig. G. 22-2. Relative radial positions of aberration parabola vertices in the Berkeley $\pi\sqrt{2}$ iron-free spectrometer: (a) before correction, (b) after correction.

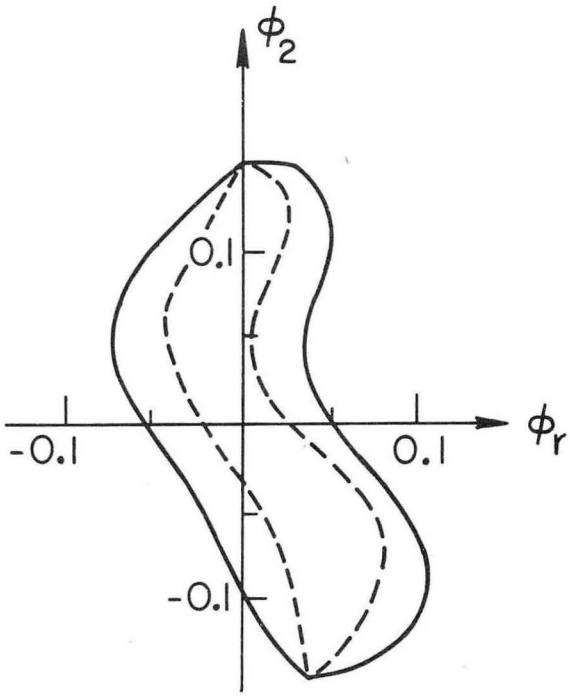

MUB-9310

Fig. G. 22-3. Entrance aperture shapes after field correction for 0.03% (dotted line) and 0.12% (solid line) maximum radial aberration. The ϕ_r and ϕ_z scales are approximate.

23. AZIMUTHALLY VARYING MAGNETIC FIELD WITH SMALL APERTURE DEFECT FOR β-SPECTROMETER APPLICATION

Karl-Erik Bergkvist† and Andrew M. Sessler

In the so-called flat magnetic β spectrometers possessing a symmetry plane and having rotational symmetry, it is impossible to obtain simultaneously second-order radial focusing in both the radial and axial aperture parameters ϕ_r and ϕ_z. In order to get rid of the limitation in transmission (for a given resolution) set by this fact it is necessary to disturb, in one way or the other, the rotational symmetry of the system. Sessler[1] suggested that an azimuthally varying magnetic field (AVF field) could be used, and demonstrated analytically for a special and somewhat idealized case that simultaneous second-order radial focusing in ϕ_r and ϕ_z could be obtained. This case involved an abrupt change of the field coefficients at a certain azimuthal angle. A computer program[2] was later developed here by Sessler and Owens for an AVF field varying smoothly and everywhere fulfilling curl $\mathbb{B} = 0$ and div $\mathbb{B} = 0$. This program, which allows orbit calculations through sixth order, has been used to establish a field which provides radial focusing to very roughly that order. During the course of the present work, a Heidelberg group[3] demonstrated that second-order aperture defect could be made to vanish in a field of type similar to that used here.

The magnetic field B_z in the symmetry plane is expressed by $B_z = B_0 (1 + a_1 x + a_2 x^2 + \cdots)$, where x is the radial departure from the central circle $r_0 = 1$, and the field coefficients a_n are assumed to vary with the azimuthal angle θ as $a_n = A_n + B_n \sin\theta + C_n \cos\theta + D_n \sin 2\theta + E_n \cos 2\theta + F_n \sin 3\theta + G_n \cos 3\theta$ (where A_n, B_n, $\cdots$ G_n are constants).

The main data for the AVF spectrometer field arrived at are given in Table G. 23-I. The radial aberration pattern as well as the shape of the entrance aperture giving an image of a point source with a radial width not exceeding 10^{-3} is shown in Fig. G. 23-1. The solid angle of the entrance aperture is close to 1% of 4π. Since the dispersion is 10 units, the width corresponds to a resolution in momentum of 10^{-4}. Although only first-order axial focusing was conditioned in the choice of the field coefficients, the axial aberration within the aperture indicated never exceeds ±0.02.

The achievement of second-order radial focusing in both ϕ_r and ϕ_z requires that the first-order radial and axial orbit solutions be made unequal (while still retaining simultaneous axial and radial focusing). Some earlier attempts had indicated that when the first-order orbit solutions were made unequal by fairly strong azimuthal dependence of the first-order field coefficient a_1, the azimuthally varying terms in the higher field coefficients tended to grow rapidly when higher-order aberration coefficients were successively made equal to zero. The starting point in this case was the rotationally symmetric field with radial and axial focusing angles equal to $\pi\sqrt{5}$. In this case the first-order radial and axial orbit solutions are already unequal without any AVF terms, since there is one intermediate axial focus between the source and the first radial focus. The simultaneous radial and axial foci were then brought to the value $\theta = 6$ (i.e., $\theta < 2\pi$) by fairly moderate AVF terms in first order. As can be seen from Table G. 23-I, the coefficients for the AVF terms in the field coefficients do not tend to grow with order in this case.

The aberration coefficients were successively made close to zero by utilizing the fact that the aberration coefficients of order n depend linearly on the field coefficients of order n and are independent of field coefficients of orders larger than n. The linear dependence was obtained by means of the computer program by observing the change in aberration pattern when the field coefficients were varied, using a set of orbits in the center of the aperture for the lowest orders and proceeding outwards with increasing order. There may still be room for improvement in the fifth- and sixth-order coefficients in Table G. 23-I. However, seventh- and higher-order terms, inaccessible for adjustment by the present program, are already becoming dominating.

The focusing of the field is very sensitive to departures from the proper field coefficients a_n, and hence an iron-free system should be used to produce the field. Laslett has shown recently[4] that the problem of realizing a given magnetic field in a region where div $\mathbb{B}$ = curl $\mathbb{B}$ = 0 can always, in principle, be solved by means of currents outside this region.

The effort so far has been concentrated upon the achievement of small aperture defect in combination with such magnitudes of the radial dispersion and radial magnification that sources of relatively favorable width can be employed. There exist methods[5] which, in principle, allow complete elimination of the influence of the source area on the resolution for a small aperture. When the aperture is increased, cross terms between source size parameters x_0, y_0 and aperture size parameters enter and ultimately limit the resolution. The lowest-order term of this type is $y_0\phi_2$. In the AVF case dealt with here the magnitude of the coefficient for this term turns out to be fairly large, around0.8—which would rather severely limit the source height at high resolution. In the case studied so far the choice of the second-order field coefficient had a certain arbitrariness, aiming only at eliminating the second-order aperture defect. It is to be expected that by using further degrees of freedom within the present computer scheme in the second-order field coefficients, it should be possible to reduce the magnitude of the $y_0\phi_2$ term. A fuller report of this work is being prepared for publication in Nuclear Instruments and Methods.

The authors are indebted to Herman Owens for generous assistance with the computations.

Footnote and References

† On leave from the Research Institute for Physics, Stockholm.

1. A. M. Sessler, Nucl. Instr. 23, 165 (1963).
2. Herman Owens, ISO--A Fortran Program for Utilizing the Strong-Focusing Principle in Beta-Ray Spectrometer Design, UCRL-16471, Oct. 21, 1965.
3. F. Schmutzler, H. Daniels, and L. Tauscher, Nucl. Instr. 35, 176 (1965).
4. L. Jackson Laslett, An Equivalent Distribution of Surface Currents: For the Generation of a Prescribed Static Magnetic Field Within the Enclosed Volume (submitted to J. Appl. Phys., 1965).
5. K.-E. Bergkvist, Arkiv Fysik 27, 383 (1964).

Table G. 23-I. Some data for an azimuthally varying magnetic field with simultaneous radial and axial focusing for β-spectrometer purposes.

Focusing angle: 6 radians
Solid angle at 0.01% point source resolution: 0.9%
Dispersion ($\Delta r/r:\Delta p/p$): 10.0
Radial magnification: -0.81
Axial magnification: 0.90
Field coefficients:

$a_1 = -1.11473 - 0.659 \cos\theta$
$a_2 = 1.223 + 1.1837 \cos\theta$
$a_3 = -1.1335 - 1.355 \cos\theta$
$a_4 = 0.8865 + 1.277 \cos\theta - 0.0066 \sin 2\theta$
$a_5 = 0.09 + 0.04 \cos\theta + 0.548 \cos 2\theta$
$a_6 = -0.22$

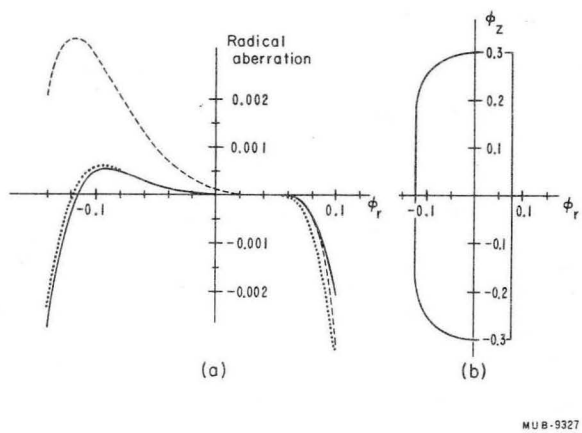

Fig. G. 23-1. (a) Radial aberrations as functions of ϕ_r for three values of ϕ_z. (b) Entrance aperture for radial image width of 0.001 (0.0001 resolution). ——— $\phi_z = 0$; ····· $\phi_z = 0.15$; ----- $\phi_z = 0.3$.

H. CHEMICAL ENGINEERING

1. KINETICS OF BACTERIAL SULFATE REDUCTION

V. H. Edwards and C. R. Wilke

Bacteria of the genus Desulfovibrio use sulfate instead of oxygen as the terminal hydrogen acceptor in their metabolism, producing sulfide. The sulfate-reducing bacteria have many activities of economic importance, including the creation of reducing environments for deposit of ions of uranium and other heavy metals. Information on kinetics of growth of these organisms is limited. Isolation, properties, and batch kinetic data have been reported previously.[1, 2] Some additional batch culture studies and continuous culture results have recently been completed[3, 4] and are summarized here.

Batch experiments were used to determine the effects of the components normally added to the environment of the cells, including ferrous sulfate, sodium sulfate, potassium phosphate, lactic acid, ammonium chloride, calcium chloride, magnesium sulfate, yeast extract, and sodium hydroxide (pH-controlling agent); the concentrations of all were adjusted to give optimum growth and sulfate reduction. A sodium chloride concentration of 10% (w/v) was used in all experiments on the basis of earlier findings.[1, 2]

Results of typical batch culture experiments, designed to determine how the initial pH of the culture affected growth and sulfate reduction, are presented in Figs. H.1-1 and H.1-2. The composition and inocula of the cultures were identical except for pH. The cultures, incubated at 30.0°C, were analyzed for soluble sulfides, cell concentration (by optical count), and pH. The pH values of the cultures at the time that growth had effectively stopped (12 days after inoculation) were 6.72, 6.88, and 6.99, respectively, in agreement with other experiments in which no growth could be obtained when the initial pH was below 7. Also, the highest yield of sulfide was obtained with the culture with the highest pH, suggesting that the higher pH permitted a longer period of growth and metabolism.

Specific rates of growth and sulfide production were calculated from these data. Figures H.1-3 and H.1-4 show that the results could be correlated as a function of specific growth rate, when the method of Luedeking and Piret[5] was used. The correlations do not apply to cultures in the lag phase of growth. Correlations of this type are commonly used to size continuous-flow reactors from batch culture data, but the method does not apply in all cases. To test the correlation in continuous culture, the continuous-flow reactor system diagrammed in Fig. H.1-5 was built. Continuous culture data were obtained by holding all control variables constant until biological variables stabilized. The sulfide concentration was kept approximately constant by continuous introduction of mixtures of nitrogen and hydrogen sulfide through a sintered-glass sparger. Three steady-state growth rates have been studied so far. The cell concentrations and specific rates of sulfide production are shown by the filled circles in Figs. H.1-3 and H.1-4 for the three growth rates studied. These values agree well with the batch data, but final confirmation of the correlation will depend on additional continuous culture experiments at higher growth rates.

A comparison of the limiting value of the specific rate of sulfide production extrapolated in Fig. H.1-4 with the limiting value from a similar correlation obtained by Leban and Wilke with the same organism in a different environment shows excellent agreement. A limiting value of 7.0×10^{-12} mM/cell-day was obtained in the earlier work,[1,2] while a value of 6.9×10^{-12} mM/cell-day was obtained in this work.[3, 4] The limiting value of the specific rate of sulfide production should be directly related to the energy required by the cell for the execution of all nongrowth processes, i.e., the maintenance energy of the cell.

References

1. Mark Leban and Charles R. Wilke, UCRL-10966, 1963.
2. Mark Leban and Charles R. Wilke, UCRL-11213, pp. 154-5.
3. Mark Leban, V. H. Edwards, and C. R. Wilke, UCRL-16420, 1965 (Presented at the U.S.–Japan Seminar on Dynamics of Microbial Populations, Kyoto, Japan, October 1965).
4. V. H. Edwards and C. R. Wilke, Kinetics of Bacterial Sulfate Reduction, UCRL-16398 (in preparation).

5. R. Luedeking and E. L. Piret, Kinetic Study of the Lactic Acid Fermentation Batch Process at Controlled pH, J. Biochem. Microbiol. Technol. Eng. 1, 393-412 (1959).

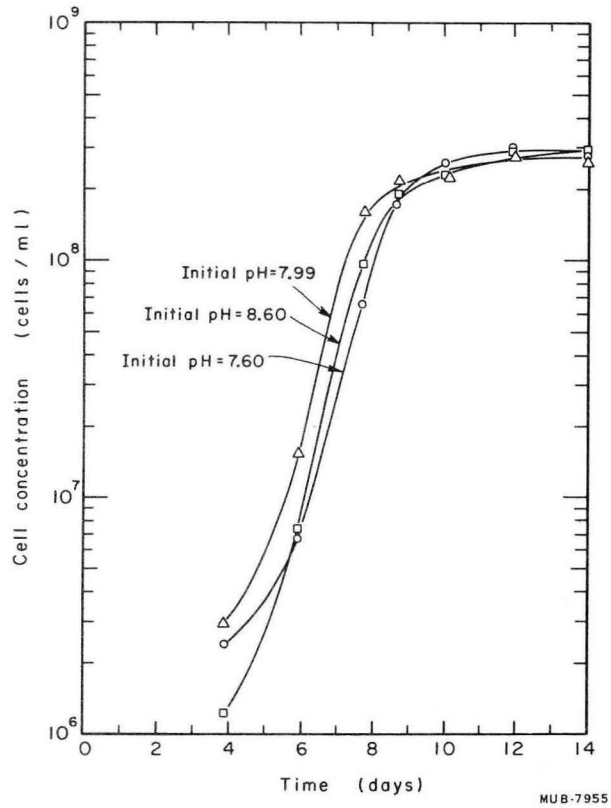

Fig. H.1-1. Cell concentration for different pH values.

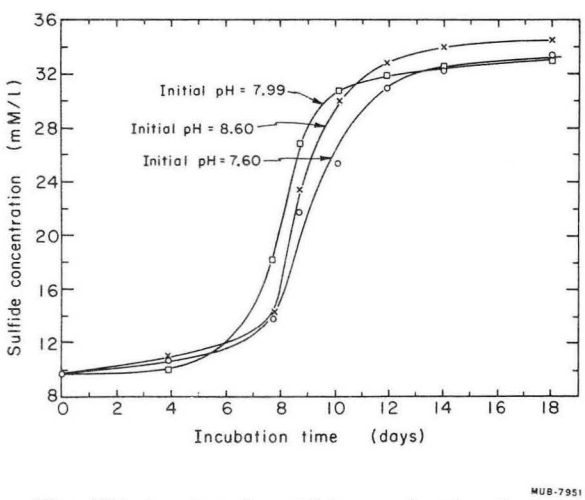

Fig. H.1-2. Batch sulfide production for different pH values.

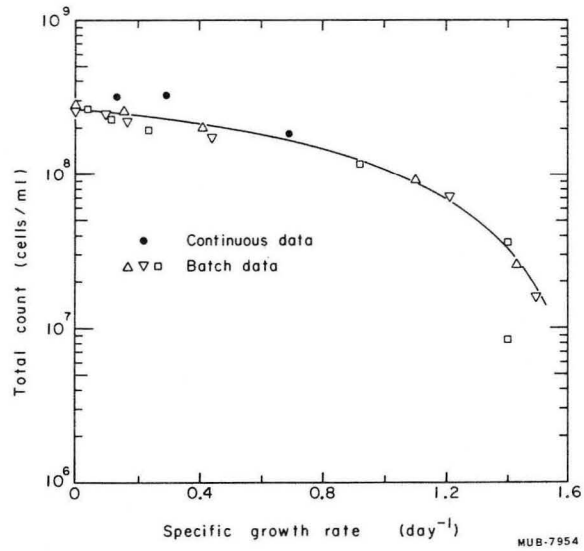

Fig. H. 1-3. Cell concentration vs specific growth rate.

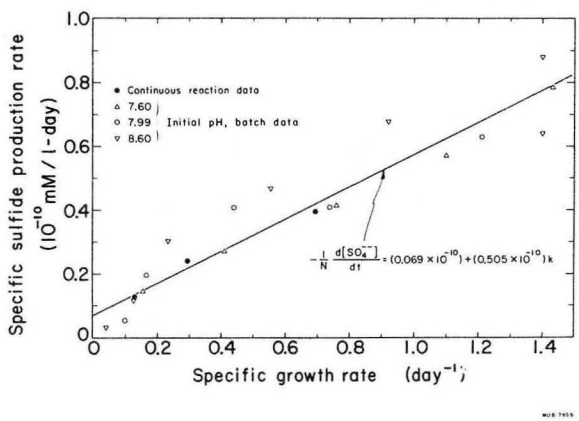

Fig. H. 1-4. Specific rate of sulfate reduction vs specific growth rate.

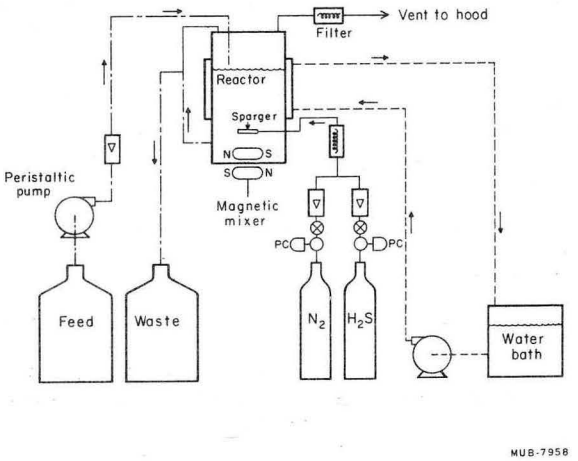

Fig. H.1-5. Flowsheet of early continuous reactor system.

2. INTERPHASE MASS AND HEAT TRANSFER IN LAMINAR FLOW

Charles H. Byers and C. Judson King

A rectangular channel has been built to study laminar interphase transfer processes in the presence of a moving interface. The overall program will encompass studies of pure mass transfer, and heat transfer, simultaneous heat and mass transfer at low fluxes, and, finally, problems of high flux. The present investigation is concerned with the construction of the basic apparatus and with the pure mass transfer aspects of the work.

The main section of the apparatus consists of a horizontal 1×3-in. polycarbonate plastic channel, which is shown in Fig. H.2-1. Two immiscible fluids pass through the channel in stratified flow. For the first 2.5 feet of travel in the channel the two fluids are kept separate by a thin metal divider plate. This allows an adequate calming section. The fluids are then exposed to each other in a 1.5-ft-long test section, after which they are once again separated in a similar 2.5-ft downstream calming section. The upper phase is gas which is taken from cylinders, brought into contact with the liquid phase in the test section, and then vented to the atmosphere. The exit gas is analyzed for the transferring component with a gas-liquid chromatograph. A closed recirculating system was found to be best for maintaining satisfactory level control upon the liquid phase. The concentration of the transferring component in the liquid is determined with either a differential interferometer or the chromatograph, depending upon which liquid system is used.

Before an interphase study was undertaken, experiments with control of the mass transfer completely residing in one or the other phase were considered. Since Tang and Himmelblau[1] have shown in a similar experiment that in the case of control in the liquid phase the penetration model is followed to within 7%, it was decided that a study of the liquid phase was unnecessary. Evaporation of a pure liquid (ethyl alcohol in this experiment) into a pure gas (oxygen) provided gas-phase mass transfer control. Mass transfer to a gas flowing in a channel over a stationary liquid is one of the classical Graetz mathematical solutions. The solution by Butler and Plewes[2] of this problem with an unsymmetric flux boundary condition correlated the experimental data with less 5% error for the series of 10 runs at different gas flows. Each point of a concentration profile taken for one flow rate agreed with the corresponding theoretical point to within 10%. The cup mixing concentration calculated from the points of the profile agreed almost perfectly with the theoretically predicted value.

Gas-phase-controlled mass-transfer studies with a moving liquid were carried out with pure ethanol used as the liquid and oxygen as the gas phase. A theoretical solution for mass transfer to a phase with a moving interface and a positive linear slope in velocity away from the interface has been presented by Beek and Bakker[3] and has been modified in this work. A computer solution has been carried out for mass transfer to a laminar flow in a confined channel with a wall moving in the direction of the flow, where the transfer occurs at the moving wall. The values for the mass-transfer coefficient by computer methods agree quite well with those obtained by the approximate analytical solution, except at concentrations close to saturation. Experiments made

with the physical system described above showed very good agreement with theory (less than 10% error), while concentration profiles taken on three of the runs agree within the same error with the profiles generated by the computer solution.

Since the case of countercurrent flow is of great industrial importance, a series of runs was made with the direction of flow of the liquid reversed but still operating with a pure liquid. Although a detailed analysis of the data has not yet been made, it may be stated that the rates of mass transfer are generally lower than those which would be found for no liquid flow.

It is interesting to note that these theoretical and experimental determinations of the effect of a moving interface give corrections in the opposite direction from the classical procedure of referring the gas velocity to the moving liquid surface velocity.

Studies have been carried out with the mass-transfer control divided between the phases. In conjunction with an experimental program, an analytical solution has been derived for co-current flow of a gas over a liquid. The solution is for a linear profile of velocity in the liquid phase and linear slope of velocity in the gas phase. When this hydrodynamic model is used, rates of mass transfer can be predicted for situations in which the resistance to transfer is distributed between the two phases. The model has been tested experimentally with use as a liquid phase of 0.5 mole % diethyl ether in alcohol transferring to two different gases, helium and carbon dioxide. Figure H.2-2 shows the experimental data for ether transferring to carbon dioxide, along with the theoretically predicted line for this system.

It was found that when ether is transferred from dilute solutions in water to a gas phase the interface almost immediately becomes stagnant. This phenomenon is discussed by Merson and Quinn.[4] It may be attributed to the rapid accumulation of trace surface-active agents at the interface.

References

1. Y. P. Tang and D. M. Himmelblau, A. I. Ch. E. J. 9, 630 (1963).
2. R. M. Butler and A. C. Plewes, CEP Symposium Series, #10, 50, 121 (1954).
3. W. J. Beek and C. A. P. Bakker, Appl. Sci. Res. 10, 241 (1961).
4. R. L. Merson and J. A. Quinn, A. I. Ch. E. J. 11, 391 (1965).

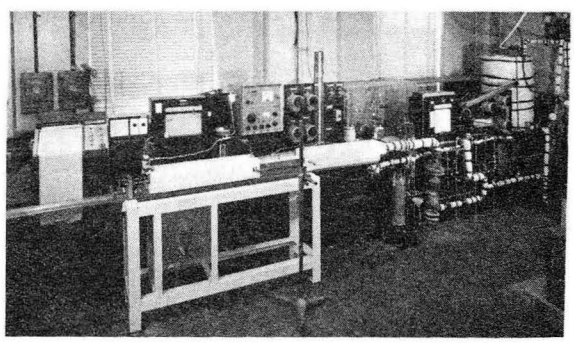

Fig. H.2-1. Overall view of two-phase laminar flow channel.

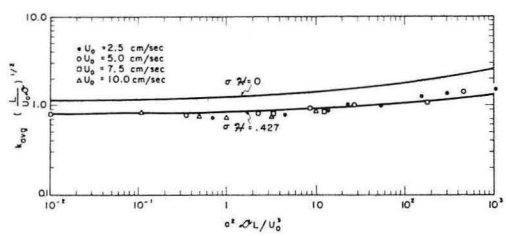

Fig. H.2-2. Overall mass-transfer data.

I. THESIS ABSTRACTS

On the following pages the abstracts of theses issued in 1965 are given as they appeared in the original documents.

1. DEVELOPMENT OF SOME HIGH-SPEED CHROMATOGRAPHIC METHODS

Sergio Ajuria-Garza
(M. S. Thesis)

(From UCRL-16015)

A thin-layer chromatography method has been developed using as stationary phase a fine mesh ion exchange resin without any admixture, thus eliminating the effects due to binding materials. The plates can be developed by the ascending, descending, horizontal or centrifugal technique. The spots obtained can be removed mechanically by several methods. An apparatus and a method of operation were developed for the centrifugal acceleration of thin-layer chromatography on 5 X 30 cm glass plates with a substantial reduction in the time of development.

A universal chromatographic chamber equally suitable for horizontal, centrifugal, ascending or descending chromatography either of paper strips or thin-layer plates is described in detail. A comparison was made of the rate of progress of the solvent front in the different chromatographic methods. The speed of the front decreases sharply as the distance from the origin increases except in the centrifugal case in which the speed remains constant.

A method of tandem horizontal or centrifugal chromatography is described which permits to increase the length of a chromatogram in order to separate two substances with very similar R_f values. The length of the chromatogram is only limited by the diffusion of the spots.

The above methods are applied to the separation of Zr^{95}-Hf^{181}, Zr^{95}-Nb^{95} and Am^{241}-Cm^{244}. The radiochromatograms were evaluated by direct scanning and autoradiography. These methods are also discussed.

2. NUCLEAR SPECTROSCOPIC STUDIES OF POLONIUM-204

Jiann-min An
(M. S. Thesis)

(From UCRL-16324)

Sources of Polonium-204 were derived from the electron capture decay of Astatine-204 made by bombarding Au^{197} with C^{12} in the Heavy Ion Linear Accelerator at Berkeley. Physical and chemical methods were adjusted to make the sources as pure as possible for the measurements.

Using scintillation crystals coupled to a 400 channel pulse-height analyzer, an investigation of some of the nuclear radiations of Po^{204} has been made. Gamma rays from Po^{204} were identified by their half life; their energies and relative intensities were carefully determined and the alpha branching ratio was measured.

3. QUADRUPOLE COUPLING IN RARE EARTH CRYSTALS

Johan Blok
(Ph.D. Thesis)

(From UCRL-16279)

The electric field gradient at the nucleus was obtained for the rare earth ethylsulfates and double nitrates of La^{+3}, Eu^{+3}, Gd^{+3}, and Lu^{+3} by measuring the quadrupole coupling constants via nuclear orientation. From a comparison with the calculated antishielding factor and the measured crystal field gradients we arrive at the ionic shielding factors for the rare earths. These shielding factors are observed to vary considerably through the rare earths. These experiments also yielded the nuclear quadrupole moment of La^{140}. We obtained $Q = +0.121(12)$ barns.

These measurements required a precise knowledge of the temperature susceptibility relationship for cerium magnesium nitrate and for neodymium ethylsulfate. The temperature scale for cerium magnesium nitrate has recently been determined quite accurately; thus it was used without reservations. For neodymium ethylsulfate, however, we determined the temperature scale at low temperatures using gamma-ray heating and nuclear orientation. We found considerable discrepancy with the previously published work.

We also made an exhaustive study of the decay of 155-day Lu^{177}. We determined the relative intensities and precise energies of many of the gamma rays in this complex decay. From nuclear orientation of the 7-day and the 155-day Lu^{177} isomers we determined the ratio of the nuclear quadrupole moments of the 155-day metastable state and the 7-day ground state. We found $Q_m/Q_g = +2.33(25)$. For gamma rays following the 1-second intermediate state in Hf^{177} we found the unattenuated value of the anisotropy. We conclude that no reorientation takes place in this 1-second state.

4. COLLECTIVE EXCITATION OF NEUTRON-DEFICIENT BARIUM, XENON, AND CERIUM ISOTOPES: CENTRIFUGAL STRETCHING TREATMENT OF NUCLEI

Jack E. Clarkson
(Ph.D. Thesis)

(From UCRL-16040)

The collective excitation of various neutron-deficient barium, xenon, and cerium isotopes by the "in-beam" method using lithium-drifted germanium counters has been obtained. The (heavy ion, xn) reaction has been used to produce Ba^{126}, Ba^{124}, Xe^{122}, Xe^{120}, and Ce^{134}. The decay of Pr^{134} to Ce^{134} was also observed, with a half life of 17±2 minutes. Partial level schemes for the ground-state rotational bands to spin 8+ or 10+ are proposed for the nuclides investigated. The lifetime of the first-excited state in Ba^{126} has been determined as an "in-beam" experiment to be $2.7 \pm 0.5 \times 10^{-10}$ seconds and, hence, gives the deformation of Ba^{126} as $\beta = 0.24 \pm 0.02$.

The implications of the rotational energies and spacings as related to deformation in this region are discussed.

A classical centrifugal stretching treatment employing realistic nuclear potentials is developed and the results of this and other works are compared to the calculated energy levels from this treatment.

5. NUCLEAR STUDIES USING SEMICONDUCTOR DETECTORS

Richard Barry Frankel
(Ph. D. Thesis)

(From UCRL-11871)

Germanium surface barrier detectors were used to measure the angular distribution of conversion electrons from the 255 keV isomeric transition in Ce^{137m} for Ce^{137m} nuclei aligned in the neodymium ethylsulfate lattice. Direct comparison with the γ-ray angular distributions gave the particle parameters $(b_2)_k = 1.061(18)$, $(b_2)_L = 1.059(20)$. From the variation of the γ-ray anisotropy with temperature, the hyperfine coupling constant for Ce^{137m} was determined to be $A = 0.0147(7)\ cm^{-1}$ using the 1957 temperature scale for this salt.

Ce^{137m} was also aligned in cerium magnesium nitrate and the variation of the 255 keV γ-ray anisotropy was studied as a function of temperature. Anomalies were shown to exist in the cerium magnesium nitrate temperature scale derived by Daniels and Robinson. A new temperature scale is proposed which goes down to 0.0019°K. To test the new scale, Pm^{144} was aligned in cerium magnesium nitrate. The anisotropies of the 615 and 695 keV γ rays were found to be attenuated, but confirmed the Ce^{137m} results.

The decay of Ce^{137m+g} to La^{137} was investigated with Ge(Li) γ-ray detectors, Si(Li) electron detectors, and nuclear alignment. Levels were found at 10, 446, 492, 708, 762, 781, 835, 925, 1004, and 1170 keV. Definite spin and parity assignments were 762 keV (11/2+), 835 keV (9/2+), and 1004 keV (11/2-). A spin of 5/2+ was tentatively assigned to the 446 keV level. The 11/2- state corresponds to a quasiparticle state predicted by Rho.

The distribution of alpha particles from E^{253} oriented in neodymium ethylsulfate was measured using germanium surface barrier detectors. The L=4 wave in the ground-state transition was found to be out of phase with the L=0 and L=2 waves. The L=4 wave was found to have a larger amplitude and the L=2 wave a smaller amplitude than predictions based on the Bohr, Froman and Mottelson coupling relations. The relative amplitudes for the ground-state transitions are $a_0 = 1$, $a_2 = 0.11$, and $a_4 = 0.016$.

6. OXYGEN INITIATED PYROLYSIS OF ETHYLBENZENE

Edwin D. Hausmann
(M. S. Thesis)

(From UCRL-16021)

The effect of small quantities of oxygen (0 to 10%) on the thermal decomposition of ethylbenzene in the temperature range of 570-650°C was investigated utilizing a flow reactor with residence times of from 0.06 to 0.18 seconds and ethylbenzene concentrations of less than 10%. Twenty-one runs were made with oxygen excluded, and the data fitted, using a multiple regression analysis, to the following form of the law of mass action:

rate of conversion to styrene =

$$4.04 \times 10^{12} \exp(-68,600/RT)\,(EB)^{0.41}\ g.mole/cm^3\ sec.$$

The liquid product yield pattern of 74 mole % styrene, 23% benzene, and 3% toluene was found to be independent of temperature and reactant concentration. A mechanism is postulated which is in accord with the reaction order, apparent activation energy and yield pattern.

Small quantities of oxygen increase the rate of thermal decomposition but this effect tapers off as the oxygen concentration is increased. With an oxygen concentration of 2.5% the same level of conversion is achieved at a temperature 10°C lower than that required when oxygen is excluded. The styrene yield selectivity increases from 74 mole % without oxygen to 81 mole %

with 10% oxygen. When the data are fitted to a law of mass action expression, oxygen is found to lower the apparent activation energy to 60,000 cal/gm-mole and to lower the order with respect to ethylbenzene slightly. Possible initiation and termination reaction steps involving oxygen are suggested to explain the results, but it is not possible to test any definite reaction mechanism for the oxygen initiated pyrolysis of ethylbenzene reliably.

7. ISOMERIC CHEMICAL SHIFTS AND ELECTRONEGATIVITY

David A. Keller
(M. S. Thesis)

(From UCRL-16436)

Mössbauer experiments were carried out at 4.2°K using Au^{197} and Sn^{119} as solutes in dilute binary alloys to study the relationship, if any, between the isomeric chemical shift and the difference in electronegativity between the solvent metal and the Mössbauer element.

Au^{197} was embedded into nineteen host lattices and the resulting isomeric chemical shifts of the Mössbauer resonance did show a positive correlation between the chemical shift and electronegativity.

However, similar experiments using Sn^{119} as the Mössbauer solute in six metallic lattices failed to show any correlation at all between chemical shift and electronegativity.

8. REACTIONS OF He^3 WITH LIGHT ELEMENTS: APPLICATIONS TO ACTIVATION ANALYSIS

John D. Mahony
(Ph.D. Thesis)

(From UCRL-11780)

A simple, rapid technique of analyzing for carbon, oxygen, and fluorine, individually and simultaneously by He^3 activation is presented. This method, which can easily be extended to other elements, is capable of analyses at the ppb level or even less in some cases and an ultimate accuracy of 5%. Milligram amounts of total sample are sufficient and are not destroyed in the analysis. The advantages of this technique with especial reference to energetics, versatility and the elimination of interferences are discussed and compared to those of other charged-particle and neutron-activation analysis procedures.

The excitation functions for the production of F^{18} from O^{16}, C^{11} and N^{13} from C^{12}, and F^{18} from F^{19} by He^3 reactions for the energy range, 0 to 31 MeV have been determined and are discussed with particular application to activation analysis.

An absolute analysis for oxygen in thorium was performed; simultaneous absolute analyses of gold, silicon, Mylar, and polyethylene for carbon and oxygen, and Teflon for carbon and fluorine are described. Results of analyses by the relative method for oxygen in thorium, beryllium, niobium, and lead are also reported.

Although the Berkeley Hilac was used for the work described, a small cyclotron is shown to be quite adequate for extensive He^3 activation analysis. The specifications of such an accelerator are given.

9. MAGNETIC PROPERTIES OF CURIUM METAL AND ITS COMPOUNDS

Sayed A. Marei
(Ph.D. Thesis)

(From UCRL-11984)

The magnetic susceptibility of curium metal has been measured from -253 to 250°C. The metal followed Curie-Weiss law above liquid nitrogen temperature up to the temperature studied. The effective magnetic moment for the metal was found to be 7.99±0.15 indicating the presence of $5f^7$ configuration in the metal. No magnetic transition was observed in the temperature range studied.

The magnetic susceptibility of Cm^{+3} in curium trifluoride, curium oxychloride, and 5.6 mole percent curium trifluoride diluted with lanthanum trifluoride has been measured. The effective moment for Cm^{+3} was found to be 7.65±0.1 Bohr magnetron, giving a Lande g factor of 1.93±0.03, pointing toward an appreciable departure from Russell-Saunders coupling. The molecular field constant Δ was found to be small and decreasing with increasing magnetic dilution. The following Δ values were found for curium compounds.

Compound	Δ^{o}
CmOCl	23±3
$CmF_3 \cdot 1/2\ H_2O$	5±3
5.6% CmF_3	5±3

10. DECAY SCHEMES OF ODD-ODD EINSTEINIUM ISOTOPES

William Charles McHarris
(Ph.D. Thesis)

(From UCRL-11784)

The radiations from the heavy odd-odd, alpha-emitting isotopes, $_{99}Es^{254}_{155}$ and $_{99}Es^{252}_{153}$, were studied and interpreted in light of the Bohr-Mottelson unified theory of deformed nuclei and the accompanying Nilsson wave functions. The study was based on their alpha-particle spectra, which were obtained both with Si alpha detectors and with a high-resolution, double-focussing magnetic spectrograph. Complementing these were gamma-ray spectra obtained with NaI scintillators and Ge gamma detectors, conversion-electron spectra obtained with Si electron detectors and precision permanent-magnet spectrographs, and various time-to-height and delayed-coincidence spectra.

Levels in the daughter nuclei were grouped into rotational bands, and the experimental properties of these were compared with predictions based on couplings of the odd-nucleon states found in neighboring odd-mass nuclei. Agreement was found to be excellent, indicating that the odd proton and odd neutron in these odd-odd states move with considerable independence of each other.

The decay scheme of Es^{254} was worked out in detail, indicating that the 6.437 MeV, favored alpha group populates a $K\pi I = 7+7$ level at 85.5 keV above the ground state of Bk^{250}. A cascade of three electromagnetic transitions is required to de-excite this level to the 2-2 ground state: (1) a 7-keV E2, with a half life of 213 μsec, that leads to a 4+5 level at 78.1 keV above ground, (2) a fast 42.6-keV M1-E2 rotational transition to the 4+4 level at 35.5 keV, and (3) branching transitions, mostly a 35.5-keV M2, that give the 4+4 level a 29 μsec half life and connect it with the ground state. Many subsidiary bands and levels were also studied and assigned.

11. AXIAL DISPERSION IN LIQUID FLOW THROUGH PACKED BEDS

Steven Frank Miller
(M. S. Thesis)

(From UCRL-11951)

Step-function injection and purging of a dilute salt tracer in water was used to measure axial dispersion for low Reynolds number liquid flow through beds of uniform sized, random packed glass spheres. The resultant data and those of several previous studies are coordinated and interpreted in terms of Reynolds number, Schmidt number, and Peclet number.

12. THE PRODUCTION OF TRITIUM LABELED METHANE AND ETHANE IN THE CH_4-T_2 SYSTEM

John B. Nash
(Ph.D. Thesis)

(From UCRL-16009)

The rates of incorporation of tritium into labeled methane and ethane in the methane-tritium system has been investigated. The production of the tritiated products can be expressed by a sum of two terms. The first term of this expression is independent of time, and is the decay-induced labeling; the other, inversely proportional to time, is the radiation-induced labeling. The rate of incorporation of tritium into product as a result of the radiation field is shown to have a dependence on the absolute molecular concentration of tritium as well as its concentration as a source of radiation. The yields of labeled methane and ethane from the decay labeling is directly proportional to the rate of decay of the tritium. The rate of incorporation of tritium into labeled ethane is larger than that for incorporation into tritiated methane. A mechanism for both series consistent with the results is proposed. The effect of additives was also determined. Addition of hydrogen elucidated the rate of labeling from the decay-induced series. Xenon was shown to enhance the product yield by 15 percent in concentrations up to 30 mole percent. Addition of ethylene in amounts less than 2 mole percent suppressed the labeling rate until the ethylene had disappeared by reaction with the radiolytic products. The effect on product formation of varying the pressure and the surface to volume ratio is also discussed.

13. THEORETICAL ALPHA DECAY RATES OF DEFORMED NUCLEI

John Kenneth Poggenburg, Jr.
(Ph.D. Thesis)

(From UCRL-16187)

The shell-model theory of alpha decay developed by Mang is summarized. The calculation of the alpha formation entails use of the pairing-force wave functions of superconductivity theory, and we briefly describe their calculation with a delta-force approximation. The penetration of the alpha particle through the anisotropic potential barrier is considered in detail. We study the approximate treatment of Fröman and the results clearly justify the method.

The particular features of the potential barrier are examined in terms of the WKB expression for barrier transmission. The Woods-Saxon potential $V = -74/(1 + \exp\{(r-1.17A^{1/3}-1.6)/(a)\})$ is chosen after a survey of recent optical model analyses of alpha scattering experiments. The Woods-Saxon potential results in penetrability factors that are $\approx$45% lower than those calculated with the Igo potential. Modification of the Coulomb potential has little effect on the penetrability.

Extensive numerical calculations are given in an appendix. The theory gives reasonable agreement with experiment, and has provided a clear example of its value in the analysis of the alpha decay of Am^{241}. The calculations predict relative amplitudes and phases of importance in interpretation of angular correlation experiments. They also predict the ℓ-wave mixing in the transition to final states of odd-mass nuclei. Comparisons of theoretical and experimental transition rates indicate the nature of the errors in the calculations. Suggestions are given for future improvement.

14. EFFECTS OF COLLECTIVE EXCITED STATES ON ALPHA PARTICLE BARRIER PENETRABILITY

Elizabeth A. Rauscher
(M. S. Thesis)

(From UCRL-11875)

For the alpha decay of Po^{212} to the ground state and various excited states of the Pb^{208} daughter, there are collective surface vibrational modes, which couple these low-lying excited states to the ground state of Pb^{208}. In the present description of the transitions between these excited states of Pb^{208} and the ground state of Pb^{208} only single phonon excitations will be considered.

Interaction of the electric multipole nature occurs between the excited state levels and the ground state of the recoil lead daughter induced by its interaction with the emitted alpha particle, affecting the latter's penetration of the nuclear barrier.

The formation of the excitation in the lead nucleus can either be produced by Po^{212} alpha decay or by (α, α') inelastic scattering on Pb^{208}, but in either case we consider that an alpha cluster exists in the nuclear surface region.

It is the purpose of the present paper to investigate the manner in which the multipole interaction affects the alpha particle penetration of the nuclear barrier.

15. THE ELECTROMAGNETIC LEVITATION OF METALS; THE DESIGN, CONSTRUCTION, AND OPERATION OF A DIFFERENTIAL MICROMANOMETER; STUDIES OF ATOMIC HYDROGEN AT LOW PRESSURES

Peter Roland Rony
(Ph.D. Thesis)

(From UCRL-16073)

This dissertation is divided into three parts for convenience of presentation. One abstract of each part is given below.

Part I

A complete theoretical description of the electromagnetic levitation of metals is given, leading to the basic equations for the lifting force and power input for a metal sphere levitated in an inhomogeneous sinusoidally alternating magnetic field. The suspended metal is suitably controlled either by operation at lower frequencies and addition of heat with an electron beam, plasma-arc torch, high-frequency induction heater, or reflection furnace, or by operation at high frequencies and employment of high-thermal-conductivity gases such as hydrogen and helium to cool the metal.

Values indicating the ease of levitation of 1-cm-radius spheres of more than 50 different metals at 0°C and at their respective melting points are given. When frequencies in the 10 to 100 kc/sec are used, the density of the metal chiefly determines the ease of levitation. Refractory, semiconducting, or dielectric materials can be levitated either by the heating of them to high temperatures to decrease their electrical resistivity or by the coating of a light and inert metal of high melting point with the material to be studied.

Liquid sodium surrounded by a mineral oil of almost identical density can be used in the study of the magnetic-field distribution of levitation coils. Liquid mercury can be used to determine the ability of levitation coils to suspend high-temperature liquid metals.

Part II

A differential micromanometer capable of measuring 100 μtorr to an accuracy of ±2% has been designed, constructed, and tested. The pressure difference is sensed by a membrane manometer constructed as a differential capacitor that forms two legs of a resonant-bridge network excited by a radio-frequency source.

The most favorable system found to date consists of a pressure transducer (Decker Corporation Model 306-2A) operated open loop with the bridge and electronics. Differential pressures as low as 50 μtorr can be measured with a zero drift of 1 μtorr per min or 30 μtorr per hour. Differential pressures of 0.5 μtorr are detectable.

The micromanometer is calibrated electrostatically. The diaphragm constant K in the formula, $\Delta P = K V^2$, is determined to ±2% by the comparison of a known voltage and a calibrated McLeod gauge.

Part III

The theoretical description of diffusion and flow tubes is extended to the following situations: (a) the discharge zone is of finite length, (b) the discharge-zone walls are inactive catalytically, (c) the end-plate sink is composed of two or more catalytic materials, and (d) the atom-recombination coefficients on the discharge- and reactor-zone walls differ in magnitude. The dimensionless groups characterizing the rate processes within the system are systematized.

A Wrede-Harteck gauge, which is capable of detecting atom concentrations of less than 0.06% at 75 mtorr, indicates that the presence of small amounts of water does not influence the yield of atomic hydrogen from a microwave or 50-MHz discharge. This result is independent of the measurement technique, the source of hydrogen, the source of water, and the discharge power.

Small amounts of oxygen stoichiometrically increase the yield of atomic hydrogen from the low-pressure discharge by a ratio of at least two atoms of hydrogen per molecule of oxygen. Molecular nitrogen has a similar but smaller effect.

The location of an active catalytic probe affects the atom concentration level throughout a diffusion tube. A cyclotron-resonant microwave discharge operates in the low-pressure system with powers as low as 250 mW. The intensity of the Balmer lines or color of low-pressure hydrogen discharges is not a reliable qualitative indication of the atomic-hydrogen yield. Requisite conditions for the proper use of an isothermal calorimeter are also discussed.

16. DECAY OF THE Zn^{64*} COMPOUND NUCLEUS FORMED BY NUCLEAR REACTIONS OF p, He^3, He^4, AND C^{12} WITH Cu^{63}, Ni^{61}, Ni^{60}, AND Cr^{52}, RESPECTIVELY

Charles F. Smith, Jr.
(Ph.D. Thesis)

(From UCRL-11862)

An experimental, radio-chemical determination of the excitation functions for reactions involving the $[Zn^{64}]^*$ compound nucleus has been performed. The reactant pairs are: $p + Cu^{63}$, $He^3 + Ni^{61}$, $He^4 + Ni^{60}$, and $C^{12} + Cr^{52}$, while the observed products for each such pair are: Zn^{63}, Zn^{62}, and Cu^{62}. Total reaction cross sections are calculated from the optical model. The ratio of the cross section for a given reaction to the total reaction cross section is compared on an excitation energy absissa for each product. The shape and magnitude of these ratio curves is essentially constant in each such comparison, suggesting a compound nuclear reaction mechanism. Range measurements for Zn^{62} recoils are made and compared to calculated ranges based on the theory of Lindhard, Scharff and Schiøtt for a compound nuclear reaction. Good agreement is found. The shapes of these curves are compared to a theoretical estimate obtained from evaporation theory, and are shown to be similar to the calculated shapes. A displacement of the

experimental curves relative to one another along the excitation energy axis is noted, and ascribed to angular momentum effects. Using the position of the Zn^{64} photoexcitation curves of Sagane as reference points, and spin averaged angular momenta of the compound system, the reduced moment of inertia is calculated for the four systems. At least two distinct values are found, indicating a difference between orbital- and spin-angular momenta, the latter causing the greater energy shift in the excitation functions. This observation is shown to be of value in understanding similar energy discrepancies in excitation function comparisons. Because of the observed relationship between the mode of formation and the mode of decay of the compound nucleus, it is concluded that the independence postulate is not strictly applicable to this system as a whole.

17. SCATTERING OF 50.9 MeV ALPHA PARTICLES FROM Ne^{20} AND Ca^{40}

Arthur Springer
(Ph.D. Thesis)

(From UCRL-11681)

More than a dozen inelastic levels of both Ne^{20} and Ca^{40} were excited by inelastic scattering of 50.9 MeV alpha particles. Differential cross sections for these excitations were measured, and by analysis with the Austern and Blair model, one-step and two-step excitation processes were distinguished from each other. Spins, parities, and reduced transition probabilities were also extracted with the aid of this model. This information was then used to discuss the collective nuclear structure of Ca^{40}, which is vibrational, and Ne^{20} which has rotational bands based on both the ground state and octupole vibrations.

J. AUTHOR INDEX

1. PAPERS PUBLISHED AND UCRL REPORTS ISSUED, 1965

AJURIA-GARZA, Sergio
Development of some high-speed chromatographic methods
UCRL-16015, June 1965

M. S. Thesis

ALAGA, G., and G. Ialongo
Semi microscopic description of $Hg^{198}I$
UCRL-16385, September 1965

ALI, Dolores, Isaac Maleh, and Richard Marrus
Hyperfine structure and nuclear moments of promethium-148 and erbium-165
UCRL-11836, January 1965

Phys. Rev. 138, B1356 (1965)

ALI, Dolores
Spins of gadolinium-153, dysprosium-159, and promethium-148
UCRL-11837, January 1965

Nucl. Phys. 71, 441 (1965)

ALSTER, Jonas, and Homer E. Conzett
Comparison between phase shift and complex potential descriptions of elastic scattering
UCRL-11975, February 1965

Phys. Rev. 139, B50 (1965)

AN, Jiann-min
Nuclear spectroscopic studies of polonium-204
UCRL-16324, August 1965

M. S. Thesis

ASARO, F. (See Gunter, K., UCRL-16582)

ASARO, F. (See Stephens, F. S., UCRL-16192)

ATKINS, Harriette L. (See Weeks, B. M., UCRL-11970 Abstract)

BANSAL, Brij M. (See Wallmann, J. C., UCRL-16468)

BAUMGARTNER, E., H. E. Conzett, E. Shield, and R. J. Slobodrian
Determination of the neutron-neutron scattering length from the reaction $T(d, He^3)2n$
UCRL-16528, December 1965

Phys. Rev. Letters

BLOK, Johan
Quadrupole coupling in rare earth crystals
UCRL-16279, July 1965

Ph.D. Thesis

BLOK, J., and D. A. Shirley
Nuclear orientation of La^{140}, Eu^{154}, Gd^{159}, Lu^{177}, and Lu^{177m} by Sternheimer antishielding
UCRL-16328, August 1965

Phys. Rev.

BLOK, J., and D. A. Shirley
Systematic variation of quadrupole crystal-field shielding in rare-earth ethylsulfates
UCRL-16318, August 1965

Phys. Rev.

BLOK, J., D. A. Shirley, and N. J. Stone
The temperature scale for neodymium ethylsulfate below $1^{o}K$
UCRL-16345, August 1965

Phys. Rev.

BOSCHITZ, E. T., M. Chabre, H. E. Conzett, and R. J. Slobodrian
Energy dependence of the polarization in p-O^{16} elastic scattering between 21 and 53 MeV
UCRL-16217, August 1965

International Conference on Polarization Phenomena of Nucleons, Kernforschungszentrum Karlsruhe, September 6-10, 1965

BOSCHITZ, E. T., M. Chabre, H. E. Conzett, E. Shield, and R. J. Slobodrian
Polarization in p-He^4 scattering between 27 and 63 MeV
UCRL-16216, August 1965

International Conference on Polarization Phenomena of Nucleons, Kernforschungszentrum Karlsruhe, September 6-10, 1965

BOSCHITZ, E. T., M. Chabre, H. E. Conzett, E. Shield, and R. J. Slobodrian
Proton polarization in small angle p-He^4 scattering at 38.7 MeV
UCRL-11964, February 1965

Phys. Rev. Letters

BOSCHITZ, E. T., M. Chabre, H. E. Conzett, and R. J. Slobodrian
Study of the $He^4(p, d)He^3$ reaction with polarized protons at 55 and 63 MeV
UCRL-16218, August 1965

International Conference on Polarization Phenomena of Nucleons, Kernforschungszentrum Karlsruhe, September 6-10, 1965

BOSCHITZ, E. T. (See Conzett, H. E., UCRL-16130 Abstract)

BOSCHITZ, E. T. (See Hendrie, D. L., UCRL-11912 Abstract)

BOSCHITZ, E. T. (See Pugh, H. G., UCRL-11940)

BOWMAN, Harry R., E. K. Hyde, Stanley G. Thompson, and Richard C. Jared
Application of high-resolution semiconductor detectors in x-ray emission spectrography
UCRL-16485, November 1965

Science

BOWMAN, Harry R., Stanley G. Thompson, Rand L. Watson, S. S. Kapoor, and John O. Rasmussen
The prompt gamma ray, prompt electron and prompt x-ray spectra associated with fission fragments of specific mass
UCRL-11902, January 1965

IAEA Symposium on the Physics and Chemistry of Fission, Salzburg, Austria, March 22-25, 1965

BOWMAN, H. R. (See Kapoor, S. S., UCRL-16208)

BOWMAN, H. R. (See Watson, R. L., UCRL-16184)

BRITT, H. C. (See Plasil, F., UCRL-11954)

BURNETT, D. S. (See Plasil, F., UCRL-11954)

BURNETT, John L., and Moshè H. Zirin
The standard EMF of $Cd_{(s)}/Cd^{++}$ at 25°C
UCRL-16257, July 1965

J. Inorg. Nucl. Chem.

BUSSIÈRE de NERCY, A. (See Harvey, B. G., UCRL-11895)

BUSSIÈRE de NERCY, A. (See Horen, D. J., UCRL-11904)

BUTLER, G. (See Cerny, J., UCRL-16575)

CERNY, Joseph, Claude Detraz, and Richard H. Pehl
Li^4 and the excited levels of He^4
UCRL-16266, July 1965

Phys. Rev. Letters 15, 300 (1965)

CERNY, J., R. H. Pehl, G. Butler, D. G. Fleming, C. Maples, and C. Detraz
The Mass 13 T=3/2 quartet
UCRL-16575, December 1965

Phys. Letters

CERNY, J., C. Detraz, and R. H. Pehl
Observation of T=3/2 states in Li^7 and Be^7 via (p, He^3) and (p, t) reactions on Be^9
UCRL-11917Abstract, February 1965

Bull. Am. Phys. Soc. 10, 439 (BA4) (1965)

CERNY, J. (See Detraz, C., UCRL-16014)

CERNY, J. (See Rivet, E., UCRL-16200)

CHABRE, M. (See Boschitz, E., UCRL-11964)

CHABRE, M. (See Boschitz, E., UCRL-16216)

CHABRE, M. (See Boschitz, E., UCRL-16217)

CHABRE, M. (See Boschitz, E., UCRL-16218)

CHABRE, M. (See Conzett, H. E., UCRL-16130Abstract)

CHABRE, M. (See Hendrie, D. L., UCRL-11912Abstract)

CHABRE, M. (See Pugh, H. G., UCRL-11940)

CLARKSON, Jack E.
Collective excitation of neutron-deficient barium, xenon, and cerium isotopes: centrifugal stretching treatment of nuclei
UCRL-16040, May 1965

Ph. D. Thesis

CLEM, Ray G., and E. H. Huffman
Spectrophotometric determination of gold with azide
UCRL-11939, February 1965

Anal. Chem. 37, 1155 (1965)

COLE, Sibyl A. (See Weeks, B. M., UCRL-11988)

CONWAY, John G.
Electronic energy levels of the f electron elements
UCRL-11872 Abstract, January 1965

American Chemical Society Meeting, Detroit, Michigan, April 4-7, 1965

CONWAY, John G., and K. Rajnak
Energy levels of Pu^{3+} in lanthanum trichloride
UCRL-16292, July 1965

J. Chem. Phys.

CONWAY, John G., Kenneth C. Ward, and Michiyuki Nakamura
Spectrographic measuring and recording equipment
UCRL-11867 Abstract, January 1965

Optical Society of America Meeting, Dallas, Texas, March 31, April 1 and 2, 1965

CONWAY, John G. (See Howard, J. C., UCRL-14139)

CONZETT, H. E., and B. G. Harvey
The modern cyclotron and nuclear research
UCRL-16007, September 1965

Nucleonics

CONZETT, H. E., E. Boschitz, M. Chabre, E. Shield, and R. J. Slobodrian
Polarization in p-He^4 scattering in the region 20 to 63 MeV
UCRL-16130 Abstract, May 1965

American Physical Society Meeting, Honolulu, September 2-4, 1965

CONZETT, H. E.
The real part of the scattering amplitude at high energies
UCRL-11967, March 1965

Phys. Letters 16, 189 (1965)

CONZETT, H. E. (See Alster, J., UCRL-11975)

CONZETT, H. E. (See Baumgartner, E., UCRL-16528)

CONZETT, H. E. (See Boschitz, E., UCRL-11964)

CONZETT, H. E. (See Boschitz, E. T., UCRL-16216)

CONZETT, H. E. (See Boschitz, E. T., UCRL-16217)

CONZETT, H. E. (See Boschitz, E. T., UCRL-16218)

CONZETT, H. E. (See Slobodrian, R. J., UCRL-16123 Abstract)

COOPER, J. A., J. M. Hollander, M. I. Kalkstein, and J. O. Rasmussen
Decay of Mo^{90}
UCRL-11923, March 1965

Nucl. Phys. 72, 113 (1965)

COOPER, J. A., J. M. Hollander, and J. O. Rasmussen
The effect of the chemical state on the lifetime of the 24-second isomer of Nb^{90}
UCRL-16319 Rev., September 1965

Phys. Rev. Letters 15, 680 (1965)

COOPER, J. A., J. M. Hollander, and J. O. Rasmussen
Very low energy isomer in the decay of Mo^{90}
UCRL-16306, July 1965

In "Internal Conversion Processes" pp. 555-563, Academic Press Inc., New York (in press)

CORNIEA, Winifred Bennett (See Sokol, H. A., UCRL-16178 Abstract)

CRIDER, John Earl, and A. S. Foss
Computational studies of transients in packed tubular chemical reactors
UCRL-11757, January 1965

CUNNINGHAM, B. B. (See Green, J. L., UCRL-16413)

DAVIS, R. M. (See Wasan, D. T., UCRL-16372)

DESHPANDE, R. Y.
Temperature dependence of conductivity of silicon-silicon dioxide interface
UCRL-11870, January 1965

DETRAZ, Claude, Joseph Cerny, and Richard H. Pehl
The observation of T=3/2 levels in Li^7-Be^7 and the uncharacterized nuclei He^7, B^7, and He^8
UCRL-16014, March 1965

Phys. Rev. Letters 14, 708 (1965)

DETRAZ, C. (See Cerny, J., UCRL-11917 Abstract)

DETRAZ, C. (See Cerny, J., UCRL-16266)

DETRAZ, C. (See Cerny, J., UCRL-16575)

DIAMOND, R. M.
Nuclear rotations and vibrations
UCRL-16156 Abstract, May 1965

National American Chemical Society Meeting, Atlantic City, N. J., September 12-17, 1965

DIAMOND, R. M. (See Jensen, C. H., UCRL-11806 Rev.)

EASLEY, Warren, Norman Edelstein, Melvin P. Klein, D. A. Shirley, and H. Hollis Wickman
Nuclear spin and moment of Ag^{110m} by paramagnetic resonance
UCRL-16002, March 1965

Phys. Rev.

EDELSTEIN, N. (See Easley, W., UCRL-16002)

EDWARDS, Victor H.
Observations of electronic counting and sizing of bacteria
UCRL-11925, February 1965

EDWARDS, V. H. (See Leban, M., UCRL-16420 preliminary)

EVANS, J. S. (See Matthias, E., UCRL-16069)

FAUST, J., R. Marrus, and W. A. Nierenberg
Direct measurement of the magnetic moment of plutonium-239

Phys. Letters 16, 71 (1965)

FLEMING, D. G. (See Cerny, J., UCRL-16575)

FOSS, A. S. (See Crider, J. E., UCRL-11757)

FRANKEL, Richard Barry
Nuclear studies using semiconductor detectors
UCRL-11871, January 1965

Ph. D. Thesis

FRANKEL, R. B., D. A. Shirley, and N. J. Stone
The cerium magnesium nitrate temperature scale from nuclear orientation
UCRL-16012, March 1965

Phys. Rev. 140, A1020 (1965)

FRANKEL, R. B., J. Huntzicker, E. Matthias, S. S. Rosenblum, D. A. Shirley, and N. J. Stone
Sign change of induced hyperfine fields in the 5p shell
UCRL-11882, January 1965

Phys. Letters 15, 163 (1965)

FRIED, S. (See Stephens, F. S., UCRL-16192)

FUGER, J. (See Wallmann, J. C., UCRL-16468)

FUGER, J. (See Wallmann, J. C., UCRL-16476)

GABRIELLI, I. (See Harvey, B. G., UCRL-16124 Abstract)

GARRISON, W. M. (See Jayko, M. E., UCRL-11972 Abstract)

GARRISON, W. M. (See Sokol, H. A., UCRL-16178 Abstract)

GARRISON, W. M. (See Weeks, B. M., UCRL-11970 Abstract)

GARRISON, W. M. (See Weeks, B. M., UCRL-11988)

GARRISON, W. M. (See Willix, R. L. S., UCRL-11969 Abstract)

GHIORSO, A. (See Sikkeland, T., UCRL-16086)

GIBSON, W. M. (See Lessler, R. M., UCRL-16421)

GLASS, R. A. (See Lessler, R. M., UCRL-16421)

GLENDENNING, N. K.
Correlations as revealed by (p, t) reactions
UCRL-16114 Abstract, May 1965

American Physical Society Meeting, Honolulu, Hawaii, September 2-4, 1965

GLENDENNING, N. K., and Marcel Veneroni
Inelastic scattering based on a microscopic description of nuclei
UCRL-16428, September 1965

Phys. Rev.

I. THESIS ABSTRACTS

On the following pages the abstracts of theses issued in 1965 are given as they appeared in the original documents.

1. DEVELOPMENT OF SOME HIGH-SPEED CHROMATOGRAPHIC METHODS

Sergio Ajuria-Garza
(M. S. Thesis)

(From UCRL-16015)

A thin-layer chromatography method has been developed using as stationary phase a fine mesh ion exchange resin without any admixture, thus eliminating the effects due to binding materials. The plates can be developed by the ascending, descending, horizontal or centrifugal technique. The spots obtained can be removed mechanically by several methods. An apparatus and a method of operation were developed for the centrifugal acceleration of thin-layer chromatography on 5 X 30 cm glass plates with a substantial reduction in the time of development.

A universal chromatographic chamber equally suitable for horizontal, centrifugal, ascending or descending chromatography either of paper strips or thin-layer plates is described in detail. A comparison was made of the rate of progress of the solvent front in the different chromatographic methods. The speed of the front decreases sharply as the distance from the origin increases except in the centrifugal case in which the speed remains constant.

A method of tandem horizontal or centrifugal chromatography is described which permits to increase the length of a chromatogram in order to separate two substances with very similar R_f values. The length of the chromatogram is only limited by the diffusion of the spots.

The above methods are applied to the separation of Zr^{95}-Hf^{181}, Zr^{95}-Nb^{95} and Am^{241}-Cm^{244}. The radiochromatograms were evaluated by direct scanning and autoradiography. These methods are also discussed.

2. NUCLEAR SPECTROSCOPIC STUDIES OF POLONIUM-204

Jiann-min An
(M. S. Thesis)

(From UCRL-16324)

Sources of Polonium-204 were derived from the electron capture decay of Astatine-204 made by bombarding Au^{197} with C^{12} in the Heavy Ion Linear Accelerator at Berkeley. Physical and chemical methods were adjusted to make the sources as pure as possible for the measurements.

Using scintillation crystals coupled to a 400 channel pulse-height analyzer, an investigation of some of the nuclear radiations of Po^{204} has been made. Gamma rays from Po^{204} were identified by their half life; their energies and relative intensities were carefully determined and the alpha branching ratio was measured.

3. QUADRUPOLE COUPLING IN RARE EARTH CRYSTALS

Johan Blok
(Ph.D. Thesis)

(From UCRL-16279)

The electric field gradient at the nucleus was obtained for the rare earth ethylsulfates and double nitrates of La^{+3}, Eu^{+3}, Gd^{+3}, and Lu^{+3} by measuring the quadrupole coupling constants via nuclear orientation. From a comparison with the calculated antishielding factor and the measured crystal field gradients we arrive at the ionic shielding factors for the rare earths. These shielding factors are observed to vary considerably through the rare earths. These experiments also yielded the nuclear quadrupole moment of La^{140}. We obtained $Q = +0.121(12)$ barns.

These measurements required a precise knowledge of the temperature susceptibility relationship for cerium magnesium nitrate and for neodymium ethylsulfate. The temperature scale for cerium magnesium nitrate has recently been determined quite accurately; thus it was used without reservations. For neodymium ethylsulfate, however, we determined the temperature scale at low temperatures using gamma-ray heating and nuclear orientation. We found considerable discrepancy with the previously published work.

We also made an exhaustive study of the decay of 155-day Lu^{177}. We determined the relative intensities and precise energies of many of the gamma rays in this complex decay. From nuclear orientation of the 7-day and the 155-day Lu^{177} isomers we determined the ratio of the nuclear quadrupole moments of the 155-day metastable state and the 7-day ground state. We found $Q_m/Q_g = +2.33(25)$. For gamma rays following the 1-second intermediate state in Hf^{177} we found the unattenuated value of the anisotropy. We conclude that no reorientation takes place in this 1-second state.

4. COLLECTIVE EXCITATION OF NEUTRON-DEFICIENT BARIUM, XENON, AND CERIUM ISOTOPES: CENTRIFUGAL STRETCHING TREATMENT OF NUCLEI

Jack E. Clarkson
(Ph.D. Thesis)

(From UCRL-16040)

The collective excitation of various neutron-deficient barium, xenon, and cerium isotopes by the "in-beam" method using lithium-drifted germanium counters has been obtained. The (heavy ion, xn) reaction has been used to produce Ba^{126}, Ba^{124}, Xe^{122}, Xe^{120}, and Ce^{134}. The decay of Pr^{134} to Ce^{134} was also observed, with a half life of 17 ± 2 minutes. Partial level schemes for the ground-state rotational bands to spin 8+ or 10+ are proposed for the nuclides investigated. The lifetime of the first-excited state in Ba^{126} has been determined as an "in-beam" experiment to be $2.7 \pm 0.5 \times 10^{-10}$ seconds and, hence, gives the deformation of Ba^{126} as $\beta = 0.24 \pm 0.02$.

The implications of the rotational energies and spacings as related to deformation in this region are discussed.

A classical centrifugal stretching treatment employing realistic nuclear potentials is developed and the results of this and other works are compared to the calculated energy levels from this treatment.

5. NUCLEAR STUDIES USING SEMICONDUCTOR DETECTORS

Richard Barry Frankel
(Ph. D. Thesis)

(From UCRL-11871)

Germanium surface barrier detectors were used to measure the angular distribution of conversion electrons from the 255 keV isomeric transition in Ce^{137m} for Ce^{137m} nuclei aligned in the neodymium ethylsulfate lattice. Direct comparison with the γ-ray angular distributions gave the particle parameters $(b_2)_k = 1.061(18)$, $(b_2)_L = 1.059(20)$. From the variation of the γ-ray anisotropy with temperature, the hyperfine coupling constant for Ce^{137m} was determined to be $A = 0.0147(7)\ cm^{-1}$ using the 1957 temperature scale for this salt.

Ce^{137m} was also aligned in cerium magnesium nitrate and the variation of the 255 keV γ-ray anisotropy was studied as a function of temperature. Anomalies were shown to exist in the cerium magnesium nitrate temperature scale derived by Daniels and Robinson. A new temperature scale is proposed which goes down to 0.0019°K. To test the new scale, Pm^{144} was aligned in cerium magnesium nitrate. The anisotropies of the 615 and 695 keV γ rays were found to be attenuated, but confirmed the Ce^{137m} results.

The decay of Ce^{137m+g} to La^{137} was investigated with Ge(Li) γ-ray detectors, Si(Li) electron detectors, and nuclear alignment. Levels were found at 10, 446, 492, 708, 762, 781, 835, 925, 1004, and 1170 keV. Definite spin and parity assignments were 762 keV (11/2+), 835 keV (9/2+), and 1004 keV (11/2-). A spin of 5/2+ was tentatively assigned to the 446 keV level. The 11/2- state corresponds to a quasiparticle state predicted by Rho.

The distribution of alpha particles from E^{253} oriented in neodymium ethylsulfate was measured using germanium surface barrier detectors. The L=4 wave in the ground-state transition was found to be out of phase with the L=0 and L=2 waves. The L=4 wave was found to have a larger amplitude and the L=2 wave a smaller amplitude than predictions based on the Bohr, Froman and Mottelson coupling relations. The relative amplitudes for the ground-state transitions are $a_0 = 1$, $a_2 = 0.11$, and $a_4 = 0.016$.

6. OXYGEN INITIATED PYROLYSIS OF ETHYLBENZENE

Edwin D. Hausmann
(M. S. Thesis)

(From UCRL-16021)

The effect of small quantities of oxygen (0 to 10%) on the thermal decomposition of ethylbenzene in the temperature range of 570-650°C was investigated utilizing a flow reactor with residence times of from 0.06 to 0.18 seconds and ethylbenzene concentrations of less than 10%. Twenty-one runs were made with oxygen excluded, and the data fitted, using a multiple regression analysis, to the following form of the law of mass action:

$$\text{rate of conversion to styrene} = 4.04 \times 10^{12} \exp(-68,600/RT)\,(EB)^{0.41}\ \text{g. mole/cm}^3\ \text{sec.}$$

The liquid product yield pattern of 74 mole % styrene, 23% benzene, and 3% toluene was found to be independent of temperature and reactant concentration. A mechanism is postulated which is in accord with the reaction order, apparent activation energy and yield pattern.

Small quantities of oxygen increase the rate of thermal decomposition but this effect tapers off as the oxygen concentration is increased. With an oxygen concentration of 2.5% the same level of conversion is achieved at a temperature 10°C lower than that required when oxygen is excluded. The styrene yield selectivity increases from 74 mole % without oxygen to 81 mole %

with 10% oxygen. When the data are fitted to a law of mass action expression, oxygen is found to lower the apparent activation energy to 60,000 cal/gm-mole and to lower the order with respect to ethylbenzene slightly. Possible initiation and termination reaction steps involving oxygen are suggested to explain the results, but it is not possible to test any definite reaction mechanism for the oxygen initiated pyrolysis of ethylbenzene reliably.

7. ISOMERIC CHEMICAL SHIFTS AND ELECTRONEGATIVITY

David A. Keller
(M. S. Thesis)

(From UCRL-16436)

Mössbauer experiments were carried out at 4.2°K using Au^{197} and Sn^{119} as solutes in dilute binary alloys to study the relationship, if any, between the isomeric chemical shift and the difference in electronegativity between the solvent metal and the Mössbauer element.

Au^{197} was embedded into nineteen host lattices and the resulting isomeric chemical shifts of the Mössbauer resonance did show a positive correlation between the chemical shift and electronegativity.

However, similar experiments using Sn^{119} as the Mössbauer solute in six metallic lattices failed to show any correlation at all between chemical shift and electronegativity.

8. REACTIONS OF He^3 WITH LIGHT ELEMENTS: APPLICATIONS TO ACTIVATION ANALYSIS

John D. Mahony
(Ph.D. Thesis)

(From UCRL-11780)

A simple, rapid technique of analyzing for carbon, oxygen, and fluorine, individually and simultaneously by He^3 activation is presented. This method, which can easily be extended to other elements, is capable of analyses at the ppb level or even less in some cases and an ultimate accuracy of 5%. Milligram amounts of total sample are sufficient and are not destroyed in the analysis. The advantages of this technique with especial reference to energetics, versatility and the elimination of interferences are discussed and compared to those of other charged-particle and neutron-activation analysis procedures.

The excitation functions for the production of F^{18} from O^{16}, C^{11} and N^{13} from C^{12}, and F^{18} from F^{19} by He^3 reactions for the energy range, 0 to 31 MeV have been determined and are discussed with particular application to activation analysis.

An absolute analysis for oxygen in thorium was performed; simultaneous absolute analyses of gold, silicon, Mylar, and polyethylene for carbon and oxygen, and Teflon for carbon and fluorine are described. Results of analyses by the relative method for oxygen in thorium, beryllium, niobium, and lead are also reported.

Although the Berkeley Hilac was used for the work described, a small cyclotron is shown to be quite adequate for extensive He^3 activation analysis. The specifications of such an accelerator are given.

9. MAGNETIC PROPERTIES OF CURIUM METAL AND ITS COMPOUNDS

Sayed A. Marei
(Ph.D. Thesis)

(From UCRL-11984)

The magnetic susceptibility of curium metal has been measured from -253 to 250°C. The metal followed Curie-Weiss law above liquid nitrogen temperature up to the temperature studied. The effective magnetic moment for the metal was found to be 7.99±0.15 indicating the presence of $5f^7$ configuration in the metal. No magnetic transition was observed in the temperature range studied.

The magnetic susceptibility of Cm^{+3} in curium trifluoride, curium oxychloride, and 5.6 mole percent curium trifluoride diluted with lanthanum trifluoride has been measured. The effective moment for Cm^{+3} was found to be 7.65±0.1 Bohr magnetron, giving a Lande g factor of 1.93±0.03, pointing toward an appreciable departure from Russell-Saunders coupling. The molecular field constant Δ was found to be small and decreasing with increasing magnetic dilution. The following Δ values were found for curium compounds.

Compound	Δ°
CmOCl	23±3
$CmF_3 \cdot 1/2\ H_2O$	5±3
5.6% CmF_3	5±3

10. DECAY SCHEMES OF ODD-ODD EINSTEINIUM ISOTOPES

William Charles McHarris
(Ph.D. Thesis)

(From UCRL-11784)

The radiations from the heavy odd-odd, alpha-emitting isotopes, $_{99}Es^{254}_{155}$ and $_{99}Es^{252}_{153}$, were studied and interpreted in light of the Bohr-Mottelson unified theory of deformed nuclei and the accompanying Nilsson wave functions. The study was based on their alpha-particle spectra, which were obtained both with Si alpha detectors and with a high-resolution, double-focussing magnetic spectrograph. Complementing these were gamma-ray spectra obtained with NaI scintillators and Ge gamma detectors, conversion-electron spectra obtained with Si electron detectors and precision permanent-magnet spectrographs, and various time-to-height and delayed-coincidence spectra.

Levels in the daughter nuclei were grouped into rotational bands, and the experimental properties of these were compared with predictions based on couplings of the odd-nucleon states found in neighboring odd-mass nuclei. Agreement was found to be excellent, indicating that the odd proton and odd neutron in these odd-odd states move with considerable independence of each other.

The decay scheme of Es^{254} was worked out in detail, indicating that the 6.437 MeV, favored alpha group populates a $K\pi I = 7+7$ level at 85.5 keV above the ground state of Bk^{250}. A cascade of three electromagnetic transitions is required to de-excite this level to the 2-2 ground state: (1) a 7-keV E2, with a half life of 213 μsec, that leads to a 4+5 level at 78.1 keV above ground, (2) a fast 42.6-keV M1-E2 rotational transition to the 4+4 level at 35.5 keV, and (3) branching transitions, mostly a 35.5-keV M2, that give the 4+4 level a 29 μsec half life and connect it with the ground state. Many subsidiary bands and levels were also studied and assigned.

11. AXIAL DISPERSION IN LIQUID FLOW THROUGH PACKED BEDS

Steven Frank Miller
(M. S. Thesis)

(From UCRL-11951)

Step-function injection and purging of a dilute salt tracer in water was used to measure axial dispersion for low Reynolds number liquid flow through beds of uniform sized, random packed glass spheres. The resultant data and those of several previous studies are coordinated and interpreted in terms of Reynolds number, Schmidt number, and Peclet number.

12. THE PRODUCTION OF TRITIUM LABELED METHANE AND ETHANE IN THE CH_4-T_2 SYSTEM

John B. Nash
(Ph.D. Thesis)

(From UCRL-16009)

The rates of incorporation of tritium into labeled methane and ethane in the methane-tritium system has been investigated. The production of the tritiated products can be expressed by a sum of two terms. The first term of this expression is independent of time, and is the decay-induced labeling; the other, inversely proportional to time, is the radiation-induced labeling. The rate of incorporation of tritium into product as a result of the radiation field is shown to have a dependence on the absolute molecular concentration of tritium as well as its concentration as a source of radiation. The yields of labeled methane and ethane from the decay labeling is directly proportional to the rate of decay of the tritium. The rate of incorporation of tritium into labeled ethane is larger than that for incorporation into tritiated methane. A mechanism for both series consistent with the results is proposed. The effect of additives was also determined. Addition of hydrogen elucidated the rate of labeling from the decay-induced series. Xenon was shown to enhance the product yield by 15 percent in concentrations up to 30 mole percent. Addition of ethylene in amounts less than 2 mole percent suppressed the labeling rate until the ethylene had disappeared by reaction with the radiolytic products. The effect on product formation of varying the pressure and the surface to volume ratio is also discussed.

13. THEORETICAL ALPHA DECAY RATES OF DEFORMED NUCLEI

John Kenneth Poggenburg, Jr.
(Ph.D. Thesis)

(From UCRL-16187)

The shell-model theory of alpha decay developed by Mang is summarized. The calculation of the alpha formation entails use of the pairing-force wave functions of superconductivity theory, and we briefly describe their calculation with a delta-force approximation. The penetration of the alpha particle through the anisotropic potential barrier is considered in detail. We study the approximate treatment of Fröman and the results clearly justify the method.

The particular features of the potential barrier are examined in terms of the WKB expression for barrier transmission. The Woods-Saxon potential $V = -74/(1 + \exp\{(r-1.17A^{1/3}-1.6)/(a)\})$ is chosen after a survey of recent optical model analyses of alpha scattering experiments. The Woods-Saxon potential results in penetrability factors that are $\approx 45\%$ lower than those calculated with the Igo potential. Modification of the Coulomb potential has little effect on the penetrability.

Extensive numerical calculations are given in an appendix. The theory gives reasonable agreement with experiment, and has provided a clear example of its value in the analysis of the alpha decay of Am^{241}. The calculations predict relative amplitudes and phases of importance in interpretation of angular correlation experiments. They also predict the ℓ-wave mixing in the transition to final states of odd-mass nuclei. Comparisons of theoretical and experimental transition rates indicate the nature of the errors in the calculations. Suggestions are given for future improvement.

14. EFFECTS OF COLLECTIVE EXCITED STATES ON ALPHA PARTICLE BARRIER PENETRABILITY

Elizabeth A. Rauscher
(M. S. Thesis)

(From UCRL-11875)

For the alpha decay of Po^{212} to the ground state and various excited states of the Pb^{208} daughter, there are collective surface vibrational modes, which couple these low-lying excited states to the ground state of Pb^{208}. In the present description of the transitions between these excited states of Pb^{208} and the ground state of Pb^{208} only single phonon excitations will be considered.

Interaction of the electric multipole nature occurs between the excited state levels and the ground state of the recoil lead daughter induced by its interaction with the emitted alpha particle, affecting the latter's penetration of the nuclear barrier.

The formation of the excitation in the lead nucleus can either be produced by Po^{212} alpha decay or by (α, α') inelastic scattering on Pb^{208}, but in either case we consider that an alpha cluster exists in the nuclear surface region.

It is the purpose of the present paper to investigate the manner in which the multipole interaction affects the alpha particle penetration of the nuclear barrier.

15. THE ELECTROMAGNETIC LEVITATION OF METALS; THE DESIGN, CONSTRUCTION, AND OPERATION OF A DIFFERENTIAL MICROMANOMETER; STUDIES OF ATOMIC HYDROGEN AT LOW PRESSURES

Peter Roland Rony
(Ph.D. Thesis)

(From UCRL-16073)

This dissertation is divided into three parts for convenience of presentation. One abstract of each part is given below.

Part I

A complete theoretical description of the electromagnetic levitation of metals is given, leading to the basic equations for the lifting force and power input for a metal sphere levitated in an inhomogeneous sinusoidally alternating magnetic field. The suspended metal is suitably controlled either by operation at lower frequencies and addition of heat with an electron beam, plasma-arc torch, high-frequency induction heater, or reflection furnace, or by operation at high frequencies and employment of high-thermal-conductivity gases such as hydrogen and helium to cool the metal.

Values indicating the ease of levitation of 1-cm-radius spheres of more than 50 different metals at 0°C and at their respective melting points are given. When frequencies in the 10 to 100 kc/sec are used, the density of the metal chiefly determines the ease of levitation. Refractory, semiconducting, or dielectric materials can be levitated either by the heating of them to high temperatures to decrease their electrical resistivity or by the coating of a light and inert metal of high melting point with the material to be studied.

Liquid sodium surrounded by a mineral oil of almost identical density can be used in the study of the magnetic-field distribution of levitation coils. Liquid mercury can be used to determine the ability of levitation coils to suspend high-temperature liquid metals.

Part II

A differential micromanometer capable of measuring 100 μtorr to an accuracy of ±2% has been designed, constructed, and tested. The pressure difference is sensed by a membrane manometer constructed as a differential capacitor that forms two legs of a resonant-bridge network excited by a radio-frequency source.

The most favorable system found to date consists of a pressure transducer (Decker Corporation Model 306-2A) operated open loop with the bridge and electronics. Differential pressures as low as 50 μtorr can be measured with a zero drift of 1 μtorr per min or 30 μtorr per hour. Differential pressures of 0.5 μtorr are detectable.

The micromanometer is calibrated electrostatically. The diaphragm constant K in the formula, $\Delta P = K V^2$, is determined to ±2% by the comparison of a known voltage and a calibrated McLeod gauge.

Part III

The theoretical description of diffusion and flow tubes is extended to the following situations: (a) the discharge zone is of finite length, (b) the discharge-zone walls are inactive catalytically, (c) the end-plate sink is composed of two or more catalytic materials, and (d) the atom-recombination coefficients on the discharge- and reactor-zone walls differ in magnitude. The dimensionless groups characterizing the rate processes within the system are systematized.

A Wrede-Harteck gauge, which is capable of detecting atom concentrations of less than 0.06% at 75 mtorr, indicates that the presence of small amounts of water does not influence the yield of atomic hydrogen from a microwave or 50-MHz discharge. This result is independent of the measurement technique, the source of hydrogen, the source of water, and the discharge power.

Small amounts of oxygen stoichiometrically increase the yield of atomic hydrogen from the low-pressure discharge by a ratio of at least two atoms of hydrogen per molecule of oxygen. Molecular nitrogen has a similar but smaller effect.

The location of an active catalytic probe affects the atom concentration level throughout a diffusion tube. A cyclotron-resonant microwave discharge operates in the low-pressure system with powers as low as 250 mW. The intensity of the Balmer lines or color of low-pressure hydrogen discharges is not a reliable qualitative indication of the atomic-hydrogen yield. Requisite conditions for the proper use of an isothermal calorimeter are also discussed.

16. DECAY OF THE Zn^{64*} COMPOUND NUCLEUS FORMED BY NUCLEAR REACTIONS OF p, He^3, He^4, AND C^{12} WITH Cu^{63}, Ni^{61}, Ni^{60}, AND Cr^{52}, RESPECTIVELY

Charles F. Smith, Jr.
(Ph.D. Thesis)

(From UCRL-11862)

An experimental, radio-chemical determination of the excitation functions for reactions involving the $[Zn^{64}]^*$ compound nucleus has been performed. The reactant pairs are: p + Cu^{63}, He^3 + Ni^{61}, He^4 + Ni^{60}, and C^{12} + Cr^{52}, while the observed products for each such pair are: Zn^{63}, Zn^{62}, and Cu^{62}. Total reaction cross sections are calculated from the optical model. The ratio of the cross section for a given reaction to the total reaction cross section is compared on an excitation energy absissa for each product. The shape and magnitude of these ratio curves is essentially constant in each such comparison, suggesting a compound nuclear reaction mechanism. Range measurements for Zn^{62} recoils are made and compared to calculated ranges based on the theory of Lindhard, Scharff and Schiøtt for a compound nuclear reaction. Good agreement is found. The shapes of these curves are compared to a theoretical estimate obtained from evaporation theory, and are shown to be similar to the calculated shapes. A displacement of the

experimental curves relative to one another along the excitation energy axis is noted, and ascribed to angular momentum effects. Using the position of the Zn^{64} photoexcitation curves of Sagane as reference points, and spin averaged angular momenta of the compound system, the reduced moment of inertia is calculated for the four systems. At least two distinct values are found, indicating a difference between orbital- and spin-angular momenta, the latter causing the greater energy shift in the excitation functions. This observation is shown to be of value in understanding similar energy discrepancies in excitation function comparisons. Because of the observed relationship between the mode of formation and the mode of decay of the compound nucleus, it is concluded that the independence postulate is not strictly applicable to this system as a whole.

17. SCATTERING OF 50.9 MeV ALPHA PARTICLES FROM Ne^{20} AND Ca^{40}

Arthur Springer
(Ph.D. Thesis)

(From UCRL-11681)

More than a dozen inelastic levels of both Ne^{20} and Ca^{40} were excited by inelastic scattering of 50.9 MeV alpha particles. Differential cross sections for these excitations were measured, and by analysis with the Austern and Blair model, one-step and two-step excitation processes were distinguished from each other. Spins, parities, and reduced transition probabilities were also extracted with the aid of this model. This information was then used to discuss the collective nuclear structure of Ca^{40}, which is vibrational, and Ne^{20} which has rotational bands based on both the ground state and octupole vibrations.

J. AUTHOR INDEX

1. PAPERS PUBLISHED AND UCRL REPORTS ISSUED, 1965

AJURIA-GARZA, Sergio
Development of some high-speed chromatographic methods
UCRL-16015, June 1965

M. S. Thesis

ALAGA, G., and G. Ialongo
Semi microscopic description of $Hg^{198}I$
UCRL-16385, September 1965

ALI, Dolores, Isaac Maleh, and Richard Marrus
Hyperfine structure and nuclear moments of promethium-148 and erbium-165
UCRL-11836, January 1965

Phys. Rev. 138, B1356 (1965)

ALI, Dolores
Spins of gadolinium-153, dysprosium-159, and promethium-148
UCRL-11837, January 1965

Nucl. Phys. 71, 441 (1965)

ALSTER, Jonas, and Homer E. Conzett
Comparison between phase shift and complex potential descriptions of elastic scattering
UCRL-11975, February 1965

Phys. Rev. 139, B50 (1965)

AN, Jiann-min
Nuclear spectroscopic studies of polonium-204
UCRL-16324, August 1965

M. S. Thesis

ASARO, F. (See Gunter, K., UCRL-16582)

ASARO, F. (See Stephens, F. S., UCRL-16192)

ATKINS, Harriette L. (See Weeks, B. M., UCRL-11970 Abstract)

BANSAL, Brij M. (See Wallmann, J. C., UCRL-16468)

BAUMGARTNER, E., H. E. Conzett, E. Shield, and R. J. Slobodrian
Determination of the neutron-neutron scattering length from the reaction $T(d, He^3)2n$
UCRL-16528, December 1965

Phys. Rev. Letters

BLOK, Johan
Quadrupole coupling in rare earth crystals
UCRL-16279, July 1965

Ph.D. Thesis

BLOK, J., and D. A. Shirley
Nuclear orientation of La^{140}, Eu^{154}, Gd^{159}, Lu^{177}, and Lu^{177m} by Sternheimer antishielding
UCRL-16328, August 1965

Phys. Rev.

BLOK, J., and D. A. Shirley
Systematic variation of quadrupole crystal-field shielding in rare-earth ethylsulfates
UCRL-16318, August 1965

Phys. Rev.

BLOK, J., D. A. Shirley, and N. J. Stone
The temperature scale for neodymium ethylsulfate below $1^{o}K$
UCRL-16345, August 1965

Phys. Rev.

BOSCHITZ, E. T., M. Chabre, H. E. Conzett, and R. J. Slobodrian
Energy dependence of the polarization in p-O^{16} elastic scattering between 21 and 53 MeV
UCRL-16217, August 1965

International Conference on Polarization Phenomena of Nucleons, Kernforschungszentrum Karlsruhe, September 6-10, 1965

BOSCHITZ, E. T., M. Chabre, H. E. Conzett, E. Shield, and R. J. Slobodrian
Polarization in p-He^4 scattering between 27 and 63 MeV
UCRL-16216, August 1965

International Conference on Polarization Phenomena of Nucleons, Kernforschungszentrum Karlsruhe, September 6-10, 1965

BOSCHITZ, E. T., M. Chabre, H. E. Conzett, E. Shield, and R. J. Slobodrian
Proton polarization in small angle p-He^4 scattering at 38.7 MeV
UCRL-11964, February 1965

Phys. Rev. Letters

BOSCHITZ, E. T., M. Chabre, H. E. Conzett, and R. J. Slobodrian
Study of the $He^4(p,d)He^3$ reaction with polarized protons at 55 and 63 MeV
UCRL-16218, August 1965

International Conference on Polarization Phenomena of Nucleons, Kernforschungszentrum Karlsruhe, September 6-10, 1965

BOSCHITZ, E. T. (See Conzett, H. E., UCRL-16130 Abstract)

BOSCHITZ, E. T. (See Hendrie, D. L., UCRL-11912 Abstract)

BOSCHITZ, E. T. (See Pugh, H. G., UCRL-11940)

BOWMAN, Harry R., E. K. Hyde, Stanley G. Thompson, and Richard C. Jared
Application of high-resolution semiconductor detectors in x-ray emission spectrography
UCRL-16485, November 1965

Science

BOWMAN, Harry R., Stanley G. Thompson, Rand L. Watson, S. S. Kapoor, and John O. Rasmussen
The prompt gamma ray, prompt electron and prompt x-ray spectra associated with fission fragments of specific mass
UCRL-11902, January 1965

IAEA Symposium on the Physics and Chemistry of Fission, Salzburg, Austria, March 22-25, 1965

BOWMAN, H. R. (See Kapoor, S. S., UCRL-16208)

BOWMAN, H. R. (See Watson, R. L., UCRL-16184)

BRITT, H. C. (See Plasil, F., UCRL-11954)

BURNETT, D. S. (See Plasil, F., UCRL-11954)

BURNETT, John L., and Moshè H. Zirin
The standard EMF of $Cd_{(s)}/Cd^{++}$ at 25°C
UCRL-16257, July 1965

J. Inorg. Nucl. Chem.

BUSSIÈRE de NERCY, A. (See Harvey, B. G., UCRL-11895)

BUSSIÈRE de NERCY, A. (See Horen, D. J., UCRL-11904)

BUTLER, G. (See Cerny, J., UCRL-16575)

CERNY, Joseph, Claude Detraz, and Richard H. Pehl
Li^4 and the excited levels of He^4
UCRL-16266, July 1965

Phys. Rev. Letters 15, 300 (1965)

CERNY, J., R. H. Pehl, G. Butler, D. G. Fleming, C. Maples, and C. Detraz
The Mass 13 T=3/2 quartet
UCRL-16575, December 1965

Phys. Letters

CERNY, J., C. Detraz, and R. H. Pehl
Observation of T=3/2 states in Li^7 and Be^7 via (p, He^3) and (p, t) reactions on Be^9
UCRL-11917Abstract, February 1965

Bull. Am. Phys. Soc. 10, 439 (BA4) (1965)

CERNY, J. (See Detraz, C., UCRL-16014)

CERNY, J. (See Rivet, E., UCRL-16200)

CHABRE, M. (See Boschitz, E., UCRL-11964)

CHABRE, M. (See Boschitz, E., UCRL-16216)

CHABRE, M. (See Boschitz, E., UCRL-16217)

CHABRE, M. (See Boschitz, E., UCRL-16218)

CHABRE, M. (See Conzett, H. E., UCRL-16130Abstract)

CHABRE, M. (See Hendrie, D. L., UCRL-11912Abstract)

CHABRE, M. (See Pugh, H. G., UCRL-11940)

CLARKSON, Jack E.
Collective excitation of neutron-deficient barium, xenon, and cerium isotopes: centrifugal stretching treatment of nuclei
UCRL-16040, May 1965

Ph. D. Thesis

CLEM, Ray G., and E. H. Huffman
Spectrophotometric determination of gold with azide
UCRL-11939, February 1965

Anal. Chem. 37, 1155 (1965)

COLE, Sibyl A. (See Weeks, B. M., UCRL-11988)

CONWAY, John G.
Electronic energy levels of the f electron elements
UCRL-11872 Abstract, January 1965

American Chemical Society Meeting, Detroit, Michigan, April 4-7, 1965

CONWAY, John G., and K. Rajnak
Energy levels of Pu^{3+} in lanthanum trichloride
UCRL-16292, July 1965

J. Chem. Phys.

CONWAY, John G., Kenneth C. Ward, and Michiyuki Nakamura
Spectrographic measuring and recording equipment
UCRL-11867 Abstract, January 1965

Optical Society of America Meeting, Dallas, Texas, March 31, April 1 and 2, 1965

CONWAY, John G. (See Howard, J. C., UCRL-14139)

CONZETT, H. E., and B. G. Harvey
The modern cyclotron and nuclear research
UCRL-16007, September 1965

Nucleonics

CONZETT, H. E., E. Boschitz, M. Chabre, E. Shield, and R. J. Slobodrian
Polarization in p-He^4 scattering in the region 20 to 63 MeV
UCRL-16130 Abstract, May 1965

American Physical Society Meeting, Honolulu, September 2-4, 1965

CONZETT, H. E.
The real part of the scattering amplitude at high energies
UCRL-11967, March 1965

Phys. Letters 16, 189 (1965)

CONZETT, H. E. (See Alster, J., UCRL-11975)

CONZETT, H. E. (See Baumgartner, E., UCRL-16528)

CONZETT, H. E. (See Boschitz, E., UCRL-11964)

CONZETT, H. E. (See Boschitz, E. T., UCRL-16216)

CONZETT, H. E. (See Boschitz, E. T., UCRL-16217)

CONZETT, H. E. (See Boschitz, E. T., UCRL-16218)

CONZETT, H. E. (See Slobodrian, R. J., UCRL-16123 Abstract)

COOPER, J. A., J. M. Hollander, M. I. Kalkstein, and J. O. Rasmussen
Decay of Mo^{90}
UCRL-11923, March 1965

Nucl. Phys. 72, 113 (1965)

COOPER, J. A., J. M. Hollander, and J. O. Rasmussen
The effect of the chemical state on the lifetime of the 24-second isomer of Nb^{90}
UCRL-16319 Rev., September 1965

Phys. Rev. Letters 15, 680 (1965)

COOPER, J. A., J. M. Hollander, and J. O. Rasmussen
Very low energy isomer in the decay of Mo^{90}
UCRL-16306, July 1965

In "Internal Conversion Processes" pp. 555-563, Academic Press Inc., New York (in press)

CORNIEA, Winifred Bennett (See Sokol, H. A., UCRL-16178 Abstract)

CRIDER, John Earl, and A. S. Foss
Computational studies of transients in packed tubular chemical reactors
UCRL-11757, January 1965

CUNNINGHAM, B. B. (See Green, J. L., UCRL-16413)

DAVIS, R. M. (See Wasan, D. T., UCRL-16372)

DESHPANDE, R. Y.
Temperature dependence of conductivity of silicon-silicon dioxide interface
UCRL-11870, January 1965

DETRAZ, Claude, Joseph Cerny, and Richard H. Pehl
The observation of T=3/2 levels in Li^7-Be^7 and the uncharacterized nuclei He^7, B^7, and He^8
UCRL-16014, March 1965

Phys. Rev. Letters 14, 708 (1965)

DETRAZ, C. (See Cerny, J., UCRL-11917 Abstract)

DETRAZ, C. (See Cerny, J., UCRL-16266)

DETRAZ, C. (See Cerny, J., UCRL-16575)

DIAMOND, R. M.
Nuclear rotations and vibrations
UCRL-16156 Abstract, May 1965

National American Chemical Society Meeting, Atlantic City, N. J., September 12-17, 1965

DIAMOND, R. M. (See Jensen, C. H., UCRL-11806 Rev.)

EASLEY, Warren, Norman Edelstein, Melvin P. Klein, D. A. Shirley, and H. Hollis Wickman
Nuclear spin and moment of Ag^{110m} by paramagnetic resonance
UCRL-16002, March 1965

Phys. Rev.

EDELSTEIN, N. (See Easley, W., UCRL-16002)

EDWARDS, Victor H.
Observations of electronic counting and sizing of bacteria
UCRL-11925, February 1965

EDWARDS, V. H. (See Leban, M., UCRL-16420 preliminary)

EVANS, J. S. (See Matthias, E., UCRL-16069)

FAUST, J., R. Marrus, and W. A. Nierenberg
Direct measurement of the magnetic moment of plutonium-239

Phys. Letters 16, 71 (1965)

FLEMING, D. G. (See Cerny, J., UCRL-16575)

FOSS, A. S. (See Crider, J. E., UCRL-11757)

FRANKEL, Richard Barry
Nuclear studies using semiconductor detectors
UCRL-11871, January 1965

Ph. D. Thesis

FRANKEL, R. B., D. A. Shirley, and N. J. Stone
The cerium magnesium nitrate temperature scale from nuclear orientation
UCRL-16012, March 1965

Phys. Rev. 140, A1020 (1965)

FRANKEL, R. B., J. Huntzicker, E. Matthias, S. S. Rosenblum, D. A. Shirley, and N. J. Stone
Sign change of induced hyperfine fields in the 5p shell
UCRL-11882, January 1965

Phys. Letters 15, 163 (1965)

FRIED, S. (See Stephens, F. S., UCRL-16192)

FUGER, J. (See Wallmann, J. C., UCRL-16468)

FUGER, J. (See Wallmann, J. C., UCRL-16476)

GABRIELLI, I. (See Harvey, B. G., UCRL-16124 Abstract)

GARRISON, W. M. (See Jayko, M. E., UCRL-11972 Abstract)

GARRISON, W. M. (See Sokol, H. A., UCRL-16178 Abstract)

GARRISON, W. M. (See Weeks, B. M., UCRL-11970 Abstract)

GARRISON, W. M. (See Weeks, B. M., UCRL-11988)

GARRISON, W. M. (See Willix, R. L. S., UCRL-11969 Abstract)

GHIORSO, A. (See Sikkeland, T., UCRL-16086)

GIBSON, W. M. (See Lessler, R. M., UCRL-16421)

GLASS, R. A. (See Lessler, R. M., UCRL-16421)

GLENDENNING, N. K.
Correlations as revealed by (p,t) reactions
UCRL-16114 Abstract, May 1965

American Physical Society Meeting, Honolulu, Hawaii, September 2-4, 1965

GLENDENNING, N. K., and Marcel Veneroni
Inelastic scattering based on a microscopic description of nuclei
UCRL-16428, September 1965

Phys. Rev.

GLENDENNING, N. K., and K. Harada
Shell-model calculation for Po^{212}
UCRL-11945, February 1965

Nucl. Phys.

GOULDING, F. S. (See Pehl, R. H., UCRL-16477)

GREEN, J. L., J. T. Haley, and B. B. Cunningham
Procedures and results of the January 1964 heavy isotopes production cave run
UCRL-16413, September 1965

GREEN, J. L. (See Wallmann, J. C., UCRL-16476)

GUNTER, K., F. Asaro, and A. C. Helmholz
Charge and energy distributions of recoils from Th^{226} alpha decay
UCRL-16582, December 1965

Phys. Rev. Letters

HALEY, J. T. (See Green, J. L., UCRL-16413)

HALEY, J. T. (See Latimer, R. M., UCRL-16191)

HANSON, D. N. (See Rony, P. R., UCRL-16211)

HARADA, K. (See Glendenning, N. K., UCRL-11945)

HARRIS, J. A. (See Prussin, S. G., UCRL-16028)

HARVEY, B. G., I. Gabrielli, D. L. Hendrie, J. Mahoney, and J. R. Meriwether
Collective levels in Cr^{52}, Cr^{53}, and V^{51} excited by inelastic alpha scattering
UCRL-16124 Abstract, May 1965

American Physical Society Meeting, Honolulu, Hawaii, September 2-4, 1965

HARVEY, B. G., J. R. Meriwether, A. Bussière, and D. J. Horen
Excitation of collective levels in Cu^{63} by 50 MeV α scattering
UCRL-11895, January 1965

Nucl. Phys. 70, 305 (1965)

HARVEY, B. G. (See Conzett, H. E., UCRL-16007)

HARVEY, B. G. (See Horen, D. J., UCRL-11904)

HARVEY, B. G. (See Rivet, E., UCRL-16200)

HARVEY, B. G. (See Springer, A., UCRL-11846)

HAUG, H. (See Wallmann, J. C., UCRL-16468)

HAUSMANN, Edwin D.
Oxygen initiated pyrolysis of ethylbenzene
UCRL-16021

M. S. Thesis

HELMHOLZ, A. C. (See Gunter, K., UCRL-16582)

HENDRIE, D. L., H. G. Pugh, Marc Chabre, and E. T. Boschitz
The $C^{12}(p, 2p)B^{11}$ reaction at 50 MeV
UCRL-11912 Abstract, February 1965

Bull. Am. Phys. Soc. 10, 526 (JA10) (1965)

HENDRIE, D. L. (See Harvey, B. G., UCRL-16124 Abstract)

HENDRIE, D. L. (See Pugh, H. G., UCRL-11940)

HOLLANDER, Jack M.
The impact of semiconductor detectors on gamma-ray and electron spectroscopy
UCRL-16307, August 1965

International Meeting on Nuclear Instrumentation, Herceg-Novi, Yugoslavia, August 20-September 3, 1965

HOLLANDER, J. M.
The use of semiconductor detectors for internal conversion coefficient measurements
UCRL-16035, March 1965

International Conference on Internal Conversion Process, Vanderbilt University, Nashville, Tennessee, May 11-13, 1965

HOLLANDER, J. M. (See Cooper, J. A., UCRL-11923)

HOLLANDER, J. M. (See Cooper, J. A., UCRL-16306)

HOLLANDER, J. M. (See Cooper, J. A., UCRL-16319 Rev.)

HOLLANDER, J. M. (See Prussin, S. G., UCRL-16028)

HOLLANDER, J. M. (See Yamazaki, T., UCRL-16064)

HOLLIDAY, R. J., D. A. Shirley, and N. J. Stone
The hyperfine magnetic fields at nuclei of indium in iron and nickel
UCRL-16437, October 1965

Phys. Rev.

HOPKINS, T. E. (See Zalkin, A., UCRL-16269)

HOREN, Daniel J., John R. Meriwether, Bernard G. Harvey, A. Bussière de Nercy, and Jeannette Mahoney
Phase variation in the scattering of alpha particles by $Ni^{58,62}$
UCRL-11904, January 1965

Nucl. Phys. 72, 97 (1965)

HOREN, D. J. (See Harvey, B. G., UCRL-11895)

HOREN, D. J. (See Hyde, E. K., UCRL-16337)

HOWARD, John C., and John G. Conway
Nitride and oxide bands of molybdenum
UCRL-14139, April 1965

J. Chem. Phys.

HUFFMAN, E. H. (See Clem, R. G., UCRL-11939)

HUNTZICKER, J. (See Frankel, R. B., UCRL-11882)

HYDE, E. K., W. J. Treytl, A. Siivola, D. H. Sisson, and D. J. Horen
The decay properties of Zr^{86}
UCRL-16337, August 1965

Phys. Rev.

HYDE, E. K. (See Bowman, H. R., UCRL-16485)

IALONGO, G. (See Alaga, G., UCRL-16385)

JARED, R. C. (See Bowman, H. R., UCRL-16485)

JARRETT, B. V. (See Pehl, R. H., UCRL-16477)

JAYKO, Michael E., and Warren M. Garrison
Radiation chemistry of peptides: mechanism of formation of peptide radicals, ~CONHĊR~, in solid poly-D, L-alanine
UCRL-11972 Abstract, February 1965

Thirteenth Annual Meeting of the Radiation Research Society, Philadelphia, May 24-26, 1965

JENSEN, C. H., and R. M. Diamond
Anion exchange in concentrated solutions
UCRL-11806 Rev

J. Phys. Chem. 69, 3440 (1965)

JUDD, B. R.
Hypersensitive transitions in rare-earth ions
UCRL-16380, August 1965

J. Chem. Phys.

JUDD, B. R.
Second quantization and atomic spectroscopy
UCRL-16098, May 1965

Rev. Mod. Phys.

JUDD, B. R.
Three-particle operators for equivalent electrons
UCRL-16321, August 1965

Phys. Rev.

JUDD, B. R.
Zeeman effect as a prototype for intra-atomic interactions
UCRL-16273, August 1965

Physica

KALKSTEIN, M. I. (See Cooper, J. A., UCRL-11923)

KAPOOR, S. S., H. R. Bowman, and S. G. Thompson
Emission of K X rays and division of nuclear charge in the spontaneous fission of Cf^{252}
UCRL-16208, June 1965

Phys. Rev.

KAPOOR, S. S. (See Bowman, H. R., UCRL-11902)

KELLER, David A.
Isomeric chemical shifts and electronegativity
UCRL-16436, October 1965

M. S. Thesis

KILIAN, G. W. (See Newton, A. S., UCRL-16584)

KING, C. J. (See Hausmann, E. D., UCRL-16021)

KING, C. J. (See Miller, S. F., UCRL-11951)

KISSLINGER, L. S.
A note on coupling schemes in odd-mass nuclei
UCRL-16341, August 1965

Phys. Rev.

KLEIN, M. P. (See Easley, W., UCRL-16002)

KUMAR, Krishna
Anharmonic terms in the potential energy of collective quadrupole motion of even nuclei
UCRL-16391 Abstract, September 1965

American Physical Society Meeting, Chicago, Illinois, October 28-30, 1965

LAMERS, K. W. (See Rony, P. R., UCRL-16212)

LANDE, Alexander
Vibrations and strength functions in Ar^{37}
UCRL-16304, July 1965

Phys. Letters

LANDIS, D. A. (See Pehl, R. H., UCRL-16477)

LARSH, A. E. (See Sikkeland, T., UCRL-16086)

LATIMER, R. M., and J. T. Haley
Procedures and results of the May 1965 heavy isotopes production cave run
UCRL-16191, June 1965

LATIMER, R. M. (See Sikkeland, T., UCRL-16086)

LEBAN, Mark, V. H. Edwards, and C. R. Wilke
Sulfate reduction by bacteria
UCRL-16420 preliminary, September 1965

LESSLER, R. M., W. M. Gibson, and R. A. Glass
Radiative capture, particle emission, and fission in heavy nuclei
UCRL-16421, September 1965

Nucl. Phys.

LEVY, R. M., and D. A. Shirley
Hyperfine structure in the 2084-keV state of Ce^{140}
UCRL-11922, January 1965

Phys. Rev. 140, B811 (1965)

MAHONEY, J. (See Harvey, B. G., UCRL-16124 Abstract)

MAHONEY, J. (See Horen, D. J., UCRL-11904)

MAHONY, John D.
Reactions of He^3 with light elements: applications to activation analysis
UCRL-11780, January 1965

Ph. D. Thesis

MALEH, Isaac
Electronic angular momentum of some low-lying states of cerium; nuclear spin of cerium-143
UCRL-11794, December 1964

Phys. Rev. 138, B766 (1965)

MALEH, I. (See Ali, D., UCRL-11836)

MANG, Hans J., John O. Rasmussen, and Mannque Rho
Comparisons of BCS nuclear wave functions with exact solutions. II. Particle number conserving method.
UCRL-16550, December 1965

Phys. Rev.

MANG, H. J. (See Rho, M., UCRL-16155)

MAPLES, C. (See Cerny, J., UCRL-16575)

MAREI, Sayed A.
Magnetic properties of curium metal and its compounds
UCRL-11984, May 1965

Ph. D. Thesis

MAREI, S. A. (See Wallmann, J. C., UCRL-16468)

MARRUS, R. (See Ali, D., UCRL-11836)

MARRUS, R. (See Faust, J., Phys. Letters 16, 71 (1965))

MATTHIAS, E., S. S. Rosenblum, and D. A. Shirley
g-factor of the 90-keV level in Ru^{99} and the paramagnetic correction in transition atoms
UCRL-11900, January 1965

Phys. Rev. 139, B532 (1965)

MATTHIAS, E., D. A. Shirley, J. S. Evans, and R. A. Naumann
Half life and g-factor of the 75-keV level in Rh^{100}
UCRL-16069, June 1965

Phys. Rev.

MATTHIAS, E., S. S. Rosenblum, and D. A. Shirley
Local moment on Ru atoms in Ni and giant induced Knight shifts above the Curie point
UCRL-16342, August 1965

Phys. Rev. Letters

MATTHIAS, E. (See Frankel, R. B., UCRL-11882)

MATTHIAS, E. (See Shirley, D. A., UCRL-16142 Abstract)

McHARRIS, William Charles
Decay schemes of odd-odd einsteinium isotopes
UCRL-11784, July 1965

Ph. D. Thesis

MERIWETHER, J. R. (See Harvey, B. G., UCRL-11895)

MERIWETHER, J. R. (See Harvey, B. G., UCRL-16124 Abstract)

MERIWETHER, J. R. (See Horen, D. J., UCRL-11904)

MILLER, Steven Frank
Axial dispersion in liquid flow through packed beds
UCRL-11951, May 1965

M. S. Thesis

MINER, Gene
Mountings and housings for lithium-drifted silicon and germanium detectors
UCRL-11946, February 1965

MÜLLER, Werner
Amine hydrohalide extraction studies
UCRL-16254, July 1965

Gordon Research Conference on Ion Exchange, New London, New Hampshire, August 2-6, 1965

NAKAMURA, M. (See Conway, J. G., UCRL-11867 Abstract)

NASH, John B.
The production of tritium labeled methane and ethane in the CH_4-T_2 system
UCRL-16009, April 1965

Ph. D. Thesis

NAUMANN, R. A. (See Matthias, E., UCRL-16069)

NEWTON, Amos S., and G. W. Kilian
Improved accuracy in measurement of low gas flow rates with a bubble meter
UCRL-16584, December 1965

Anal. Chem.

NEWTON, Amos S.
Metastable ion peak shapes in dempster type mass spectrometers
UCRL-16483, November 1965

J. Chem. Phys.

NEWTON, Amos S., and A. F. Sciamanna
Metastable peaks in the mass spectra of N_2O and NO_2
UCRL-16567, December 1965

J. Chem. Phys.

NIERENBERG, W. A. (See Faust, J., Phys. Letters 16, 71 (1965))

PEHL, Richard H.
(d, α) reactions on C^{12}, N^{14}, and O^{16} induced by 24 MeV deuterons
UCRL-11947, February 1965

Phys. Rev. 140, B605 (1965)

PEHL, Richard H., Donald A. Landis, Fred S. Goulding, and Blair V. Jarrett
Detection of 30- and 40-MeV protons by a windowless lithium-drifted germanium counter
UCRL-16477, October 1965

Phys. Letters

PEHL, R. H. (See Cerny, J., UCRL-11917 Abstract)

PEHL, R. H. (See Cerny, J., UCRL-16266)

PEHL, R. H. (See Cerny, J., UCRL-16575)

PEHL, R. H. (See Detraz, C., UCRL-16014)

PEHL, R. H. (See Rivet, E., UCRL-16200)

PERLMAN, I. (See Stephens, F. S., UCRL-16192)

PETERSON, J. R. (See Wallman, J. C., UCRL-16476)

PLASIL, F., D. S. Burnett, H. C. Britt, and S. G. Thompson
Kinetic energy-mass distributions from the fission of nuclei lighter than radium
UCRL-11954, July 1965

Phys. Rev.

POGGENBURG, John Kenneth, Jr.
Theoretical alpha decay rates of deformed nuclei
UCRL-16187, August 1965

Ph. D. Thesis

PRUSSIN, S. G., J. A. Harris, and J. M. Hollander
Application of lithium-drifted germanium gamma-ray detectors to neutron activation analysis: nondestructive analysis of aluminum
UCRL-16028, April 1965

Anal. Chem. 37, 1127 (1965)

PUGH, H. G., D. L. Hendrie, Marc Chabre, and E. Boschitz
High-resolution study of the $C^{12}(p, 2p)B^{11}$ reaction at 50 MeV
UCRL-11940, February 1965

Phys. Rev. Letters 14, 434 (1965)

PUGH, H. G. (See Hendrie, D. L., UCRL-11912 Abstract)

RAJNAK, K.
Configuration interaction effects on the "free ion" energy levels of Nd^{3+} and Er^{3+}
UCRL-11826, December 1964

J. Chem. Phys. 43, 847 (1965)

RAJNAK, K. (See Conway, J. G., UCRL-16292)

RASMUSSEN, John O.
Nuclear models and nuclear structure chemistry today
UCRL-11868 Abstract, January 1965

American Chemical Society Meeting, Detroit, Michigan, April 4-7, 1965

RASMUSSEN, J. O. (See Bowman, H. R., UCRL-11902)

RASMUSSEN, J. O. (See Cooper, J. A., UCRL-11923)

RASMUSSEN, J. O. (See Cooper, J. A., UCRL-16306)

RASMUSSEN, J. O. (See Cooper, J. A., UCRL-16319 Rev)

RASMUSSEN, J. O. (See Mang, H. J., UCRL-16550)

RASMUSSEN, J. O. (See Rho, M., UCRL-16155)

RASMUSSEN, J. O. (See Struble, G. L., UCRL-16102 Rev)

RAUSCHER, Elizabeth A.
Effects of collective excited states on alpha particle barrier penetrability
UCRL-11875, January 1965

M. S. Thesis

RAWITSCHER, G.
Ingoing wave boundary condition analysis of α-Ni^{62} elastic scattering cross section
UCRL-11893, January 1965

Phys. Rev. Letters 14, 150 (1965)

REDLICH, Martin G.
Energy levels of Pb^{210} from shell theory
UCRL-11735, October 1964

Phys. Rev. 138, B544 (1965)

REYNOLDS, F. L.
Helium leak detector probe
UCRL-16004, March 1965

Rev. Sci. Instr. 36, 1260 (1965)

RHO, Mannque, Hans J. Mang, and John O. Rasmussen
Comparisons of BCS nuclear wave functions with exact solutions
UCRL-16155, May 1965

Phys. Rev.

RHO, Mannque (See Mang, H. J., UCRL-16550)

RIVET, Ernest, Richard H. Pehl, Joseph Cerny, and Bernard G. Harvey
Investigation of high spin levels preferentially populated by the (α, d) reaction
UCRL-16200, July 1965

Phys. Rev.

ROBINSON, Herman P.
Gear ratios
UCRL-16226, June 1965

Mathematics of Computation

ROBINSON, Herman P.
Ruling quartz with a diamond
UCRL-16356, August 1965

Rev. Sci. Instr.

RONY, Peter R.
Atom production from cyclotron-resonant discharges
UCRL-16215, June 1965

Rev. Sci. Instr.

RONY, Peter R., and D. N. Hanson
The effect of oxygen, nitrogen, and water in low-pressure hydrogen discharges
UCRL-16211, June 1965

J. Chem. Phys.

RONY, Peter R.
The electromagnetic levitation of metals; the design, construction, and operation of a differential micromanometer; studies of atomic hydrogen at low pressures
UCRL-16073, April 1965

Ph. D. Thesis

RONY, Peter R.
Studies of atomic hydrogen at low pressures
UCRL-16050, April 1965

RONY, Peter R., and Kenneth W. Lamers
Vacuum measurement techniques. I. An electronic differential micromanometer
UCRL-16212, June 1965

J. Vacuum Sci. Tech.

RONY, Peter R.
Vacuum measurement techniques. II. Secondary microtorr pressure standards
UCRL-16213, June 1965

J. Vacuum Sci. Tech.

RONY, Peter R.
A water-cooled Wrede-Harteck gauge fitting
UCRL-16214, June 1965

Rev. Sci. Instr.

ROSENBLUM, S. S. (See Frankel, R. B., UCRL-11882)

ROSENBLUM, S. S. (See Matthias, E., UCRL-11900)

ROSENBLUM, S. S. (See Matthias, E., UCRL-16342)

SCIAMANNA, A. F. (See Newton, A. S., UCRL-16567)

SHIELD, E., and R. J. Slobodrian
Exchange processes and $^1S_0$ n-p scattering length
UCRL-11985, March 1965

Phys. Letters

SHIELD, E. (See Baumgartner, E., UCRL-16528)

SHIELD, E. (See Boschitz, E., UCRL-11964)

SHIELD, E. (See Boschitz, E., UCRL-16216)

SHIELD, E. (See Conzett, H. E., UCRL-16130 Abstract)

SHIELD, E. (See Slobodrian, R. J., UCRL-16123 Abstract)

SHIRLEY, D. A.
Applications of germanium gamma-ray detectors
UCRL-11865, December 1964
Nucleonics 23 No. 3, 62 (1965)

SHIRLEY, D. A., N. J. Stone, and E. Matthias
Nuclear orientation of Fm^{255}
UCRL-16142 Abstract, May 1965

American Physical Society Meeting, Honolulu, Hawaii, September 2-4, 1965

SHIRLEY, D. A. (See Blok, J., UCRL-16318)

SHIRLEY, D. A. (See Blok, J., UCRL-16328)

SHIRLEY, D. A. (See Blok, J., UCRL-16345)

SHIRLEY, D. A. (See Easley, W., UCRL-16002)

SHIRLEY, D. A. (See Frankel, R. B., UCRL-11882)

SHIRLEY, D. A. (See Frankel, R. B., UCRL-16012)

SHIRLEY, D. A. (See Holliday, R. J., UCRL-16437)

SHIRLEY, D. A. (See Levy, R. M., UCRL-11922)

SHIRLEY, D. A. (See Matthias, E., UCRL-11900)

SHIRLEY, D. A. (See Matthias, E., UCRL-16069)

SHIRLEY, D. A. (See Matthias, E., UCRL-16342)

SIIVOLA, A. (See Hyde, E. K., UCRL-16337)

SIKKELAND, T., A. Ghiorso, R. Latimer, and A. E. Larsh
Decay properties of the nuclides fermium-256 and -257 and mendelevium-255, -256, and -257
UCRL-16086, April 1965

Phys. Rev. 140, B277 (1965)

SIKKELAND, Torbjørn
Energy degradation and energy straggling of argon-40 ions in aluminum
UCRL-16453, October 1965

SIKKELAND, Torbjørn
Γ_n/Γ_f systematics and its implication in the synthesis of the heaviest nuclides
UCRL-16348, August 1965

Phys. Rev.

SISSON, D. H. (See Hyde, E. K., UCRL-16337)

SLOBODRIAN, R. J.
On the determination of the proton-proton $^1S_0$ shape parameter
UCRL-16408, September 1965

Phys. Rev.

SLOBODRIAN, R. J.
Extended charge effects on low energy proton-proton scattering
UCRL-16322 Rev, August 1965

Phys. Rev. Letters

SLOBODRIAN, R. J., H. E. Conzett, E. Shield, and S. Yamabe
Threshold effects in the α-α elastic scattering near 40 MeV
UCRL-16123 Abstract, May 1965

American Physical Society Meeting, Honolulu, Hawaii, September 2-4, 1965

SLOBODRIAN, R. J. (See Baumgartner, E., UCRL-16528)

SLOBODRIAN, R. J. (See Boschitz, E., UCRL-11964)

SLOBODRIAN, R. J. (See Boschitz, E., UCRL-16216)

SLOBODRIAN, R. J. (See Boschitz, E., UCRL-16217)

SLOBODRIAN, R. J. (See Boschitz, E., UCRL-16218)

SLOBODRIAN, R. J. (See Conzett, H. E., UCRL-16130 Abstract)

SLOBODRIAN, R. J. (See Shield, E., UCRL-11985)

SMITH, Charles F., Jr.
Decay of the Zn^{64*} compound nucleus formed by nuclear reactions of p, He^3, He^4, and C^{12} with Cu^{63}, Ni^{61}, Ni^{60}, and Cr^{52}, respectively
UCRL-11862, January 1965

Ph. D. Thesis

SOKOL, Harvey A., Winifred Bennett-Corniea, and Warren M. Garrison
Effect of conformation on the mechanism of the radiation-induced oxidation of poly-2-α-glutamic acid in aqueous solution
UCRL-16178 Abstract, June 1965

American Chemical Society Meeting, Atlantic City, September 12-17, 1965

SPRINGER, Arthur
Scattering of 50.9 MeV alpha particles from Ne^{20} and Ca^{40}
UCRL-11681, May 1965

Ph. D. Thesis

SPRINGER, A., and B. G. Harvey
Inelastic scattering of 50.9 MeV alpha particles from Ne^{20}
UCRL-11846, December 1964

Phys. Rev. Letters 14, 316 (1965)

STEPHENS, F. S., Frank Asaro, Sherman Fried, and I. Perlman
Odd-parity rotational bands in Cm^{246}
UCRL-16192, July 1965

Phys. Rev. Letters 15, 420 (1965)

STONE, N. J. (See Blok, J., UCRL-16345)

STONE, N. J. (See Frankel, R. B., UCRL-11882)

STONE, N. J. (See Frankel, R. B., UCRL-16012)

STONE, N. J. (See Holliday, R. J., UCRL-16437)

STONE, N. J. (See Shirley, D. A., UCRL-16142 Abstract)

STRUBLE, G. L., and J. O. Rasmussen
On the violation of Gallagher and Moszkowski's coupling rules in Ho^{166}
UCRL-16102 Rev, May 1965

Phys. Letters 17, 283 (1965)

TEMPLETON, D. H. (See Ueki, T., UCRL-16438)

TEMPLETON, D. H. (See Vogt, Jr., L. H., UCRL-16549)

TEMPLETON, D. H. (See Zalkin, A., UCRL-16269)

THOMPSON, S. G. (See Bowman, H. R., UCRL-11902)

THOMPSON, S. G. (See Bowman, H. R., UCRL-16485)

THOMPSON, S. G. (See Kapoor, S. S., UCRL-16208)

THOMPSON, S. G. (See Plasil, F., UCRL-11954)

THOMPSON, S. G. (See Watson, R. L., UCRL-16184)

TREYTL, W. J. (See Hyde, E. K., UCRL-16337)

UEKI, Tatzuo, Allan Zalkin, and David H. Templeton
Crystal structure of thorium nitrate pentahydrate by x-ray diffraction
UCRL-16438, October 1965

Acta Cryst.

VENERONI, M. (See Glendenning, N. K., UCRL-16428)

VOGT, Lester H., Jr., Allan Zalkin, and David H. Templeton
Crystal and molecular structure of a double complex of manganese with phthalocyanate and pyridine
UCRL-16549, November 1965

Science

WALLMANN, J. C., J. Fuger, J. R. Peterson, and J. L. Green
Crystal structure and lattice parameters of curium trichloride
UCRL-16476, October 1965

J. Inorg. Nucl. Chem.

WALLMANN, J. C., J. Fuger, Hermann Haug, Sayed A. Marei, and Brij M. Bansal
The heat of solution of curium metal and the heats of formation of $Cm^{+3}_{(aq)}$ and $CmCl_{3(c)}$
UCRL-16468, October 1965

J. Inorg. Nucl. Chem.

WARD, K. C. (See Conway, J. G., UCRL-11867 Abstract)

WASAN, D. T., R. M. Davis, and C. R. Wilke
Measurement of the velocity of gases with variable fluid properties
UCRL-16372, August 1965

A. I. Ch. E. J.

WATSON, R. L., H. R. Bowman, and S. G. Thompson
Internal conversion electrons from primary fission fragments
UCRL-16184, June 1965

International Conference on Internal Conversion Process, Vanderbilt University, Nashville, Tennessee, May 11-13, 1965

WATSON, R. L. (See Bowman, H. R., UCRL-11902)

WEEKS, Boyd M., Harriette L. Atkins, and Warren M. Garrison
Enhancement of water decomposition yields in the radiolysis of solutions of the anion and cation forms of the α-amino acids
UCRL-11970 Abstract, February 1965

Thirteenth Annual Meeting of the Radiation Research Society, Philadelphia, May 24-26, 1965

WEEKS, Boyd M., Sibyl A. Cole, and Warren M. Garrison
Reactions of alanine with the reducing species formed in water radiolysis
UCRL-11988, March 1965

J. Phys. Chem. 69, 4131 (1965)

WEEKS, B. M. (See Willix, R. L. S., UCRL-11969 Abstract)

WICKMAN, H. H. (See Easley, W., UCRL-16002)

WILKE, C. R. (See Leban, M., UCRL-16420 preliminary)

WILKE, C. R. (See Wasan, D. T., UCRL-16372)

WILLIX, Rodney L. S., Boyd M. Weeks, and Warren M. Garrison
Influence of chemical form on the reactions of amines with the hydrated electron
UCRL-11969 Abstract, February 1965

Thirteenth Annual Meeting of the Radiation Research Society, Philadelphia, May 24-26, 1965

YAMABE, S. (See Slobodrian, R. J., UCRL-16123 Abstract)

YAMAZAKI, T.
Angular correlations involving conversion electrons
UCRL-16027, March 1965

International Conference on Internal Conversion Process, Vanderbilt University, Nashville, Tennessee, May 11-13, 1965

YAMAZAKI, T., and J. M. Hollander
Measurement of pair production cross section near threshold
UCRL-16064, May 1965

Phys. Rev. 140, B630 (1965)

ZALKIN, A., David H. Templeton, and Ted E. Hopkins
The crystal and molecular structure of $C_5H_5FeC_2B_9H_{11}$
UCRL-16269, June 1965

J. Am. Chem. Soc. 87, 3988 (1965)

ZALKIN, A. (See Ueki, T., UCRL-16438)

ZALKIN, A. (See Vogt, Jr., L. H., UCRL-16549)

ZIRIN, M. H. (See Burnett, J. L., UCRL-16257)

2. CONTRIBUTIONS TO THIS REPORT

AHMAD, I.
A.9

ALI, D.
A.7

ALSTER, J.
C.4

ANTMAN, S. O. W.
D.14

ARMSTRONG, L., Jr.
A.5

ASARO, F.
A.8, 9, 10, 28

BABA, H.
B.3

BANSAL, B. M.
D.10

BERGKVIST, K. E.
G.22, 23

BLOK, J.
D.1, 8

BOSCHITZ, E. T.
A.25
C.5, 6, 7, 9, 11

BOWMAN, H. R.
B.1, 2
D.24

BUCHER, J. J.
F.1

BURDE, J.
A.15

BUSSIÈRE de NERCY, A.
C.3

BUTLER, G.
A.29

BYERS, C. H.
H.2

CERNY, J.
A.19, 20, 22, 23, 24, 29
G.18

CHABRE, M.
A.25, 26
C.5, 6, 7, 9, 11, 13, 17

CINGOLANI, H.
G.13

CLARK, D. J.
G.1

CLEM, R. G.
F.2

CLOSE, E.
G.1

CONWAY, J. G.
G.2, 8

CONZETT, H. E.
A.18
C.4, 5, 6, 7, 8, 9

COOPER, J. A.
A.13

CUNNINGHAM, B. B.
D.11

DARRIVLAT, P.
A.18

DÉTRAZ, C.
A.23, 24, 26, 29

DIAMOND, R. M.
A.15
F.1

EASLEY, W.
A.4
D.15

EDELSTEIN, N.
A.4
D.15

EDWARDS, V. H.
H.1

ELAD, E.
G.3

EMMOTT, M. J.
A.16

ENGLISH, M. K.
E.2

EVANS, J. S.
A.3

FALTENS, M. O.
D.12

FAUST, J.
A.6

FLEMING, D. G.
A.29

FRANCO, V.
C.14, 15

FRIED, S.
A.10

FUGER, J.
D.9, 10

GABRIELLI, I.
A.27
C.12

GARRISON, W. M.
E.1, 2

GATTI, R. C.
B.4

GIN, F.
G.5

GLAUBER, R. J.
C.14

GLENDENNING, N. K.
A.32
C.1, 2

GOLDSWORTHY, W.
G.4

GOULDING, F. S.
G.5, 6, 9, 12, 18

GREEN, J. L.
D.9, 11

GUNTER, K.
A.28

HANSEN, W. L.
G.7

HARADA, K.
A.32

HARRIS, J. A.
G.19

HARVEY, B. G.
A.19, 20, 27
C.3, 12

HAUG, H.
D.10

HAVERFIELD, A. J.
G.21

HELMHOLZ, A. C.
A.28

HENDRIE, D. L.
A.17, 25, 26, 27
C.11, 12, 13, 17

HOLLANDER, J. M.
A.12, 13, 14, 36, 37
G.17, 19, 21, 22

HOLLIDAY, R. J.
D.7

HOPKINS, T. E.
D.18

HOREN, D. J.
A.31
C.3

HOWARD, J. C.
G.8

HUFFMAN, E. H.
F.2

HYDE, E. K.
A.30, 31, 33, 34, 35
D.24

JARED, R. C.
D.24

JARRET, B. V.
G.7, 11, 12

JOHNS, O.
A.11

JUDD, B. R.
D.3, 4, 5, 6

KAPOOR, S. S.
B.3

KHODAI-JOOPARI, A.
B.4

KILIAN, G. W.
G.16

KIM, H.
G.1

KING, C. J.
H.2

KLEIN, M. P.
A.4

LAMB, J.
G.19

LANDIS, D. A.
D.14
G.6, 9, 12, 17, 18

LaPIERRE, R.
G.20

LEE, K. S.
D.20

LEIGH, J. R.
A.16

LERES, R. G.
G.10

LOTHROP, R. P.
G.11

MAHONEY, J.
A.27
C.3, 12
G.14

MALEH, I.
A.7

MAPLES, C.
A.29

MAREI, S. A.
D.10

MARRUS, R.
A.5, 6, 7
D.13, 16

MATTHIAS, E.
A.1, 2, 3

McCOLM, D.
D.13

McHARRIS, W.
A.8

McLAUGHLIN, R.
D.15

MENG, J.
G.13

MERIWETHER, J. R.
A.17, 27
C.3, 12

MYERS, M.
G.13

NAKAMURA, M.
G.3, 20

NAUMANN, R. A.
A.3

NEWTON, A. S.
D.22, 23
G.16

NEWTON, J. O.
A.16

NIERENBERG, W. A.
A.6

NITSCHKE, J. M.
A.34, 35

NURMIA, M.
A.30

PALMER, K. J.
D.20

PEHL, R. H.
A.19, 20, 22, 23, 24, 29
D.14
G.12, 18

PERLMAN, I.
A.8, 9, 10

PETERSON, J. R.
D.9

PRUSSIN, S. G.
G.19

PUGH, H. G.
A.18, 25, 26
C.11, 13, 17

RAJNAK, K.
G.2

RASMUSSEN, J. O.
A.11, 13
B.2

REDLICH, M. G.
A.21

REYNOLDS, F. L.
D.21

RIVET, E.
A.19, 20

ROACH, M. D.
G.11

ROBINSON, L. B.
G.5, 13, 14

ROSENBLUM, S. S.
A.2

SAKAI, M.
A.14, 17, 37

SCHAEFFER, T.
G.14

SCHURR, D.
G.6

SCIAMANNA, A. F.
D.22

SESSLER, A. M.
G.23

SHIELD, E.
A.18
C.6, 7

SHIRLEY, D. A.
A.1, 2, 3, 4
D.1, 2, 7, 8, 12

SIIVOLA, A.
A.31

SIKKELAND, T.
B.5

SISSON, D. H.
A.31

SLOBODRIAN, R. J.
A.18
C.5, 6, 7, 9, 10, 16

SMITH, H. E.
G.11

SPRINGER, A.
C.13

STEPHENS, F. S.
A.8, 10, 15

STONE, N. J.
D.7, 8

STONE, R. S.
G.17

TEMPLETON, D. H.
D.17, 18, 19

THOMPSON, S. G.
B.1, 2, 3, 4
D.24

TREYTL, W. J.
A.31

UEKI, T.
D.19

VALENTIN, J.
C.12

VALLI, K.
A.30, 33

VENERONI, M.
C.2

VOGT, L. H., Jr.
D.17

WALLMANN, J. C.
D.9, 10

WARD, D.
A.16

WARD, K.
G.20

WATSON, R. L.
B.2

WICKMAN, H. H.
A.4

WILKE, C. R.
H.1

WILLIX, R. L. S.
E.1

WRIGHT, S.
G.6

WYDLER, A. A.
G.15

YAMAZAKI, T.
A.12, 14, 17, 36, 37
G.17

YELLIN, J.
D.16

ZALKIN, A.
D.17, 18, 19

This report was prepared as an account of Government sponsored work. Neither the United States, nor the Commission, nor any person acting on behalf of the Commission:

A. Makes any warranty or representation, expressed or implied, with respect to the accuracy, completeness, or usefulness of the information contained in this report, or that the use of any information, apparatus, method, or process disclosed in this report may not infringe privately owned rights; or

B. Assumes any liabilities with respect to the use of, or for damages resulting from the use of any information, apparatus, method, or process disclosed in this report.

As used in the above, "person acting on behalf of the Commission" includes any employee or contractor of the Commission, or employee of such contractor, to the extent that such employee or contractor of the Commission, or employee of such contractor prepares, disseminates, or provides access to, any information pursuant to his employment or contract with the Commission, or his employment with such contractor.